Micro-contactors for Kinetic Estimation of Multiphase Chemistries

By

EVGENIA APOSTOLOPOULOU

A THESIS SUBMITTED IN FULFILLMENT OF THE REQUIREMENTS
FOR THE DEGREE OF DOCTOR OF PHILOSOPHY
UNIVERSITY COLLEGE LONDON, DECEMBER 2012

I, Evgenia Apostolopoulou, confirm that the work presented in this thesis is my own. Where information has been derived from other sources, I confirm that this has been indicated in the thesis.

Evgenia Apostolopoulou

Acknowledgements

The Author would like to thank Lucite International for the project funding and in particular Dr Graham Eastham and Dr Darren Gobby. She also acknowledges the lab personnel at the Wilton site (LI) for the execution of the autoclave experiments and Dr Jon Iggo at the university of Liverpool for the provision of the gas solubility data. The Author is very grateful to Dr George Manos, Dr Panagiota Angeli and Dr Lazaros Papageorgiou for their help and guidance during this project. Finally, the Author likes to acknowledge her husband, parents and brother but most of all her children for being fountains of motivation and inspiration.

Abstract

The revolutionary Alpha process developed by Lucite International (LI) is an industrially advantageous process over the traditional route of acetone cyanhydrin for the production of methyl methacrylate (MMA). The Alpha process entails two stages. The first stage is an homogeneous catalysis process, a methoxycarbonylation reaction which produces methyl propionate (MeP) from ethylene, CO and methanol using a Pd catalyst stabilised with the 1,2-bis(di-tert-butylphosphinomethyl)benzene (d^tbpx) phosphine ligand developed by LI. As it is known, kinetics are important for reactor modelling and simulation, interpretation of reaction mechanisms and catalytic phenomena. The kinetics of the methoxycarbonylation reaction are the subject of this research project and have been studied using a 2 L autoclave reactor and a 0.573 ml volume and 11.7 m length capillary microreactor with similar results. A bespoke experimental rig was designed and built to accommodate the micro devices. A theoretical investigation on the significance of mass transfer effects was undertaken to assess the significance of mass transfer limitations and both reactors were found to operate in the kinetic regime. A hydrodynamics study of Taylor flow under reaction conditions in a 6 m, 0.25 mm ID capillary microreactor was conducted to provide better understanding of the flow and improve its characteristics before the execution of kinetic experiments. The effect of methanol and Pd concentration, CO and ethylene partial pressure on the reaction rate have been studied. The reaction was found to be first and zero order with respect to methanol and ethylene respectively while the fractional order of 0.74 was derived with respect to Pd. CO inhibition kinetics were observed for high CO partial pressures and the reaction order was found to shift from positive to negative at p_{CO} equal to 1.8 bar.

The effect of temperature has been investigated in the range 80-120 ^{o}C and the activation energy was found to be 53 KJ/mol. A molecular level approach was used to derive a rate equation assuming the methanolysis step as the rate-controlling step. A software package was employed for the estimation of the rate parameters at the reaction conditions of 100 ^{o}C and 10 bar of gas pressure. Finally, a significant part of this research was spent on the design and development of a mesh microreactor of rectangular shape with dimensions 3 cm x 3 cm x 1.4 mm incorporating a 2 μm silicon nitride mesh with the aim to perform kinetic experiments but unfortunately this device was proved unsuitable for operation at high pressure.

Table of Contents

List of Figures

CHAPTER 1

CHAPTER 2

CHAPTER 3

CHAPTER 4

CHAPTER 5

CHAPTER 6

CHAPTER 7

CHAPTER 8

List of Tables

CHAPTER 2

CHAPTER 3

CHAPTER 4

CHAPTER 5

CHAPTER 6

CHAPTER 7

CHAPTER 8

Abbreviations

ACH	Acetone cyanhydrin
ACM	Aspen Custom Modeller
BHF	Buffered Hydrogen Fluoride
BR	Batch Reactor
CFD	Computational Fluid Dynamics
CSTR	Continuous Stirred Tank Reactor
DRIE	Deep Reactive Ion Etching
FEP	Fluorenated ethylene propylene
FID	Flame Ionisation Detector
GC	Gas Chromatography
ID	Inside diameter
IR	Infra-Red
LI	Lucite International
MEMS	Micro-Electro-Mechanical Systems
MeOH	Methanol
MeP	Methyl propanoate
MMA	Methyl methacrylate
MRI	Magnetic Resonance Imaging
OD	Outside diameter

PFR	Plug Flow Reactor
PR	Pressure Regulator
PTFE	Polytetrafluoroethylene
RTD	Residence Time Distribution
SS	Stainless Steel
STP	Standard Temperature and Pressure conditions (20^{o}C 1bara pressure)
T/C	Thermocouple
TCD	Thermal Conductivity Detector
TON	Turnover Number (molMeP/molPd)
TOF	Turnover Frequency (molMeP/molPd/h)
WGSR	Water Gas Shift Reaction

Nomenclature

Symbol	Definition	Units (SI)
A	Cross sectional area of the capillary channel	m^2
A_B	Cross sectional area of the gas bubble	m^2
A^*	Solubility of gaseous reactant *A* in the liquid reactant *B*	mol m^{-3}
B_0	Concentration of liquid reactant *B* in large excess	mol m^{-3}
C_{MeOH_0}	Concentration of methanol in the liquid mixture at the reactor inlet	mol m^{-3}
C_{MeOH}	Concentration of methanol in the liquid mixture at the reactor outlet	mol m^{-3}
D	Diffusion coefficient of CO in the liquid mixture	m^2 s^{-1}
d	Diameter of the capillary tube	m
C^*_{Eth}	Ethylene solubility in the liquid mixture	mol m^{-3}
C^*_{CO}	CO solubility in the liquid mixture	mol m^{-3}
d	Diameter	m
d_I	Impeller diameter (for autoclaves)	m
d_T	Tank diameter (for autoclaves)	m
E_α	Activation energy	kJ mol^{-1}
E_{abs}	Absolute experimental	-

	error	
E_{rel}	Relative experimental error	-
e_s	Systematic error	-
e_r	Random error	-
e_b	Gross error	-
F_B	Frequency of gas bubbles	s^{-1}
f_S	Slug friction factor	-
h_1	Height of impeller from bottom of tank (for autoclaves)	m
h_2	Height of liquid in the autoclave from the bottom of the tank	m
$k_{L,cap}$	Mass transfer coefficient, contribution of the bubble cap	$m\ s^{-1}$
$k_{L,film}$	Mass transfer coefficient, contribution of the liquid film	$m\ s^{-1}$
$k_L\alpha$	Specific mass transfer coefficient, all contributions	s^{-1}
L	Length of capillary channel	m
L_B	Length of gas bubble	m
L_S	Length of liquid slug	m
M_{mx}	Molality of the liquid mixture	$mol\ m^{-3}$
m_{Eth}	Solubility (in terms of	mol/ mol

	molar fraction) of Ethylene in the liquid mixture	
m_{CO}	Solubility (in terms of molar fraction) of CO in the liquid mixture	mol/ mol
n	Reaction order with respect to reactant *I*	-
N	Agitation speed (for autoclaves)	Hz
p	Partial pressure	bar
Q_{in}	Flow rate of the dispersed phase in a t-junction	
Q_{out}	Flow rate of the carrier phase in a t-junction	
Q_G	Gas flow rate	$m^3 s^{-1}$
Q_L	Liquid flow rate	$m^3 s^{-1}$
Q_m	Mixture flow rate= gas flow rate + liquid flow rate	$m^3 s^{-1}$
R	Reaction rate	$mol\ m^{-3}\ s^{-1}$
R	Gas constant =8.314	$J\ mol^{-1}\ K^{-1}$
S	Slip ratio-ratio of gas to liquid velocity	
t	time	s
T_v	True value of property	
U_b	Bubble velocity	$m\ s^{-1}$
U_{ls}	Liquid slug velocity	$m\ s^{-1}$
U_G	Velocity of the gas	$m\ s^{-1}$
U_L	Velocity of the liquid	$m\ s^{-1}$
U_m	Mixture velocity=velocity of gas + velocity of liquid	$m\ s^{-1}$
V	Volume	m^3

V_R	Reactor volume	m^3
V_{SG}	Surface aeration speed	m/s
w	Catalyst loading	mol m^{-3}
w_c	Width of the microfluidic channel	m
X_m	Measured of calculated value of property	
$\overline{X}$	Mean of sample of observations	

Greek Letters

α_{cap}	Specific area of the bubble cap	m^{-1}
α_{film}	Specific area of the liquid film	m^{-1}
γ	Ratio of reaction rate over rate of mass transfer	mol m^{-3} s^{-1}/ mol m^{-3} s^{-1}
δ	Thickness of liquid film in Taylor flow	m
δ_x	Relative systematic error	
ε_A	Relative area of the bubble in the cross area of the capillary	-
ε_G	Gas fraction (or void fraction) in the reactor	-
ε_L	Liquid fraction in the reactor	

ε_{Length}	Relative length of the bubble in the capillary	-
λ	Curvature ratio of capillary channel	-
μ_L	Viscocity of liquid	Ns/m^2
ρ_L	Density of liquid	kg/m^3
σ	Surface tension	N/m
τ_{in}	Reactor space time referring to the reactor inlet conditions	s
τ_{out}	Reactor space time referring to the reactor inlet conditions	s
χ	Methanol conversion	-
χ_{Eth}	Ethylene conversion	-
χ_{CO}	CO conversion	-

Subscripts

B	Relates to the gas bubble of Taylor flow
S	Relates to the liquid slug of Taylor flow
CO	Carbon Monoxide
Eth	Ethylene
film	film

fl	Relates to the fluid segment	
G	Gas	
L	Liquid	
mx	Gas-liquid mixture	
block	Relates to the blocking of the cross section of the duct in a t-contactor by the formed droplet	
squeeze	Relates to the squeezing of the immiscible thread in a t-contactor	
in	Refers to inlet	
out	Refers to outlet	
MeOH	Methanol	
I	With respect to reactant I	
NC	Complete gas dispersion (refers to the autoclaves)	
UC	Refers to the unit cell=1 bubble+1 slug	

Physical Constants

R	Gas constant, 8.314	J mol $^{-1}$ K^{-1}
h	Planck's constant, 6.626 10^{-34}	J s
k_b	Boltzmann's constant, 1.381 10^{-23}	J K^{-1}

Dimensionless numbers

Ha	Hatta number $Ha = \frac{(D\ \kappa)^{\frac{1}{2}}}{\kappa_L}$ (first order reaction)

Ca	Capillary number $Ca = \frac{\mu_L U_m}{\sigma}$
Dean	$\mathrm{Re}\sqrt{1/\lambda}$
We	Weber number $We = Ca \cdot \mathrm{Re}$
Fo	Fourier number $Fo = \frac{Dt_{film}}{\delta^2}$
ϕ	Enhancement factor $\phi = \frac{Ha}{\tanh Ha}$

CHAPTER 1

Introduction

The kinetics of the methoxycarbonylation of ethylene with a Pd homogeneous catalyst as the first stage of the production of methyl methyl acrylate (MMA) using the Lucite International (LI) Alpha Process is the subject of this study. The development of the reaction rate model suitable for reactor design is the ultimate goal of this project. MMA is the methyl ester of methacrylic acid, has the commercial name 'Perspex' and is a glass-like material with high hardness, resistance to fracture and chemical stability. It is an important monomer and intermediate. Almost half of the MMA global production is used in the manufacturing of polymethylmethacrylate (acrylic) resins. Other important uses include the production of surface coatings, impact modifiers and emulsion polymers.

MMA is mainly produced via the acetone cyanhydrin (ACH) route; reaction of acetone with HCN produces ACH, which is further treated with sulphuric acid to produce methacrylamide sulphate. The sulphate is then esterified with methanol to produce MMA and ammonium bisulphate as a by-product. The disadvantages of this process are the extreme operating conditions and the high volume of by-products. An overview of the numerous processes industrially used for the production of MMA and the various feedstocks are shown in Figure 1.1.

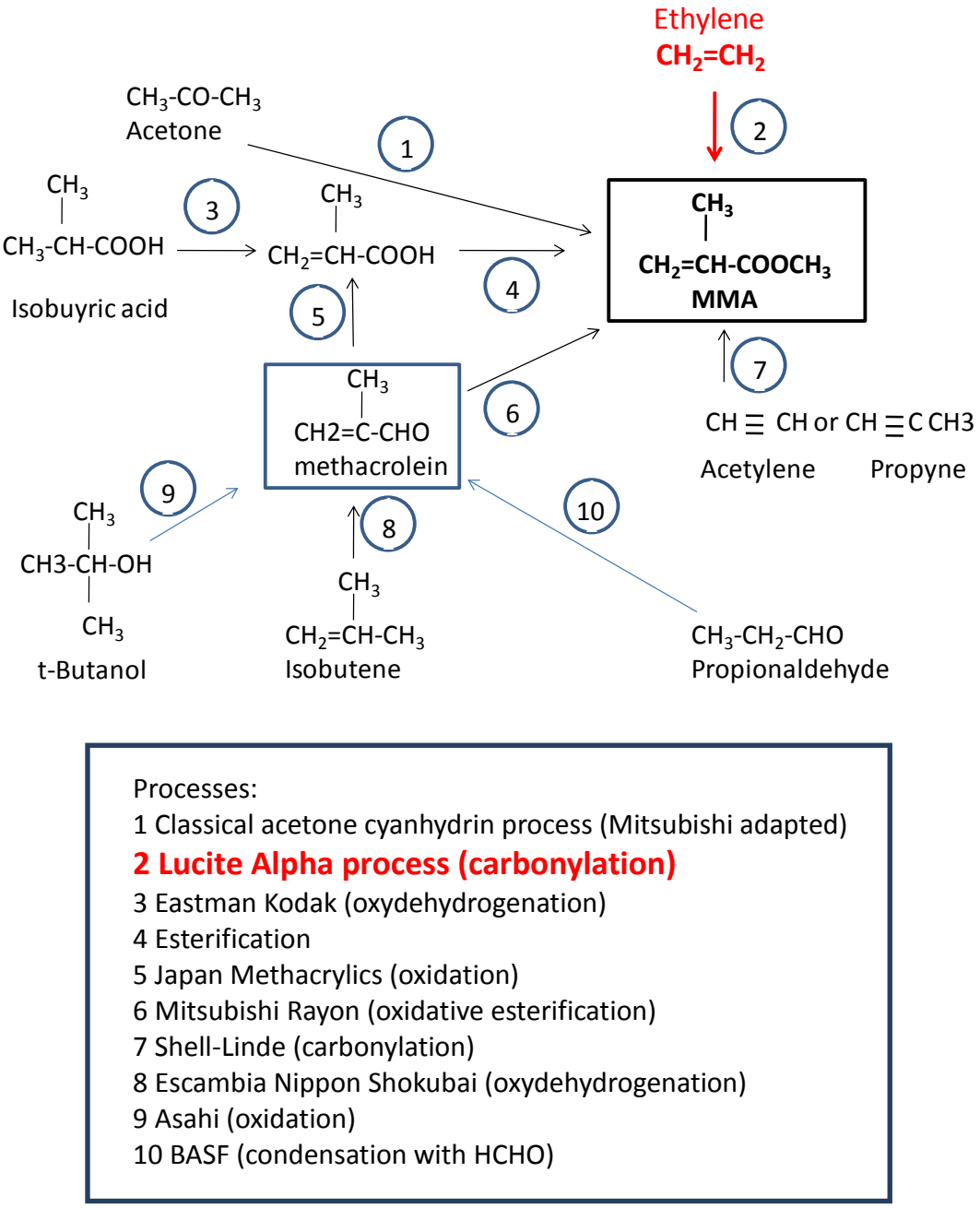

Figure 1.1. Different feedstocks/processes for MMA production.

The Alpha process for the production of MMA is a revolutionary route with no by-products, at milder conditions and with around 40% less production costs compared to the ACH process. The Alpha process comprises the following two stages:

- **Stage 1 is the synthesis of methyl propionate (MeP)** from ethylene, CO and methanol over homogeneous Pd catalyst with a selectivity greater than 99.8 %. It is a methoxycarbonylation reaction as follows:

$$CH_2 = CH_2 + CO + CH_3OH \rightarrow CH_3CH_2COOCH_3 \quad \Delta_r H^{\ominus} = -174.5 \text{ kJ mol}^{-1} \qquad (1.1)$$

Even though the reaction above is shown in one step, it is actually a series of elementary consecutive steps which compose the catalytic cycle.

- **Stage 2 is the formation of MMA** from MeP and formaldehyde over heterogeneous catalyst with a selectivity of 50 %:

$$CH_3CH_2COOCH_3 + HCHO \rightarrow CH_2 = CH(CH_3)COOCH_3 \qquad (1.2)$$

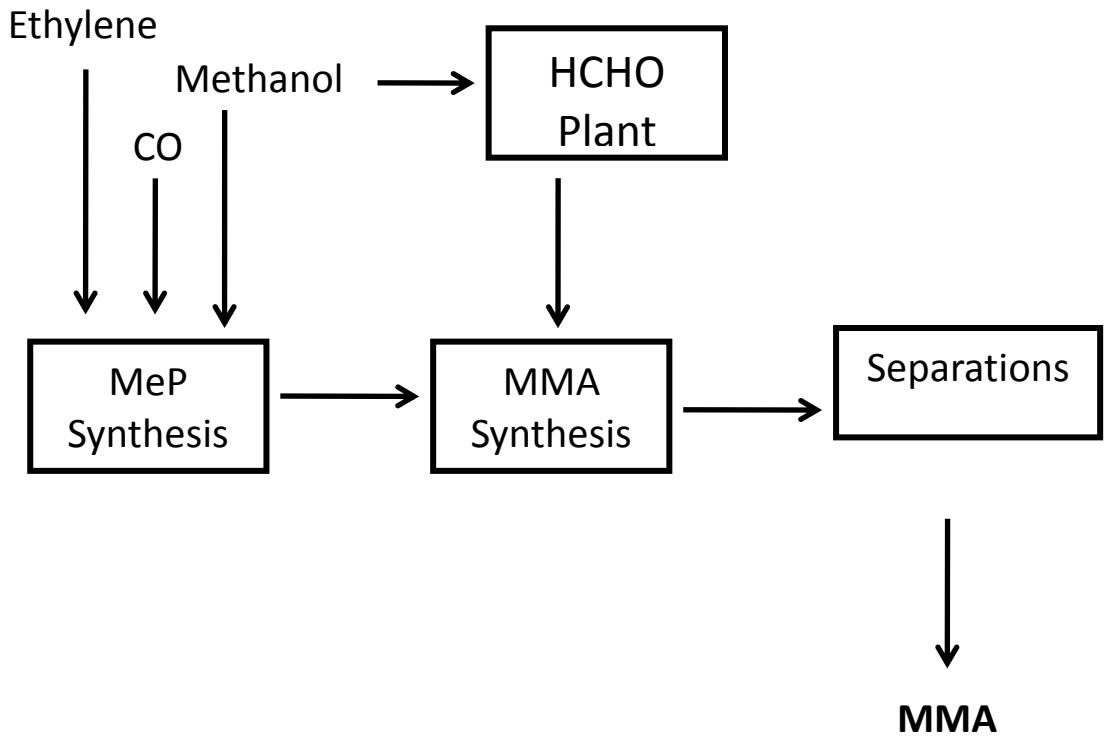

Figure 1.2. The Alpha Process.

LI is the sole proprietor of the Alpha process for MMA. Following the successful operation of a Stage 1 pilot plant reactor at LI, the first industrial plant ever built using this technology became a reality in Singapore for an annual capacity of 120,000 tonnes of MMA. A second plant is currently in the design stage with the nameplate capacity of 200,000t/y and is scheduled to come on-stream in the short-term, again in Singapore, while a third plant is in the company's plans to be constructed either in Asia or in the Middle East (www.luciteinternational.com).

As it is known, the importance of having good reaction kinetics for the design of chemical reactors is vital. Even though the first plant is already built, the MeP reactor design was based on empirical observations and preliminary experiments as the kinetics was unknown. However, the findings of this research study could be valuable to the design of the second and third MMA plants.

1.1 Description of the Chemical System

This research study focuses on Stage 1 of the Alpha Process which introduced a new catalytic system with two main characteristics: high activity and high selectivity to MeP. The miniscule amounts of catalyst necessary was one of the important factors that determined the viability of this technology for industrial application on a large scale. Process operating conditions are 100 ^{o}C and 10 bar of pressure of gas mixture.

The catalytic system is based on the zero valent palladium complex [Pd(L-L)(dba)] where L_2 is the C_4 –bridged bidentate phosphine ligand 1,2-bis(di-tert-

butylphosphinomethyl)benzene(d^tbpx) or $L-L=1,2(CH_2PBu^t_2)_2C_6H_4$ and dba=trans,trans,-dibenzylideneacetone or $dba=trans,trans(PhCH=CH)_2CO$. The complex is formed in situ from the salt $[Pd_2(dba)_3]$. The catalyst is quite stable and under continuous operation gives a turnover frequency or TOF (mol MeP formed per mol of Pd used per h) of 100,000 with 99.8% selectivity to MeP (Clegg et al., 1999, 2002a).

Other ligands were investigated for their suitability in the Alpha process but did not match the selectivity and activity of d^tbpx. For example, the ligand 1,3-bis(di-tert-butylphosphino)propane(d^tbpp) gave selectivity of 98.0% but a TOF of 15,000 (Clegg et al., 1999, Wolowska et al., 2002 and Eastham et al., 2002).

The ligands are surrounding molecules whose donor atoms are bound to a central metal atom or ion in coordinating compounds. 'Coordination' means that the ligands form a polyhedron with the metal in the center. Coordination number is the number of neutral or charged ligands. When the coordination number is 1 the ligand is called homoheleptic. A bi- or multi-dentate is the ligand that has two or multiple bonds to the metal and forms chelate complexes. The angle between two bonds is called the bite angle. (Cornils, 2003).

Phosphines are P, H compounds of the form P_nH_{n+2} and their organic derivatives. They are the most versatile group of ligands in coordination chemistry. In accordance to the amount of organic substituents they are called primary, secondary and tertiary phosphines. The latter are used as modifiers in homogeneous catalysis

because they affect the activity and selectivity of the catalyst. The extent of the modifying effect depends on the reactant and ligand properties and ligand concentration. The ligand properties depend on the electro-donating or -withdrawing character of the substituents and on the geometry and chain length of the bridging units. Tailoring of the ligand allows the control of chemo-, regio- and enantio-selectivity in homogeneous catalytic reactions (Cornils, 2003 and Kiss, 2001).

Monodentate phosphine ligands is the type used extensively in homogeneous catalytic reactions as they are easy to prepare and low cost while bidentate ligands which contain two P atoms are not so commonly used. Using a bidentate ligand for MeP synthesis is a new approach as in the past bidentate ligands were utilized for the formation of polyketones and monodentate ones for MeP (Clegg et al., 2002 and Eastman et al., 2000).

Pd is a 4-d transition metal together with Mo, Ru, Rh, Ag and the main catalyst for carbonylation reactions but also used in the Heck reaction, the Wacker and other processes (Cornils et al., 2003). It forms complexes or organometallic compounds together with ligands which allow the tuning of the catalyst properties. Pd is the only element with d^{10} electronic ground state and thus a unique catalytic metal. Pd complexes are stable, easy to handle and non-toxic. Moreover, Pd is less expensive than Rh or Pt. Homogeneous Pd catalysed reactions can be classified into oxidative reactions of Pd^{II} and Pd^{0} –mediated coupling reactions. In the case of Pd^{II}, it is reduced to Pd^{0} in the course of the reaction and has to be re-oxidized in situ. In the case of Pd^{0}, like the catalyst used in the Alpha process, the catalytic cycle must start and end with Pd^{0} and must be stabilised with ligands. However, these catalysts suffer

from decomposition to aggregates of elemental Pd. The colloidal particles obtained are usually less reactive and can exhibit different chemo- and regioselectivities. Pd black is the aggregate form that is observed in most cases, although sometimes colloids or even Pd particles with metallic cluster can be obtained. Kinetically, the precipitation process is initiated by the formation of a nucleus followed by growth processes. Pd's ability to change the oxidation state during a catalytic cycle and the formation of low-energy intermediates leads to a reduction of the activation energy of the catalytic reactions.

In homogeneous catalysis with phosphine ligands, a strong acid with weakly coordinating anions is used in order to protonate the phosphine. In the methoxycarbonylation of ethylene with the Alpha process, methanesulphonic acid, $MeSO_3H$, is used as it is more suitable for industrial applications because it increases the stability of the Pd-hydride species. It was found that at room temperature the Pd-hydride can stay for days without decomposing while at 353 K the decomposition starts after a few hours. When p-toluenesulfonic acid ($TfOH$), was used instead of $MeSO_3H$, the hydride formation was more facile but at 353 K decomposition started after 20 min. (Clegg et al., 2002).

An excess of $MeSO_3H$ is used in the catalytic acid as well as an excess of the phosphine ligand. The rate-promoting and stabilizing effect of the acid is caused not only by the preservation of the Pd in the active divalent form as Pd black can be dissolved in strong acids to Pd^{II} but also increases the concentration of the Pd-hydride complex which is the catalytic precursor, therefore acting as a catalytic

promoter. The phosphine ligand is kept in excess as it helps to maintain the Pd catalyst in solution and improves the catalyst selectivity. Previous research efforts showed that when only excess of ligand was used and not acid, this led to a very significant loss of catalytic activity even though precipitation of Pd black did not occur. (Kiss, 2001).

Methanol is the nucleophilic reagent used in the Alpha process. It was chosen because it is very reactive and cheap feedstock. Methanol's strong necleophilic character helps the reaction rate as it is known that in the case of nucleophils with attacking oxygen atom, increased nucleophilicity increases the reaction rate. (Kiss, 2001)

In the Alpha process, methanol (MeOH) fulfills four different roles:

- It is a reactant for the formation of MeP.
- It is involved in the formation of the Pd-hydride complex $[Pd(d^tbpx)H(MeOH)]^+$ which is the most important intermediate in the catalytic cycle.
- It stabilizes the Pd-hydride by keeping H^+ in solution.
- It is the solvent.

MeOH is not used on its own in the liquid mixture but is rather a component at 30 % (w/w) concentration; the second component being MeP at 70 % (w/w). The reasons for keeping MeP in excess are:

- The CO solubility in the MeP:MeOH liquid mixture is higher than in pure MeOH.
- Faster catalyst deactivation at very high MeOH concentrations has been noted from previous experimental results obtained at LI.
- The MeP:MeOH mixture forms an azeotrope at 50:50 (w/w) composition and the 70:30 ratio facilitates separation of the MeP produced at a later stage of flash separation.

The other two reactants in the Alpha process are CO and ethylene which dissolve in the liquid MeOH:MeP mixture where the reaction occurs. CO is an important building block in homogeneous catalysis. A large number of large scale industrial processes use CO in catalytic reactions involving the C-C bond formation between CO and the substrate (reactant). The high π-acceptor capacity of CO makes it a strongly coordinating molecule and this causes the stability of carbonyl complexes of low valent late transition metals like Pd. The formation of stable species is a catalyst poisoning effect and CO is a known catalyst poison for most low-valent metal complex catalysts (Nakamura, 1980). For example, the following reaction explains the deactivation of the catalyst for the Wilkinson hydrogenation by CO:

$$RhCl(PPh_3)_3 \xrightarrow{CO} RhCl(CO)(PPh_3)_2 \qquad (1.3)$$

Ethylene is an important building block for industrial manufacturing of polymers and chemicals. It is mainly co-produced with propylene from the steam reforming of naptha, gas oils, pygas (pyrolysis of gasoline) or condensates. The two carbon atoms of the ethene share two pairs of electrons; the double bond C-C. The double bond

comprises a σ and a π bond. The latter is weak which facilitates insertion reactions (Solomons, 2000 and Bailey, 1985).

Chapter 2 – Literature Review: Chemical Systems and Kinetics gives a summary of previous work on the chemistry of the methoxycarbonylation of ethylene and reviews the kinetic studies of other carbonylation reactions.

1.2 Kinetics with Conventional Laboratory Devices: Autoclave Reactor

A 2 L autoclave reactor, located at the research facility of LI was the first equipment used for the kinetic study. Following the elimination of mass transfer resistances, verified experimentally and by calculations, the collection of kinetic data took precedence and the results were analyzed. The work with the autoclave reactor is detailed in **Chapter 5 – Kinetics from Autoclave Experiments**.

1.3 Microreactors: the Principal Devices for this Study

Apart for autoclave reactors, micro-reactors were chosen as the preferred type of reactor for the work described in this Thesis. Microreactors are equipment which merit increased interest by the research community, particularly in the last years. They are considered advantageous over conventional reactors because (Hessel, 2005):

- They are particularly useful for diffusion limited reactions.
- The reactions are carried out with high heat and mass-transfer under safe conditions.
- They are characterised by high selectivity and productivity.
- There is significant scaling potential by arrays of microreactors.
- They involve low material inventories.
- They are cost effective.
- There is a variety of materials to be used for their fabrication.

Their main characteristic is the small dimensions in the order of the diffusion distances which enables fast equilibrium, fast heat and mass transfer and in the case where micro channels are used and laminar flow is the predominant flow pattern. As previously described, the methoxycarbonylation of ethylene involves two gaseous reactants; CO and ethylene which must dissolve in the liquid medium (a mixture of methanol and methyl propionate) where the reaction takes place. With the solubility of CO in the liquid mixture low and the constraint that the CO concentration in the gas mixture fed to the reactor must remain at a minimum level due to the fact that the CO deactivates the Pd catalyst, there is increased risk that the reaction can be diffusion limited. As a result, reactor operation at the Stage 1 pilot plant at LI was believed to be under mass transfer control and in addition to that observations from a number of autoclave experiments performed in 2000-2001 at LI pointed to the that mass transfer being problematic. Therefore, microreactors were favoured as the main tool for this kinetic study mainly for their potential of improved mass transfer which stems from their micro dimensions, enabling in this way operation in the kinetic regime and collection of intrinsic kinetic experimental data.

Different microreactor systems have been designed e.g. for very fast reactions and residence time in the order of s at atmospheric pressures as well as for reaction time min to h at high pressures. However, there is one consideration to be kept in mind regarding these reactors in general, which is ensuring sufficient interface area and contact time between the phases, which was addressed in this study with the conception, design, manufacture of three novel micro reactors; the first one being a mesh micro reactor whose additional characteristic to those mentioned above is the known gas-liquid contact area, which is effectively the open area of the pores of the mesh.

Even though this device was initially thought to be very promising for this study, in practice its operation was found to be problematic under the reaction conditions of high pressure. Suggestions for additional research to be conducted with the mesh micro reactor are provided in order to verify its suitability and effectiveness as a gas-liquid reactor but for other chemical systems requiring milder reaction conditions. A summary of past research conducted on mesh reactors is given in **Chapter 3 – Literature Review: Microreactors with Particular Focus on Mesh Microreactors**. Details of the design, development and experimental work done on the mesh reactors as well as trials with other micro-contactors can be found in **Chapter 6- Mesh Microreactors and other Reactor Trials** of this Thesis.

Two novel capillary microreactors were developed and utilised in this kinetic study. The first one which has the shape of a spiral, therefore called ‘spiral reactor’, was used in the context of a hydrodynamics study including flow visualisation and characterisation, bubble and size measurements, size distributions and flow

repeatability check, as well as improvement of the experimental set-up in order to achieve homogeneous gas-liquid flow prior to the execution of kinetic experiments with the second capillary reactor. The literature review on the hydronamics of Taylor flow with emphasis on important issues faced in this research is included in **Chapter 4 – Literature Review: Hydrodynamics of Taylor Flow with Particular Focus on Bubble, Slug Size and Flow Homogeneity.** The hydrodynamics study conducted in the framework of this project can be found in **Chapter 7 – Hydrodynamics Study**.

Numerous experiments were conducted and intrinsic kinetic data were gathered with the second capillary microreactor, part of a bespoke apparatus, as it is explained in **Chapter 8- Kinetics Study from Microreactor Experiments**. Kinetic modelling based on the catalytic cycle of the methoxycarbonylation of ethylene and the quasi-state approximation also forms part of this chapter. The analysis of this work with the capillary reactor provided kinetics which agrees with kinetic results obtained via autoclave experiments. Finally, **Chapter 9 – Summary and Conclusions** reviews the results**,** confers the meaning of this study, relates the findings of current work to previous research as well as discusses the additional research that this study suggests is needed.

1.4 Novelty of this Work

When one works with capillary reactors, the measurement of bubble and slug sizes can be essential to her work and at the same time prove to be a difficult task, particularly under reaction conditions of high temperature and pressure. In the

context of this work, a spiral capillary reactor was developed which proved to be a very useful tool for flow visualisation and characterisation, bubble and size measurements not only at the reactor inlet and outlet but also at any intermediate position along the capillary under reaction conditions. The microreactor was used in conjunction with a camera-microscope and flow analysis software system. Furthermore, the microreactor system is suitable for high pressure and temperature operation under safe conditions, provides for temperature homogeneity and is problem-free regarding channel blockage. It is designed to hold 1/16'' OD capillary tube of variable ID and maximum length of 7.6 m. A capillary tube with 0.25 mm ID and 6 m length was used in the experiments presented in this Thesis.

As a new kinetic study is undertaken, two possible approaches exist according to Santacesaria (1999). The first one is the empirical approach, when the determination of partial reaction orders based on the power law is attempted from the reaction rate data gathered and then a kinetic law equation of first attempt is derived from the experimental results. The second one is the theoretical approach, when a kinetic law equation is proposed based on a theoretical suggestion after one makes the hypothesis of a reaction mechanism for the reaction to be studied, the hypothesis of the slow step as well as the hypothesis of the steady state. Subsequently a kinetic law in agreement with the two approaches is derived followed by the determination of the kinetic parameters and examination of their consistency. This methodology was followed in the work reported in this Thesis but with some new elements.

Partial reaction orders for the methoxycarbonylation of ethylene whose kinetics were largely unknown prior to this study were determined experimentally using a capillary

microreactor with 0.25 mm ID and 0.573 ml volume and the results were found in very good agreement with autoclave data. When batch reactors are the most commonly used equipment by researchers active in the field of kinetics, only few studies of reactions have been reported in the literature to have been carried out with capillary microreactors and in these cases the ID of the capillary tubing was 0.5 mm and above.

A kinetic law equation was established theoretically from a proposed reaction mechanism scheme based on the hydride catalytic cycle - the most plausible mechanism for the chemical reaction system in question - but which also includes the novel element of the catalyst deactivation reaction route. The methanolysis, i.e. the step where methanol reacts and yields the ester, is assumed to be the rate determining step in the suggested reaction mechanism scheme (also suggested by Jimenez et al, 2004). The results from the two approaches were firstly coupled together and then parameter estimation followed for the determination of the kinetic parameters.

As was mentioned in the previous section, there were strong indications that the methoxycarbonylation of ethylene could be diffusion limited, originating mostly from observations during past autoclave experiments rather than being the product of a systematic study. In the context of this project, a theoretical exercise entailing the characterisation of the autoclave reactor operating regime, evaluation of mass transfer coefficient and mass transfer rate as compared to reaction rate was completed prior to the onset of the main experimental program. Measures were proposed in order to avoid mass transfer resistances and results from preliminary

experiments verified the soundness of these conclusions. Equivalent calculations were executed for the experiments performed with the capillary reactor but with the additional input of hydrodynamic experimental data also taking into account previous relevant research conducted on gas-liquid flows in micro channels.

The various tasks involved in this research project, how they are interconnected with each other and the way in which they have been incorporated in this Thesis is depicted in Figure 1.3. It can be seen that autoclaves and microreactors were the main reactors used in this study. The mesh microreactors developed for this project were proven to be unsuitable equipment for operation under pressure and therefore inappropriate for the reaction under study. Two capillary microreactors were developed and used satisfactorily. The one with the spiral form was used for the Taylor flow hydrodynamics study and the collection of data which were very useful in the kinetic experiments performed with the second capillary. The research conducted with the second capillary reactor and the experimental data collected agree very well with the data obtained with the autoclave reactor. Coupling of these two sets of data provided kinetics for the methoxycarbonylation of ethylene in the LI Alpha process. Kinetic modelling and parameter estimation led to the derivation of the reaction rate law, as it is illustrated in Figure 1.3.

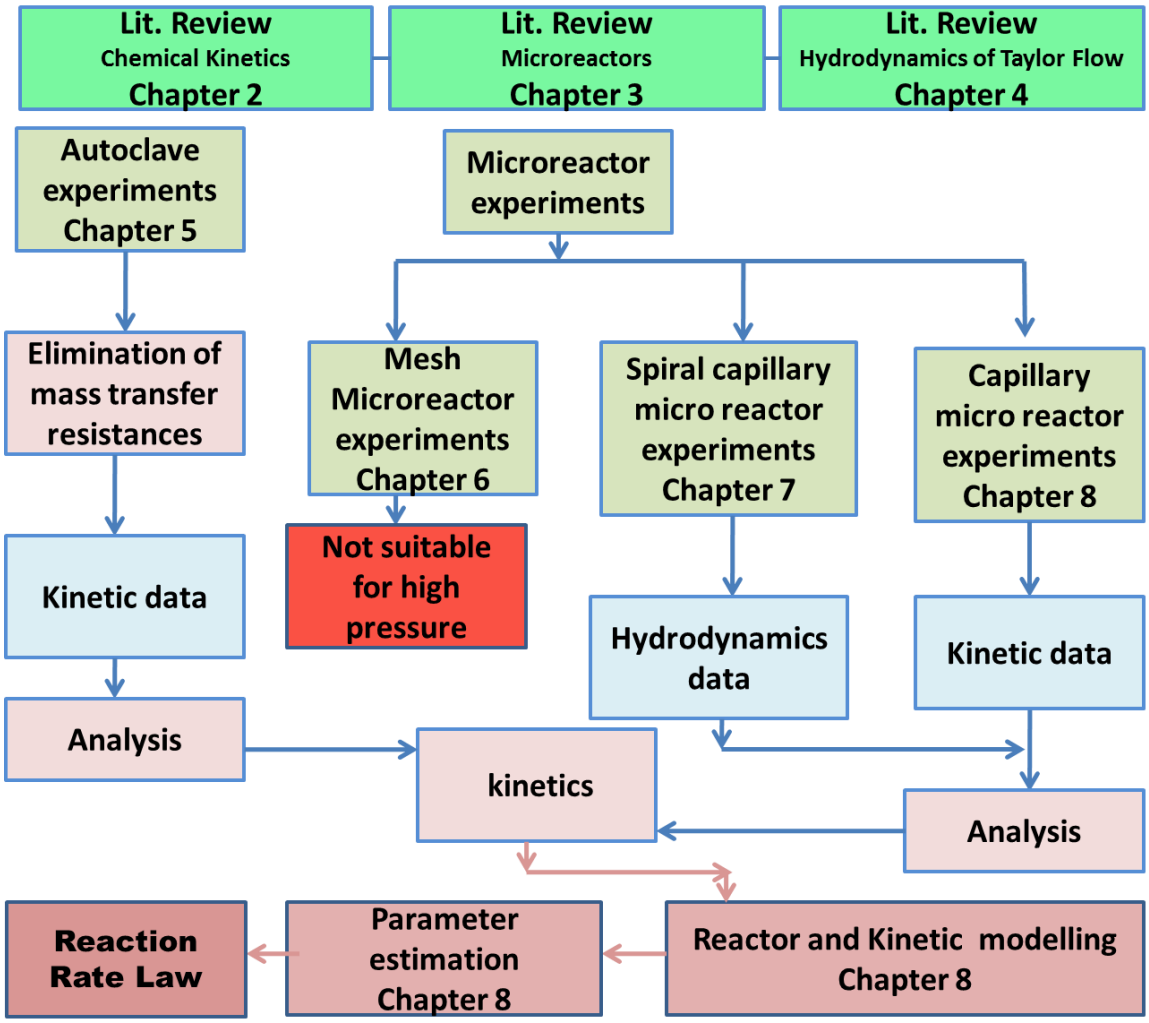

Figure 1.3. Work presented in this Thesis.

--//--

CHAPTER 2

Literature Review: Chemical Systems and Kinetics

The Pd- catalysed methoxycarbonylation of ethylene is of growing importance as it produces a variety of products through four industrial processes according to the following scheme (Clegg et al., 1999, Cornils et al. 2003):

$$CH_2 = CH_2 + CO + CH_3OH \rightarrow H[CH_2CH_2CO]_n OCH_3 \qquad (2.1)$$

These industrial processes are:

1. *Methoxycarbonylation*: Formation of MeP for (n=1 in eq. 2.1).
2. *Diethyloketone production* (DEK) (for n=2 in eq. 2.1).
3. *Copolymerization*; Formation of CO/C_2H_4 copolymer.
4. *Polyketones production*; Polyketones are high molecular weight products with useful thermoplastic properties like flexibility, high impact and wear resistance as well as high strength. They are manufactured and marketed by Shell under the commercial name *Carilon.*

For the formation of polyketones or MeP, a palladium complex, an excess of phosphine ligand and a Bronsted acid of weakly or non-coordinating anions like for

example methanosulphunic acid, must be present (Makamura & Tsutsui, 1980). The methanol is acting as a solvent and a reactant.

Methoxycarbonylation and copolymerization are intimately related. They involve similar initiation and propagation steps but methoxycarbonylation has no chain propagation and termination occurs after a single turnover (Knight et al, 2000).

The choice of the phosphine ligand determines the production of the monomer or the polymer. Traditionally, monodentate ligands like PPh_3 give MeP while bi-dentate ligands give high molecular weight co-polymers. However, the proprietary Alpha process of LI is based on the bi-dentate phosphine ligand 1,2(di-*tert*-butylphosphinomethyl)benzene or (d^{t}bpx) which gives high activity, selectivity and stability for MeP production (Clegg et al., 1999). Early experimental work showed that the rates produced with the d^{t}bpx ligand were in the range of 100,000 molMeP/molPd/h and 99.8% selectivity. d^{t}bpx belongs to the group of di-phosphines which are a class of chelating ligands containing two posphine groups connected to each other by a bridge also referred to as backbone. The bridge, for instance, might consist of one or more methyl groups or multiple aromatic rings with heteroatoms attached. In the case of d^{t}bpx, the backbone consists of a benzene ring and two methyl groups. The two phosphorus atoms of the diphosphine bond to the metal. The structure of the backbone and the substituents attached to the phosphorus atoms influence the chemical reactivity of the diphosphine ligand in metal complexes through steric and electronic effects. The natural bite angle of diphosphines, obtained

using molecular mechanics calculations, is defined as the selective chelation angle (P-Metal-P bond angle) that is determined by the diphosphine ligand backbone.

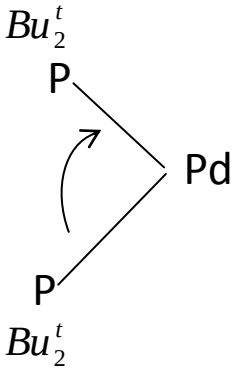

Figure 2.1. Bite angle for the d^{t}bpx ligand.

2.1 Carbonylation Reaction-General Overview

Acylation is the introduction of acyl groups such as –CO-R or –SO_2-R in organic compounds containing C-H acid groups such as –OH, -SH, -NH (Cornils, 2003). Carbonylation is the catalytic reaction that introduces $C=O$ into an organic molecule. Reppe carbonylation is the reaction that combines three reactants: an unsaturated hydrocarbon, CO and a nucleophile. The substances studied mostly are alkenes, alkynes, dienes (mostly butadiene) and aryl-substituted dienes (e.g. styrene). The nucleophile can be water, alcohol or acid and the products are saturated or unsaturated acids, esters or anyhydrides. The Pd-catalysed carbonylation of alkenes with CO and water is referred to as hydroxycarbonylation and it yields carboxylic acids. When the nucleophile is alcohol the process is called hydroesterification and sometimes hydroalcoxycarbonylation, hydrocarbalcoxylation or alcoxycarbonylation

(Kiss, 2001) and it allows the formation of carboxylic acid esters. When the alcohol is methanol, the reaction is called methoxycarbonylation.

Depending on the reactions conditions, the catalyst used (ligand type, bite angle e.t.c.) alcoxycarbonylation reactions can lead to branched or linear esters. Bisalcoxycarbonylation yields diesters. Hydroxycarbonylation and alcoxycarbonylation reactions have similarities in terms of activity and regioselectivity because the nucleophile is not involved in the selectivity determining step. However, alcoxycarbonylation is more interesting for academic purposes because of the highest product purification achievable.

The general reaction scheme of alcoxycarbonylation which can lead to two isomers is the following:

$$R-CH=CH_2+CO+Nu-H \rightarrow R-CH_2-CH_2-CO-Nu+R-CH(CO-Nu)-CH_3 \qquad (2.2)$$

Apart from Pd, other metals like Co, Pt, Ni, Rh and Ru have been used for hydrocarboxylation and alcoxycarbonylation reactions but for reasons of working with mild reaction conditions (for instance 20-80 ^{o}C and 1-10 bar CO), only Pd and Rh have received significant interest (Chiusoli, 1991).

As mentioned before, the ligand and the reaction conditions play a major role in determining the chemoselectivity and regioselectivity of carbonylation reactions but in the past, primarily ligand-free Pd catalysts, for example $PdCl_2$/HCL were used to synthesize esters from alkenes at harsh pressure conditions like 100 bar of CO. However, in the last ten years, Pd^0 or Pd^{II} with phosphine ligands have received

increased interest in the formation of linear esters with improved regioselectivity. The fact that chelating phosphine ligands are a particularly useful tool to control regioselectivity has been identified by much earlier. Ligands like these are for example bis(phosphanoadamantyl)-alkanes, 1,2-bis(di-tert-butylphosphanylmethyl) benzene, 1,1-bis(diphenyl phosphanyl) metallocenes or others. Carbonylation reactions in recent years have been improved in terms of mildness of conditions and catalyst stability and selectivity. However, more catalyst and reaction conditions optimization is necessary for many carbonylation processes so that the efficiency can be improved. (Chiusoli, 1991).

The most plausible mechanism of the carbonylation of alkenes using Pd-complexes, consists of the alkene insertion into the bond of Pd-hydride which is the catalytic precursor, to create a Pd-alkyl intermediate followed by the migratory insertion of CO into the Pd-alkyl bond to give a Pd-acyl complex. Finally, the Pd-acyl undergoes nucleophilic attack by the alcohol to give the ester and the Pd-hydride is re-formed. The role of the acidity is important for the cleavage of the Pd-acyl bond. Furthermore, the balance between the acid and the phosphine ligand helps the stabilisation of the Pd-hydride which in turn determines the efficiency of the catalytic system. An alternative mechanism which is not as widely accepted as the one just described, does not start with the Pd-hydride but with a Pd-alkoxy-carbonyl intermediate (for more information on catalytic cycles please see the following Section).

When Pd^0 species are used as catalysts in carbonylation reactions, these are usually formed in-situ by Pd^{II} precursors when a reducing agent is present in the system, like

for instance OR^-, F^- or OH^-. During the numerous repetitions of the catalytic cycle, it is possible that the Pd^0 will lose the phosphine ligand and form phosphine-free Pd^0 colloidal nano-particles which are regarded as good catalysts for carbonylation, especially when applied in an ammonium salt or anionic liquid medium. However, bigger size clusters are considered to have limited activity. Mono-molecular Pd^0 species have been found to exist in equilibrium with Pd^0 colloid nano-particles in phosphine-free systems but more research is necessary to see if this is the case in phosphine systems (Trzeciak, 2005).

CO is the main component in carbonylation reactions. However, there are some drawbacks associated with its use like its high toxicity and also difficulty in handling and storing due to its gaseous nature. Many research efforts have concentrated in replacing the CO with other C1 building blocks and significant improvements have been made in terms of efficiency and yields but the new methods generally require more severe reaction conditions, include more by-products which are discarded as waste and often these C1 building blocks are as toxic as CO. Nevertheless, these new carbonylation reactions can have applications in the fields of microreactor synthesis, combinatorial synthesis and other, on the back of the demand for automated handling of liquids rather than gases.

Alkyl formates, and in particular methyl formate, have been used as alternative to CO C1 building block. The alkyl formates dissociate in the presence of a strong base and yield highly pure CO and the corresponding alcohol. MeP has been formed from methyl formate which decarbonylates and yields CO and methanol using a Ru-catalyst and then reacts with ehylene. The reaction is as follows:

$$CH_2 = CH_2 + HOOCH_3 \xrightarrow{RuCl_2(PPh_3)_3,(0.14mmol),190^0C,18h,N_2 15bar,C_2H_4 10bar} CH_3CH_2COOCH_3 \quad (2.3)$$

Recently formates with pyridyl group have been used for the carbonylation of various alkenes and alkynes. (Morimoto & Kakiuchi, 2004).

2.2 Catalytic Cycle Analysis

Two catalytic cycles have been proposed by several authors concerning the methoxycarbonylation of ethylene with Pd homogeneous catalysts, (Eastman et al., 2000, Clegg et al., 2002, Kiss 2001, Pugh et al., 2001, Pugh et al, 2002, Vavasori et al. 2001, Vavasori et al. 2003, Bhaduri & Mukesh, 2000).

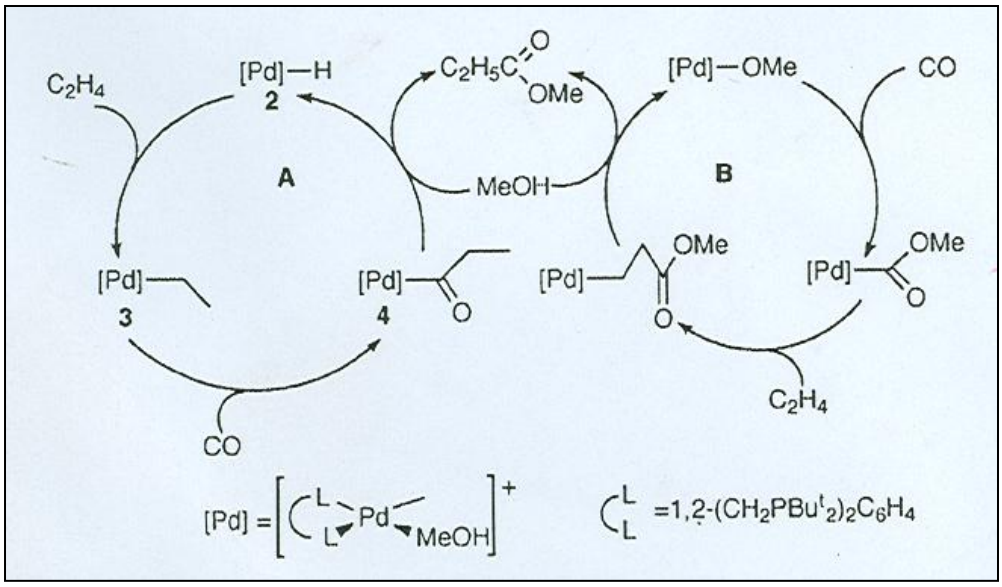

Figure 2.2. The possible catalytic cycles for the methoxycarbonylation of ethylene to methyl propanoate. A: Hydride cycle, B: Methoxy cycle.

2.2.1 The methoxy cycle

This is proposed to be followed in the hydroesterification of propyne in the Shell process for MMA. It starts with the Pd-methoxy complex $[Pd-OCH_3]^+$ which reacts with CO to form the Pd-alcoxy-carbonyl intermediate $[Pd-COOCH_3]^+$ which in turn reacts with $CH_2=CH_2$ (insertion of the alkene into the Pd-carbon bond) yielding a Pd-alkyl complex $[Pd(L-L)(C(O)Et)(MeOH)]^+$. Protonolysis with methanol gives the product MeP $EtCOOMe$ and the initial Pd-methoxy complex (Bharuri & Mukesh, 2000 and Clegg et al., 2000).

2.2.2 The hydride cycle

The cycle starts with the formation of the $[Pd(L-L)H(MeOH)]^+$ by oxidation of $[Pd(L-L)(dba)]$. This hydride structure is shown in Figure 2.4. The hydride complex, was initially believed to give the methoxy-complex $[Pd-OCH_3]^+$ in the presence of an oxidant. However, in this case, the hydride is quite stable, which is a rare case, even if oxygen is pumped through the reactive solution for 10 min or in the presence of BQ (benzoquinone). One of its characteristics is that at room temperature the Pd-hydride can stay for days without decomposing. At 353 K the decomposition starts after a few hours. When another acid, $TfOH$ is used instead of $MeSO_3H$, the hydride formation is more facile but at 353 K decomposition starts after 20 min. Thus, $MeSO_3H$ is more suitable for industrial applications because in this case the Pd-hydride species is more stable (Clegg et al., 2002).

The transformations of the catalyst which lead to the formation of the Pd-hydride, the complex believed to be the catalyst precursor in the Alpha Process, were reported by Clegg et al., 2002:

$$[Pd(d^tbpx)(dba)] \xrightarrow{+H^+} [Pd(d^tbpx)(dbaH)]^+ \quad (2.4)$$

$$[Pd(d^tbpx)(dbaH)]^+ \xrightarrow{+BQ/O_2} [Pd(d^tbpx)(n^2-RSO_3)]^+ \quad (2.5)$$

$$[Pd(d^tbpx)(n^2-RSO_3)]^+ \leftrightarrow [Pd(d^tbpx)(solv)_2]^{-2} \quad (2.6)$$

$$[Pd(d^tbpx)(solv)_2]^{-2} \rightarrow \underset{\textbf{Pd-hydride}}{[Pd(d^tbpx)H(solv)]^+} \quad (2.7)$$

In the above reaction scheme, *solv* denotes the solvent which is methanol while R is methyl. Reaction (2.4) is a protonation reaction. Reaction (2.5) is a very fast oxidation reaction at high temperatures and even traces of oxygen are sufficient for this reaction to take place. Reaction (2.6) is a displacement reaction of the anion RSO_3^-. It was found that the position of the equilibrium depends on the solvent used and the R. Polar solvents, like methanol, shift the equilibrium to the right. The opposite happens when very basic R groups are employed. Reaction (2.7) is a redox reaction which happens only with primary and secondary alcohols and is a β-hydride elimination reaction.

The Pd-hydride reacts with ethylene to form the alkyl complex $[Pd(L-L)CH_2CH_3]^+$ which is an agostic compound and in reality not a single substance but a 1:1 mixture of two isomers $[Pd(L-L)(CH_2{}^{13}CH_3)]^+$ and $[Pd(L-L)(^{13}CH_2CH_3)]^+$ as it was shown by ^{13}C experiments reported in the study by Clegg et al. in 2002. The alkyl complex, subsequently reacts with CO to form the acyl-complex $[Pd(L-L)(C(O)Et)(MeOH)]^+$. These two steps are believed to be

facile equilibrium. The acyl complex is very reactive and undergoes methanol nucleophilic addition to yield the product and regenerate the Pd-hydride complex. This methanolysis step is believed to be the rate determining step in the catalytic cycle. The same catalytic system is believed to be active for the methoxycarbonylation of terminal and internal alkenes (Jimenez et al., 2004). The nucleophilic attack on the acyl complex has been found to be the rate-limiting step in the carbonylation of iodo- and bromo-compounds (Beller et al., 1995). The complex $[Pd(L-L)H(CO)]^{+}$ could form in a competitive reaction and is very unstable even at low temperatures. It could cause further decomposition of the Pd-hydride by more addition of CO. Consequently, the efficiency of the catalytic cycle depends on the competition of $CH_2 = CH_2$ and CO for the Pd-hydride (Clegg et al, 2002). In addition to d^tbpx ,the catalytic system of the phosphine d^tbpp (please refer to Figure 2.3) was proposed to follow the hydride catalytic cycle. Isotope scrambling experiments also confirmed the hydride-cycle. Furthermore, other studies using different Pd catalytic systems have concluded that the process follows the hydride cycle. Example is the mehoxycarbonylation of ethylene to produce MeP when $[Pd(p-CH_3C_6H_4SO_3)_2(PPh_3)_2]$ is used as catalytic precursor (Cavinato et al, 2004). The fact that the Pd-hydro-route is operative has also been concluded by different studies for ethane (Cavinato et al., 2004) as well as for the hydroalkoxycarbonylation of styrene and α-methylstyrene (Benedeck et al., 1999).

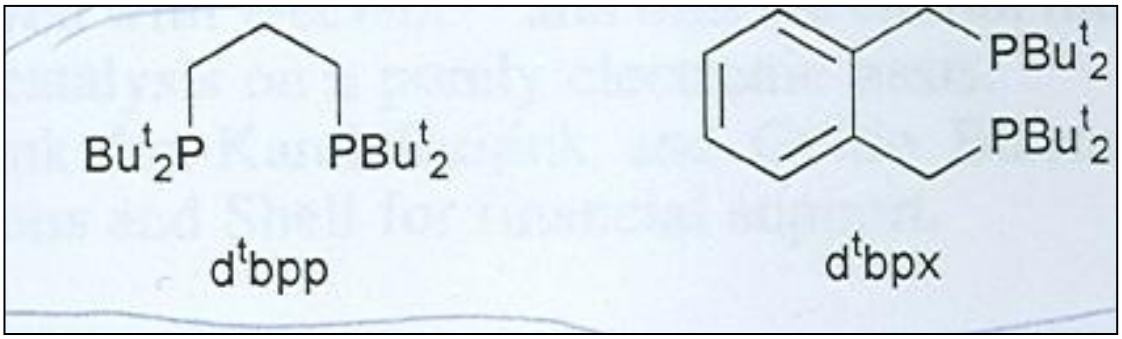

Figure 2.3. Ligand Structures.

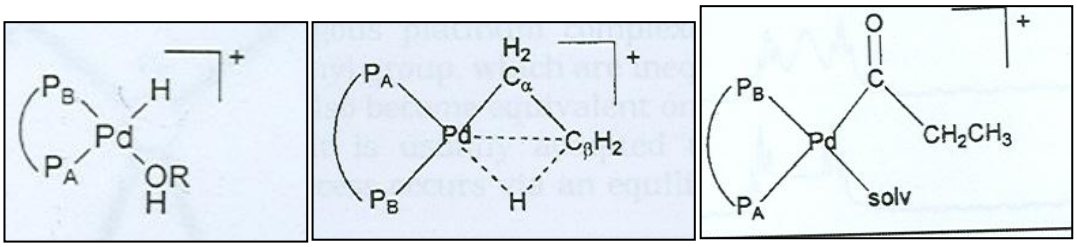

(A) (B) (C)

Figure 2.4. The complexes: (A) The hydride, (B) the alkyl, (C) the acyl complex (Clegg et al., 2002a).

2.3 Kinetics-General Overview

2.3.1 Different factors affecting the reaction

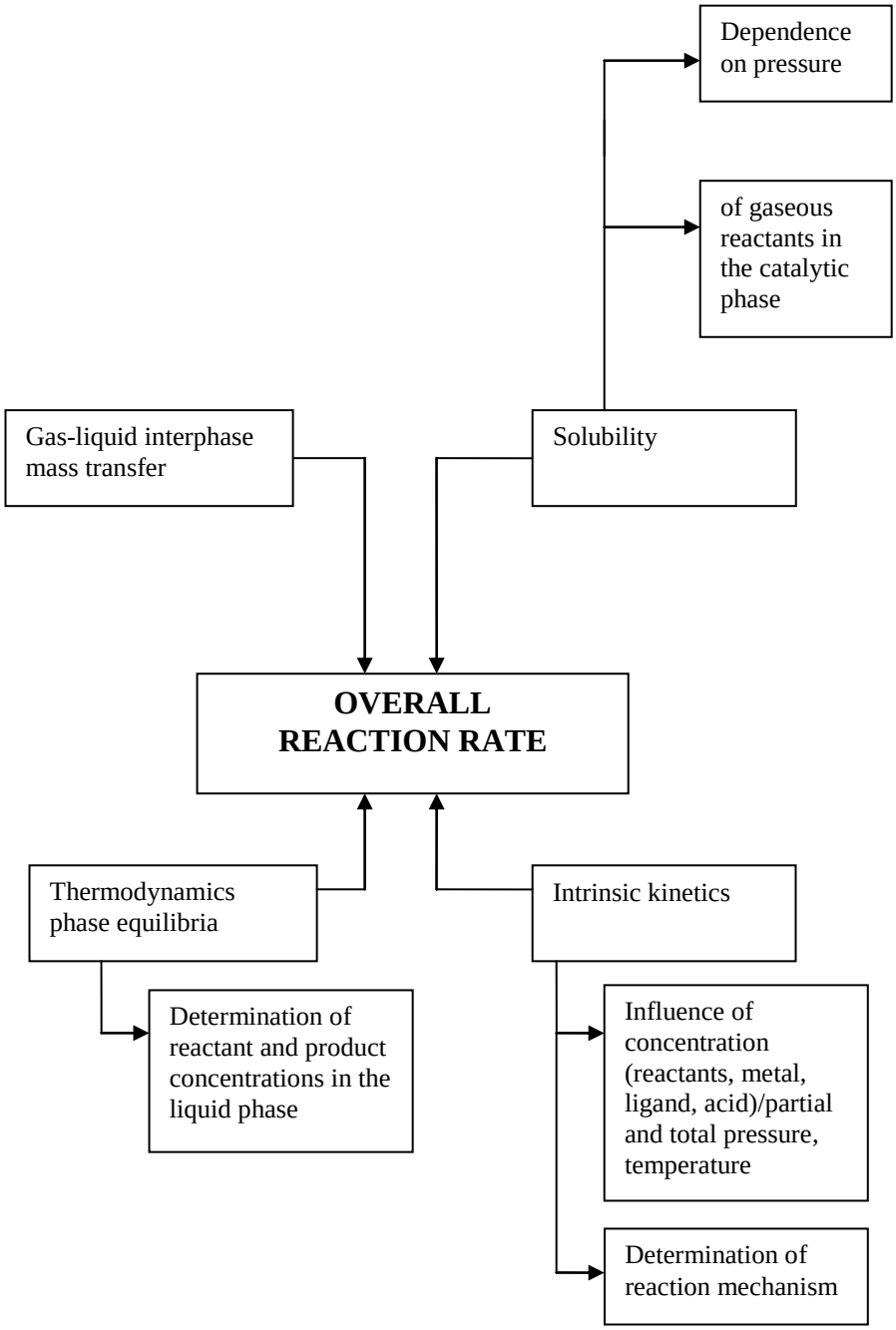

Figure 2.5. Factors influencing the overall reaction rate of homogeneously catalysed gas-liquid reactions (Cornils et al., 2003).

Whilst a kinetic study is being undertaken, two problems must be overcome:

1. Selection of the experimental techniques to gather reliable data of reaction rates at different conditions.
2. Selection of the appropriate method for the elaboration of the data in order to evaluate the kinetic law that fits the data collected.

2.3.2 Methods for the Elaboration of Kinetic Data

There are several approaches that can be used for the analysis of kinetic data (time, concentration) for reactions involving more than one reactants; for instance the Initial Rates Method, the Integral Method and the Differential Method. The first two were the methods used for the analysis of the autoclave data as it is presented in Chapter Five while the latter was used for the elaboration of the capillary microreactor data shown in Chapter Eight.

Initial Rates Method

Let us consider the logarithm of the rate law equation with respect to a reactant *I*:

$$-R_I = kC_I^n \rightarrow \ln(-R_I) = \ln k + n \ln C_I \tag{2.8}$$

According to the Method of Initial Rates, one can perform several runs at constant temperature using different initial concentration of one reactant *I* at each run while the initial concentration of the others are maintained constant. Reaction rate for each run is then extrapolated back to the initial conditions to find the initial reaction rate.

Next, the double-logarithmic plot of initial rates and initial concentrations gives a straight line whose slope is the order of the reaction with respect to the reactant *I*. The order found need not always be an integer, sometimes fractional orders are computed, especially half order reactions (Espenson, 1981 and 1995, Smith 1981). The most important advantage of the Initial Rates Method is that the reaction order found is the *true* order without influence from product inhibition or autocatalytic phenomena. Furthermore, it does not require reactants to be in excess and it is simple. But apart from advantages, there are certain disadvantages associated with this method.

One of its drawbacks is the difficulty in determining the reaction rate at true t=0, the time when the reaction actually initiated. This is particularly true in some cases, for example when a reaction has a long induction time. Induction time is a *time delay*, the time interval between the moment when all the reactants were introduced into the reactor and the moment when significant reaction ensues. It can be associated with a system of consecutive reactions or a system of at least two reactions happening in coupled parallel reactions occurring at different rates, autocatalytic reactions and thermal explosions (Lente et al., 2007). Reactant concentrations and temperature are the main factors affecting the length of the induction period. Another disadvantage of the Initial Rates Method is that it can be quite cumbersome requiring many runs. Nevertheless, it is one of the most popular methods - if not the most popular - amongst chemists and researchers involved in the subject of reaction kinetics.

Integral Method

The Integral method always puts a particular rate equation to the test by integrating it and subsequently comparing the predicted (concentration, time) curve to the experimental concentration versus time data. If *I* is a reactant, the reaction rate can be expressed in terms of *I*'s disappearance as follows:

$$-R_I = kf(C) = -\frac{dC_I}{dt} \rightarrow -\frac{dC_I}{f(C_I)} = kdt \rightarrow -\int_{C_{A_0}}^{C_A} \frac{dC_I}{f(C_I)} = k\int_0^t t = kt \tag{2.9}$$

which gives a linear plot of slope k.

From experiments, we calculate values for the integral $\int_{C_{I_0}}^{C_I} \frac{dC_I}{f(C_I)}$ and plot them at the corresponding t. If the plot gives a reasonable straight line passing through the origin, then the rate equation tested satisfactorily fits the data. If not, the chosen equation and its mechanism are rejected, another rate equation is selected and the procedure is repeated.

The method of Integration is useful for simple reaction types of elementary reactions. It is an easy method when testing particular mechanisms or simple rate expressions as well as when there is a limited amount of data or when the data are scattered and their calculated derivatives are not reliable. Table 2.1 has a summary of all the integrated rate expressions for selected single-term equations.

$-d[A]/dt =$	Integrated rate law
1. k	$[A] = [A]_0 - kt$
2. $k[A]^{1/2}$	$[A]^{1/2} = [A]_0^{1/2} - (k/2)t$
3. $k[A]$	$\ln([A]/[A]_0) = -kt$
4. $k[A]^{3/2}$	$[A]^{1/2} = [A]_0^{1/2} - (k[A]_0^{1/2}/2)([A]^{1/2}t)$
5. $k[A]^2$	$[A] = [A]_0 - (k[A]_0)([A]t)$
6. $k[A]^n\ (n \neq 1)$	$[A]^{n-1} = [A]_0^{n-1} - (k[A]_0^{n-1})(n-1)([A]^{n-1}t)$
7. $k[B]$	$\ln(\Delta_0 + [A]) = \ln[B] = \ln[B]_0 - kt$
8. $k[A][B]$	$\ln([B]/[A]) = \ln([B]_0/[A]_0) + k\,\Delta_0 t$
9. $k[A][C]$	$\ln\left(\frac{[A]}{[A]_0 + [C]_0 - [A]}\frac{[C]_0}{[A]_0}\right) = -k([A]_0 + [C]_0)t$

[a] A and B react with 1:1 stoichiometry; $[B]_0 > [A]_0$. C is used to represent a product of the reaction; $[C] = [A]_0 - [A] + [C]_0$. Reaction 9 is autocatalytic. $\Delta_0 = [B]_0 - [A]_0$.

Table 2.1. Summary of integrated rate expressions (Espenson, 1981).

Differential Method

The Differential Method of analysis is a very useful technique for the treatment of kinetic data even for complicated kinetic systems with or without the use of excess. It is based on the fact that the reaction rate with respect to a reactant I is relative to the $C_I^{\,n}$:

$$-\frac{dC_I}{dt} = k_i C_I^{n_i} \tag{2.10}$$

where $k_i = kC_A^{\alpha}C_B^{\beta}\cdots/C_I^{n_i}$ and n_i is the reaction order with respect to I. If the concentrations of the other components are constant (e.g. large excess) then k_i is constant.

Taking the logarithm of the equation of the rate law we obtain:

$$\ln(-\frac{dC_I}{dt}) = \ln k_i + n \ln C_I \tag{2.11}$$

Since the rate expression is a differential equation, one has to find first the concentration derivatives or reaction rates. After plotting $\ln(-\frac{dC_I}{dt})$ versus $\ln C_I$, one should obtain a straight line whose slope will give the order of the reaction with respect to component I. If the experiment is repeated for other components keeping the rest of the concentrations constant the overall reaction order can be obtained as the sum of the components' orders. The intercept gives $\ln k_i$.

2.4 Kinetics of Hydroesterification Reactions

In the case of multiple reactions taking place in a chemical system, the first step could be the determination of an acceptable reaction scheme. Then, the kinetic study can be oriented to find the parameters of each reaction in the reaction pattern (Santacesaria, 1999):

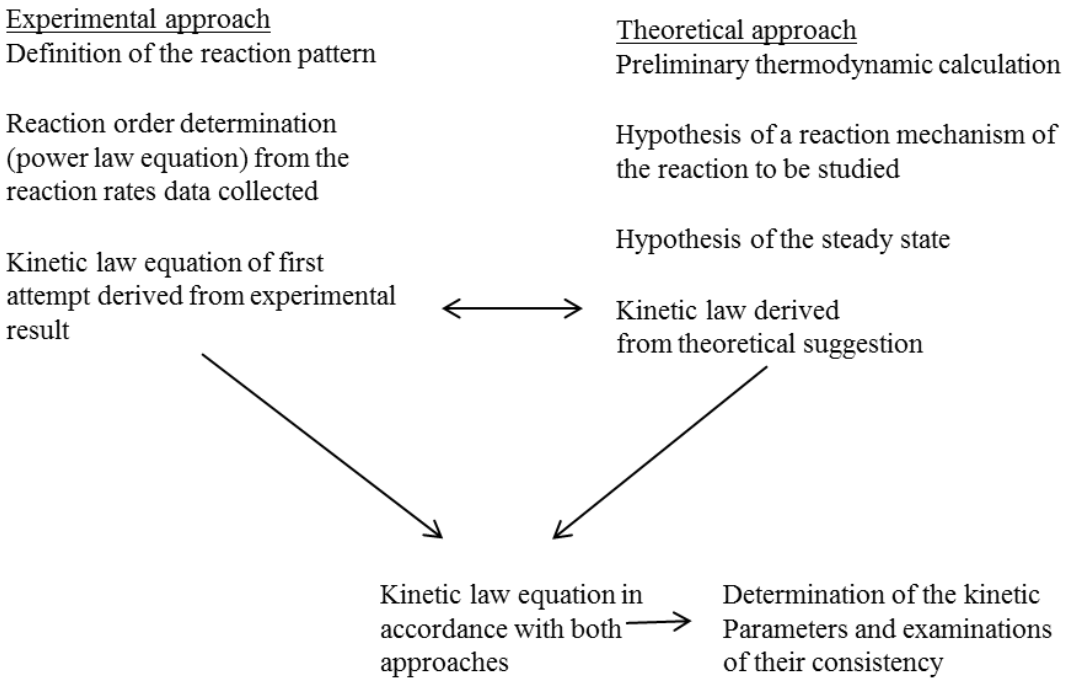

Figure 2.6. Scheme of the phases occurring in the kinetic study of a reaction (Santacesaria, 1999).

The alkocarbonylation of ethylene with methanol using Pd-catalysts, a reaction with particular industrial and academic interest, is particularly sensitive to the reaction conditions but even more to the phosphine ligand used (Breefuhrer at el., 2009). Since the methoxycarbonylation of ethylene with the homogeneous Pd catalyst based on the bidentate phosphine ligand d^{t}bpx (otherwise called the Alpha ligand) had not been the subject of a kinetic study before, an effort was made to collect information from kinetic studies of similar reactions like for example other alcoxycarbonylation and hydroformylation reactions.

Hydroformylation is the addition CO and H_2 (syngas) to the double bond of alkenes or their functionalised derivatives:

$$RCH=CH_2+CO+H_2 \rightarrow RCH_2CH_2CHO(n-aldehyde)+RCH(CH_3)CHO(iso-aldehyde) \quad (2.12)$$

Hydroformylation uses as reactant cheaper syngas rather than pure CO. Moreover, it does not require an acidic promoter which can be corrosive. The drawback is that it requires one more step for the production of the ester. While alcoxycarbonylation is relatively new and has been the subject of only few kinetic studies, hydroformylation is a mature industrial process. Notwithstanding that, new ligands and highly selective and efficient catalytic systems make hydroesterification competitive with great potential (Kiss, 2001).

Studies of the reaction rate of the methoxycarbonylation of 1-heptene with methanol by solutions of $\left[(C_6H_5)_3P\right]_2PdCl_2-SnCl_2$ yielding methyl octanoate at reaction conditions of 70 ^{o}C and 134 bar of CO, showed a first order dependence on [*Pd*] until a threshold value above which the rate approaches an asymptotic value. The observed rate was also first order with respect to CO, zero-order with respect to methanol provided that there was an excess of the stoichiometric amount and zero-order with respect to the olefin. However, a decrease in rate was observed for low olefin/Pd ratios. The formulated rate law was:

$$\frac{d[ester]}{dt}=\frac{k[Pd]P_{CO}}{(1+K[Pd])} \quad (2.13)$$

k was calculated equal to 0.34 $M^{-1}h^{-1}$ and the activation energy was found from Arrhenius plot in the temperature range 38-70 ^{o}C to be 130 kJ mol^{-1} (Knifton, 1976).

Other studies have shown a reaction order with respect to CO that shifts from positive at low concentrations to negative as CO is found to inhibit the reaction of hydroformylation above a threshold value (Kiss et al., 1999). From the study of the catalyzed hydroformylation of 1-octene by supported aqueous phase catalysis with Rh-complexes published by Jaurequi-Haza et al. in 2003, it was found that the reaction rate increased with increasing CO partial pressure and passed through a maximum. Substrate-inhibited kinetic behavior was found to occur for higher partial pressures of CO due to the formation of inactive Rh species and thus, lower reaction rates were recorded. Regarding the effect of the olefin concentration on the reaction rate, the rate was found to increase with an increase of the substrate concentration up to a threshold value beyond which inhibition kinetics were observed. A first order dependence with respect to the catalyst concentration was also concluded while the positive partial order dependence on hydrogen was observed and was attributed to possible solvent interactions without providing further explanation. A kinetic model was developed based on the experimental observations and an optimization sequential routine was used for the evaluation of the reaction rate parameters (parameter fitting).

A study on the methoxycarbonylation of benzyl chloride by Gavino et al. in 2001 concluded that CO deactivates the catalyst by formation of palladium carbonyl species that are very electron poor due to the presence of the carbonyl ligand. It was therefore concluded that the reaction should be fast enough to reduce the concentration of CO in the catalytic phase in order to prevent deactivation of the catalyst but not too fast in order for operation to remain in the kinetic regime and mass transfer resistances to be eliminated.

Hydroformylation of 1-hexene with a *HRh(CO)(PPh$_3$)$_3$* catalyst showed strong inhibition with an increase in the dissolved concentration of *CO*, mild substrate inhibition with the olefin and increase of the reaction rate with an increase of the H_2 and catalyst concentration (Deshpande et al., 1988).

The negative effect of CO was also concluded in the study of hydroformylation of 1-decene using a Rh homogeneous catalyst by Divekar et al. in 1993. Inhibition of hyroformylation with increase at CO partial pressure was attributed to side reactions leading to the formation of inactive carbonyl species. The oxidative addition of H_2 to the acyl complex was assumed to be the rate determining step. The effect of the olefin on the reaction rate was found to be marginal at high olefin concentration while a first order dependency was found at moderate concentrations. A 1.2 and 1.5 reaction order with respect to the catalyst and the hydrogen concentration respectively was found. The following kinetic rate equation was proposed based on the experimental data:

$$R = \frac{k(P_{H_2}H_A)^{1.5}(P_{CO}H_B)[RhCat]^{1.2}[decene]}{(1+K_BP_{CO}H_B)^3(1+K_D[decene])} \tag{2.14}$$

A kinetic model was derived using a molecular level approach based on the hydroformylation catalytic cycle and assuming the H_2 addition step as rate determining:

$$R = \frac{\kappa' K_1K_2(P_{H_2}H_A)(P_{CO}H_{CO})[RhCat][decene]}{1+K_2P_{CO}H_{CO}+K_1K_2P_{CO}H_{CO}[decene]+K_1K_2K_3(P_{CO}H_{CO})^2[decene]+K_1K_2K_3K_4(P_{CO}H_{CO})^3[decene]} \tag{2.15}$$

Equation (2.15) was consistent with the general experimental trends even though the predictions were not in exact agreement with the experimental data performed in an autoclave reactor. The various coefficients were calculated by means of an optimization routine.

Table 2.2 provides a summary of kinetic studies in homogeneous catalysis (Chaudhari et al., 2001):

No	Reaction	Catalyst	Rate equation
1	Carbonylation of methanol	$RhCl_3$/HI	$R = k[Rh][CH_3I]$, zero order with CO and methanol
2	Carbonylation of methanol	$RhCl_3$/HI	$R = \frac{k[catalyst][I][MeOH]}{[H_2O] + K_1[MeOH] + K_2[MeOH][I][CH_3COOH]}$
3	Carbonylation of methanol	NiCl2/iso-quinoline	$R = \frac{k[CO][substrate]}{(1+K_1[CO])(1+K_2[substrate])(1+K_3[H_2O])^2}$
4	Carbonylation of styrene	$PdCl_2(PPh_3)_2$	See below*
5	Carbonylation of styrene	$Pd(OAc)_2$/PPh_3/ TsOH	$R = \frac{kP_{CO}(1+K_1[styrene])^2[catalyst][H_2O]}{(1+K_2P_{CO})(1+K_3[H_2O])^2}$
6	Hydrogenation of cyclohexane	$RhCl(PPh_3)_3$	$R = \frac{kK_1[H_2][substrate][catalyst]}{1+K_1[H_2]+K_2[substrate]}$
7	Hydrogenation of allyl alcohol	$RhCl(PPh_3)_3$	$R = \frac{kK_1[H_2][substrate][catalyst]}{1+K_1[substrate]+K_1K_2[substrate]^2+[PPh_3]/K_3}$
8	Hydroformyla-tion of propylene	$HCo(CO)_4$	$R = \frac{k[substrate][catalyst][H_2]}{[CO]}$
9	Hydroformyla-tion of propylene	$Co_2(CO)_8$	$R_n = \frac{k[H_2]^{0.55}[CO][catalyst]^{0.75}[substrate]^{0.87}}{(1+K_2[CO])^2}$ $R_{iso} = \frac{k[H_2]^{0.32}[CO[catalyst]^{0.62}[substrate]}{(1+K_2[CO])^2}$
10	Hydroformyla-tion of 1-hexene, allyl alcohol, vinyl acetate	$HRhCO(PPh_3)_3$	$R = \frac{k[H_2]^m[CO][catalyst][substrate]}{(1+K_1[substrate])^n(1+K_2[CO])^p}$

No	Reaction – Continued…	Catalyst	Rate equation
11	Hydroformylation of 1-decene or styrene	$HRhCO(PPh_3)_3$	See below*
12	Hydroformylation of ethylene	$Rh(acac)(CO)_2$/ PPh_3	$TOF = \frac{k_1(P_{C_2H_4}/[PPh_3])}{1+K_1(P_{CO}/[PPh_3])+K_2([PPh_3]/P_{CO})}$
13	Hydroformylation of 1-octene	[RhCl(1,5-COD)]2/TPPTS	$R = \frac{k[H_2][CO][catalyst][substrate]}{(1+K_1[CO])^2(1+K_2[H_2])}$
14	Hydroformylation under supercritical CO_2	$HRh(CO)[p\text{-}CF_3C_6H_4)_3]_3$	$R = \frac{k[H_2]^{0.48}[catalyst]^{0.84}[octene]^{0.5}}{1+K_1[CO]^{2.2}}$
15	Oxidation of cyclohexane	$Mn(OAc)_2$	$R = \frac{k[substrate][catalyst]}{K_1+K_2[catalyst]}$
16	Heck coupling of iodobenzene and methyl acrylate	$Pd(OAc)_2/PPh_3$	$R = \frac{k[PhI][olefin]^2[Me_3N][catalyst]}{(1+K_1[olefin]^2)(1+K_2[Me_3N]^4)(1+K_3[catalyst])^3}\times$ $\times(1+K_4[PPh_3])$ (2.31)

* $R = \frac{kK_1K_2[H_2][CO][catalyst][substrate]}{1+K_2[CO]+K_1K_2[CO][substrate]+K_1K_2K_3[CO]^2[substrate]+K_1K_2K_3[CO]^2[substrate]+K_1K_2K_3K_4[CO]^3[substrate]}$

Table 2.2. Summary of kinetic rate equations in homogeneous catalysis (Chaudari et al., 2001).

2.5 Conclusions

The novel LI Alpha process for the methoxycarbonylation of ethylene belongs to the family of carbonylation reactions referring to the introduction of C=O into an organic molecule. The Alpha process entails ethylene, CO and methanol as reactants forming a methyl propionate ester. It is a homogenously catalysed process using Pd combined with a bi-dentate phosphine ligand developed by LI. The process involves a series of consecutive steps comprising the catalytic cycle where the active catalytic precursor has the form of a hydride complex. Previous research conducted by LI has identified the transformations of the catalyst which lead to the formation of the Pd-hydride complex as well as the other important intermediates in the cycle.

Kinetic investigations of other carbonylation reactions have been reported in the literature and some main conclusions have been derived, like mainly partial reaction orders with respect to the reactants and occasionally reaction rates and activation energy data. Hydroformylation is one type of carbonylation reaction of particular interest entailing H_2 as a reactant rather than an alcohol. It is a mature industrial process forming the subject of a number of kinetic studies involving different substrates. These have been reviewed in order to collect information relevant to the Alpha process.

--//--

CHAPTER 3

Literature Review: Microreactors with Particular Focus on Mesh Microreactors

In the last 15 years there has been increased research interest in microreactors; a fact that is evidenced by the large amount of reference papers on the subject (for instance the review of Hessel et al., 2005). Microreactors are advantageous because:

- They are particularly useful for diffusion limited reactions.
- They are characterised by inherent reactor safety.
- The reactions are carried out with improved high heat and mass-transfer characteristics under safe conditions.
- Broader reaction conditions can be used, including up to the explosion regime.
- They allow faster process development.
- They can be used as means of process intensification.
- They are characterised by high selectivity and productivity.
- There is significant scaling potential by arrays of microreactors.
- They involve low material inventories.
- They are cost effective.
- Are easier to scale-up.
- They enable on-site and on-demand production of hazardous chemicals.

- They are tools for implementation of high throughput screening techniques.
- They constitute integral components within the framework of process miniaturisation.
- Of the variety of materials to be used for their fabrication.

Their characteristics have been identified as follows:

- Small dimensions in the order of the diffusion distances which enable fast equilibrium.
- Laminar flow in microchannels.
- Diffusion process complete in time t if $t > \frac{l_D^2}{D}$ or $\frac{Dt}{l_D^2} > 1$ where D is the diffusion coefficient and l_D the distance through which the material has to travel.
- Contact times can be very small.
- Two immiscible phases can be brought in contact and then separated without phase mixing.

This Chapter pays special attention to mesh microreactors whose main characteristic is the known interfacial area stabilised in the pores of the mesh. The mesh has a high porosity and the pore sizes vary between 1-5 μm which give stability and good diffusive transport. Diffusive resistance is minimised by ensuring that the diffusive distance (length of the pores) is short. Usually the ratio width: length of pores is 1:1. In addition, they give a high volumetric ratio (volume/solid structural area). Furthermore, there are many possibilities for different geometries and fabrication processes to be utilised.

3.1 Advantages of Microreactors against Traditional Contactors

Microreactors are tools that facilitate reactions by passing reactants through channels with dimensions 10-1000 μm (Mason et al., 2007, Kiwi-Minsker & Renken, 2005). The narrow channel dimensions combined with static mixers provide millisecond mixing times. They can also allow for relatively short distances between the cathode and the anode, thus decreasing the energy requirements for performing redox chemistry. Microreactors achieve efficient input or removal of heat and nearly constant reaction temperatures because of the high surface to volume ratios which can go up to 30,000 m^2/m^3_{liq} compared to more traditional chemical reactors. The specific surface to-volume ratio in traditional lab reactors and production vessels are usually in the range of 100 m^2/m^3_{liq} and seldom exceed 1,000 m^2/m^3_{liq}. The prevention of hotspots, elimination of large exotherms, better selectivity and yield for organic reactions are offered versus batch reactors due to their small size enabling rapid cooling. Furthermore, the large surface-to-volume ratios and small dimensions increase the heat transfer out of the reaction zone and enhance the wall quenching of free radicals that in conventional reactors participate in chain branching reactions leading to runaway conditions. Hence, microreactors enable the development of new processes that would not be possible in conventional reactors due to the danger of runaway reactions (Ming Hsing et al., 2000). For instance, nitrations of aromatic species can be uncontrollably exothermic, can generate explosive products and they have been used to illustrate control of exothermicity, yield and selectivity in microreactors. Waste generation is minimal as a consequence of fast mixing and heat transfer which make possible the use of highly concentrated

reactant streams (Mason et al., 2007). Partial oxidation reactions are also particularly interesting candidates for application of microchemical systems since they typically have short reaction times, are constrained by heat transfer considerations, are of particular exothermic nature and produce important intermediates and products (Hsing et al, 2000). Furthermore, microreactors offer the ease of creating parallel systems for higher data throughput and improved workflow efficiency (Milles et al., 2007). Finally, the higher reaction temperatures without hot spot formation lead to improved energy efficiency and less amounts of catalyst reducing the operating costs (Kiwi-Minsker & Renken, 2005).

Unlike the case of macroscale laboratory equipment, fluid behaviour in microreactors is dominated by non-convective laminar flow where, in the absence of enhancement by electric or magnetic fields, diffusion alone affects mixing, making hydrodynamics and mass transfer characterisation of these devices simpler when qualitative studies such as kinetic investigation are targeted. The laminar flows are more easily quantified than the turbulent flows characteristic of conventional reactors (Ming Hsing et al., 2000). In addition, due to the small dimensions, the radial diffusion time in a microchannel is of the order of milliseconds and the axial dispersion can be efficiently suppressed, as shown by recent theoretical and experimental studies (Kiwi-Minsker & Renken, 2005).

According to Wenn et al. (2003), the physical parameters that define the characteristics of the microreactor are the channel dimensions, number of channels, channel arrangement, channel internals and layers, wall thickness and profiles, fluid-flow paths, materials of construction, thickness of layers, surface roughness, etc.

These parameters affect the transport phenomena, hydrodynamics and kinetics and their proper choice will increase the yield, selectivity, energy efficiency or a combination of them.

In order to increase production of a desired substance from grams to kilograms, multiple microreactors can be used in parallel and more reactors can be brought on-line as necessary. Thus, the notion of 'numbering-up' is applied instead of 'scaling-up' for conventional apparatuses which is impossible to implement here as many of the properties of microreactors are unique to their micron sized dimensions. Multi-step synthesis, where relatively simple reagents can be fed into a series of microreactors to produce relatively complex and synthetically difficult products, is also viable. Most micro-reactors are designed and fabricated using methods borrowed from the well established field of semi-conductor electronics. In most cases, the small size of microreactors is combined with a modular design that enables mass production and as material of consistent quality is attained from one unit or many, time and cost savings can be realised because a reaction does not require additional optimization once it is moved onto production scale. Furthermore, by adopting the appropriate microfabrication strategy, it is feasible to integrate sensors with the reactor so that simulations can be checked and subsequently used to extract unknown reaction parameters.

A short radial diffusion time, characteristic of the smaller tubing diameter, leads to narrow residence time and thus, improved selectivity to a desired product is achieved when one deals with consecutive reactions. Isothermal conditions, short and narrow RTD are the main characteristics of microreactors according to Kiwi-Minsker &

Renken (2005). Productivity can also be boosted in comparison to using large batch reactors as micro-reactors often offer greater amount of product per unit volume and unit time (kg m^{-3} s^{-1}). Due to the small material inventories, safety is enhanced.

Microreactors can be employed as a useful tool to generate libraries of related compounds, for quick catalyst screening or for conduction of low-volume, low waste kinetic investigation as was made obvious by the research of de Bellefon and co-workers in 2003. The potential for catalytic recycling and the opportunity for low volume optimisation make them ideal for doing more environmentally benign chemistry.

Microreactors, with the increased process intensification they offer, can replace more traditional pilot-scale reactor systems and pilot plant systems in some cases, by smaller, faster responding, more flexible mini plants with reduced capital and operating costs as stated by Milles et al. (2007). The researchers also mentioned that the use of microreactors has intensified in the last fifteen years as tools for combinatorial material science. Prototype microreactors were first constructed towards the end of 1980s by the chemical industry using micromechanical systems fabrication techniques. Microreactors although were initially used for single phase reactions (important for pharmaceutical and fine chemicals synthesis) were later used for multiphase reactions, gas-liquid-solid, gas-gas-solid, gas-liquid and immiscible organic-aqueous liquid systems. Drivers behind reactions done on a miniature scale in these early years were cost related:

- The transport of hazardous chemicals was constrained by governmental regulation.

- The quantities of chemicals/reagents required for new product development was much smaller than the minimum quantities typically provided by chemical suppliers. Smaller quantities meant lower emissions and posed lesser risks for the workers and the community in general.
- The cost of disposal by incineration of waste material or of unused substances increased significantly and hence the need for smaller material inventories was generated. The use of miniaturised continuous systems did not produce the large amount of waste related to the start-up, shut-down and cleaning of batch reactors.
- Scale-up of hazardous reactions to pilot plant scale was costlier in order to satisfy the safety standards and shielding versus the continuous operation in a smaller scale in a laboratory.
- Some very reactive substances (nitro-compounds, azo-compounds e.t.c.) had limited shelf-life, were unstable or required special handling techniques, therefore providing these compounds in-situ using microreactors eliminated extra costs.

A reduction in the characteristic size, normal to the flow leads to increased surface area per unit volume of fluid which in turn increases the heat and mass transfer rates. The advantage in using microscale when performing reactions is really achieved when the channel dimensions approach the characteristic length for heat and mass transfer. The characteristic length for heat transfer is given by (Milles et al., 2007):

$$l_H = \sqrt{\alpha_H \cdot t_H} \tag{3.1}$$

where l_H is the characteristic length of heat transfer, α_H is the thermal diffusivity of the liquid and t_H is the characteristic time for heat transfer.

Similarly, the characteristic length scale for mass transfer is given by:

$$l_D = \sqrt{D \cdot t_D} \tag{3.2}$$

where l_D is the characteristic diffusion path length of component A in B, D is the diffusion coefficient of component A in B and t_D is the characteristic time for mass transfer.

There are certain drawbacks however, like the unease and expense of micro-fabrication in some cases, lack of straight-forward approach for creating integrated, flexible systems but progress is being made (Milles et al., 2007). Another disadvantage of using microreactors for chemical synthesis is that solid-forming reactions can clog the small reactor channels. Other identified problems that could be encountered are catalyst deactivation and incompatibility with reagents and intermediates, back-pressures developed in flow and the removal or elimination of unwanted side products. However, as the advantages outweigh the disadvantages, there is definitely a potential for more efficient organic synthesis and other applications using microreactors.

Indicative reactions that have been used with microreactors are listed in Table 3.1:

Reaction	Reference
Fluorination of B-dicarbonyl compounds	Chambers et al. (1999)
Direct fluorination of toluene	Jahnisch et al. (2000)
Hydrolysis of colourless fluorescein diacetate in toluene with transfer as fluorescein anion to aqueous alkali and oxygen absorption into aqueous alkaline pyrogallol solution to generate a coloured compound piurpurogallin	Wenn et. al (2003)
Reversible addition-fragmentation chain-transfer polymerisation (RAFT)	Russum et al. (2006)
Nitroxide-mediated polymerisation (NMP)	Enright et al. (2005)
Sonogashira and Mizoroki-Heck reactions in high yields	S. Liu et al. (2004)
Assymetric hydrogenation of methyl Z-acetamidocinamate (MAC) with a [Rh (S,S-BDPPTS]$^{+}$ water-soluble catalyst	de Bellefon et al. (2003)
Hydrogenation of a-methylstyrene with Rh/γ-alumina catalyst.	Abdallah et al. (2006)

Table 3.1. Indicative reactions used with microreactors.

3.2 Different Types of Multiphase Microreactors

Gas-liquid micro-reactors can be classified into the following main categories:

- **Microreactor with gas-liquid interface stabilised by physical structures like meshes of micro-porous plates.** Liquid and gas flow in adjacent microchannels separated by the physical structures. The main advantage of these microreactors is that the gas-liquid interface which is equal to the openings of the physical structures is well established and known. Another advantage is that it enables fast gas-liquid separation.

- **Microchannel contactor**. Gas and liquid channel flow together either in a single channel or in a multitude of channels. Various flow patterns can be achieved depending on the hydrodynamic and other parameters. When a cluster of parallel microchannels is used, the flow distribution at the inlet becomes critical.
- **Falling film microreactor**. By means of the gravitational force, liquid flows in thin films in microchannels. Gas flows above the microchannels in concurrent or countercurrent mode. One of the advantages of this structure is the very low pressure across the reactor.
- **Micro packed bed reactor**. Offers a solution when solid catalyst particles have to be incorporated directly in the reactor. The solid catalyst is retained in the reactor with the help of a microfilter at the outlet of the reaction microchannel.

The subsequent sections of this Chapter focus on the former type presented above, i.e the mesh microreactor while the succeeding Chapter concentrates on the microchannel contactor.

3.3 Advantages of the Mesh Reactor versus other Microreactors

For single phase processes, mass transfer limitations can be reduced or even eliminated by efficient mixing or by contacting short streams under laminar

conditions and that is why microreactors are a useful tool for studying reaction kinetics. Other ways could be dispersing one phase into the other in droplet form but there is a degree of uncertainty about the inter-phase surface areas. This is where the mesh microreactor becomes advantageous where the surface area is equal to the open pores. Furthermore, chemical processes usually lead to the formation of more than one products which will need to be separated from the reactants and solvents in the chemical system. It is known that reaction and separation if combined in one process reduces the process costs but microreactors are not efficient separators in terms of density. This is another advantage of the mesh microreactor in which two phases come in contact, reaction takes place without phase mixing and then the two phases separate after the mesh and can be used for sampling in various analytical techniques.

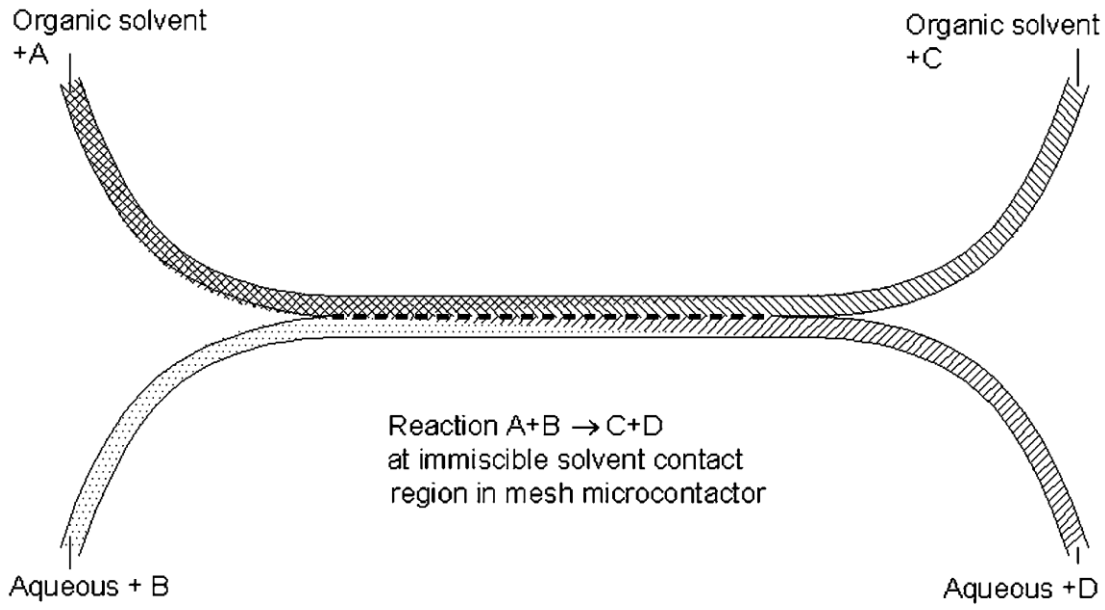

Figure 3.1. Principle of a 2-phase mesh microreactor (Wenn, 2003).

In the mesh/membrane microreactor the gas-liquid interface is defined, in contrast to the micro-bubble column and the packed bed reactor where various flow patterns can be observed depending on the gas and liquid fluid rates which could adversely impact the reaction conversion. In addition in these devices, feed can be inhomogeneous and can cause a reduction of the gas-liquid interface and of the liquid film and thus a drop in the achieved conversion. The mesh ensures also the stability of the interface for a large range of liquid flow and provides better control of the gas-liquid and gas-liquid-solid contact. With regards to fixed-bed reactors, the mesh reactor offers much better mass transfer efficiency. The specific G-L interfacial area and the liquid thickness are constant in the mesh reactor, thus a constant volumetric mass transfer coefficient is considered over all the reactor. However, the interfacial area in a mesh microreactor at around 2,000 m^2/m^3 is less than in other microreactors which can go up to 30,000 m^2/m^3. Finally, safe operation is achieved with this tool due to lower material inventories and fast start-up and shut-down and can be ideal when working with exothermic, fast reactions or those entailing toxic or expensive reagents (Abdallah et al., 2006).

In comparison to other devices which also show a stable G-L interface like the falling film microreactor, Abdallah et al. (2006) stated that the mesh microreactor is more beneficial because it can operate in a wider range of liquid flow whereas the falling film miroreactor is limited as the liquid film thickness depends on the liquid flow due to the gravity effect.

The recognised disadvantages of mesh microreactors are firstly that the mesh can present additional resistance to mass transfer in cases when the resistance of the

pores is similar to the resistances of the bulk phases. In order to minimise this effect, the thickness of the mesh should be the smallest possible without compromising mechanical stability. Secondly, operation can be difficult because the two phases meet at the pores of the mesh but they are not supposed to disperse in one another. This is realised with the application of a pressure differential, ΔP, between the phases, derived by the Laplace equation and called the break-through pressure. In this way, the non-wetting (or the wetting fluid) does not pass the pores of the mesh. However, when pore size is not uniform or when impurities or surfactants are present, the break-through pressure decreases and operation can be problematic. A solution to this problem can be uniform, small and straight pores. (Zanfir et al., 2008).

3.4 Studies using Mesh Microreactors

Abdallah and co-workers in a study published in 2004, demonstrated the use of a mesh microreactor for catalyst/chiral inductor screening and for kinetic data acquisition. The characteristics of the mesh were: 20-25 % open area, the sizes of the mesh pores 5 μm and an estimated gas-liquid interfacial area of 2000 m^3/m^2liq. This design allowed a good mass transfer between the cavities while stabilising the interface hence ensuring gas-liquid interaction. In the first series of experiments, the mass transfer capability of the mesh microreactor was evaluated by determining experimentally the activation energy of a known reaction. A mass transfer coefficient for a fast reaction of around 1-2 s^{-1} was evaluated for the mesh microreactor applying

the ‘in-series mass transfer resistances’ concept, a value which is close to those found in traditional contactors equipped with baffles and turbines. In a second series of experiments the researchers performed a well-known reaction, the gas-liquid asymmetric hydrogenation of 2-methyl acetamidocinnamate with Rh chiral diphosphine complexes and found fairly good agreement between measured enantioselectivity and published data which confirmed that mesh reactors can be used for catalyst screening. It was also concluded from this research that the mesh microreactor is a valuable tool for the accurate investigation of gas-liquid and gas-liquid-solid catalytic reactions.

In a later study in 2006, Abdallah et al. worked with a mesh reactor entailing a 155 μm liquid thickness and 123 μl liquid phase volume. The device also incorporated a15 μm thin catalytic layer and a mesh with 5 μm pores. The researchers performed a kinetic study on the very fast hydrogenation of α-methylstyrene with Rh/γ-alumina catalyst. Mass transfer investigations are necessary when qualitative studies like kinetic investigations are targeted and chemical, physical methods or computational fluid dynamics can be used for this purpose. Using CFD, the concentration of the gas below the mesh was calculated equal to 96 % of the equilibrium concentration. By considering the boundary conditions at reactor inlet and outlet:

Inlet: $F_A = F_A^i = C_A^i Q_L$ (3.3)

Outlet: $F_A = F_A^o = C_A^o Q_L$ (3.4)

And after integrating the steady state plug flow reactor model equation

$$-\bar{r} \cdot dV_{cata} = dF_A \quad (3.5)$$

they obtained the relation between the apparent rate of reaction ($\bar{r}$), the operating conditions, and the measured conversion as follows:

$$\bar{r} = \frac{F_A^i - F_A^o}{V_{cata}} = \frac{\chi \cdot F_A^i}{V_{cata}} = \frac{\chi \cdot C_A^i \cdot Q_L}{V_{cata}} \tag{3.6}$$

where F_A is molar flow rate, Q_L is volumetric liquid flow rate, C_A is the a-methylstyrene concentration and V_{cata} is the volume of the catalytic layer. The superscripts ^{i} and ^{o} denote the reactor inlet and outlet respectively.

Using a small concentration of the Pd catalyst, an activation energy of 40 kJ/mol was derived from the experiments which led the authors to conclude that the operation of the reactor was in the kinetic regime. Below is a schematic of the experimental set-up.

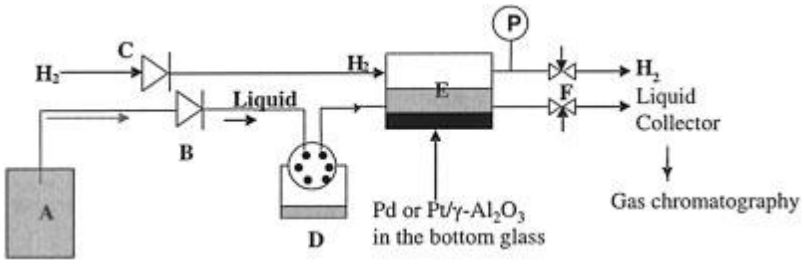

Figure 3.2. Experimental set-up for the mesh microreactor: (A) Liquid reservoir , (B) HPLC pump, (c) gas flow-meter, (D) valve equipped with a micro-injection loop, (E) microreactor, (F) needle valve, (P) pressure gauge. Catalyst Pd or Pt on γ-alumina (Abdallah et al., 2006).

Kulkarni et al., in a paper published in 2007, focused on the experimental analysis of residence time distribution and phase hold up in a mesh microreactor built without the need for precision micromachining. The polypropelene mesh was sandwiched between two acrylic plates 5 mm thick allowing the formation of microvolumes and

specific inlets for the gas and the liquid (air and tap-water). Four different types of mesh (100 mm x 200 mm x mesh thickness) were utilised and the mesh acted as a separator between the two plates maintaining a gap equal to the mesh thickness. Details about the mesh and the microreactors can be found in Figures 3.3 and 3.4. The whole microreactor was transparent for the study of hydrodynamics by means of a high-speed camera. The phase distribution for four different mesh types was obtained, and the liquid RTD was studied by tracer pulse experiments and measurements of the liquid side connectivity at the reactor outlet. The authors concluded that operation with meshes of smaller open area was strongly affected by channelling. Furthermore, RTD showed hysterisis when the gas flow was kept constant but the liquid flow was increased and then decreased for all four mesh types. This was attributed to the wetting characteristics of the mesh. The operating range of the liquid depended on the flow area available for each mesh type. Finally, the hydrodynamics of the reactor were strongly influenced by the mesh design and open area.

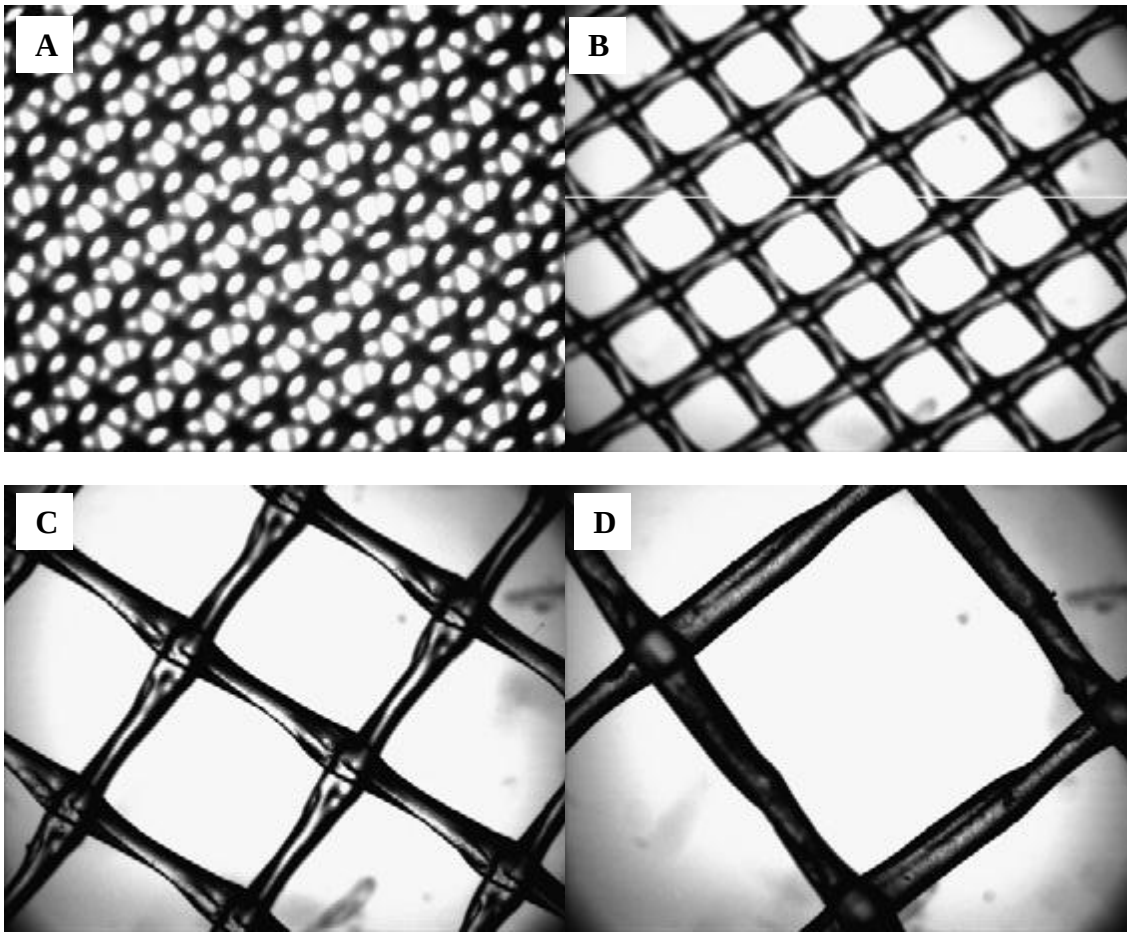

Figure 3.3. Meshes (mesh thickness, size of the pore and open area) used for the research of Kulkarni et al. (2007): (A) 100 µm, 0.25 mm and 20 % open area, (B) 200 µm, 1 mm and 40 %, (C) 400 µm, 2 mm and 60 %, (D) 700 µm, 3 mm and 96 %.

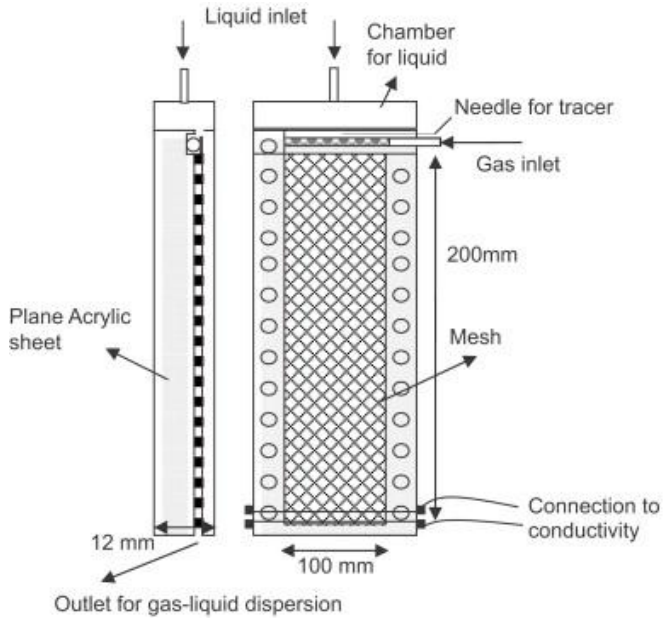

Figure 3.4. Schematic of the mesh microreactor (Kulkarni et al., 2007).

Wenn et al. (2003) worked with a micromesh with pore diameter, depth and spacing of 5 μm formed by means of electrodeposition of Ni onto substrates. The passages on each side of the mesh were generated from milled glass and metal components (please refer to section 4.4 for more microfabrication details). The mesh microreactor was used in flow-through mode and static mode. The reactions studied was the liquid/liquid hydrolysis of colourless fluorescein diacetate in toluene with transfer of fluorescein anion to aqueous alkali and the gas/liquid oxygen absorption into aqueous alkaline pyrogallol solution generating a coloured product, piurpurogallin, for UV/UV spectrometric measurement of product formation. The processes chosen here were initially thought slow enough to proceed within the mesh microreactor at rates controlled by inherent kinetics rather by diffusive transport. For the liquid/liquid operation, the authors found a linear relation of ln(1/(1-F)) (F is conversion) with time and concluded a pseudo-first order process and they also estimated an activation energy of 28 kJ/mol. For the gas/liquid operation, Wenn and

his co-workers concluded that due to the fact that the process was fast, significant reaction occurred within 30 s and therefore some diffusive limitation existed. A more extensive analysis of the kinetics of the G-L reaction was not possible for this reason (for instance, measurement of the rate dependence on oxygen concentration in order to find the reaction order with respect to oxygen was not feasible). It was concluded that higher gas rates or higher gas pressures could obviate those limitations.

Zanfir and co-workers in 2008 researched the acetone stripping from binary mixtures of acetone and isopropanol wih N_2 as inert gas using a microstructured mesh contactor. Furthermore, the asymmetric transfer hydrogenation of acetophenone with isopropanol as the hydrogen donor to chiral alcohol 1-phenylethanol in the presence of an homogeneous catalyst was also studied experimentally with the mesh microreactor. A model was formulated, solved and showed good agreement with the experimental data. The microreactor consisted of parallel SS metal plates (width x length equal to 3 cm x 8 cm), copper gaskets (thickness 200 μm) and a microstructured SS mesh (pore size 76 μm and thickness 50 μm) which allowed passages for the gas and liquid flows. The open area was approximately 23 %. The operation of the mesh reactor for acetone stripping was compared against that of a batch reactor. The improved efficiency of the mesh reactor in terms of shorter reaction times to attain the same conversion, was attributed to the higher G-L contact area. Theoretical and experimental investigation revealed that the amount of acetone removed depended on the G-L flow ratio, however increasing this ratio in a batch microreactor results in flooding of the impeller whereas in the mesh contactor, the thin mesh does not allow the two phases to disperse in one another and hence obviate this problem. Overall, increased reactor efficiency using a mesh microreactor, means

that reaction time can be significantly reduced as compared to using a conventional lab batch reactor.

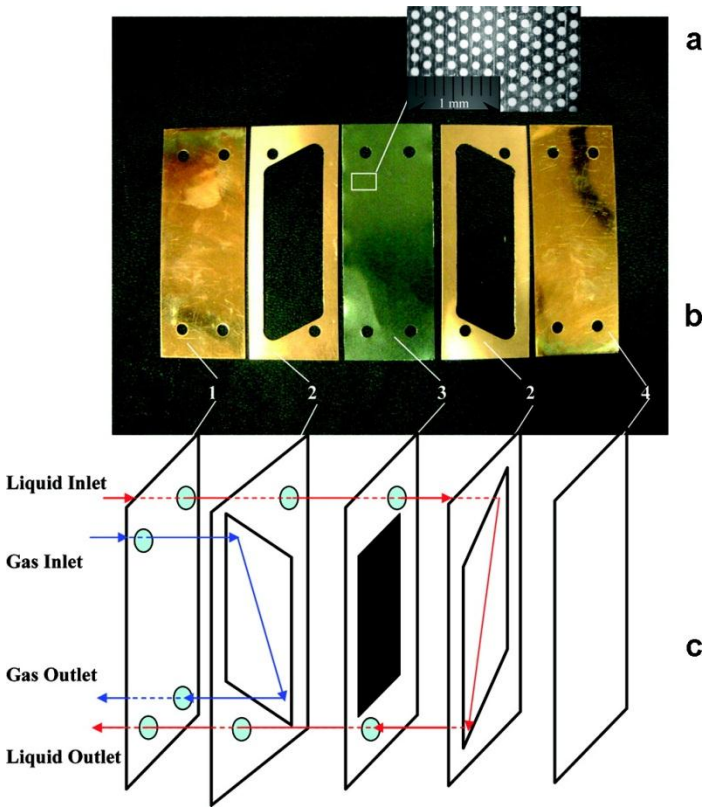

Figure 3.5. Microstructured mesh contactor design. (a) Magnified picture of the mesh. (b) Components of the contactor. (c) Flow arrangement: (1) top plate, (2) gasket, (3) mesh, (4) bottom plate (Zanfir et al., 2008).

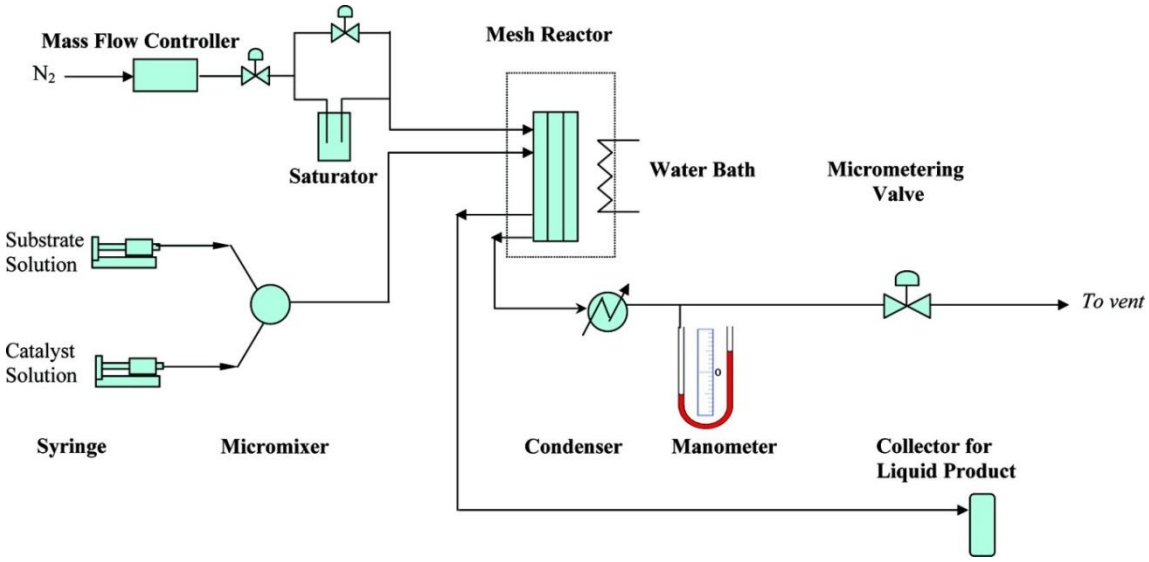

Figure 3.6. Schematic of experimental setup for the mesh microreactor (Zanfir et al., 2008).

3.5 Microfabrication Techniques for Micromeshes/micro-sieves

3.5.1 Silicon Nitride Micro-sieves for Microfiltration Purposes

The microfiltration regime is defined as filtration through a sieve with pore sizes between 100 nm and 5 μm. It has applications in the pharmaceutical and food/beverage industry where sieves with a pore size <5 μm are required to retain bacteria.

Polymeric as well as inorganic materials have been used to manufacture these membranes employing different techniques. Inorganic microfiltration membranes have a higher chemical and thermal resistance than polymeric materials. However, there are certain disadvantages like limited clean water flow because the membrane

is thick compared to the pore size and poses a resistance to the flow. In addition, there is poor control over the pore size distribution. Other problems with the inorganic membranes include the inadequate cleaning methods due to the large inner surface area of the membrane and the support. In an ideal microfiltration system:

- The sieve should be as thin as possible.
- The pore density should be high but not compromising the strength.
- The pore density should be uniform because small pores give small fluxes.
- The support should have large openings so it will not interfere with the flux through the membrane (Wenn et al., 2003 and Abdallah et al., 2004). The support is necessary because the membrane is thin and consequently weak.

For the fabrication of microsieves, Si micromachining was used due to its capabilities to make very thin films and very small structures.

Different steps in wafer processing were used depending on the pore size; either smaller or larger than 1 μm. In the former case, interference lithography was used which a fast, inexpensive, suitable for large areas method allowing the fabrication of pores as small as 0.1 μm (van Rijn et al., 1999). In the latter case, standard photolithography and patterning were employed. Standard mask lithography is limited to 1 μm minimum pore size because of the dispersion of the 400 nm UV light through the holes. The fabrication process for pores larger than 1 μm is shown in the following Figure (Kuiper et al., 1998 and van Rijn et al., 1999).

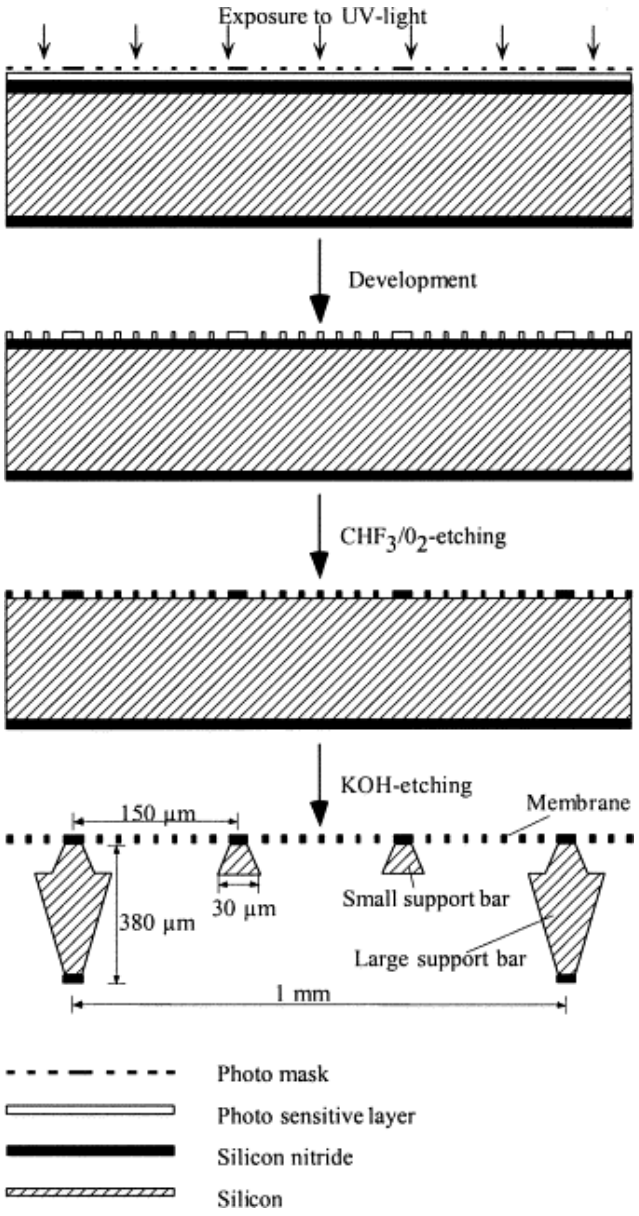

Figure 3.7. Fabrication process of a microsieve with pores >1µm (Kuiper et al., 1998).

A review of the process steps is the following:

- Start with a polished Si wafer with a thickness of 380 µm.
- A layer of Si_3N_4 is deposited with Low Pressure Chemical Vapour Deposition (LPCVD).
- Application of a photosensitive lacquer layer.
- Pattern the lacquer layer through a mask with holes>1 µm with UV light.

- Pattern transfer by means of Reactive Ion Etching (RIE) with CHF_3/plasma.
- Silicon support etched by KOH(25% at 70^oC) to form the support bars (Kuiper et al., 1998).

3.5.2 Silicon Nitride Micro-membranes with Slits

In order to increase further the flux through the membrane further research was conducted on manufacturing membranes with slits instead of circular pores. Ceramic membranes were compared in terms of flow resistance and membrane strength (Kuiper et al., 2002). It was concluded the membranes with slits posed five times less flow resistance than circular perforated membranes for comparable strength. Another advantage of the slits is that they cannot be blocked completely by cells in industrial microfiltration applications. It was also found that the membrane strength depends on the orientation of the slits. Furthermore, the membrane is stronger when the slits are patterned vertically to the longer edges of the membrane in a non-alternating pattern.

Finally, fracture of the membrane happens at the edge of the membrane that is connected to the support because that is where the stress is the highest as the sum of tensile and bending stress. Thus, the stiffer the membrane, the higher the strength it can withstand because it gives less deflection and less bending at the edge. The fabrication process was similar to that described in Section 3.5.1 and shown in Figure 3.8. The micro-membranes with slits are compared to those having circular pores in Figure 3.9.

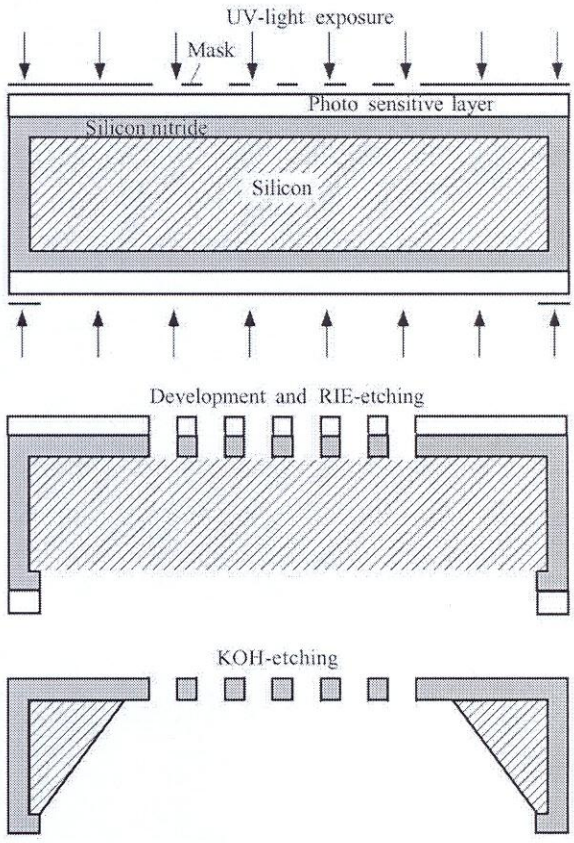

Figure 3.8 Fabrication process of the micromembranes with slits (Kuiper et al., 2002).

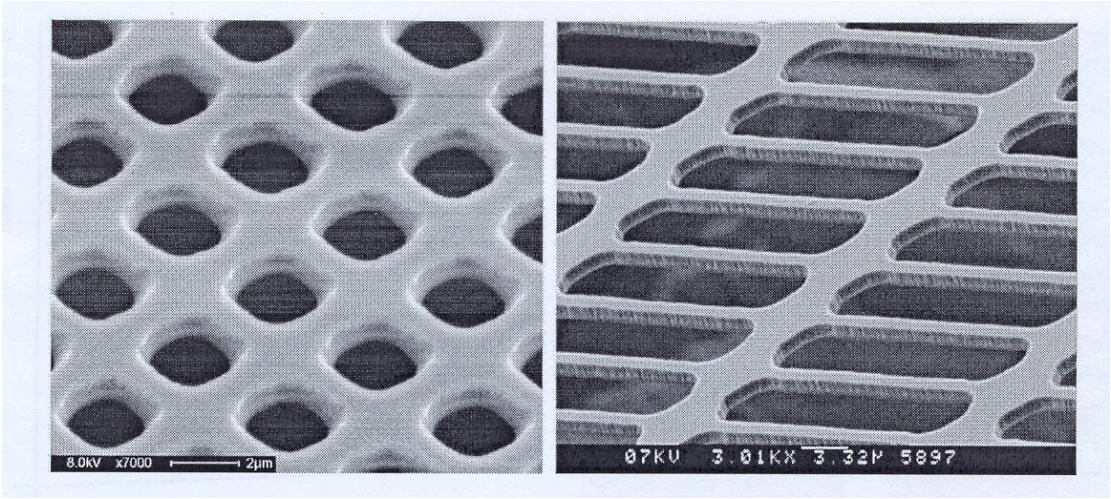

Figure 3.9. Comparison of membranes with slits and circular pores (Kuiper et al., 2002).

3.5.3 Silicon Nitride Micro-membranes for Hydrogen Separation

Extensive research in the last few years has been dedicated to the fabrication of micromembranes for hydrogen separation (Gielens et al, 2002, 2003 Tong et al., 2003 and 2005, Wilhite et al., 2004). These silicon nitride membranes have been used with microfabrication techniques and have many advantages compared to previously made efforts; they use a Pd/Ag film to facilitate H_2 separation, they are thin and with small support bars that pose little resistance to the flow of the gas. In addition, the Pd/Ag layer covers the silicon nitride in a uniform manner. Compared to literature, these membranes showed higher permeability and H_2 fluxes. The fabrication process in steps is shown in Figure 3.10 and is as follows:

- Start with a 3 inch diameter and 350 μm thickness silicon wafer <110>.
- Grow a film of silicon dioxide of 0.3 μm by thermal oxidation on both sides of the wafer.
- Deposit a silicon nitride film of 1 μm on both sides of the wafer.
- Pattern with standard lithography the back side of the wafer parallelogram shapes 350 μm x 2100 μm.
- Pattern transfer by etching of the silicon nitride and the silicon dioxide.
- Wet etching of Si with KOH solution until 300 μm of Si are etched away.
- At the front side of the wafer circular openings of 5 μm were patterned by standard lithography.
- Pattern transfer onto the silicon nitride by dry etching (probably plasma etching with CHF_3 oxide gas) to create the membrane pores.
- Wet etching with KOH the back side of the membrane to remove the remaining 50 μm of Si substrate so that the SiO_2 layer is reached.

- A Ti layer sputtered as adhesion layer.
- Co-sputtering of Pd/Ag alloy (77/23 %) inside the parallelogram shaped slits and formation of a layer with thickness between 0.5-1 μm.
- On the front side of the wafer, the SiO_2 layer is removed by etching with BHF to release the membrane.
- Channels 200 μm deep were etched with powder blasting in two 5in thick glass plates. These channels end at previously drilled holes for the inlet-outlet.
- The membrane was sandwiched between the two glass plates with 4-electrode anodic bonding to create the 3D structure shown in Figure 3.10.

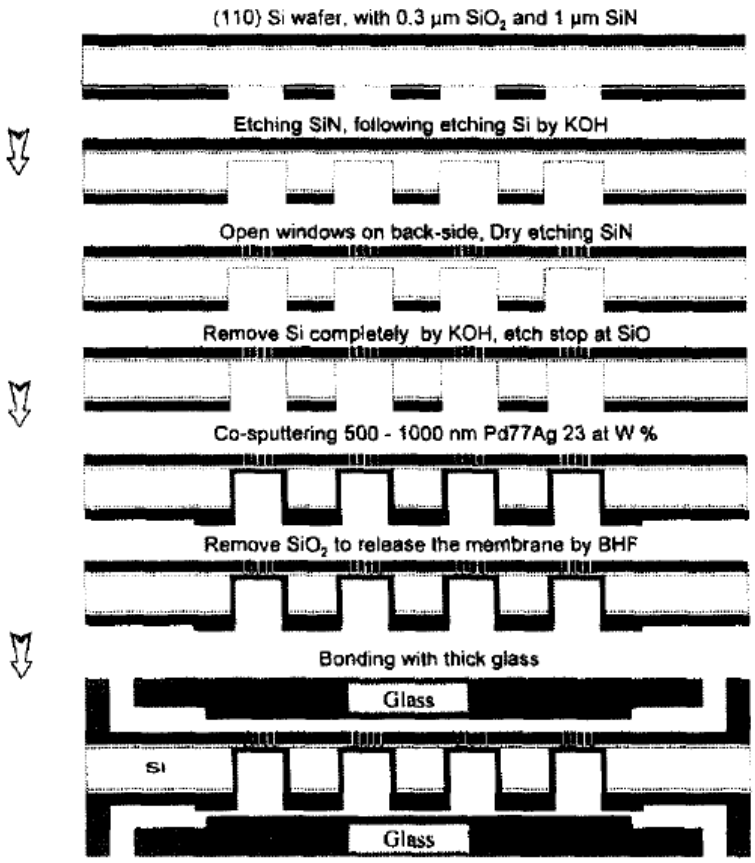

Figure 3.10. Fabrication process of the silicon nitride microsieve for H_2 separation (Gielens et al., 2002).

The experimental set-up used for conducting the experiments is shown in Figure 3.11.

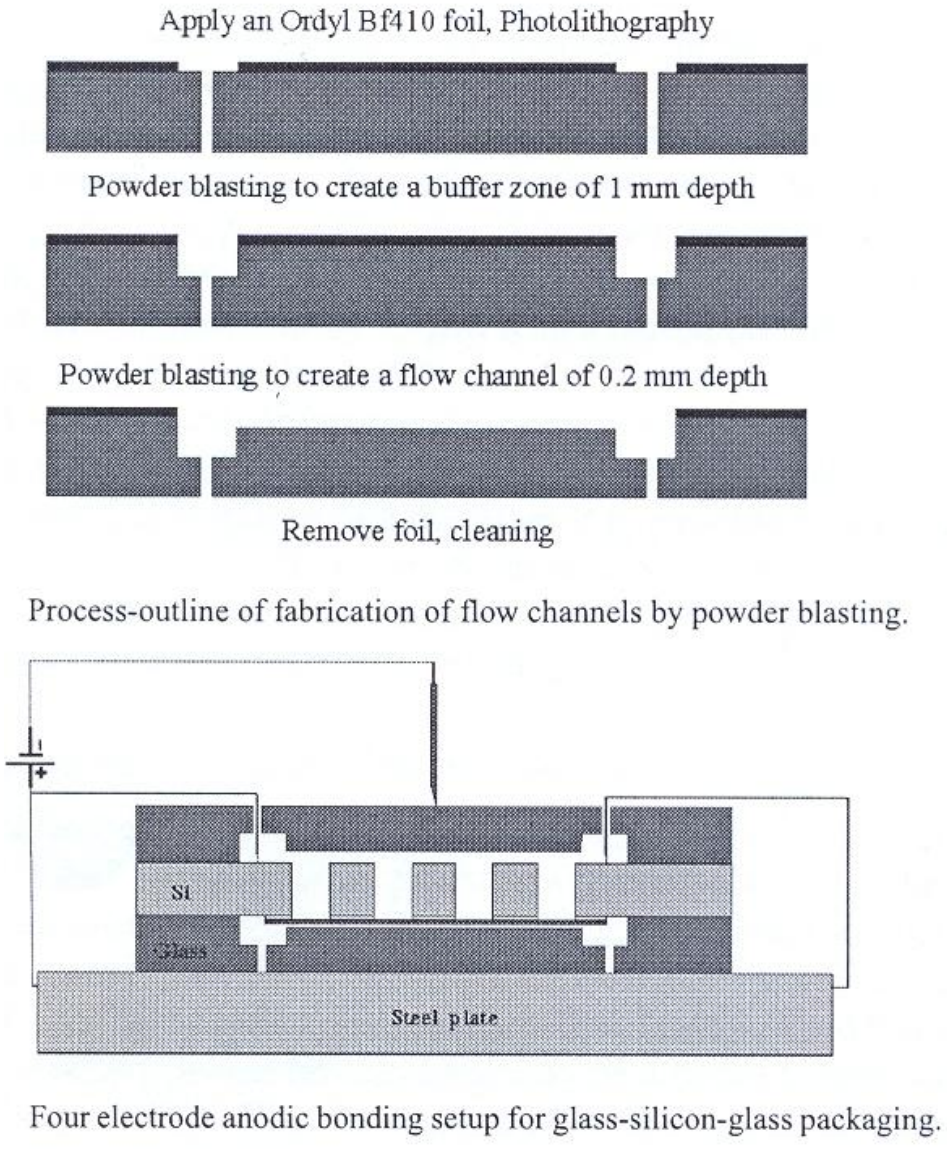

Figure 3.11. Fabrication steps and microreactor assembly (Tong et al., 2003).

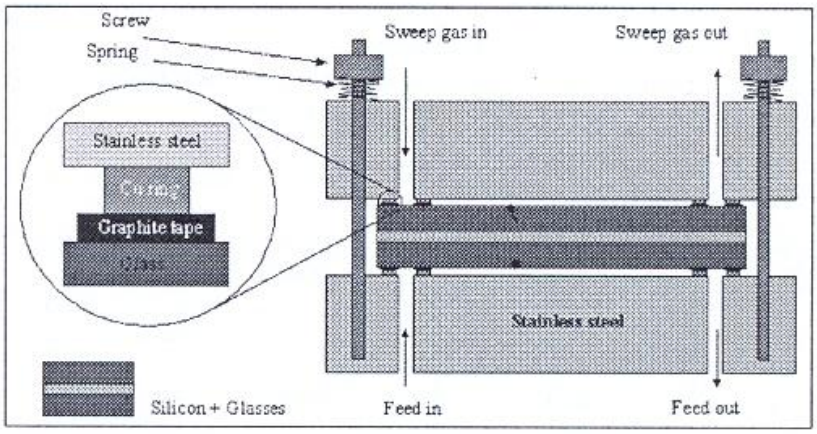

Figure 3.12. Microreactor assembly with the stainless steel holder. The structure is held together tightly by screws and springs. Graphite rings were used to prevent gas leakage (Tong et al., 2003).

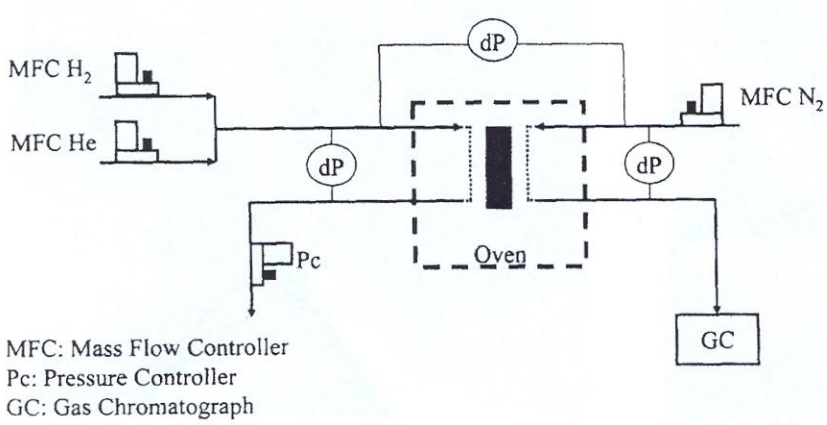

Figure 3.13. Experimental layout of the microreactor (Gielens et al., 2002).

3.5.4 Nickel Mesh Reactors for Gas-liquid and Gas-liquid-solid Reactions

Microreactors with a mesh made out of Ni were developed and used to study reactions in the areas of gas-liquid–solid hydrogenations (e.g. methylstyrene, unsaturated carbonyls) and gas-liquid asymmetric hydrogenations of cinnamate

derivatives and ketones. Ni was chosen as the material for the mesh because of its robustness, ease of fabrication by plating and compatibility with a wide range of chemicals (Wenn et al., 2003).

The reactor consisted of a micromesh sandwiched between two 100 μm cavities. The upper cavity served for the gas flow and the lower for the liquid flow. The pores were 5 μm in diameter which provided an interface of 2,000 m^2/m^3. The schematic of the fabrication procedure for the micromesh is shown in Figure 3.14 and it basically comprisesthe following steps:

- Start with a Si wafer.
- Sputtering of a Cu layer on the Si.
- Application of photo resist and standard lithography to produce an array of hexagonal 5 μm pillars.
- Ni plated onto Cu around photoresist.
- Photoresist removal.
- Thick photoresist applied and patterned.
- Second Ni electroplating for the formation of the membrane support and the frame.
- Photoresist removal.
- Etching of the Cu to release the frame and the membrane.
- Enclosure of the mesh between two structural blocks from Cu and glass.

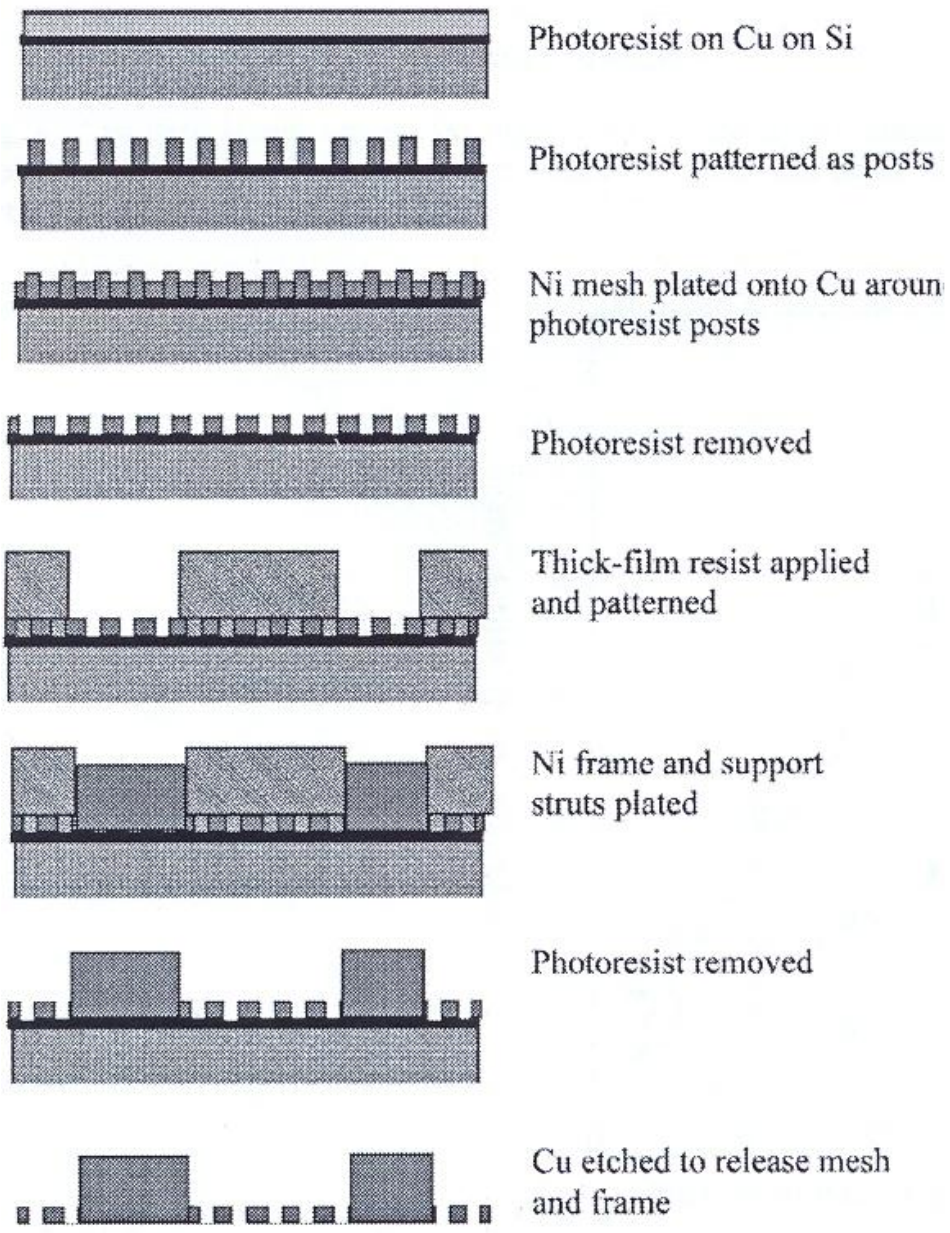

Figure 3.14. Mesh microfabrication procedure (Wenn et al., 2003).

A picture of the microreactor is given in Figure 3.15.

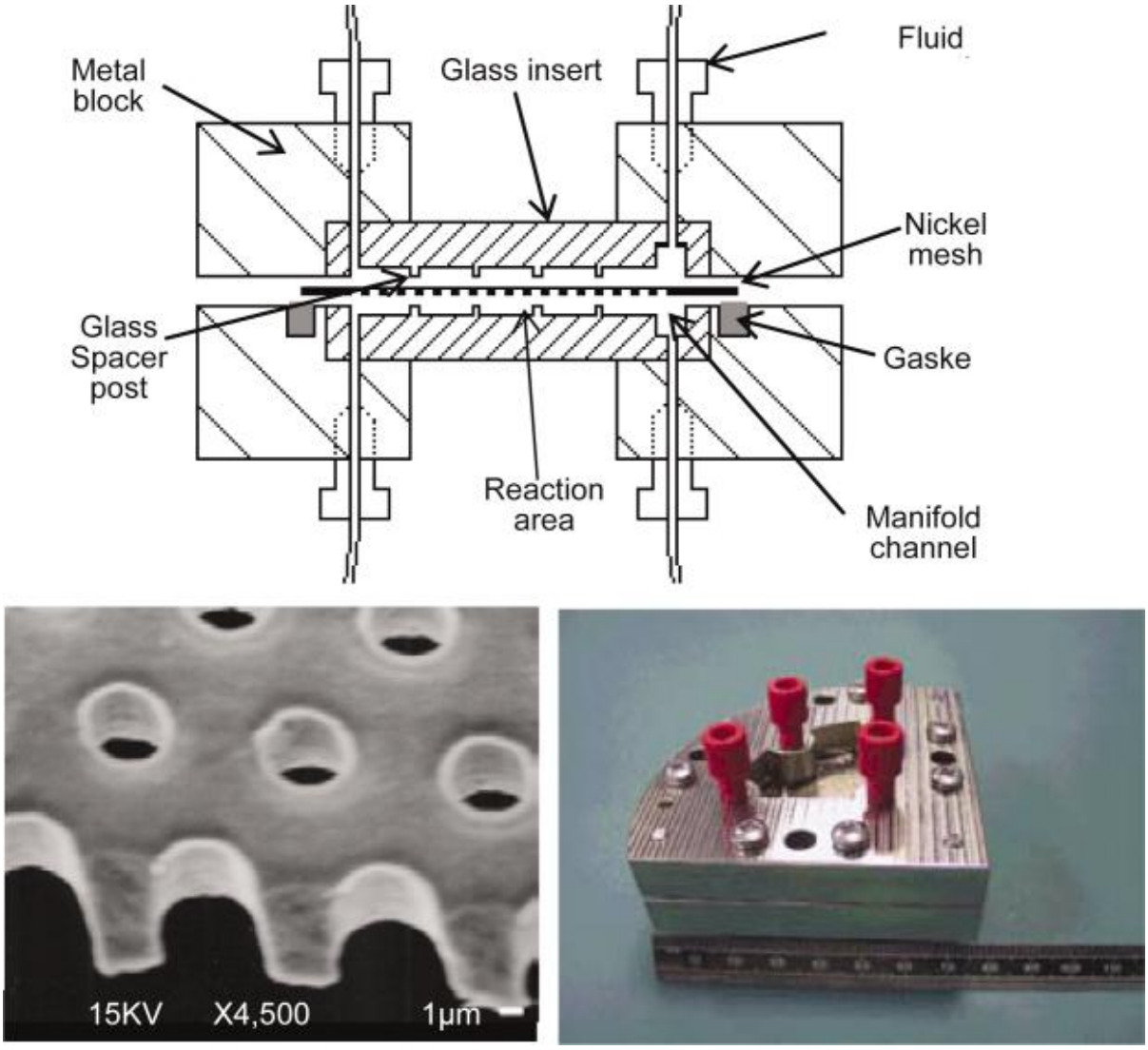

Figure 3.15. Mesh microreactor (a) diagrammatic cross-section, partially exploded view, (b) photograph of the mesh showing the micro-holes (5µm) (c) assembled device (Wenn et al., 2003 and Abdallah et al., 2004).

These microreactors were used to collect data for kinetic estimation as well as catalyst and ligand screening (Wenn et al., 2003 and Abdallah et al., 2004).

3.6 Conclusions

Since their first appearance in the late 1980s, microreactors have developed into powerful research tools for catalyst screening, combinatorial chemistry, creation of compound libraries, kinetic and hydrodynamic studies because of their numerous advantages against conventional lab contactors. One particular type of these micro-devices is the mesh microreactor which benefited from particular interest by the research community in the 2000s. It adopts the concept of contact of two phases through membrane or mesh which has been used in industrial processes like reverse osmosis, absorption, stripping, distillation and others (Zanfir et al., 2008). The main technological driver behind the development of mesh microreactor is the known interfacial area, equal to the open pore area, where the two phases meet without dispersion in one another, hence enabling separation and sampling downstream the process. Numerous published papers have investigated the potential use of mesh for kinetic studies and catalyst screening in static or continuous operation using gas-liquid, gas-liquid-solid or liquid-liquid immiscible reactions. Microfabrication methods developed by the micro-electronics industry involving Si micromachining have been utilised for the mesh usually made of silicon nitride or occasionally from nickel or other materials. The advantages of the mesh compared to other types of microreactors which also show stable interfacial have been demonstrated. But on the other hand, mesh microreactors can present certain drawbacks which relate mostly to the maintenance of the pressure differential between the two fluids so there is no phase breakthrough. Non-uniformity in pore size and the presence of contaminants can greatly reduce this ΔP and make reactor performance problematic. Moreover, the mesh thickness, if too large, can present significant resistance to the heat and mass

transfer, thus careful selection of mesh material and design is crucial. On the whole, advantages seem to outnumber the disadvantages of mesh microreactors rendering them useful devices for research and development or even small scale production. Considering the progress of MEMS, integration of mesh and other types of microreactors in general, with on-board sensors and micro-process units like micro-valves, fluid micro-transport systems, micro-separation units etc for the creation of mini-plants remain challenging research areas for the future.

--//--

CHAPTER 4

Literature Review: Hydrodynamics of Taylor Flow with Particular Focus on Bubble, Slug Sizes and Flow Homogeneity

The challenges faced by the modern chemical industry are to implement processes with improved energy efficiency, less pollution and improved chemistry. Microchemical engineering, an independent discipline in chemical and process engineering has much to offer in this context. First of all, the high mass and heat transfer rates allow highly exothermic, fast reactions to be operated under isothermal conditions with improved yield and selectivity as compared to using conventional technologies. Intensification of heat and mass transfer phenomena is due to the short diffusion/ conduction distances, large concentration/temperature gradients and high surface/volume ratio. In particular, mass transfer limited reactions can also benefit from the high mass transfer rates achieved in micro-structured reactors. Minimal reactant inventories lead to improved safety particularly when explosive, hazardous or toxic substances are involved in the chemical process. Finally, scaling-up of micro-chemical technology is easier through the addition of similar micro-structures units and enables production volume flexibility according to the market needs.

Out of the different types of microreactors presented in Section 3.2 of the preceding Chapter, the microchannel contactor is the most promising for industrial applications as it can offer high heat and mass transfer under a wide range of gas and liquid flow rates. When solid catalyst has to be used, wall coating techniques like sol-gel or anodic oxidation can be implemented (Yue et al., 2007).

Type of contactor	$k_L \times 10^5$ **(m s^{-1})**	a **(m^2 m^{-3})**	$k_L a \times 10^2$ **(s^{-1})**
Bubble columns	10–40	50–600	0.5–24
Couette–Taylor flow reactor	9–20	200–1200	3–21
Impinging jet absorbers	29–66	90–2050	2.5–122
Packed columns, cocurrent	4–60	10–1700	0.04–102
Packed columns, countercurrent	4–20	10–350	0.04–7
Spray column	12–19	75–170	1.5–2.2
Stirred tank	0.3–80	100–2000	3–40
Tube reactors, horizontal and coiled	10–100	50–700	0.5–70
Tube reactors, vertical	20-50	100-2000	2-100
Gas-liquid microchannel contactor	40-160	3400-9000	30-2100

Table 4.1. Comparison different gas-liquid contactors in terms of mass transfer performance, as summarized by Yue et al. (2007).

Direct fluorination of aromatics (toluene and 4-nitrotoluene) and hydrogenation reactions, like for instance the hydrogenation of benzalacetone with Pd as catalyst, are just two examples of reaction categories which have been conducted using microchannel reactors (Guangwen et al., 2008).

4.1 Flow in Microchannels

Depending on the superficial gas and liquid velocities a variety of patterns can be observed in a microchannel reactor (Hessel et al., 2005, and Liu et al., 2005). These are:

- **Film flow**: This type of flow is only observed for downward flow of the liquid. At very low liquid velocities, the liquid flows downwards on the walls of the channel while the gas flows in the channel's core either upwards or downwards.
- **Bubbly flow** is achieved at low gas fractions at moderate gas velocities. One can see small non-wetting bubbles in a continuous wetting fluid. This pattern is governed by surface tension.
- **Slug flow** (also found as plug flow, bubble-train flow, segmented flow or intermittent flow in the literature) is the flow pattern of long bubbles that span most of the cross-section of the channel. Two regimes can be distinguished; Taylor flow and unsteady slug flow. The lengths of bubbles and slugs depend on the inlet conditions and the operating parameters. This type of flow is dominated by surface tension.
- At higher velocities, small satellite bubbles appear at the rear of the slugs and the slugs are eventually aerated. The chaotic pattern that emerges when the gas velocity is increased further is called **churn flow**. This flow pattern occurs at relatively high liquid velocities. Liu et al., 2005, observed churn flow in 0.9-3 mm capillaries while in a study conducted in 2007, Yue et al. observed churn flow in a 0.667 mm capillary.

- When the liquid velocity is at low levels, the rise of gas velocity will lead to the development firstly of **slug-annular** and then **annular flow**. Annular flow occurs at high velocities and low liquid fraction. In this pattern, a thin wavy liquid film flows along the wall while the gas with some entrained liquid in the core. Annular flow is dominated by inertia.
- Other researchers also include **spray flow** as an additional category (Sobieszuk et al., 2010).

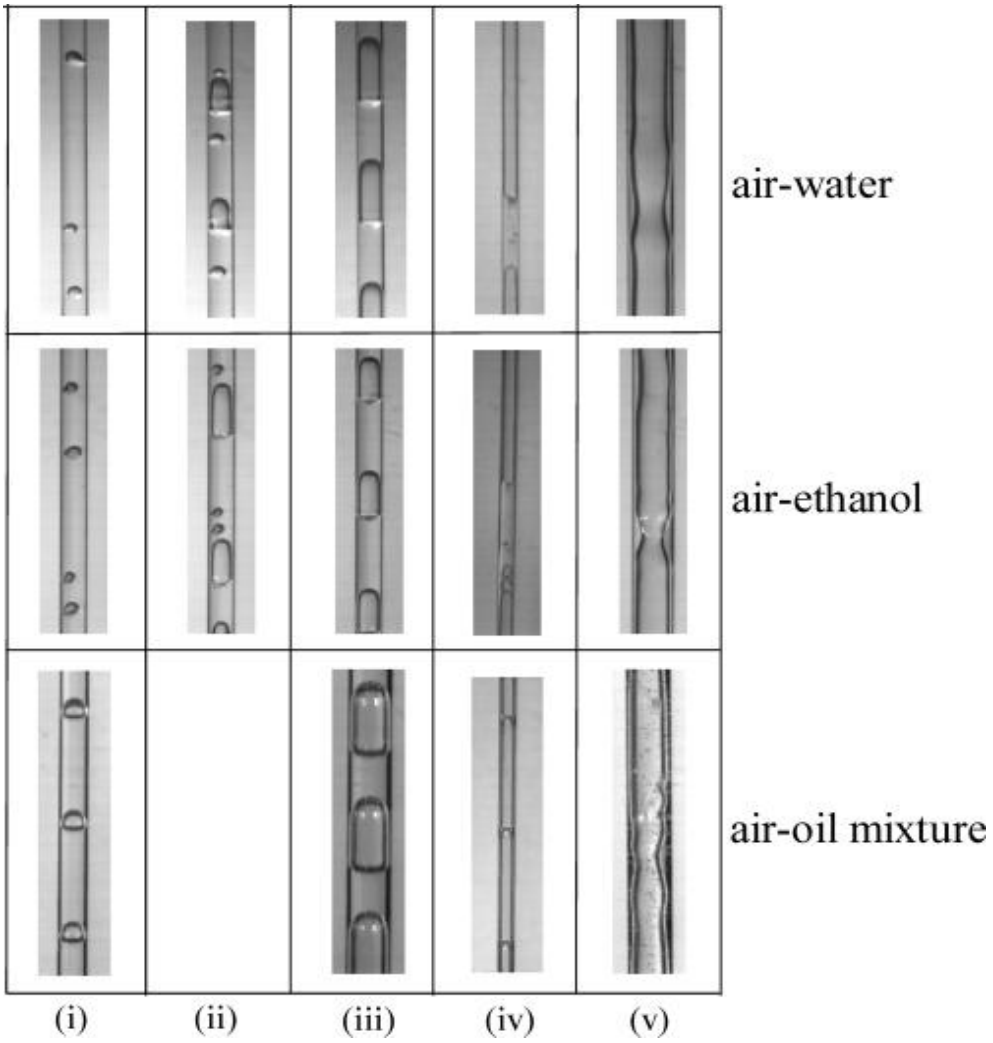

Figure 4.1 Flow regimes observed for various gas-liquid mixtures in vertical capillaries. (i) bubbly, (ii) slug—bubbly, (iii) Taylor, (iv) churn and (v) annular flow. (Liu et al., 2005).

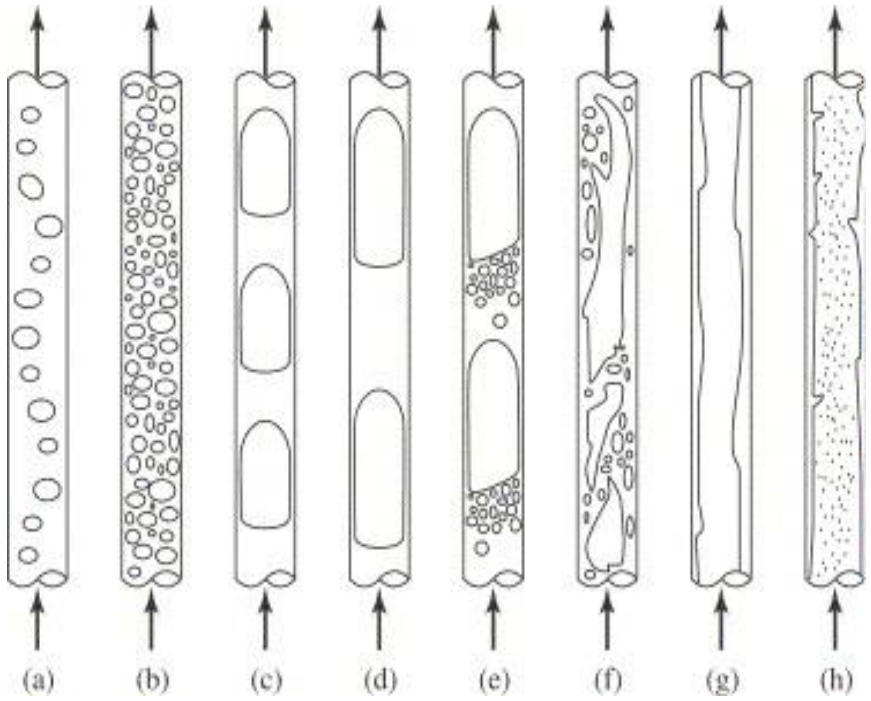

Figure 4.2. Sketch of observed flow patterns in capillary channels. (a, b) bubbly flow, (c, d) segmented slug (a.k.a bubble train flow, Taylor flow, capillary slug flow (e) , (iv) transitional slug/churn flow (f) churn flow, (g) film flow (downflow only). (Kreutzer et al., 2005c).

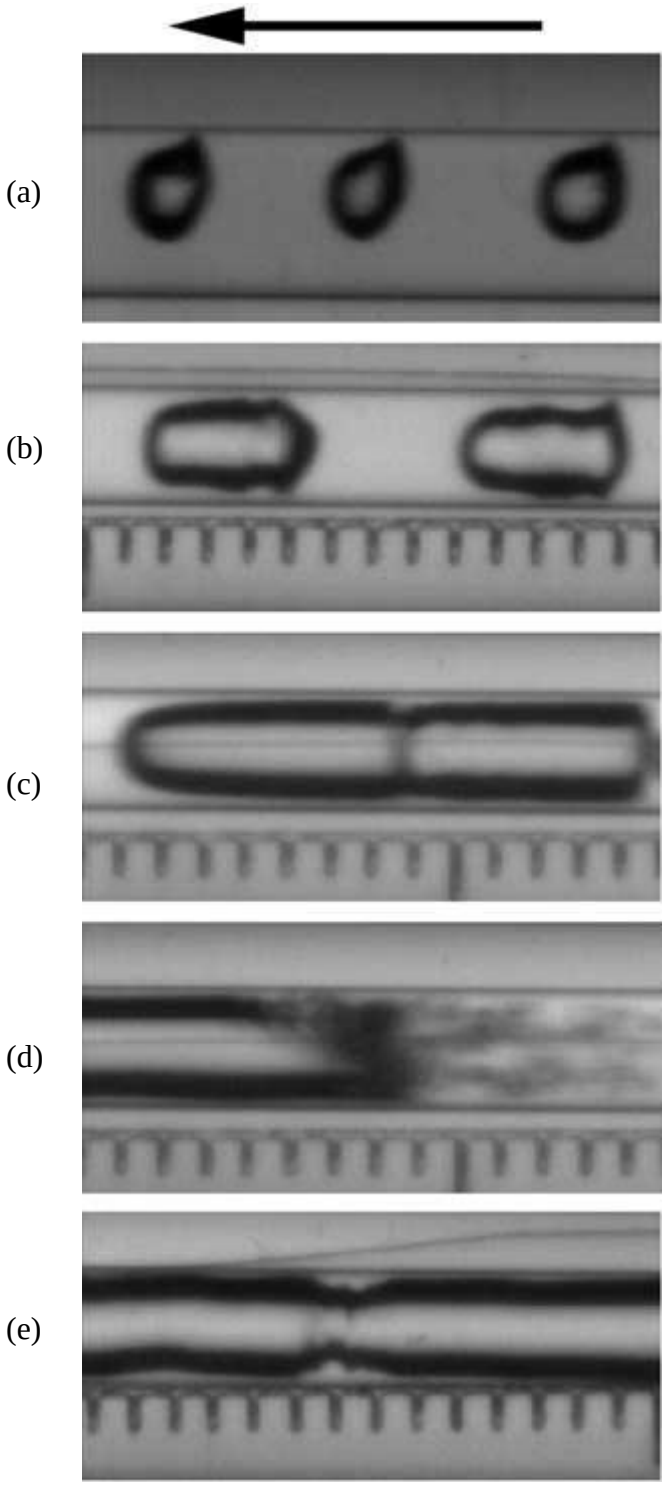

Figure 4.3. Flow regimes observed for the system nitrogen- water in capillaries of diameter 1.0 and 1.5 mm capillaries. (a) bubbly, (b) slug, (c) bubble train slug, (d) churn and (e) annular. (Chen et al., 2002). The arrow indicates the direction of the flow.

Apart from the gas and liquid velocities, there is a number of additional parameters that determine the gas-liquid pattern:

- Ratio of the gas over the liquid flow rate.
- Physical properties of the gas and the liquid.
- Geometry of the mixing or inlet section.
- Channel geometry.
- Material of the channel.

Two-phase flow in capillary channels is different than flow in large channels:

- Viscous effects are inversely proportional to the diameter $\propto \frac{\mu u}{d}$ and are important in microchannels.
- Interfacial stresses are also inversely proportional to the diameter $\propto \frac{\gamma}{d}$ and are also important in microchannels.
- On the contrary, gravitational effects are $\propto \rho g H$ and the same is true for inertial stresses $\propto \rho u^2$ and those are not significant in microchannels (Kreutzer, 2005c).
- Inertial effects are not important if $We = Ca \cdot \mathrm{Re} << 1$.
- Gravitational effects are insignificant in microchannels and therefore, the flow is independent of channel orientation with respect to gravity.

A condition necessary for the channel to be considered capillary is the dominance of surface tension forces over gravitational forces. Eötvös number or otherwise called

Bond number is a measure of the surface tension over gravity. A variety of values of Eö below which the channel is characterised small, has been suggested in the literature. In general the most acceptable condition is Eö<4 because in this case, the bubble terminal velocity which is the rise velocity in a vertical channel filled with stagnant fluid is zero. The Eötvös number is defined as (Angeli & Gavriilidis, 2008):

$$Eö = \frac{(\rho_L - \rho_G)d^2 g}{\sigma} \tag{4.1}$$

It should be mentioned that *Eö* for the microchannel of diameter 250 μm used in the current experimental study was 0.021.

Taylor flow offers some advantages like low axial mixing and high radial mixing as compared to other flow patterns and single-phase laminar flow. The low axial mixing is achieved because the capillary channel is intermittently filled with the bubbles and liquid slugs. The only means of communication between the slugs is a thin liquid film surrounding the bubbles. The high radial mixing is fulfilled due to the recirculation patterns within the liquid slugs which refresh the gas-liquid interface continuously and therefore improve mass transfer from the liquid to the wall and interfacial mass transfer from gas to the liquid. The smaller the liquid slugs, the higher the mass transfer rate due to the higher interfacial area and also the more intense radial mixing inside the liquid slugs, as found by research studies like for instance that by Bercic & Pintar, 1997, and Heiszwolf et al., 2001. The former concluded that the volumetric mass transfer coefficient increases with decreasing

slug length and increasing the velocity of the unit cell based on absorption experiments using methane and water. They also found that the length of the liquid slugs influences much more the mass transfer than the length of the bubbles. They fitted their data to a correlation relating the volumetric mass transfer coefficient with the mixture velocity and the length of liquid slug.

Due to the high radial mixing but low axial mixing, Taylor flow is the preferred flow pattern for two-phase applications, like for example fast multiphase reactions which can be mass transfer limited, or for single phase applications which suffer from large back-mixing. Furthermore, the enhanced heat and mass transfer possible in Taylor flow in microchannels would enable a kinetically operating regime to be established for the evaluation of reaction kinetics.

Mass transfer characteristics depend on the following hydrodynamic properties of the flow:

- Thickness of the liquid film that surrounds the bubbles.
- Bubble velocity.
- Bubble length.
- Slug length.
- Mixing and flow circulation in the liquid slugs.

Knowledge of Taylor flow hydrodynamics is necessary for understanding the behaviour and improving the performance of the micro chemical systems that operate in this regime (Pohorecki, 2007). According to Kreutzer, 2005, Taylor flow

is fully characterised in a capillary and determined when the bubble frequency, the gas and liquid velocities and the fluid properties are known.

Flow transition correlations for larger channels do not have applicability in microchannels due to the fact that flow in microchannels is mostly laminar and governed by surface tension. Several diagrams, called flow-pattern maps have been presented in the literature to depict the region in which a given flow pattern occurs. For example, Triplett et al. (1999) prepared a flow-map based on superficial velocities and Akbar et al. (2003) proposed one based the Weber number. However, in a later study in 2008, Yue et al. argued that these flow maps are applicable for microchannels with diameters of 1 mm and above and suggested that further research is required in order to produce flow maps for microchannels of smaller dimensions.

In detail, Yue argued that the experiments conducted with two micro channels of 667 and 400 μm diameter showed good agreement with the predictions of Triplett et al. (1999) developed for 1.097 mm diameter circular microchannel for all flow transitions. Conversely, a poor agreement between the experimental data and the predictions of the flow-map has been found for the smaller micro channel of 200 μm diameter. The same conclusions were drawn in comparison to the experimental data with the flow-maps having We_G and We_L as coordinates produced by Akbar et al. (2003). For the 200 μm micro channel the transition from slug flow to slug-annular was not well defined while the predictions for the larger channels were successful.

Efforts to develop a universal flow-map to cover different microchannels and gas-liquid systems have bared limited fruits. Notwithstanding this, it is evident that the Taylor flow regime occupies a significant proportion of the flow map, is obtainable for the majority of gas-liquid systems and is the most suitable regime to conduct gas-liquid reactions.

Significant research on Taylor flow has application in monoliths which are usually catalyst support structures comprising of small parallel channels and are interesting alternatives to three-phase slurry reactors and trickle bed reactors. They are offering advantages like the small pressure drop and the suitability for gas cleaning purposes like in Selective Catalytic Reaction (SCR) applications. The operating mode is determined by the channel size; in smaller channels, the flow is slug flow or bubble train flow with elongated bubbles.

4.2 Mass transfer in Taylor Flow

The improved mass transfer in Taylor flow make it an attractive flow pattern for carrying out gas-liquid operations in microchannels. In Taylor flow, gas components from the bubbles get transferred to the flat film region and the liquid slugs. As previously mentioned, one of the characteristics of Taylor flow is that the two successive liquid slugs do not mix and mass transfer between them occurs by diffusion from the film to the liquid slug. The turbulent convective flow responsible

for mixing in macroreactors is non-existent in micro-reactors, as said by Qian & Lawal (2006).

Yue et al. in a study published in 2007, summarised that mass transfer in microchannels is strongly affected by the operating conditions:

- At a fixed superficial liquid velocity, an increase in the gas velocity increases the interfacial area and the liquid side volumetric mass transfer coefficient while the effect on the liquid side coefficient is insignificant as it was concluded from CO_2 absorption experiments in a NaOH solution.
- At a fixed superficial gas velocity, an increase in the liquid superficial velocity increases drastically the liquid side mass transfer coefficient and the volumetric mass transfer coefficient while the effect on the interfacial area is not very marked.
- The volumetric mass transfer coefficients in micro-channels are at least two orders of magnitude larger than those in conventional macroreactors (for example bubble columns, packed columns). Due to the very high mass transfer achieved in micro-channels, a certain gas-liquid system can fall into a different operating regime in a micro-reactor as compared to the conventional reactors depending on the relative rates of diffusion and reaction.

The dominant resistance in mass transfer is the lubricating film. For instance, this was the conclusion of Kreutzer (2003) when he used a model to verify that the dominant resistance for hydrogen transfer to the catalyst was in the lubricating film for the hydrogenation reaction of α-methylsterene over a Pd catalyst.

The film resistance, estimated by the film theory as $\frac{D}{\delta}$ is found between the bubble and the wall and between the slug and the wall. For Ca<0.01, the difference in thickness between the film around the slug and the film around the bubble vanishes and the mass transfer of the gas through the film is as fast for the slug as for the bubble.

For short slugs and typical hydrogenation conditions of organic liquids in square channels, the slug is almost saturated and the gaseous concentration in the slug is equal to the equilibrium solubility ($C_{slug} \approx C^*$) as the majority of the circulation zone is characterised by a region of equal concentration. In conclusion, if the slugs are short, the slugs are saturated with the gas component, and if additionally the film thickness is the same for the bubble and the slug, then the mass transfer is independent of the liquid hold-up as supported by Kreutzer (2005c).

When the velocity is decreasing, the film thickness is reducing and mass transfer is improved. Additionally, the pressure drop along the channels declines. Enhancement of mass transfer comes at the cost of an increase in pressure drop in large channels. This analogy is based on the dominance of eddy transport in turbulent flows. Microchannels provide an escape to the usual compromise between pressure drop and mass transfer with minimal energy input (Kreutzer, 2005a).

4.3 Liquid Film

In Taylor flow, if the liquid shows good wettability of the channel wall (small contact angle), then the wall is covered by a thin liquid layer and the bubbles are sliding over this lubricating layer.

For round capillaries at low *Ca*, the film is very thin, the cross-section of the bubble is almost equal to the cross-section of the channel and the following applies (Kreutzer, 2005a):

$$\frac{U_b}{U_{ls}} = 1 + \frac{4\delta}{d} \tag{4.2}$$

In general, the thickness of the lubricating film around the bubble can be given by various expressions found in the literature, like those below. Please note that a summary of expressions is given in Table 4.3:

$$\frac{\delta}{d} = \frac{0.66Ca^{2/3}}{1 + 3.33Ca^{2/3}} \quad \text{For } 10^{-3}<Ca<1.4 \quad \text{(Schwartz et al., 1986)} \tag{4.3}$$

$$\frac{\delta}{d} = 0.25Ca^{1/2} \quad \text{For } 10^{-3}<Ca<3\ 10^{-1} \quad \text{(Aussilous \& Quéré, 2000)} \tag{4.4}$$

$$\frac{\delta}{d} = 0.67Ca^{2/3} \quad \text{For } 10^{-3}<Ca<10^{-2} \quad \text{(Bretherton, 1961)} \tag{4.5}$$

The interfacial gas-liquid area is then composed of two parts: the lateral part (the lubricating layer between the bubble and the wall) and the perpendicular part

(between the bubble and the adjacent liquid slug). As the length of the bubble is often many times that of the channel diameter, the lateral part is many times greater than the perpendicular one and often contributes more than 90 % of the total interfacial area. The lubricating film is usually very thin of the order of 10^{-6} m. According to Pohorecki (2007), the criterion to ensure that the lubricating film around the bubbles is always saturated with the gaseous components in the case of slow catalysed reactions is:

$$\frac{L_B D}{U_b \delta^2} >> 1 \qquad (4.6)$$

L_B: bubble length

U_b: bubble velocity

D: Diffusivity for physical absorption

It should be noted this criterion was always satisfied in the experiments described in this Thesis.

It is therefore essential when one designs microreactors to take into account not only gas (or liquid) hold-up and interfacial area but also size and frequency of gas bubbles so that this criterion is fulfilled.

Edvisson & Irandoust (1996), studied the effect of inertia on the lubricating film using finite elements. The conclusions from this study are included in the following Table.

Range studied		
Ca	**Re**	**Fr**
0.1-1	20-200	0 or 1

Condition	**Result/Conclusion**
Re ↑	• δ ↑ • Bubble velocity ↑
Fr ↑ And high *Ca*	• δ ↑ • Bubble velocity ↑ For upwards flow the increase was significant but for downwards flow the effect was only slight
Ca ↑	The bubble shape at the back changes from convex to concave
Ca ↑ And high Re	Ripples appear at the back of the bubble Amplitude and wavelength of these ripples go through a maximum with increasing *Ca*.

Table 4.1a. Factors affecting the lubricating film, the bubble and shape velocity. From the study by Edvinsson and Irandoust (1996).

Giavedoni & Saita in 1997 and 1999 also studied the effect of inertia. *Re* was found to affect the film thickness slightly in a non-monotonic way. When *Re* was increasing, film thickness initially decreased and then increased. However, for $Ca<10^{-2}$ inertial forces were not found to have an effect on the film thickness. This is the viscocapillary regime when the film thickness depends only on the *Ca*. Aussilus & Queré (2000), suggested that when inertia effects become important - this regime is referred to as the visco inertial regime - the film thickness depends on the *We* number as well:

$$\frac{\delta}{r} \propto \frac{Ca^{2/3}}{\left(1+Ca^{2/3}-We\right)} \tag{4.7}$$

where $We = \rho_L U_b^2 \left(r-\delta\right)/\sigma$ (4.8)

The Table below lists the various correlations found in the literature for the film thickness:

Correlation for film thickness	**Range of *Cα***	**Reference**
$\frac{\delta}{d} = \frac{0.66Ca^{2/3}}{1+3.33Ca^{2/3}}$	$10^{-3} \leq C\alpha \leq 1.4$	Schwartz et al. (1986)
$\frac{\delta}{d} = 0.25Ca^{1/2}$	$510^{-5} \leq C\alpha \leq 3\ 10^{-1}$	Aussillous & Queré (2000)
$\frac{\delta}{d} = 0.67Ca^{2/3}$	$10^{-3} \leq C\alpha \leq 10^{-2}$ For lower capillary numbers the film thickness is larger than the theoretical value. The presence of surface contaminants that are absorbed on the interface may affect the thickness. Conversely, surface roughness, intermolecular forces or non-zero dispersed phase velocity could not explain the discrepancy.	Bretherton (1961)

Correlation for film thickness – *Continued…*	**Range of *Cα***	**Reference**
$\frac{\delta}{d} = \sqrt{\frac{\mu_L}{\sigma}}\left[-0.1 + 0.89\sqrt{U_b}\right]$ U_g in cm s^{-1} μ_L in poise σ in dynes cm^{-1}	$710^{-6} \leq C\alpha \leq 2\ 10^{-4}$	Marchessault & Mason (1960)
$\frac{\delta}{d} = 0.18[1 - \exp(-3.08(Ca^{0.54}))]$	$9.5\ 10^{-4} \leq C\alpha \leq 1.4$	Irandoust & Andersson (1989)

Table 4.2. Correlations for liquid film.

The bubble is separated by the channel wall by a thin film that also prevents the contact between the slug and the wall. When the *Ca* is low, the film separating the slug and the wall is almost equal to the film between the bubble and the wall and this can be an assumption to be used in the first approximation. The circulating vortex in the slug is never in direct contact with the wall and the mass or heat can be transferred to the wall by diffusion (conduction) through the film. If *Ca*>0.01, the film between the slug and the wall is thicker and for values higher than 0.7 the recirculating pattern in the slug completely vanishes.

The flow developed in a tube is Hagen-Poisseuille flow. The recirculation pattern is still found for short slugs even when the length of the liquid slug is less than 25 % of the capillary diameter. The film thickness for these short slugs is larger (Fujioka &

Grotberg, 2004). For the experiments performed in this Thesis, Ls/d>0.25 and *Ca* was within the range [9.5 10^{-5}-7.8 10^{-4}] which means there was a recirculation pattern inside the slugs and the concentration of the gas component is uniform inside the liquid slug and equal to the saturation solubility.

4.4 Bubble velocity

The drift flux model is frequently used in the literature to evaluate the bubble velocity as follows:

$$U_b = CU_{ls} + U_0 \tag{4.9}$$

where C is an experimentally determined coefficient, U_{ls} is the liquid slug velocity and U_0 is the bubble rise velocity in a stagnant liquid (it is called the terminal velocity if the tube is vertical). U_0 is very small or zero in very small capillaries due to the surface tension effects and can be neglected from the above equation which becomes (Angeli & Gavriilidis, 2008):

$$U_b = CU_{ls} \tag{4.10}$$

Various correlations found in the literature used to evaluate the bubble velocity are listed in the subsequent Table:

Correlation for bubble velocity	Range	Reference
$U_b = C_0 U_m + C_1\sqrt{gd}$	C_0=2.27 for laminar flow 1.2<C0<1.4 for turbulent flow C1=0.35	Developed for upward flow in a vertical capillary, (Collins, 1978)
$U_b = C_0 U_m + V_\infty$ $U_m = U_G + U_L$ is the mean flow velocity $V_\infty = C_\infty(Ga, Eö)\sqrt{gd}$ (Zukoski, 1966) $Ga = \frac{(\rho_L - \rho_G)\rho_L d^3 g}{\mu_L^2}$ Galileo number $Eö = \frac{(\rho_L - \rho_G) d^2 g}{\sigma_L}$ Eötvös number $C_\infty(Ga, Eö) = 0.344 \frac{1 - 0.96e^{-0.0165 Eö}}{\left(1 - 0.52e^{-0.0165 Eö}\right)^{3/2}} \sqrt{1 + \frac{20}{Eö}\left(1 - \frac{6.8}{Eö}\right)}$ Developed by Bendiksen, 1985, assuming an inertial controlled patterned. This condition is satisfied i.e.when d>2.5 10^{-3} m for a gas bubble rising in water.		Developed for inclined tubes (Bendiksen, 1984) but extended to vertical tubes as well (Bendiksen, 1985). Tube diameter was 2.42 cm. Zukoski (1966) developed the relationship between the V_∞ and the Galileo and Eötvös numbers.

<table>
<tr><th>Correlation for bubble velocity – Continued…</th><th>Range</th><th>Reference</th></tr>
<tr><td>$U_b = C_0 U_m + V_\infty$
When Eö<4, then $V_\infty = 0$ (from experiments).
Without any gas or liquid circulation gas bubbles in a motionless liquid do not move.
C_0 is a function of Eö:
$E\ddot{o} \to 0$ then $C_0 = 1.7$
$E\ddot{o} > 0$ then $C_0 = \alpha E\ddot{o}^b$
α and b depend on the fluid property number $N_f = g\mu_L^4 / \sigma^3 \rho_L$
<table>
<tr><th>N_f</th><th>α</th><th>b</th></tr>
<tr><td>4.7 10-11</td><td>0.95</td><td>-0.10</td></tr>
<tr><td>9 10-11</td><td>0.89</td><td>-0.09</td></tr>
<tr><td>3.2 10-10</td><td>1.17</td><td>-0.11</td></tr>
<tr><td>6.9 10-8</td><td>1.08</td><td>-0.07</td></tr>
</table>
</td><td>1.5 10^{-3}≤Cα≤0.1
55<Re<2000
0.13<Eö<5</td><td>Laborie et al. (1999)</td></tr>
<tr><td>$\frac{U_b}{U_m} = \frac{1}{1 - 0.61 Ca_m^{0.33}}$
$Ca_m = \frac{\mu_L U_m}{\sigma}$</td><td>2 10^{-4}≤Cα≤0.39</td><td>Liu et al. (2005)</td></tr>
</table>

Table 4.3. Correlations for the bubble velocity.

The difference between U_b and the mean flow velocity is equal to mU_b. m signifies the relative velocity between the bubble and the liquid slug and is defined as:

$$m = \frac{U_b - U_{ls}}{U_b} \tag{4.11}$$

Its determination has always been based on experiments (Laborie et al., 1999). Table 4.4 summarizes the correlations found in the literature for *m*.

Correlation for relative velocity between the bubble and the liquid	**Range of Cα**	**Reference**
$m = \sqrt{Ca}$	$7\ 10^{-5} \leq C\alpha \leq 0.1$ Correlation validated for capillary numbers<0.015 by Fairbrother and Stubbs (1935) and later Taylor (1961) extended its validity to 0.1	Fairbrother & Stubbs (1935) Taylor (1961)
Constant value 0.58	Large *Ca*	Cox (1964)
Constant value 0.592	$C\alpha = 10$	Giavedoni & Saita (1997)
$m = \left(\frac{\mu}{\sigma}\right)^{1/2}\left[-0.10 + 1.78\sqrt{U_b}\right]$	$710^{-6} \leq C\alpha \leq 210^{-4}$	Marchessault & Mason (1960) Capillary diameter: 1.484 10^{-3} m. Capillary placed at different inclinations and filled with water at different flow rates.
$m = 3.87Ca^{2/3}$ Correction factor for vertical tubes and • upward flow $\left(1+1/6\,E\ddot{o}\right)$ • downward flow $\left(1-1/6\,E\ddot{o}\right)$		Bretherton (1961) Capillary diameter: 1 10^{-3} m. Horizontal capillary.

Table 4.4. Correlations for relative velocity between the bubble and the liquid slug.

4.5 Pressure drop

A variety of models have been suggested for calculation of the pressure drop in microchannels. Pressure drop correlations are based either on the homogeneous flow model (for bubble flow), the separated flow model (for slug-annular, churn and annular flows) and the two-phase frictional pressure drop (for Taylor flow).

Three terms must be taken into account when calculating the pressure drop in Taylor flow; the viscous term (the friction between the slugs and the wall), the gravity term (in the case of upflow/ downflow) and the Laplace term. The latter is significant if Ls/d<10. Fujioka & Grotberg (2004) calculated numerically the pressure drop across the slug and found that for short slugs the Laplace term dominates and that the pressure drop is slug length dependent.

Kreutzer (2003), calculated pressure drop over the bubble length using numerical simulations and he found that pressure drop increases when *Re* increases and *Cα* decreases. Experimental data in a 2.3 mm capillary showed that the pressure drop depends on the slug length. Keutzer found that the only contribution of the bubbles to the pressure drop occurs at the caps and is unrelated to the length of the bubble. f_{app}*Re is independent of the bubble length. On the contrary, f_{app}*Re depends very much on the slug length and he proposed the following relationship:

$$f_{app} = \frac{16}{\mathrm{Re}}\left[1+\frac{d}{L_S}\cdot\frac{0.465}{Ca^{1/3}}\right], \text{ applicable for Re<10.} \qquad (4.12)$$

If the length of the slug is very long (approaches infinity), the f_{app} approaches $\frac{16}{\mathrm{Re}}$.

In a study published in 2005a, Kreutzer showed that inertia can be taken into account with the dimensionless group $\frac{\mathrm{Re}}{Ca} = \frac{\mu^2}{\rho d \gamma}$ which is independent of velocities and all data can be represented accurately by the semi-empirical model:

$$f_{app} = \frac{16}{\mathrm{Re}}\left[1 + 0.17\frac{d}{L_S}\cdot\left(\frac{\mathrm{Re}}{Ca}\right)^{1/3}\right], \text{ valid for Re>100 and for We>0.1.} \quad (4.13)$$

Experimental data showed that the friction factor depends on the fluid properties and slug length and not on velocities. The factor 0.17 was not verified by CFD calculations and it represents the maximum increase per bubble (a factor of $4^{2/3}$) due to the Marangoni effect. In the absence of impurities, the factor of 0.07 must be used instead. Kreutzer supported the view that liquid slug lengths can be determined from pressure measurements, particularly for slug lengths that otherwise could not be measured easily like in monoliths or closed microreactors.

Warnier et al. (2010), developed a model for the pressure drop for gas-liquid Taylor flow in a capillary channel with diameter smaller than 1 mm. Experimental results using a glass capillary with diameter 250 μm showed good agreement with the model. The model takes into account two contributions for the pressure drop; the first one is due to the laminar flow in the liquid slugs and the second one is due to the bubbles disturbing the parabolic velocity profile in the liquid slugs. The model was developed using the theory by Betherton (1961) and the scaling analysis of

Aussillous & Quéré (2000), and also a mass balance based Taylor flow model. The model and the experimental results were compared with the Lockhart-Martinelli-Chisholm model (Chisholm, 1967) and the Kreutzer model (Kreutzer, 2005b).

The main difference of the Warnier model (Warnier et al., 2010) and the Kreutzer model (Kreutzer, 2005) is that the latter does not take into account the effect of the bubble velocity on the pressure drop and was found to under-predict the pressure drop for low *Re* numbers. However, the convergence of the Kreutzer model with the experimental data was improved greatly as *Re* approached 150.

The Lockhart-Martinelli-Chisholm model does not take into account any hydrodynamic properties of Taylor flow or surface tension and its predictions were found to deviate from the experimental data as compared to the Kreutzer (2005b) or Warnier et al. (2010) models.

In conclusion, the pressure drop can be decomposed into a viscous term because of friction and a Laplace term due to surface tension - the pressure difference between the adjacent gas bubble and liquid slug is the Laplace pressure -. In addition, pressure drop depends on the slug length. Finally, the more bubbles per unit length, the shorter the slugs and the higher the pressure drop (Qian & Laval, 2006).

Correlation for pressure drop	Range	Reference
Pressure drop over a single Taylor bubble: $\Delta P_B = 7.16(3Ca_B)^{2/3}\frac{\sigma}{d}$	<1.1Hydraulic diameter<1.5 $S \approx 1$ Film thickness is negligible	Bretherton (1961)
$f_{app} = \frac{16}{\mathrm{Re}}\left[1+\frac{d}{L_S}\cdot\frac{0.465}{Ca^{1/3}}\right]$	Re<10	Kreutzer (2003)
Friction factor for the flow in the liquid slugs: $f_S = \frac{16}{\mathrm{Re}}\left[1+\alpha\frac{d}{L_S}\left(\frac{\mathrm{Re}_{GL}}{Ca_{GL}}\right)^{1/3}\right]$ Pressure drop over the liquid slugs: $-\left(\frac{dP}{dz}\right)_S = f_S\left(\frac{1}{2}\rho_L(U_G+U_L)^2\right)\frac{4}{d} = \frac{2f_S\,\mathrm{Re}_{GL}\,\rho_L\mu_L(U_G+U_L)}{d^2}$ Pressure drop per unit of channel length: $-\left(\frac{dP}{dz}\right)_C = -\left(\frac{dP}{dz}\right)_S\left(\frac{L_S}{L_B+L_S}\right)$ α is a constant with a value of 0.07 from numerical calculations and 0.17 from experiments. The difference was attributed to Marangoni effects due to impurities in the flow. Re and *Ca* numbers are calculated using the sum of the superficial gas and liquid velocities.	$2\ 10^{-3} < Ca_{GL} < 4\ 10^{-2}$ $\mathrm{Re}_{GL} > 150$	Kreutzer (2005a)

Correlation for pressure drop – *Continued…*	**Range**	**Reference**
$f = \frac{16}{\mathrm{Re}}\left[1 + \frac{d}{L_S}\frac{0.465}{Ca_B^{1/3}}\right]$ Pressure drop per unit of channel length: $-\left(\frac{dP}{dz}\right)_C = \frac{2fU_m^2\rho_L}{d}\varepsilon_L$	$Ca_B << 1$ $Ca_B \times \mathrm{Re}_B << 1$ Extended for *Ca* numbers up to 10^{-2} and Re in the order of 100 with the scaling analysis of Aussilous and Quéré	Bretherton (1961) Aussilous & Quéré (2000)
$F_E = \frac{C_f}{\mathrm{Re}_E} S^{-0.5}\left[\exp\left(-0.02\,\mathrm{Re}_E\right) + 0.07\,\mathrm{Re}_E^{0.34}\right]$ $\mathrm{Re}_E = \frac{\rho_L U_E d}{\mu_L}$ $U_E = U_m + U_e = U_m + \left(\frac{d^2}{32\mu_L}\right)\rho_L g$ S is the slip ratio C_f is a constant relating the Fannning factor to laminar flow Reynolds number Pressure drop per unit of channel length: $-\left(\frac{dP}{dz}\right)_C = \frac{2F_E U_E^2 \rho_L}{d}$ $U_E = U_G + U_L + U_e$ is the two-phase velocity U_e is the gravity equivalent velocity	$\frac{U_G}{U_L} > 0.5$	Liu et al. (2005)

Correlation for pressure drop – *Continued…*	**Range**	**Reference**
Gas phase pressure drop per unit length of channel: $-\left(\frac{dP}{dz}\right)_G = \frac{32\mu_G U_G}{d_h^2}$ Liquid phase pressure drop per unit length of channel: $-\left(\frac{dP}{dz}\right)_L = \frac{32\mu_L U_L}{d_h^2}$ Lockhart-Martinelli parameter X : $X^2 = \frac{\left(\frac{dP}{dz}\right)_L}{\left(\frac{dP}{dz}\right)_G}$ Lockhart-Martinelli parameter Φ_L^2: $\Phi_L^2 = 1 + \frac{c}{X} + \frac{1}{X^2}$, c=5 when the gas flow and laminar flow are both laminar. Two-phase pressure drop: $-\left(\frac{dP}{dz}\right)_C = \Phi_L^2 \left(\frac{dP}{dz}\right)_L$	This model was not developed to describe pressure drop in Taylor flow but it has been used by other authors to calculate pressure drop in this regime.	Chisholm (1967)

Correlation for pressure drop – *Continued…*	**Range**	**Reference**
Pressure drop over a single Taylor bubble: $\Delta P_b = 7.16\frac{\sigma_L (3Ca_b)^{2/3}}{d\left(1+3.34Ca_b^{2/3}\right)}$ Frictional pressure loss in one liquid slug: $\Delta P_S = \frac{32\mu_L (U_G + U_L)}{d^2}(L_S + \delta)$ Pressure drop over a unit cell: $\Delta P_{UC} = \Delta P_S + \Delta P_b$ Pressure drop over a unit length of channel: $-\left(\frac{dP}{dz}\right)_C = \frac{32\mu_L U_L}{d^2}\left(1+\frac{7.16\cdot 3^{2/3}}{32}\frac{d}{(L_S+\delta)}\left(\frac{A}{A_b}\right)\frac{1}{\left(Ca_b^{1/3}+3.34Ca_b\right)}\right)$ or $-\left(\frac{dP}{dz}\right)_C = \frac{32\mu_L U_L}{d^2}\left(1+\frac{7.16\cdot 3^{2/3}}{32}\frac{d\cdot F_b}{U_L}\frac{1}{\left(Ca_b^{1/3}+3.34Ca_b\right)}\right)$ Slug friction factor: $f_S = \frac{16}{\mathrm{Re}_{GL}}\left(1+\frac{7.16\cdot 3^{2/3}}{32}\frac{d}{(L_S+\delta)}\left(\frac{A}{A_b}\right)\frac{1}{\left(Ca_b^{1/3}+3.34Ca_b\right)}\right)$ or $f_S = \frac{16}{\mathrm{Re}_{GL}}\left(1+\frac{7.16\cdot 3^{2/3}}{32}\frac{d\cdot F_b}{U_L}\frac{1}{\left(Ca_b^{1/3}+3.34Ca_b\right)}\right)$	$Ca_B < 10^{-2}$ $\mathrm{Re}_B < 150$ Negligible velocity of the liquid film surrounding the bubbles.	Warnier et al. (2010)

Table 4.5. Correlations for the pressure drop.

4.6 Bubble formation process

Two descriptions for bubble or droplet formation are found in the literature corresponding to microdevices; the dripping and the squeezing regime. The *Ca* is the criterion to distinguish between the two regimes (Garstecki et al., 2006):

- When the *Ca* <0.01, the interface force dominates the shear stress and the squeezing regime appears. The dispersed fluid in this case will fill the entire cross-section and will block the continuous phase until it breaks off. The squeezing regime was considered to be specific to microdevices.
- When *Ca* >0.01, shear stress plays a leading role and the dripping regime appears. In this case, the dispersed fluid occupies only part of the cross-section when it enters the main channel and this regime is similar to the unbounded case.

According to studies by Garstecki et al. (2006) and Dai et al. (2009), bubble formation in microchannels includes three stages; expansion, collapse and pinching off. Three kinds of forces were considered to be involved in the formation process with different effects; the pressure, shear stress and surface tension. The former two are destabilising forces while the latter is a stabilising force. The pressure and surface tension are at least two orders of magnitude larger than the shear stress in microchannels.

The bubble formation process starts when the gas expands mainly in the Y- direction (please refer to Figure 4.4) and the contracting zone is gradually occupied by the gas

phase. When the gas thread reaches the opposite site of the main channel, the liquid phase is blocked almost completely; from then on the liquid phase starts to squeeze the gas thread and the collapse phase begins, a neck of the gas thread forms and the interface pushes both downstream to the exit and upstream to the gas inlet. Finally, the neck is pinched off and a bubble forms in a very short time.

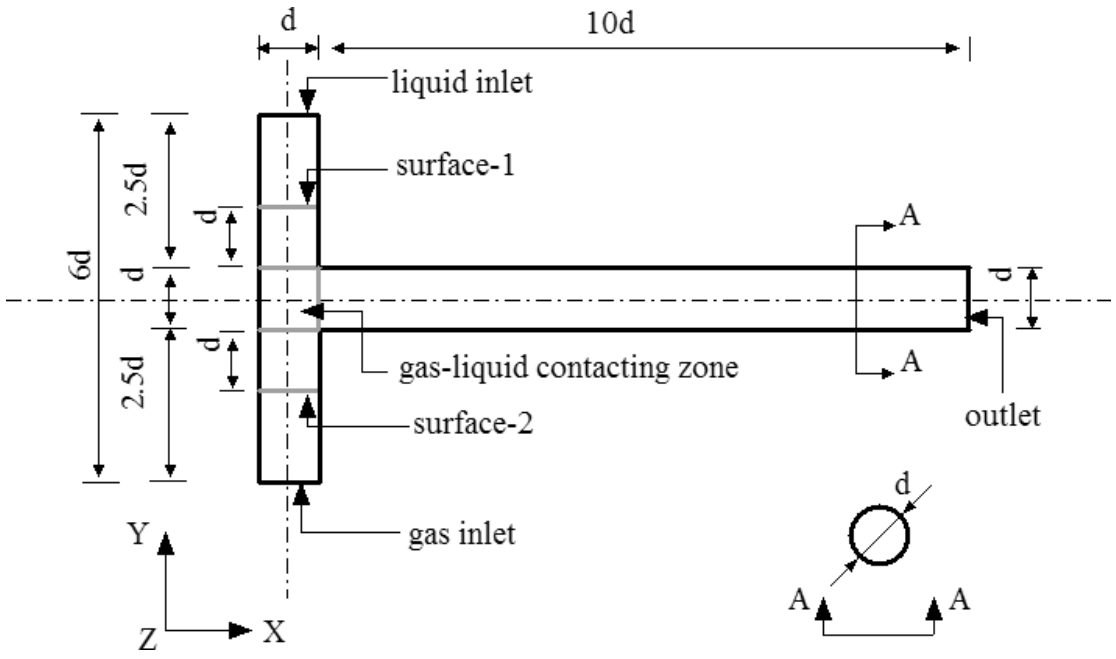

Figure 4.4. Schematic of microdevice used by Dai et al. (2009).

Gastercki et al. (2006), thought that the dynamics of break-up can be entirely controlled by the rate of the continuous fluid in the micro channel. Compared with the classical theory of capillary break-up, the collapse rate in a micro channel is at least one order of magnitude lower and Gastercki considered that the slow collapse is helpful to produce uniform bubbles and slugs. Other parameters that affect the bubble formation process are the orientation of the T-junction, the lengths of the inlet channels for the gas and liquid and the contacting zone for the two phases.

Dai et al. (2009) derived some very interesting conclusions about the bubble formation process:

- The surface tension dominates at the expansion stage.
- The pressure at the liquid inlet dominates at the collapse stage.
- The pressure at the liquid inlet is always lower than in the gas inlet in the micro channel.
- The shear stress participates in dragging the gas thread downstream for only part of the expansion stage; however, it might influence the bubble formation stage.
- The collapse rate $\frac{\Delta W_m}{\Delta t}$ increases approximately linearly and the collapse time τ_c decreases exponentially with the liquid superficial velocity as it induces a larger pressure rise in the liquid inlet and a larger squeezing action on the gas thread.
- There is no significant influence of the ratio of the liquid velocity over the gas velocity ($\frac{U_L}{U_G}$) on the bubble formation process.
- Increasing the viscosity or decreasing the surface tension accelerates the collapse process. As the liquid velocity increases, this acceleration becomes more significant.
- The effects of the 10-fold increase of viscosity and a 10-fold decrease of surface tension are similar which means that the collapse rate can be correlated with the *Ca*.

W_m was defined as the maximum distance between the gas-liquid interface and point D in the expansion stage and the minimum distance in the collapse stage (please refer to the subsequent Figure).

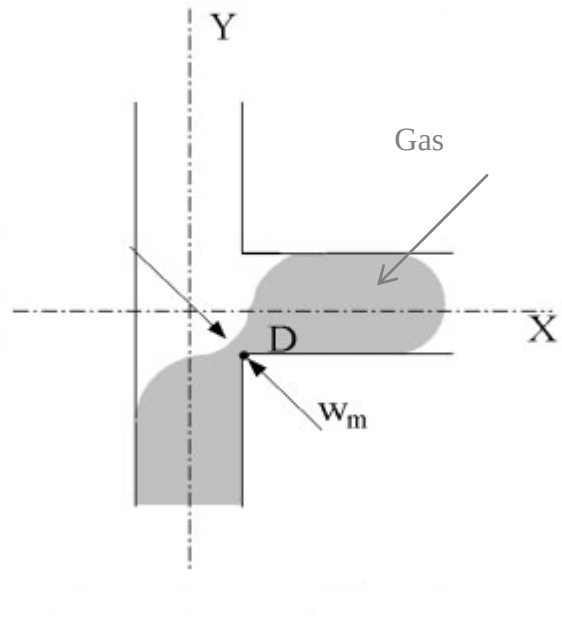

Figure 4.5. Schematic of Wm at the collapse stage in the bubble formation process, Dai et al. (2009).

In summary, out of the three stages, collapse was the most important for bubble formation and was found to be mostly influenced by the liquid superficial velocity. The rate and time of collapse can be correlated with empirical correlations including the liquid superficial velocity, the *Ca* and the *Re*.

A correlation was proposed for the collapse rate:

$$\frac{\Delta W_m}{\Delta t} = 1.24 \cdot U_L Ca_L^{0.103} \tag{4.14}$$

And the collapse time:

$$\frac{\tau_c}{\left(\frac{d}{U_L}\right)} = 0.4394 \cdot Ca_L^{-0.1197} \mathrm{Re}_L^{0.0464} \quad (4.15)$$

In the study by Fu et al. (2009) the break-up rate and time were correlated as a function of the ratio of the gas over liquid flow rates and the *Re*. The microchannel utilised was a 600 μm x 600 μm rectangular microchannel and μ-PIV (micro-particle image velocimetry) and a high speed camera were used to investigate the bubble formation and the factors affecting it. From this research effort it was derived that:

- The formation of the slug at the cross-section is dominated by the collapse stage.
- When the viscosity of the continuous phase increases, the collapse time decreases. The increase in liquid viscosity accelerates the formation of bubble by intensifying the shear stress. Therefore, higher viscosity results in shorter formation time and higher collapse rate.
- There is a sharp increase of the collapse rate when increasing the liquid flow rate. As the liquid flow rate is increased, the collapse time is decreased non-linearly.
- The measured collapse rate in the microfluidic device is smaller than the theoretical prediction based on classical capillary driven theory. This is explicable by the fact that the surface tension has no effect on the bubble formation and rather the shear stress and elongation should mostly contribute to the thread breakup in microdevices.

Empirical correlations were proposed for predicting the breakup rate and time based on several dimensionless numbers. The normalized collapse rate can be correlated by the following equation which displays a mean relative deviation of 14.31 %:

$$\frac{\left(\Delta W_m/\Delta t\right)}{U_l} = 0.27\left(\frac{Q_G}{Q_L}\right)^{-0.35} \mathrm{Re}^{-0.39} \tag{4.16}$$

A dimensionless number equal to the ratio of the collapse time t_c over the characteristic time t_l of the liquid passing through the cross-section was employed to correlate the experimental data. t_l is defined as:

$t_l = \frac{w_c}{U_L}$, where w_c is the width of the channel

(4.17)

The following correlation was obtained by linear regression with a mean relative deviation of 27.87 %:

$$\frac{t_c}{t_l} = 1.10\left(\frac{Q_G}{Q_L}\right)^{0.85} \mathrm{Re}^{0.53} \tag{4.18}$$

Where Q_L and Q_G are the liquid and gas volumetric flow rates.

These correlations could be used to predict rate and time during a bubble formation process by flow-focusing technology. Furthermore, these two expressions could be applied to predict bubble size and formation frequency.

4.7 Techniques for Measuring Bubble and Slug Sizes

The bubble and slug lengths are usually measured along the channel axis using the photographic method. Results from numerical simulations also refer to measurements along the channel axis. Only in a few papers these parameters are measured with other methods like conductivity, which makes the results difficult to compare with those obtained from the photographs (Heiswolf et al., 2001).

When conductivity or Infra Red (IR) sensors are used, those are mounted in the middle of the capillary channel allowing the discrimination of passing bubbles from passing slugs by the difference in absorption between the gas and the liquid. IR sensors have the advantage over conductivity sensors that they can efficiently detect other liquids than water. The signal from the sensors is usually then processed by a binary gate (1=bubble and 0=slug). The slug and bubble velocities can be calculated from cross correlation of the binary signals and finally, using the calculated velocities the length of the slug and the bubble can be determined (Kreutzer, 2005b).

A variety of methods which have been used in the literature to conduct measurements of bubble and slug lengths:

- Mantle et al. (2002) measured the slug lengths using MRI (Magnetic Resonance Imaging) and found a wide range of size distributions. MRI has also been used to measure film thickness.
- Heiszwolf (2001) and Kreutzer (2005c) used conductivity to measure bubble and slug lengths. They found that the slug length was highly dependent on

the inlet geometry. There was a considerable variation of gas bubbles and liquid slugs' sizes even for the same experimental set-up. A variation of 30 % was quite common. Hence, they proposed to measure the pressure drop and then compute the slug lengths for short slugs.

- Thulasidas (1995 and 1999) measured bubble and slug sizes using the flow visualisation method. The same method was used by Vandu et al. (2004), Laborie et al. (1999), Haverkamp (2006) and Chen et al. (2002).
- Kreutzer (2005a) also used IR to measure bubble and slug lengths. Two IR sensors mounted in the middle of the capillary channel allowed the discrimination of passing bubbles from passing slugs by the difference in IR absorption between the gas and the liquid.
- Xia et al. (2009) used U-type optical probes to measure the slug lengths. The signals were recorded and analysed by PC.
- Fu et al. (2009) used μ-PIV (micro-particle image velocimetry) and a high speed camera to measure bubble and slug sizes.

4.8 Factors Affecting Bubble and Slug Sizes

As discussed in preceding sections of this Chapter, mass transfer and pressure drop in Taylor flow depend on the bubble and slug sizes. In recent years, various studies have focused on the hydrodynamics of Taylor flow with significant effort dedicated on the aspect of bubble and slug sizes.

Laborie at al. (1999) investigated experimentally Taylor flow in capillaries with 1-4 mm diameter. Well established Taylor flow was observed only for small capillaries while bubble coalescence was seen in larger capillaries. With regards to the various factors affecting bubble and slug lengths, it was concluded that:

- The surface tension was found to affect the bubble length but not the liquid slug length. Much higher bubble lengths were observed when the surface tension of the liquid used increased significantly.
- The liquid viscosity was found to have a small effect on the average bubble and slug lengths. For given gas and liquid superficial velocities a slight decrease of bubble and liquid slug length was observed when the viscosity of the liquid increased (also in the study be Qian & Lawal, 2006).
- The diameter of the capillary was found to have an effect on the bubble length. For the same liquid and gas superficial velocities, bubble length decreased when the diameter increased. Indeed, when the inner diameter increased three-fold the bubble length decreased 20 times. This was also verified for the mean liquid slug length.

- The diameter of the capillary has an effect on the observed flow. For the smaller capillaries of 1 mm and 2 mm diameter the flow was fully established, gas bubbles were fully formed, no coalescence was observed in the tube and the liquid slugs contained no bubbles. For the largest capillaries of 3 mm and 4 mm diameter, the bubbles were coalescing along the pipe and it was difficult to distinguish between gas and liquid slugs because the latter were aerated.
- The average bubble length increases when the gas superficial velocity increases for a given liquid superficial velocity and the relationship was found to be linear (Also found in the study by Kumar et al., 2007, and Qian & Lawal, 2006). Moreover, the higher the gas proportion in the flow, the longer are the gas bubbles. This was also concluded in the current study presented in this Thesis.
- On the contrary, when the gas velocity increases, the slug length decreases. This is in agreement with the results from the current research in this Thesis.
- The superficial liquid velocity does not affect the bubble and liquid slug lengths. Conversely, Qian & Lawal (2006) and Kumar et al. (2007) found that when the liquid velocity rises, slug size increases and bubble size decreases. This is in-line with findings from this work too.

With regards to the bubble frequency, it was inferred in the study of Laborie that this depends on the fluid properties, the gas and liquid velocities and the capillary inner diameter. When the capillary diameter increases the bubbles become smaller but more frequent. When the diameter increased three times, the bubble frequency

increased 10-fold. For a given *Re*, the higher the viscosity, the higher is the frequency. Conversely, surface tension did not seem to have any influence on the bubble frequency.

The effect of inlet configuration on bubble and slug size was investigated by Amador et al., 2004. In this study, T- and Y- inlet configurations with different inlet channel dimensions and fluid joining angles were used. Bubble pairing was observed at the inlet and when small Taylor bubbles formed there was bubble coalescence in the main channel. From this research work it was concluded that:

- The ratio of gas to liquid superficial velocity is the factor which determines the bubble length.
- The size of the gas inlet was found to affect the bubble size.
- The size of the liquid inlet did not have an affect the bubble size.
- The joining angle of the two liquids had only a slight effect on the bubble size.

Bercic & Pintar (1997), measured the oxygen absorption in water by means of oxygen probes and also measured the liquid slug and bubble lengths using platinum probes inside one of the monolith channels. They found that liquid slug length remains more or less constant when liquid hold-up decreases. The increase of the gas velocity does not seem to affect the slug length substantially unlike the findings presented in the current Thesis. They found that the length of the liquid slugs influences mass transport much more than the length of bubbles. They developed an

equation for bubble and slug size derived from a single capillary but may also be applied to monoliths.

The inlet geometry strongly affects the slug length as it was concluded by Qian & Laval in 2006. Non-uniformity of the slugs was observed in their experiments and was also found from simulation results. The researchers argued that this is due to time-dependent toroidal vortices generated in the mixing section which subsequently propagate throughout the length of the channel. The non-uniformity increases when the gas or liquid velocity increases. This was also observed during the experiments of the present study detailed in this Thesis – in general the increase of gas velocity increased the flow non-uniformity. However, it was also found that flow was non-uniform below a threshold value of the gas velocity. Therefore, in order to achieve uniformity, the ratio of the gas over liquid velocity should be within a certain range. Additionally, the findings of the current study support the conclusion of Qian & Laval that the inlet geometry affect bubble and slug sizes.

Furthermore, Qian & Laval found that the degree of pre-mixing has a strong effect on slug length and the higher the degree of pre-mixing the shorter the slug length. This is because the smaller mixing zone generates larger velocity, hence bigger toroidal vortices are produced in the mixing zone, making it easier for the slug to detach. The same conclusion was made in the present study; shorter slugs were observed using the static mixing tee which incorporates a micro-frit to facilitate micro-mixing.

Qian & Laval (2006) studied different inlet orientations of the gas and liquid streams into the tee-junction:

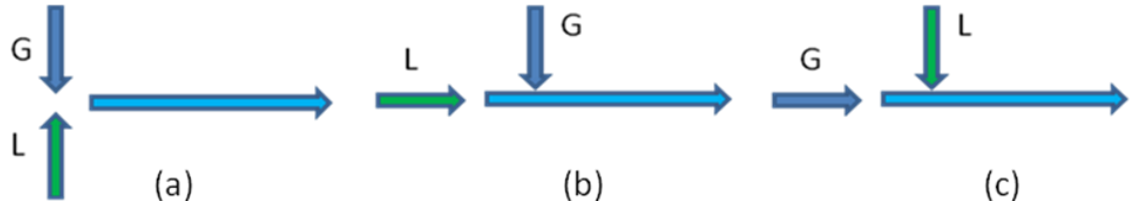

Figure 4 6. Different inlet configurations tested by Qian & Lawal, 2006.

Case (c) was found to provide longer slugs because this case has smoother stream at the mixing section and the slug is more difficult to detach. In the study by Qian & Laval it was concluded that scheme (c) should be avoided and the schemes (a) and (b) are preferable. Contrary to the conclusion from Qian & Laval, case (c) was proved to be beneficial as it improved flow homogeneity according to the research presented in this Thesis.

Regarding the fluid properties, no effect of the viscosity on the slug lengths was observed by Qian & Lawal but the slug length increases with an increase of the surface tension. It was mentioned that when the surface tension is very small it is difficult to create slug flow. The surface tension effect is much stronger than the viscous effect on the flow.

It was observed that the size of the channel affects the uniformity of the flow; the 1 mm and sub-millimetre channels produced more uniform flow than the 2 mm and 3 mm channels in the experiments of Qian & Lawal (2006).

The dimensionless slug length depends mainly on the liquid phase hold-up and the *Ca* and *Re* numbers have small affect. That is why the dimensionless slug length falls within a narrow range even for wide operating conditions. The gravity does not have much effect in microchannels, so the Froude number can be ignored.

Yue et al. (2007) performed experiments of physical absorption of carbon dioxide in water in a rectangular microchannel. Photographs of the two-phase flow were obtained and analysed and some interesting conclusions were derived. A stable Taylor flow was observed when the gas superficial velocity was at its lowest value. As the gas superficial velocity increased while the liquid superficial velocity remained constant, the length of the bubbles increased while the length of the liquid slugs shortened. After a certain gas superficial velocity, the gas bubbles approached each other and the slug length was not uniform. The very long bubbles sometimes break to smaller parts. This phenomenon was also observed in the experiments demonstrated in this Thesis. In detail, it was observed that Taylor flow was stable within a range of gas superficial velocities as liquid velocity remained constant. When the gas velocity fell outside these limits, the flow became bubble train flow consisting of long bubbles broken in several parts whilst the slug length was not uniform as slugs in-between very long bubbles were shorter.

Kumar et al. (2007) in a study focused on Taylor flow in curved microchannels of various curvature ratios observed that the curvature ratio affects the slug length. The higher the curvature ratio, the larger is the length of the slug. This is due to the lower centrifuge force at higher curvature ratio. When the curvature ratio becomes lower, the centrifuge force becomes stronger and slug length reduces. In the same research effort it was concluded that the slug length is determined by the phase hold-up with a slight effect of *De* (Dean number= $\mathrm{Re}\sqrt{1/\lambda}$) and *Ca*. It was further observed that the effects of liquid viscosity are more dominant in curved than in straight micro channels. The effects of surface tension and wall adhesion moderately affect the slug length. In many microdevices the use of curved microchannels is very common due to the high heat and mass transfer rates, narrower residence time distributions and compactness. The enhanced performance in curved tubes is due to secondary flows called Dean vortices. Secondary flows are generated when fluid flows across the curved channel due to unbalanced centrifugal forces.

According to Haverkamp et al. (2006) the most influential parameter for bubble formation is the ratio of gas flow rate to total flow rate:

$$U_r = \frac{U_G}{U_G + U_L} \tag{4.19}$$

Initially increasing U_r by increasing U_G when increasing the amount of gas in the flow, this leads to higher probability of bubbles coalescing and colliding to yield a broader bubble size distribution. An increase of the liquid flow rate yields a smaller bubble size distribution as one can expect the higher stress between gas and liquid

will result in a decrease of bubble coalescence. Therefore, an increase of the liquid flow rate while the gas flow rate is kept constant narrows the bubble size distribution. Additionally, a rise of the shear stress leads to smaller bubbles. The mean bubble length is seen to increase with increasing gas velocity despite the spread in the data. The bubble size did not seem to be affected to a major extent by the liquid flow rate. However, the authors mentioned that further measurements were needed to confirm this observation. The same conclusion was derived from the current study. An increase in gas velocity yielded a broader bubble size distribution.

Haverkamp et al. (2006) also concluded that the mechanism of bubble size formation affects the bubble size distribution. In the same study, the absolute geometry and the channel aspect ratio were found to affect the formation of the different flow regimes. Furthermore, initial broad size distributions were improved by new mixer designs. In particular, smooth mixer design gave narrower size distribution but larger bubbles as compared to the T-mixer.

Fu et al. (2009) reported that unlike in conventional devices, bubbles or droplets, rarely coalesce with each other in microfluidic systems. In flow-focusing devices, the bubble size depends mainly on the ratio of the gas flow rate to the liquid flow rate and is independent of the *Ca* for both low and high *Re* numbers.

Tan et al. (2009) observed that the bubble length increased when the gas flow rate increased and decreased when the liquid flow rate increased. Furthermore, the gas

bubble length decreased when the liquid viscosity increased. Conversely, the gas bubble length increased when the surface tension of the liquid increased.

Fries & von Rohr (2009) discussed the influence of the gas inlet on gas-liquid flow characteristics in rectangular microchannels. Varying the ratio of the gas inlet width compared to the main channel width as well as changing the angle of the gas inlet showed different characteristics of the gas-liquid flow. While the bubble-slug size ratio is not affected by the geometry at a given volumetric flow ratio, the lengths of the gas bubble as well as of the liquid slug and thus the pressure drop change with the geometry. They observed variations of the unit cell length for a given flow ratio of a factor 4. If the gas phase is injected in the flow direction of the liquid phase, gas bubbles are shorter that in the opposite case. This observation, can be explained using the interfacial pressure at the breakup point. Decreasing the gas inlet width at a constant main channel width also results in decreasing gas bubble lengths. If the gas inlet has a smaller width than the main channel, the liquid slug length is shorter as compared to a gas inlet with the same width as the main channel.

The diameter of the capillary tube also affects the flow as well as the bubble and slug lengths. This was one of the conclusions derived from the study of Laborie et al. (1999) focused on characterisation and understanding of 2-phase flow inside capillaries in the context of a wider study dealing with improvement of drinking water treatment. For the smaller diameter (1 and 2 mm), the flow was well established, no coalescence of the bubbles was observed and no bubbles inside the liquid slugs. For the larger capillaries (3 and 4 mm diameter) and particularly for the

4 mm capillary, there was coalescence of the bubble along the tube, difficult to distinguish between the liquid slugs and the bubbles because the slugs were aerated.

The conclusions from various studies using different T configurations under a plethora of operating conditions are summarised in the next Table:

Condition	Result/Conclusion	Reference
U_G ↑	• L_B ↑ • L_S ↓	Laborie et al. (1999) Kumar et al. (2007) Qian & Laval (2006) Tan et al. (2009)
U_L ↑	• L_B ↓ • L_S ↑	Laborie et al. (1999) Qian & Laval (2006) Kumar et al. (2007)
ratio of gas velocity over liquid velocity ↑	• L_B ↑	Amador et al. (2004) Fu et al. (2009)
ε_L ↑	Affects strongly L_S, L_B ↑	Kumar et al. (2007)
Curvature ratio ↑	L_S ↑	Kumar et al. (2007)
Size of the inlet, configuration, t-orientation	Affects strongly L_S, L_B	Amador et al (2004) Haverkamp et al. (2006) Fries & von Rohr (2009)
Channel diameter d ↑	Affects strongly L_S, L_B ↓	Laborie et al. (1999)
Surface tension and wall surface adhension (wetting or non-wetting liquid) ↑	Affects moderately L_B, L_S ↑ The effect on L_S is less pronounced than that on L_B.	Laborie et al. (1999) Qian & Lawal (2006)
Liquid viscosity ↑	• L_S for curved microchannels. ↓ • L_B ↓ For straight microchannels, the effect is small. The liquid viscosity affects mostly the gas bubble size while the effect on the liquid slug is limited.	Laborie et al. (1999) Tan et al. (2009)
Ca, *Re*	The effect on L_S is small	Kumar et al. (2007)

Condition - *Continued …*	Result/Conclusion	Reference
Liquid density	• $L_S \approx$ The effect on L_S is negligible	Qian & Lawal (2006)

Table 4.6. Factors affecting slug and bubble lengths.

4.9 Stability of Taylor flow

Obtaining uniform stable Taylor flow has been marked as a critical requirement for the application of monoliths (Dudukovic et al., 2002).

According to Kreutzer (2005b), Taylor flow can exhibit highly undesired dynamic oscillations that may grow to significant instability. This behaviour can be predicted if the gradients of pressure drop versus gas and liquid flowrates are accurately known and stability criteria for monoliths can be formulated.

Non-uniformity of slug flow (sometimes mentioned as unsteady slug flow) was found by various researchers. For instance, the stability of the Taylor flow was discussed by Grolman et al. (1996) and by Reinecke et al. (1997) and they both arrived at similar conclusions. If the pressure drop in a channel is dominated by friction, an increase in flow rate will create a pressure drop. As a result, the dynamic response to the perturbation of the velocity will dampen out to the equilibrium situation. If other contributions to the pressure drop such as hydrodynamic contributions become important, an increase in flow rate can cause a decrease in

pressure drop. Then the liquid will continue to accelerate upon a slight increase of the superficial velocity and the flow can become unstable and behaviours such as oscillating behaviour are observed. The condition of stability is as follows:

$$\frac{\partial(\Delta P/L)}{\partial u_F} < 0 \qquad (4.20)$$

F: Gas or Liquid which holds for both upflow and downflow. For all upflow conditions, Taylor flow is unstable.

Kumar et al. in 2007 performed a hydrodynamic study on slug flow in curved microreactors with curvature ratios 5-30. Non-uniformity of the slugs was observed for all the geometries considered. The non-uniformity in the slug formation was observed more at low curvature ratios as compared to the higher curvature ratios. The slug length is not uniform because of the Dean vortices which form in the mixing section when the two streams meet and then propagate along the channel length. The bubble and liquid slug is relatively stable, it rarely breaks or coalesces unless it is very short.

Yue et al. (2008) studied Taylor flow in three Y-type rectangular microchannels of 667, 400 and 200 μm. Two-phase flow patterns in these microchannels were recorded by means of a high-speed photography system. During this study, two sub-regimes were found in slug flow:

- Taylor flow emerged when the gas superficial velocity was relatively small. At rather low gas and liquid velocities, *Re* and *Ca* numbers were so small that the interfacial tension was large enough to maintain the hemispherical shapes of

Taylor bubble caps. At high gas and liquid velocities, both *Ca* and *Re* increased significantly and the effect of inertia became to play an important role. As a result the nose of the bubble became elongated and the rear part turned more flattened. Contrary to the phenomenon observed in large pipes, smaller bubbles were seldom seen in liquid slugs.

- Unstable Taylor Flow emerged when the gas velocity was relatively high. Under this circumstance, two adjacent bubbles were so close to each other that the gas-liquid flow exhibited significant randomness. The rupture of an extremely long bubble was seen in some occasions, while sometimes a specific flow pattern called ***bubble-train slug flow*** appeared.

The authors of the aforementioned study argued that the two phase flow pattern at the entrance may gradually evolve along the micro channel due to the interaction between two competitive factors. On one hand, the pressure drop along the microchannel leads to a decline in gas density from the entrance until the channel outlet. On the other hand, mass transfer process and absorption of the gas into the liquid leads to a decrease of the gas mass flow rate along the channel. Consequently, it is expected, that under some conditions, there will be relatively big change in the gas velocity along the microchannel so that different flow patterns can exist at the entrance and in the middle section of the micro channel. For instance in Taylor flow, the gas expansion due to the pressure drop will increase the length of the Taylor bubble while the gas absorption will cause a decrease in Taylor bubble length.

For the experiments conducted with the smaller square microchannels, 200 and 400 μm, an axial increase of the Taylor bubble was observed. The authors observed that the compressibility effect was more significant in this case but more future work was necessary to clarify this because mass transfer data were not available at the time. Higher pressure drop was encountered in the smaller microchannel of 200 μm.

For the biggest micro channel with 667 μm size, the Taylor bubble was always larger at the entrance than in the middle section. This was attributed to the dominance of mass transfer effect. The pressure drop was relatively small in the order of several kPa as compared to the absolute pressure measured in the micro channel, while the amount of gas absorption was significant.

Finally Yue et al. (2008) concluded that the transition from Taylor flow to unstable slug flow can be represented by the following correlation which compares favourably with the experimental data obtained for microchannels with diameters 667, 400 and 200 μm:

$$We_G = 0.0172 We_L^{0.25} \tag{4.21}$$

Chen et al. (2002) performed experiments with the system N_2-water in a glass microchannel of 1 mm and 1.5 mm diameter. The two-phase flow patterns, bubble speed and void fraction were observed and analysed through visualisation. Bubble train flow, slug flow, slug-annular and churn flow were observed. They mentioned that the bubble train flow pattern is unique in micro channels. For this flow pattern, typically 2-4 bubbles and possibly up to 10 or more are in contact like a train with a

clear interface or 'membrane' between the connecting bubbles. The number of bubbles is random, irregular manner indicating its inherent turbulent nature. Fukano and Kariyasaki (1993) as well as Mishima & Hibiki (1996) have also reported the presence of such a bubble train flow in their experiments but did not distinguish it from the regular slug flow. This bubble-train flow appears also in large channels under micro-gravity conditions (Zhao & Rezkallah, 1993). They named it as frothy slug flow. The existence of a "membrane" between two-fast moving bubbles is characteristic of this flow pattern. Though the inertial force of the second bubble is large enough to overcome surface tension and break through the liquid to coalesce together, it is still small to rupture the interface. Chen argued that when the transition from slug to bubble train flow occurs the Weber number based on the bubble inertial force is in the order of one:

$$We = \frac{\rho_G d u_B^2}{\sigma} \approx 1 \tag{4.22}$$

This means that the bubble inertial force is as high as the surface tension. The features of the bubble-train slug flow in micro-channels under earth gravity and in large channels under micro-gravity conditions are not the same. However, in both situations, the gravity and so the buoyancy force, is negligibly small compared to the surface tension force. Zhao & Rezkallah (1993) also adopted *We=1* as the criterion for the flow transition between slug flow and bubble train flow. However, they supported that the randomness of the bubble number in a train deserves further investigation.

The number of bubbles in the train decrease with an increase in liquid superficial velocity. Large liquid superficial velocities seem to hinder the formation of bubble trains. It should be mentioned that bubble train flow was also observed in the research presented in the current Thesis.

Xia et al. (2009) studied upward vertical slug flow in a 10 m Perspex channel with 24 mm ID. U-type optical probes were used to measure the slug length. The signals were recorded and analysed by the PC. Xia and co-workers found from their experimental study that the liquid slug length changes during the flow process and they identified a minimum stable slug length L_{stab} equal to *14d* (*d* is the ID of the channel). In detail, they concluded the following:

- The increase or decrease of the slug length as the flow moves upwards depends on the velocities of the leading Taylor bubble and the trailing Taylor bubble. If the leading Taylor bubble moves faster than the trailing one, the liquid slug between them increases and vice versa. The length of liquid slugs behind these expanding as mentioned earlier, tends to diminish and as a result shorter slugs eventually disappear and the related liquid goes into the slug behind while the two bubbles coalesce.
- The liquid slugs or bubbles coalesce near the pipe entrance and shorter slugs gradually disappear far away from the entrance. Eventually, the liquid slugs shorter than the minimum stable slug length become very scarce as the merging process is very slow when the slugs are close or exceed $L_{stab.}$

- It was concluded that the average slug length, standard deviation, maximum length increase moving away from the inlet. This conclusion is in line with the findings of the current research presented in this Thesis.

Tan et al. (2009) studied the effect of the intersection angle between the gas and the liquid phase ranging between 30^{o} and 150^{o} in T-junction micro fluidic devices. The authors found that when the channels near the intersections were not narrower than the main channels, the bubbles were non-uniform because of the instability of the pressure at the intersection. In addition, when surfactant was not added to the liquid consistent Taylor flow was achieved only sporadically. The surfactant used helped to decrease the surface tension. Thus, with these modifications, ordered gas flow with polydispersity index values of less than 2 % was achieved. Prior research from the same group indicated that the size of the dispersed phase is independent of the surfactant concentration once the surfactant concentration is higher than the critical micelle concentration.

Other researchers who observed Taylor flow instability are as follows:

- Haverkamp et al. (2006) studying the hydrodynamics and bubble formation in micro bubble columns with single and multiple channels.
- Heiszwolf et al. (2001) with their study on gas-liquid mass transfer of Taylor flow in monoliths using the air-water system. The non-uniformity of the bubbles is exhibited by the photographs and the data presented in the study. They also observed that the standard deviation of the average liquid slug length increases as the liquid hold-up increased.

- Qian & Lawal (2006) found that for certain liquid and gas velocities, a distribution of bubble sizes was found and this non-uniformity was more pronounced at increased velocities although no bubble coalescence was observed. Coalesence was observed in the main channel when bubbles were small.
- Yue et al. (2008) observed Taylor-flow non-uniformity during a study on hydrodynamics and mass transfer characteristics in gas-liquid flow through a rectangular microchannel. Photographs included in this reference showed non-homogeneity of slugs and bubbles under certain operating conditions (U_G =0.92 m/s U_L =0.5 m/s) and (U_G =2.14 m/s and U_L =1 m/s).
- Laborie et al. (1999) when conducted the study of hydrodynamics of gas-liquid flow in glass capillaries of 1, 2, 3 and 4 mm inner diameter. They measured a dispersion of gas bubble lengths in a particular liquid for given values of gas and liquid superficial velocities and capillary diameter. For each condition of gas and liquid velocities, 100 bubbles and slugs were filmed and measured. From the hundred values of L_B measured, and arithmetic mean value $\langle L_B \rangle$ and a standard deviation δ_{st} were calculated. The relative error was then found from:

$$\varepsilon_r = \frac{\Delta}{\langle L_B \rangle} \text{ and } \Delta = \frac{t_a \delta_{st}}{\sqrt{n_m}} \tag{4.23}$$

where n_m is the number of measurements and t_α is the t-statistic for a probability α. Values of the relative error ranged from 0.4%-27.0% and 1.5%-18% for the slugs and bubbles sizes respectively, depending on the operating conditions. The same approach for the calculation of the dispersion

of the bubble and slug sizes, the standard deviations and relative errors was followed in the research in the present Thesis.

- Grolman et al. (1996) studied the instabilities in Taylor flow in down flow and defined the area of unstable flow.
- Mantle et al. (2002) revealed instabilities in Taylor flow with MRI tomography and obtained bubble size and bubble velocity distributions.
- Lebens et al. (1997) reported instabilities in Taylor up flow in a commercial monolith under certain operating conditions.
- In the study by Kreutzer (2005a) it was mentioned that when the liquid velocity is very low or very high, the bubbles started to coalesce straight away upon entering the main channel. Roughly stable slug and bubble sizes were found when:

$$0.25 < \frac{U_L}{U_G} < 2 \quad \text{or} \quad 0.5 < \frac{U_G}{U_L} < 4 \tag{4.24}$$

- Liu et al. (2005) observed that homogeneous flow occurs generally when

$$\frac{U_G}{U_G + U_L} < 0.5 \tag{4.25}$$

which is characterised by a slip ratio close to unity. When the slip ratio was higher than one, the flow was found to deviate from homogeneity.

- Bubble pairing was observed at the inlet and when small Taylor bubbles formed there was bubble coalescence in the main channel, (Amador et al., 2004).

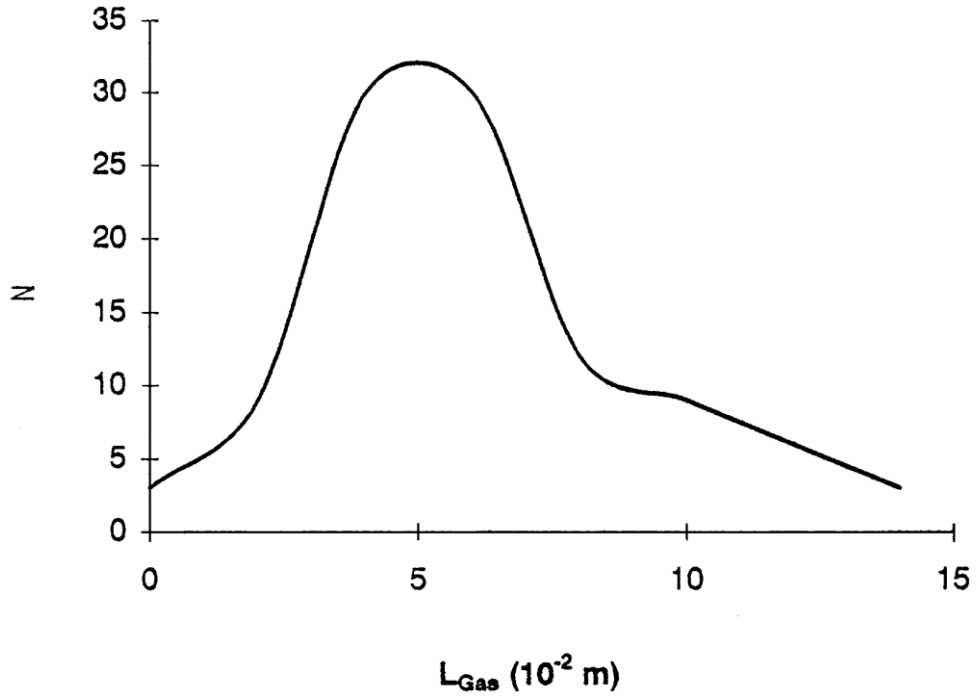

Figure 4 7. Dispersion of length of gas bubbles (d=1 10^{-3} m, liquid: water at 15° C, U_L=0.48 m s^{-1} and U_G=0.18 m s^{-1}). N is the number of gas bubbles corresponding to a given value of L_B. Laborie et al. (1999).

4.10 Bubble and Slug Sizes - Correlations

Bubble and slug lengths play a very important role in mass transfer and back mixing in Taylor flow and few researchers have conducted studies of bubble and slug lengths in microchannels.

Laborie et al. in a study published in 1999, measured bubble and slug length created in vertical gas capillaries with 1, 2, 3 and 4 mm diameter. The correlations they proposed are the following, firstly for the bubble length:

$$\frac{L_B}{d} = 0.0878 \frac{[\mathrm{Re}(U_b)]^{0.63}}{Eo^{1.26}} \tag{4.26}$$

from where is derived that L_B is proportional to $d^{-0.89}$ (*Eö* and *Re* are proportional to d^2 and d respectively). As for the slug length:

$$\frac{L_S}{d} = 3451 \frac{[\mathrm{Re}(U_G)]^{-1.27}}{Eo^{1.27}} \tag{4.27}$$

from where is derived that L_S is proportional to $d^{-2.81}$.

It follows from these correlations that L_B is inversely proportional to d while L_S is inversely proportional to the third power of d.

Qian & Lawal in 2006, performed numerical simulation of the Taylor flow in microchannels with 0.25 to 1 mm diameter, using the commercial CFD package FLUENT (release 6.1.22.2003) and derived correlations for the bubble and slug lengths. In this package, the volume of fluid (VOF) model was used to simulate the two-phase fluid-fluid flows. The correlations, for which the researchers concluded that they are not applicable to larger channels of 2-3 mm diameter due to more scatter of the simulation data for capillaries of larger diameters versus the sub-millimetre channels, are shown below:

$$\frac{(L_B + L_S)}{d} = 1.637 \varepsilon_G^{-0.893} (1 - \varepsilon_G)^{-1.05} \mathrm{Re}^{-0.075} Ca^{-0.0687} \tag{4.28}$$

$$\frac{L_B}{d} = 1.637 \varepsilon_G^{0.107} (1 - \varepsilon_G)^{-1.05} \mathrm{Re}^{-0.075} Ca^{-0.0687} \tag{4.29}$$

$$\frac{L_S}{d} = 1.637\varepsilon_G^{-0.893}\left(1-\varepsilon_G\right)^{-0.05}\mathrm{Re}^{-0.075}Ca^{-0.0687} \tag{4.30}$$

The correlations (4.28-30) show that the determinant factor of the bubble and slug lengths is the phase hold-up while the *Cα* and Re have little effect. In the study, the two fluids were either brought together in a T-junction or were premixed. The T-orientation, the size of the inlet channels as well as the size of the main channel were found to affect bubble and slug lengths. Small mixing zones and the higher the degree of pre-mixing produced smaller bubble and slug sizes. For certain liquid and gas velocities, a distribution of bubble sizes was found and this non-uniformity was more pronounced at increased velocities although no bubble coalescence was observed.

This form of correlation like the one developed by Qian & Lawal can be justified by the 'switching mechanism' for a bubble or drop break up, proposed by Pohorecki & Kula (2008). This mechanism is based on the simple assumption that each phase (gas or liquid) flows into the capillary passage and therefore fills a bubble or a slug until the other phase blocks completely the passage. In order to block the passage, the second phase element must grow at least until its radius is equal to the radius of the channel.

In another study, Sobieszuk et al. (2010) used a high speed camera system that allowed to record high resolution frames of the flow. An automatic computer system was developed for the bubble and slug measurements. The bubble and slug sizes

were measured along the channel axis as it is customary in the literature and for every set of experimental conditions about 100 bubbles and slug lengths were measured. The experimental results obtained disagreed with the correlation of Laborie et al. (1999) but showed good agreement with that proposed by Qian & Lawal (2006). Sobieszuk et al. proposed a correlation of the form developed by Qian & Lawal but with new corrected values of the pre-exponential constant and the exponents as it is shown below:

$$\frac{L_B}{d} = 1.3\varepsilon_G^{0.073}\left(1-\varepsilon_G\right)^{-1.01}\mathrm{Re}^{-0.098}Ca^{-0.108} \tag{4.31}$$

This correlation was compiled by using the least squares method separately for three different sets of experimental data, subsequently developing three different correlation-one for each experimental set and finally taking the average values of the constants from the these correlations. The average deviation of the correlation for all microchannels and systems studied was 17.2%.

It was noticed that the exponents of the *Re* and *Ca* numbers were very close. This suggested that the Weber number can be used instead as:

$$We = \mathrm{Re}\cdot Ca \tag{4.32}$$

Taking this into account and truncating the values of the constants, the Sobieszuk correlation was simplified to the form:

$$\frac{L_B}{d} = 1.3\varepsilon_G^{0.07}\left(1-\varepsilon_G\right)^{-1.01}We^{-0.1} \tag{4.33}$$

Its average deviation was found to be 16.8% for the all microchannels and systems studied.

Tan et al. (2009) considered the equilibrium between the shear force of the continuous flow and the interfacial tension, and also the influence of the two-phase flow ratio on the shape of the interface, and proposed that the plug length could be expressed as:

$$\frac{L}{w_c} = K\left(\frac{Q_d}{Q_c}\right)^{\alpha} Ca^{\beta} \tag{4.34}$$

Where L is the dispersed phase plug length, Q_d, Q_c are the volumetric flow rates of the dispersed and continuous phases respectively.

Linear regression was used to determine the parameters K, α and β:

$$\frac{L}{w_c} = \frac{1}{2}\left(\frac{Q_G}{Q_L}\right)^{1/2} Ca^{-1/5} \tag{4.35}$$

and the capillary number is $Ca = \frac{U_L \mu}{\gamma}$ (4.36)

where U_L is the velocity of the liquid phase in the main straight channel.

It was found from these experiments that the entrance channel angle makes the shape of the interface and rupturing time different. When the intersection angle between the two flows is θ, the gas bubble length can be correlated as:

$$\frac{L}{w_c} = k\left(\frac{Q_G}{Q_L \sin\theta} + \lambda \cot\theta\right)^{\alpha} Ca^{\beta} \tag{4.37}$$

A linear regression was used to evaluate the λ for θ=60° and 120°. It was determined as λ=0.4.

Hence, the gas bubble formed in a T-junction microfluidic device with angle θ is predicted as follows:

$$\frac{L_B}{w_c} = \frac{1}{2}\left(\frac{Q_G}{Q_L \sin\theta} + \frac{2}{5}\cot\theta\right)^{1/2} Ca^{-1/5} \tag{4.38}$$

A good prediction was provided for intersecting angles of θ=30° and 150°.

Fries & von Rohr (2009) investigated the parameters channel width w_c, the ratio γ of the width of the main channel w to the width of the gas inlet, and the inlet angle β. This study demonstrated that enhanced mass transfer within the liquid slugs of short length can be obtained by injecting the gas phase in the flow direction of the main channel and bulding a gas inlet with a smaller channel width than the one of the main channel. It should be mentioned that injecting the gas phase in the flow direction was also used in the present study as it was found to be the best tee orientation. In order to predict the gas bubble length, Fries & von Rohr modified the equation below:

$$\frac{L_B}{w_c} = 1 + \alpha \frac{Q_G}{Q_L} \tag{4.39}$$

which was developed by Garstecki and co-workers in 2006. Based on literature, α is assumed to be close to one. Since α strongly depends on the inlet geometry, the researchers found a correlation to fit this geometrical value:

$$\alpha = 17.2131\gamma^{-1}\beta^{-0.5} \tag{4.40}$$

The authors proposed the following correlation:

$$\frac{L_S}{w} = k \cdot l \cdot n\left[\left(\frac{\mathrm{Re}}{Ca}\right)^{0.33} \frac{\varepsilon_L}{\gamma^l \beta^m}\right] + n \tag{4.41}$$

$k = 0.369$

$l = 2.5$

$m = 1$

$n = 3.15$

The following Table summarizes the correlations found in the literature for the prediction of bubble and slug lengths:

Correlation for bubble and slug length	Range	Type of microchannel used	Reference	Type of study
○ $\frac{L_B}{d} = 0.0878\frac{[\mathrm{Re}(U_b)]^{0.63}}{Eo^{1.26}}$ ○ $\mathrm{Re}(U_b) = \frac{U_s \rho_L d}{\mu_L}$ ○ $E\ddot{o} = \frac{(\rho_L - \rho_G) d^2 g}{\sigma}$ ○ $\frac{L_S}{d} = 3451\frac{[\mathrm{Re}(U_G)]^{-1.27}}{Eo^{1.27}}$ ○ $\mathrm{Re}(U_G) = \frac{U_G \rho_L d}{\mu_L}$ ○ U_G is the superficial gas velocity ○ U_b is the bubble velocity	55<Re<2000 0.13<Eö<5 1.5 10-3<Cα<0.1	Vertical glass capillaries of 1, 2, 3, 4 mm diameter Applicable for circular capillaries	Laborie et al. (1999)	Experimental Well established Taylor flow was found only for small capillaries. Bubble coalescence was observed in larger capillaries.

Correlation for bubble and slug length –*Continued*…	Range	Type of microchannel used	Reference	Type of study
○ $\frac{L_B}{d}=1.637\varepsilon_G^{0.107}(1-\varepsilon_G)^{-1.05}\mathrm{Re}^{-0.075}Ca^{-0.0687}$ ○ $\frac{L_S}{d}=1.637\varepsilon_G^{-0.893}(1-\varepsilon_G)^{-0.05}\mathrm{Re}^{-0.075}Ca^{-0.0687}$ ○ $\frac{(L_B+L_S)}{d}=1.637\varepsilon_G^{-0.893}(1-\varepsilon_G)^{-1.05}\mathrm{Re}^{-0.075}Ca^{-0.0687}$ ○ $\mathrm{Re}=\frac{\rho_L U_m d}{\mu_L}$ ○ $Ca=\frac{\mu_L U_m}{\sigma}$ ○ $U_m=U_G+U_L$ ○ $\varepsilon_G \sim \frac{U_G}{U_m}$ ○ $\varepsilon_L \sim \frac{U_L}{U_m}$	0.01 m s^{-1}< U_G <0.25 m s^{-1} 0.01 m s^{-1}< U_L <0.25 m s^{-1} 0.09< ε_G <0.91 15<Re<1500 0.000278<*Cα*<0.01	0.25-1mm diameter. Not applicable for channels with diameters of 2mm and above	Qian & Lawal (2006)	Theoretical (CFD simulation using FLUENT)
$\frac{L_B}{d}=1.3\varepsilon_G^{0.073}(1-\varepsilon_G)^{-1.01}\mathrm{Re}^{-0.098}Ca^{-0.108}$ Or the simplified form: $\frac{L_B}{d}=1.3\varepsilon_G^{0.07}(1-\varepsilon_G)^{-1.01}We^{-0.1}$	Heptane-nitrogen Ethanol-nitrogen 0.1<We<26 0.06< ε_G <0.85 0.02 m s^{-1}< U_G <1.2 m s^{-1} 0.004 m s^{-1}< U_L <0.7 m s^{-1}	PDMS polydimethysiloxan W=0.15mm H=0.15mm L=25mm Shape:Y Glass W=0.15mm H=0.15mm L=100mm	Sobieszuk et al. (2010)	Experimental

Correlation for bubble and slug length –*Continued…*	Range	Type of microchannel used	Reference	Type of study
$\frac{U_m}{\sqrt{L_S}} = 0.088\,\mathrm{Re}_G^{0.72}\,\mathrm{Re}_L^{0.19}$ Or $L_S = \left[\frac{U_G + U_L}{0.088\,\mathrm{Re}_G^{0.72}\,\mathrm{Re}_L^{0.19}}\right]^2$ $\mathrm{Re}_G = \frac{\rho_G U_G d}{\mu_G}$ $\mathrm{Re}_L = \frac{\rho_L U_L d}{\mu_L}$ U_L is the superficial liquid velocity U_G is the superficial gas velocity		The gas and liquid were introduced at opposite sides of a T-junction. Capillaries studied 0.9-3mm It can be used for circular and square channels.	Liu et al. (2005)	Experimental
$\frac{U_m^{-0.33}}{\sqrt{L_S}} = 142.6\varepsilon_G^{0.56}\left(\frac{d}{L_{UC}}\right)^{0.42}\mathrm{Re}_G^{-0.252}$ $U_m = U_G + U_L$ $L_{UC} = L_S + L_B$, length of unit cell			Akbar & Ghiaasiaan, (2006)	Theoretical study: CFD axisymmetric simulations
$\frac{L_S}{d} = \frac{\varepsilon_L}{-0.00141 - 1.556\varepsilon_L^2\ln(\varepsilon_L)}$		-For square channels -For monoliths	Kreutzer (2003)	Theoretical

Correlation for bubble and slug length – *Continued…*	Range	Type of microchannel used	Reference	Type of study
$\frac{L_B}{w_c} = 1 + \alpha\left(\frac{Q_G}{Q_L}\right)$ w_c is the width of the main α a geometry-dependent constant in the order of 1 Q_L, Q_G are the volumetric flow rates	For $Ca<10^{-2}$	-Rectangular microchannels -Main channel width higher than the channel's height -Gas inlet height at least half that of the main channel. -For $\alpha = 1$ -Width of main channel 50-200µm -Height of main channel 33-79µm. -The discontinuous phase in injected into the continuous via a smaller channel at a right angle. The width of the inlet channel for the disperse phase was 50 and 100 µm. -This model did not fit for gas-liquid flow at higher gas flow rates ($Q_G>Q_L$). -The equation predicts the bubble length obtained in mixing sections of cross geometry with square channels and co-flow geometry.	Garstecki et al. (2006)	Experimental

Correlation for bubble and slug length – *Continued…*	Range	Type of microchannel used	Reference	Type of study
$\frac{L_B}{d_h} = 0.0878\left(\frac{\mathrm{Re}_L(U_b)}{Bo^2}\right)^{0.63}$ $\frac{L_S}{d_h} = 3451\left(\frac{1}{\mathrm{Re}_L(U_G)Bo}\right)^{1.2688}$ d_h is the hydraulic diameter Bo is the Bond numer $Bo = \frac{(\rho_L - \rho_G)gd_h^2}{\sigma}$ $\mathrm{Re}_L(U_b) = \frac{\rho_L U_b d_h}{\mu_L}$ $\mathrm{Re}_L(U_G) = \frac{\rho_L U_G d_h}{\mu_L}$		-For circular capillaries	Laborie et al. (1999)	Experimental
$\frac{L_S}{d_h} = \varepsilon_L \frac{L_S + L_B}{d_h}$ $\varepsilon_L = \frac{U_L}{U_G + U_L}$			Heiszwolf (2001)	
$\frac{L_B}{w_c} = \frac{1}{2}\left(\frac{Q_G}{Q_L \sin\theta} + \frac{2}{5}\cot\theta\right)^{1/2} Ca^{-1/5}$		-Square microchannels Two phases meet at a T-junction at angle θ	Tan et al. (2009)	Experimental

Correlation for bubble and slug length – *Continued…*	Range	Type of microchannel used	Reference	Type of study
$\frac{L_B}{w_c} = 1 + \alpha \frac{Q_G}{Q_L}$ $\alpha = 17.2131 \gamma^{-1} \beta^{-0.5}$ $\frac{L_S}{w_c} = k \cdot l \cdot n \left[\left(\frac{\mathrm{Re}}{Ca} \right)^{0.33} \frac{\varepsilon_L}{\gamma^l \beta^m} \right] + n$ $k = 0.369$ $l = 2.5$ $m = 1$ $n = 3.15$		-Rectangular microchannels	Fries & von Rohr (2009)	Experimental

Table 4.7. Correlations for bubble and slug lengths.

4.11 Conclusions

Taylor flow consists of gas bubbles with lengths longer than the tube diameter separated by liquid slugs. The bubbles travel at a velocity greater than the volume-average liquid velocity and remain disconnected from the capillary wall by a very thin liquid film. The most important characteristic of this pattern is the good mass and heat transfer, a particularly useful feature for the study of multiphase reactions which can be transfer limited. The fact that each liquid slug is confined between two bubbles significantly reduces the axial mixing while the recirculation pattern inside the slugs improves the radial mixing. Mass transfer has been found to be closely related to the length of the liquid slug. Factors that affect slug and bubble length are the gas and liquid velocity, the velocity ratio, the inlet size, the configuration and orientation of the t-contactor, the channel diameter, the curvature ratio, the liquid viscosity and wall surface adhesion. The mechanism of bubble formation depends on parameters like the properties of fluids, inlet geometry and operating conditions.

Previous studies have been reviewed also in terms of homogeneity and stability of Taylor flow. The gas and liquid velocities have been identified as the main factors affecting the uniformity of the flow and stability criteria have been proposed.

Hydrodynamic properties of Taylor flow like liquid film, bubble velocity, pressure drop, bubble and slug lengths can be calculated from correlations provided in the literature.

--//--

CHAPTER 5

Kinetics from Autoclave Experiments

The work with autoclave reactors presented in this Chapter was done in the context of the kinetic study of the methoxycarbonylation of ethylene with the aim to develop the experimental rate law equation entailing the determination of the partial reaction orders and kinetic rate constant(s). The experiments were performed by designated personnel for health and safety reasons at the LI research facility at Teeside using a 2 L autoclave reactor while the experimental design and the data analysis was done by the Author of this Thesis. Three series of experiments were completed to establish the effect of the concentration of the three reactants on the reaction rate; namely methanol, carbon monoxide and ethylene. Early work done by LI had also shown that treatment of the MeOH:MeP liquid mixture under an ethylene atmosphere prior to the initiation of the experimental run enhances the reaction rate. This procedure has been labelled as *pre-treatment*. Hence, a series of experiments was conducted to verify also this effect. Conditions for the pre-treatment are:

Condition	Value
Temperature	100^{o}C
Ethylene Pressure	8 bar
Time	30 min
Reactor stirrer	ON

Table 5.1. Conditions for ethylene pre-treatment of the liquid mixture.

Some interesting features of the kinetics of the methoxycarbonylation of ethylene in the Alpha process are reported in this Chapter which starts with a description of the autoclave reactor and its operation as well as a summary of the main points of the experimental procedure followed in the course of these experiments. Next, the kinetic results are presented and finally, this Chapter draws upon some interesting conclusions.

5.1 Experimental

5.1.1 Description of the Autoclave and its Operation

A 2 L high pressure autoclave reactor has been used for this study. The reactor is fitted with a hollow stirrer shaft to allow the gas from the reactor overhead to be directed under the base of the stirrer where is effectively mixed in the liquid mixture by means of the 4-blade stirrer turbine. The rotating speed of the blades which are driven by an electrical motor is in the range 0-2330 rpm with 2000 rpm used as agitation speed for the kinetic experiments performed in this study in order to achieve good dispersion of the carbon monoxide and ethylene gas bubbles into the

liquid mixture where the reaction occurs. Two ceramic coils on the reactor outer surface provide efficient heating while a stainless steel cooling coil positioned internally in the reactor is used for temperature control. The reactor temperature is monitored by an internal thermocouple. If the temperature is increased by two degrees above the set-point, the flow of cooling water is activated until the temperature decreases by two degrees. On the other hand, current is supplied to the heating coils to heat up the reactor if the temperature falls two degrees below the set-point. In this manner, the reactor remains in the range of two degrees below and one degree above the programmed temperature. A description of the autoclave reactor set-up is illustrated in Figure 5.1.

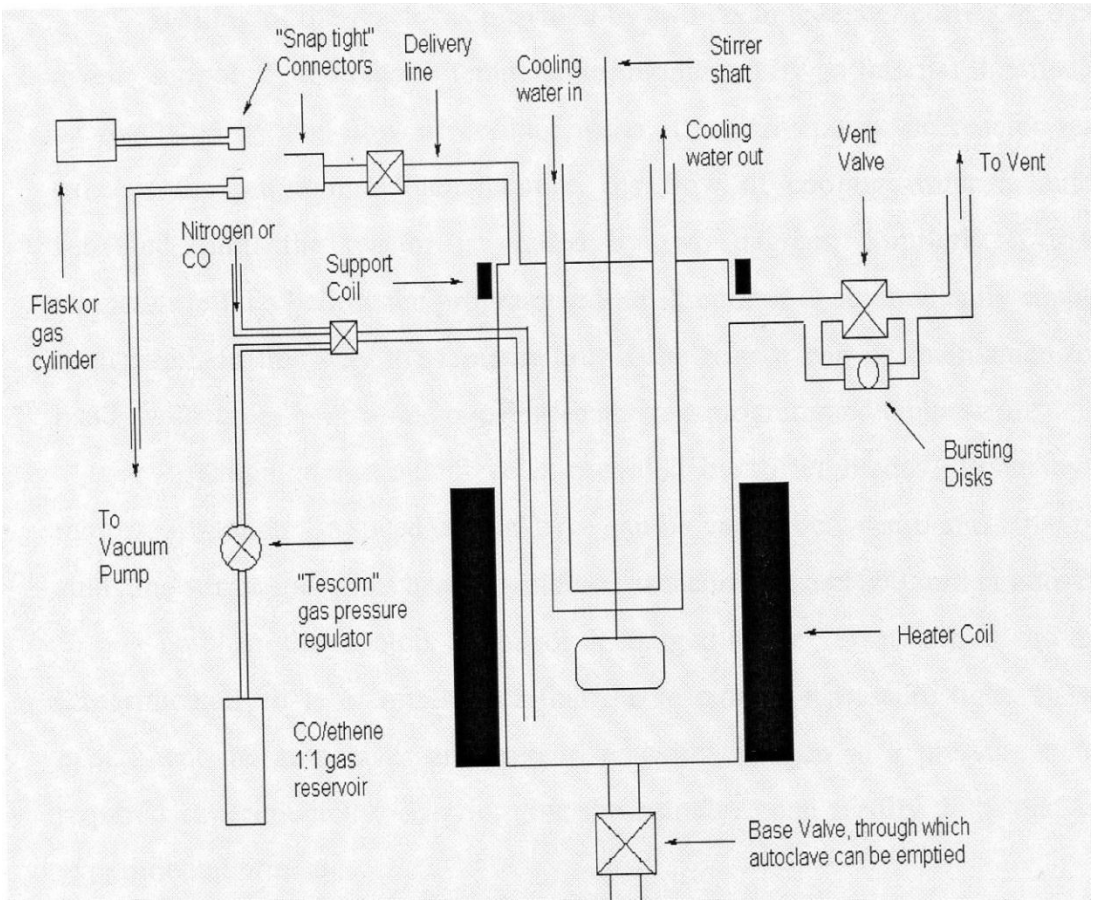

Figure 5.1. Schematic of the experimental layout for the autoclave reactor.

The autoclave is a pressure -tight vessel and can withstand a maximum pressure of 100 bar at atmospheric temperature. In order to avoid the pressure exceeding the maximum allowed of 100 bar, the reactor is equipped with two thin metal disks, called the 'bursting disks' designed to rupture at 100 bar. In the unlikely event of over-pressurisation, the disks will burst resulting in a fast venting of the autoclave avoiding the development of a hazardous situation. Maximum recommended operating pressure equates two thirds of the maximum pressure. Oxygen is excluded at all times as catalytic reacting solutions are air sensitive. The reactor is pressurised with nitrogen to a pressure two times higher than the required one experimentally between two consecutive experiments for pressure testing. This is done to ensure that there is no leak of gas and that the reactor can withstand the experimental pressure. The autoclave is normally charged by evacuating the autoclave and allowing the reactant solution to be sucked via a delivery line. The autoclave can be pressurised either at ambient temperature or at reaction temperature. The feed gas normally consists of a mixture of carbon monoxide and ethylene but small amounts of hydrogen can also be added on some occasions. The autoclave pressure is regulated by a 'Tescom' regulator valve which is connected to a 1:1 ethylene:CO gas mixture reservoir corresponding to the reactor stoichiometry, so that the gas which gets consumed by the reaction in the course of the experiment is replenished and the reactor pressure is maintained at the programmed set-point. Details of the reactor temperature and the pressure of the gas reservoir are logged every 5 s throughout the reaction in (mA) electric current values which are converted to give (T, P) readings via formula. An example of temperature and pressure reading logged in the course of an experiment is shown in Figure 5.2.

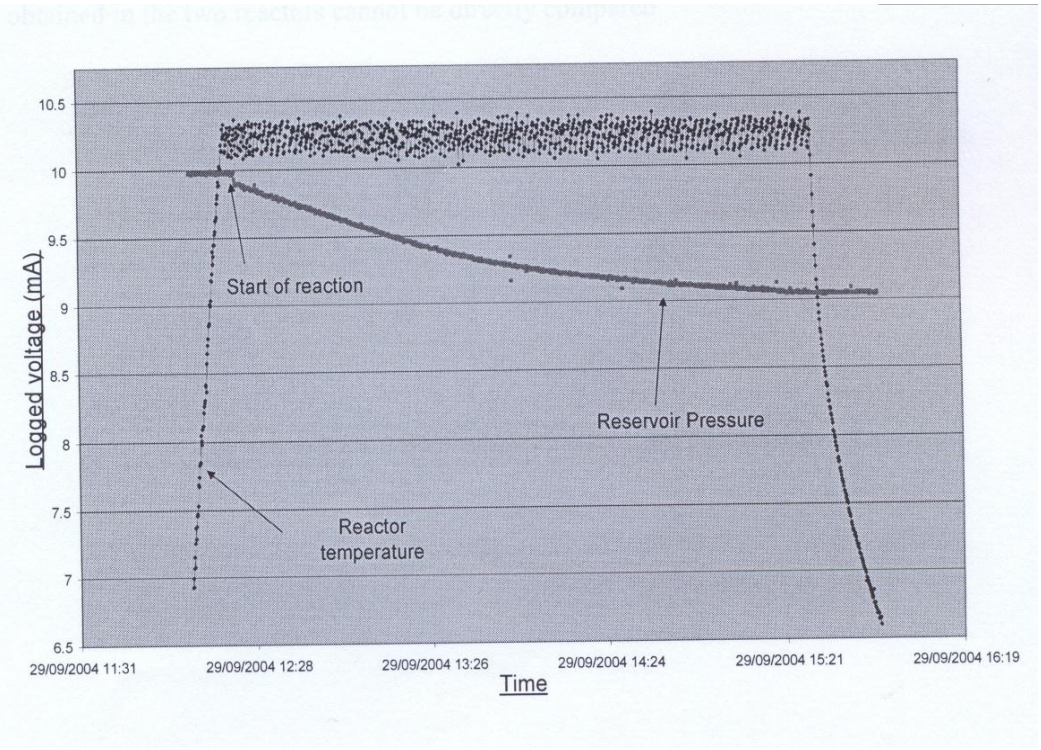

Figure 5.2. Reaction temperature and gas reservoir pressure readings logged during a typical experimental run.

The number of mol of MeP produced which is half the number of mol of gas consumed can be calculated from the pressure drop in the 1:1 composition 10 L gas reservoir using the equation of state for an ideal gas and 100 % selectivity for MeP. Other assumptions are that the gas composition in the reactor overhead, consisting of CO, ethylene and MeOH and MeP vapours (please refer to Appendix D for calculations of reactor overhead composition), and the gas solubilities in the reacting liquid mixture remain constant due to the very small changes in MeP, MeOH concentrations during the course of the reaction. To find the reaction rate profile, a plot of mol of MeP formed versus reaction time is produced. A trend line is generated by fitting an appropriate equation to the data with the help of the software program TableCurve. The trend line is then differentiated to give rate data (as mol of product/time) for the whole duration of the experiment. The rate values are then

converted to TOF (mol product/mol of Pd/h) which is then plotted against reaction time to give the reaction rate profile, an example of which is illustrated in Figure 5.3. The MeP produced in mol is also plotted against the reaction time.

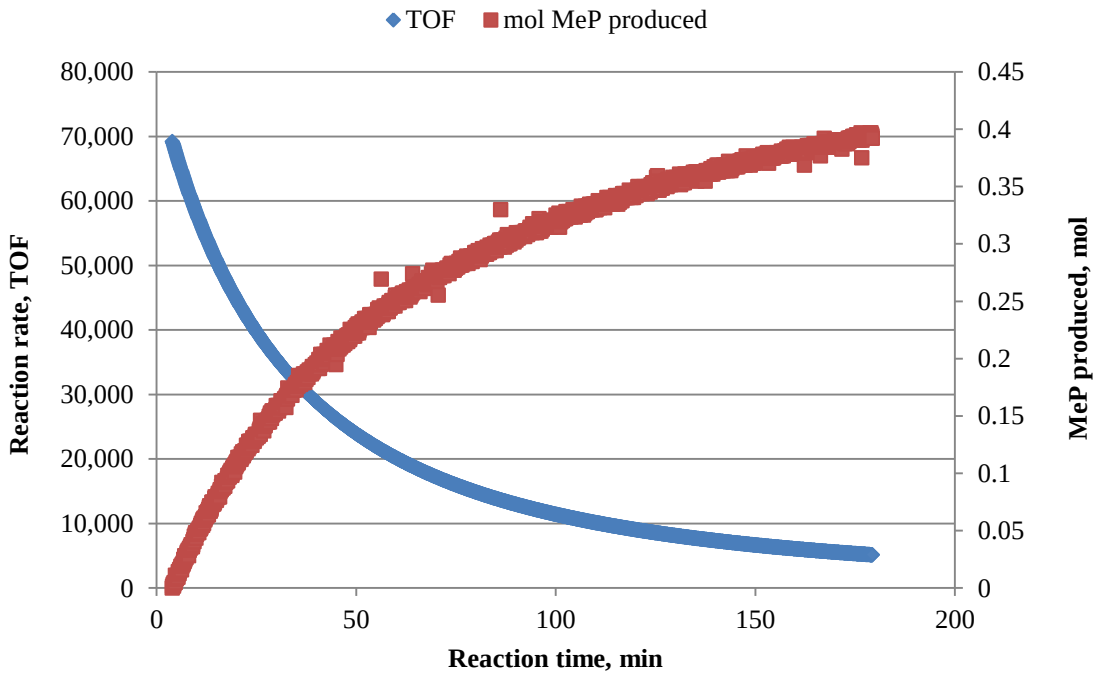

Figure 5.3. Example of reaction rate profile.

Another way in which the autoclave reactor can be operated is firstly to be charged with the liquid solution, pressurised and heated to the desired conditions and then allow the reaction to proceed in a closed system configuration. In this way, the gas which gets consumed is not replenished resulting in a drop of reactor pressure which is measured via a pressure transducer. This mode of operation was not utilised for the experiments presented in this Chapter. The geometrical characteristics as well as operating conditions of the autoclave reactor are listed in Table 5.2.

Autoclave Reactor	**19F**	
Charasteristic/Condition	**Value**	**Comments**
Methanol (MeOH)	30%	Initial mixture
Methanopropionic acid (MeP)	70%	Initial mixture
Methanosulfonic acid ($MeSO_3H$)	ratio acid/ligand=90/1 acid/Pd=450/1	Initial mixture
Ligand (dtbpx)	ratio ligand/Pd=5/1 or 6/1	Initial mixture
Pd	7.1E-6 mol or 2.4 10^{-5} mol/L for the 0.3 L reacting mixture	Initial mixture
Carbon monoxide	1 bar	Constant by means of a back pressure regulator
Ethylene	9 bar	8 bar is the pre-treatment P and 1 bar extra is added just before the start of the experimental run. ethylene pressure is kept constant by means of a back pressure regulator.
Pre-treatment	8 bar ethylene, 100^{o}C, 30 min	
Pressure	12.2 bar	10 bar above the methanol vapour pressure
Temperature	100 ^{o}C	
Stirrer Speed	1750-2000 rpm	
Stirrer	single impeller, 4 blade turbine	The reactor is an aspirating unit
Baffles	no baffles	The cooling coil around the stirrer acts as a baffle
Capacity	2L	Liquid reactant mixture 0.3 L
Geometrical Characteristics	D=2in=5.08cm, T=4in=10.16cm, h_1/h_2=1/3	D=impeller diameter, T=tank diameter,h_1/h_2= clearance of impeller from bottom of tank
Maximum Pressure	100bar	
Reactor Type	Batch for the liquid and semi-batch for the gas	Gas consumed by the reaction is replenished with gas sourced from the gas reservoir

Table 5.2. Geometrical characteristics and operating conditions of autoclave reactors.

5.1.2 Experimental Procedure

It should be noted that catalyst preparation was always performed under nitrogen and exclusion of oxygen was accounted for in every step of the operating and experimental procedure.

The main steps of the standard procedure for catalyst preparation and execution of a typical experiment are as follows:

- Firstly, in a glove box weight measurements of the specified amount of salt Pd_2dba_3 and phosphine ligand are taken and subsequently the substances are transferred in a glass flask.
- Addition of MeP in the flask happens next, followed by stirring maintained for 45 min under a nitrogen atmosphere. No contact with air is allowed to prevent oxidation of the phosphine. The colour from dark red becomes yellow after stirring due to the formation of the complex [P-P-Pd^0dba] (personal communication with Dr Eastham from LI, 2006).
- Addition of azeotrope solution 50:50 MeP and MeOH in the flask.
- Addition of acid. The solution turns red because of the protonation of the oxygen atom in the dba molecule. The dba molecule disassociates and the complex of [P-P-Pd^{II}-H-MeOH] is formed at this stage (personal communication with Dr Graham Eastman from LI, 2006).
- The reactant solution is transferred by vacuum into the reactor.
- The reactor stirrer is turned-on at this point.

- The reactor temperature starts rising to the set-point of 100 ^{o}C. Once the temperature is at set-point the pressure inside the reactor is 2.2 bar which corresponds to the vapour pressure of the reactants.
- Manual addition of ethylene corresponding to ethylene partial pressure of 8 bar in a gradual and careful manner to bring reactor pressure to 10.2 bar.
- Maintenance of the liquid reactant under the ethylene atmosphere for 30 min for pre-treatment.
- Further addition of the mixture ethylene/CO 1:1 until the pressure reaches 12.2 bar and the time and the pressure in the gas mixture reservoir when addition is complete is noted. The pressure in the gas reservoir shortly afterwards starts dropping, signalling the start of the reaction.
- During the 3 h duration of the reaction, pressure and temperature are recorded on-line every 5 s and stored in a personal computer. Reactor stirrer speed of 2000 rpm is maintained throughout the experiment.
- When run is complete, the heater is turned off and the temperature set-point is set to zero. This will allow the cooling water to cool down the reactor.
- When reactor is at ambient temperature the stirrer is turned off, the reactor gas is vented off and the liquid is emptied from the draining valve into a sample bottle for weighing.
- Methanol is charged into the reactor to clean the vessel, stirred and then gets discharged.

The experimental conditions under which a standard experiment is carried out are called the *Alpha Standards* (LI report No 91, 2001) and are included in Table 5.3

Apart from MeP and methanol, the standard liquid reacting mixture also contains the Pd catalyst as well as methanosulphonic acid and ligand in excess. The standard amount of catalyst used for was 7.12 10^{-6} mol for preparation of 0.3 L of reacting mixture, which resulted in a concentration of 0.024 mol/m^3 so that the reaction was slow enough to allow for reactor operation in the kinetic regime and collection of intrinsic kinetic data. Reaction conditions are 100 ^{o}C and 12.2 bar pressure.

Lucite International Alpha Standards	
CO partial pressure	1 bar
Ethylene/CO molar ratio in the reactor headspace	9:1
Reaction Temperature	100 ^{o}C
Reaction Pressure	12.2 bar
Liquid composition	30 % MeOH, 70 % MeP (w/w)
Pd catalyst concentration in the liquid mixture	2.4 10^{-5} mol/L
Pd/L_2 ratio (L_2 is the bi-dentate d^{t}bpx ligand) in the liquid mixture	1:5
Pd/acid (acid is the methanosulphonic acid)	1:450

Table 5.3. Alpha standards.

There is an excess of ethylene in the reactor overhead space, resulting from initially adding ethylene to increase the reactor pressure from 2.2 to 10.2 bar and after the conclusion of pre-treatment a further gas addition but this time of a 1:1 (v/v) mixture of ethylene and CO to bring the pressure to a final 12.2 bar. The pressure in the reactor is monitored with accuracy by means of a digital pressure gauge situated on the reaction control panel. The reactor stirrer is maintained on at the high speed of 2000 rpm during the gas additions and the liquid mixture becomes saturated in both ethylene and CO. From the pressure increments, the initial gas feed to the reactor

was ethylene:CO=9:1. Once the reaction has started, one mol of CO, one mol of ethylene and one mol of MeOH are consumed for every mol of MeP produced according to the stoichiometry of the reaction:

$$CH_2 = CH_2 + CO + CH_3OH \rightarrow CH_3CH_2COOCH_3 \quad (5.1)$$

The total pressure in the reactor is maintained constant at 12.2 bar via the 'Tescom' regulator valve connected to the 10 L gas reservoir containing 1:1 ethylene:CO mixture. In addition, when reaction is initiated, the liquid mixture is saturated with the reactant gases and the high speed stirrer maintains gas bubbles dispersed in the liquid at all times even though the solubility of CO is low and at 100 ^{o}C five times less compared to that of ethylene (Torres, 2009). To verify that the liquid mixture is indeed fully saturated with CO gas at t=0, two blank experiments were performed under the Alpha conditions for 30 % and 70 % methanol concentration in the reactant mixture. No gas uptake was observed which means that the liquid is saturated at the beginning of the experiment. It is known that solubility apart from temperature and pressure depends also in the liquid composition.

Furthermore, the gas solubility depends on the liquid composition which changes in the course of the experiment as methanol gets consumed and MeP is formed. This would also mean a change in the partial pressures of the gas in the reactor overhead space. Notwithstanding this, taking into account that the methanol conversions achieved in the autoclave experiments range in 0-16% in addition to the lack of CO and ethylene solubility data obtained at variable MeP:MeOH liquid compositions led us to assume that the solubility of gases remain approximately unchanged during the experimental run. The availability of solubility data at other compositions apart from

the MeP:MeOH 70:30 % wt would allow for the validity of this statement to be checked.

It is reasonable to wonder whether the solubility of gases could create a small change in the reaction volume. However, according to Torres, 2009, who used the standard *Alpha* composition to experimentally determine the CO and ethylene solubility using NMR, the composition of the liquid phase was assumed constant and always close to 70 % wt of MeP and 30 % wt methanol and only small deviations occurred due to the low solubility of the gases.

Overall, it is thus reasonable to make the hypothesis that whilst the reaction is taking place, the ratio of ethylene:CO in the overhead reactor space as well as the gas solubilities in the liquid mixture remain approximately constant.

5.1.3 Experimental Conditions

Several experiments were carried out with the autoclave reactor in order to study the kinetics of the methoxycarbonylation of ethylene with the d^{t}bpx ligand whose range of conditions is shown in Table 5.4:

Condition	Range
Concentration of methanol in the MeP:MeOH initial reacting solution (%w)	15-70%
Partial pressure of ethylene in the reactor overhead (bar)	1.0-6.0
Partial pressure of CO in the reactor overhead (bar)	0.4-5.95
Pre-treatmeant temperature (^{o}C)	50-100

Table 5.4. Range of conditions for the experiments using the autoclave reactor.

Two methods were employed for the treatment of the data collected from the autoclave experiments; the Initial Rates Method and the Integral Method of Analysis (Laidler, 1965). Details of those can be found in the Chapter Two, Section 2.3.2.

5.2 Investigation of Mass Transfer Effects

5.2.1 Calculation of Mass Transfer Coefficient

Intrinsic kinetic data were necessary for the conduction of the kinetic study and the establishment of the effect of various factors on the reaction rate (carbon monoxide, ethylene, methanol concentrations and temperature). For the characterisation of experimental data as kinetic we had to cancel out the existence of mass transfer resistances.

Correlations from the literature were employed as a first step in order to evaluate the mass transfer coefficient for the LI autoclave reactors. The mechanical characteristics of the autoclave reactors, the fluid properties of the gases and liquid mixture in the reactors as well as the operating conditions were used for these calculations in order to evaluate the mass transfer coefficients $k_L\alpha$ and k_L.

All the results obtained for $k_L\alpha$ and k_L are summarised in Table 5.5. Detailed calculations can be found in Appendix J:

Correlation	Mass transfer coefficient	Value	Reference
$k_L\alpha = 1.48\times10^{-3} N^{2.18}\left(\frac{V_G}{V_L}\right)^{1.88}\left(\frac{d_I}{d_T}\right)^{2.16}\left(\frac{h_1}{h_2}\right)^{1.66}$	$k_L\alpha$ (s^{-1})	0.64	Chaudhari & Gholap (1987)
$\frac{k_L\alpha d_I^2}{D} = 0.06\left(\frac{d_I^2 N\rho_L}{\mu_L}\right)^{1.5}\left(\frac{d_I N^2}{g}\right)^{0.19}\left(\frac{\mu_L}{\rho_L D}\right)^{0.5}\left(\frac{\mu_L V_{SG}}{\sigma}\right)^{0.6}\left(\frac{N d_I}{V_{SG}}\right)^{0.32}$	$k_L\alpha$ (s^{-1})	0.64	Trambouze et al. (1983)
$k_L\alpha = AN^B$	$k_L\alpha$ (s^{-1})	0.62	Meille et al. (2004)
$k_L = 0.31\left(\frac{g\mu_L}{\rho_L}\right)^{\frac{1}{3}}\left(\frac{D_L\rho_L}{\mu_L}\right)^{\frac{2}{3}}$	k_L (ms^{-1})	$1.4\ 10^{-4}$ for small bubbles (<25mm) Applicable for sieve trays	Calderbank (1961)
$k_L = 0.42\left(\frac{g\mu_L}{\rho_L}\right)^{\frac{1}{3}}\left(\frac{D_L\rho_L}{\mu_L}\right)^{\frac{1}{2}}$	k_L (ms^{-1})	$4.6\ 10^{-4}$ for large bubbles (>25mm) Applicable for sieve trays	Reith (1968)
$\alpha = \frac{6\varepsilon_G}{d_b}$ $\frac{\varepsilon_G}{1-\varepsilon_G} = 0.819\frac{V_{SG}^{2/3}N^{2/5}d_I^{4/15}}{g^{1/3}}\left(\frac{\rho_L}{\sigma}\right)^{1/5}\left(\frac{\rho_L}{\rho_L-\rho_G}\right)\left(\frac{\rho_L}{\rho_G}\right)^{-1/15}$ $d_b = \frac{4.15\sigma^{0.6}\varepsilon_G^{0.5}}{\left(\frac{P_G}{V_L}\right)^{0.4}\rho_L^{0.2}} + 0.0009$ $\frac{P_G}{V_L} = \frac{0.83}{V_L}\left[\frac{N_p d_I^8 \rho_L N^4 V_L}{V_{SG}^{0.56}}\right]^{0.45}$ $k_L = \frac{k_L\alpha}{a}$	k_L (ms^{-1})	$5.4\ 10^{-3}$ Applicable for autoclaves with Rushton turbines	Stenberg & Anderson, (1988) Calderbank (1959) Lemoine & Morsi (2005)

Correlation – ***Continued…***	**Mass transfer coefficient**	**Value**	**Reference**
VISIMIX	k_L (ms^{-1})	$3.5\ 10^{-3}$	
$k_L = 0.448\left(\frac{P_g \mu_L}{V_L \rho_L^2}\right)^{0.25}\left(\frac{D_L \rho_L}{\mu_L}\right)^{0.5}$ $k_L\alpha = 0.04\left(\frac{P_g}{V_L}\right)^{0.47} V_{SG}^{0.6}$	k_L (ms^{-1})	$2.16\ 10^{-3}$ Applicable for mechanically agitated reactors	Linek et al., (2005) Kapic & Heindel (2006)
$k_L = 0.448\left(\frac{P_g \mu_L}{V_L \rho_L^2}\right)^{0.25}\left(\frac{D_L \rho_L}{\mu_L}\right)^{0.5}$ $k_L\alpha = 0.01\left(\frac{P_g}{V_L}\right)^{0.475} V_{SG}^{0.4}$	k_L (ms^{-1})	$2.93\ 10^{-3}$ Applicable for mechanically agitated reactors	Linek et al., (2005) Smith et al. (1977)
$k_L = 0.448\left(\frac{P_g \mu_L}{V_L \rho_L^2}\right)^{0.25}\left(\frac{D_L \rho_L}{\mu_L}\right)^{0.5}$ $k_L\alpha = 0.00326\left(\frac{P_g}{V_L}\right)^{0.55} V_{SG}^{0.25}$	k_L (ms^{-1})	$2.51\ 10^{-3}$ Applicable for mechanically agitated reactors	Linek et al. (2005) Joshi & Sharma (1977)

Table 5.5. Values of $k_L\alpha$, k_L using different correlations.

The three correlations for $k_L\alpha$ produced almost the same result of 0.64 s^{-1}; however, different values of k_L were calculated depending on the methodology adopted. Considering that the correlations for sieve trays probably underestimate mass transfer while the opposite may be true for the approach assuming a Rushton turbine and after disregarding the corresponding results, the value of 2.98 10^{-3} ms^{-1} for k_L can be accepted as the average of the remaining figures.

5.2.2 Operating Regime Criteria

For gas-liquid systems where mass-transfer is accompanied by chemical reaction in the liquid phase, for example when the gas *A* reacts with liquid *B*, we distinguish four operating regimes depending on the relative rates of diffusion and reaction (Levenspiel, 1992) :

Regime 1: This is the kinetic regime. It is valid for very slow reactions where the reaction rate is much smaller that the mass-transfer rate. The rate of product formation will depend exclusively on the reaction kinetics.

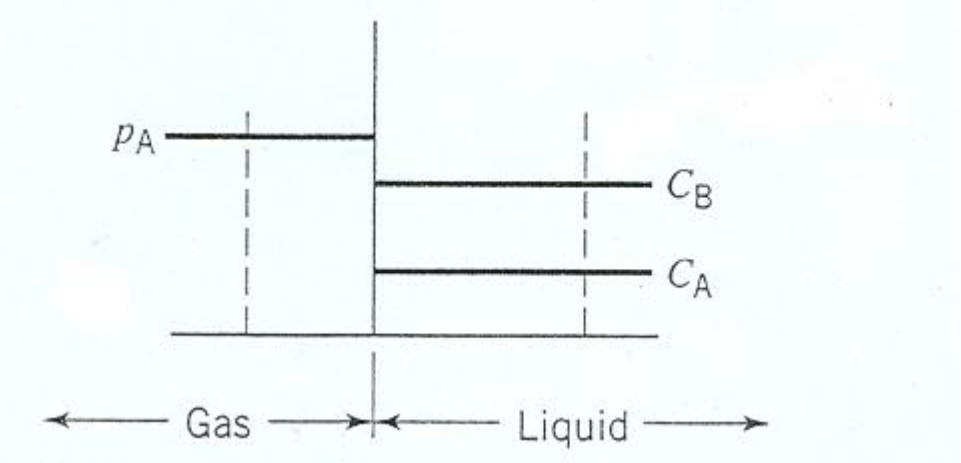

Figure 5.4. Very slow reaction (regime 1). The gaseous reactant A dissolves in the liquid where it reacts with liquid reactant B.

Regime 2: It occurs for slow reactions where the reaction rate is faster than the mass-transfer rate of the gas into the liquid. The concentration of dissolved gas in the liquid is zero or small. The reaction happens in the liquid film and the liquid bulk. The process is controlled by diffusion.

Regime 3: It is valid for fast reactions. The reaction rate is much faster than the mass-transfer. The reaction occurs solely in the film. The process is controlled by diffusion.

Regime 4: It occurs for very fast (instantaneous) reactions. The reaction is so fast that the gas solute and the liquid reactant cannot coexist and at a distance from the interface both substances are instantaneously consumed.

Two criteria were examined to assess the autoclave reactor operating regime:

Criterion 1 was using the Hatta number (Ha) which is defined as:

$$\left(\frac{Maximum\_possible\_conversion\_in\_the\_film}{Maximum\_diffusion\_transport\_through\_the\_film}\right)^{0.5} = \left(\frac{R\cdot\delta}{\frac{D_L}{\delta}[A]^*}\right)^{0.5} = \left(\frac{\frac{R}{[A]^*}}{k_L^2}\right)^{0.5} == = Ha = \frac{\sqrt{D_L\frac{R}{[A]^*}}}{k_L} \quad (5.2)$$

and according to its value a reaction can be characterised as slow, fast or instantaneous (Levenspiel, 1992).

If Ha>>1, all reaction happens in the film and surface area is the controlling rate factor. Conversely, if Ha<<1, no reaction occurs in the film and bulk volume becomes the controlling rate factor. In detail:

1. If Ha<0.02, the reaction is infinitely slow
2. If 0.02<Ha<2, part of the reaction occurs in the film and part of the reaction in the liquid bulk.

3. If 2<Ha<5, the reaction is fast and occurs in the film.
4. If Ha>5, the reaction is instantaneous.

Infinitely slow reaction *Reaction happens entirely in the liquid bulk*	**Intermediate case** *Reaction happens in the film and the liquid bulk*	**Fast reaction** *Reaction happens entirely in the film*	**Instantaneous reaction** *Reaction happens at the gas-liquid interface and both reactants cannot coexist*
Ha<0.02	0.02<Ha<2	2<Ha<5	Ha>5

Table 5.6. Values of Hatta number (Levenspiel, 1992).

Other sources define three reaction regimes based on the Ha number and specify that the reaction is considered slow when Ha is less than 0.3, as follows:

Slow reaction	**Fast reaction**	**Instantaneous reaction**
Ha<0.3	0.3<Ha<5	Ha>5

Table 5.7. Values of Hatta number (Trambouze et al., 1988).

We can define the enhancement factor ϕ, as the ratio of mass exchange between the gas and the liquid phase with and without chemical reaction (Ramachandran & Chaudhari, 1983, Doraiswamy & Sharma, 1984 and Levenspiel 1992):

$$\phi = \frac{rate\_with\_reaction}{rate\_for\_mass\_transfer\_alone} \tag{5.3}$$

When Ha<0.3, the rate of mass exchange is not enhanced by the chemical reaction and the enhancement factor is 1. If 0.3<Ha<5, the mass exchange is enhanced by the chemical reaction, the enhancement factor is greater than 1 and is given by:

$$\phi = \frac{Ha}{\tanh Ha} \tag{5.4}$$

For reactions that proceed only in the boundary layer, Ha>5 and the enhancement factor is equal to Ha (Trambouze et al., 1983).

Criterion 2 is the factor γ which is defined as the ratio of the reaction rate divided by the rate of reaction conforming to regime 2:

$$\gamma = \frac{R}{k_L \alpha [A^*]} \tag{5.5}$$

If the following condition is satisfied:

$$\gamma = \frac{R}{k_L \alpha [A^*]} < 0.1 \tag{5.6}$$

the operating regime is regime 1, the kinetic regime.

To sum up, in order to determine if the autoclave reactor operation was in the kinetic regime two criteria were checked (Ramachandran & Chaudhari, 1983, Vavasori et al., 2003):

Criterion	Formula
1	$\text{Ha} = \frac{\sqrt{D_L \frac{R}{[A]^*}}}{k_L} = (0.02 + 0.3)/2 = 0.16$ *Note: average between the values given by Trambouze (1988) and Levenspiel (1992).*
2	$\frac{R}{\kappa_L \alpha C_{CO}^*} << 1$

Table 5.8. Operating regime criteria.

For the calculations of criteria 1 and 2, the values of the estimated specific mass transfer coefficient $k_L\alpha$ and mass transfer coefficient k_L were used. Details of the calculations are shown in Appendix I.

Parameter	Value
$\gamma = \frac{R}{\kappa_L \alpha C_{CO}^*}$	0.26
$\text{Ha} = \frac{\sqrt{D_L \frac{R}{[A]^*}}}{k_L}$	0.006
Enhancement factor ϕ	1.0

Table 5.9. Operating regime criteria-calculated values.

The conclusions derived from this analysis are that firstly, even though the Ha is smaller than 0.002 which means that the reaction is slow, factor $\gamma = \frac{R}{\kappa_L \alpha C_{CO}^*}$ is

greater than 0.1 which signifies that at the agitation speed of 1000 rpm, reactor operation is between regimes 1 and 2. This means that a part of the reaction is taking place at the liquid film while the rest in the liquid bulk. Secondly, in order for the mass transfer resistances to be eliminated, the specific mass transfer $k_L\alpha$ must be increased to the value of 1.72 s^{-1}. This could be achieved by increasing the agitation speed to 1600 rpm. These conclusions were verified by experiments conducted under the same *Alpha* conditions but using different agitation speeds and they are presented in the next section.

5.3 Experimental Results

5.3.1 Preliminary Results

The effect of the agitation speed on the methoxycarbonylation rate was studied at 100 ^oC to determine the significance of mass transfer. This method has been used by other researchers as well to check whether mass transfer limitations exist or not in autoclave reactors used for kinetic studies (for example Deshpande & Chaudhari, 1988 and Seayad et al., 1998).

Various experiments were conducted under the same Alpha standards conditions but the stirrer speed was altered in the range of 1500 rpm to the maximum speed of 2330 rpm. It was found that the agitation speed of 1500 rpm gave significantly lower reaction rates (TOF=60,000 mol MeP/ mol Pd/h) compared to the speeds 1750 rpm and above (TOF=90,000-100,000) as shown in Table 5.10. The differences in

reaction rates obtained for 1750 rpm, 2000 rpm and 2330 rpm can be attributed to experimental error. No significant increase in reaction rate was obtained when the agitation speed was raised from 1750 rpm to 2000 rpm or 2330 rpm which denotes reactor operation in the kinetic regime.

No	Stirring speed (rpm)	Initial rate, TOF, mol/mol/h
1	1500	62,376
2	1750	97,292
3	2000	101,707
4	2000	91,009
5	2330	88,220

Table 5.10. Initial rates obtained at different agitation speeds.

The figure presented next, includes the reaction rate profiles obtained under different agitation speeds.

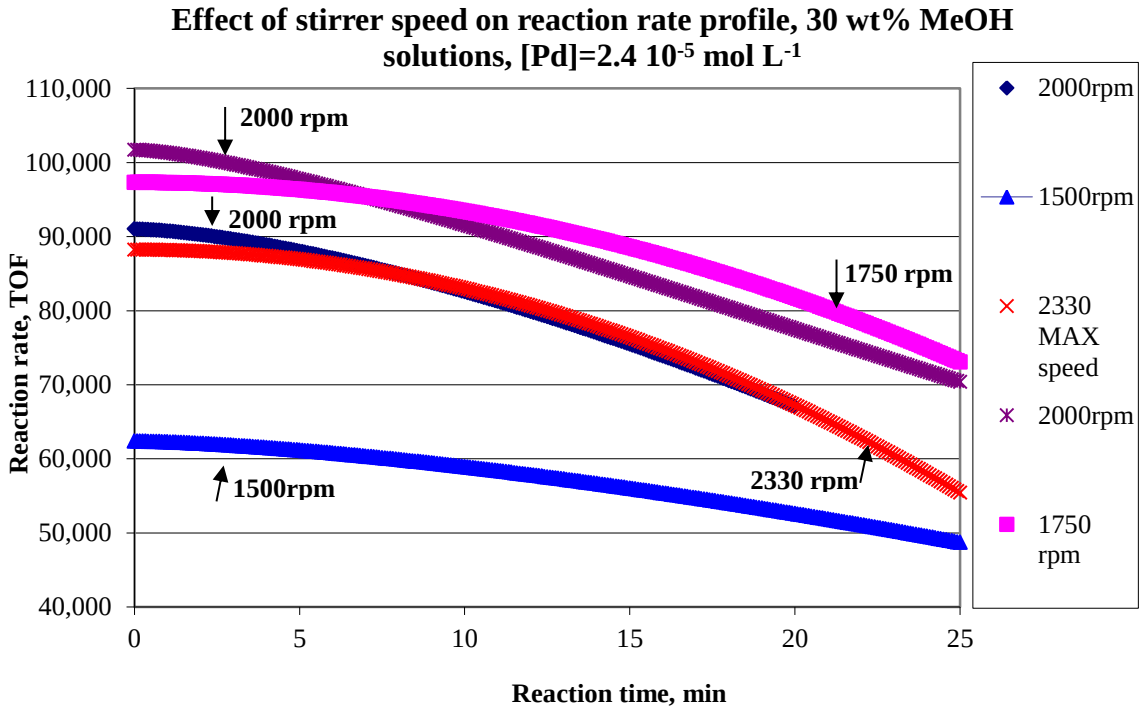

Figure 5.5. Effect of stirrer speed on reaction rate.

Using a higher stirrer speed and lower catalyst concentration, the reaction rate profile of a standard experiment changed shape slightly as it is depicted from Figure 5.6.

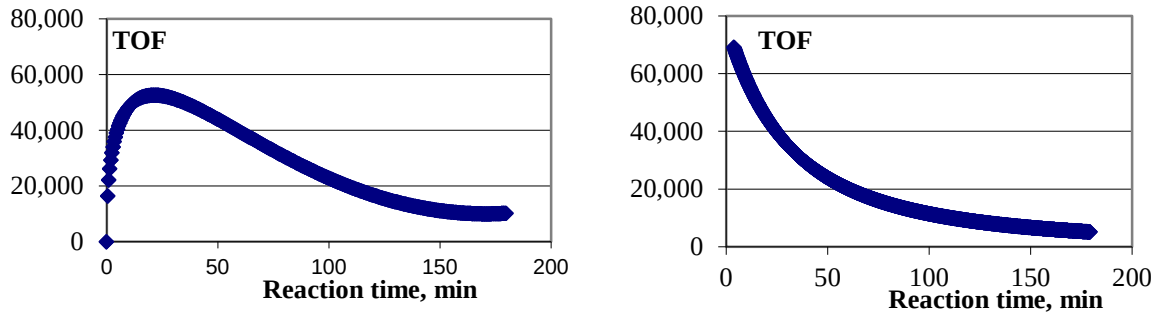

(A) Stirring speed: 1000 rpm
Pd concentration 4.7 10^{-5} mol L^{-1}
$k_L\alpha$=0.642 s^{-1} (calculated)

(B) Stirring speed: 1750 rpm
Pd concentration 2.4 10^{-5} mol L^{-1}
$k_L\alpha$=2.17 s^{-1} (calculated)

Figure 5.6. Reaction rate profile for standard experimenent before (A) and after (B) the modifications to the experimental conditions.

Based on these experimental results, the agitation speed of 2000 rpm was utilised for all the kinetic experiments which were presented in the remainder of this Chapter.

5.3.2 Pre-treatment Series

Prior to the reaction initiation in all the autoclave experiments presented in this Chapter, the MeOH: MeP liquid mixture in the reactor had remained under an ethylene atmosphere at 100 ^{o}C for 30 min. This procedure has been labelled as *pre-treatment* and during previous research by LI, although not exactly under the same experimental conditions, it was found to increase the reaction productivity/ yield (communication with G. Eastman from LI, 2005). In order to quantify the importance of pre-treatment in reaction yield and also investigate the importance of temperature at which the pre-treatment take place, a series of experiments was completed effectively comparing the effect of applying pre-treatment at 100 ^{o}C, at 50 ^{o}C and foregoing pre-treatment completely. A list of all the experiments

performed together with the methanol conversion attained is included in the following Table.

Experiment	Name of experiment	Pre-treatment	Initial Rate (TOF)	Induction time (min)	MeOH conversion after 3h reaction time (%)
1	30mins pre-treatment _1 100C	Yes, at 100^{o}C	93,924	2	15.66
2	**30mins pre-treatment _2 100C**	**Yes, at 100^{o}C**	**63,267**	**16**	**11.14**
3	No_pre-treatment _1	No	67,636	4	13.15
4	No_pretreatment_2	No	55,740	12	10.12
5	30mins_pretreatment at 50C_1	Yes, at 50^{o}C	69,347	8	12.43
6	30mins_pretreatment at 50C_2	Yes, at 50^{o}C	71,799	5	13.40

Table 5.11. Overview of the autoclave pre-treatment experiments.

Not all the experiments gave reproducible results. In detail, the results of the standard experiments 1 and 2 are very different as can be seen from Figure 5.10. Appendix H concluded that the initial rate achieved from a standard experiment lies in the range 84,354±9,534 with a 90 % confidence limit and therefore the TOF of 63,267 obtained in Experiment 2 is extremely low suggesting gross experimental error. Experiments 5 and 6 gave very similar results while the results obtained from experiments 3 and 4 showed a difference in induction time and TOF of 8 min and 11,896 respectively (please refer to Figures 5.9 and 5.8) which are inexplicable and could be attributed to experimental errors. In detail, Experiment 3 (no pre-treatment was applied) gave analogous results with Experiments 5 and 6 (pre-treatment at 50 ^{o}C) while the results of Experiment 4 are much inferior. Judging from the data overall and ignoring Experiment 2, it could be supported that pre-treatment has a positive effect on the reaction rate but not conclusively. The extent of this effect

could not be derived with accuracy due to discrepancies in the results obtained from experiments performed supposedly under the same conditions.

A deduction to be made is that no pre-treatment with ethylene gives an average initial rate of around 60,000 mol MeP/mol Pd/h. There is some evidence suggesting that pre-treatment at 50 ^{o}C increases the initial rate slightly as compared to having no-pretreatment at all, to approximately 71,000 mol MeP/mol Pd/h but this hypothesis could not be validated unless more experiments foregoing pre-treatment are performed. Finally, pre-treatment at 100 ^{o}C could result in higher initial rates, close to 94,000 mol MeP/mol Pd/h. (A TOF of 90,000-100,000 is typical under the standard Alpha conditions).

Pre-treatment seems to have a positive effect at the initial stages of the reaction. This could be explained by the fact that the formation of MeP is the final step in a series of consecutive reactions occurring at different speeds. Having a large ethylene excess pushes the equilibrium of the first reaction in the catalytic cycle, that is the ethylene addition and the formation of the alkyl intermediate, far to the right, thus speeding up the whole cycle once the CO is introduced into the reactor. There is no effect on the reaction rate observed after approximately 50 min of reaction time and from then on all the reaction rate profiles coincide as it can be seen from Figure 5.7. This means that the ethylene addition is faster than the methanolysis reaction which yields MeP. Jimenez et al. (2004) also suggested that the alkyl formation is fast equilibria.

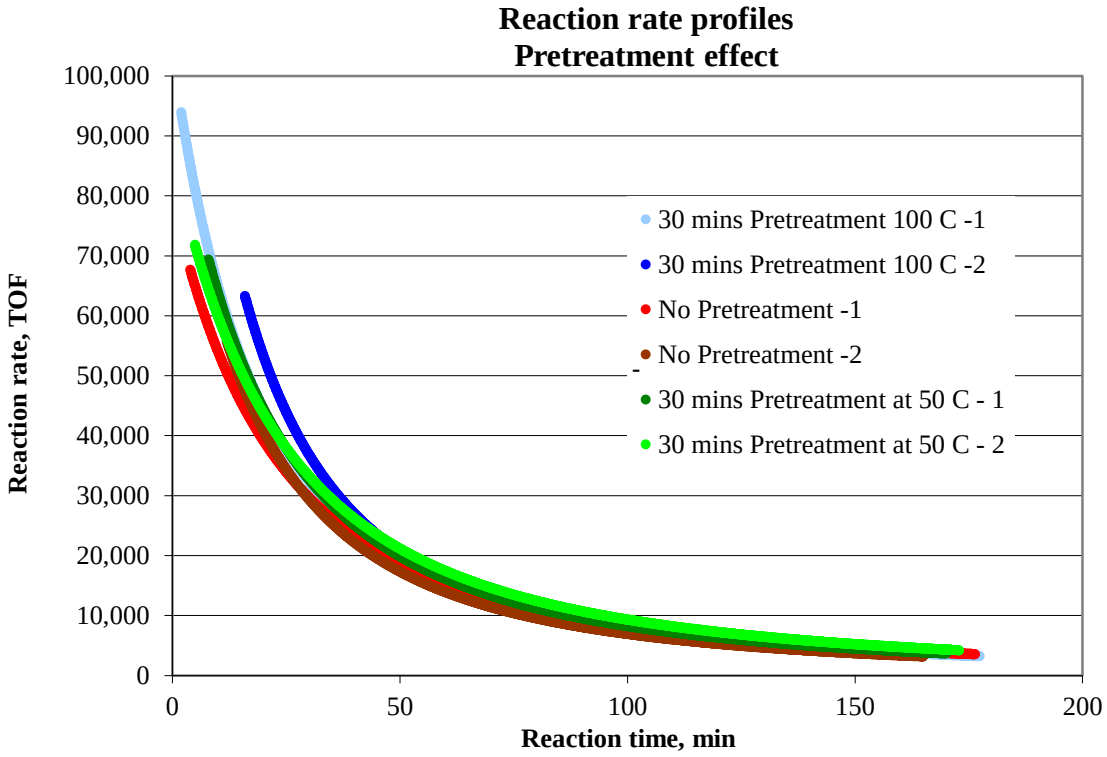

Figure 5.7. Reaction rate profiles. Pretreament experiments.

An induction time of 8 min was noted when no pre-treatment was applied (Figure 5.8).

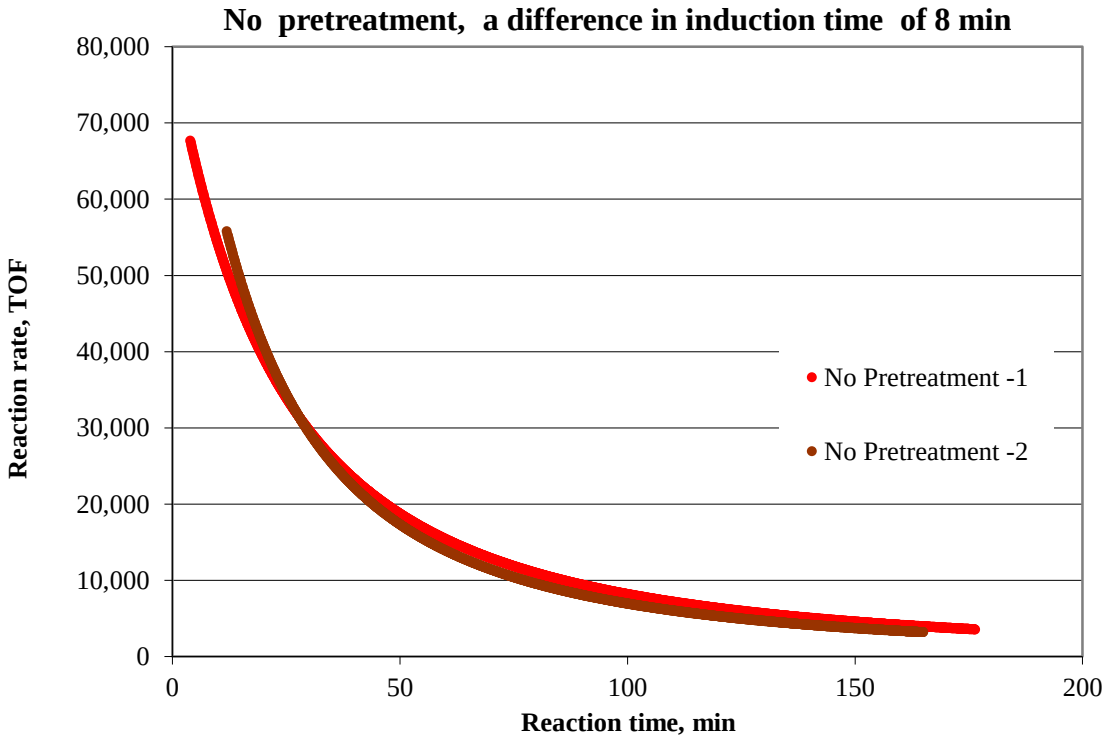

Figure 5.8. Reaction rate versus time for No-pretreatment.

Figure 5.9 illustrates the experimental data obtained when pre-treatment of the liquid mixture with ethylene was applied for the set time of 30 min but at 50 ^{o}C temperature. It can be seen that the induction time is reduced to 2-3 min but the initial reaction rate, was only in the range of 70,000 mol MeP/molPd/h. The methanol conversion attained was only 12.4-13.4 %, a very small increase of 0-3 % compared to applying no-pretreatment at all.

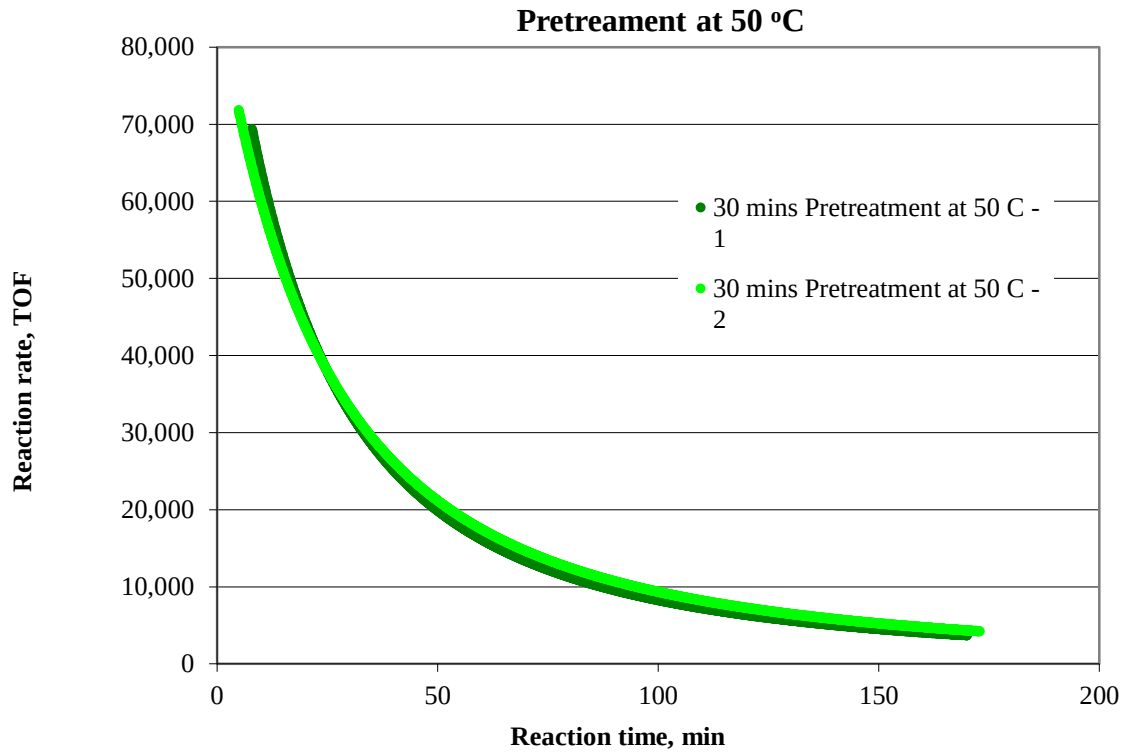

Figure 5.9. Reaction rate versus reaction time for 30mins pre-treatment at 50 ^{o}C.

Experiments 1 and 2 were conducted under the same experimental conditions but they produced incomparable results. There is reason to believe that there was experimental error involved in Experiment 2 as it produced inexplicably long induction time and very low initial rate compared to Experiment 1 and other standard experiments performed in the past (unfortunately, the resources were unavailable for the Experiment 2 to be repeated). On the contrary, the reaction rate profile of Experiment 1 is the reaction rate profile which one would expect from a standard experiment under the Alpha standards.

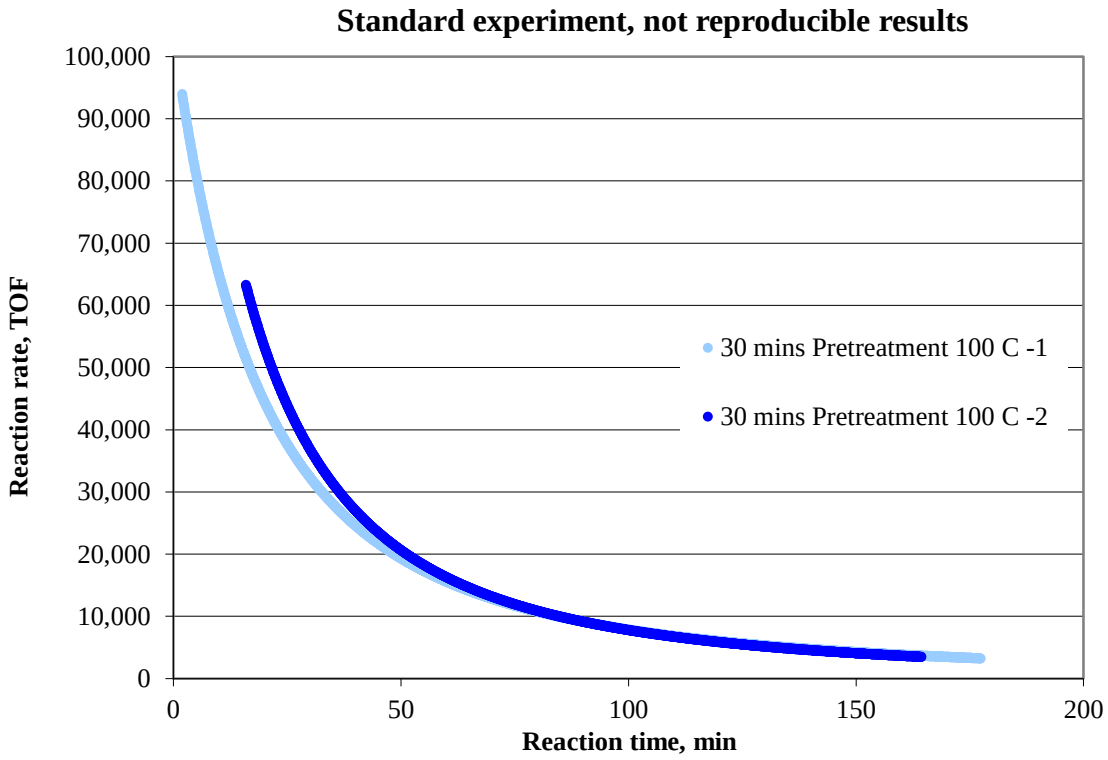

Figure 5.10. Reaction rate versus time for 30mins Pre-treatment at 100 ^{o}C.

Even though not all experiments in this series gave reproducible results, judging from the data overall and excluding Experiment 2, there is suggesting evidence that pre-treatment has a positive effect on the reaction rate by improving the product yield through an enhancement of reaction rate and shrinkage of induction time. The extent of this effect cannot be derived exactly due to discrepancies in the results obtained under the same conditions. However, a conclusion to be drawn is that no pre-treatment with Ethylene gave an initial rate in the range of 60,000mol MeP/mol Pd/h while the reaction induction time was raised to around an average 8 min. Pre-treatment at 50 ^{o}C increased the initial rate by approximately 20% compared to having no-pretreatment at all to the level of 70,000 mol MeP/mol Pd/h while on the other hand the induction time was diminished to the level of 6 min on average. Pre-treatment for 30 min at 100 ^{o}C resulted in an initial rate increase by a third to a value

exceeding 90,000 mol MeP/mol Pd/h. Pre-treatment had a positive effect at the initial stages of the reaction by reducing the induction time, thus, enabling a *head-start* of the catalytic cycle. The fact that the higher the pre-treatment temperature, the higher the initial rate can also be explained by the fact the equilibrium reaction constant is increased with temperature according to Van't Hoff law (Santacesaria et al., 1999):

$$K_E = K_E^0 \exp((-H / R_g)(1/T - 1/T^0) \quad (5.8)$$

Where K_E and K_E^0 are the equilibrium constants at a temperature T and T^0 respectively, H is the reaction enthalpy and R_g is the constant of gases.

There is no promotional effect on the reaction rate observed after approximately 50 min of reaction time and from then on all the reaction rate profiles coincide. This can be explained by the fact that MeP formation happens at a slower rate compared to the ethylene addition reaction.

As it has been shown, pre-treatment seems to have a beneficial effect by increasing the initial rate/ product yield on the back of a reduced reaction induction time. However, the experiments presented in this section are not 100 % conclusive due to the discrepancy observed between results obtained from runs conducted under presumed identical conditions. In order to elucidate beyond reasonable doubt and quantify the effect of pre-treatment at 50 and 100^{o}C as compared to foregoing pre-treatment altogether, this experimental series should be expanded with more runs.

Pre-treating the liquid mixture under an ethylene atmosphere at 100°C for 30 min was developed as the standard practice when working with autoclaves based on conclusions from a past experimental study performed by LI prior to the initiation of the research effort described in this Thesis. The experiments detailed in this section do not advocate that this procedure ought to be altered, on the contrary there is evidence suggesting that pre-treatment has a favourable effect when conducting autoclave experiments in terms of product yield via increasing conversion and reducing reaction *dead time*.

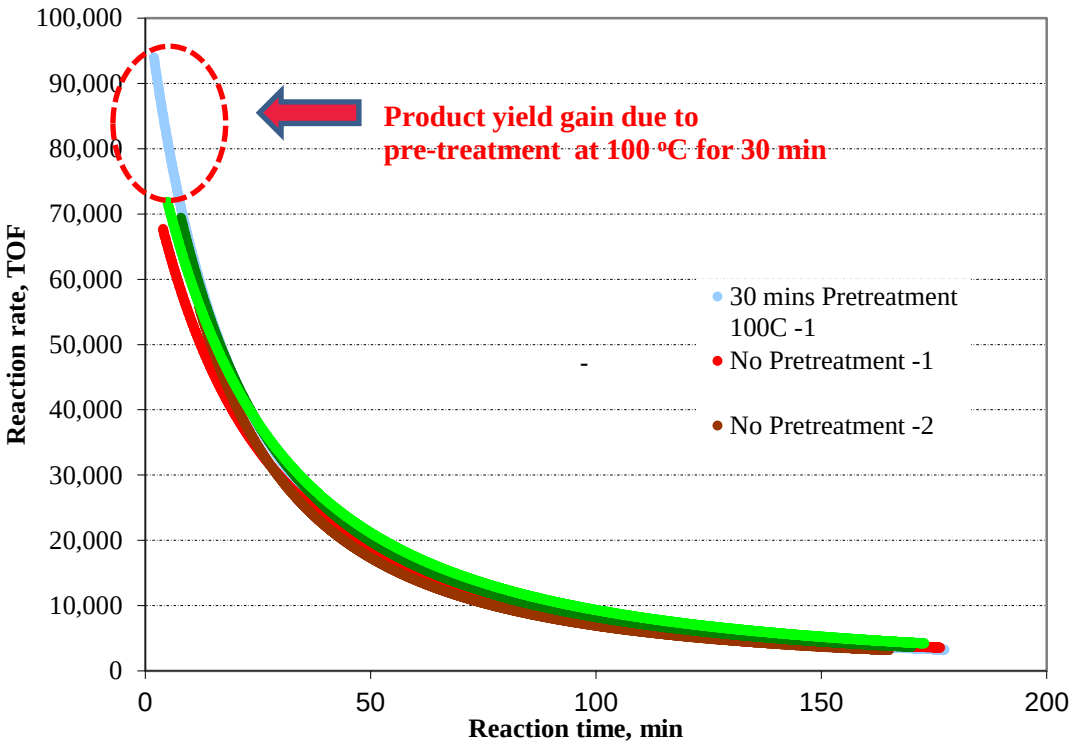

Figure 5.11. Positive effect of pre-treatment on product yield and induction time.

5.3.3 Methanol Series

A series of experiments was conducted with the autoclave reactor in order to establish the partial reaction order with respect to methanol. All experiments were performed under the Alpha Standard conditions apart from the concentration of methanol in the reaction mixture which was varied; 15 %, 20 %, 25 %, 30 %, 40 %, 50 %, 60 %, 70 %. The remaining of the liquid volume was made by MeP. The pressure drop in the gas reservoir was recorded every 5 s for 30 min or 1h of reaction time.

Methanol Autoclave Experiments Conditions	
CO partial pressure	1 bar
Ethylene/CO ratio in the reactor headspace	9:1
Methanol composition in the methanol: methyl propionate liquid mixture	15 %, 20 %, 25 %, 30 %, 40 %, 50 %, 60 %, 70 % (w/w).
Methyl propionate composition in the methanol: methyl propionate liquid mixture	8 5%, 80 %, 75 %, 70 %, 60 %, 50 %, 40 %, 30 % (w/w)
Temperature	100 ^{o}C
Pressure	12.2 bar
Pd catalyst concentration	2.4 10^{-5} mol/L
Pd/(phosphine ligand L2) ratio	1:5
Pd/acid	1:450

Table 5.12. Experimental conditions for the methanol series autoclave experiments.

It should be reminded that in order to use the Initial Rates method, the initial concentration of one reactant - methanol in this series - is varied while the initial

concentrations for the other reactants are maintained unchanged for all the experimental runs. It is expected that the methanol and MeP concentration of the liquid mixture will have an affect the solubility of the CO and ethylene and therefore the composition of the reactor headspace will not be exactly the same for all experiments in this series even though the nominal gas ratio was the same for all experimental runs and equal to ethylene:CO=9:1. However, due to the absence of gas solubility data corresponding to other compositions apart from the standard one (MeP:MeOH=70:30 % wt), it had to be assumed that the composition of the liquid mixture has no effect on the gas solubility. It should be noted that this assumption was backed up by the findings by Torres (2009). Considering that the nominal gas ratio utilised was constant, the reactor total pressure was maintained unchanged due to the back pressure regulator, the liquid was always saturated with gas at the absence of mass transfer effects and finally the reaction was extremely slow due to the miniscule amounts of Pd used leads us to believe that this assumption would not have significantly skewed the experimental results.

The following figure shows the reaction rate profiles obtained from the various autoclave experiments. It is evident that a drop of in methanol concentration in the reaction mixture, decreases the reaction rate. In addition, the induction time became significant and reached 13 min for methanol concentrations of 25 % and below.

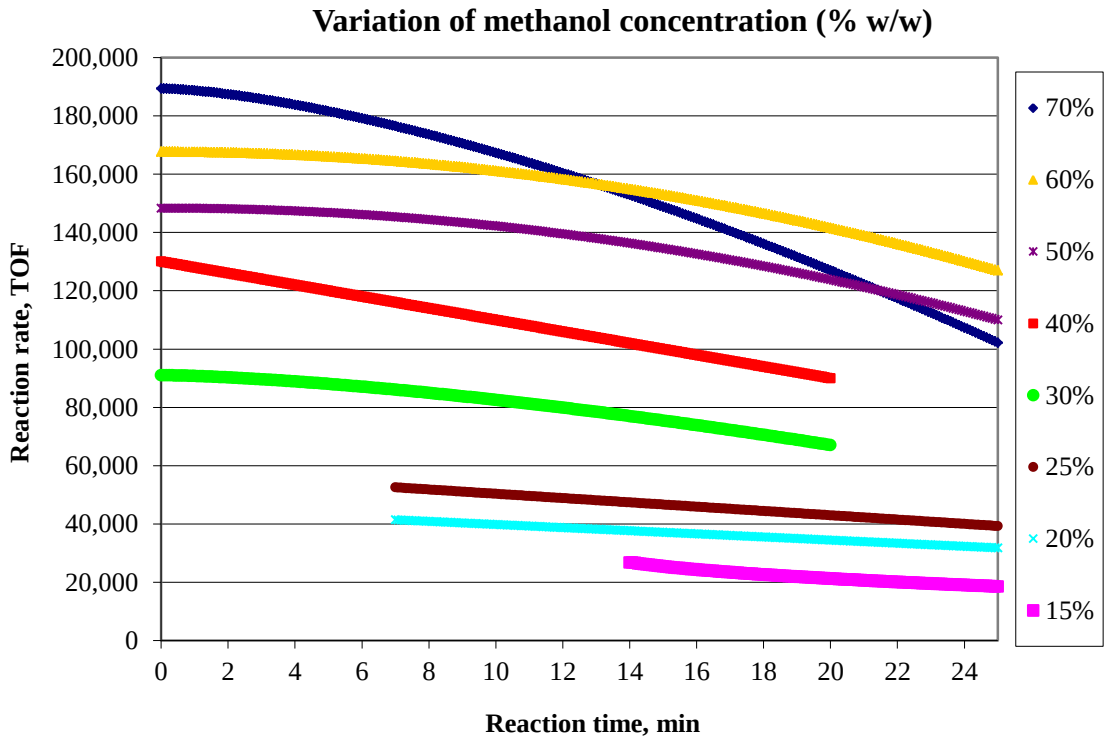

Figure 5.12. Reaction rate profiles for the methanol series autoclave experiments.

The experimental results obtained were analysed using the Initial Rates Method and the Integral Method. Both methods concluded that the reaction is first order with respect to methanol as it is shown in the next pages.

Figure 5.13 illustrates the analysis of the data with the Initial Rates Method for low methanol concentrations, i.e 15-25 % (w/w) in the liquid mixture while Figure 5.14 demonstrates the results obtained from experiments where methanol composition in the reaction mixture was in the range of 30-70 %. The reaction order with respect to methanol it was found to be +1.1 and +0.9 at low and high methanol concentrations respectively. First order dependence on methanol was also concluded from previous studies at LI conducted prior to 2005.

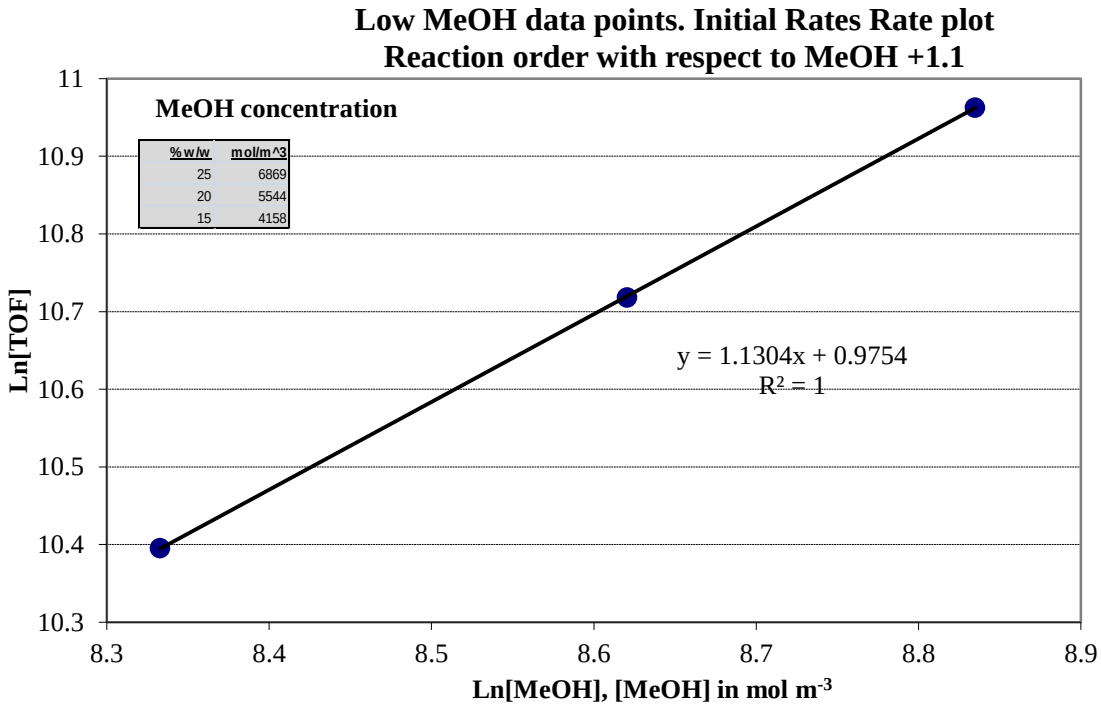

Figure 5.13. Initial rates data. methanol concentration in the liquid mixture <30 %.

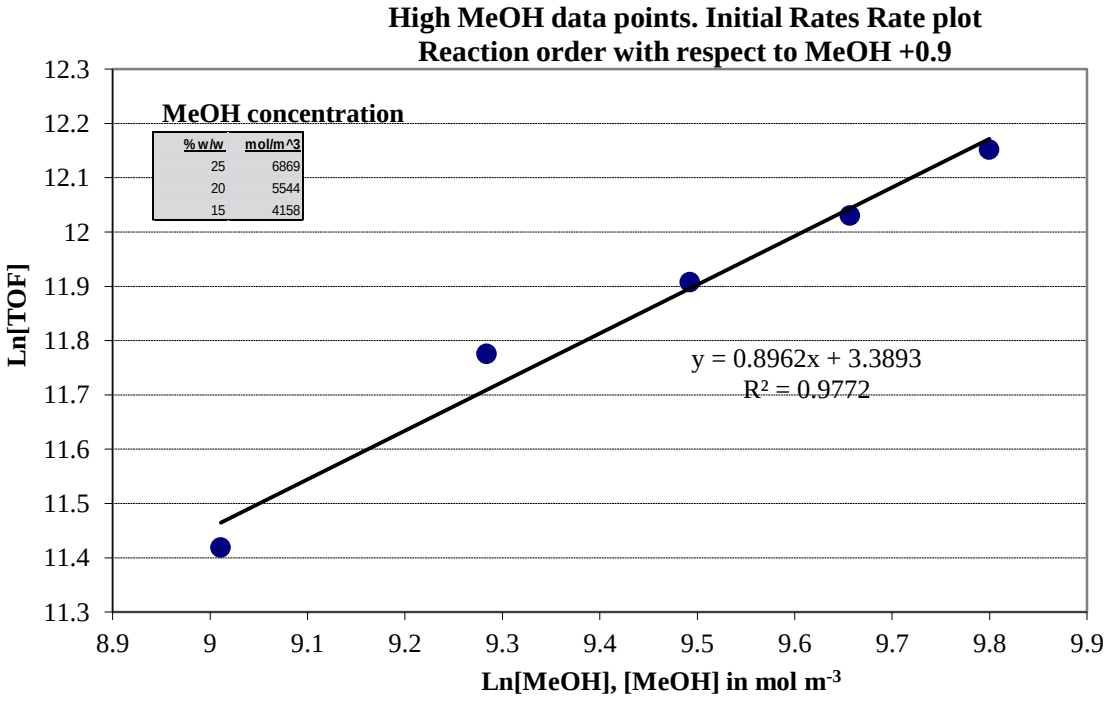

Figure 5.14. Initial rates method data. methanol concentration in the liquid mixture >=30 %.

In addition to the Initial Rates Method, the Integral Method of Analysis was used for treatment of the methanol data. Plotting the $\ln\left(\frac{[MeOH]_0}{[MeOH]}\right)$ against reaction time produced a straight line which means that the reaction is first order with respect to methanol and the pseudo-reaction rate constant is equal to the line slope (please refer to Figures 5.15-17).

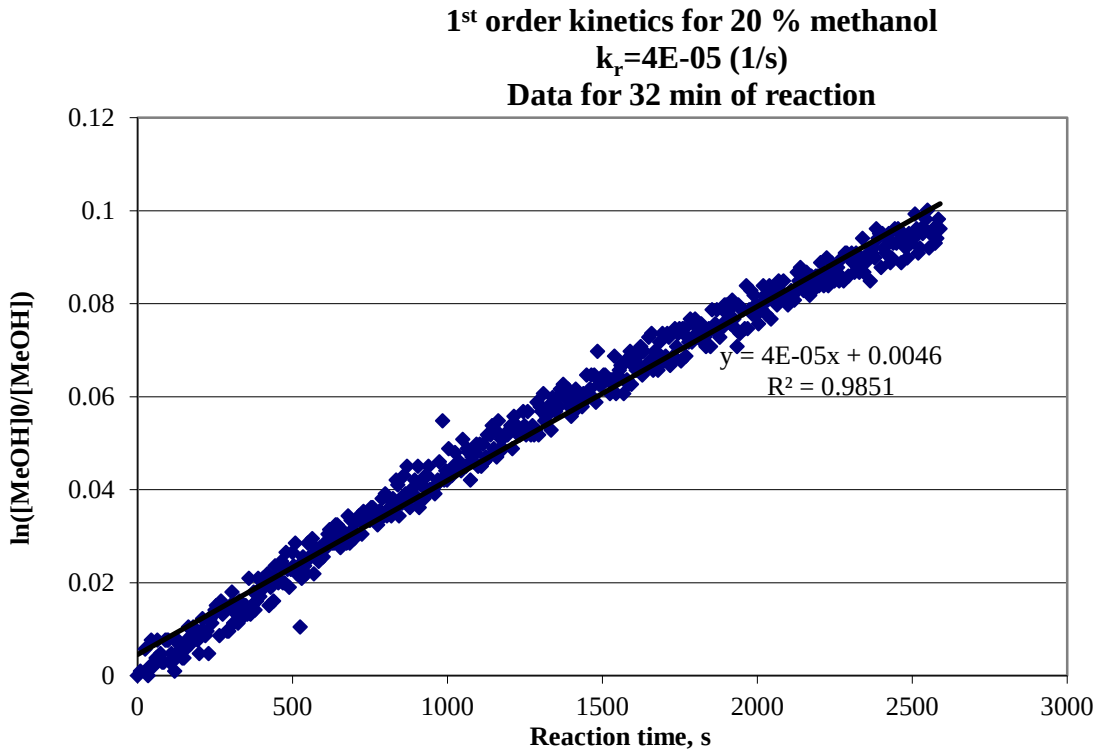

Figure 5.15. Test 1st order kinetics for 20 % methanol.

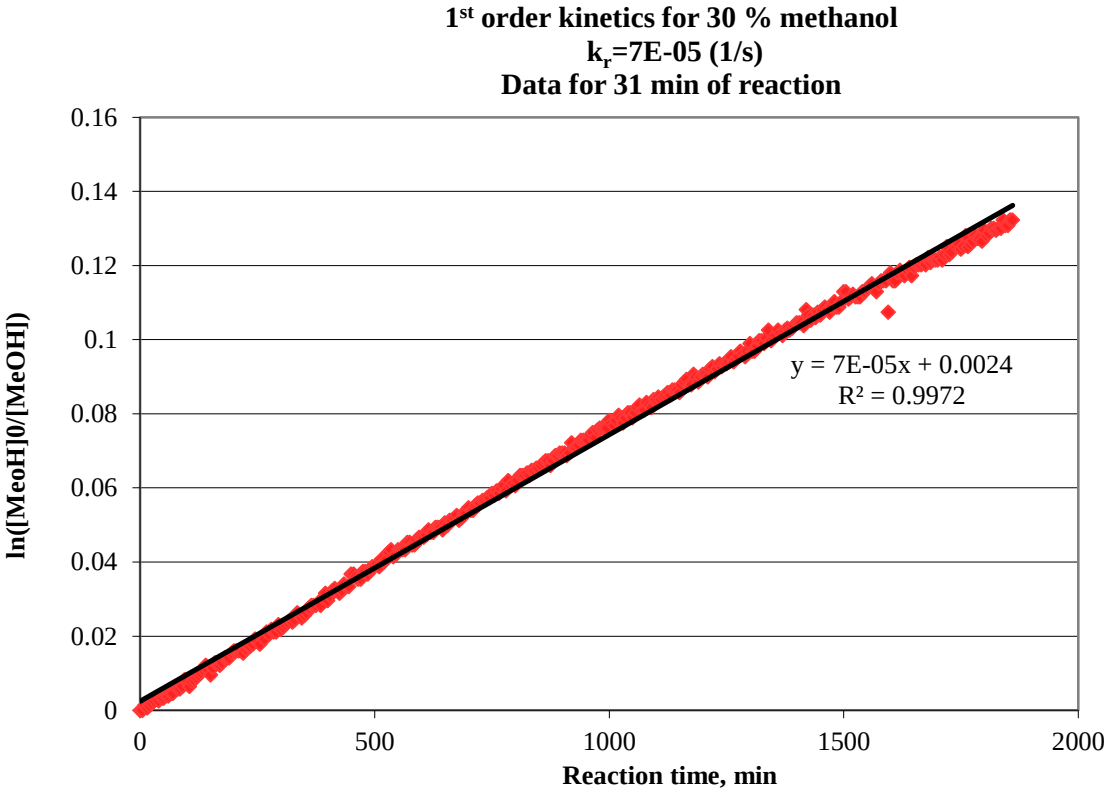

Figure 5.16. Test for 1st order kinetics for 31min of reaction and 30 % methanol.

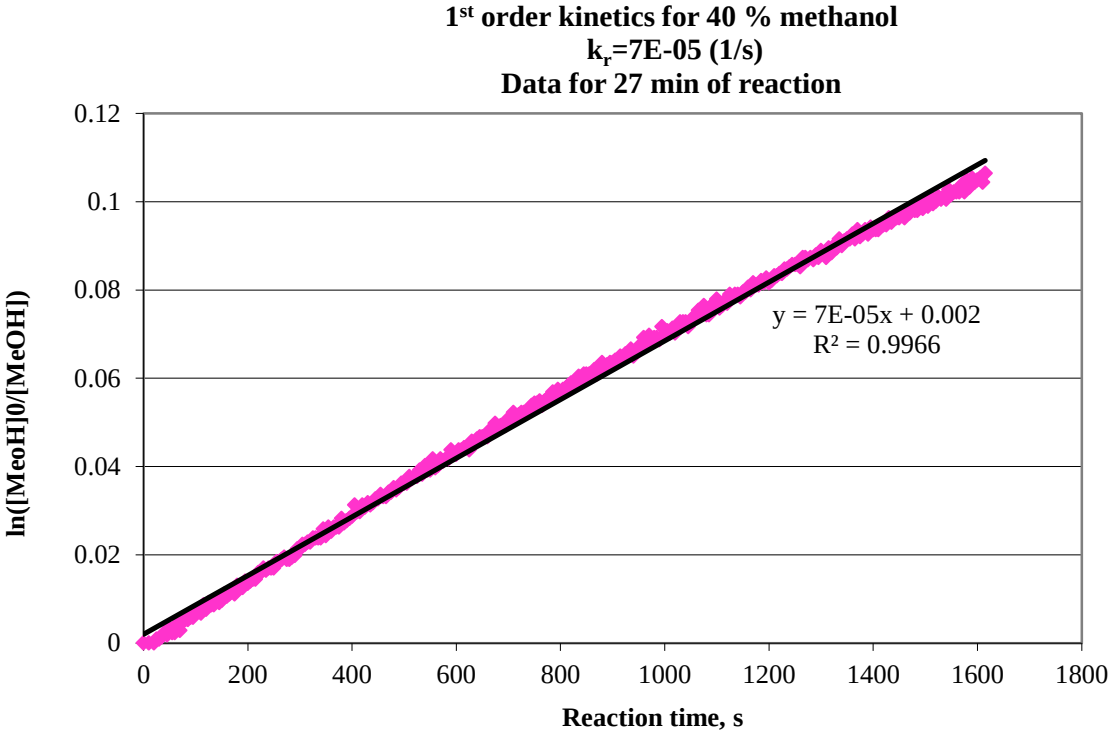

Figure 5.17. Test for first order kinetics for 27min of reaction and 40 % methanol.

Similar graphs were produced for all the experiments and the results showed a first order dependency with respect to methanol. In the methanol concentration range 30-60 % (w %) in particular, the reaction rate has the empirical form $R = k_r[MeOH] = -\frac{d[MeOH]}{dt}$ with an average k_r=6.85 10^{-5} ± 3.21 10^{-6} (s^{-1}) (or ±4.69 %). (5.9)

The value of k_r is given in the following table for the whole methanol range studied:

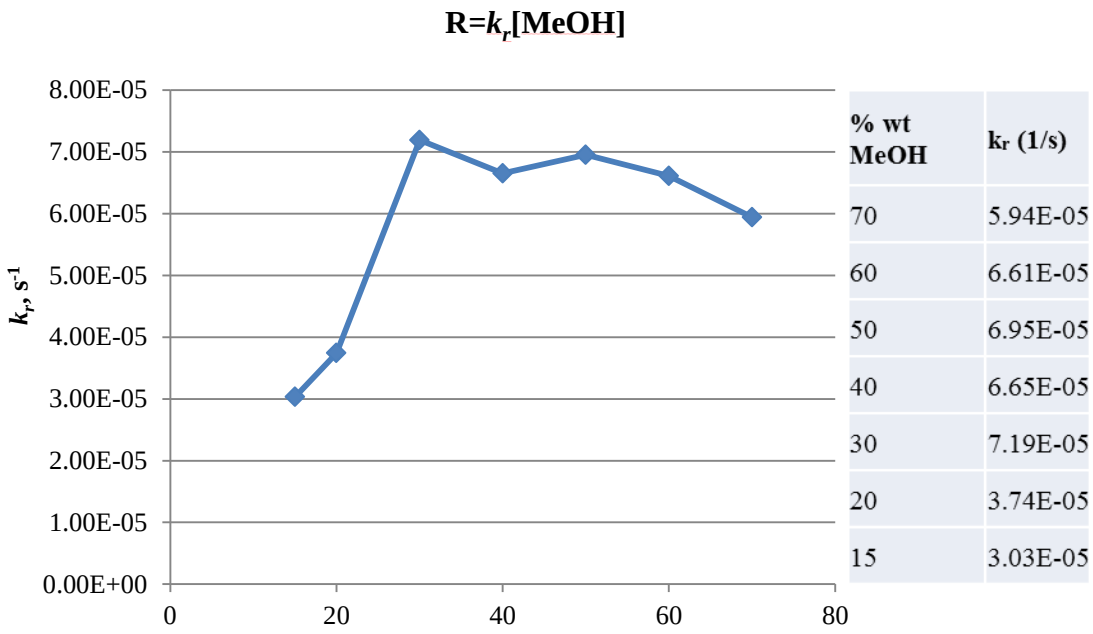

% wt MeOH	k_r (1/s)
70	5.94E-05
60	6.61E-05
50	6.95E-05
40	6.65E-05
30	7.19E-05
20	3.74E-05
15	3.03E-05

Figure 5.18. Variance of k_r with the % initial concentration of MeOH in the liquid mixture.

From the data presented above we can distinguish two concentration ranges; 15-30 % and 30 %-70 % MeOH (% w). Even at the very high concentration of 70 % first order kinetics is still a good assumption but a more pronounced influence of MeOH on the reaction rate was observed. Two phenomena may interfere with the kinetics at the concentration of 70 %:

- k_r includes the contribution from the solubility of CO which is inhibited by the high percentage of MeOH in the liquid mixture. The contribution of ethylene is assumed negligible as it was concluded by other autoclave experiments.
- k_r also includes the contribution of the active catalyst. It is known from early experiments performed at LI (LI Report #88, 2000) that at very high MeOH concentration the activity of the catalyst is adversely affected. Methanol is a polar molecule, a reactant and a solvent in this reaction and it is known from chemistry textbooks that the polarity of the solvent may affect the catalyst activity and/or selectivity (Cornils & Hermann, 2002).

The fact that k_r is practically constant in the range 30-60 % MeOH means that the CO solubility does not affect the rate significantly, at least for the first 30 min of reaction, and the kinetic law equation has the simplified form of a first order reaction with regards to methanol. It is known that the lower the MeOH concentration, the higher the CO solubility in the liquid mixture. Figure 5.18 shows that for MeOH concentration below 30 %, k_r decreases drastically and this might be an indication of CO adversely affecting the reaction rate or maybe a change in reaction mechanism. It should be noted that the findings of the present research agree with earlier experiments described in LI Report #88 where it was concluded that the reaction rate with respect to MeOH is one at concentrations above 20 %. First order reaction with respect to methanol has also been observed for other carbonylation reactions like the methoxycarbonylation of propyne (A. Nakamura & M. Tsutsui, 1980).

5.3.4 CO Series

A series of experiments were conducted at different CO partial pressures ranging from 0.4 bar to 5.95 bar with the purpose of finding the reaction order with respect to CO. The pressure of the autoclave was kept constant at 10 bar above the vapour pressure of the reactants which was approximately 2.2 bar. Thus, the total pressure was kept at 12.2 bar. The pressure was raised above 12.2 bar to 14.2 bar approximately, only for the last experiment at 5.95 bar CO partial pressure (higher partial pressure used). The reason for this was for the ethylene to be at 6.05 bar partial pressure and thus in excess against CO, for consistency with the rest of the experimental data. Table 5.13 lists the experimental conditions:

CO autoclave experiments **Conditions**	
CO partial pressure range	0.4 bar -5.95 bar
Ethylene/CO ratio in the reactor headspace	Variable. Ethylene was making up for the remaining of the total pressure of the gas reacting mixture.
Liquid composition	30 % MeOH, 70 % MeP (w/w)
Temperature	100^{o}C
Pressure	12.2 bar
Pd catalyst concentration	2.4 10^{-5} mol/L
Pd/L2 ratio	1:5
Pd/acid	1:450
Reactor stirrer speed	2000 rpm
Pre-treatment under an ethylene atmosphere at 100^{o}C for 30 min.	YES

Table 5.13. Experimental conditions for the CO autoclave data.

Figure 5.19 and Figure 5.20 show the reaction rate profiles obtained from the various autoclave experiments conducted at low (CO partial pressure 0.4-2.1 bar) and high CO concentrations (CO partial pressure 2.35-5.95 bar).

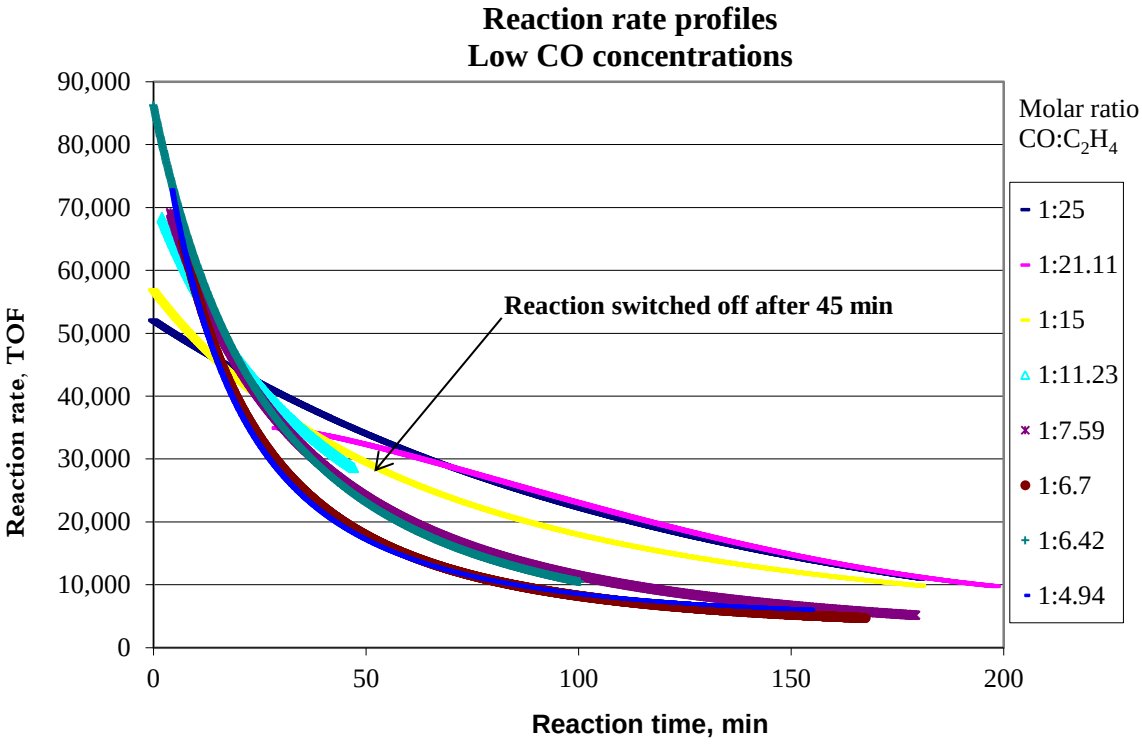

Figure 5.19. Reaction rate profiles for low CO concentration experiments; CO p. pressure 0.4-2.1 bar.

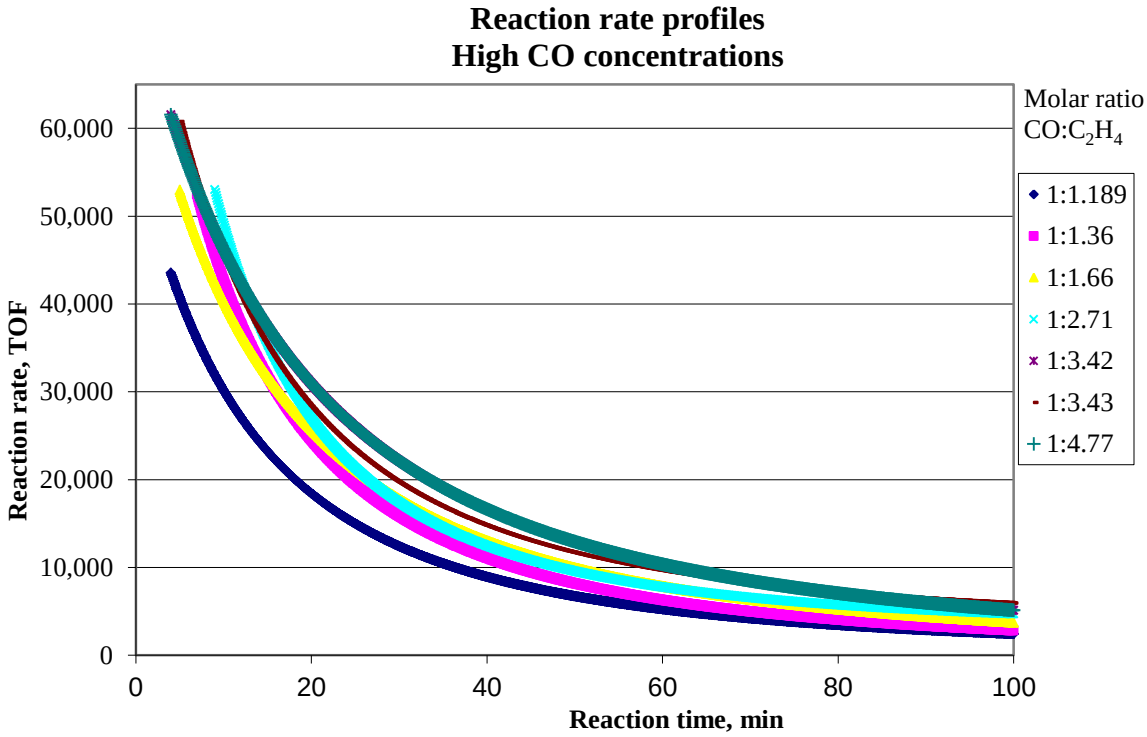

Figure 5.20. Reaction rate profiles for high CO concentration experiments; CO p. pressure 2.1-5.95 bar.

Analysis of the results with the method of Initial Rates showed a shift of the reaction order with respect to CO from positive (+0.4) to negative (-0.9) It must be noted that substrate inhibition kinetics, in detail the shift in CO dependency from positive to negative with maximum obtained at CO partial pressures between 1-2 bar was also noted in past studies conducted by LI (LI report #91, 2000). Figure 5.21 shows a slight scattering of the data at low CO pressures compared to the data obtained at high pressure. However, it can be derived that the order at low pressures is in the range of +0.4 and the shift in the reaction order takes place between 1.75 and 2.1 bar of CO partial pressure. There is a certain degree of uncertainty related to the interpretation of the experimental results obtained from experiments conducted at high CO concentrations. The experiments conducted at 2.35 bar of CO and above

showed an induction time of several minutes (up to 8 min). This can be explained by the fact that CO acts like a ligand and binds to Pd and thus the higher the CO concentration, the higher the amount of catalyst in inactive form and thus the longer it takes for the reaction onset to be recorded. It was mentioned before that one challenge faced by the researchers using the Initial Rates method is to extrapolate the reaction rate to the true $t = 0$ when the reaction started. From Figure 5.22, which depicts the extrapolated rate values to $t = 0$ for experiments conducted above 2.35 bar CO partial pressure, the reaction order was found to be -0.9. It should be mentioned that if the reaction rate data were not extrapolated to $t = 0$, the Initial Rates Method gives a reaction order at high CO partial pressures equal to (-1.5) instead of (-0.9).

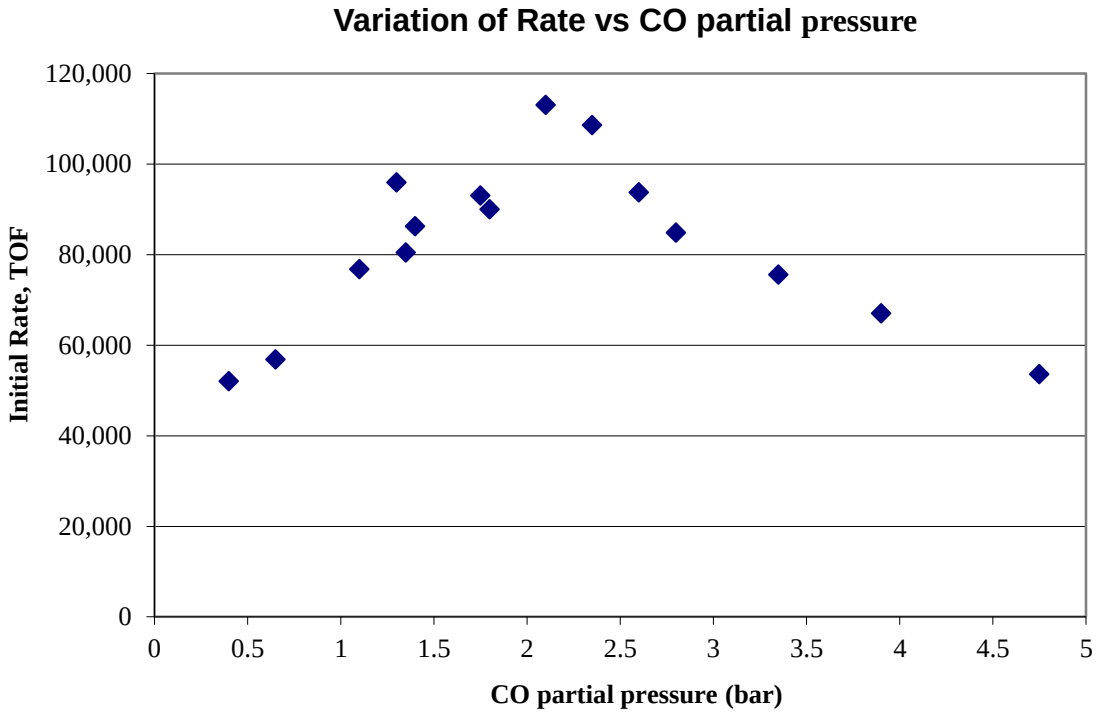

Figure 5.21. Variation of reaction rate with CO partial pressure.

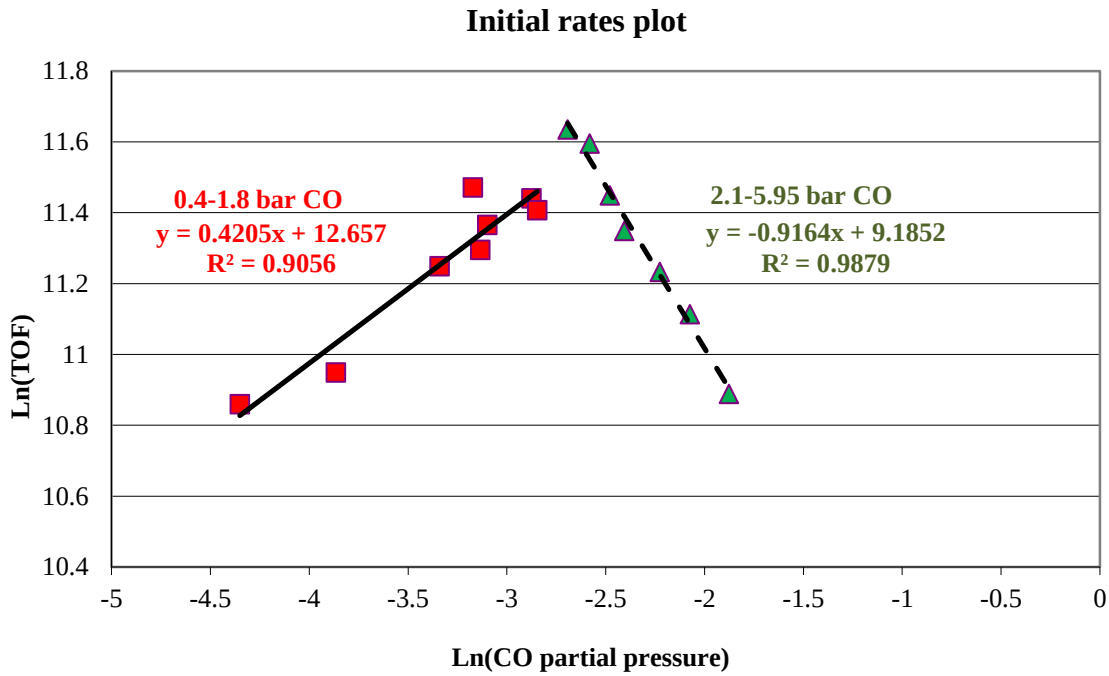

Figure 5.22. Initial rates plot for CO experiments.

Inhibition kinetics for CO and a reaction order which shifts from positive to negative has been observed for other carbonylation reactions (Gavino et al., 2001, Kiss et al., 1999, Divekar et al., 1993, Nakamura & Tsutsui, 1980). The reaction rate initially increases as the CO concentration increases and then it decreases as the CO - a known Pd catalyst poison - becomes abundant in the liquid mixture. Apart from Pd, CO deactivates most low-valent metal complex catalysts like Rh. CO is a strongly coordinating and electron poor molecule which removes the active catalyst from the chemical system by the formation of stable species. According to LI report #91, CO coordinates to Pd and reduces the active form of Pd^{II} to Pd^{0} which is inactive. It was also found that the CO concentration is linked to productivity and small increments in CO concentration decrease significantly the productivity but on the other hand minimum CO concentration leads to the inhibition of the reaction. It was concluded from these experiments that the highest productivity after 4 h of reaction was

obtained at partial pressure equal to 0.5 bar CO and the higher the CO partial pressure above this value the more extensive the catalyst decay.

5.3.5 Ethylene series

A series of experiments were performed in order to determine the partial reaction order with respect to ethylene using the method of initial rates. The experimental conditions used for this series of experiments are included in Table 2.15:

Ethylene autoclave experiments **Conditions**	
CO partial pressure	1 bar
Ethylene partial pressure	Variable in the range [3 bar-9 bar]
Liquid composition	30 % MeOH, 70 % MeP (w/w)
Temperature	100 ^{o}C
Pressure	12.2 bar
Pd catalyst concentration	2.4 10^{-5} mol/L
Pd/L_2 ratio	1:5
Pd/acid	1:450
Reactor stirrer speed	2000 rpm
Pre-treatment under an ethylene atmosphere at 100^{o}C for 30 min.	YES

Table 5.14. Experimental conditions for the ethylene autoclave experiments.

The reaction rate profiles obtained from this series of experiments are included in Figure 5.23. No significant difference can be observed between the various different

reaction rate profiles obtained from experiments conducted at different ethylene concentrations.

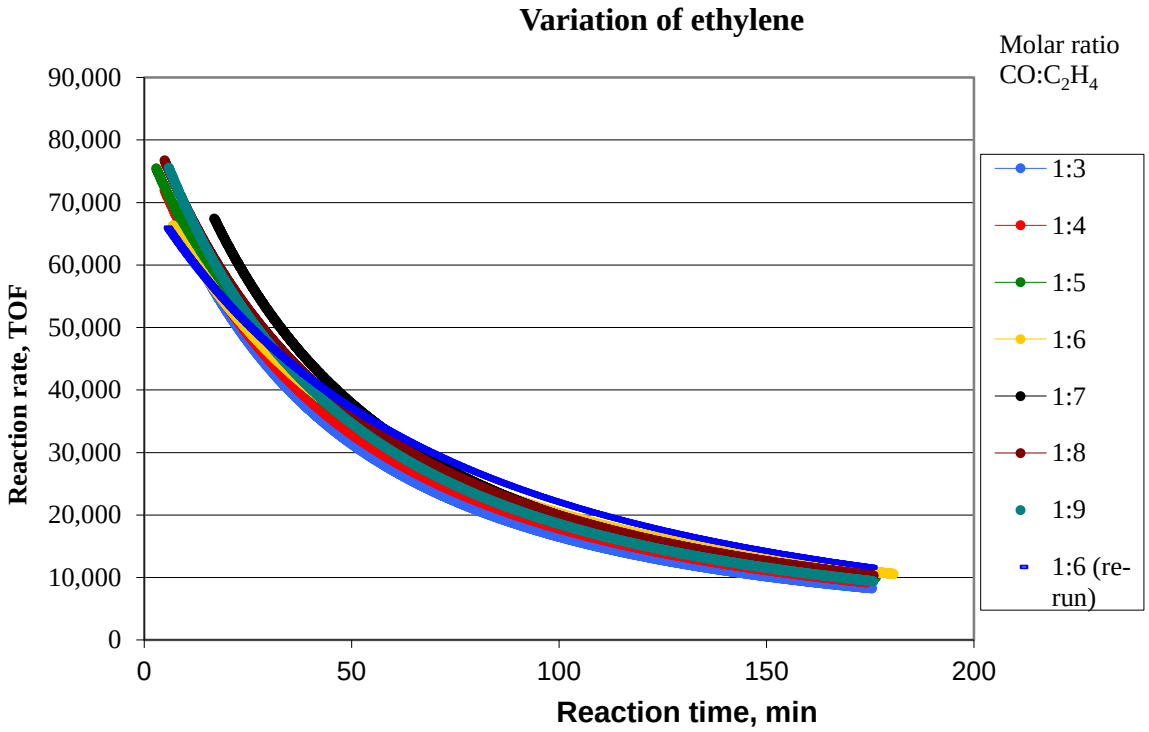

Figure 5.23. Reaction rate profiles for the ethylene autoclave data. The partial pressure of ethylene was varied in the range (3-9 bar) while the CO pressure was kept at 1 bar and the total reactor pressure was 12.2 bar (balance N_2). The liquid mixture concentration was the standard MeP:MeOH=70:30 (% w/w).

Figure 5.24 presents the experimental results analysed by the Initial Rates Method. The increase of the ethylene concentration has only a marginal positive effect on the reaction and the reaction order with respect to ethylene is found to be +0.08. This observation is in line with previous studies by LI conducted prior to 2005 (LI report #89) conducted at similar conditions (CO partial pressure 1 bar, ethylene partial pressure 3-15 bar and temperature 80-110 ^{o}C).

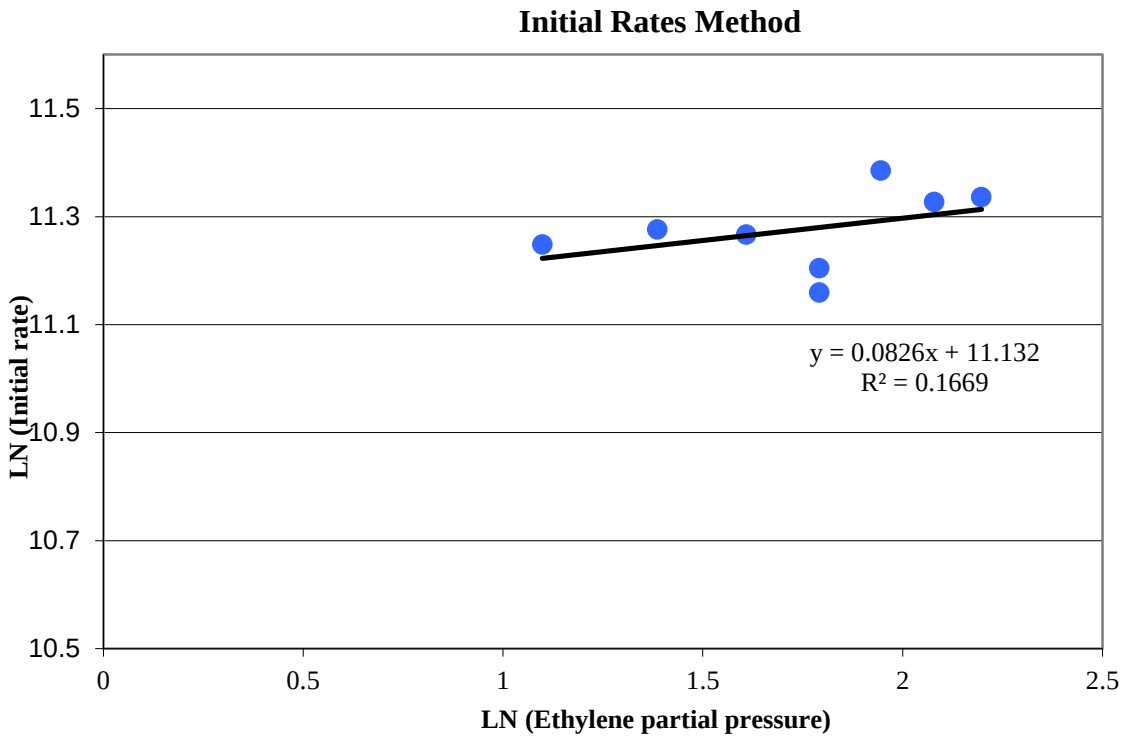

Figure 5.24. Method of initial rates for determination of partial order with respect to ethylene. Only marginal the effect of ethylene on the reaction rate. CO partial pressure 1 bar. Liquid concentration MeOH:MeP=30:70 (% w/w).

5.4 Conclusions

Shedding light on the kinetics of the methoxycarbolylation of ethylene using a Pd homogeneous catalyst based on the 1,2-bis(di-tert-butylphosphinomethyl)benzene ligand is the purpose of this project. The determination of the kinetic law equation of the form:

$$R = f(composition, temperature) \tag{5.10}$$

is the final goal of this research Thesis. Kinetic law equations in homogeneous catalysis are often complex expressions incorporating various constants (kinetic and

equilibrium constants). Early autoclave experiments performed by LI indicated that the same was true for the reaction under study.

An experimental program was developed to determine the apparent reaction orders assuming a power law kinetic equation with respect to the various reactants; methanol, CO, ethylene and the reaction rate constant(s) using an autoclave reactor as these values would provide suggestions on the form that should be assigned to the true kinetic law equation (also suggested as a general methodology by Santacesaria, 1999). The experiments were performed in kinetic regime conditions, that is conditions not affected by diffusional limitations as it was demonstrated theoretically by calculations. In addition, the effect of the reactor agitation speed on the methoxycarbonylation rate was checked to verify the significance of mass transfer effects. It was found that beyond 1750 rpm the rate is independent of the agitation speed. All the experiments were carried out at 2000 rpm to ensure reactor operation in the kinetic regime. Therefore, the data collected were intrinsic kinetic data which can be used for parameter estimation. For the estimation, a theoretically derived model based on the reaction mechanistic scheme will be used to fit the experimental data and find the best fit parameters for the constants appearing in the kinetic law equation. Initial rate data from autoclaves using very similar experimental procedure with the one described in this Chapter have been used to derive empirical kinetic law equations (for example Seayad et al, 1998).

The 2 L autoclave reactor situated at the research facility of LI at Teeside, UK, was used for these experiments which produced very interesting results. The autoclave

operates as a batch reactor with relation to the liquid and as semi-batch with relation to the gas.

The experiments performed in the context of the methanol series showed a first order reaction order with respect to methanol and a pseudo-reaction rate constant k_r =6.85 10^{-5} ± 3.21 10^{-6} s^{-1}. The Integral Method was used in addition to the Initial Rates Method for the analysis of the kinetic data. Both methods produced similar results. The methanolysis step, i.e. the nucleophilic attack of the methanol which yields the ester, is the final step in the catalytic cycle for the methoxycarbonylation of ethylene (detailed explanation was given in Chapter Two, Section 2.2.2) and is presumed to be the rate-determining step. This assumption is verified by the autoclave results showing a first-order reaction with respect to methanol as it is known that nothing can be found on the kinetics of elementary reactions following the rate-determining step (also suggested by Jimenez et al., 2004). Thus, if either the ethylene or the CO addition which precedes methanol addition was the rate-limiting step, the discovery of first order kinetics with respect to methanol would not be possible. In hydroformylation reactions, the nucleophilic agent is H_2 instead of methanol. It was often found that the H_2 addition step is rate-controlling and the reaction is first order with respect to H_2 (for example Divekar et al., 2003).

From the experimental results of the CO series and the analysis previously presented, it can be concluded that the reaction order with respect to CO shifts from positive (+0.4) for CO partial pressures up to 1.75 bar to negative (in the range [-0.9 to -1.5]) for pressures above 2.10 bar. This behaviour has been observed for other

carbonylation reactions[1]. The reaction rate initially increases at low CO concentrations and then it decreases at higher concentrations due to the increased importance of side reactions in which the Pd catalyst reacts with the strongly coordinating and electron poor molecule CO forming inactive species.

The relative scattering of the data at low partial pressures is due to random or systematic experimental errors probably related to the accuracy of the amount of CO initially introduced in the autoclave due to fluctuations of the pressure indicator. In addition, the slight fluctuations of the reactor temperature can influence the reactor pressure and in effect, the correct amount of CO fed to the reactor.

As it was mentioned in the section before, longer induction times were evident with experiments performed under high CO concentration in the reactor head space. In order to obtain the necessary initial rate data for the Initial Rates Method, rate values were extrapolated to t=0. It is not quite clear whether or not the extrapolation to t=0 was necessary. Furthermore, the extrapolation introduces a factor of objectivity related to the amount of data required for this procedure. Extrapolation or not produces different results; reaction order with respect to CO, (-0.9) or (-1.5).

Ethylene was found to have only a marginal effect on the reaction rate and the partial reaction order was derived to be (+0.08), showing practically a zero-order reaction, using the Initial Rates Method. The carbonylation of styrene with the homogeneous $Pd(OAc)_2/PPh_3$/*p*-toluenesulfonic acid catalytic system studied by Seayad et al.

[1] For example Deshpande & Chaudhary, 1998 and Divekar et al., 1993, Jaurequi-Haza et al., 2003, Kiss et al., 1999, Nakamura et al. , 1980.

(1998) also concluded zero-order with respect to the styrene. Studies of kinetics of other carbonylation or hydroformylation reactions have shown various behaviours; first order, zero order or substrate inhibition kinetics depending on the chemical system and the experimental conditions.

Pre-treatment of the liquid mixture fed to reactor at 100 ^{o}C for 30 min under an ethylene atmosphere prior to reactor initiation seemed to have a positive contribution to the reaction rate as it increased the product yield and reduced the induction time. There is supporting evidence that pre-treatment at 50 ^{o}C could be effective in reducing the induction time by even halving it and in improving the initial reaction rate by almost 20 %. However, these results were not conclusive because of inexplicable discrepancies between results obtained from runs performed under identical conditions. The findings suggest that pre-treatment with ethylene makes a difference at the initial stages of the reaction pushing the equilibrium of the formation of the alkyl catalytic intermediate far to the right in equation 5.11 (also please refer to Chapter Two, Section 2.2.2) and thus, enabling a speeding up of the reaction rate once CO is introduced into the system. This is evident by a noticeable faster formation of MeP which is produced after a series of elementary steps; ethylene addition, CO addition and methanolysis.

$$(L-L)Pd(H)]^{+} + CH_2 = CH_2 \xleftrightarrow{K_5} (L-L)Pd(CH_2CH_3)]^{+} \qquad (5.11)$$

Currently, pre-treatment at 100^{o}C is the established practice when one performs autoclave experiments at Lucite International based on the conclusions of past experimental study by LI. The results depicted in this Thesis do not substantiate a modification in the standard practice.

--//--

CHAPTER 6

Mesh Microreactors and other Reactor Trials

This Chapter describes the work done with microreactors, the largest part dedicated to mesh microreactors, with the purpose on one hand to assess their suitability as tools for this kinetic study and on the other hand to test the bespoke experimental set-up. A novel mesh microreactor was designed and developed using a unique microfabrication process, and with much smaller characteristics in terms of channel sizes, liquid volume and pore size compared to previous research found in the literature. This Chapters starts by presenting the calculations forming the basis behind the design and then depicts the detailed path followed to the development of the final reactor design. Experimental work is presented next and results are illustrated. Unfortunately, pressure testing of the mesh reactor revealed that is not suited for purpose under reaction conditions at 10 bar pressure and 100 ^{o}C temperature. The second part of this Chapter explains the trial runs using two different types of reactors; the CRL mesh reactor and the Micronit channel reactor. Detailed illustration of these microreactors is provided first, followed by the description of the experimental work conducted. Although most of these attempts did not bear any fruit for a number of reasons explained in the last sections of the Chapter, valuable insight into the chemistry of the system was obtained and the functionality of custom-built rig was proven.

6.1 Mesh Microreactor- Theoretical

6.1.1 Calculations of the Diffusion Time

Where reactions are mass transfer limited there is scope of increasing rates by constraining reactant fluids to microdimensions. Generally, a purely diffusive process will be near complete in time *t* if $D \cdot t / l^2 > 1$ where *D* is the diffusion coefficient and *l* is the distance the material has to travel. For small molecules (molecular weight <500) in liquids, concentration gradients across a layer of 100 μm thickness are usually removed by diffusion in less than 30 s (Kulkarni et al., 2007). Indeed, in the mesh microreactor developed here, as the diffusive distance is only 120 μm, diffusion is complete in less than 8 s as it is shown below.

The diffusion time for the CO is given by:

$$t_D = \frac{l^2}{D_{C2H4}} = (1.2 \times 10^{-4}\text{m})^2 / 1.87 \times 10^{-9}\text{m}^2/\text{s} = 7.7 \text{ s}.$$

The diffusion time for the ethylene is calculated as previously done for the CO:

$$t_D = \frac{l^2}{D_{C2H4}} = (1.2 \times 10^{-4}\text{m})^2 / 0.95 \times 10^{-8}\text{m}^2/\text{s} = 1.5 \text{ s}.$$

6.1.2 Determination of the Maximum Acceptable Depth of the Liquid Channel

The prerequisite for the liquid channel is an approximately flat gas concentration profile. This means that the gas concentration should not drop below 95% of the concentration at the interface. A maximum depth of 143 μm was determined by the calculations shown in the next few pages. The gas concentration profile in the liquid is given in the following Figure.

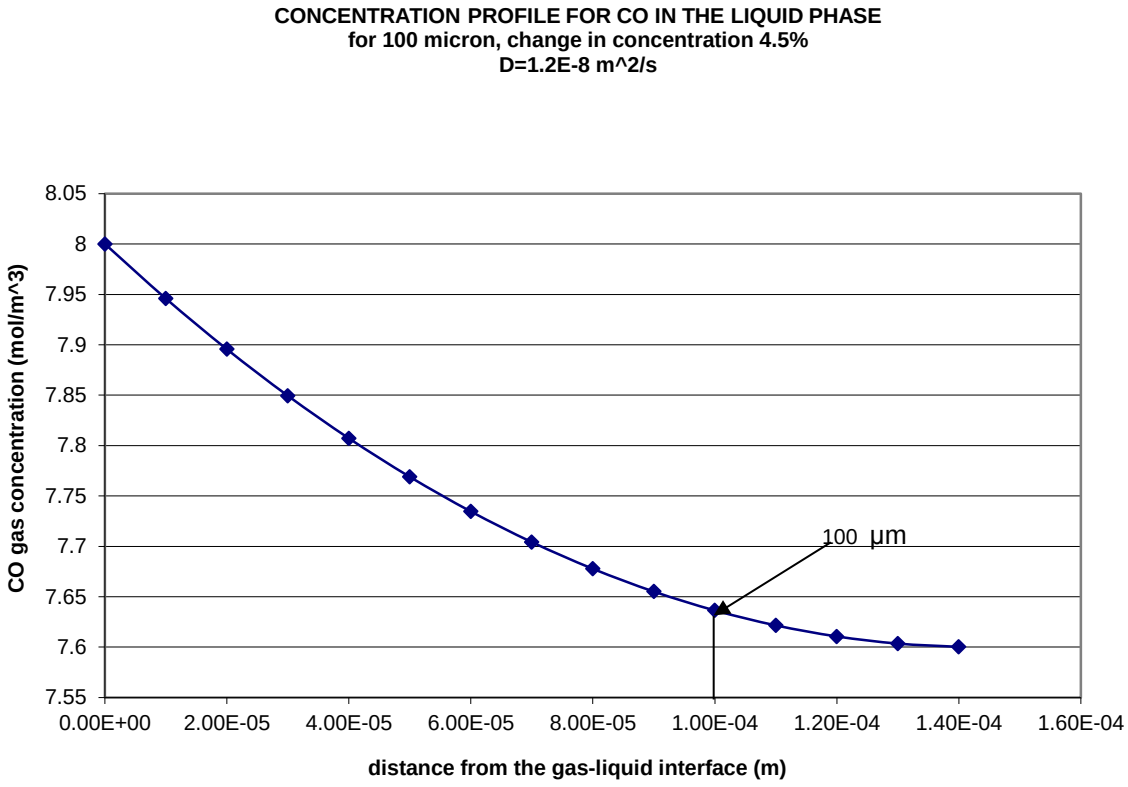

Figure 6.1. CO concentration profile in the liquid phase.

Detailed calculations in the liquid layer

Steady state operation is assumed.

The diffusion equation for a *n*-order reaction is:

$$\frac{d_{C_A}^2}{d_y^2} - \kappa C_A^n = 0 \qquad (6.1)$$

If the reaction is assumed to be first order, n=1, and the diffusion equation becomes:

$$\frac{d_{C_A}^2}{d_y^2} - \kappa C_A = 0 \qquad (6.2)$$

Equation (6.2) can be integrated using the appropriate boundary conditions.

From Coulson & Richardson (1999), equation (6.2) has the solution:

$$C_A = B_1' \cdot e^{\sqrt{\left(\frac{\kappa}{D}\right)}y} + B_2' \cdot e^{\sqrt{\left(\frac{\kappa}{D}\right)}y} \qquad (6.3)$$

D: is the diffusion coefficient

y: distance from the gas/liquid interface

C_A: concentration of gas *A* in the liquid.

B_1' and B_2' are parameters to be evaluated using the appropriate boundary conditions:

First boundary condition is that the concentration of gas at the gas-liquid interface is equal to the equilibrium concentration:

For $y=0 \rightarrow C_A = C_{A_i}$

Equation (6.3) then becomes:

$$C_{A_i} = B_1' + B_2' \Leftrightarrow B_2' = C_{A_i} - B_1' \qquad (6.4)$$

Second boundary condition is that at the bottom of the channel (distance from the gas-liquid interface is equal to L_c), the concentration of gas is equal to C_{A_0} :

For $y=L_c \rightarrow C_A = C_{A_0}$ and $\frac{d_{C_A}}{dy}|_{y=L_c} = 0$.

Substitution in equation (3) gives:

$$C_{A_0} = B_1' \cdot e^{\sqrt{\frac{\kappa}{D_c}}L_c} + B_2' \cdot e^{-\sqrt{\frac{\kappa}{D_A}}L_c}$$

After substituting B_2' from equation (6.4), we obtain:

$C_{A_0} = B_1' \cdot e^{\sqrt{\frac{\kappa}{D}}L_c} + \left(C_{A_i} - B_1'\right) \cdot e^{-\sqrt{\frac{\kappa}{D_A}}L_c}$ and after rearranging:

$$B_1' = \frac{C_{A_0} \cdot e^{\sqrt{\frac{\kappa}{D}}L_c} - C_{A_i}}{e^{2\sqrt{\frac{\kappa}{D}}L_c} - 1} \tag{6.5}$$

From equation (6.4), B_2' becomes:

$$B_2' = \frac{C_{A_i} \cdot e^{2\sqrt{\frac{\kappa}{D}}L_c} - C_{A_0} e^{\sqrt{\frac{\kappa}{D}}L_c}}{e^{2\sqrt{\frac{\kappa}{D}}L_c} - 1} \tag{6.6}$$

From equation (6.3) we get:

$$\frac{dC_A}{dy} = \sqrt{\frac{\kappa}{D}} \cdot B_1' \cdot e^{\sqrt{\frac{\kappa}{D}}y} - \sqrt{\frac{\kappa}{D}} \cdot B_2' \cdot e^{-\sqrt{\frac{\kappa}{D}}y} \tag{6.7}$$

After applying the second boundary condition $\frac{d_{C_A}}{dy}|_{y=L_c} = 0$, we obtain:

$$B_1' \cdot e^{\sqrt{\frac{\kappa}{D}}L_c} - B_2' \cdot e^{-\sqrt{\frac{\kappa}{D}}L_c} = 0 \Leftrightarrow e^{2\sqrt{\frac{\kappa}{D}}L_c} = \frac{B_2'}{B_1'} \tag{6.8}$$

$$e^{2\sqrt{\frac{\kappa}{D}}L_c} = \frac{C_{A_i} e^{2\sqrt{\frac{\kappa}{D}}L_c} - C_{A_0} e^{\sqrt{\frac{\kappa}{D}}L_c}}{C_{A_0} e^{\sqrt{\frac{\kappa}{D}}L_c} - C_{A_i}} \Leftrightarrow e^{\sqrt{\frac{\kappa}{D}}L_c} = \frac{C_{A_i} e^{\sqrt{\frac{\kappa}{D}}L_c} - C_{A_0}}{C_{A_0} e^{\sqrt{\frac{\kappa}{D}}L_c} - C_{A_i}} \Leftrightarrow$$

$$\Leftrightarrow C_{A_0} e^{2\sqrt{\frac{\kappa}{D}}L_c} - 2C_{A_i} e^{\sqrt{\frac{\kappa}{D}}L_c} + C_{A_0} = 0 \Leftrightarrow e^{2\sqrt{\frac{\kappa}{D}}L_c} - 2\left(\frac{C_{A_i}}{C_{A_0}}\right) \cdot e^{\sqrt{\frac{\kappa}{D}}L_c} + C_{A_0} = 0 \qquad (6.9)$$

By substituting $e^{\sqrt{\frac{\kappa}{D}}} = \psi$, we get:

$$\psi^2 - 2\left(\frac{C_{A_i}}{C_{A_0}}\right) \cdot \psi + 1 = 0 \qquad (6.10)$$

$$\Delta = 4 \cdot \left(\frac{C_{A_i}}{C_{A_0}}\right)^2 - 4$$

For $C_{A_i} = 8$ mol m^{-3} and $C_{A_0} = 0.95 \cdot C_{A_i}$ =7.6 mol m^{-3}, we calculate that

$$\Delta = 0.432 \Rightarrow \sqrt{\Delta} = 0.657$$

The solution of equation (6.10) is:

$$S_{1,2} = \frac{2\left(\frac{C_{A_i}}{C_{A_0}}\right) \pm \sqrt{\Delta}}{2} = \frac{2(0.95) \pm 0.657}{2} =$$

1.381, solution accepted

0.724, solution rejected

Thus, $e^{\sqrt{\frac{\kappa}{D}}L_c} = \psi = 1.381 \Rightarrow L_c = \frac{LN(\psi)}{\sqrt{\frac{\kappa}{D}}}$ (6.11)

After substitution of the values:

$\kappa = 0.061\,\text{s}^{-1}$

D=1.2 10^{-8} m^2 s^{-1}

Then, $\sqrt{\frac{\kappa}{D}}$ =2.25 10^3 m^{-1}.

Subsequently, L_c is calculated as:

L_c=143 10^{-6} m or L_c=143 μm.

Hence, the depth of the liquid channel for a 5 % drop in gas concentration as compared to the concentration at the gas-liquid interface is 143 μm.

Due to the very small thickness of the mesh (1.2 μm) and if the gas concentration at the gas-liquid interface inside the pores is C^*, the calculated concentration right below the mesh from Figure 6.1 was found to be C^*_{below}=0.992 C^*. A schematic of the flow inside the liquid channel is shown subsequently:

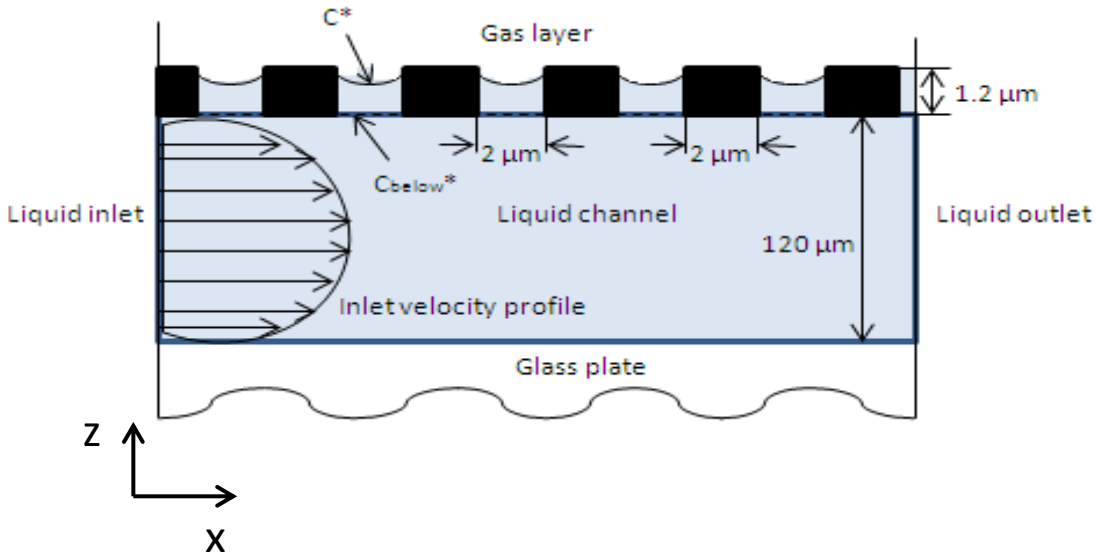

Figure 6.2. Schematic of the flow inside the liquid channel.

6.1.3 Estimation of the Breakthrough Pressure

The critical issue in operating the mesh microreactor is the maintenance of the gas/liquid interface. In general, when we have two immiscible phases which we call non-wetting and wetting phases or P_{NW} and P_W respectively flowing on the sides of a mesh (refer to Figure 6.3), the interface is stabilised in the pores as long as the transmembrane pressure does not exceed a ΔP given by:

$$P_{NW} - P_W = \Delta P = \frac{2\gamma \cos\theta}{r} \tag{6.12}$$

This equation is valid for cylindrical capillaries in the absence of gravity.

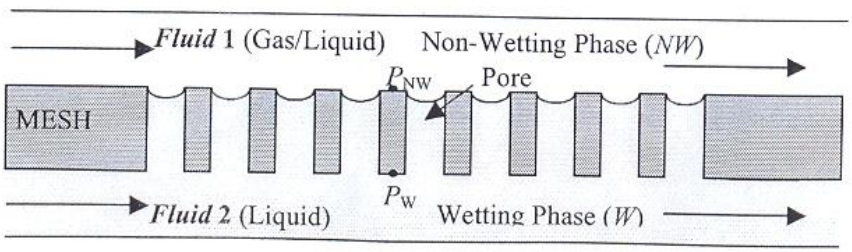

Figure 6.3. Schematic Diagram of a mesh microreactor (Amador et al., 2005).

In the present case P_{NW} is the gas phase (CO, ethylene) while the P_W is the liquid phase (MeP/ MeOH). θ is the contact angle, γ is the surface tension of the liquid and r is the radius of the pores.

In order to find the contact angle θ wetting experiments were conducted with the following procedure;

1. Try to form drops of the reaction mixture MeP/ MeOH 70:30 with methanosulphonic acid on a piece of silicon nitride (Si_3N_4).

2. Take photographs of the drops by a camera that had been set-up for this purpose.
3. Measure with an angle meter the contact angle θ between the liquid and the silicon nitride.

The same method was used to find the contact angle between the liquid and a piece of nickel.

The result was that no drops could be formed either on the Si_3N_4 piece or on the Ni piece. This means that θ is zero and both materials show complete wettability.

Since $\theta = 0, \cos\theta = 1$. From the Laplace equation is derived that the bigger the pores, the more difficult is to maintain the pressure. For the chosen 2 μm pores (diameter) $r = 1$ μm.

In order to estimate the remaining parameter, the surface tension, the Detherm Database was utilised:

For MeOH at 373 K the surface tension was given as 0.0157 N/m.

For MeP, the following data were obtained:

- At T=351 K the surface tension was 0.0172 N m^{-1};
- At T=333 K the surface tension was 0.0195 N m^{-1}.

With extrapolation, the surface tension is calculated at T=373 K equal to 0.0144 N m^{-1}.

By using the formula obtained from Perry's Chem. Eng. Handbook:

$\gamma = \sum \chi_i \gamma_i$ we find:

γ =0.3 x 0.0157+0.7 x 0.0144=0.0148 N m^{-1}

Finally, from the Laplace equation we obtain ΔP =296 mbar. This means that if the pressure difference between the two sides of the membrane increases more than 296 mbar (higher pressure would be on the gas side), the gas will break into the liquid. However, this is only an estimate because researchers have reported deviations from the breakthrough pressure predicted (Amador et al., 2005). Nevertheless, the small allowed ΔP set the requirement for a good pressure control system.

6.1.4 Calculation of the Strength of a Membrane

The maximum allowed transmembrane pressure is given by the formula (Kuiper et al., 1998):

$$P_{\max} = 0.58 \frac{h \cdot \sigma^{\frac{3}{2}}}{l E^{\frac{1}{2}}} \tag{6.13}$$

where h is the membrane thickness, σ is the yield stress of the membrane material, l is the distance between the support bars and E is the Young's Modulus of the material.

For the case of a membrane with a porosity k %, the above formula is slightly altered:

$$P'_{\max} = 0.58 \frac{h \cdot \sigma^{\frac{3}{2}}}{l E^{\frac{1}{2}}} k^{\frac{1}{2}} \tag{6.14}$$

For example for a membrane with porosity 25 % the strength of the perforated membrane is half of the imperforated one.

Symbol	Parameter	Units	Value
σ	Yield stress	Pa	$4.0\ 10^{9}$
h	Membrane thickness	m	$1.0\ 10^{-6}$
l	Distance between support bars	m	$1.0\ 10^{-4}$
l	Distance between support bars	m	$2.0\ 10^{-4}$
E	Young's modulus	Pa	$2.9\ 10^{11}$
k	Membrane porosity	%	30
Calculation of membrane strength for distance between support bars l=1.0 10^{-4} m			
Symbol	**Parameter**	**Unit**	**Value**
P_{max}	Strength of imperforated membrane	Pa	$2.72\ 10^{6}$
P_{max}	Strength of imperforated membrane	bar	27.2
P'_{max}	Strength of perforated membrane	bar	14.9
$\frac{P'_{max}}{P_{max}}$	Ratio of strength (perforated/imperforated membrane)		0.55
Calculation of membrane strength for distance between support bars l=2.0 10^{-4} m			
P_{max}	Strength of imperforated membrane	Pa	$2.72\ 10^{6}$
P_{max}	Strength of imperforated membrane	bar	13.6
P'_{max}	Strength of perforated membrane	bar	7.5
$\frac{P'_{max}}{P_{max}}$	Ratio of strength (perforated/imperforated membrane)		0.55

Table 6.1a. Calculation of the membrane strength for the support bars (a) 100 μm and (b) 200 μm apart.

6.1.5 Calculation of the Pressure Drop across the Liquid Channel

Table 6.1 shows the calculation of the pressure drop in a serpentine channel with rectangular cross section 200 μm x 120 μm.

Calculation of pressure drop along a serpentine channel with rectangular cross section 200μm x 120μm. Size of the microreactor chip 3cm x 3cm.

Symbol	Parameter	Units	Value
e_c	Depth of channel	m	120 10^{-6}
w_c	Width of channel	m	200 10^{-6}
$A = e_c \cdot w_c$	Cross sectional area of channel	m^2	2.40 10^{-8}
$D_h = \frac{4A}{(2e_c + 2w_c)}$	Hydraulic diameter of channel	m	150 10^{-6}
Total volume of the microreactor chip	Volume of the 3 cm x 3 cm chip and the depth of channel is 120 μm	m^3	0.03*0.03*0.00012= =10.80 10^{-8}
$V_{serpentine}$	Effective volume of serpentine channel calculated from the actual mesh area of the microreactor of 1.5cm x 1.5 cm and the depth of channel is 120 μm	m^3	0.015*0.015*0.00012= =2.70 10^{-8}
q_{min}	Minimum flow rate – Equipment specifications	μl min^{-1}	1.5
q_{max}	Minimum flow rate – equipment specifications	μl min^{-1}	6.0
$L_{serpentine} = V_{serpentine}/(e_c \cdot w_c)$	Estimation of length of serpentine channel	m	1.125
$N_o = L_{serpentine}/(0.85 \cdot w_c)$	Number of short channels completing the serpentine if 85 % of the width of the 3cm chip is used to etch the channels	-	45

Calculation of pressure drop along a serpentine channel with rectangular cross section 200μm x 120μm. Size of the microreactor chip 3cm x 3cm.- *Continued…*			
Symbol	**Parameter**	**Units**	**Value**
$L_{serpentine} = V_{serpentine}/(e_c \cdot w_c)$	Estimation of length of serpentine channel	m	1.125
$N_o = L_{serpentine}/(0.85 \cdot w_c)$	Number of short channels completing the serpentine if 85 % of the width of the 3cm chip is used to etch the channels	-	45
ρ_L	Density of multiphase volume	Kg m^{-3}	777
μ_L	Liquid viscosity	Pa s	$2.20\ 10^{-4}$
D	Diffusion coefficient of CO in the liquid	$m^2\ s^{-1}$	$1.20\ 10^{-8}$
$u = q/A$ for $q = q_{\max}$	Velocity of liquid in serpentine	m s^{-1}	$4.17\ 10^{-3}$
$\mathrm{Re} = \frac{\rho_L u D_h}{\mu_L}$	Reynolds number	-	1.77 → The flow is laminar
$\frac{e_c}{w_c}$	Ratio depth/width of channel		0.6
$\lambda_{nc} = \frac{3/2}{(1-0.351*(e_c/w_c))^2(1+(e_c/w_c))^2}$	Non-circularity coefficient		0.94
$\Delta P = \frac{128 \cdot \mu_L \cdot L_{serpentine} \cdot q_{ave}}{\lambda_{nc} \cdot \pi \cdot D_h^4}$ $q_{ave} = \frac{q_{\min} + q_{\max}}{2}$	Hagen-Poiseuille equation for fully developed flow in circular and long channels (length of channel>>channel diameter) corrected with the non-circularity coefficient. Flow is assumed fully formed.	Pa	1379
ΔP		bar	0.01379

Table 6.1. Calculation for the pressure drop in the liquid channel. The non-circularity coefficient is defined as: $\lambda_{nc} = \frac{3/2}{(1-0.351*(e_c/w_c))^2(1+(e_c/w_c))^2}$ **for e/w<1. If e/w >1 then it is replaced by w/e (Commenge et al, 2002).**

Thus, the pressure drop along the liquid channel is estimated at 13.8 mbar.

6.1.6 Proposed Designs for the Mesh Microreactor

After the main calculations were complete, the next task was the design of the mesh microreactor. In the framework of this work, an initial microreactor design was proposed by Aquamarijn Ltd (a microfabrication company based in the Netherlands) that comprised eight microfabrication steps.

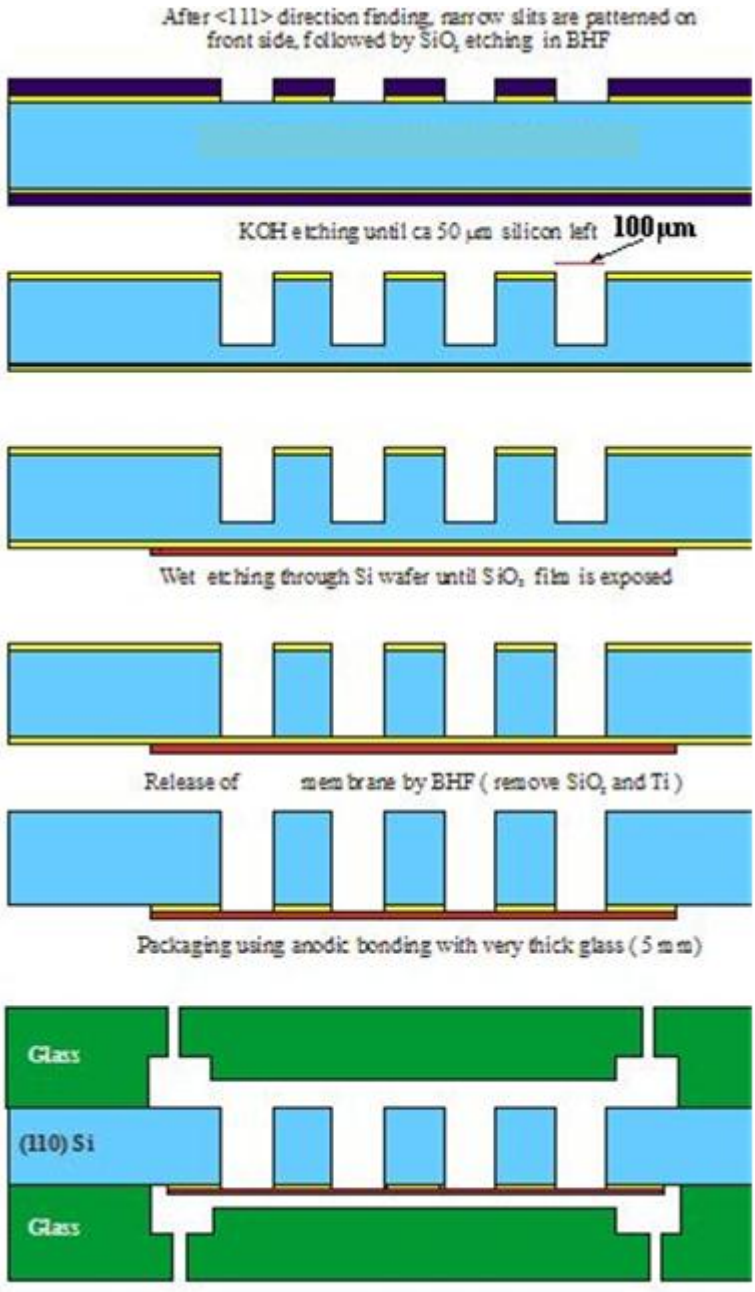

Figure 6.4. Schematic of the initial proposal regarding the microfabrication process. Blue is the <110> Si, yellow is the SiO_2, red is the Si_3N_4 and green is the glass. Design by Aquamarijn Ltd.

The microfabrication sequence would be as follows:

1. Thermal growth of silicon dioxide ($SiO_{2)}$ and deposition of silicon nitride (Si_3N_4) on a Si wafer .
2. Pattern the membrane pores with standard photolithography.
3. Transfer the pattern onto the silicon nitride using wet etching (buffered oxide etch otherwise known as buffered HF or BHF).
4. Etch the Si with KOH etching from the other side of the wafer all the way through until the silicon dioxide layer is exposed.
5. Release the membrane by etching the silicon dioxide with BHF through the pores of the membrane.
6. Etch the liquid channel on a glass plate using powder blasting.
7. Etch the gas channel on another glass plate using powder blasting.
8. Sandwich the membrane between the two etched glass plates to make a solid structure by means of four-electrode anodic bonding.

The above proposal was unsuitable for the current application because the KOH etching would not produce the desired result of the gas and the liquid channels mirroring each other. Hence, the initial design was changed and two possibilities resulted from this process:

Design 1

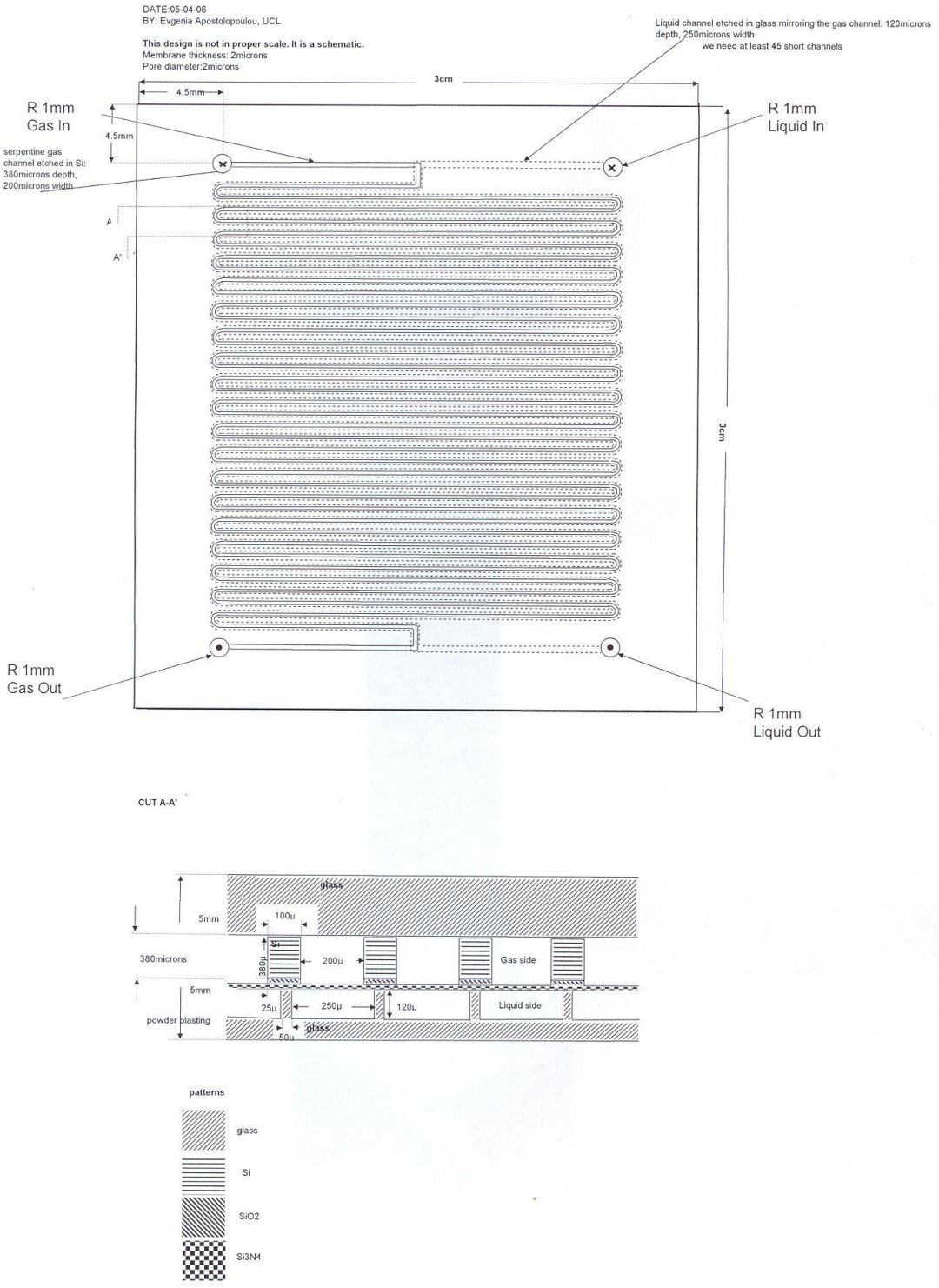

Figure 6.5. Microreactor design No 1. Design by Evgenia Apostolopoulou, 2006, UCL.

The microfabrication process would entail the following steps:

1. Thermal growth of SiO_2 and deposition of Si_3N_4 on a Si wafer.
2. Pattern the membrane pores with standard photolithography.
3. Transfer the pattern onto the silicon nitride with plasma etching.
4. Etch the Si with Deep Reactive Ion Etching (DRIE) from the other side of the wafer all the way through until the silicon oxide layer is reached. In this way the gas channel will be created.
5. Release the membrane by etching the silicon dioxide with BHF through the pores of the membrane.
6. Etch the liquid channel on a glass plate using powder blasting. The liquid channel will mirror the gas one.
7. Sandwich the membrane between the etched and another glass plate to make a solid structure by means of four-electrode anodic bonding.

The main differences between this design and the previous one proposed by Aquamarijn Ltd (Figure 6.4) was the use of plasma etching instead of BHF to transfer the pore pattern on the silicon nitride and secondly, the etching of the Si wafer would be accomplished via DRIE instead of KOH etching which would result in a gas channel with vertical walls mirroring the liquid one. Other differences were the dimensions of the gas and liquid channels. The micromesh would be similar to:

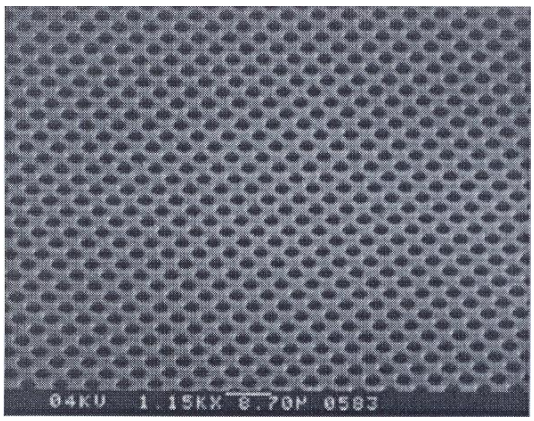

Figure 6.6. SEM photo of a Silicon Nitride microsieve (Kuiper et al., 1998).

Design 2

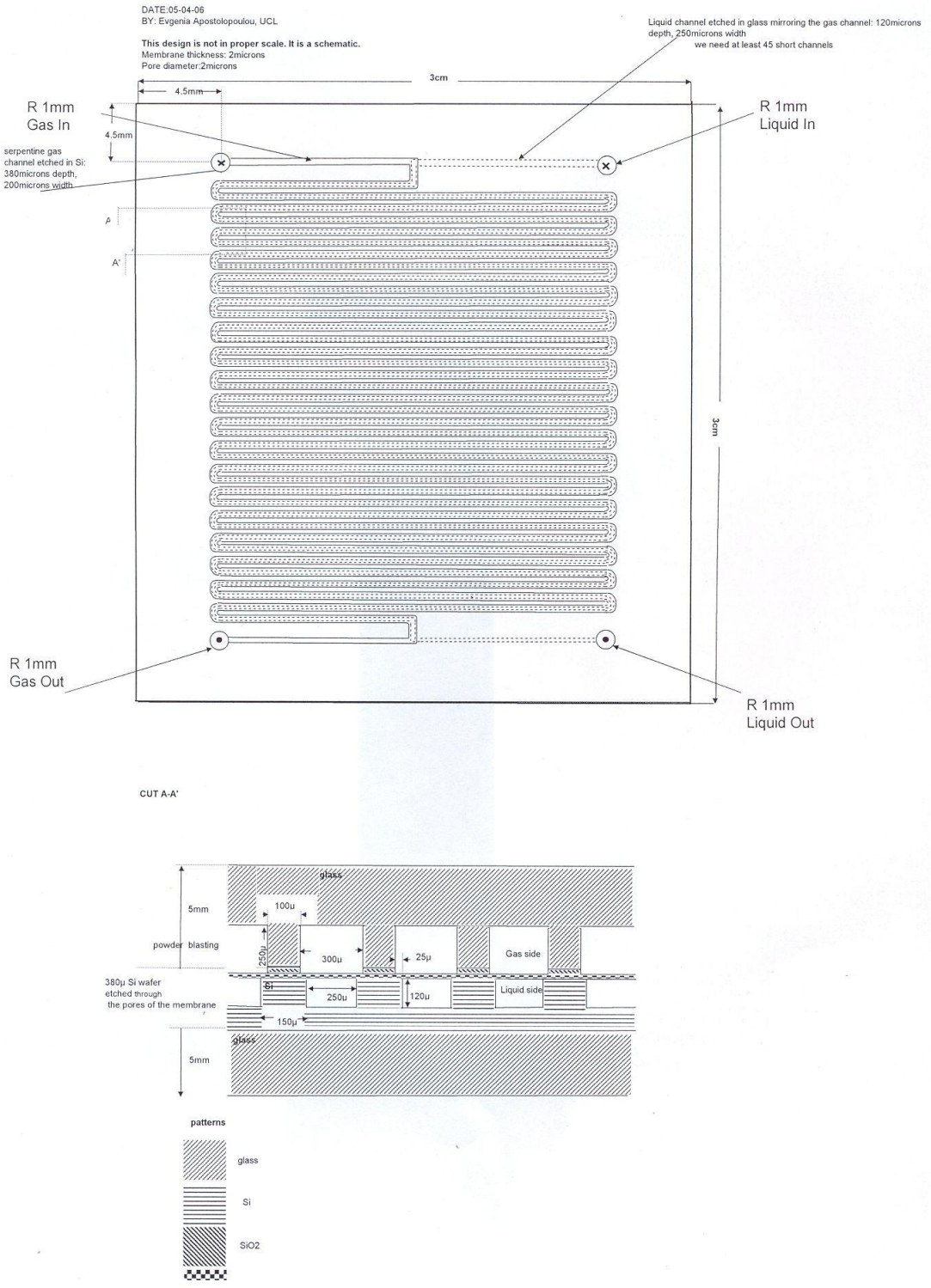

Figure 6.7. Microreactor design No2. Design by Evgenia Apostolopoulou 2006 UCL.

The microfabrication process would involve these steps in sequence:

1. Thermal growth of SiO_2 and deposition of Si_3N_4 on a Si wafer .
2. Pattern the membrane pores with standard photolithography.
3. Transfer the pattern onto the silicon nitride with plasma etching.
4. Etch the Si with plasma etching through the pores of the membrane to create the liquid channel.
5. Etch the gas channel on a glass plate by powder blasting. The gas channel will be mirroring the liquid channel.
6. Sandwich the membrane between the etched and another glass plate to make a solid structure by means of four-electrode anodic bonding.

The main difference between this design and the previous one (Figures 6.5) was to create the liquid channel in Si and the gas channel using powder blasting of a glass plate instead of the other way around. Other differences were the dimensions of the gas and liquid channels.

6.1.7 Microreactor Characteristics and Requirements

Table 6. 2 lists all the desired characteristics of the mesh microreactor.

Characteristic	Value	Remarks
Pore size (μm)	2	Small pores help avoid breakthrough of one phase into the other. Too small pores (<1 μm) are more expensive to fabricate.
Membrane thickness (μm)	1	From previous experience this thickness will withstand the pressure of 13 bar. Small thickness for fast diffusion of gas into the liquid. Too large thickness might cause the pores to behave like short channels which is undesirable. Too thin membrane compromises strength and makes maintenance of the gas-liquid interface difficult.
Porosity (%)	30	25-30% is typical for those membranes.
Operating pressure(bar)	12 bar	The design pressure wouldl be 20 bar.
Pore walls	vertical	
pitch	1:1	Typical value.
Material for the membrane	Silicon nitride	Strong, chemically inert, environmental friendly. It is an important material in microfabrication. Membranes with this kind of material have been successfully fabricated previously.

Table 6. 2. Micromesh requirements.

After several communications between UCL and Aquamarijn, Design No 1 was chosen as the one to be made. The reason for this was that Aquamarijn had enough experience and expertise with similar designs to No1 and consequently the

manufacturing process would have been shorter. A few changes were made in the initial design as requested by the manufacturer. The first one was that the width of the supporting walls in the liquid side will be 75 μm instead of 50 μm due to the tolerance of the powder blasting process. Another change was that the thickness of the silicon nitride film was going to be 1.2 μm instead of 2 μm in order to avoid the formation of internal stresses frequent in the thick films. Furthermore, the increased thickness to 2 μm would not add to the mechanically strength of the membrane as initially thought. The final design of the microreactor cross section is shown in Figure 6.8.

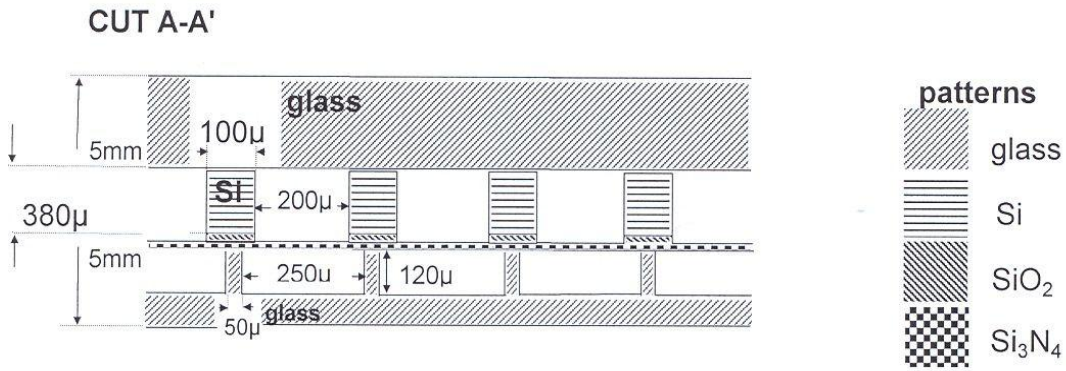

Figure 6.8. Final microreactor design. by Evgenia Apostolopoulou, 2006, UCL

Finally, the thickness of the glass plates bonded on either side of the silicon wafer would have a width of 1 mm instead of 5 mm due to limitations of the wafer handling equipment at Aquamarijn Ltd.

6.1.8 Problems Encountered during Manufacturing

The initial promised delivery time was greatly exceeded for reasons concerning mainly unforeseen problems that occurred during the manufacturing process due to the novelty of the process:

- **Beam buckling**: for the first fabrication batch, the channels were dry etched and because the channels were long, they were buckling and causing breakage of the silicon nitride membrane. During the second attempt, the manufacturers at Aquamarijn Ltd etched almost through the silicon wafer, they then patterned the membrane from the other side of the channels before bonding it with the glass wafer. When they tried to do dry etching to release the channels, they discovered that the process would not work due to unstable temperature at the back of the wafer. The problem was solved by adding five support walls (partially etched silicon) on the silicon side.
- **Low yield**: one defect on the glass wafer or the silicon wafer makes the wafer obsolete. Therefore, they had to process several wafers in order to manufacture four reactors.
- **Dicing machine**: The maximum thickness of the substrate that the machine could handle was 2 mm. Initial plans of using 1 mm thick glass on both sides of the wafer were abandoned after it was discovered that the dicing machine was not working properly. Aquamarijn resorted in using only 0.5 mm thick glass for both sides. At this point concerns were expressed regarding the mechanical strength of the microreactors as the 0.5 mm glass was very thin.
- **Masks change**: Even though it had been specified according to the final design (please refer to Figure 6.5) that the four inlet-outlet ports must be on

the top side (gas side), Aquamarijn altered the design and placed two ports on either side of the microreactor. Once this was realised, demands were made for the design to be changed back to the original because otherwise the microreactor holder as well as the microreactor heating system would not be suitable.

6.1.9 Channel Characteristics and Changes of the Original Design

Gas (silicon) serpentine channel

- Even though the design was for a width of 200 μm, the dry etching procedure produced 215 μm possibly due to the 2% lateral etching of approximately 7 μm at each side of the channels.
- The depth was 370 μm which is basically the depth of the silicon wafer.
- The length was as follows:
  - 52 sections, 23.6 mm length each.
  - 6 sections of 18.4 mm length each
  - 2 short channels of 10 mm length each. No sieves were patterned for these channels as they were just for inletting purposes. In this way, the fluids would travel a short distance before they came into contact which according to Aquamarijn's previous experience proved to be beneficial.

Liquid (glass) serpentine channel

- The width is 250 μm. In the original design it was 225 μm and in the course of the manufacturing process it was increased by Aquamarijn to allow more flexibility for the wafer alignment.
- The depth was 120 μm as in the original design.
- The width of the vertical walls was designed to be 100 μm but the result was actually 90 μm, possibly due to the side reduction effect during powder blasting.
- The length was almost identical to the one of the silicon channel. The only difference is the length of the 2 inletting short channels which is 10.8 mm instead of 10mm.

From the above dimensions we can calculate that the effective reactor volume on the gas side is 106.4 μl whilst on the liquid side is 40.1 μl. The calculated interfacial area is 3,184.0 m^2/m_{liq}^3 and the porosity at 19.6% (pitch as well as pore diameter equal to 2 μm.

6.1.10 Microreactor Characteristics and Photos

The following picture shows the cross section of the powder blasted glass channel. Two measurements were taken to verify the width of the channel (shown in Figure 6.9):

- measurement 1: 257.7 μm
- measurement 2: 256.4 μm.

This decrease in width was expected as we know that powder blasting does not create completely vertical walls.

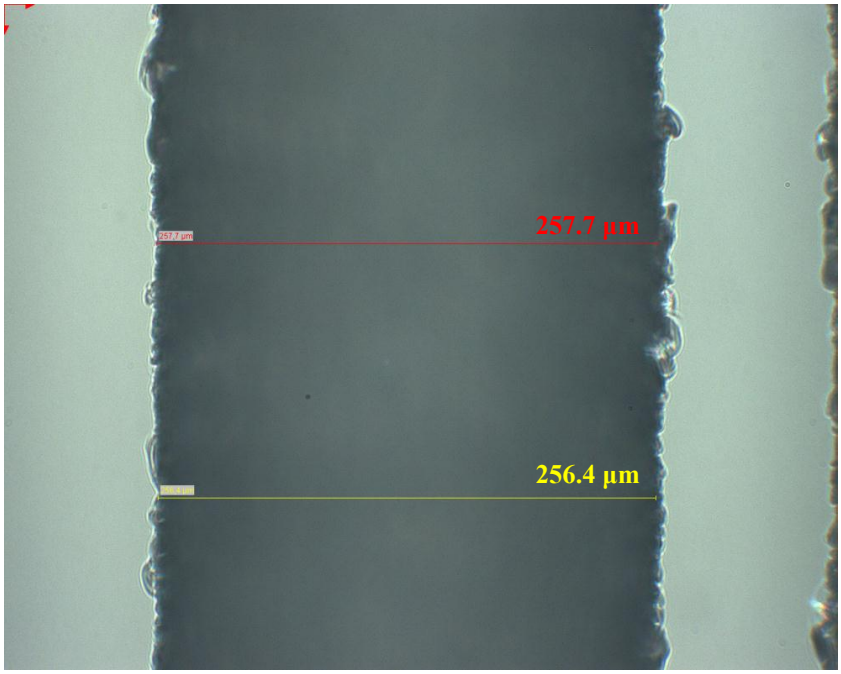

Figure 6.9. Cross section of the glass channel.

Next picture shows the vertical walls of the glass channel with a thickness measured to be 89.3 µm.

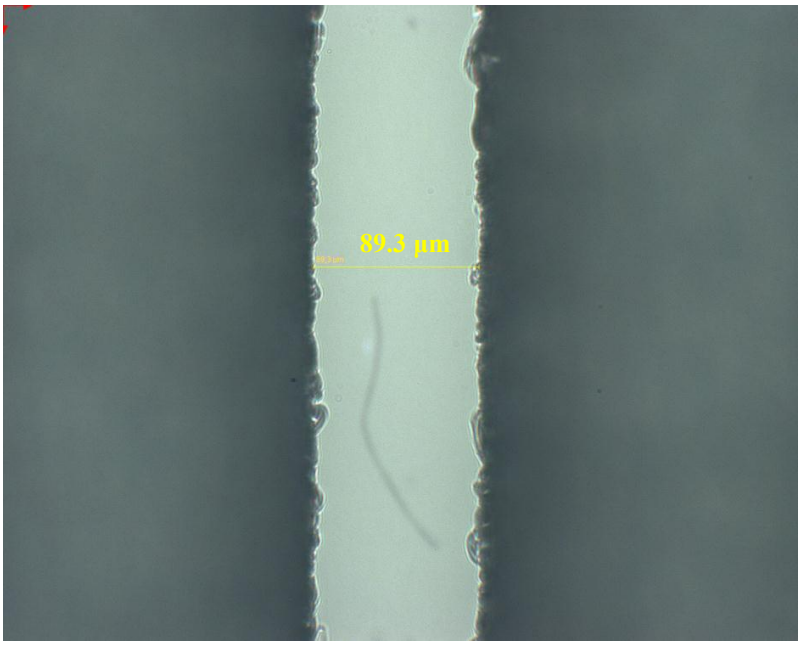

Figure 6.10. Cross section of the vertical walls of the glass channel.

The silicon nitride microsieve is shown in Figure 6.11. The diameter of the mesh pores is 2 μm and the pitch (distance between two pores) is also 2 μm. The sieve is characterised by a very good uniformity.

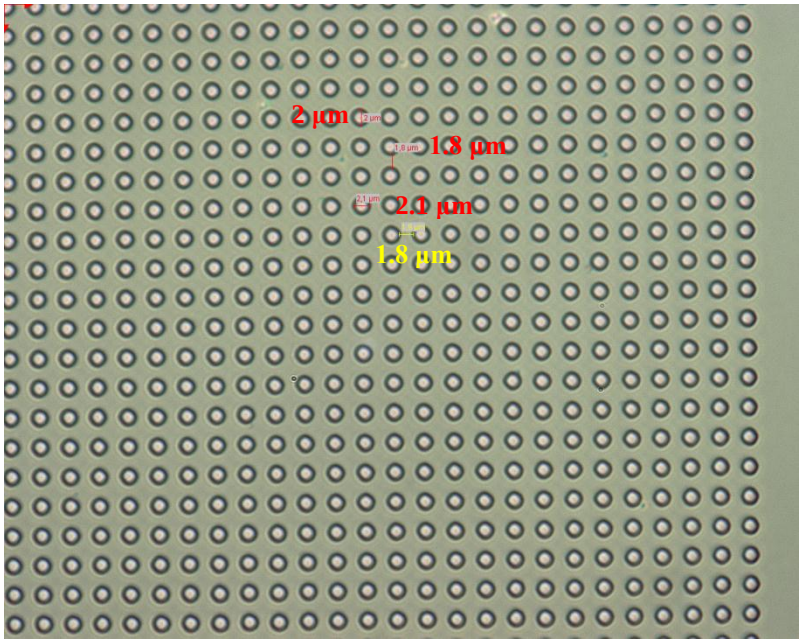

Figure 6.11. Microsieve with 2 μm pore size.

Figure 6.12 is a cross section of the serpentine silicon channel. We can see the perfectly vertical walls produced by dry etching. The thickness of the vertical walls is measured 125.3 μm while the width of the channel is 215.5 μm (measurements seen in Figure 6.12). These numbers are very close to the process set points of 125 and 215 μm respectively.

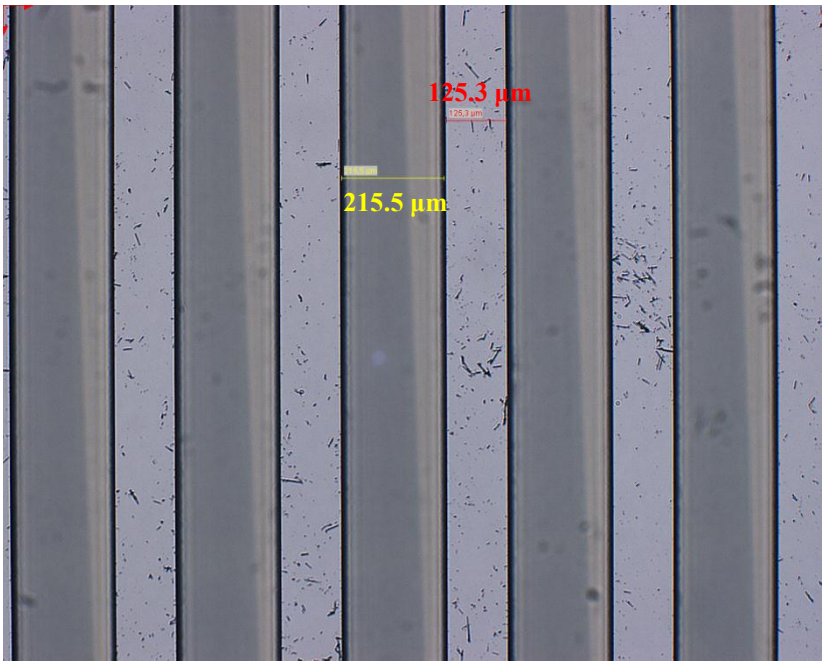

Figure 6.12. Silicon structure.

Figure 6.13 shows a photograph of the complete mesh microreactor.

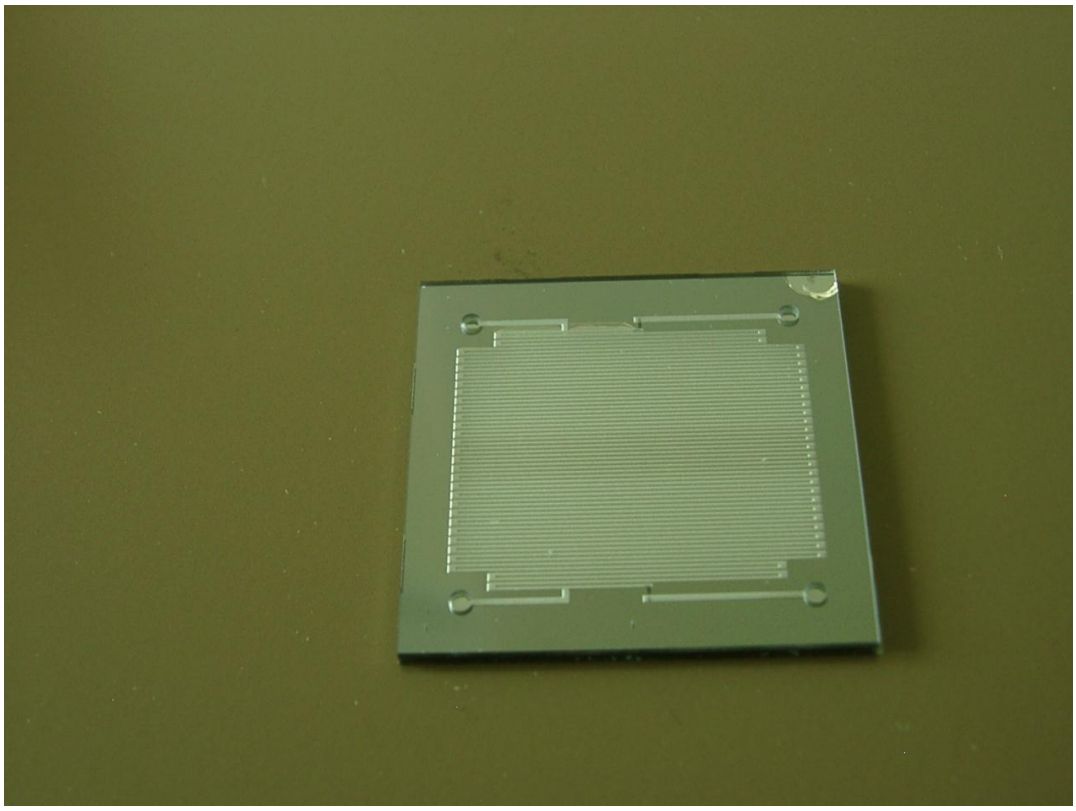

Figure 6.13. Mesh microreactor fabricated by Aquamarijn Ltd.

6.1.11 Microreactor Holder

The purpose of the holder was firstly to support the microreactor, secondly to provide the connection interface between the tubing and the microreactor and thirdly to provide a form of insulation and reduce heat losses to the environment. The material chosen was stainless steel for its robustness, medium heat capacity, chemical and thermal resistance. The design of the holder is depicted in Figure 6.14.

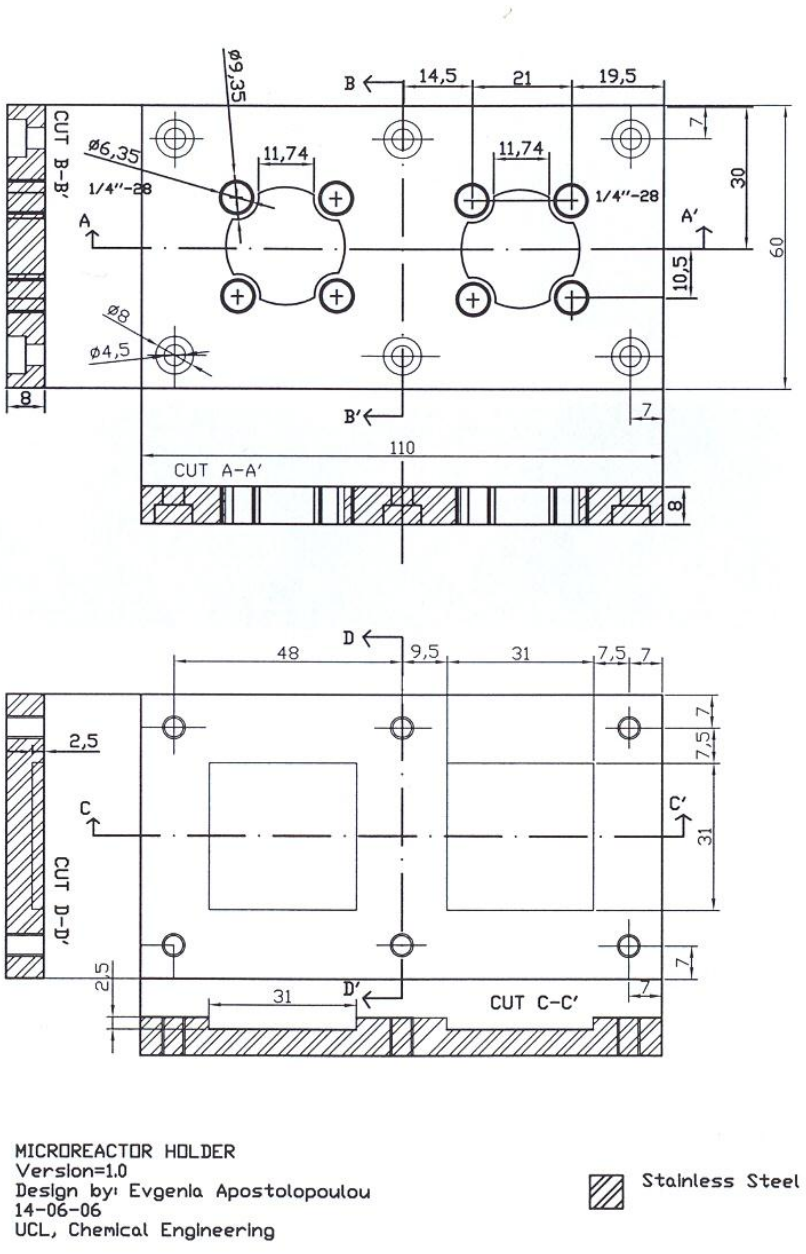

Figure 6.14. Microreactor holder. Design by Evgenia Apostolopoulou.

The holder consists of a top and a bottom plate. The inlet-outlet ports on the top plate are ¼”-28 threaded and the thickness of the top plate is 8 mm. With the above design provision for ethylene pre-treatment is made as the holder can accommodate a maximum of two microreactors in the two separate cavities etched in the bottom plate. The two plates eventually would be screwed together with six screws in the periphery as shown in Figure 6.15 to make one solid structure. The holder was manufactured at the UCL Chemical Engineering Workshop. Six channels were opened in the bottom plate at a second stage to accommodate thermocouples for temperature homogeneity investigation.

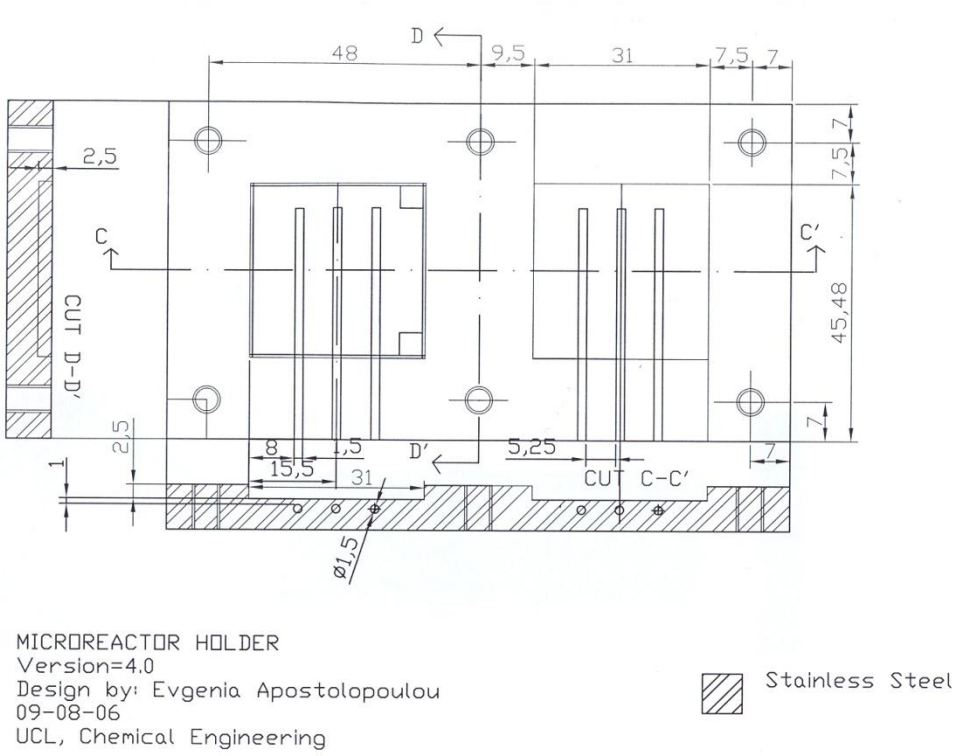

Figure 6.15. Microreactor holder- bottom plate modification. Design by Evgenia Apostolopoulou.

A detailed flow-chart of the bespoke experimental set-up used for the mesh microreactor is depicted in Figure 6.16.

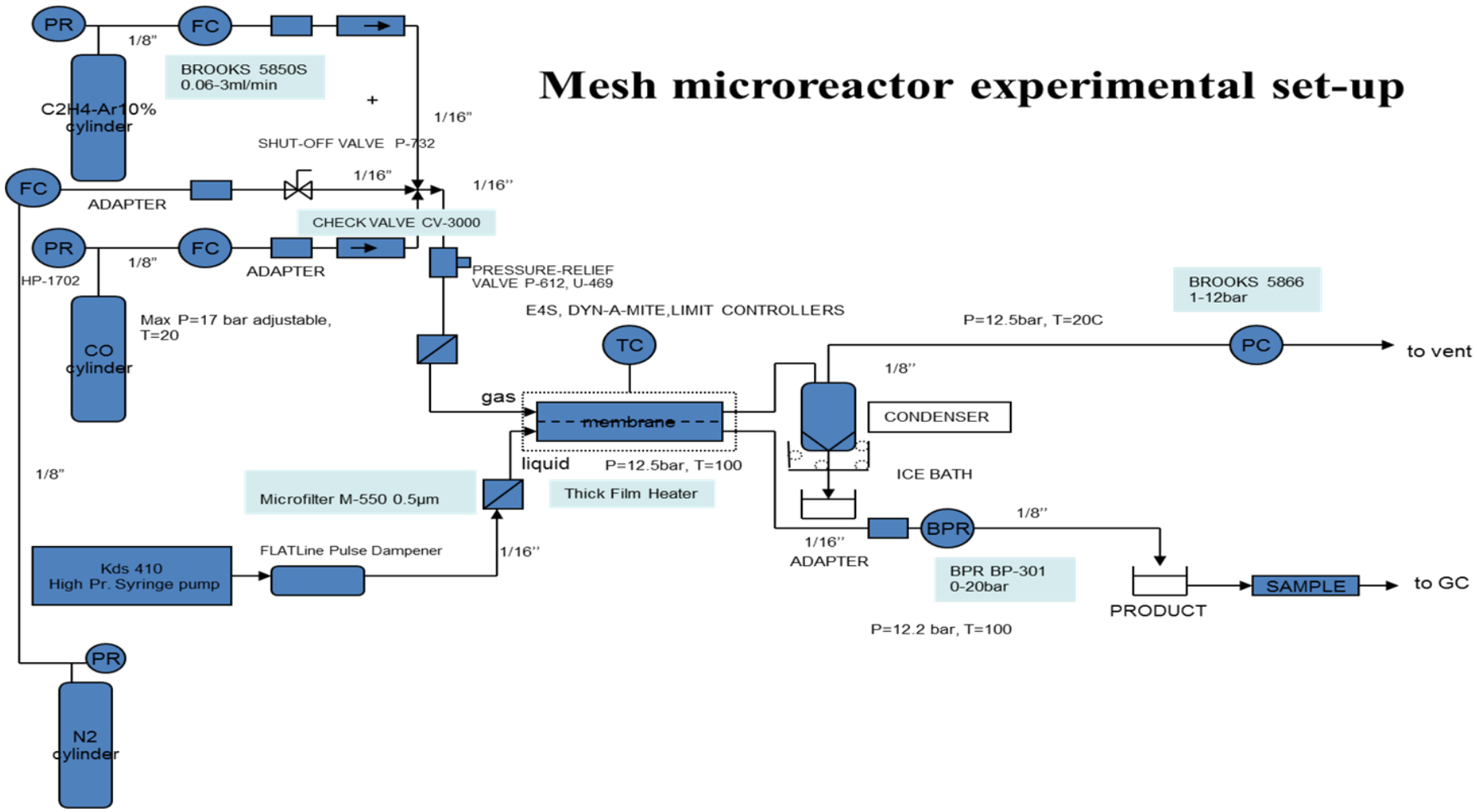

Figure 6.16. Detailed flow-sheet of the mesh experimental set-up.

6.1.12 Mesh Reactor Experimental Arrangement

A photograph of the experimental arrangement and a schematic of the set-up is shown below:

(a)

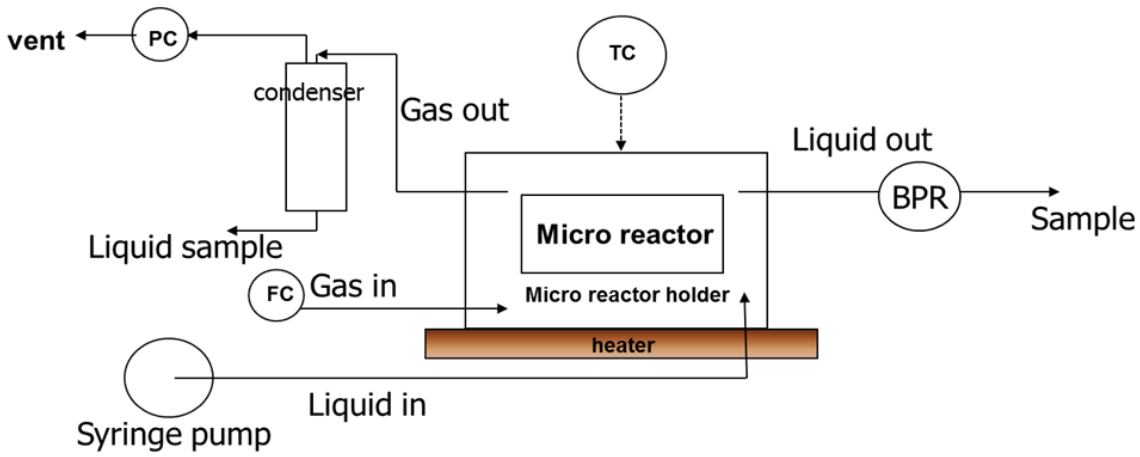

(b)

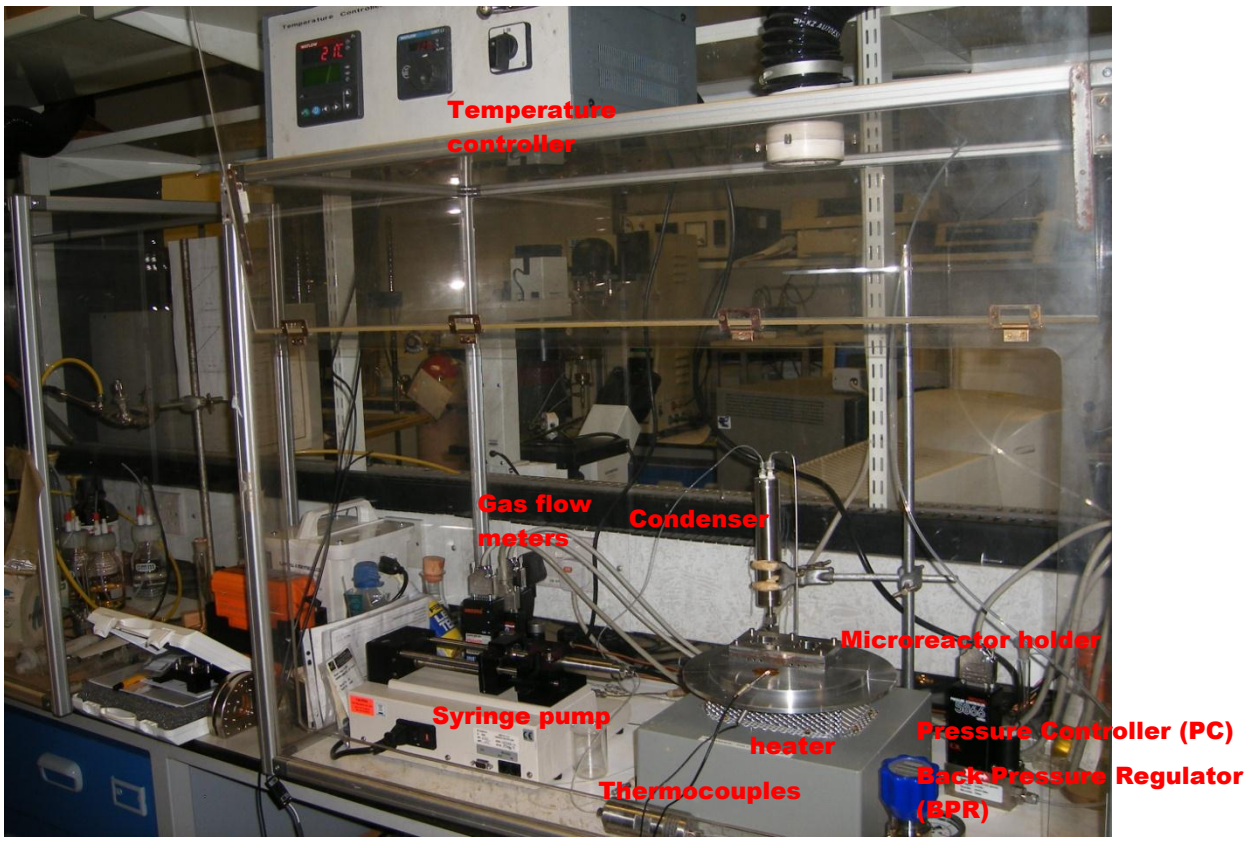

Figure 6.17. Mesh microreactor set-up. (a) Concise schematic, (b) photograph.

6.2 Mesh Microreactor- Experimental

6.2.1 Choice of Material for the Mesh – Corrosion Experiments

In order to determine the suitable material for the microreactor membrane a corrosion experiment had to be conducted. The materials used were a silicon nitride piece and a nickel piece. The reaction solution was made with MeP/ MeOH and methanosulfonic cid. The ratio of MeP: MeOH was 70: 30 (as in standard solution) but the acid was 10 times higher that the concentration used in the batch experiments as the Author wanted to observe the corrosion in severe conditions.

The results were:

- After 24 h no corrosion was seen with the naked eye on either material.
- After 48 h, no corrosion was observed on the silicon nitride piece but the Ni piece showed signs of corrosion (a portion of one surface was blackened).

Thus, silicon nitride was found to be the most appropriate material for the membrane.

6.2.2 Temperature Uniformity Experiments

The tests were performed on two consecutive days. The purpose of the first test was to determine the accuracy of the temperature controlling system. The procedure followed was firstly to give a set-point to the controller, place the thermocouple (T/C) in one of the wells and then place the thermometer T/Cs in the remaining two wells, wait a short period of time for stability to be attained, record the temperature

measurements and finally make a comparison. The temperature set-point was increased from 55 to 135 ^{o}C and then decreased again in order to find the hysteresis of the controller. The data and the resulting graphs are shown as follows:

	INCREASING TEMPERATURE				DECREASING TEMPERATURE			
controller SP	controller	thermometer T1	thermometer T2	ΔT= T1-T2	controller	thermometer T1	thermometer T2	ΔT= T1-T2
55	55	56	56	0	54	55	55	0
65	65	65	65	0	64	65	65	0
75	76	78	78	0	74	75	75	0
85	86	88	88	0	84	85	85	0
95	94	96	96	0	94	95	95	0
100	99	100	100	0	99	100	100	0
105	104	106	106	0	104	105	105	0
115	114	115	115	0	114	116	115	1
125	124	125	125	0	124	125	125	0
135	133	135	135	0				

Table 6.3. Comparative temperature data.

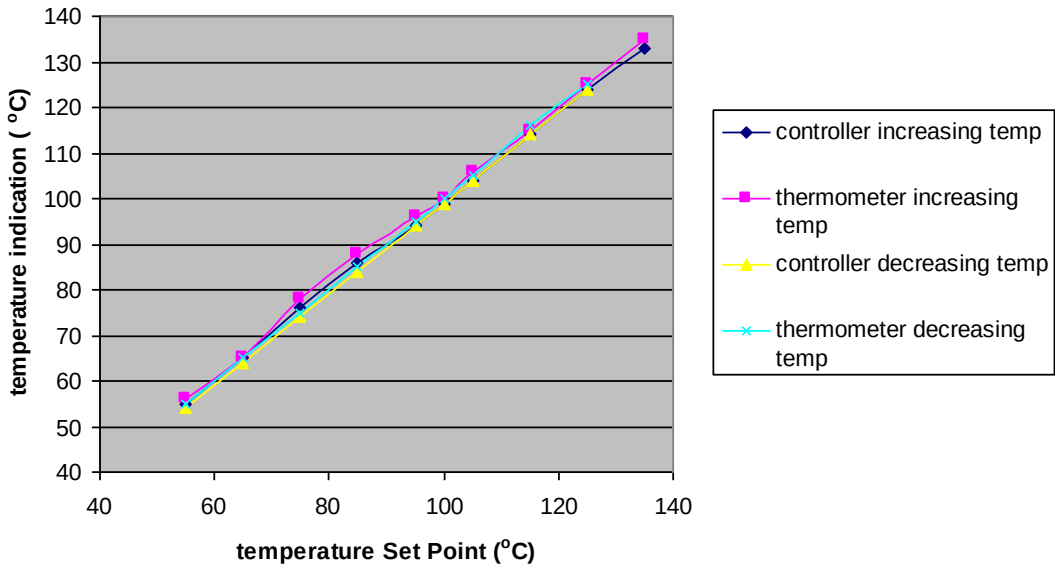

Figure 6.18. Response curves for temperature controller and thermometer.

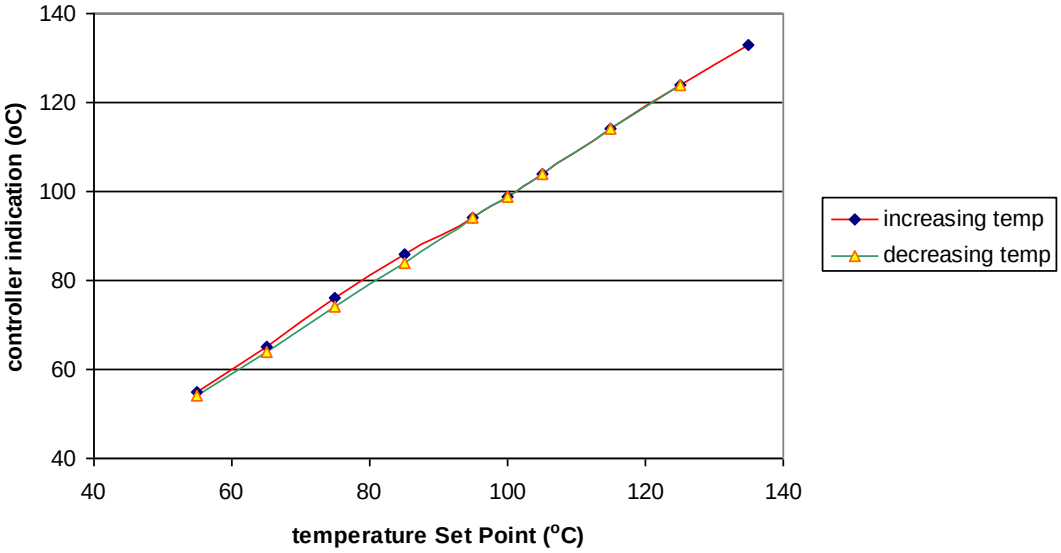

Figure 6.19. Response curve for the controller.

It can be concluded from this test that the controller does not show hysteresis. The Author performed a pair t-test for equality of means between the measurements taken by the thermometer and the controller display. The hypothesis for equality of means was rejected at 95% level of significance and we found an offset of 1°C (thermometer measurement higher). Moreover, by interchanging the position of the controlling and thermometer T/Cs, it was concluded that there is temperature homogeneity across the length of the microreactor.

In order to find out the required controller set point for the microreactor to be at 100 °C, a thermometer T/C was placed inside the holder and was secured between the bottom side of the reactor and the sealing material. It was found that the controller set point should be at 103 °C for the reactor to be at 100°C.

The purpose of the last test was to find any temperature differences across the microreactor width. A thermometer T/C was placed in each well and three measurements were taken along the depth of the well as shown in Table 6.4. The results depict that there is temperature homogeneity along the well.

	SP	well 1	well 2	well 3	SP	well 1	well 2	well 3	SP	well 1	well 2	well 3	SP	well 1	well 2	well 3
in	65	64	66	66	75	74	76	76	85	84	85	85	95	93	95	95
mid	65	65	66	66	75	74	75	75	85	84	85	85	95	94	95	95
out	65	65	66	66	75	74	75	75	85	84	85	85	95	94	95	95

	SP	well 1	well 2	well 3	SP	well 1	well 2	well 3	SP	well 1	well 2	well 3	SP	well 1	well 2	well 3
in	100	99	101	101	105	105	105	105	115	113	115	115	125	124	125	124
mid	100	99	101	101	105	105	105	105	115	114	116	116	125	124	124	124
out	100	99	101	101	105	106	106	106	115	114	115	115	125	124	124	124

Table 6.4. Temperature uniformity measurements along the microreactor width.

6.2.3 Pressure Testing

The Aquamarijn mesh microreactor was pressure tested firstly by increasing the pressure very slowly at room temperature. Unfortunately, it broke when the pressure reached 4.2 bar. Subsequently, we tried to separate the exit streams from the second microreactor at various operating conditions. This endeavour was successful in the temperature range [20-80 ^{o}C] and for pressure [1-2 bar]. The fluid flow rates applied were; L=0.1-0.8 ml/min, G=1-3 ml/min. Unfortunately, after a short period of time the microreactor started leaking from the periphery at 2.7 bar and 80 ^{o}C. The reason for the leak is unknown but one possible explanation could be a defect in the bonding. From the pressure testing experiments we can conclude that the mesh microreactor is unsafe for operation at reaction conditions (10 bar and 100^{o}C). SEM

photographs of the broken microreactor allowed identification and measurement of the dimensions of the channels and the pore size.

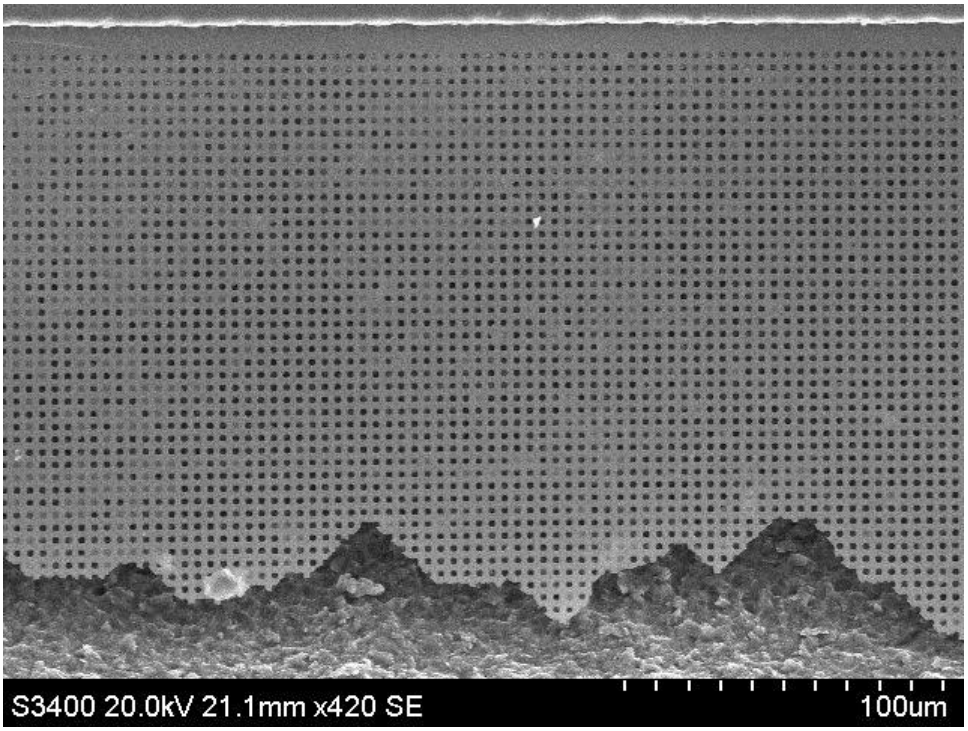

Figure 6.20. Picture of the broken mesh.

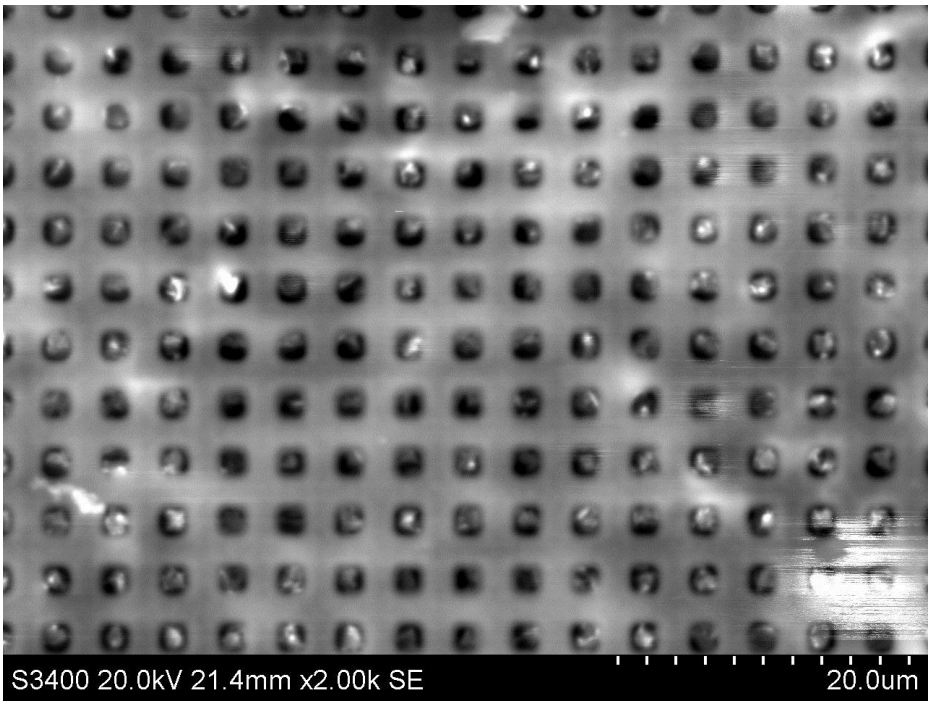

Figure 6.21. SEM photo showing detail of the broken mesh. Pores clogged up by particles and fragments.

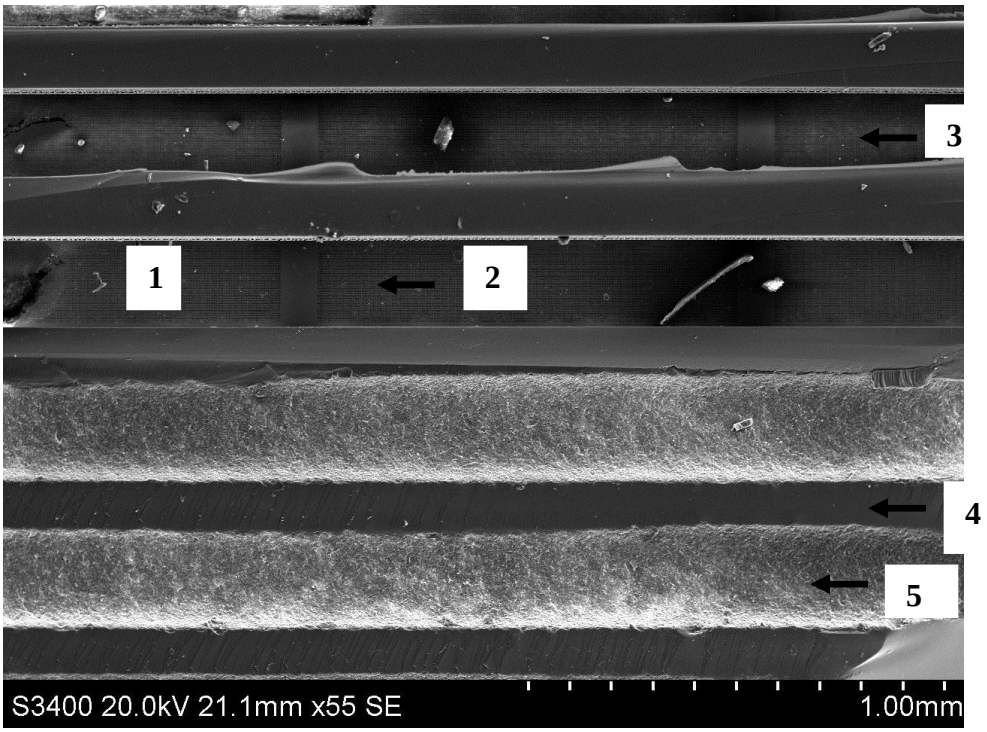

Figure 6.22. SEM photograph of the broken mesh microreactor. Internal parts are clearly seen: 1) silicon nitride mesh, 2) mesh support bar, 3) silicon channel for the gas flow, 4) wall of glass channel for the liquid flow, 5) glass channel for the liquid flow.

6.3 Other Reactor Trials

Two different reactors; the CRL and the Micronit reactors were tried in order to assess their suitability as tools for the collection of kinetic data. These attempts were unsuccessful for a variety of reasons which are explained in the following sections.

6.3.1 CRL Reactor

Description

The microreactor (please refer to Figure 6.23) was designed and built by CRL (Central Research Laboratories, London) as part of the KEMiCC project G1RD-CT2000-00469. It consists of two cavities separated by a nickel micromesh fabricated by a two-stage electroplating method. The mesh has 5 μm pores and an open area of approximately 20-25 % which is translated into an interfacial area of approximately 2000 m^2/m^3liq compared to 100-200 m^2/m^3liq of traditional tank reactors (Wenn et al., 2003). The mesh is shown in Figure 6.24. The upper cavity can be fed with gas for gas-liquid reactions or a liquid phase for liquid-liquid reactions. The bottom cavity is the reacting chamber and is fed with liquid. It must be mentioned that there is epoxy between the glass window and the metal housing to prevent leaks.

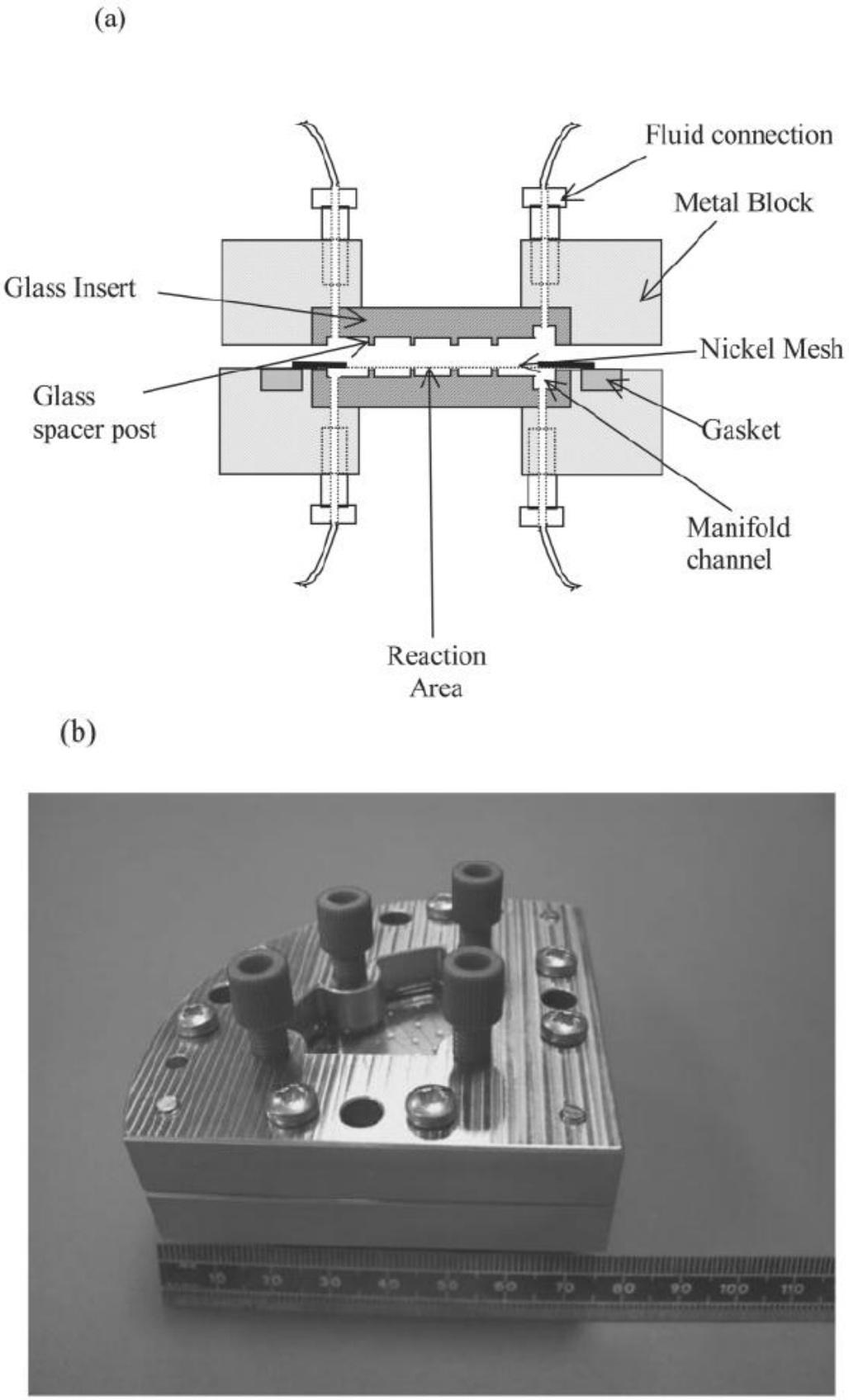

Figure 6.23. CRL reactor. (a) Diagrammatic cross cection. (b) Assembled device (Wenn et al., 2003).

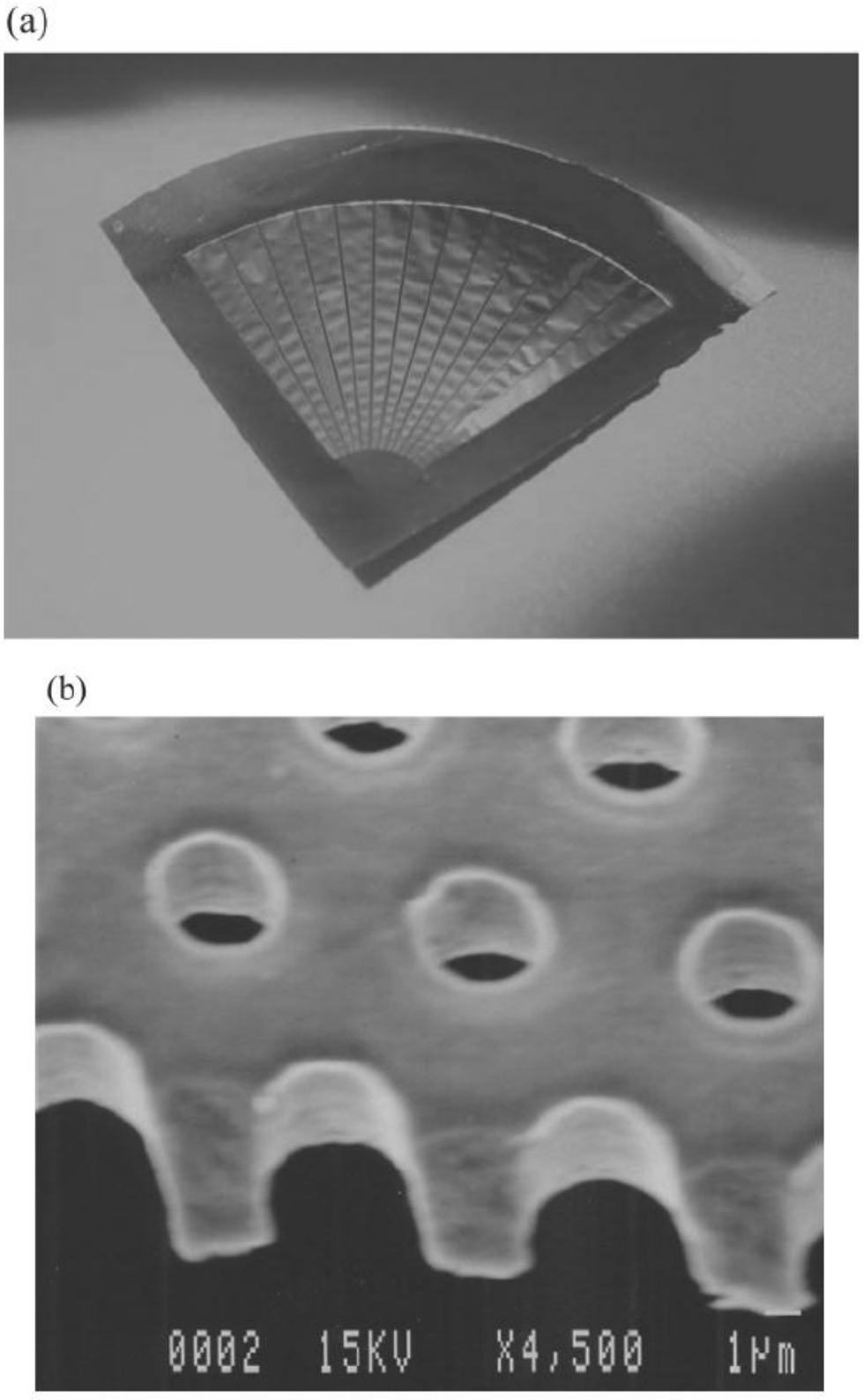

Figure 6.24. (a) Nickel mesh. (b) SEM photograph of the mesh (Wenn et al., 2003).

Each reactor block has one inlet port and three outlet ports. For the purpose of the preliminary experiments that we performed only the middle outlet port was used; the remaining two were blocked with plugs for 1.6 mm OD tubing, provided by Bohlender, code: F 705-02 made of PTFE, with a high chemical compatibility and a range of operating temperatures (-200, +260 ^{o}C).

Objectives

The purpose of these experiments was firstly to test the set-up incorporating the condenser, the back-pressure regulator (BPR, liquid-side) and the pressure controller (gas-side) and secondly to study the gas-liquid breakthrough pressure.

Experiments performed

The back pressure-regulator on the liquid side was tested. Initially, the Swagelok fittings at the inlet and outlet ports were leaking. Once they were tightened the BPR was tested to 12 bar successfully. When all the connections were made to the microreactor with the aim to test the gas pressure controller we noticed that the fittings were leaking. After they were tightened and the test continued, it was noticed that the reactor was leaking around the periphery. The nuts on the metallic blocks were tightened but they were quite short and even when they were tightened to the maximum there was still leakage. The nuts were subsequently replaced by longer ones and after proper tightening the leakage stopped. The condenser and the pressure controller were connected to the gas exit side. The set-point on the pressure controller was 10 bar and soon the pressure started increasing but when the pressure reached 2.7 bar above the atmospheric the microreactor started leaking again; this

time between the epoxy and the glass housing. The same type of leakage was encountered in the past in the course of the KEMiCC project when this reactor was used at pressure 3 bar above the atmospheric. This led to the conclusion that the CRL reactor with the epoxy sealing is not suitable for operation at high pressure.

6.3.2 Micronit lab-on-a-chip 4515 Kit

Description

The kit was bought for the study of the methoxycarbonylation of ethylene using a single channel capillary microreactor operating under Taylor flow conditions. It was a standard, in-stock product provided by the company Micronit Microfluidics DV based in the Netherlands. It consists of the microreactor holder, the microreactor chip (x 2), the fittings and the tubing.

Chip holder 4515 Flat-Bottom Teflon

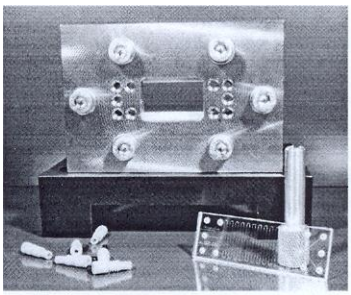

It is designed for fast and easy interconnections between the chip and the capillaries. Maximum operating pressure and temperature are 100 bar and 100 ^{o}C. It comprises of two plates, the bottom is PEEK while the top one is stainless steel. The fittings and the tubing provided are Teflon (1/16”OD and 0.25 mm ID).

Figure 6.25. Kit components

The limitation of the operating temperature is due to the ferrules that might deform at higher temperatures and cause leakage. The dimensions of the holder, l x w x h, are 85 x 55 x 35 mm. The Teflon fittings are preferable as they offer low friction connections. It should also be mentioned that the connections are extremely low-volume; maximum 0.9 µl per connection.

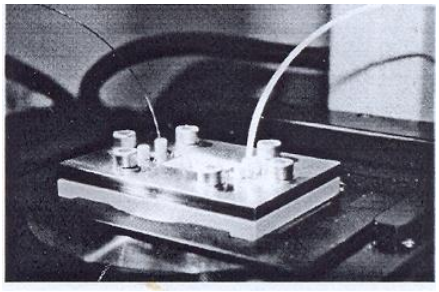

Figure 6.26. Micronit 4515 lab-on-a chip kit assembled.

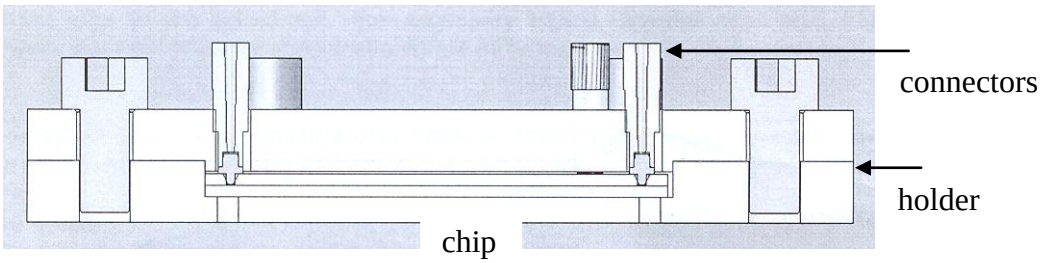

Figure 6.27. Schematic showing the holder, microreactor chip and the connections (www.micronit.com).

The burst pressure of Teflon tubing is a function of the thickness of the wall, the tubing diameter and the operating temperature. The following plot was produced at 20 ^{o}C. In order to find the burst pressure at 100 ^{o}C, one has to multiply the value at 20 ^{o}C with the factor 0.68 (see Figure 6.28).

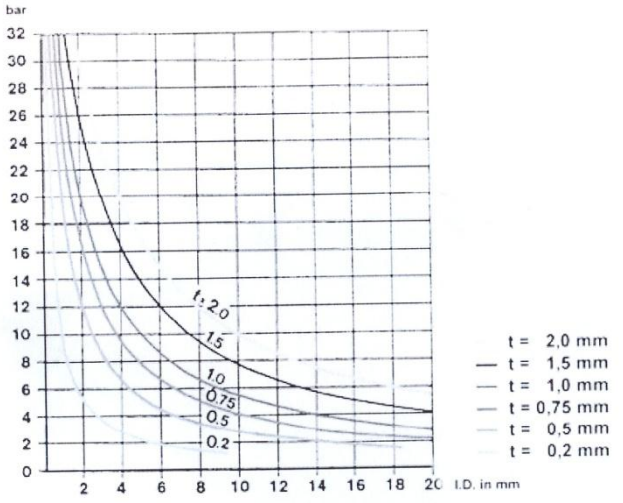

Temperature °C	Reduction factor
50°	0,87
75°	0,77
100°	0,68
150°	0,53
200°	0,39
250°	0,28

(i) (ii)

Figure 6.28. i)PTFE (Teflon) burst pressures for different wall thickness (t) and tube ID. (ii) temperature reduction factor (www.micronit.com).

Microreactor chips

The lab-on-a-chip kit comes complete with two microreactor chips made from borofloat glass whose properties are shown in Table 6.5. Its characteristics are hydrophilicity, optical transparency and chemical inertness.

Density	ρ	$2{,}2 \cdot 10^{3}$	$kg\ m^{-3}$	(at 25 °C)
Young's modulus	E	$63 \cdot 10^{9}$	Pa	
Poisson's ratio	μ	0,2		
Coefficient of thermal exp.	α	$3{,}3 \cdot 10^{-6}$	K^{-1}	(at 20 - 300 °C)
Thermal conductivity	λ	1,2	$W\ m^{-1}\ K^{-1}$	(at 20 °C)
Specific heat	c_p	$0{,}9 \cdot 10^{3}$	$J\ kg^{-1}\ K^{-1}$	(at 20 - 300 °C)
Maximum op. temperature	T_{max}	500	°C	(< 10 hours)
	T_{max}	450	°C	(> 10 hours)

Table 6.5. Properties of borosilicate glass (www.micronit.com).

Type	Characteristics					
	Technique	Channel width	Channel depth	Channel length	Size (mm)	Bottom
R50.332.2	HF etching	50 µm	20 µm	332 mm	45.0 x 15.0 x 1.8	0.7 mm
R50.332.3	HF etching	50 µm	20 µm	332 mm	45.0 x 15.0 x 1.3	175 µm
R100.332.2	Powderbl.	100 µm	150 µm	332 mm	45.0 x 15.0 x 1.8	0.7 mm
R100.332.3	Powderbl.	100 µm	150 µm	332 mm	45.0 x 15.0 x 1.3	175 µm
R50.676.2	HF etching	50 µm	20 µm	676 mm	45.0 x 15.0 x 1.8	0.7 mm
R50.676.3	HF etching	50 µm	20 µm	676 mm	45.0 x 15.0 x 1.3	175 µm
R150.676.2	Powderbl.	150 µm	150 µm	676 mm	45.0 x 15.0 x 1.8	0.7 mm
R150.676.3	Powderbl.	150 µm	150 µm	676 mm	45.0 x 15.0 x 1.3	175 µm

Table 6.6. Standard Micronit microreactors. Model R150.676.2 was used in the current study (www.micronit.com).

The standard microreactor chip that was chosen is the one with the highest volume channel; type: R150.672.2 (see Table 6.6). The channel is created by powder blasting and its dimensions, l x w x d, are 676 x 0.15 x 0.15 mm which gives a volume of 15 µl. The chip size is, l x w x d, 45 x 15 x 1.8 mm and comprises of two plates. The structured bottom plate has a thickness of 0.7 mm. Two standard reactors are shown in Figure 6.29.

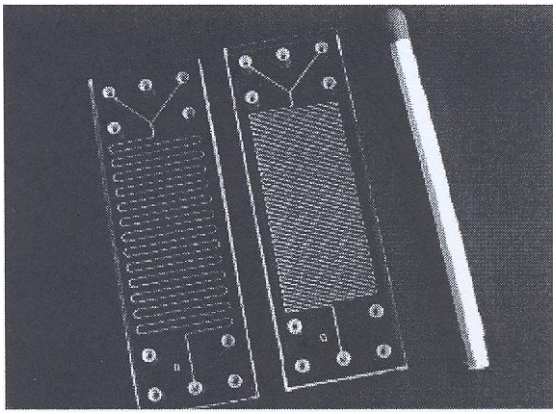

Figure 6.29. Micronit standard reactors with 30 and 60 cm chamber length (www.micronit.com).

Objectives

It was one of the objectives of the project to study the reaction using Taylor flow in a capillary reactor. The extent of the reaction theoretically could be measured by the length of the bubbles as the decrease of the length of the bubbles is relative to the conversion. Results of these experiments could lead to preliminary kinetics. The kit as a product in-stock and off-the-shelve could allow for immediate start of performing experiments.

Experiments performed - Cold runs

The cold runs were performed in order to familiarize oneself with the micronit reactor and to determine the appropriate ranges of flow on the gas and liquid side for good reactor operation. The liquid flow was deionised water driven by the syringe pump with a 20 ml syringe and a very wide potential range, theoretically from 0.052 µl/min to 54.7 ml/min. The gas used was nitrogen and the potential flow range was 0-100 ml/min through a 5850 Brooks Mass flow controller. The liquid flow rate was altered from 0.2 ml to 1 ml and the gas flow rate used ranged from 3.6 ml/min to 100 ml/min. It was observed that above 0.4 ml/min liquid flow rate the liquid flowed backwards through the tubing on the gas side instead of through the micronit reactor even if the gas flow rate was increased to 100 ml/min and the pressure on the gas side to 10 bar. By changing the liquid flow rate in the range 0.2-0.4 ml/min and the gas rate from 3.6 to 10 ml/min Taylor, churn and annular flow patterns were recorded. All the tests were performed at atmospheric pressure and ambient temperature.

Experiments performed - Reaction runs

With the reacting mixture provided by LI, the Author proceeded with performing the reaction in the micronit reactor. The gases used were CO and ethylene, through the pressure regulators on the gas cylinders and the Brooks Mass flow controllers for regulating the flow. The flow used for each of the gases was 1-2 ml/min. The flow used for the liquid solution was in the range 5 μl/min-0.3 ml/min. Numerous experiments were performed with at least two samples taken through each run but a measurable conversion was achieved only when the liquid flow was lowered to 10 μl/min and the flow rate for each of the gases was 2 ml/min in which case the MeOH conversion was calculated as 2.86 %, the average of two samples. Formation of formaldehyde or a formaldehyde by-product was also observed. Further oxidation of formaldehyde gives formic acid may have been present in very small values as the GC analysis of the product sample showed many small unidentified peaks.

The liquid flow rate was further decreased to 5 μl/min while each gas flow rate was 2 ml/min. When the experiment was to be repeated for 7.5 μl/min liquid flow, the Author faced problems with blockage of the micronit reactor by particles of Pd black resulting from precipitation of the catalyst and it was impossible to operate. Optically the phenomenon was evident as the glass channel had changed colour from being clear to brown. The liquid instead of going through the reactor was flowing backwards through the gas tubing. The gas flow was increased but with no success. The effort to try to clean the micronit reactor by using the ultrasonic bath with deionised water at 40 ^{o}C was not successful either. The Author further tried using 20 % nitric acid solution (made by adding 100 ml of HNO_3 69 % in 200 ml deionised water) in the bath with the same result. Subsequently, an effort was made to pump

nitric acid solution 20 % at 60 ^{o}C which gave partially a good result but when the Author tried to use the reactor it blocked again. Finally, a 35 % v/v nitric acid (made by adding 100 ml HNO_3 69 % in 100 ml de-ionised water) solution was produced and was pumped through the micronit reactor at 60 ^{o}C which cleaned the channel quite well and made it again transparent. Subsequently, operation of the micronit reactor was attempted, the effect of the cleaning was short-lived and although operation was initially successful, channel blockage occurred again maybe due to the presence of Pd particles in the liquid mixture or Pd deposition. These experiments were conducted at atmospheric pressure and at 10 bar and 100 ^{o}C (reaction conditions) and no catalyst pre-treatment with ethylene took place.

6.4 Conclusions

A bespoke mesh microreactor with dimensions 3 cm x 3 cm and silicon nitride mesh with 2 μm pore size was designed for the puspose of this study. The microfabrication was outsourced to Aquamarijn Ltd (Netherlands) as UCL was not equipped with the necessary facilities. The process from conception to reactor delivery lasted more than a year mainly due to problems with the fabrication. Although this device was designed to operate at reaction conditions (10 bar and 100 ^{o}C), unfortunately pressure testing showed that the mesh microreactor was only suitable for operation below 4 bar at atmospheric temperature or less than 2.7 bar pressure at 80^{o}C as breakage or leakage occurred at more aggressive conditions. Microfabrication defect(s) like flaws with the anodic bonding utilised to sandwich the various components together might be one reason behind this failure. Investigation of the broken microreactor pieces using SEM did not provide any evidence to establish the reason why the operation failed but rather allowed measurement, comparison and verification of channel dimensions and pore size against the final design.

The suitability of two more types of microreactors was assessed in the context of this study. The first one was a mesh micreactor developed by CRL, containing a nickel mesh with 5 μm pore size and the second was a glass channel reactor developed by Micronit (Netherlands). Both reactors were found to be unsuitable to operate under reaction conditions. The former because it leaked from the periphery at pressure 2.7 bar and the latter because it suffered from channel clogging. Despite the failure in lasting continuous operation, the Micronit reactor was useful as it enabled testing of the experimental set-up during cold runs (using de-ionised water and N_2 gas) and

under actual reaction conditions. During the latter, formation not only of the desired product MeP but also of the by-product formaldehyde was observed. The deposition of Pd black in the channel – an anticipated phenomenon in Pd catalysis - caused blockage and no further reaction was possible. Pumping hot concentrated acid solution at 60 ^{o}C through the micronit reactor seemed to clean the channel satisfactorily but unfortunately the effect did not last long. Thus, plans for further experimentation with the Micronit reactor were abandoned.

--//--

CHAPTER 7

Hydrodynamics Study

Various flow patterns can predominate in gas-liquid flow in capillaries. Their occurrence depends on the gas/liquid inlet flow rate ratio, gas inlet opening (size and orientation), the superficial velocities and the properties (for example surface tension, liquid viscosity etc) of the two phases. A number of different flow regimes can be observed at the gradual increase of the gas flow rate (Hessel et al., 2005, Liu et al., 2005) out of which **Taylor Flow** is the most important and has been the subject of various studies as it is the operating regime of monolithic reactors. It is also referred to in the literature as slug flow and is characterised by long bubbles whose length is longer that the tube diameter separated by liquid slugs. They occupy most of the capillary cross section and are separated by the tube wall by a very thin layer of liquid. The bubbles have hemispherically shaped tops and in most cases flattened tails. This flow arrangement is considered to yield superior mass-transfer performance.

One of the most important characteristics of Taylor flow is the good mass and heat transfer due to the thin film separating the slugs and bubbles from the tube wall as well as the recirculation pattern in the slugs. Other characteristics include the elongated bubbles and the slugs which are isolated between two consecutive bubbles. Since the bubbles exert a much smaller shear stress on the film than the wall does,

they usually travel at a velocity slightly greater than the volume average liquid velocity. Mass transfer in Taylor flow has been found closely related to the length of the liquid slug.

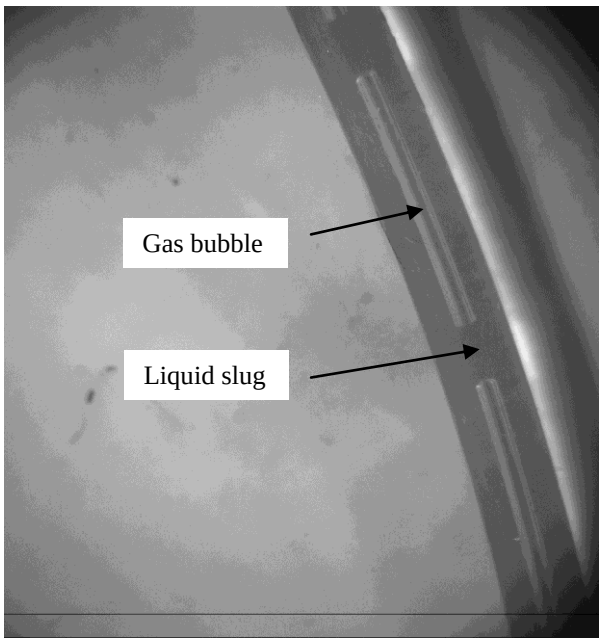

Figure 7.1. Taylor flow in 250 µm capillary.

Taylor flow has many applications. One of the first was in flow measurements where bubbles acted as tracers to measure liquid velocity in capillaries (Kreutzer, 2003). It was later recognised than the bubble velocity was slightly different to the liquid one. The fact that each slug is confined between two gas bubbles reduces significantly the axial mixing between liquid slugs. On the contrary, the recirculation pattern improves radial mixing which in turn improves heat and mass transfer, a fact that can be particularly useful in the study of multiphase reactions which can be mass transfer limited. Due to this property, capillary microreactors were chosen as one of the tools for the kinetic study of methoxycarbonylation of ethylene in this project. However, as mentioned before, various factors can affect the flow characteristics.

The work presented in this chapter was done in an attempt to understand the characteristics of the flow produced when the gas and liquid meet in a 250 μm=0.25 mm capillary tube and how this flow develops along the very long capillary, how the contactor used and other equipment (for instance the syringe pump) affect the characteristics of the flow and under what flow rates for the gas and the liquid, the produced Taylor flow is homogeneous. All experiments were carried out under the reaction conditions of 10 bar and 100^{o}C. The findings from this hydrodynamics study would prove useful to the kinetic experiments which were to be conducted with the second capillary reactor of 0.25 mm ID and 11.7 m length at the next stage of work which are described in the next Chapter of this Thesis.

A capillary reactor, in the shape of a spiral, which from now will be called the 'spiral reactor' was developed to allow for flow visualisation in the framework of the hydrodynamics study mainly for two reasons; firstly, to investigate the characteristics of the gas-liquid flow under Alpha reaction conditions (10 bar and 100 ^{o}C) achieved in the capillary tube. Even though bubble sizes were also measured, the slug sizes were of particular importance due to the fact that the smallest slug size possible was the most desirable in order to minimise mass transfer resistances during the reaction. The quality of the gas-liquid flow in terms of homogeneity was also to be studied in a capillary microreactor under the Alpha experimental conditions. It should be noted that flow homogeneity would render measurements easier but it was of secondary importance as compared to the sizes of the liquid slugs. Secondly, to establish whether or not the extent of the reaction could be measurable from the determination of the decrease of the bubble size as the gas

gets consumed along the capillary tube. It was thought that results from these experiments could lead to preliminary kinetics for the reaction under study.

The system microscope-camera was placed on top of the spiral microreactor to enable the measurement of bubble and slug size not only at the reactor inlet and outlet but also at intermediate positions.

7.1 Spiral Reactor

7.1.1 Design

The Spiral Reactor consists of the FEP tube with 0.25 mm ID and 1.6 mm OD, has a maximum length of 7.6m and is enclosed in a pan type structure which comprises of two plates; the bottom one is made of stainless steel and the top one from Perspex for optical transparency. Each one is ¼'' thick and has a diameter of 7''. A spiral channel of 1.6 mm depth whose purpose is to accommodate the capillary tubing is etched on the stainless steel plate. The length of the etched channel is approximately 7.6 m. The two plates are sealed by means of 6 screws on their periphery. The stainless steel plate has also two channels etched along the radius on the top and on the bottom surface respectively for the inlet and the outlet (please refer to Figure 7.2).

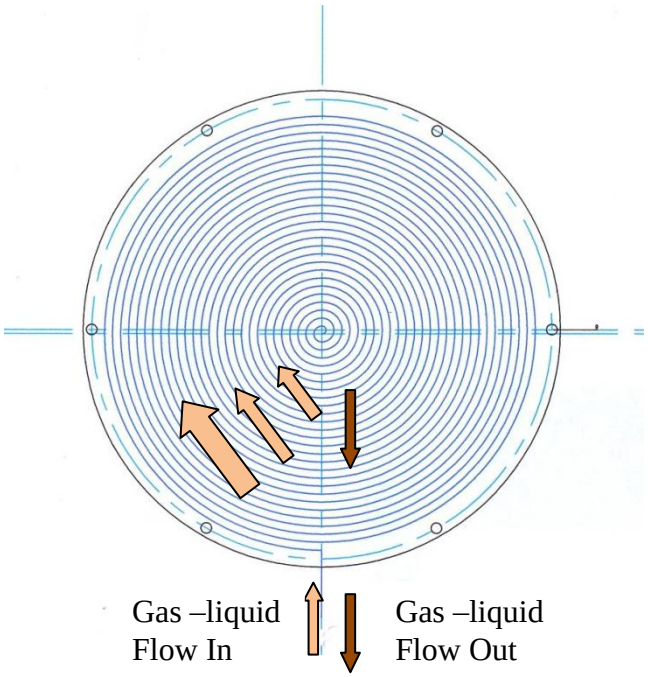

Figure 7. 2. Schematic of the spiral reactor.

Spiral Reactor Characteristics	
Length	Variable, maximum allowable 7.6 m *(6 m used for the flow visualisation experiments presented here)*
Volume	Variable *(295 μl for 6 m tube length)*
Tubing OD	1/16''=1.6 mm or smaller
Tubing ID	0.25 mm
Operating conditions	T=100 ^{o}C P=10 bar or higher
Advantages	Gives the ability to see inside the reactor and study the hydrodynamics with the aid of microscope-camera system

Table 7.1. Spiral reactor characteristics.

7.2 Experimental Set-Up

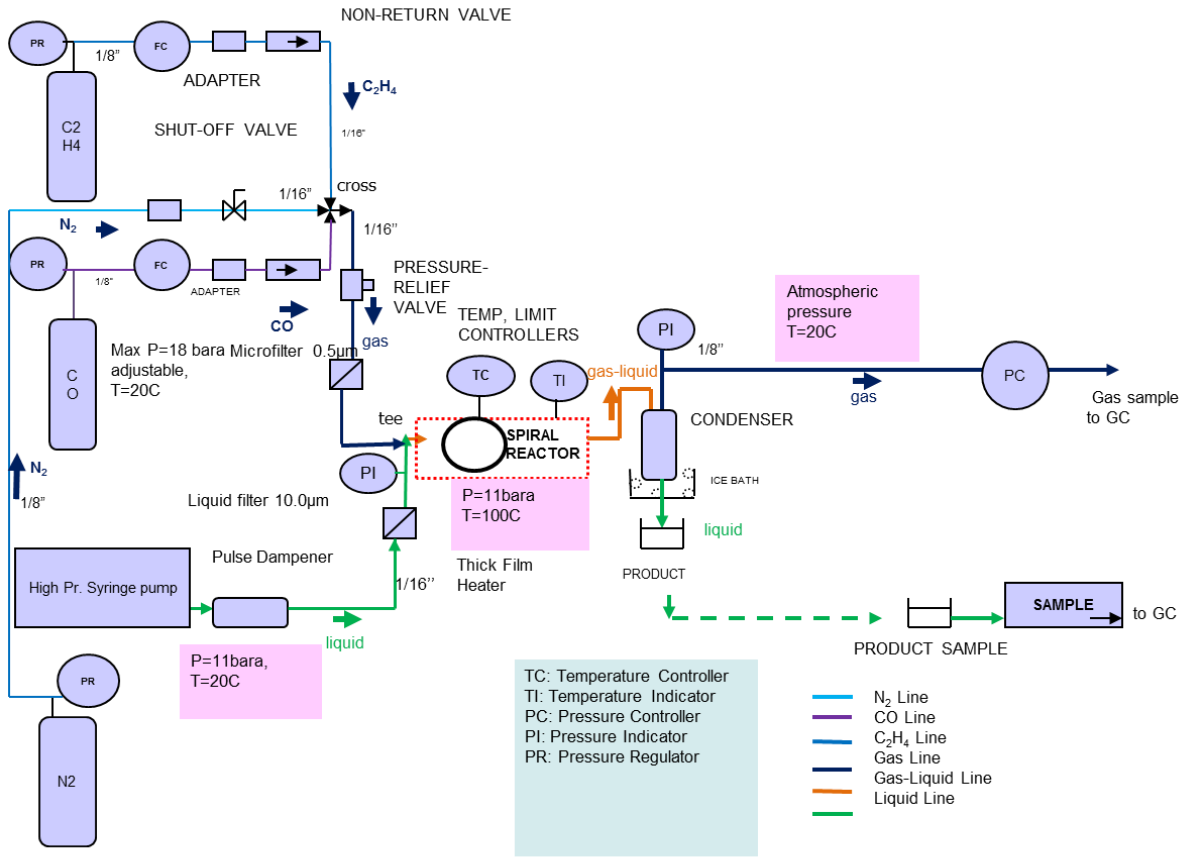

Figure 7. 3. Schematic of the Experimental Layout for the Spiral Reactor.

.

The experimental set-up used for the hydrodynamics study (Figure 7.3) comprised:

Upstream of the Spiral Reactor:

- The CO is fed by the gas cylinder at the pressure of 17 bar, controlled by a high Pressure Regulator (PR), through the mass flow controller and through the non-return valve to the cross junction.

- The ethylene is fed by the gas cylinder at the pressure of 17 bar, controlled by a high PR, through the mass flow controller and through the non-return valve to the cross junction where it meets the CO gas.
- The experimental set-up allows for use of N_2 as inert gas to built-up the pressure of the system quickly to 10 bar. The N_2 is fed from the gas cylinder at the pressure of 17 bar through a mass flow controller and a shut-off valve to the cross junction when it meets the CO and the ethylene.
- The mixture of the gases passes through a pressure relief valve, which serves as a safety precaution and its role is to open in case of over-pressurisation of the system to avoid a burst of tubing of other equipment.
- The gas mixture subsequently passes through a microfilter for removal of any microparticles present in the gas flow and then it reaches the tee junction which is the gas-liquid contactor where it meets the liquid flow. The liquid flow is a 70:30 MeP:MeOH (w/w, %) mixture. The gas- liquid Taylor flow then enters the Spiral Reactor.

Downstream of the Spiral Reactor exit:

- The gas-liquid stream enters the top of the condenser, where the liquid vapours condensate. The liquid accumulates at the condenser bottom which has an inverted conical shape, while the gas exits the condenser from the top part and thereafter enters the GC for a possible analysis with the Thermal Conductivity Detector (TCD).
- A liquid sample can be collected manually from the bottom of the condenser for analysis with the GC using the Flame Ionisation Detector (FID).

7.3 Taylor Flow Measurements

The arrangement used for the Taylor flow measurements incorporated the microscope (PRIOR Scientific Instruments Ltd, model: Z6T101) with a fitted camera (Kodak MegaPlus Camera, model: ES1.0\TH by Oxford Laser Ltd) connected to the computer. The VISIFLOW software was used for flow analysis of the gas-liquid flow. Various photographs of bubbles and slugs were obtained and subsequently the slug and bubble sizes were measured in relation to the photo of a ruler (the ruler length was 1cm) and a suitable software package.

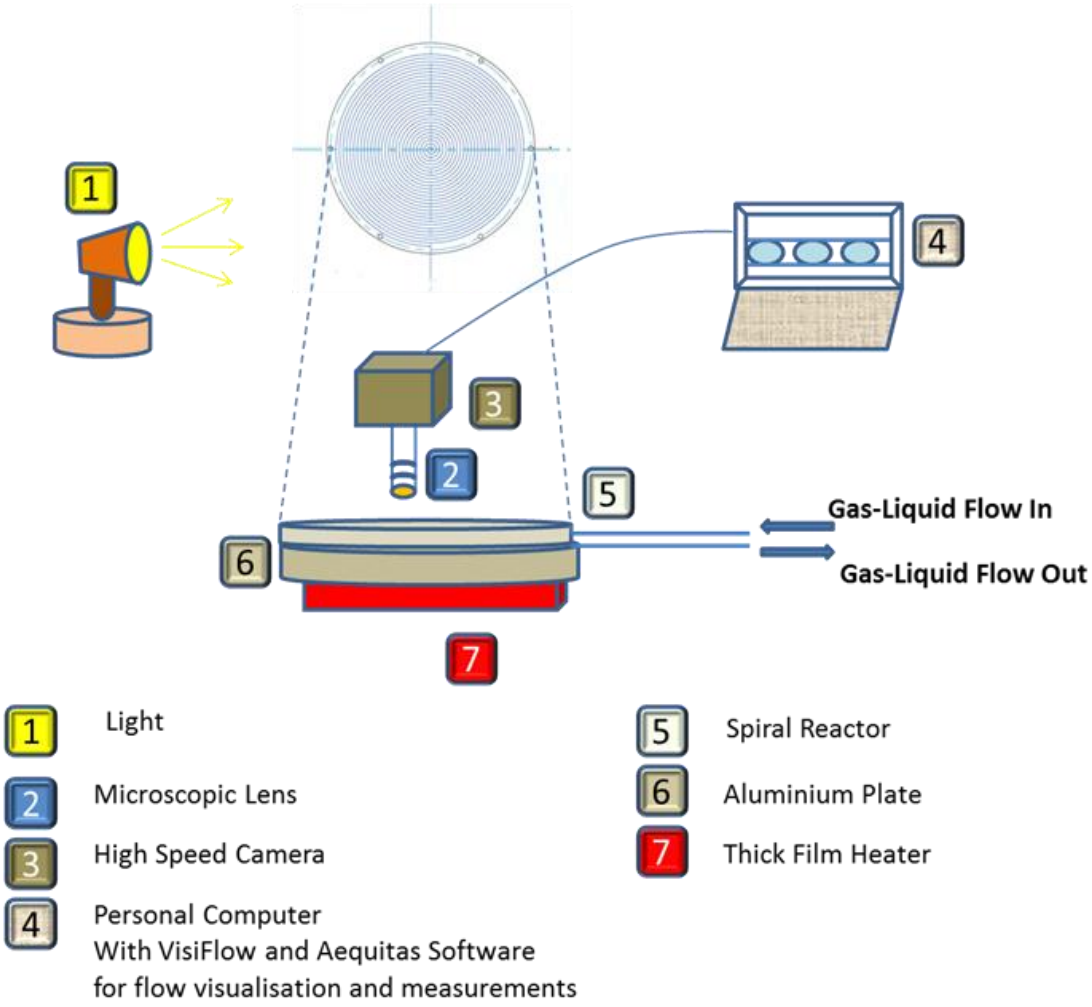

Figure 7.4. Experimental set-up for the spiral reactor utilized for flow visualization and measurements.

7.4 Gas-Liquid Contactors (Tees) Trials

Preliminary experiments showed that the type of gas-liquid contactor used has an effect on the experimental results obtained. As this was attributed to possible non-uniformities present in the gas-liquid flow, an attempt was launched to establish which was the best tee contactor to achieve homogeneous Taylor flow but with the additional requirement of producing small slugs for avoidance of gas concentration gradients inside the slugs. It has been reported in the literature that the recirculation zone inside the liquid slugs in Taylor flow is characterised by constant gas concentration and this is particularly true for short slugs (Kreutzer, 2003).

The tee contactors examined were the following five:

- ✓ **Static Mixing Tee**

  The tee U-466S, purchased from Upchurch Scientific has a PEEK body and is characterised by low swept volume of 2.2 μl (including frit volume). The thru-holes are 0.508 mm (0.020") and the centre port features a 10 μm stainless steel frit that creates high turbulent mixing. It is designed to operate for flows 0.5-3 ml/min at a maximum of 414 bar pressure.

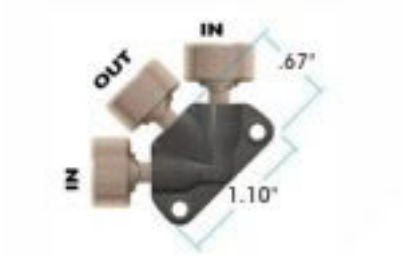

Figure 7.5 U-466S static mixing tee.

- ✓ **1.0 mm and 0.50 mm**

The tee that was initially used with the capillary microreactor was the U-429 from Upchurch Scientific with a thru-hole of 0.040”=1.0 mm and a swept volume 2.1 μl. It was later replaced by U-428 (Upchurch Scientific) with the same outside dimensions but with the smaller thru-hole 0.020”=0.50 mm and a swept volume 0.57 μl in order to get smaller liquid slugs.

Figure 7.6. U-428 tee with 0.50 mm borehole.

- ✓ **0.25 mm and 0.15 mm**

Two stainless steel tees 300 series, manufactured by Valco Ltd were purchased from Thames Restek Ltd and tried. The first one was the ZT1C for 1/16” tubing with a 0.25 mm bore. The second one was the MT1XCS6 for 1/16” tube and 0.15 mm bore.

Figure 7.7. Valco stainless steel tees.

7.5 Size Distributions and Repeatability Study

In order to find out the repeatability of the gas-liquid flow achieved in the spiral capillary reactor, a large amount of bubble and slug size measurements at the reactor inlet and outlet, were taken during experiments performed on different dates but under identical reaction conditions. The data presented here are slug and bubble size normal distributions obtained during experiments on 01-08-07 and 14-08-07 under the same reaction conditions using the static mixing tee U-466S. The flows correspond to Standard Pressure and Temperature conditions (STP) which are 20 ^{o}C and atmospheric pressure. At least 100 bubble end slug size measurements were taken for each set of data presented.

Experimental Conditions		
Parameter	Unit	Value
CO flow rate	ml/min, STP	0.10
C_2H_4 flow rate	ml/min, STP	0.30
Liquid flow rate	μl/min	5
G/L (STP) G/L (10 bar, 100C)		80 10.02
Pressure	bar	10
Temperature	^{o}C	100
Contactor	**Static mixing tee**	

Table 7.2. Experimental conditions for bubble and slug size measurements.

For the size distributions shown in the Diagrams below, the probability function is calculated using the formula for a specified mean and standard deviation:

$$f(x,\mu,\sigma) = \frac{1}{\sqrt{2\pi}\sigma} e^{-\left(\frac{(x-\mu)^2}{2\sigma^2}\right)}$$

The numbering 1, 2 corresponds to different experiments performed on a specific date.

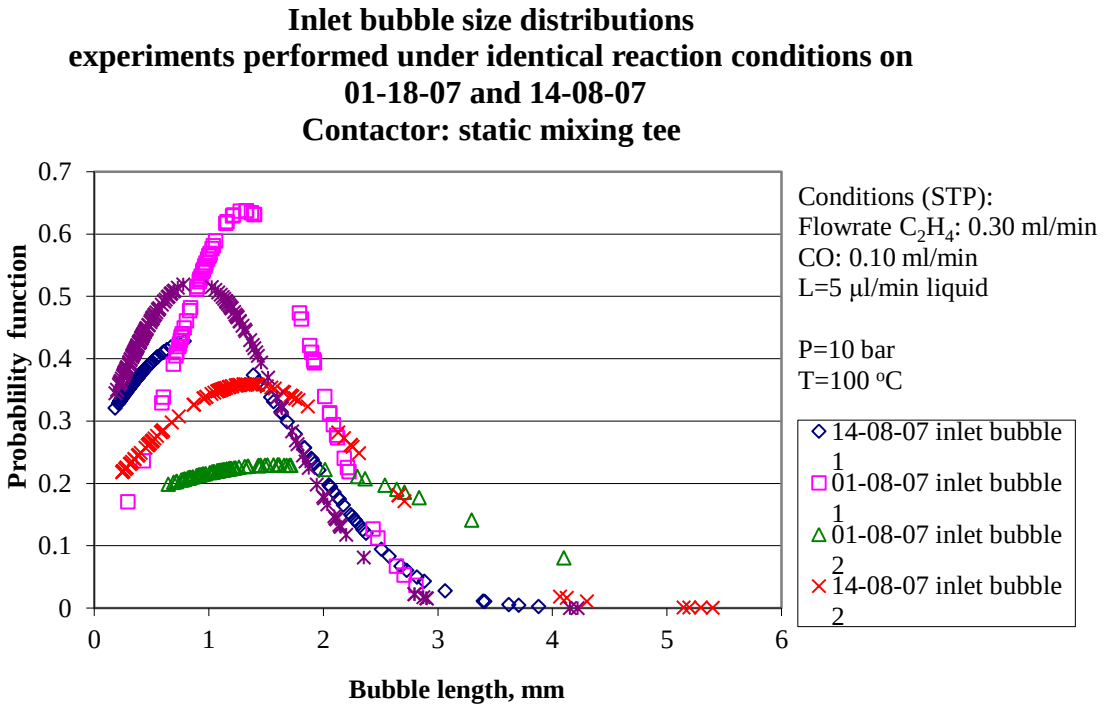

Figure 7.8. Size distributions of the bubbles at the reactor inlet. Contactor: Static mixing tee.

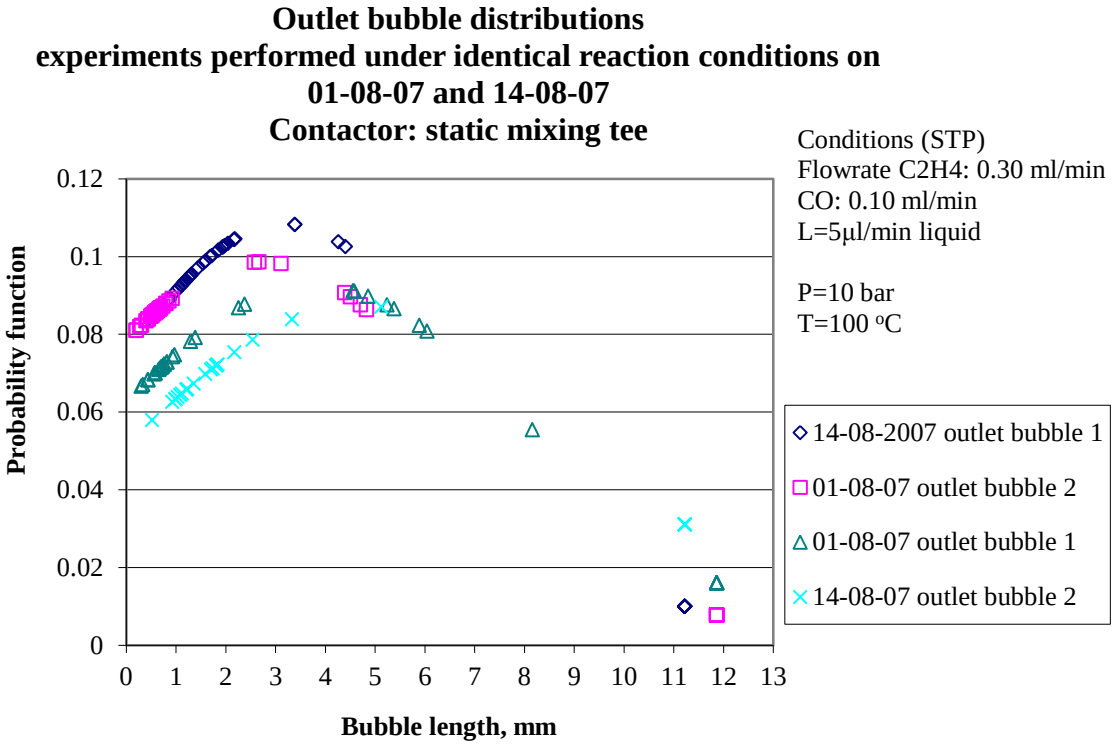

Figure 7.9. Size distributions of the bubbles at the reactor outlet. Contactor: Static mixing tee.

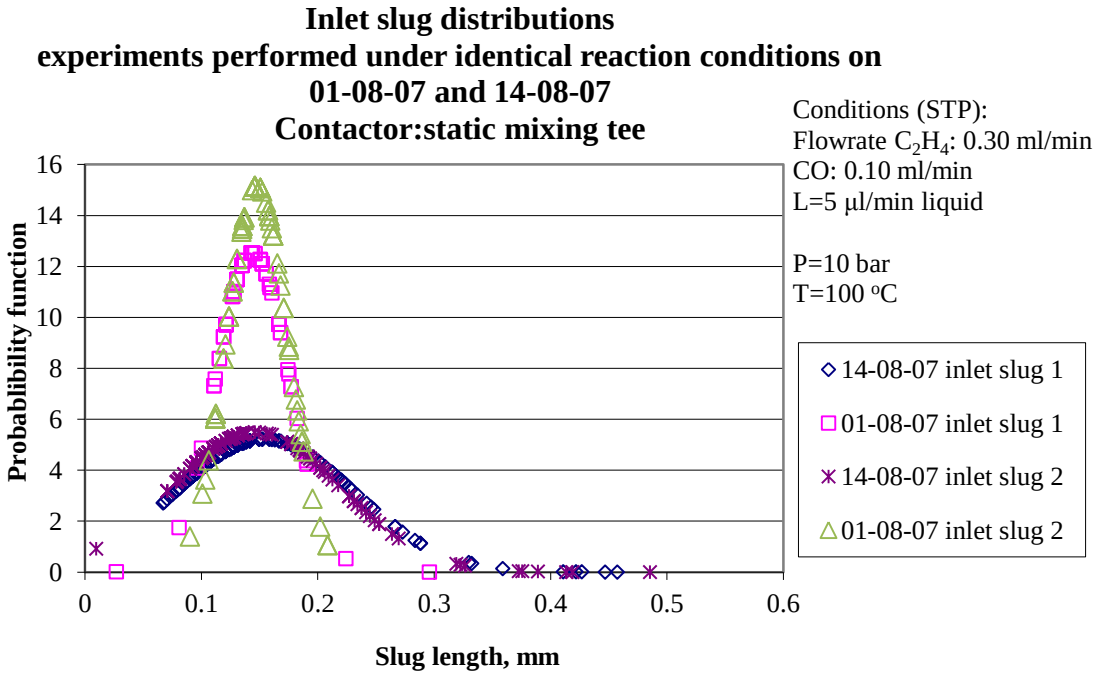

Figure 7.10. Size distributions of the slugs at the reactor inlet. Contactor: Static mixing tee.

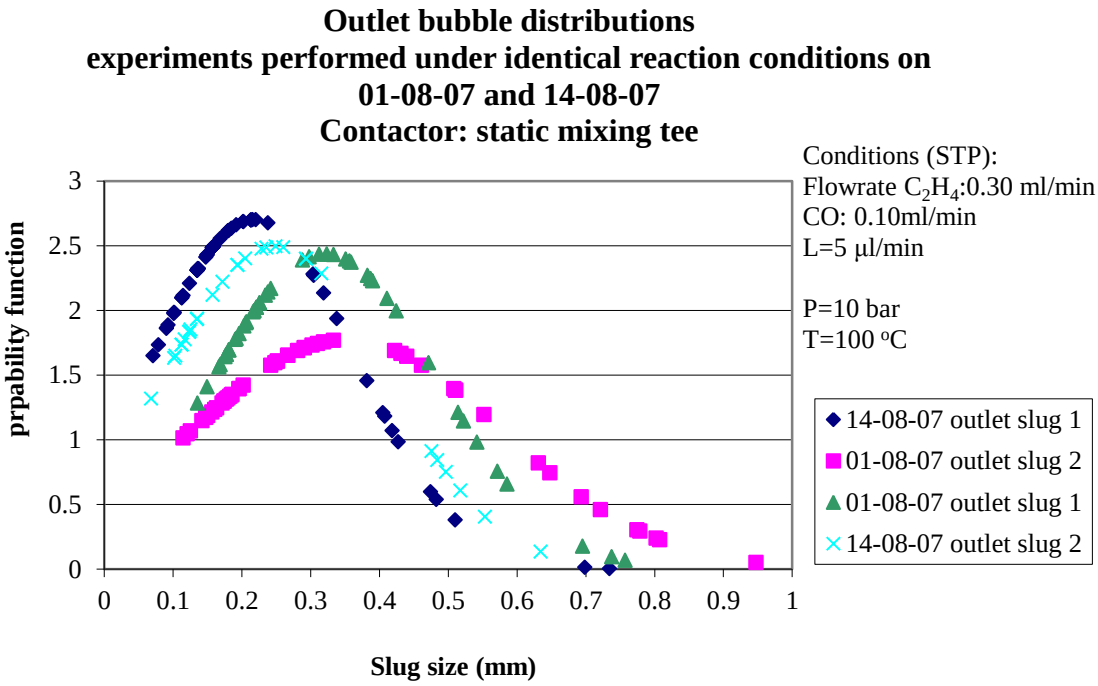

Figure 7.11. Size distributions of the slugs at the reactor outlet. Contactor: Static mixing tee.

The slug and bubble size measurements were carried out through flow visualization using the camera-microscope-computer system illustrated in Figure 7.4. A plethora of photographs of the flow were obtained, a sample of those is shown below, corresponding to the reactor inlet, outlet and at various intermediate positions of the spiral reactor. Homogeneous Taylor flow consisting of long bubbles many times the capillary tube diameter and tiny slugs are evident at the reactor inlet as well as at intermediate positions. Bubble and slug coalescence is also present along the tube and the farther to the reactor inlet, the more profound this phenomenon is. Figure 7.12 shows photographs of the flow obtained using the static mixing tee at conditions of 0.3 ml/min and 0.1 ml/min (STP) for the flow rates of ethylene and CO_2 respectively, while the liquid flow rate was 5 µl/min (STP).

(a) Inlet (b) Intermediate positions in the spiral

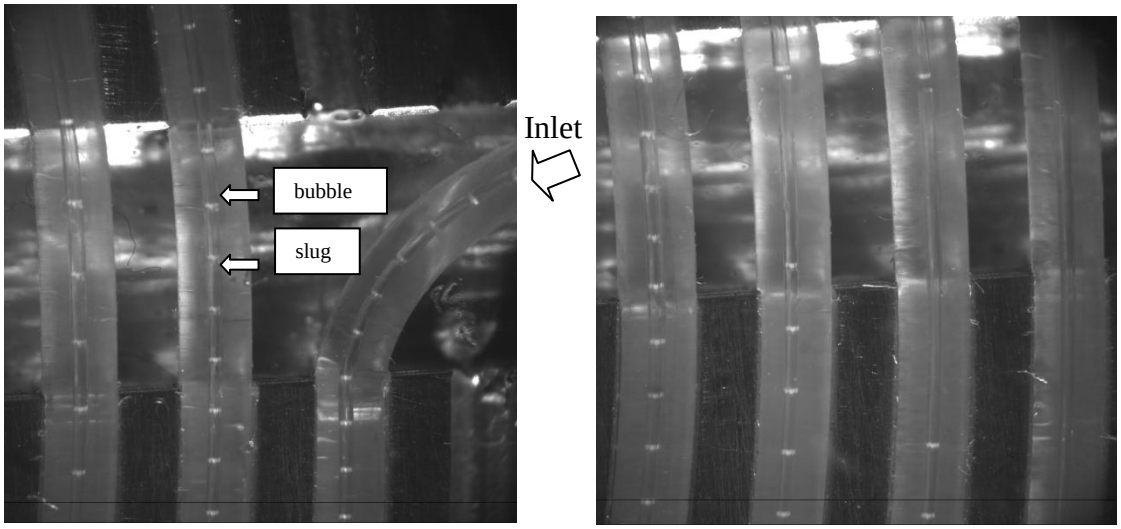

(e) Intermediate positions (d) Intermediate positions

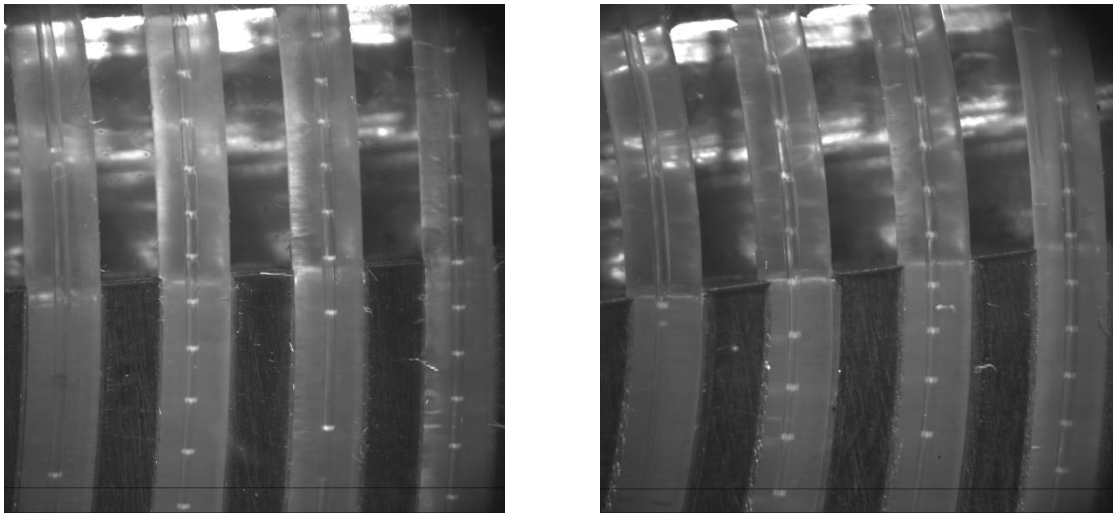

(e) Intermediate positions close to the outlet (f) Spiral outlet

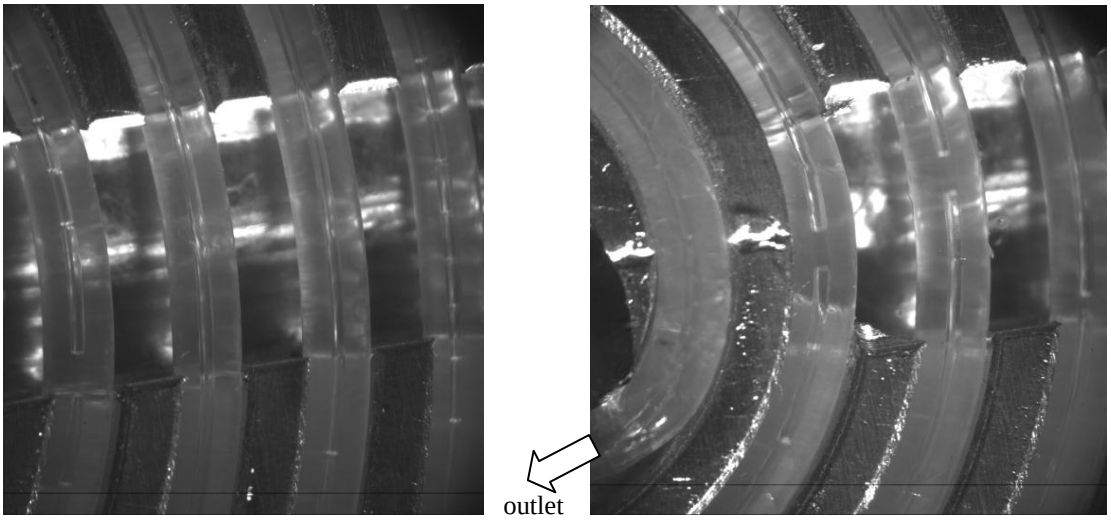

Figure 7.12. Photographs obtained through flow visualization using the spiral reactor.

Figures 7.7 to 7.11 show better agreement between the size distributions of slug and bubbles obtained from different experiments performed under the same conditions on the same day rather on different dates. Homogeneous Taylor flow was the predominant gas-liquid pattern at the reactor inlet and at intermediate positions near the reactor entrance. Bubble and slug coalescence and size increase was observed along the spiral reactor as it can be seen from the following Table and Figures 7.13 and 7.14. It was measured that for a G/L flow ratio at reaction conditions equal to 10.02, the ratio (bubble length/slug length) was 10.67 at the inlet.

	Inlet 1(mm)	**Inlet 2(mm)**	**Outlet 1(mm)**	**Outlet 2 (mm)**
Mean bubble size	1.3	1.58	3.80	2.73
Mean slug size	0.144	0.148	0.32	0.35
Stand. Deviation bubble size	0.63	1.74	4.3	4.0
Stand. Deviation slug size	0.032	0.026	0.16	0.22
Conditions: C2H4: 0.3 ml/min, CO: 0.1 ml/min, L=5 μl/min(STP), P=10 bar, T=100 ^{o}C, contactor: static mixing tee				

Table 7.3. Mean bubble and slug sizes, at reactor inlet and outlet. 1 and 2 denote different experiments.

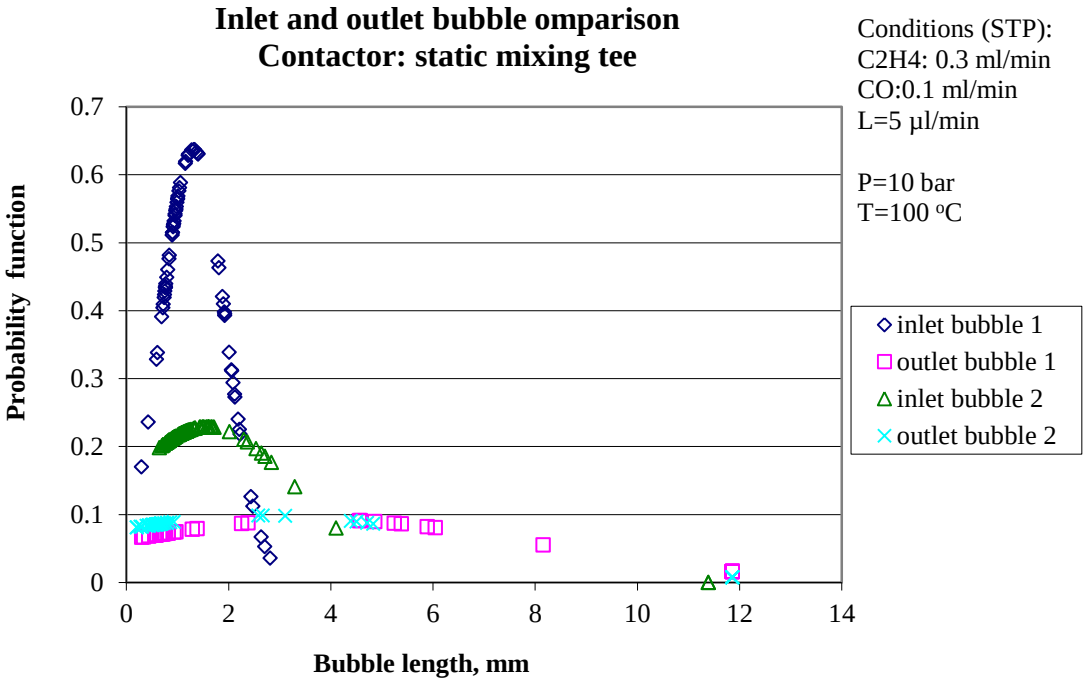

Figure 7.13. Measurements of bubble sizes at the reactor inlet and outlet for comparison.

Contactor: Static mixing tee.

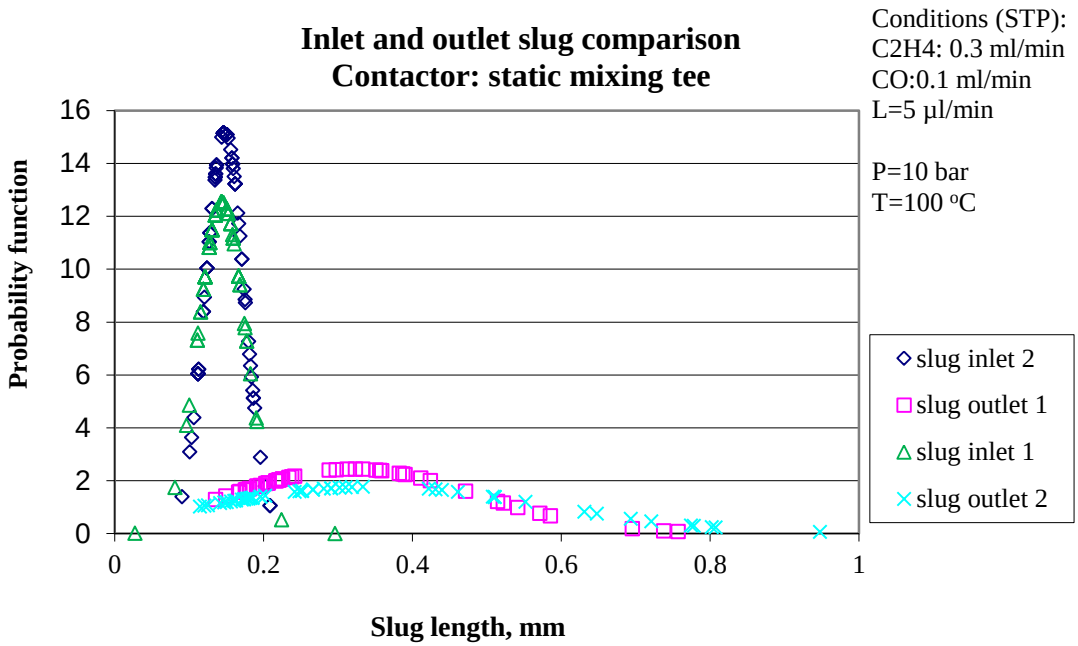

Figure 7.14. Measurements of slug sizes at the reactor inlet and outlet for comparison.

Contactor: Static mixing tee.

From the results of the experiments conducted we can conclude that the flow shows satisfactory repeatability. In addition, the size distribution is very narrow at the inlet but broad at the outlet for the slugs and the bubbles due to bubble and slug coalescence.

The evolution of the slug size as the slugs move along the spiral reactor is shown in the following Figure for distances up to 4.1 m from the inlet. As it can be seen, slugs have a narrow distribution which broadens substantially after 1m distance from the inlet. Data for up to 6 m was collected and the distributions were similar to the ones taken at 3.8 m and 4.1 m from the inlet. These data is not presented in Figure 7.15 for clarification purposes.

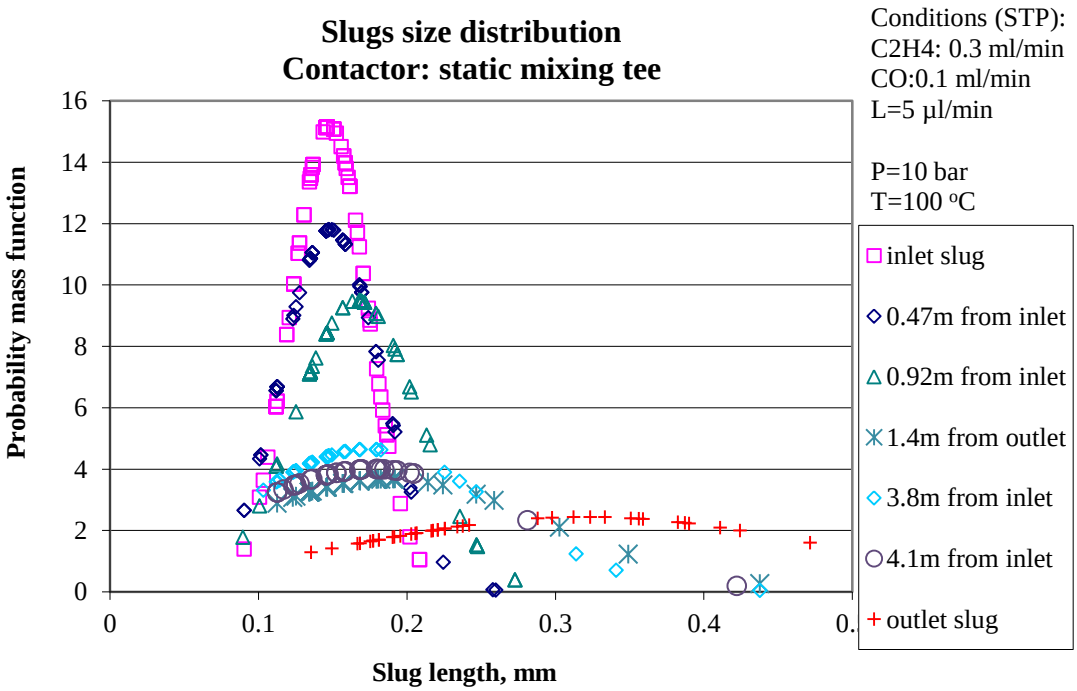

Figure 7.15. Size evolution of the slugs as they travel along the spiral reactor.

Similar results were obtained for the bubbles as depicted in Figure 7.16. The distribution of the inlet bubbles entering the spiral reactor is narrow at the spiral inlet but due to bubble coalescence larger bubbles start appearing from around 0.5 m distance from the inlet. The size distribution does not change substantially from 1.8 m from the spiral inlet. Data corresponding to the distance 1.8 to 6 m was also gathered but was omitted as it would merely add to the complexity of the Figure below without providing any new information.

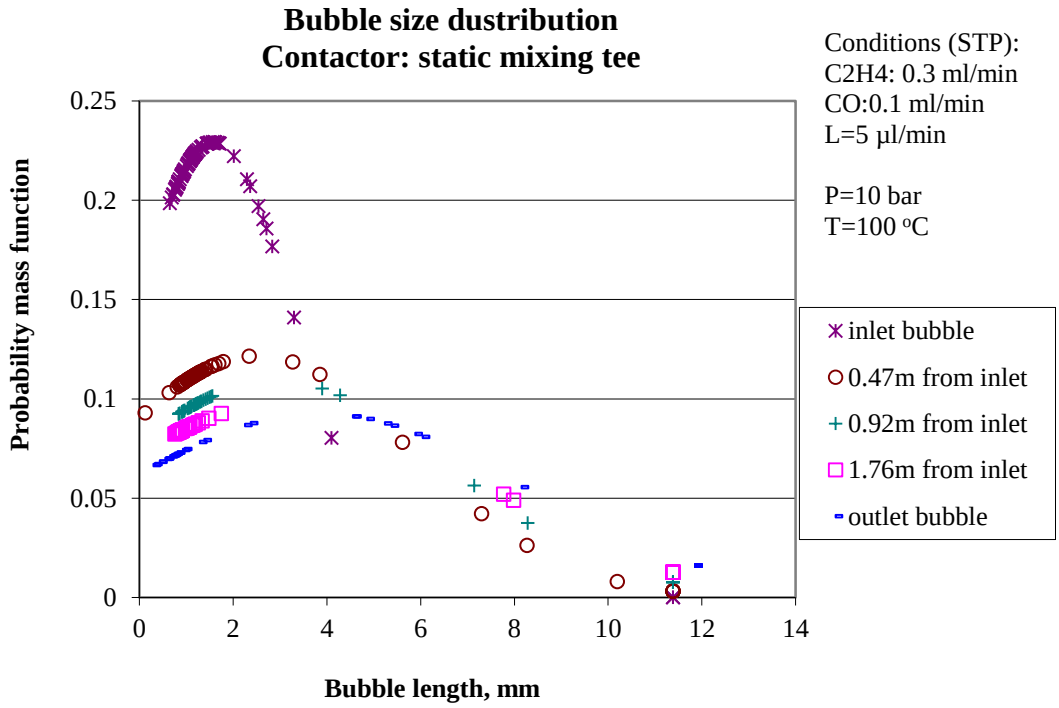

Figure 7.16. Size evolution of the bubbles as they move along the spiral.

Figure 7.17 shows the bubble and the slug size evolution as they travel along the Spiral Reactor. Data presented cover the reactor inlet until round 12 which corresponds to 3.5 m distance from the spiral reactor inlet. The average bubble size

was found to increase from 1.58 mm at the inlet to 3.66 mm at round 4 (1.35 m from the inlet) after which it was decreased through to round 7 (2.53 m from the inlet) to 2.64 mm. The size increased from that distance onwards and reached 3.78 mm at round 11 which coincides with 3.5 m from the inlet. Flow homogeneity is lost along the reactor due of bubble coalescence resulting in an increase of bubble size of 121 % to 3.49 mm from the spiral inlet to round 12. Therefore, it is rather impossible to measure the extent of the reaction by measuring bubble size changes.

Data showed that the mean slug size follows a wave trend as the slugs travel along the spiral. The mean slug size was measured to increase from 0.148 mm reaching 0.218 mm at round 6 which corresponds to 2.16 m from the spiral inlet. Subsequently, the mean slug size declined through to round 10 (3.21 m from the inlet) after which it increased again to 0.178 mm at round 12.

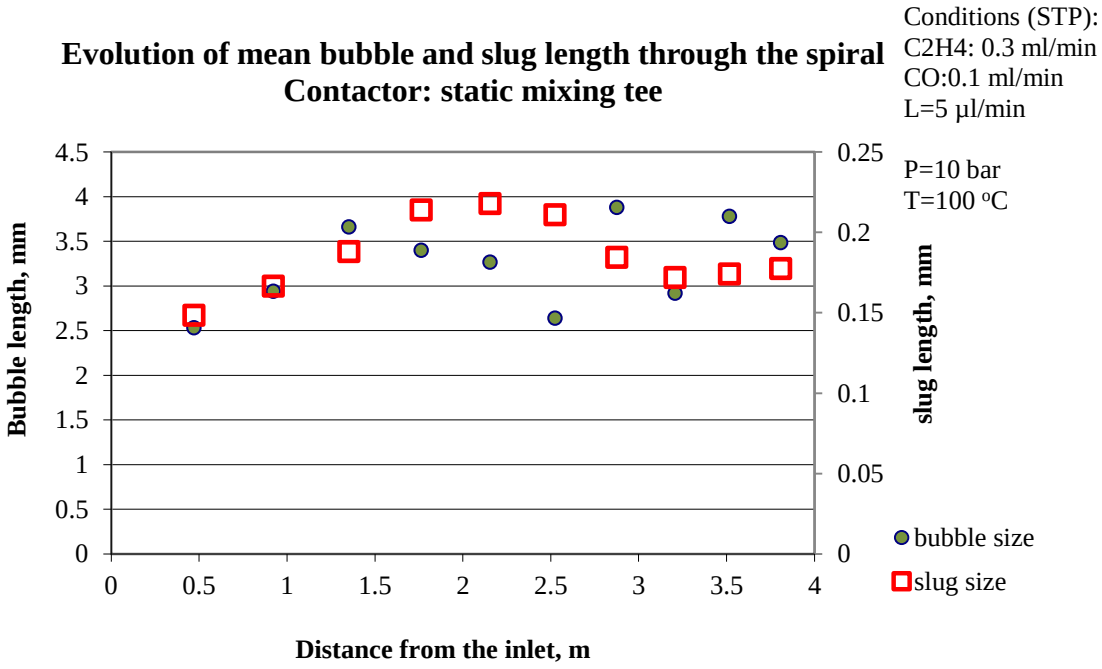

Figure 7.17. Bubble and slug size evolution through the spiral.

According to Kreutzer, 2003, Taylor flow does not exhibit coalescence but in our system and for our experimental conditions, slug coalescence was observed starting at distances above 1 m from the spiral inlet and at around 0.5 m for the bubbles. A possible reason for that might have been the pressure fluctuations at the capillary inlet or outlet. The former are created at the point when the break-up of the fluid segments in the tee-junction. The latter are caused by the pressure controller whose valve opens and closes slightly around three-four times per hour in order to maintain the pressure at the 10 bar set-point. Experimental observations in the framework of this study showed that the pressure fluctuations in the reactor outlet are more significant. Another factor which might be causing the coalescence is the slight flow rate fluctuations caused by the gas flow meters or the syringe pump. Finally, the curvature of the capillary in spiral form probably played a role as compared to using straight tubing as increased curvature leads to increased flow inhomogeneity (Kumar et al., 2007). Due to the phenomenon of bubble coalescence, the idea of obtaining preliminary kinetics for the methoxycarbonylation of ethylene by measuring the decrease of bubble size as the gas gets consumed along the capillary and thus determining the extent of reaction, did not bear any fruit.

One explanation of the up and down trend in average bubble and slug lengths along the spiral depicted in Figure 7.17 could be competition amongst different phenomena:

- Coalescence increases the bubble and slug lengths.
- Reaction, which occurs only in the liquid phase, decreases the bubble length and increases the slug length.
- Pressure drop increases the bubble length and decreases the slug length.

7.6 Flow Homogeneity Investigation

- The flow conditions affect the performance of small borehole gas-liquid contactor in producing homogeneous flow. A comparison between the 0.15 mm and 0.25 mm tee-junctions, showed that for the same gas/liquid rate ratio the former gives better results at lower gas flow rates. It was found that, for the experiments performed at G/L=10 at STP conditions, the 0.15 mm tee produced narrower size distribution of slugs and bubbles at the lower combined gas flow (CO and ethylene) of 1.1ml/min (STP) while the same was true for the larger thru-hole contactor of 0.25 mm when the 1.5ml/min gas flow was utilised. Furthermore, the 0.15 mm tee produced more homogeneous flow against the 0.25 mm tee at low gas flow rates as it is evident in the subsequent comparative photographs of the gas-liquid flow.

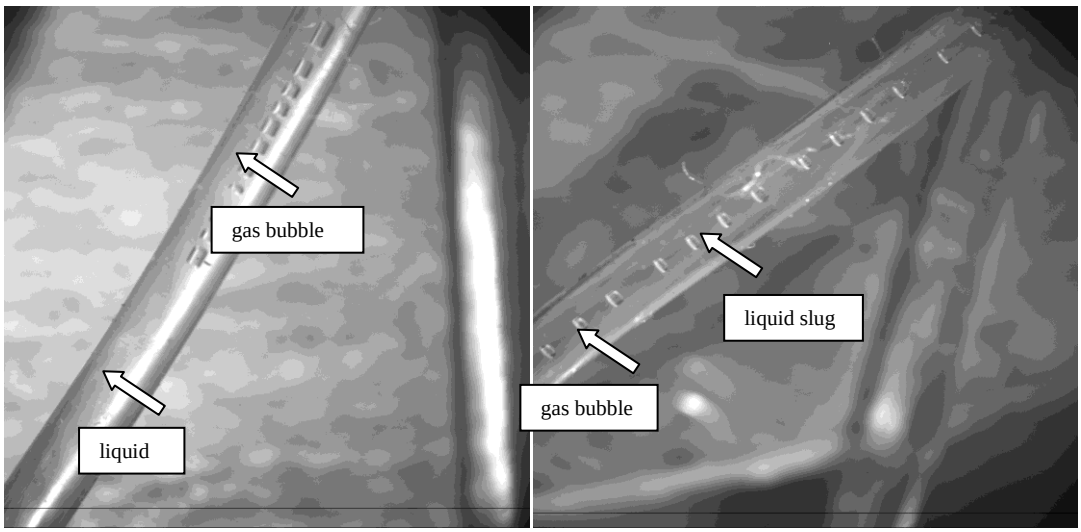

0.25mm tee **0.15mm tee**

Conditions STP: C2H4:0.3ml/min, CO: 0.3ml/min, L: 0.06ml/min, 100^{o}C, 10 bar.

Figure 7.18. Comparison of flow patterns obtained with different tees under the same operating conditions.

- The SS 0.25 mm and 0.15 mm tee-junctions produced very small slugs but did not produce homogeneous Taylor flow and therefore their use is not recommended under the experimental conditions applied for this study. A comparison of the results obtained with the various tee contactors are included in Appendix F.
- The static mixing tee performed better amongst the small bore tees.
- The best results regarding flow homogeneity were produced with the 1 mm and 0.50 mm tees. The drawback of the former one was that it generated large slugs (2-3 mm in length).

Figures 7.19-7.20 show the comparison between the slug and bubble distributions obtained with the 0.25 mm and 0.15 mm tee. The flow rate of ethylene and CO was 1.0 ml/min (STP) and 0.5 ml/min (STP) respectively while the liquid flow rate was 0.15 ml/min (STP). The gas/liquid flow rate ratio was equal to 10 measured at STP conditions or at the reaction conditions of 10 bar pressure and 100 ^{o}C temperature that is equal to 1.27. As it can be seen from the experimental data, 0.25 mm gave a narrower distribution of bubbles compared to the 0.15 mm tee contactor. Even better were the results of the 0.25 mm tee compared to those of 0.15 mm regarding the slugs. Furthermore, even though one would expect the size of slugs produced with the 0.15 mm to be smaller compared to those of 0.25 mm, this did not look the case. The 0.15 mm tee produced a range of slug sizes from 0.13 to 2.2 mm. It seems that the larger size borehole of the 0.25 mm contactor is beneficial at high flow rates.

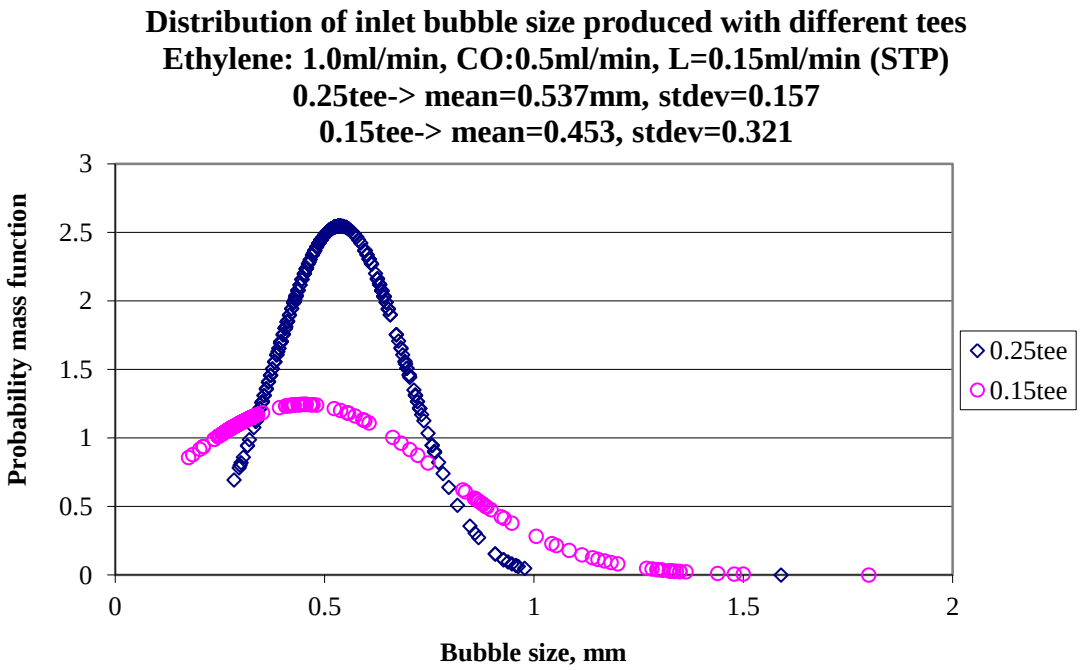

Figure 7.19. Comparison of inlet bubble size distributions produced with the 0.25 and 0.15mm tees.

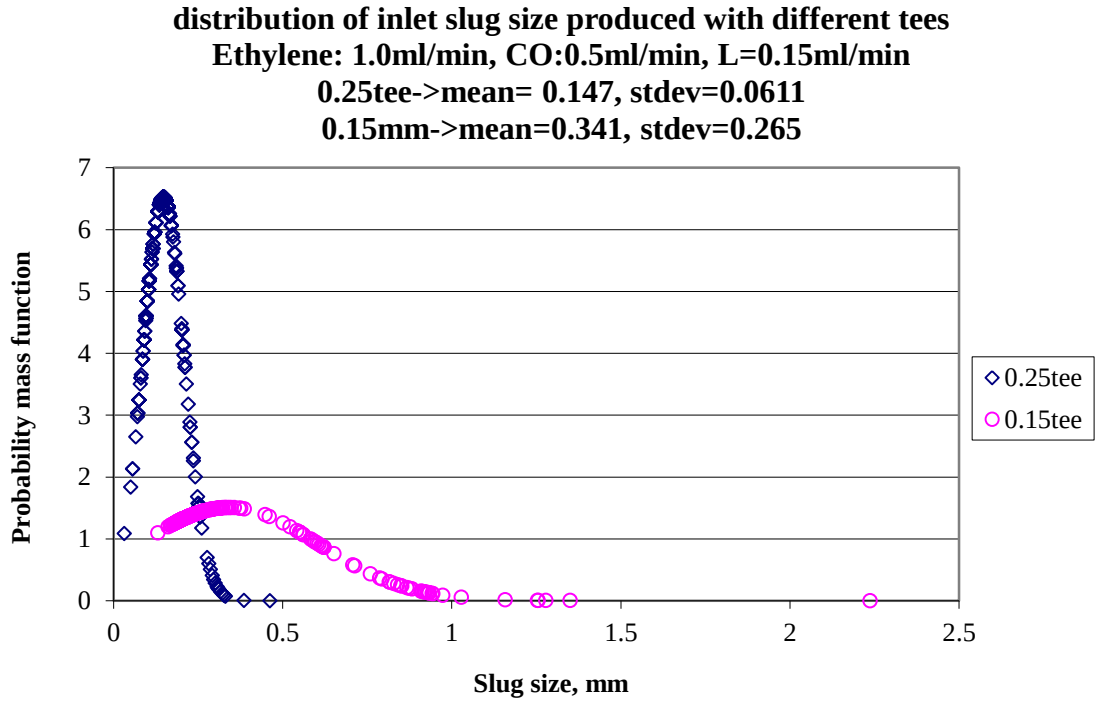

Figure 7.20. Comparison of inlet slug size distributions produced with the 0.25 and 0.15mm tees.

Figures 7.21-7.22 show the comparative results between the two tee contactors at the lower flow rates of 1.0 and 0.1 ml/min (STP) for the ethylene and CO and 0.11 ml/min for the liquid mixture. The gas/liquid flow rate ratio is 10 measured at STP conditions and 1.21 at reaction conditions. Here we see the opposite situation to that explained earlier. The 0.15 mm tee was the contactor which gave the best results compared to the larger tee at lower flow rates.

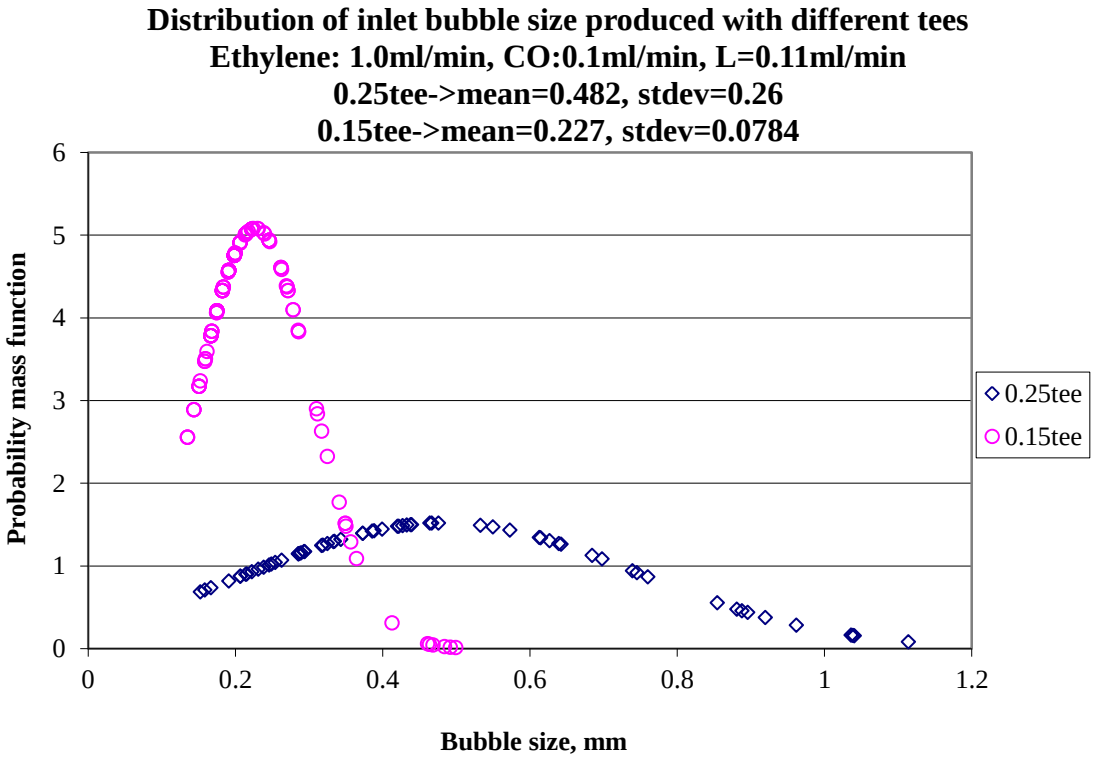

Figure 7.21. Comparison of inlet bubble size distributions produced with the 0.25 and 0.15mm tees.

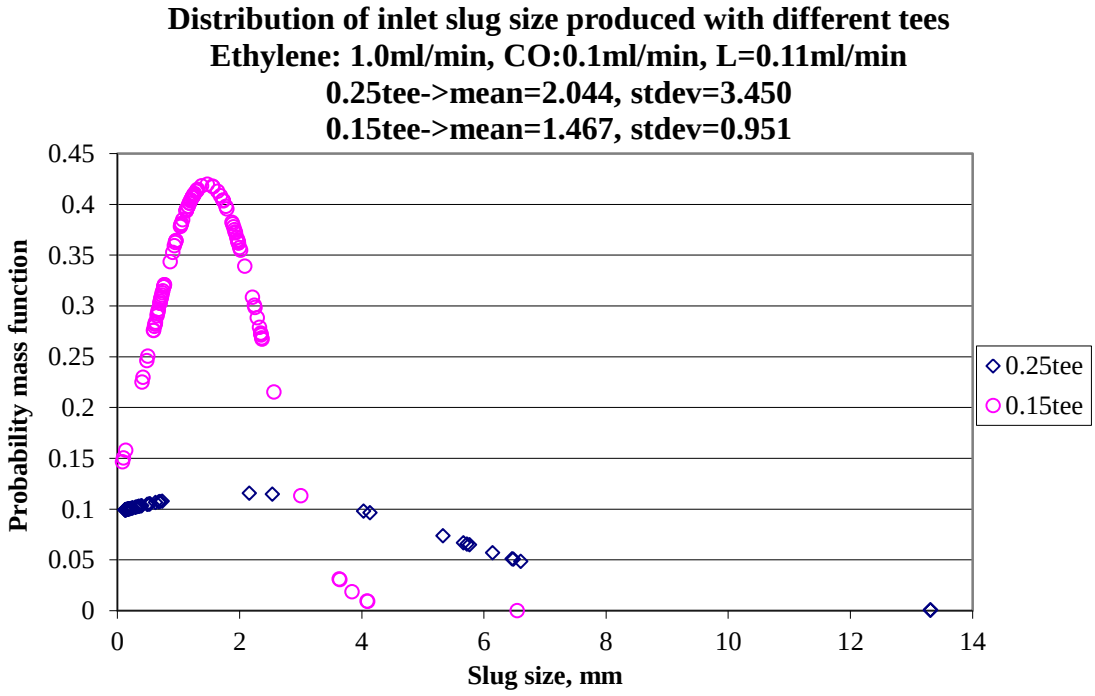

Figure 7.22. Comparison of slug size distributions produced with the 0.25 and 0.15mm tee contactors.

The photographs which are presented below correspond to experiments performed with the 0.50 tee-junction. It was observed that for G/L (STP) ratio of 40, Taylor flow is very homogeneous as it can be seen from Figure 7.23 (e). By 'homogeneous Taylor flow' in this study we mean, a structured flow consisting of one bubble followed by a slug, followed by the same size bubble, followed by a same size liquid slug etc. Through experimentation, it was also found that when higher gas flow rates were utilised the flow was a repeating pattern of 2-11 bubbles of unequal sizes separated by minuscule slugs in the μm scale (Fig. 7.23 a-d).

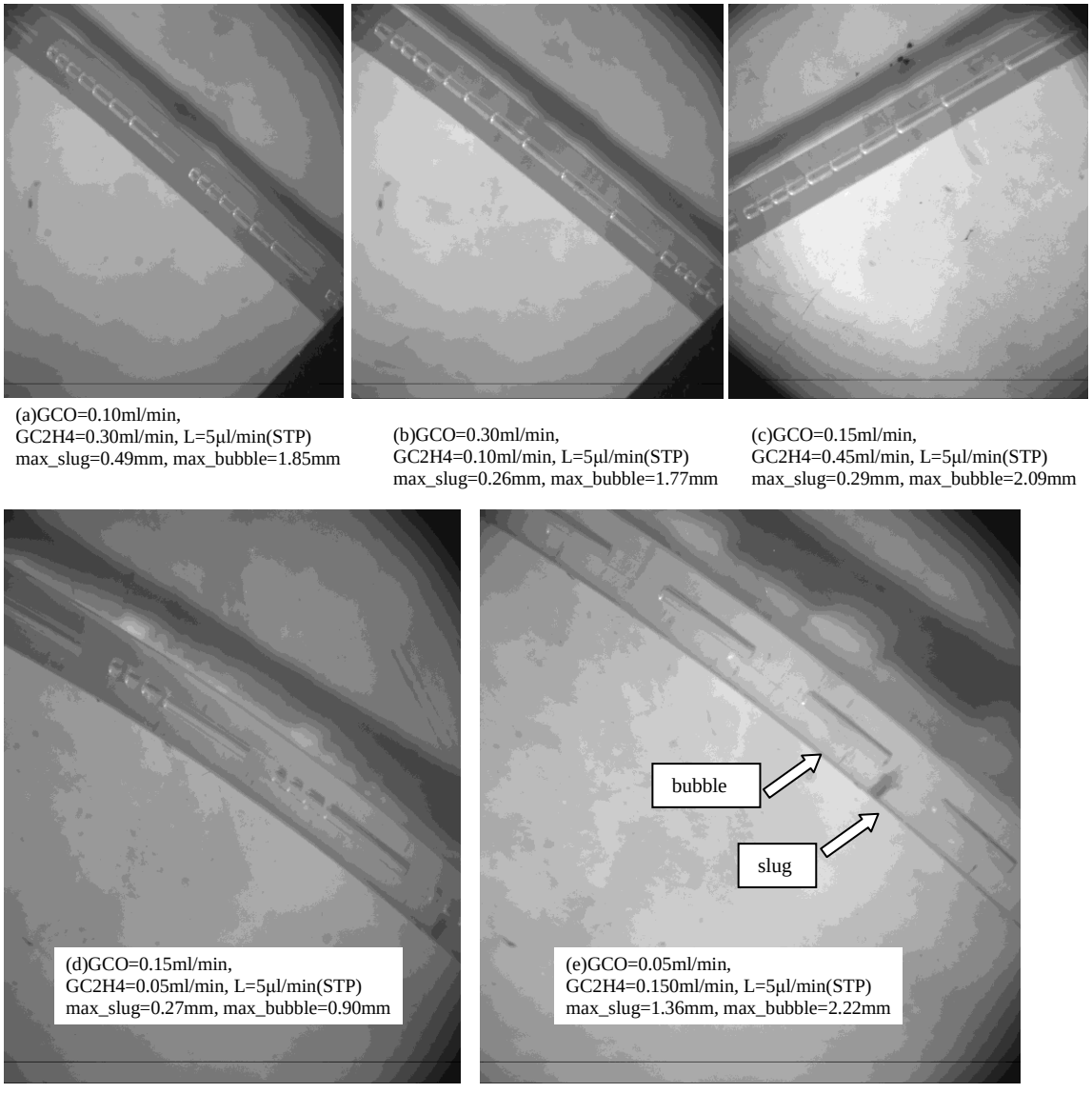

Figure 7.23. Flow visualization and measurements using 0.50mm t-junction.

In conclusion, the 0.50 mm tee was chosen to be used for the kinetic experiments as it performed the best in terms of small slug length and Taylor flow homogeneity.

7.7 Set-Up Improvements

Bubble and slug sizes in Taylor flow emerging from a tee-contactor depend on a number of parameters like tee inlet orientation and geometry, channel sizes, wettability of materials and gas and liquid superficial velocities with the gas velocities being more important (Garstecki et al., 2006 and Hessel, 2005). In addition, inlet pre-mixing results in smaller bubbles and slugs.

Taking the above into consideration, different configurations of the experimental set-up were tried with the aim to improve the homogeneity of Taylor flow:

- **Different inlet orientation of the 0.50 mm tee**

Numerous experiments were performed initially using the configuration below for gas-liquid contact in the tee:

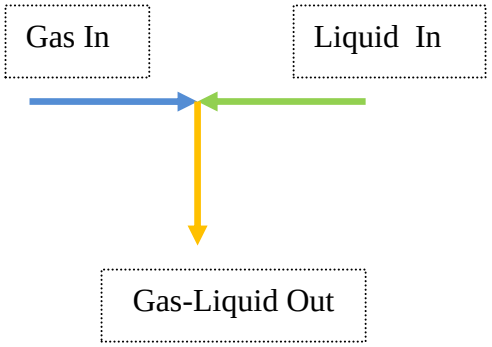

The following configuration was tried and it was found to improve flow homogeneity. The gas-liquid flow produced after the tee, consisted of more equally sized bubbles when high gas/liquid ratios were utilised.

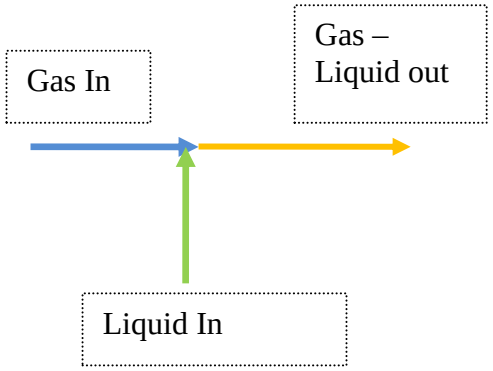

- **The pulse dampener was placed after the capillary reactor but there was no improvement of the flow.**

- **Different pump**

The pumping system NEMESYS was tried against the KdS 410 High Pressure pump regarding flow pulsations. The manufacturing company of the NEMESYS claimed that their syringe pump produces less pulsations than most syringe pumps in the market. Comparative tests were performed and photographs were taken but NEMESYS did not seem to improve the homogeneity of the flow. In addition, pulsations were also observed. Another disadvantage of the NEMESYS was that due to the fact that its linear force was 60 lbs compared to 100 lbs (at least) of the KdS 410, the former proved inadequate to pump at 10 bar and the reaction pressure had to be lowered to 9 bar.

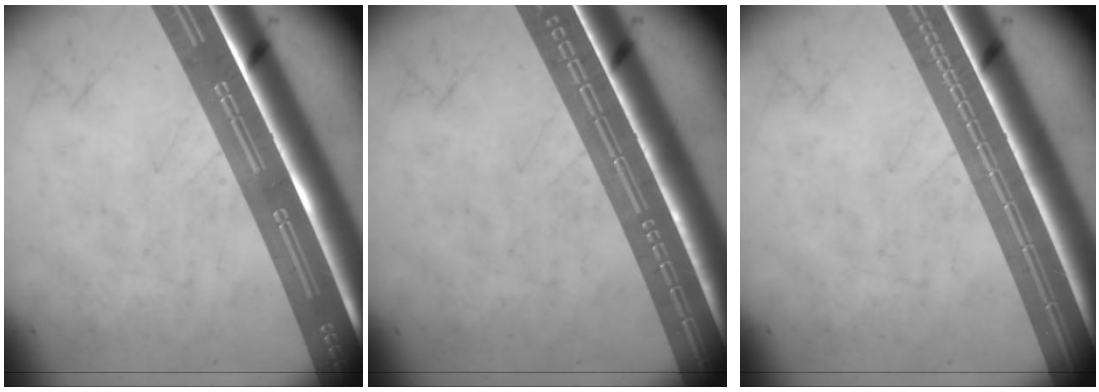

Gas flow increasing

Figure 7.24. Flow pictures obtained using the NEMESYS pump. Flow inhomogeneous.

- **Tubing replacement**

The tubing before the tee contactor for the gas and the liquid streams used to be 0.80 mm ID and 1/16'' OD. It was replaced with the same tubing used for the reactor, that is 0.25mm ID, 1/16" OD. This improved the flow homogeneity.

- **Pressure transducers were incorporated in the set-up**

The first one was placed before the reactor and was tried at the gas inlet as well as the liquid inlet and the pressure was measured and monitored for fluctuations. The second one was placed and tried after the condenser, just before the pressure controller. Again the pressure was measured and the pressure fluctuations monitored. The pressure differential between reactor inlet (liquid side) and condenser outlet was measured and was found to be close to calculated estimates (please refer to Section 7.10 of this Chapter). The pressure fluctuations at the inlet are not major but the pressure fluctuations at the outlet can be large when the valve of the pressure controller opens and then closes again to regulate the pressure. This was found to

happen every 19 min for a typical experiment. The homogeneity of the flow is instantly lost and the flow accelerates due to the sudden pressure drop but then equilibrium is reached fast and the Taylor flow is re-stabilised. It was found that pressure fluctuation effects on the flow were minimal in the few cases where all the gas had been consumed by the reaction and the stream exiting the reactor was full of liquid.

In conclusion, the successful steps taken to improve the flow homogeneity were firstly the use of the correct tee for gas-liquid contact, secondly the change of the tee orientation and finally the replacement of the tubing. It was also found that homogeneous Taylor flow is achieved at low gas flow rates. If the gas flow is increased, instead of the Taylor flow we get a repeating pattern of two bubbles (not of same size) separated by a slug which is referred to as bubble train flow. This is evident in the photographs which follow (please refer to Figure 7.25 (a) and (b)). If we increase the gas flow even further we get a repeating pattern consisting of three or more bubbles.

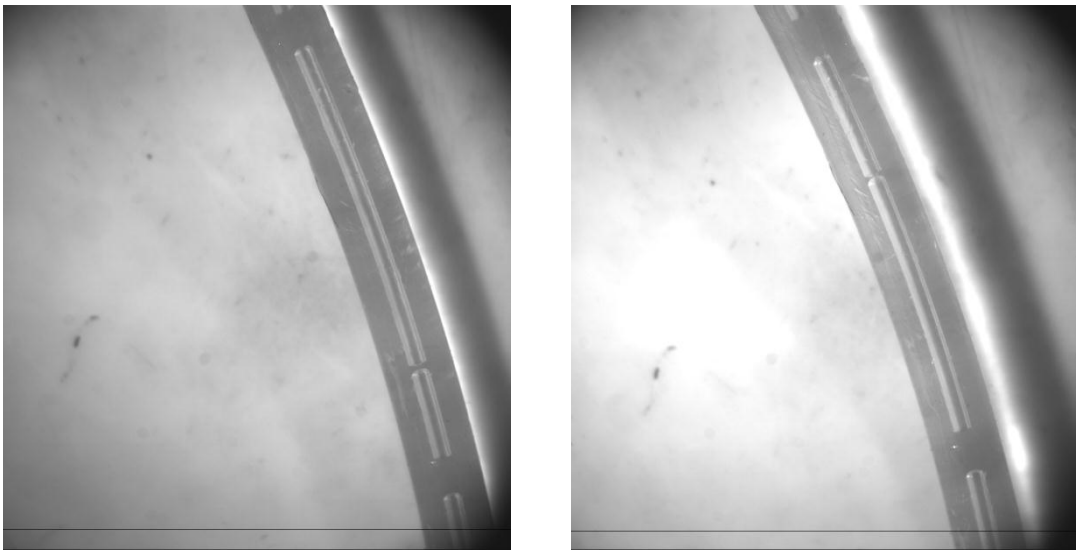

(a)Date: 08-01-08

G_CO=0.15 ml/min

G_C2H4=0.45 ml/min

L=5 μl/min (STP)

Aver. bubble=9.05 mm

Aver. slug=0.90 mm

Aver. slug=0.90 mm

(b)Date: 10-01-08

G_CO=0.10 ml/min

G_C2H4=0.50 ml/min

L=5 μl/min (STP)

Aver. bubble=8.40 mm

Aver. slug=0.95 mm

Aver. slug=0.95 mm

Figure 7.25. Flow visualization with 0.50mm tee-junction after set-up improvements. The flow pattern is bubble-train flow.

Examples of homogeneous flow are seen in the subsequent photographs of Figure 7.25a:

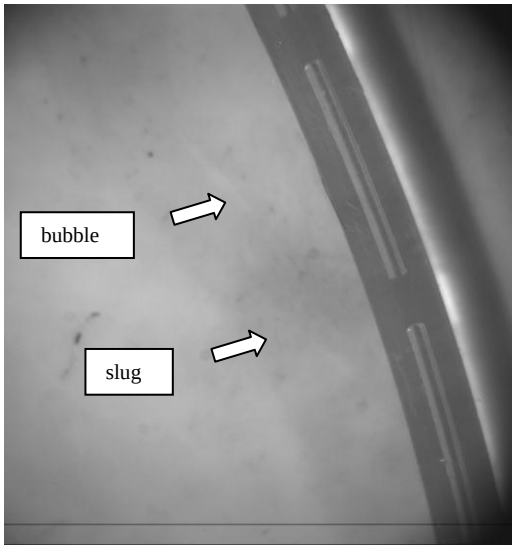

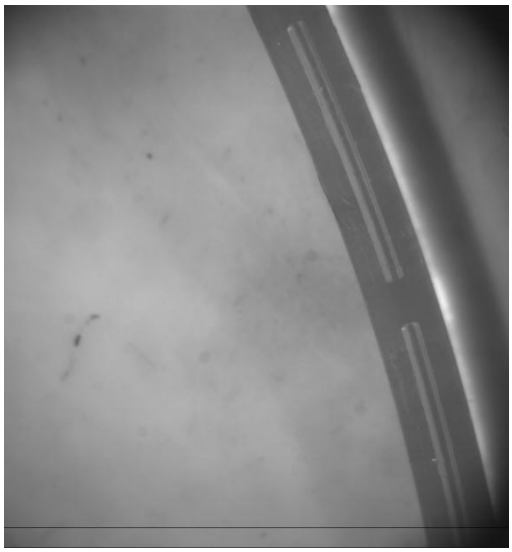

(a)Date: 07-01-08

G_CO=0.10 ml/min

G_C2H4=0.30 ml/min

L=5 μl/min (STP)

Aver. bubble=5.03 mm

Aver. slug=1.07 mm

(b)Date: 07-01-08

G_CO=0.12 ml/min

G_C2H4=0.36 ml/min

L=5 μl/min (STP)

Aver. bubble=6.03 mm

Aver. slug= 0.94 mm

Figure 7.25a. Flow visualization with 0.50mm tee-junction after set-up improvements. The flow pattern is Taylor flow.

The photographs of Figures 7.25 and 7.25a were taken at the reactor entrance under reaction conditions and the liquid flow rate at 5 μl/min. The factors that differ are the gas flows for CO and for C_2H_4. The 0.50 mm tee junction was used for these experiments.

The flow improvement is evident after the set-up modifications if for example Figure 7.25a (a) is compared to Figure 7.23(a).

A summary of the set-up improvements and their outcome is given in Table 7.4.

Action	Improvement?	Comment
The pulse dampener was placed after the capillary reactor	×	
Different orientation of the 0.50mm tee	✓	
Different syringe pump used for the liquid feed	×	
Tubing replacement	✓	
Pressure transducers were incorporated in the set-up	✓	Enabled capability to investigate whether fluctuations of the system pressure disturb the flow or not; pressure fluctuations exist at the reactor inlet and outlet but the latter perturb the flow the most.

Table 7.4. Summary of set-up improvement attempts and outcomes.

7.8 Liquid Slug Length

The average liquid slug length decreases when the gas superficial velocity increases for a given liquid superficial velocity equal to 1.48 10^{-3} m/s at reaction conditions (corresponding to 5 μl/min liquid flow STP) and the relationship was found to be linear with correlation coefficient 0.824 as it is depicted in Figure 7.26 below.

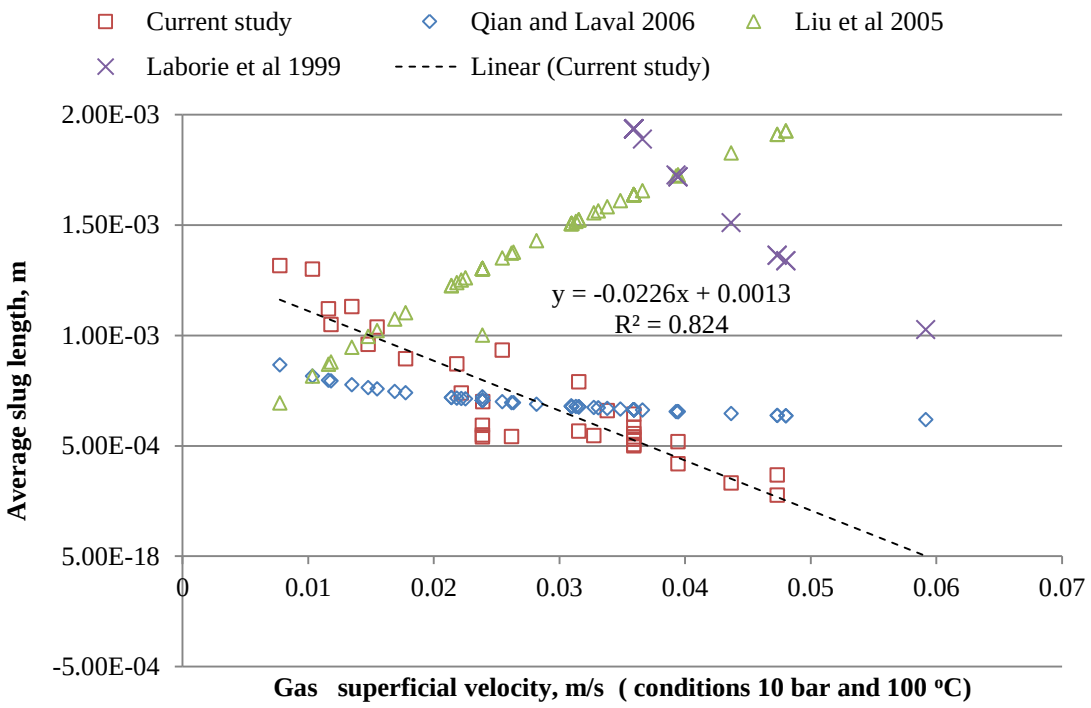

Figure 7.26. Effect of gas superficial velocity on liquid slug length.

A comparison of the experimental data with the calculated values using the correlations reported in the literature suggests a relative agreement with the one proposed by Qian and Laval, 2006, applicable for capillaries with diameter 0.25-1.0 mm.

$$\frac{L_S}{d} = 1.637\varepsilon_G^{-0.893}\left(1-\varepsilon_G\right)^{-0.05}\mathrm{Re}^{-0.075}Ca^{-0.0687}$$ (Qian & Laval, 2006)

$$\frac{L_S}{d} = 3451\frac{\left[\mathrm{Re}(U_G)\right]^{-1.27}}{Eo^{1.27}}$$ (Laborie et al., 1999)

$$L_S = \left[\frac{U_G + U_L}{0.088 \mathrm{Re}_G^{0.72} \mathrm{Re}_L^{0.19}} \right]^2$$ (Liu et al., 2005)

The correlations brought forward by Laborie et al., 1999 and Liu et al., 2005 do not agree with the experimental data. Particularly the latter showed the opposite trend with slug length increasing with the gas superficial velocity instead of decreasing. These correlations were developed for larger capillaries; the former for 1-3 mm and the latter for 0.9-3 mm capillary.

7.9 Flow Map

For the extremely low range of superficial velocities used in the present study, the observed flow pattern was expected to fall within the boundaries of the slug flow regime and indeed, this was found to be true. However, it is worth noting that there was not previous research conducted within the limits or even near the operating conditions chosen for this study, namely 0.0059 m/s<U_G<0.047 m/s and U_L=0.00148 m/s at reaction conditions, as it is evident from the subsequent Figure which depicts the flow map produced by Yue et al. (2008) for three microchannels with different diameters (667 μm, 400 μm and 200 μm).

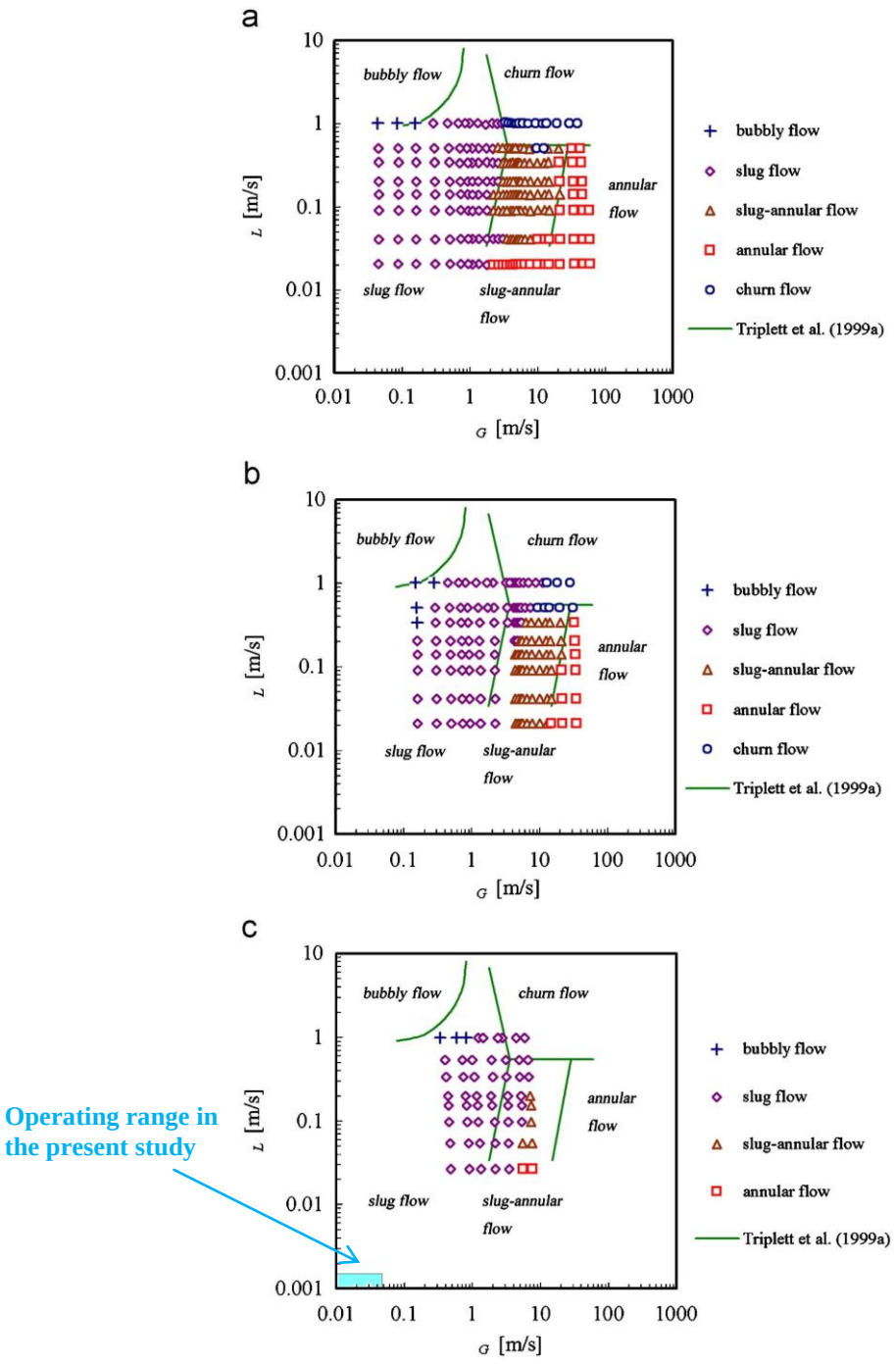

Figure 7.27. Flow maps with coordinates the gas and liquid superficial velocities calculated at the channel entrance for three microchannels with different diameters by Yue et al. (2008) and comparison with the pattern regimes suggested by Triplett at al. (1999). (a) 667µm, (b) 400 µm, (c) 200 µm channel diameter.

In the current study presented in this Thesis, Taylor flow was not encountered at gas superficial velocities higher than 0.025 m/s or G/L ratio greater than 17 (equivalent to a gas flow rate of 0.68 ml/min and liquid flow rate of 5μl/min at STP conditions). Furthermore, Taylor flow was not seen for gas velocities less than 0.007 m/s or G/L ratio lower than 5 (equivalent to a gas flow rate of 0.20 ml/min and liquid flow rate of 5μl/min at STP conditions). Finally, not only the total gas velocity but also the ratio of ethylene over CO was found to play a role as well in the flow pattern obtained due to the solubility of the former in the liquid reaction mixture being around seven times higher against the latter. Thus, the higher was the proportion of CO in the gas, the higher the chance of seeing bubble train flow instead of Taylor flow. The flow map produced from these experiments is presented below and it must be mentioned that the gas superficial velocities were calculated at reaction conditions at the channel entrance. Annular flow was not observed at the 10 bar pressure for the gas and liquid velocities used in this study. However, when the pressure dropped to 4 bar annular flow appeared due to the fact that the gas velocity became much faster at the lower pressure.

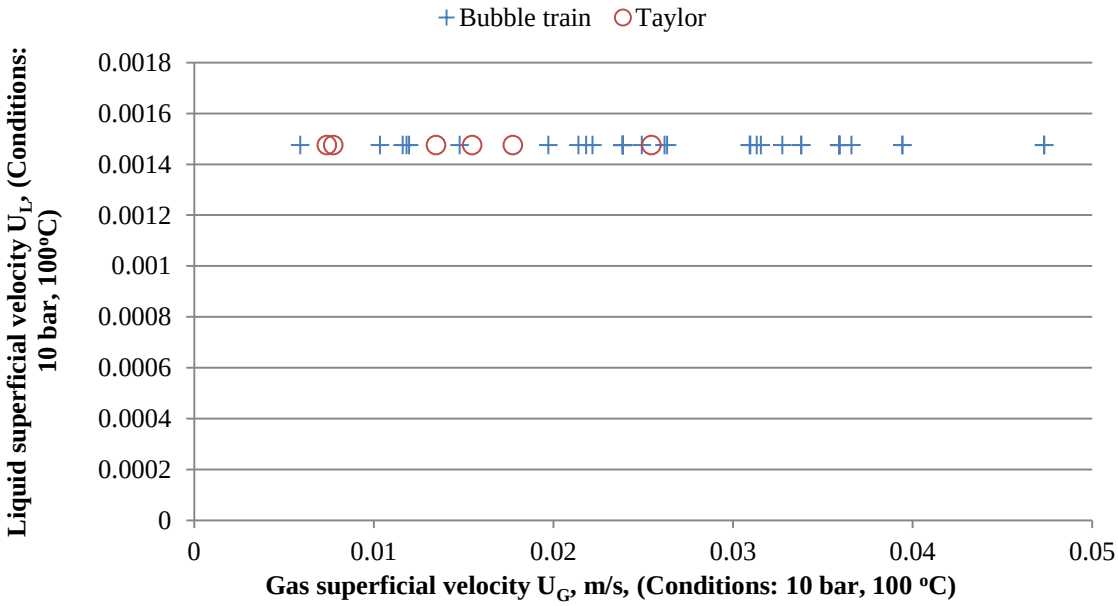

Figure 7.28. Flow map showing the type of flow based on gas and liquid superficial velocities.

Figure 7.29 illustrates the difference between Taylor and bubble train flow while a collection of representative photographs of flow patterns for the various experiments performed with the 250 µm capillary can be found in Appendix K.

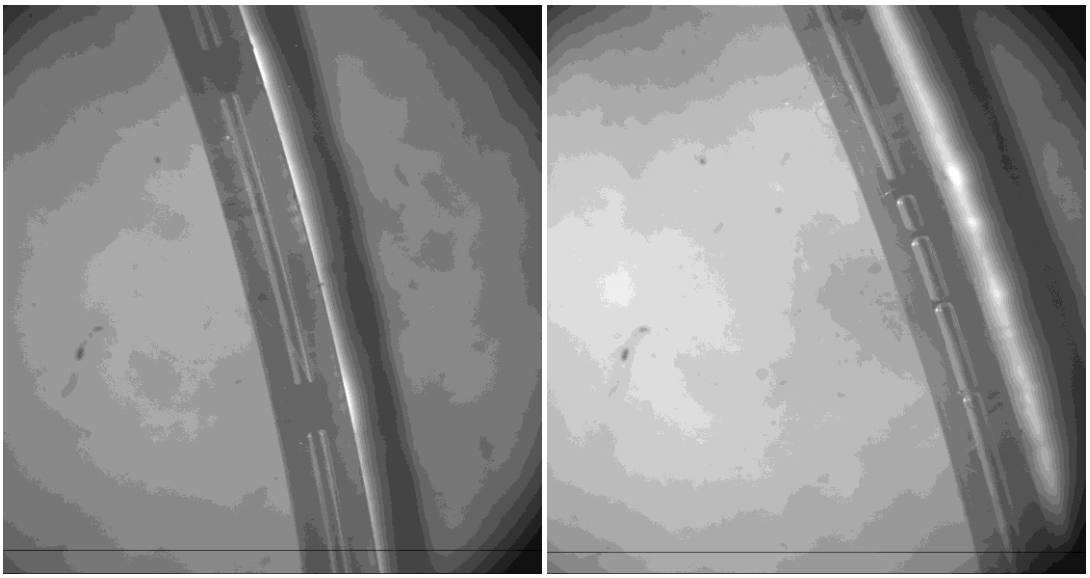

(a) Taylor flow **(b) Bubble train flow**

Figure 7.29. (a) Taylor flow; liquid flow rate L=5µl/min, G_C2H4=0.2ml/min, G_CO2=0.2 ml/min (STP). Date: 11/12/07. (b) Bubble train flow; liquid flow rate L=5 µl/min, G_C2H4=0.6 ml/min,G_CO2=0.3 ml/min (STP). Date: 18/12/2007.

The present study concluded that stable Taylor flow was achieved in the 250 µm microchannel when:

Condition of stability	Comment
$5 < \frac{U_G}{U_L} < 17$	U_G, U_L are the superficial velocities calculated at reaction conditions

Table 7.5. Range of conditions under which Taylor flow was observed.

Different criteria of stable Taylor flow have been reported in the literature but are not endorsed from the findings of the current study.

Condition of stability	Capillary/ies studied	Reference	Comparative findings from present study
$0.5 < \frac{U_G}{U_L} < 4$	1.1-2.3 mm	Kreutzer et al. (2005a)	Stable Taylor flow was observed at $5 < U_G/U_L < 17$.
$\frac{U_G}{U_G + U_L} < 0.5$	0.9-3.0 mm	Liu et al. (2005)	Stable Taylor flow was observed at $\frac{U_G}{U_G + U_L}$ up to 0.95.
$We = \frac{\rho_G d U_B^2}{\sigma} \approx 1$	1 mm and 1.5mm	Chen et al. (2002)	Stable Taylor flow was observed at *We* at 0.006 or lower.

Table 7.6. Comparative stability criteria between this work and literature. Note: The velocities in the various conditions are superficial.

7.10 Pressure Drop

The pressure drop between the liquid inlet at the tee-junction and the pressure controller downstream of the reactor was measured and the results are shown in the following Table:

Pressure at liquid inlet, bar	Pressure at P controller , bar	ΔP, bar
3.57	1.00	2.57
3.95	2.10	1.85
4.6	3.00	1.60
4.86	4.00	0.86
5.53	5.00	0.53
7.16	6.00	1.16
8.82	7.00	1.82
9.46	9.00	0.46
10.45	10.00	0.45

Table 7.7. Pressure drop along the 250 μm capillary.

At 10 bar, the pressure drop between the two pressure transducers upstream and downstream of the reactor was measured at 0.38 bar (reaction conditions: C_2H_4: 0.30 ml/min, CO=0.10 ml/min, L=5μl/min, T=100^{o}C and P=10 bar) and was compared with correlations proposed in the literature. The correlations by Aussilous & Quéré (2000) and Warnier (2010) produced values close the experimental. Particularly, the former one predicted most closely the experimental pressure drop. The advantage of the correlation of Aussilous & Quéré might be that it incorporates the liquid hold up which in this study was on average 10 %. Conversely, the model proposed by Chisholm (1967) deviated from experiment because it was not developed for Taylor

flow in the first place and does not take into account hydrodynamics parameters although it has been used in the past by other researchers to predict the pressure drops in this regime (please also refer to Chapter Four for more information on correlations found in the literature).

Correlation for the pressure drop per unit channel length	**Reference**	**Value obtained**
$-\left(\frac{dP}{dz}\right)_C = \Phi_L^2\left(\frac{dP}{dz}\right)_L$	Chisholm (1967)	Very high pressure drop
$-\left(\frac{dP}{dz}\right)_C = \frac{2fU_m^2\rho_L}{d}\varepsilon_L$	Aussilous & Quéré (2000)	3,310 Pa/m
$-\left(\frac{dP}{dz}\right)_C = \frac{32\mu_L U_L}{d^2}\left(1+\frac{7.16\cdot 3^{2/3}}{32}\frac{d}{(L_S+\delta)}\left(\frac{A}{A_b}\right)\frac{1}{\left(Ca_b^{1/3}+3.34Ca_b\right)}\right)$	Warnier (2010)	1,709 Pa/m
$-\left(\frac{dP}{dz}\right)_C = 9.86\cdot 10^{-11}\left(\frac{F\mu}{d^4}\right)$ Theoretical pressure drop in tubing. *F*: flow rate in ml/min The viscosity μ is is assumed the viscosity of the gas because gas hold-up was calculated at 91%.	www.upchurch-scientific.com Capillary manufacturer	2,639 Pa/m
Measured experimentally		**3,260 Pa/m**

Table 7.8. Values of pressure drop calculated using correlations from the literature and comparison with experiment.

7.11 Device for Slug Size and Speed Measurements

A device for measurements of slug speed as well as the slug length and liquid hold-up in the capillary reactor was developed by Mr Simon Barass with some insight from the Author of this Thesis. The main elements of this device are two conductivity censors both placed above the capillary tubing at different positions. The methodology of the system is that each sensor takes a scan of the liquid slug flowing in the capillary, then a next scan of the same slug is obtained by the second sensor further down the tube length and finally the scans are superimposed to allow for the calculation of the slug velocity. Furthermore, the system distinguishes between gas bubble and liquid slug and permits the calculation of the liquid hold-up. The device is operated through the LabView software. The results of two of the experiments performed with this device are shown below. The 0.25 mm diameter of capillary reactor tubing was too small for the device to operate properly and therefore measurements were taken on the 0.8 mm ID tubing which is connected to the 0.25 mm tubing through a union. The slug and bubbles sizes for the 0.25 mm tubing were back calculated from the experimental results obtained. The experimental conditions and which the experiments were performed are shown below:

No of Experiment		**1**	**2**
Date of experiment		17/06/08	23/06/08
Parameter	**Unit**	**Value**	**Value**
Contactor used		0.50 mm tee	0.50 mm tee
CO flow rate	ml/min, STP	0.1	0.1
C_2H_4 flow rate	ml/min, STP	0.9	0.9
Liquid flow rate	μl/min	5	5
MeOH composition in the liquid mixture	%w	19.41	27.93
MeP composition in the liquid mixture	%w	80.59	72.97
Pressure	bar	10	10
Temperature	^oC	100	100

Table 7.9. Experimental conditions for slug size measurements at the reactor exit.

Regarding the bubble speed measurements, the device needs to be calibrated in order for its accuracy to be determined. As for the measured slug length at the reactor exit, it was found from the size distribution that 9 5% of the slugs are in the ranges 1.81±0.5 mm and 2.38±0.68 mm for the experiments 1 and 2 respectively. The liquid hold-up in the capillary reactor was measured to be 6.2 % and 7.5 % for the two experiments. The calculated liquid hold up was 8.7 % (based on the formula $\varepsilon_L = 1 - \frac{U_G}{U_b}$) for both cases. The MeOH conversion achieved experimentally was 1.78 % in experiment 1 while a slightly higher conversion of 2.06 % was achieved in experiment 2.

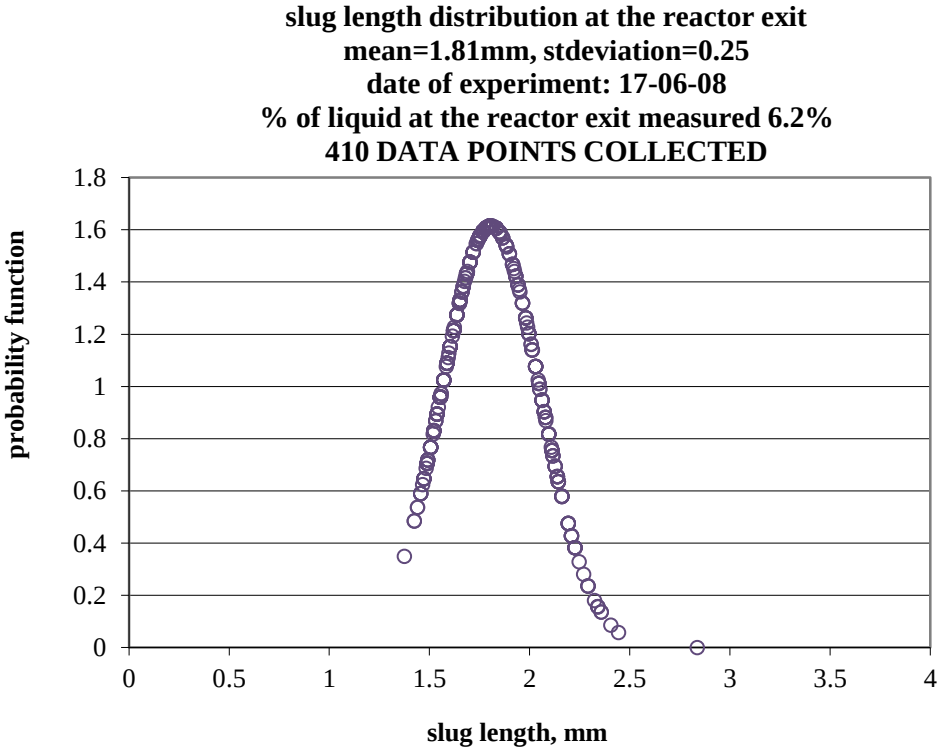

Figure 7.30. Slug length distribution and % of liquid in the capillary. Data from Experiment 1.

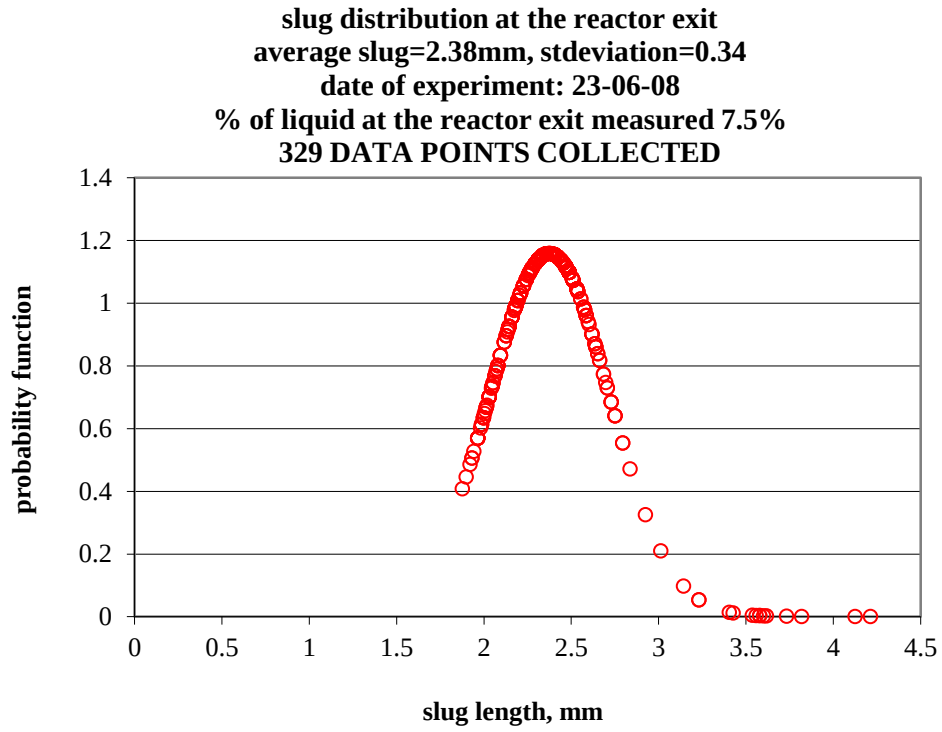

Figure 7.31. Slug length distribution and % of liquid in the capillary. Data from Experiment 2.

7.12 Conclusions

A bespoke reactor Spiral capillary reactor was developed to accommodate capillary tubing to a maximum length of 7.6 m and became operational to a very satisfactory degree for flow visualization and measurement of slug and bubble sizes under reaction conditions. The system of the microscope equipped with a high speed camera positioned on top of the spiral reactor allowed for flow visualization at various positions of the spiral including reactor inlet and outlet. The good repeatability of the gas-liquid flow achieved by the spiral reactor under reaction conditions was established after the completion of a series of experiments performed at various dates utilizing different gas flow rates while the liquid flow rate was maintained at 5 μl/min for all experiments.

Numerous photographs of the flow were obtained at the reactor inlet and outlet as well as at various intermediate positions along the spiral. Bubble and slug coalescence was evident and therefore size increase was observed and measured along the capillary tube. Size distributions of bubbles and slugs were derived from these experiments (on average 100 data points collected for each distribution) and were proven to be narrow at the reactor inlet but due to the coalescence phenomenon very wide at the reactor outlet.

As it is known, the type of the gas-liquid contactor plays a very important role in the size of slugs and bubbles formed as well the degree of the homogeneity of Taylor flow. Therefore, a number of various tee-contactors with bore holes ranging from 0.15 mm to 1mm were tried and compared to distinguish which contactor provides

the most homogeneous flow in conjunction to small slugs which would facilitate good mass transfer. The experimental results showed that under reaction conditions at10 bar and 100 ^{o}C:

- The SS tee-junctions with boreholes of 0.15 mm and 0.25 mm even though they produce small slugs, the flow was inhomogeneous. 0.15 mm was found to perform better at smaller gas flow rates compared to 0.25 mm. The opposite happened when high rates were utilised.
- The plastic static mixing tee with the 10 μm SS internal mixing frit performed the best amongst the small thru-hole tee-junctions in terms of flow homogeneity. The turbulence created by the frit resulted in shorter bubble and slug lengths versus the other contactors.
- The SS 1.0 mm borehole tee-junction produced homogeneous Taylor flow but the size of the slugs was in the range of a few mm.
- The SS 0.50 mm borehole tee-junction produced homogeneous Taylor flow with slug sizes of 1mm or below.

The results obtained with the static mixing tee suggest that the ratio of the gas over the liquid flow rate almost matches the ratio of the bubble to slug length. The ratio of gas to liquid flow rate was equal to 10.02 while the bubble to slug average length was measured slightly higher at 10.67 in line with expectations due to the existence of the liquid film surrounding the bubbles. The results produced with the SS 0.25 and 0.15 tee do not agree as well with the scaling equation. A reason for could be that these contactors showed a wider distribution of slug and liquid sizes. In addition, the geometry of the tee plays a role as well as the material used for the manufacturing of the tee and its wettability properties.

The SS 0.50 mm tee performed the best in terms of Taylor low homogeneity and slug size and thus, it was chosen as the gas-liquid contactor to be used for the kinetic experiments.

Once the most suitable gas-liquid contactor was established, various steps were taken to improve the experimental set-up - not all of them successful - in order to widen the range of G/L ratio in which the Taylor flow is homogeneous. By materialising the set-up improvements, the range of $\frac{U_G}{U_L}$ ratio under which the Taylor flow was homogeneous was expanded significantly.

Winding up the parameters which were found to have an effect on the gas-liquid flow pattern in microchannels, these were:

- The gas superficial velocity.
- The geometry and size of the tee-contactor.
- The size of the main channel as compared to the inlet.
- The orientation of gas and liquid streams at the inlet.
- The degree of gas-liquid pre-mixing.
- Pressure fluctuations, particularly at the reactor outlet.

Concerning bubble and slug sizes, the following factors were noted to have an effect:

- An increase of gas velocity increases the length of the bubbles. Conversely, the opposite is true regarding the size of the liquid slugs. The correlation by Qian & Laval (2006) showed relative agreement with the experimental measurements Furthermore, apart for very low gas velocity levels, an

increase in the gas velocity increased the non-uniformity of the gas bubbles and also yielded a broader bubble and slug size distribution. To sum up, stable Taylor flow was not observed for gas velocities lower than 0.2 ml/min (STP) or higher than 0.7 ml/min (STP).

- Gas-liquid pre-mixing produced smaller bubble and slug sizes.
- The smaller the size of the inlet, the smaller the bubble and slug sizes.
- Non-uniformity of bubble and slug sizes was noted along the capillary channel due to coalescence leading to an increase of the average and maximum bubble and slug lengths and standard deviations.

The correlation by Qian & Laval (2006) for liquid slug length showed relative agreement with the experimental measurements as it is applicable for capillaries 0.25 mm-1 mm. On the contrary, the correlations by Liu et a.l (2005) and Laborie et al. (1999) diverge from the experimental values.

Steady Taylor flow was observed in some cases under the operating conditions examined in this study. In detail, this flow pattern was marked in the range of $5 < \frac{U_G}{U_L} < 17$ at reaction conditions or 40<G/L<136 at STP conditions. In the remainder of cases, the type of flow encountered was bubble train flow consisting of bubbles broken in various parts in a random manner with very short liquid slugs in-between. The number of bubbles pertaining to the train seems to increase with the proportion of gas in the flow.

Regarding pressure drop, the correlation by Aussilous & Quéré (2000) predicted very well the experimental data. The model by Warnier et al. (2010) also produced good results but on the contrary the Lockhart-Martinelli-Chisholm model (1967) greatly over-predicted the pressure drop.

A device for slug size and speed measurements as well as for measurements of liquid ratio at the rector exit was developed at UCL and tried and found to operate well. Two sensors are the main components of this system together with the measurements acquisition system which is connected to a personal computer equipped with the LabView software. The slug size distributions measures at the reactor exit showed that the mean outlet slug size was around 2 mm and the standard deviation of the measurements was around 0.3 mm. In addition, the percentage of liquid in the reactor was measured and it was found to agree very well with calculations. Finally, the device needs to be calibrated in terms of slug speed determination.

--//--

CHAPTER 8

Kinetics from Microreactor Experiments

This Chapter reports on the experimental work conducted using the capillary micro reactor of 250 μm internal diameter (ID) and 11.7 m length as the tool for studying the kinetics the methoxycarbonylation of ethylene with the Alpha process. Numerous experiments were carried out in order to derive the partial reaction orders with respect to the three reactants (ethylene, CO, methanol) and the Pd catalyst. Additionally, the effect of temperature on the reaction rate was studied and the activation energy was calculated from the Arrhenius plot. Calculations performed with the purpose of assessing the importance of mass transfer effects and identifying the capillary reactor operating regime are also presented in this Chapter. Based on the analysis of the experimental data, a rate equation assuming the methanolysis step as rate determining was proposed and the kinetic parameters were evaluated. The rate equation was found to represent the experimental data satisfactorily.

Batch Reactors (BR) are the reactors most commonly used for kinetic studies. Very few studies have used capillary continuous flow reactors and in particular micro capillary reactors for the same purpose. Capillary microreactors, manufactured from PTFE, with diameters ranging from 500-1000 μm were used for the study of the

selective hydrogenation of α,β-unsaturated aldehydes in aqueous multiphase catalysis in a Taylor flow L/L system of immiscible fluids. The catalyst Ru^{II}-TPPTS (triphenylphosphantrisulfonat-sodium) was dissolved in the aqueous phase and it was physically separated from the reactant and product in the organic phase. Hydrogen was used as a reducing agent. Taylor flow consisted of alternatively organic and aqueous slugs with gas bubbles in the organic phase (please refer to the Figure 8.1). The influence of the catalyst phase volume rate on the overall reaction rate as well as the low value of the activation energy found (E=32.3 kJ/mol), counted for a mass transfer limited reaction. The experiments were conducted at atmospheric pressure and temperature of 60 ^{o}C (Önal et al., 2005). It was also concluded in this study that mass transfer can be improved by decreasing the capillary diameter not only because the specific transfer area is increased but also the Taylor flow characteristics are improved (internal recirculation in the organic phase intensified rendering the diffusion path even shorter than expected). A 3-fold increase of the reaction rate was observed by reducing the capillary diameter from 1000 μm to 500 μm. The capillary microreactor was rated as an excellent tool to investigate and model the effect of mass transport on reaction rate and selectivity due to the flexibility of adjusting flow rates and droplets dimensions by adjusting the capillary diameter.

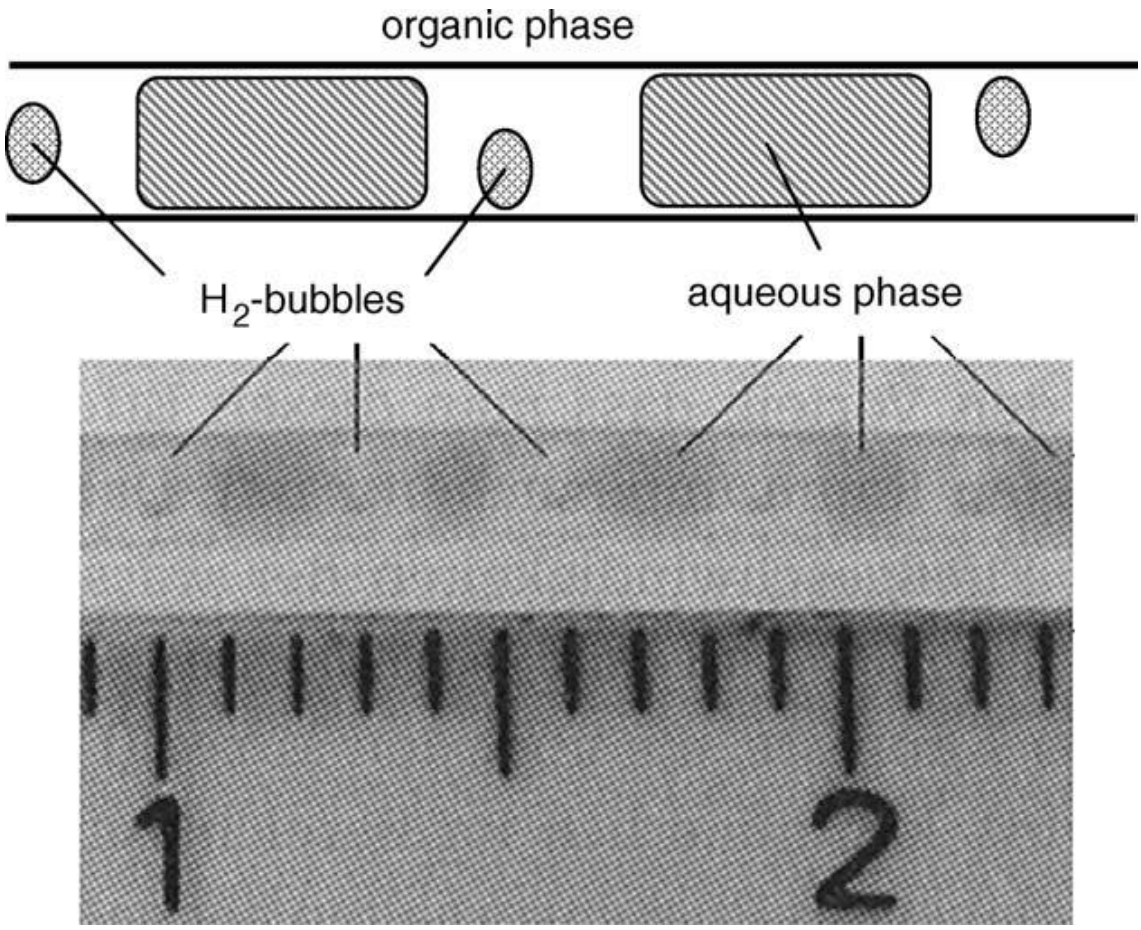

Figure 8.1. Three phase gas-liquid-liquid flow in a capillary microreactor developed by Önal et al. (2005).

The capillary microreactor with a diameter between 500-1000 μm was used for the study of the nitration of a single ring aromatic in a L/L two- phase reaction. Reaction conditions were atmospheric pressure and temperature 60-120 ^{o}C. The homogeneously catalysed reactions occur in the aqueous phase which consists of a mixture of concentrated sulphuric and nitrophosphan acids. Mass transfer experiments with different flow rates but identical residence time, suggested that mass transfer is enhanced by flow velocity and this enhancement could be interpreted in terms of internal recirculation within the liquid slugs. In the capillary

microreactor, isothermal behavior was assumed due to the high mass transfer rates. A L/L plug flow with a well-developed flow pattern of alternating plugs was observed giving a constant uniform specific area for mass transfer between the two phases. The nitration reaction leads to the formation not only of the mononitrated (desired) product but also a variety of side-products as a consequence of the occurrence of parallel and consecutive reactions. Hence, product yield and selectivity depends greatly on the interfacial mass transfer and residence time distribution. The capillary microreactor was shown to behave like a plug flow reactor allowing high mass transfer between the phases (Dummann et al., 2003).

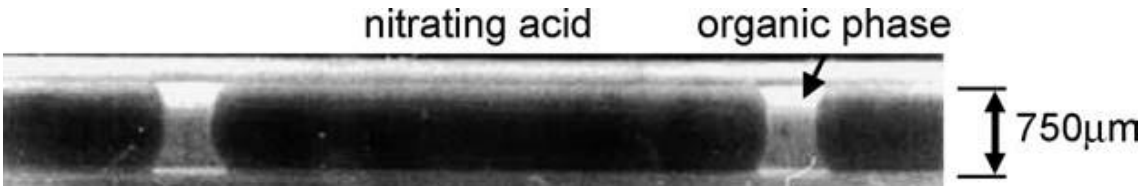

Figure 8.2. **L-L two-phase plug-flow with plugs of nitrating acid and organic phase in a capillary microreactor (Dummann et al., 2003).**

De Bellefon and co-workers in 2003, conducted a kinetic study using a micro-machined device for molecular gas-liquid reactions. The new high-throughput concept described was based on sequential operations with a combination of pulse injections and a micromachined mixer. The reaction studied was the asymmetric hydrogenation of methyl Z-(a) acetamidocinamate with a rhodium /(S,S-BDPPTS) catalyst in an aqueous phase. They authors concluded a first order reaction with respect to the catalyst, the reagent and H_2. The activation energy was evaluated in the microreactor as (31±4 kJ/mol) or 9 kJ/mol less than the value obtained using a batch reactor. The authors attributed these differences to the difficulties to perform

experiments with low inventories of material and also to the poor control of the temperature and of the residence time in the microreactor.

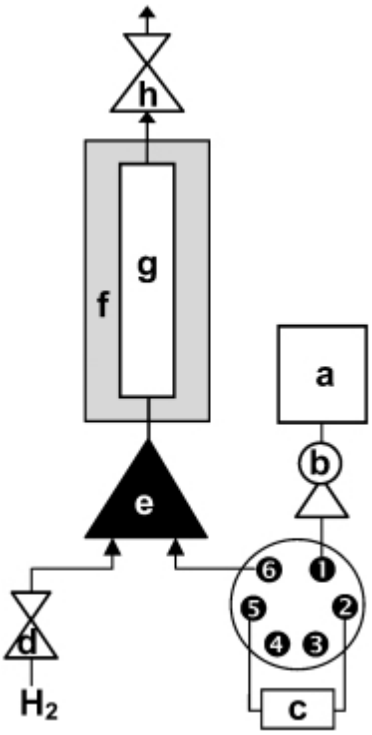

Figure 8.3. Experimental set-up: (a) water/substrate reservoir, (b) high-pressure liquid pump, (c) catalyst/substrate injection with then HPLC valve, (d) hydrogen supply and mass flow controller, (e) micromixer, (f) heating mantel, (g) tubular glass or quartz reactor (0.4 cm ID, 80 cm length, (h) back pressure regulator (de Bellefon et al., 2003).

The experimental evaluation of a three-phase capillary reactor with 3.86 mm internal diameter studying the resorcinol hydrogenation concluded a first order reaction with respect to H_2 and a positive effect of the G/L ratio on the reaction rate. The apparent activation energy was found to be 38 ± 2 kJ/mol and the reactor operation under kinetic control was concluded by the high linearity of the Arrhenius plot (Enache et al., 2005).

A pyrex glass capillary with 400 μm internal diameter and 5 cm length was developed and used by Basheer at al., 2004. The Suzuki coupling reactions with catalyst Pd nanoparticles, prepared from Pd acetate, were used as model reactions for this system. The mobility of the reactants was driven by electro osmotic flow which was controlled by applied potential. The capillary reactor was assessed to be a convenient tool for optimization of catalyst performance offering also good precision, reproducibility and high reaction yield versus conventional apparatuses. A similar rector design was employed for the study of the oxidation of glucose to gluconic acid with a Au^0 sponge used as catalyst.

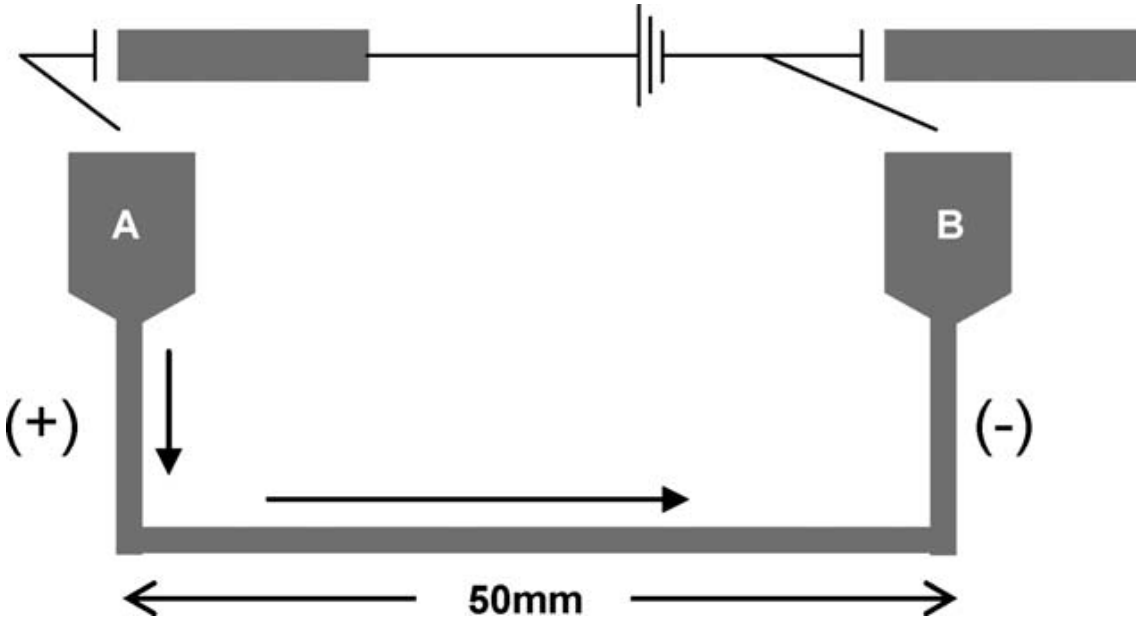

Figure 8.4. Schematic diagram of the capillary microreactor system for Suzuki coupling (Basheer at al., 2004).

As it was previously mentioned, reaction rates in capillary reactors can be limited by mass transport. However, the measured rate values presented in this Chapter are intrinsic reaction rate values as it was proven by calculations. The novelty of this

work also lies on the fact that kinetic studies for a gas-liquid complex homogeneous catalysis reaction system under high pressure and temperature, using a micro capillary reaction with 250 μm internal diameter operating under kinetic control have not been reported before.

This Chapter starts by giving a description of the capillary reactor used for these experiments followed by a detailed outline of the experimental set-up and the experimental procedure. The aim of every kinetic study is to elucidate the effect of various factors, e.g. reactant concentrations, temperature etc, on the reaction rate. For this purpose, reaction rates have to be calculated under various experimental conditions. The method followed for reaction rate calculation is explicitly described in this Chapter. A kinetic study also involves the collection of intrinsic kinetic data. The calculations performed to verify that the capillary reactor operated under kinetic control for the purpose of this study are explained in sequence. Numerous experiments were conducted in order to find out the partial reaction order with respect to carbon monoxide, ethylene, methanol and the palladium catalyst. The aim of these experiments was to throw light on the effect of each reactant on the reaction rate by changing the concentration of this particular reactant while keeping the other reactants in excess. The differential method was used for the analysis of the experimental data which are presented here. In addition, the influence of temperature on the reaction rate, the calculation of the apparent activation energy and the comparison between the capillary and autoclave data is presented. One of the observations made in the course of this experimental work with the capillary reactor was the catalyst degradation by precipitation of Pd black particles and reduction of the catalytic activity after prolonged storage. A series of experiments was performed

to shed light on the catalyst degradation and the results with a short discussion are included in this chapter. A kinetic model based on the hydride catalytic cycle assuming the methanolysis step as rate controlling is later proposed. This model also accounts for catalyst deactivation by the formation of catalytic intermediates which lead to the formation of palladium black. The kinetic parameters were determined by means of a statistical software package. Finally, the last section in this Chapter summarises the main findings from this work conducted with the capillary reactor.

8.1 Experimental

8.1.1 Capillary Reactor Description

The capillary microreactor consists of a transparent FEP polymeric tube with an OD 1.6 mm and ID 0.25 mm wrapped in a coil form. The tubing is colourless with optical transparency and has a maximum operating pressure of 120 bar (for operation at 100 ^{o}C). The gas and liquid meet at a tee-junction with a 0.50 mm bore hole at the reactor entrance.

Capillary Reactor Characteristics and Operating Conditions	
Characteristics	
Length	11.7 m
Material	FEP
OD	1/16" in=1.6 mm
ID	0.25 mm
Volume	573 μl
Conditions	
T	100 ^{o}C
P	9-10 bar
Liquid flow rate (at 20^{o}C and atmospheric pressure)	3-50 μl/min
CO flow rate (at 20^{o}C and atmospheric pressure)	0.05-3 ml/min
C_2H_4 flow rate (at 20^{o}C and atmospheric pressure)	0.05-3 ml/min

Table 8.1. Capillary reactor characteristics and operating conditions.

The reactor is wrapped in a coil form and immersed in a concentrated aqueous solution of ethylene glycol contained in a custom-made stainless steel vessel. The vessel has cylindrical form with dimensions 6.5 cm diameter x 9 cm height and is positioned on top of the heater. The vessel has a cover of 0.3 cm thickness with a special holder for a thermocouple dipped inside the thermal bath for measuring the temperature, and is connected to the PID temperature controller which regulates the heater's temperature in order to maintain a constant temperature inside the thermal bath. A custom-made 3.3 mm borosilicate glass cover is fitted on top of the heater encasing the stainless-steel vessel to minimise heat losses. The reactor is considered to operate in isothermal mode since the reaction heat is low and moreover it is placed in the thermal bath kept at constant temperature. The same assumption was made by

Zanfir et al. (2008) for the study of an asymmetric transfer hydrogenation reaction using a microstrustructed reactor, from Önal et al. (2005), Dummann et al. (2003) and also from Russum and co-workers (2006) due to the inherent high heat transfer rates in the microreactor and the small size of the tubing relative to the thermal bath.

Ethylene glycol, $C_2H_6O_2$, was the chosen material for the thermal bath because of its high boiling point of 197^{o}C and also because of its thermal conductivity at 0.258 W/(m K) at 25 ^{o}C. The exit of the capillary microreactor is connected to the inlet of the condenser. The vapours condense and the gas leaves the condenser from the top while the liquid accumulates inside the condenser. The sample is collected from the bottom of the condenser. The exit gas stream of the condenser is connected to the pressure controller in order to keep the pressure at the required set point of 10 bar.

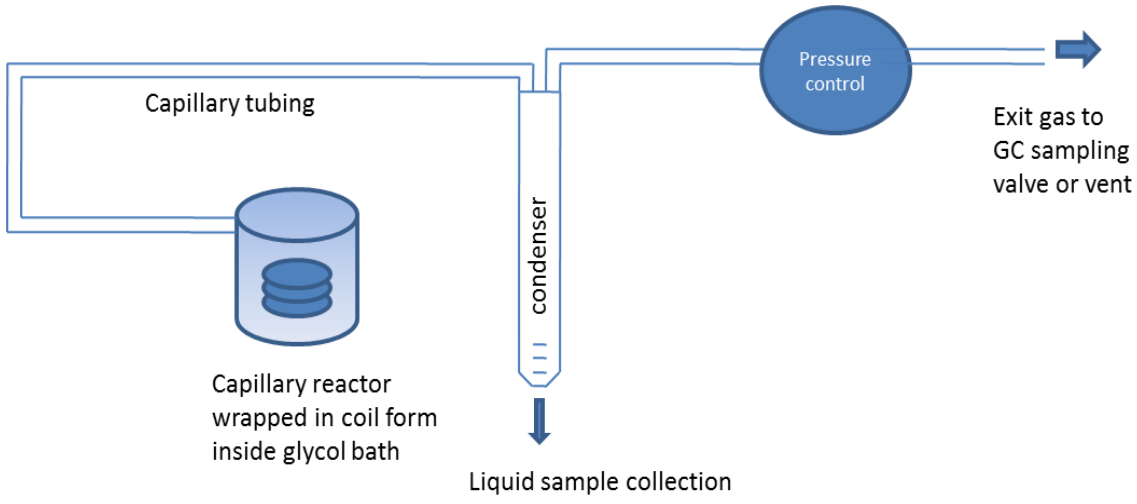

Figure 8.5. Schematic of capillary reactor layout.

Prior to the development of the capillary microreactor, preliminary experimentation and reactor trials were performed using the glass capillary microreactor

manufactured by *Micronit* as well as mesh microreactors. The capillary reactor has certain advantages compared to other microreactors used before:

- Adjustable volume by increasing or decreasing the tube length.
- Easy liquid sampling from the bottom of the condenser.
- Safe operation at desirable conditions of pressure and temperature without problems.
- Ease of operation.
- Can be operated as a differential reactor.
- No channel blockage observed probably. This problem prevented proper operation of the *Micronit* capillary microreactor due to Pd black deposition.
- Flow characteristics easily adjustable by changing the gas and liquid flow rates and the tee-junction geometrical characteristics.

8.1.2 Experimental Set-Up Description

The capillary microreactor experimental set-up was designed and built in order to satisfy the following objectives:

- Perform experiments under the conditions specified by the reaction under study; in the (P,T) range around 10 bar and 80-120 ^{o}C.
- Accommodate microreactors (equipment suitable for micro-scale flows, micro-dimensions etc).
- Reliable pressure and temperature control.
- Satisfactory repeatability.
- Safe operation.

The experimental set-up was a bespoke apparatus whose flow sheet is depicted in Figure 8.6. Colour codes were used to distinguish the different flows.

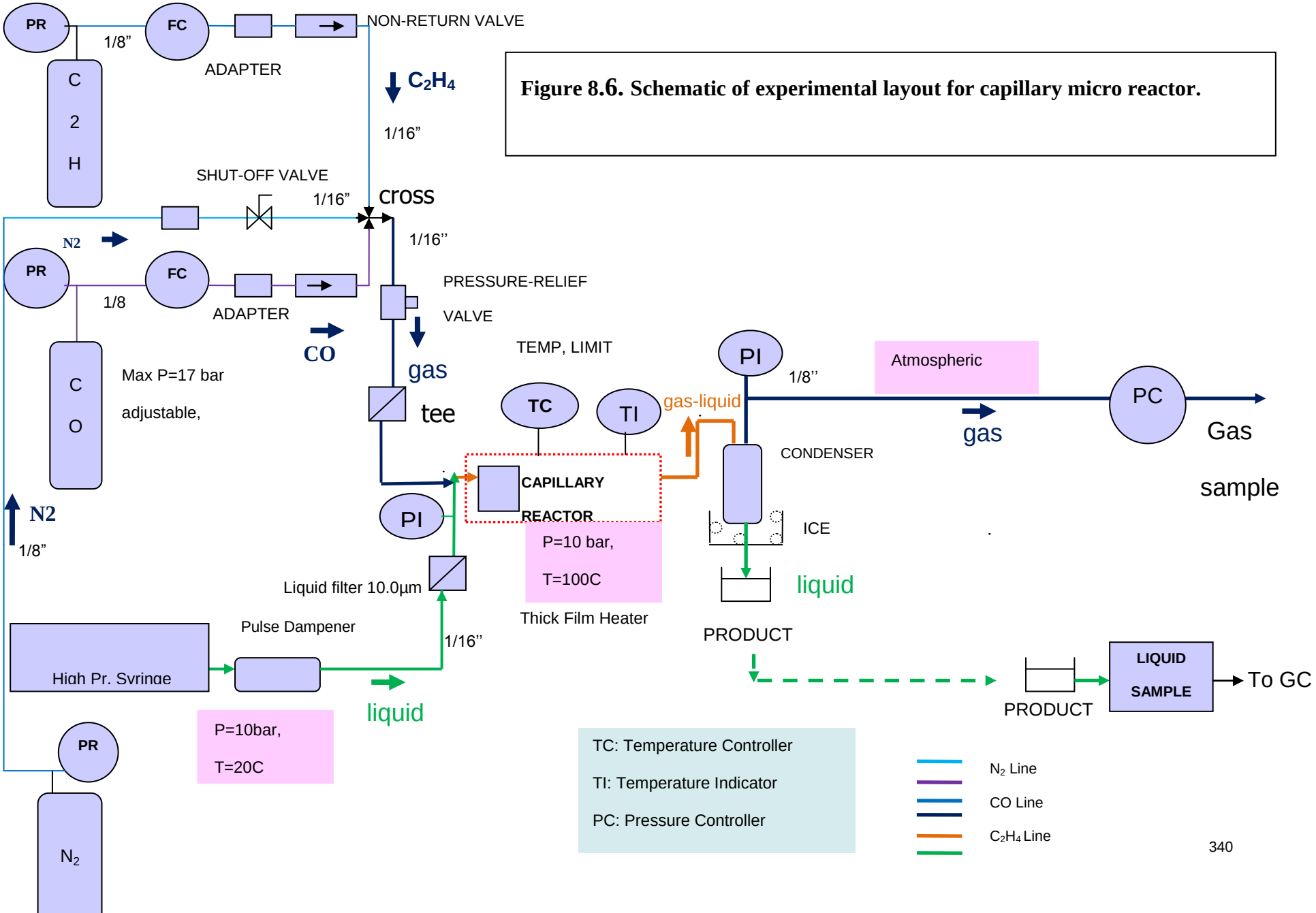

Figure 8.6. Schematic of experimental layout for capillary micro reactor.

The layout of the experimental set-up consists of two parts; upstream and downstream of the capillary microreactor as follows:

Upstream of the microreactor:

- The first gas line is for the ethylene. The ethylene from the cylinder passes through a BROOKS mass flow meter, then an adapter 1/8''-1/16'' and then a non-return valve and meets the other gases in a cross junction. The pressure in the line is maintained at 10bar by means of a Pressure Regulator (PR).
- The second gas line is for the carbon dioxide. The carbon dioxide from the cylinder passes through a BROOKS mass flow meter, then an adapter 1/8''-1/16'' and then a non-return valve and meets the other gases in a cross junction. The pressure in the line is maintained at 10bar by means of a Pressure Regulator (PR).
- The third gas line is for the nitrogen. The nitrogen from the cylinder passes through an adapter 1/8''-1/16'', then a shut-off valve and meets the other gases at a cross junction. The pressure in the line is maintained at 10bar by means of a Pressure Regulator.
- After the cross junction, the gas line for the gas mixture (ethylene, carbon monoxide, nitrogen) passes through a pressure-relief valve which was placed in the set-up as a safety precaution and will open if the pressure in the system rises above 17 bar in case of a malfunction of the pressure controlling system. Subsequently, the gas mixture passes through a microfilter to remove any particles above 0.5 μm and then it passes through a tee junction where it meets the liquid.

- The liquid comes from the high pressure syringe pump, through a pulse dampener to reduce the pump pulsations, then a liquid filter to remove any particles above 10 μm before it passes through the tee-junction where it meets the gas mixture.
- The gas-liquid mixture leaves the tee-junction and enters the 11.7 m capillary micro reactor which is wrapped in a coil form and is placed inside a stainless steel vessel (SS) filled with ethylene glycol. The SS vessel is also fitted with a thermocouple, part of the Temperature Control System (TCS) whose main parts are described in the Appendix A. The SS vessel is considered to be isothermal.

Downstream of the microreactor:

- The gas-liquid mixture exits the ethylene glycol bath and enters the condenser where the methanol and methyl propionate condense, the liquid accumulates at the bottom of the instrument while the gas exits the condenser from the top.
- The gas exiting the condenser passes through the Pressure Controller which maintains the pressure at 10 bar and then through the GC from where a gas sample can be obtained through the gas-sampling valve and be analysed by means of the Thermal Conductivity Detector (TCD).
- A liquid sample is collected from the bottom of the condenser and analysed via the Flame Ionization Detector (FID) in the GC.

8.1.3 Experimental Procedure

Figure 8.7 shows the experimental apparatus for gas-liquid flow visualisation and measurements. The microscopic lens with the high-speed camera was positioned above the capillary tubing just before the ethylene glycol bath. The camera was connected to the computer. By means of the Visiflow Software, the magnified flow could be seen on the computer screen and photographs of the slugs and bubbles could subsequently be taken and then the dimensions of the bubbles and slugs could be determined.

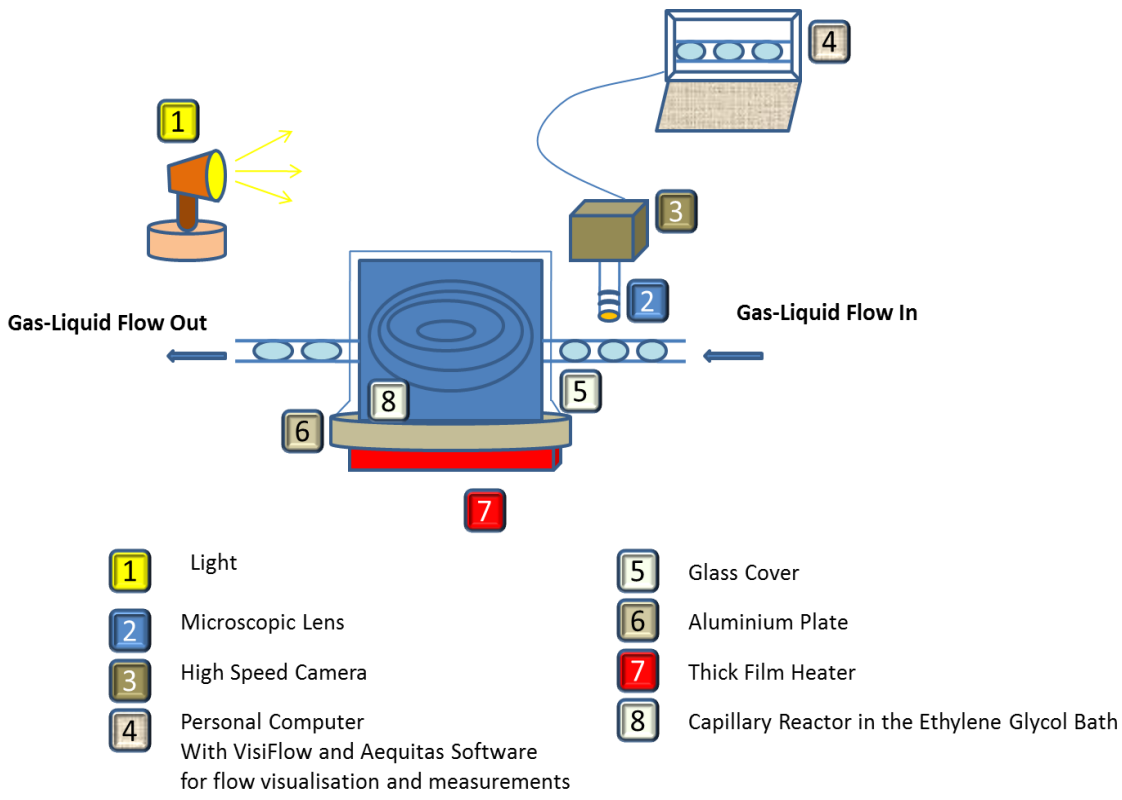

Figure 8.7. Experimental apparatus for flow visualisation and investigation.

The same experimental procedure was followed strictly for all experiments in order to avoid discrepancies and random errors and it entailed a step sequence whose detailed description is included in Appendix E. The main steps are outlined below:

- A sample from the liquid in the pump syringe is taken before the start of the experiment and is analysed in the GC to find the initial Methanol concentration C_{MeOH_0}.
- Subsequently, the experiment is initiated and once steady state is established under the required conditions the experiment is run for 30 min-1 h and then the liquid in the phase separator is discarded. This will create a small pressure drop in the range of 0.3 bar but the pressure will soon build up again to the required set point of 10 bar.
- The experiment is continued for 1 h, photographs of the bubbles and slugs are taken for size determination.
- A liquid sample from the bottom of the phase separator is collected. After analysis with the GC using the FID, the concentrations of methanol and MeP at the exit of the reactor are measured, C_{MeOH} and C_{MeP}.

8.1.4 Experimental Strategy for the Kinetic Study

A kinetic study usually entails the following steps:

- The first step is measurements of concentration of reactant(s) or product(s) as a function of time and the development of the kinetic reaction profile which is a plot of concentration of reactant(s) or product(s) as a function of time.

- The second step is the treatment of the kinetic data with the appropriate method(s) in order to determine the reaction order and rate contants(s).

The stoichiometry of the methoxycarbonylation of ethylene using the Alpha process is known from Lucite International (Clegg et al., 1997). With regards to obtaining the kinetic reaction profile for the methoxycarbonylation of ethylene theoretically the concentration of methanol, methyl propionate, carbon monoxide or ethylene could be monitored. The concentration measurements could be taken as a function of reactor residence time under isothermal conditions by means of Gas Chromatography. A method was developed for the FID for liquid samples which enabled the concentration measurement of methanol or methyl propionate. Although the concentrations of both methanol and MeP were monitored, because of the fact that the liquid reacting mixture consisted mostly of MeP in the ratio 70:30 MeP:MeOH (% w/w), it was chosen to use the methanol concentration measurements to calculate the reaction rates as this data would provide better analytical accuracy (Open University, Inorganic Chemistry). It is known from autoclave experiments that the reaction is practically stopped when the temperature drops below 60^{o}C which means that the reaction was quenched once the gas-liquid stream left the microreactor. The capillary reactor was kept under isothermal conditions at 100 ^{o}C as it was immersed in an ethylene glycol bath and the temperature was accurately controlled by means of the Temperature Controlling System.

The repeatability and the systematic error of the analysis method to measure % concentration (wt/wt) with the GC were measured and are presented in Appendix H.

Liquid sampling points were firstly the outlet of the syringe pump before the reactor to find the inlet methanol concentration and secondly the bottom of the condenser to determine the outlet methanol concentration. Inlet samples were obtained at the start of each experimental run while samples at the outlet were collected after 1 h of operation which was usually 12 space times, as the space time had the typical value of 5 min. The difference in mol (or concentration) of methanol between the inlet and the outlet were equal to the mol of methanol consumed. Blank experiments (performed in the absence of catalyst) showed zero change in methanol concentration, in line with the Author's expectations.

There are several approaches that can be used for analysis of kinetic data (time, concentration) for reactions involving more than one reactants as explained in more detail in a precedent Chapter, (please refer to Section 2.3.2) like the differential method which was used for the analysis of the capillary data presented in this Chapter.

Initial rates can identify reaction mechanisms before any complications due to reverse reactions or inhibition by formation of by-products. Differential reactors can be used to study the initial stages of the reaction by observation of changes in conversion close to zero (typically below 10 %). BR, PFR and CSTR can be operated as differential reactors but not without problems. In the case of BR, taking concentration measurements at the very beginning of the reaction can be very problematic. Regarding PFR, very small conversions can be achieved using very high flow rates which means high pressure drop and also the uncertainty of adequate mixing and adequate homogeneity at such high flow rates. In addition, the dead

volume should be minimised so that the reaction does not take place outside the reactor volume. Regarding the CSTR, the requirement for fast heat and mass transfer still holds at high flow rates so that space time is minimal. In addition, there are cost and size issues involved.

The advantage of capillary microreactor that was developed for studying the initial stages of a reaction is that due to the very small residence time the conversions obtained are very small. In addition, the micro dimensions of the capillary reactor facilitate mixing, heat and mass transfer at small Reynolds numbers and consequently small pressure drops. As it will be shown in the next sections of this Chapter, the capillary experimental data show good agreement with the autoclave initial rates data but with less scattering when experiments were performed at low CO partial pressures.

8.2 Modelling and Calculations

8.2.1 Reactor Modelling

We make the assumption that the unit cell (one bubble and one slug) is a plug flow reactor and hence, if N is the number of unit cells then the capillary reactor is a series of N plug flow reactors with X_1, X_2, X_3, …X_N is the fractional conversion of component A (methanol) leaving the reactor 1,2, 3.. N. The material balance for steady state plug flow reactor *i* is:

$$\frac{V_i}{F_0} = \int_{X_{i-1}}^{Xi} \frac{dX}{-r} \tag{8.1}$$

Or for the series of N plug reactors according to Levenspiel (1992):

$$\frac{V}{F_0} = \sum_{i=1}^{N} \frac{V_i}{F_0} = \frac{V_1 + V_2 + ... + V_N}{F_0} = \int_0^{X_1} \frac{dX}{-r} + \int_{X_1}^{X_2} \frac{dX}{-r} + ... + \int_{X_{N-1}}^{X_N} \frac{dX}{-r} = \int_0^{X_N} \frac{dX}{-r} \tag{8.2}$$

$$\frac{V}{F_0} = \int_0^{X_N} \frac{dX}{-r} \tag{8.3}$$

Hence, a series of N plug flow reactors with total volume V gives the same conversion as a single plug flow reactor with volume V.

The reaction rate is a function of the concentrations of the reactants and temperature. The concentration of the liquid reactant methanol is in large excess and the methanol conversion is less than 10% in all experiments while the concentrations of the dissolved gases, ethylene and carbon monoxide in the liquid are equal to the equilibrium concentrations as defined by the Henry's law for the reactor pressure because there are no mass transfer resistances and the reaction is infinitely slow. Furthermore, the lubricating film around the gas bubbles is always saturated with gas as the Pohorecki criterion is satisfied in every experiment (please refer to Chapter Four). Therefore, we can assume that the reaction happens with the same rate in all the unit cells. It is worth mentioning that Divekar et al. (1993) who studied the kinetics of hydroformylation of 1-decene also observed that the hydroformylation rate was constant in the low conversion range (<10-20 %).

It should be noted that the analysis of Bercik & Pintar (1997) who proposed a CSTR-by-pass model, cannot be used for the experiments presented in this Chapter because it ignores the amount of reaction which occurs in the liquid film. In the current work, the slugs are very short and the liquid hold-up in the capillary is an average of 10% and hence the liquid film is also significant by comparison.

Thus, integration of equation (8.3) gives the relationship (8.4) between the apparent rate of reaction, the operating conditions and the measured conversion (the same equation was also derived by Abdallah and co-workers in 2006):

$$\frac{V}{F_0} = \frac{X_N}{-\bar{r}} \tag{8.4}$$

or

$$-r = \frac{X_N \cdot F_0}{V} = \frac{X_N}{V} \cdot \frac{V \cdot C_0}{\tau} = \frac{X_N \cdot C_0}{\tau} \quad \text{or} \tag{8.5}$$

$$R = \frac{C_0 - C_{out}}{\tau} = \frac{C_0 X}{\tau} \tag{8.6}$$

8.2.2 Calculation of Reaction Rates

In our case component *A* is methanol and reaction rates were calculated as the rates of its disappearance i.e. the difference in methanol concentration between reactor inlet and outlet, which is essentially equal to the difference in concentration between the two sampling points, over reactor space time $R = \frac{C_{MeOH_0} X}{\tau}$. The reactor space time could be calculated with reference to the reactor inlet or outlet.

The reactor space time calculated at the reactor inlet conditions was $\tau_{in} = \frac{V_R}{Q_m}$ while at the outlet conditions was $\tau_{out} = \frac{V_R}{Q_{m\_out}}$. The conditions and in particular the gas flows under which the capillary experiments were conducted were chosen so that there was never a significant difference whether the space time was calculated at the inlet or outlet. The maximum difference of 12 % between τ_{out} and τ_{in} was found for all the experiments reported in this chapter. Experimentally measured residence time data were found to agree with the calculated reactor space time corresponding to the reactor outlet (please refer to Section 8.3.1). That is why the reactor space at the reactor outlet was used for the calculation of reaction rates.

The real flow rates at the reactor inlet and outlet are calculated using the known initial flow rates at STP corrected at reaction (P,T) and also taking into account the evaporation of methanol and methyl propionate and the CO and ethylene disappearance due to their solubility in the reactant mixture. To calculate the flow rate at the reactor outlet, the reactants' consumption due to the reaction taking place is also been used.

Ethylene has five times higher solubility compared to CO in the MeP:MeOH mixture at 100^{o}C. In addition, the solubility of ethylene decreases with temperature while that of CO increases. That is why the solubility of ethylene becomes seven and nine times higher than the solubility of CO at 70 ^{o}C and 50 ^{o}C respectively as reported in the study by Torres (2009).

The amount of CO and ethylene which disappears into the liquid due to gas solubility can be calculated using the solubility data obtained by the University of Liverpool (a partner institution in this project) under the experimental conditions.

Solubility data for CO and ethylene in the reaction mixture MeOH: MeP 30:70 were obtained by the University of Liverpool at different temperatures and various gas ratios C_2H_4:CO 0.54:1, 2.5:1, 5.7:1, 7.8:1, 14:1 and 25:1.

Examples of the solubility data are presented in Figures 8.8-8.9 for two gas ratios; 7.8:1 and 14:1. The horizontal axis represents the pressure of the system in absolute pressure (barA) while the vertical axis gives the mole fraction of the gas (CO or ethylene) in the liquid mixture under reaction conditions.

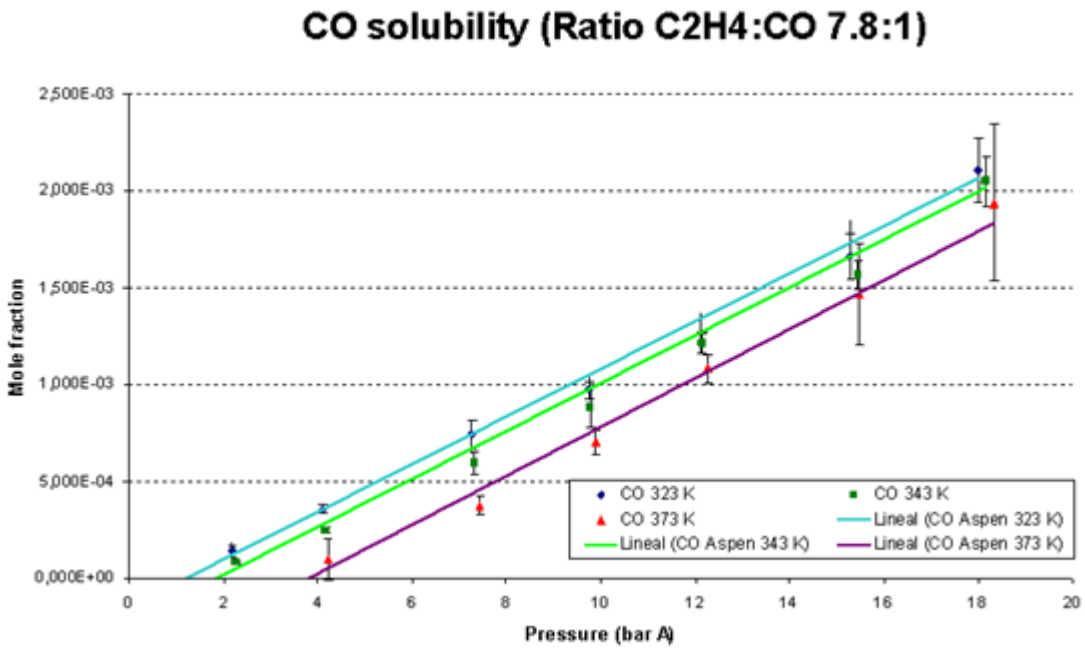

Figure 8.8. CO solubility data for C_2H_4:CO molar ratio=7.8:1. Data provided by LI.

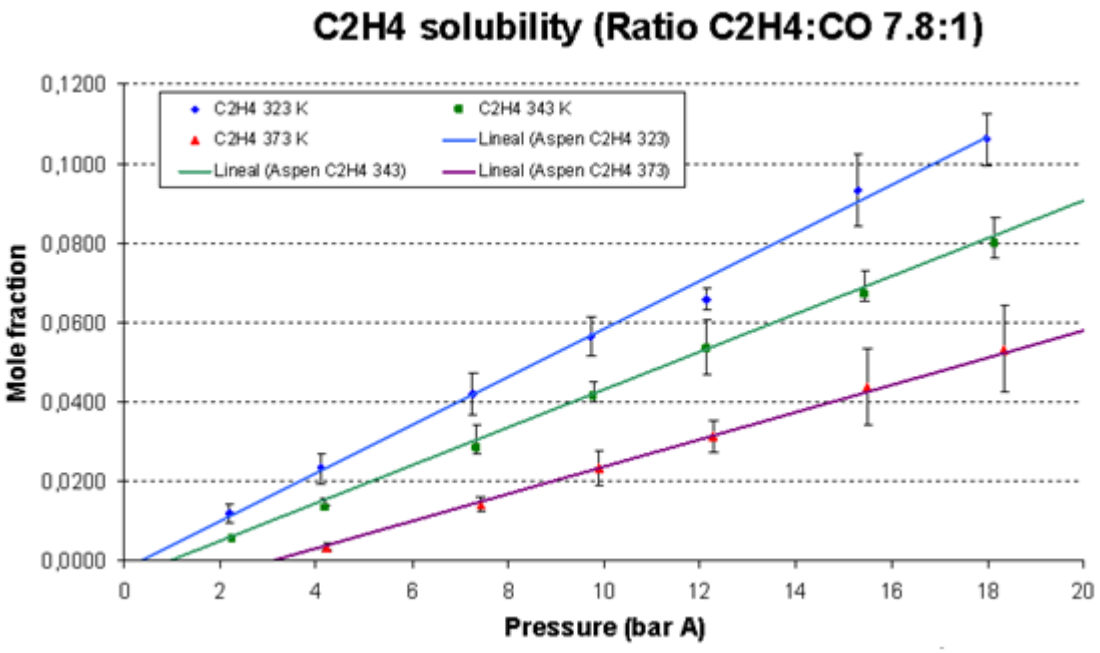

Figure 8.9. Ethylene solubility data. C_2H_4:CO molar ratio=7.8:1. Data provided by LI.

y_{C2H4}/y_{CO} = 7.8			
T / K	**P / barA**	**x(CO)**	**x(C_2H_4)**
323	0.6	0.00E+00	0.00E+00
	2.2	1.40E-04	7.45E-03
	4.1	3.56E-04	1.58E-02
	7.3	7.40E-04	4.21E-02
	9.7	9.71E-04	5.66E-02
	12.1	1.21E-03	6.54E-02
	15.3	1.66E-03	9.32E-02
	18.0	2.11E-03	1.06E-01
343	1.4	0.00E+00	0.00E+00
	2.3	7.87E-05	3.94E-03
	4.2	2.46E-04	1.16E-02
	7.3	5.94E-04	2.85E-02
	9.8	8.78E-04	4.16E-02
	12.1	1.21E-03	5.36E-02
	15.4	1.57E-03	6.73E-02
	18.2	2.05E-03	9.05E-02
373	3.7	0.00E+00	0.00E+00
	4.2	9.70E-05	4.36E-03
	7.4	3.74E-04	1.34E-02
	9.9	7.00E-04	2.13E-02
	12.3	1.08E-03	3.06E-02
	15.5	1.47E-03	4.67E-02
	18.3	1.94E-03	6.36E-02

Table 8.2. Solubility of C_2H_4 and CO mixed in a molar ratio 7.8:1, respectively, in solvent MeP/MeOH [70:30 % wt.] using NMR at different temperatures and pressures. Provided by LI.

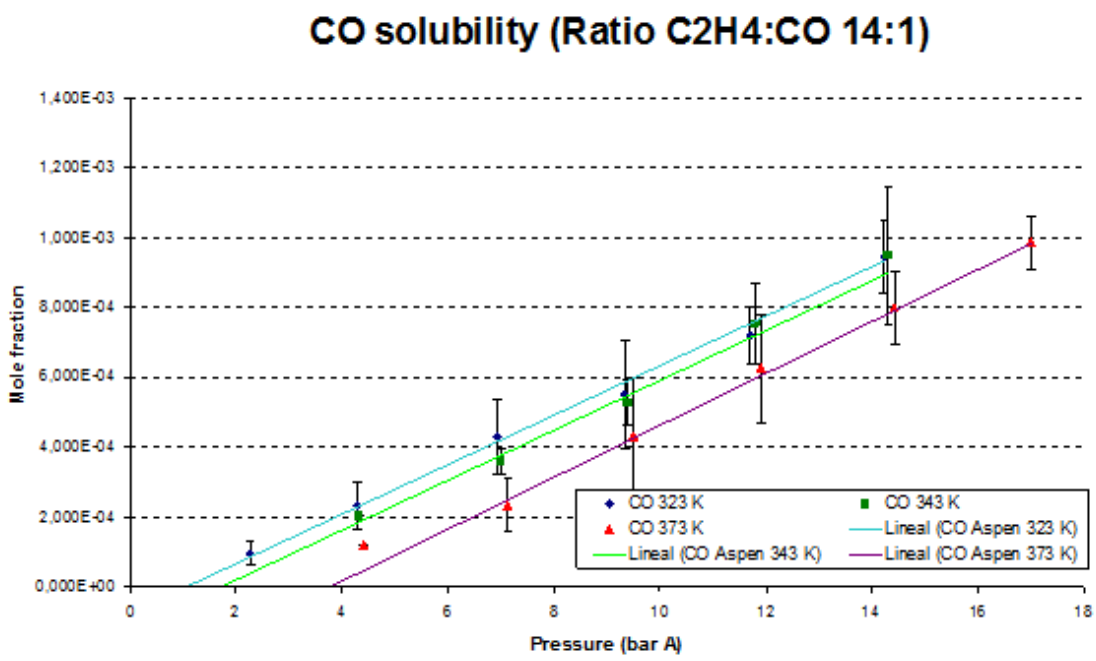

Figure 8.10. CO solubility data. C_2H_4:CO molar ratio=14:1. Data provided by LI.

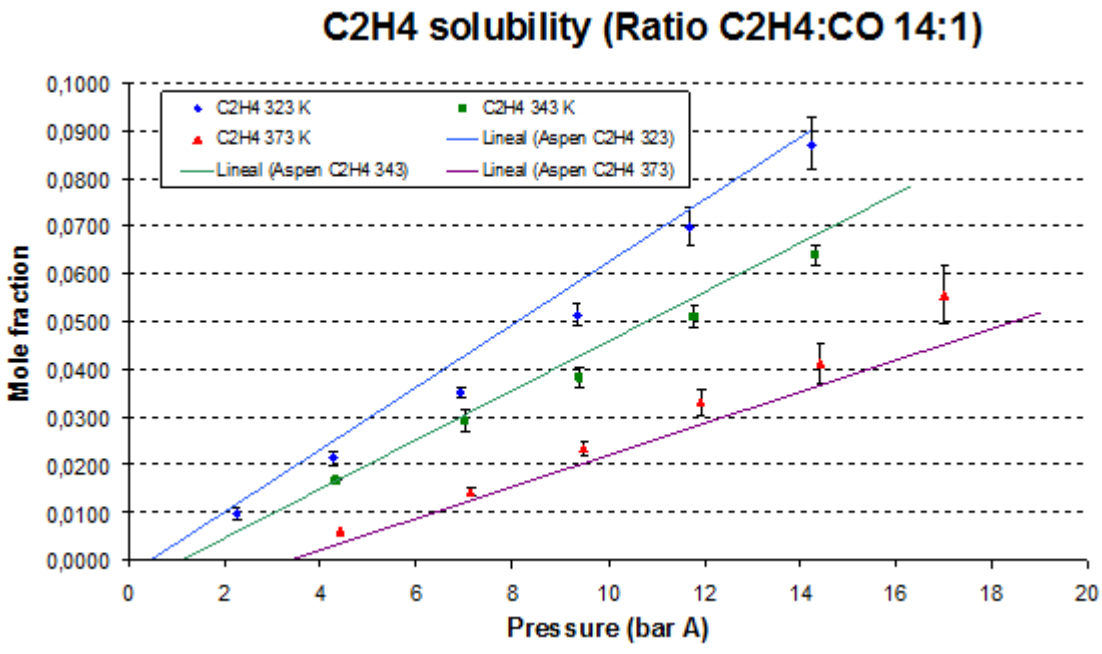

Figure 8.11. Ethylene solubility data. C2H4:CO molar ratio=14:1. Data provided by LI.

y_{C2H4}/y_{CO} = 14			
T / K	**P / barA**	**x(CO)**	**x(C_2H_4)**
323	0.6	0.00E+00	0.00E+00
	2.3	9.47E-05	9.79E-03
	4.3	2.34E-04	2.14E-02
	6.9	4.28E-04	3.52E-02
	9.3	5.50E-04	5.15E-02
	11.7	7.20E-04	7.00E-02
	14.2	9.45E-04	8.73E-02
343	1.4	0.00E+00	0.00E+00
	4.3	2.03E-04	1.68E-02
	7.0	3.59E-04	2.94E-02
	9.4	5.29E-04	3.83E-02
	11.8	7.54E-04	5.11E-02
	14.3	9.47E-04	6.38E-02
373	3.7	0.00E+00	0.00E+00
	4.4	1.18E-04	6.12E-03
	7.1	2.35E-04	1.43E-02
	9.5	4.34E-04	2.35E-02
	11.9	6.27E-04	3.32E-02
	14.4	7.99E-04	4.13E-02
	17.0	9.85E-04	5.57E-02

Table 8.3. Solubility of C_2H_4 and CO mixed in a molar ratio 14:1, respectively, in solvent MeP/MeOH [70:30 % wt.] using NMR at different temperatures and pressures. Provided by LI.

Calculations of the gas disappearance due to reaction

The concentration of MeOH in the reactor inlet is C_{MeOH_0} while the concentration of methanol at the reactor exit is $C_{MeOH} = C_{MeOH_0}(1-\chi)$ (8.6a)

The reactor feed with MeOH is $N_{MeOH} = C_{MeOH_0} Q_L \quad N_{MeOH} = C_{MeOH} Q_L$ (mol/s) (8.6b)

τ_{in} is used as base for the calculations. In one space time $\tau_{in} = \frac{V_R}{Q_m}$ the number of moles of Methanol fed to the reactor is ($N_{MeOH}\tau_{in}$) and the consumption of MeOH is $(N_{MeOH}\tau_{in}\chi)$ mol.

In one space time τ_{in}, the amount of C_2H_4 fed to the reactor is ($N_{Eth}\tau_{in}$). It is known that the stoichiometry of the reaction is 1:1 MeOH: C_2H_4. Thus, the amount of mol of ethylene consumed should be equal to the amount of mol of methanol consumed. The amount of ethylene exiting the reactor must be:

$(N_{Eth}\tau_{in} - N_{MeOH}\tau_{in}\chi)$ (8.7)

and the conversion of ethylene is $\chi_{Eth} = \frac{N_{Eth}\tau_{in} - N_{MeOH}\tau_{in}\chi}{N_{Eth}\tau_{in}}$. (8.8)

In the same manner the conversion of CO is $\chi_{CO} = \frac{N_{CO}\tau_{in} - N_{MeOH}\tau_{in}\chi}{N_{CO}\tau_{in}}$ (8.9)

Conversion of gases due to reaction	
Conversion of ethylene due to reaction	$\chi_{Eth} = \frac{N_{Eth}\tau_{in} - N_{MeOH}\tau_{in}\chi}{N_{Eth}\tau_{in}}$
Conversion of CO due to reaction	$\chi_{CO} = \frac{N_{CO}\tau_{in} - N_{MeOH}\tau_{in}\chi}{N_{CO}\tau_{in}}$

Table 8.4. Conversion of gases due to reaction.

8.2.3 Mass Transfer Resistances Investigation

Wern et al., in a study published in 2003, stated that if the time for significant reaction was sufficiently long that the condition $D \cdot t / d^2 > 1$ is satisfied, the results are expected to reflect inherent activation controlled kinetics. In the capillary microreactor presented here because the diffusive distance is only 250 μm, diffusion is complete in 33 s or 9% of the average reaction time of 6 min. Although, this condition is a useful indication that there is no diffusive limitation, it was decided to examine more complex criteria in order to verify that the capillary reactor operated under kinetic control for the purpose of this study. Table 8.5 lists the criteria to verify reactor operation in the kinetic regime as reported in the literature.

Criterion		**Reference**
Hatta number	$Ha < 0.3$	Trambouze et al. (1983)
Hatta number	$Ha < 0.02$	Levenspiel (1992)
Ratio of reaction rate over rate of mass transfer	$\gamma = \dfrac{R}{\kappa_L \alpha C_{CO}^*} < 0.1$	Chaudari et al. (1987)

Table 8.5 Criteria to establish reactor operation in the kinetic regime found in literature.

For this work we accepted 0.16 (average of 0.3 and 0.02) as the limit of the Ha number below which the reaction can be considered slow. Additionally, we accepted the criterion proposed by Chaudari et al. (1987).

Criteria to establish reactor operation in the kinetic regime in this work	
Hatta number	$Ha < 0.16$
Ratio of reaction rate over rate of mass transfer	$\gamma = \frac{R}{\kappa_L \alpha C_{CO}^*} < 0.1$

Table 8.6. Criteria to establish reactor operation in the kinetic regime in current study.

Formulas reported in previous studies on the hydrodynamics of Taylor Flow (Liu et al., 2005, Vandu et al., 2005 and Abiev, 2010) were used for the calculation of the mass transfer as it is shown below:

Steps of Calculations	Formulas
Step 1: Calculation of the Mixture Velocity	$U_m = (Q_G + Q_L)/A$
Step 2: Calculation of the Capillary Number	$Ca = \frac{\mu U_m}{\sigma}$
Step 3: Calculation of the Bubble Velocity	$U_b = \frac{U_m}{1 - 0.61 Ca^{0.33}}$
Step 4: Calculation of the film thickness	$\delta = \frac{0.66 d Ca^{2/3}}{1 + 3.35 Ca^{2/3}}$
Step 5: Calculation of the relative area of a bubble in the cross area of the capillary	$\varepsilon_A = \left(\frac{d - 2\delta}{d}\right)^2$
Step 6: Calculation of the gas fraction in the capillary	$\varepsilon_G = \frac{U_G}{U_b}$
Step 7: Calculation of the relative length of the bubble	$\varepsilon_{Length} = \frac{\varepsilon_G}{\varepsilon_A}$
Step 8: Calculation of the Length of the unit cell=length of bubble + length of slug	$L_{UC} = L_{slug} / (1 - \varepsilon_{Length})$

Steps of Calculations – *Continued…*	**Formulas**
Step 9: Calculation of the Mass transfer coefficient: contribution from the bubble cap	$k_{L,cap} = 2\sqrt{\frac{DU_b}{d}}$
Step 10: Calculation of the Specific area for the bubble cup	$a_{cap} = 4/L_{UC}$
Step 11: Calculation of the Mass transfer coefficient: contribution from the bubble cup from the liquid film	$k_{L,film} = 2\sqrt{\frac{DU_b}{\varepsilon_G L_{UC}}}$
Step 12: Calculation of the Specific area for the liquid film	$a_{film} = 4\varepsilon_G / d$
Step 13: Calculation of the Specific Mass transfer coefficient (all contributions)	$k_L a = k_{L,cap}\alpha_{cap} + k_{L,film}\alpha_{film}$

Table 8.7. Formulas used and steps of calculations.

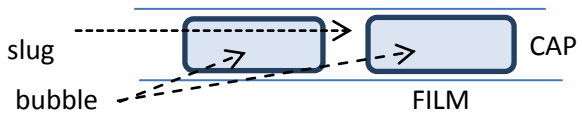

Figure 8.12. Schematic of Taylor flow.

The $k_L\alpha$ model described in the study by Vandu et al. (2005) assumes that the dominant contribution is due to the film surrounding the Taylor bubble and is applicable in the range where the condition $((U_G + U_L)/L_{slug})^{0.5} > 3s^{-0.5}$ is satisfied. Below this range, the contribution of the liquid film is decreased as the film begins approaching saturation. This condition was found to be satisfied for all the experimental data obtained with the capillary reactor and the calculated $((U_G + U_L)/L_{slug})^{0.5}$ was in the range [82 $s^{-0.5}$-2147 s^{-05}].

The experimental study of Vandu et al. (2005) agreed well with the CFD simulations of gas absorption in Taylor flow by van Baten & Krishna (2004) who developed a mass transfer model based on penetration theory also considering two contributions:

$$k_{L,cap} = \frac{8\sqrt{2}}{\pi L_{UC}} \sqrt{\frac{U_b}{d}} \frac{4}{L_{UC}} \tag{8.10}$$

$$k_{L,film} = \begin{cases} 3.41 \dfrac{D}{\delta} : Fo > 1 \\ 2\sqrt{\dfrac{D}{\pi \cdot t_{film}}} \cdot \dfrac{\ln(1/\Delta)}{1-\Delta} : Fo < 0.1 \end{cases} \tag{8.11}$$

The Fourier number Fo and the parameter Δ are calculated by the formulas:

$$Fo = \frac{D t_{film}}{\delta^2}, \; t_{film} = \frac{L_{film}}{U_B} \text{ and}$$

$$\Delta = 0.7857 \exp(-5.212 Fo) + 0.1001 \exp(-39.21 Fo) + \ldots \tag{8.12}$$

For all the experiments conducted, the criteria for operation in the kinetic regime (Table 8.6) were checked and were satisfied. An example of these calculations can be found in the Appendix C.

8.3 Experimental Results

8.3.1 Residence Time Experimental Measurement

The reaction time was experimentally measured using an injection valve. The pulse with the blue dye was introduced as the capillary reactor was on steady state under the following conditions:

Experimental Conditions		
Parameter	**Unit**	**Value**
CO flow rate	ml/min, STP	0.040
C_2H_4 flow rate	ml/min, STP	0.63
Liquid flow rate	μl/min	5
Pressure	bar	10
Temperature	^oC	100

Table 8.8. Experimental Conditions for Reaction Time Measurement.

The time between the coloured liquid slug entering and exiting the reactor was measured using a stop-watch. It should be noted that as the coloured slug travelled along the 11.7 m capillary reactor there was a small degree of back-mixing involved possibly due to the fact that the capillary reactor was stacked up vertically in coil form inside the thermal bath. At the reactor exit, a couple of very small size slugs left the reactor first, followed by a large coloured slug and two very small slugs not so deeply coloured appeared closely in sequence. The time corresponding to the time difference between the coloured slug entering the reactor and the large slug exiting the reactor was accepted as the reaction time. The space time for the above conditions is as below:

Space Time Calculated and Comparison with Experiment		
1	Space time calculated at the inlet conditions (min)	7.67
2	Space time calculated at the outlet conditions taking into account disappearance of the gas due to reaction (min)	7.90
3	Space time calculated at the outlet conditions taking into account disappearance of the gas due to reaction and solubility (min)	8.51
4	Average space time=(**1**+**2**)/2 (min)	7.79
5	Average space time=(**1**+**3**)/2 (min)	8.09
6	**Reaction time experimentally measured (min)**	**7 min 55 s=7.9**

Table 8.9. Space time calculated and experimental - comparison.

The experimental reaction time result is practically the same as the space time calculated at the reactor outlet taking into account the gas consumption due to reaction without correcting for the gas solubility. The flow rate of the gas and liquid mixture was used to calculate the reactor space and that is why the dissolution of one phase into the other (evaporation of volatiles into the gas phase and solvation of the gases into the liquid) does not need to be accounted for - a fact which is verified by the experimental results. This is why for the calculation of the rates in all experiments, the calculated space time at the reactor outlet without the solubility calculation was used for all the experimental results presented in this Chapter.

It should be noted that observations indicated some axial dispersion and hence a residence time distribution, although a very narrow one, as not more than 2 s were necessary for all the coloured slug fragments to exit the reactor. The RTD was neglected for the reactor/kinetic modelling (please note that the same approached was used by de Bellefon et al., 2003).

8.3.2 Experiments at Variable Gas Ratios

Numerous experiments under the Alpha conditions of pressure, temperature and liquid mixture composition but variable the gas ratio ethylene:CO were performed. Each series of experiments corresponded to a particular gas ratio and the reactor space time was varied by alternation of the gas flow rates. The gas ratios investigated are C_2H_4:CO 1:1, 2:1, 3:1, 5:1, 10:1 which were achieved by varying the initial gas flow rates 10-fold; in the ranges 0.04-0.35 ml/min (STP) and 0.1-1.5 ml/min (STP) for the CO and C_2H_4 respectively. The experimental conditions used are included in the Table below:

Experimental Conditions		
Parameter	**Unit**	**Value**
CO flow rate	ml/min, STP	0.04-0.35
C_2H_4 flow rate	ml/min, STP	0.1-1.5
Total gas flow rate	ml/min, STP	0.16-1.65
Liquid flow rate	μl/min	5
Pressure	bar	10
Temperature	^oC	100

Table 8.10. Experimental conditions.

The liquid flow rate used for all the experiments was constant at 5 μl/min for the following reasons:

- The minimum flow rate which the pump could deliver is 4 μl/min at the pressure of 10 bar as it was found in preliminary experiments. 5 μl/min was selected as it is close to the minimum but provides also a margin

against possible problems as it is not wise to work a piece of equipment at its lowest 10 % of its operating range where accuracy suffers.

- The reaction was very slow (due to the minimum amount of catalyst used) and that is why flow rates at the lower equipment operating range were chosen so that the reaction time is the highest possible.
- The liquid flow rate needed to be the lowest possible as it was one of the factors which determined the length of the liquid slug. The main aim was to maintain the smallest possible slugs so that the diffusion of the gas into the liquid is the fastest possible and mass transfer effects were avoided.

Figure 8.13 shows all the experimental data obtained at various gas ratios. The following conclusions can be made:

- The methanol conversion varies linearly with the reactor space time for every gas ratio. This means that for each gas ratio, the reaction rate remains constant.
- For the gas ratio of 1:1 which means lowest ethylene concentration, the plot does not pass through the origin of the axis. This can be due to the reaction induction time. Rapid start of the catalytic cycle is facilitated in the autoclave experiments by pre-treatment of the catalyst with ethylene before reaction initiation. A lag time of several min was also observed during autoclave experiments performed at high CO concentrations.
- As with the data for gas ratio 1:1, the data for f 3:1 do not fit with the general pattern followed by the rest of the data. This gas ratio corresponds to the

critical CO pressure when the swift in reaction order occurs. But this merits further investigation.

Carbon balance was closed for two experiments, at gas ratios ethylene:CO 1:1 and 2:1 with -1.27% and 1.91% discrepancy between reactor outlet and inlet. Details are given in the Appendix G.

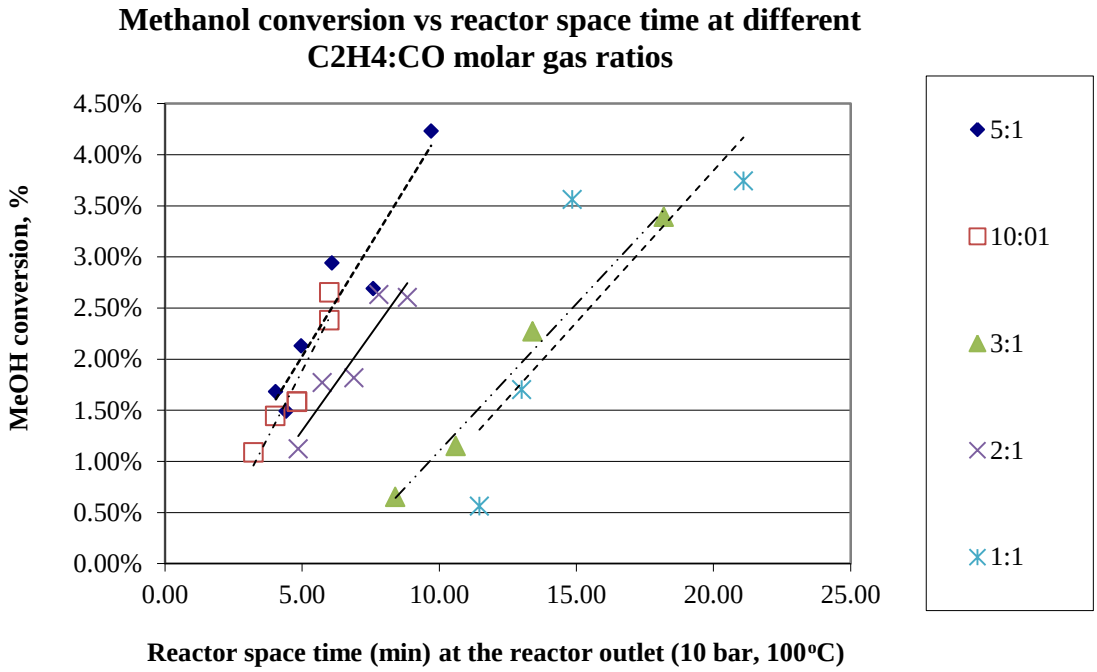

Figure 8.13. Methanol conversion as a function of reactor space time at various gas ratios.

8.3.3 Ethylene Series of Experiments

Series 1- Experiments under CO and methanol excess

A series of experiments were conducted with the purpose of shedding light on the dependence of reaction rate on the ethylene concentration. For this purpose, the flow rate of CO was kept constant at 0.7 ml/min (STP) while the ethylene flow rate was varied from 0.04 to 0.2 ml/min (STP) (please refer to Table 8.11). The methanol

conversion was obtained after sampling from the bottom of the condenser and GC analysis. The gas consumption was calculated at the reaction conditions (P,T) using the 1:1 reaction stoichiometry. The value of 0.7 ml/min as CO flow rate (STP) was chosen for it gives for every case a CO conversion of less than 3%. The space time calculated at the inlet at 10 bar and 100^{o}C varied from 5.11 to 6 min, the space time calculated at the outlet varied from 5.21 to 6.14 min while the average space time=(inlet res. time+outlet res. time)/2 varied from 5.16 to 6.07 min. The difference between the space time calculated at the inlet and the outlet was less than 3%.

Experimental Conditions		
Parameter	**Unit**	**Value**
CO flow rate	ml/min, STP	0.7
C_2H_4 flow rate	ml/min, STP	0.04-2.0
Liquid flow rate	µl/min	5
Pressure	bar	10
Temperature	^{o}C	100

Table 8.11. Experimental conditions for series 1-ethylene.

Figure 8.14 below shows that the ethylene conversion varies linearly with the space time which means that the reaction rate is constant even though the concentration of ethylene in the gas phase changed for each experiment due to its changing flow rate. The CO and methanol were in excess and their concentrations remained constant for this series of experiments. This leads us to believe that the partial reaction order with respect to ethylene is zero. This was also concluded from autoclave experiments. As mass transfer processes obeying Fick's law are first order processes, the reaction rate is not limited by mass transfer (Kreutzer, 2003).

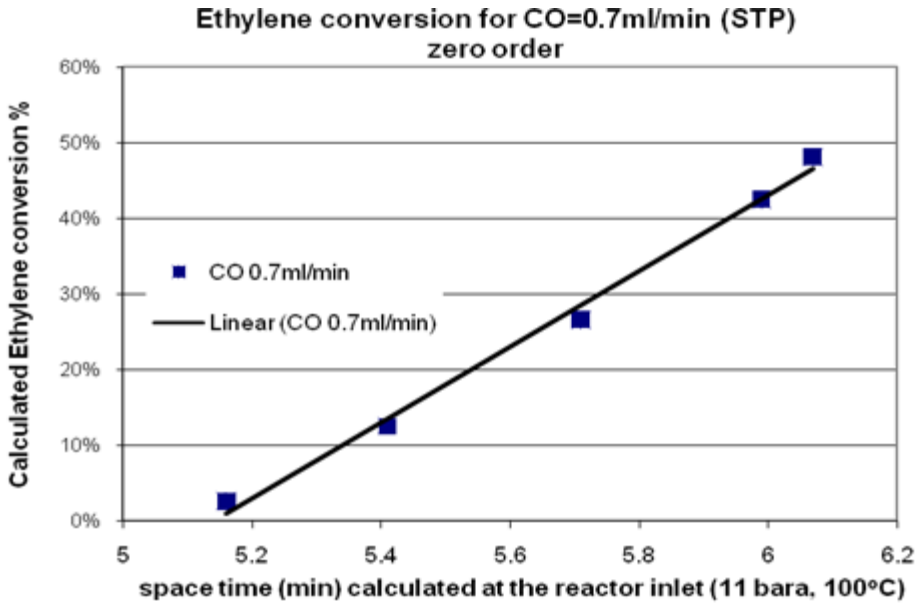

Figure 8.14. Ethylene conversion versus space time at various CO flow rates.

As it can be seen from the graph above, the ethylene conversion line does not pass through the origin. This can be attributed to the fact that the reaction shows an induction time of several min. Figure 8.15 that follows, shows the length of the induction period for a series of experiments performed with the autoclave reactors at variable ethylene concentrations and at the constant CO partial pressure of 1bar. N_2 gas was added in the gas mixture to make up for the total pressure of the reactor. These experiments were presented in Section 5.3.5 of Chapter Five.

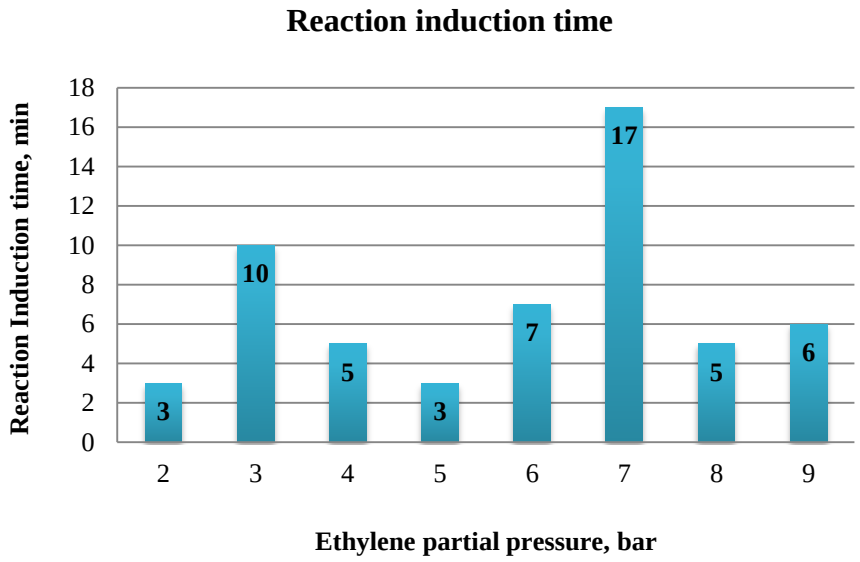

Figure 8.15. Reaction induction time at variable ethylene concentrations.

The induction time recorded between experiments performed in the autoclaves when pre-treatment is applied and the capillary reactor when pre-tretment is not applied are comparable.Thefore, as a first attempt it can be said that pre-tretmeant is not necessary for experiments performed with the capillary microreactor possibly due to the capillary's micro dimensions enabling the liquid to become rapidly saturated with the ethylene gas under our experimental conditions.

Series 2- Experiments at constant reactor space time

A second series of experiments was conducted at the identical reactor space time of 6 min calculated at the reactor inlet conditions. CO and ethylene flow rates were varied but CO in addition to methanol remained in excess for all the experiments of this series. Temperature and pressure conditions as well as the composition of the liquid mixture were according to the Alpha standards. The following Table includes the experimental conditions under which this series of experiments was performed.

Experimental Conditions		
Parameter	**Unit**	**Value**
CO flow rate	ml/min, STP	0.524-0.692
C2H4 flow rate	ml/min, STP	0.05-0.25
MeOH:MeP composition of reactant mixture	%(w/w)	70:30
Pd catalyst	mol/lt	$2.4\ 10^{-5}$
Liquid flow rate	μl/min	5
Pressure	bar	10
Temperature	^{o}C	100

Table 8.12. Experimental Conditions for the Ethylene Series.

Table 8.13 includes all the data obtained with the capillary reactor in this series of experiments.

Ethylene Capillary Data –Constant reactor space time									
Experi-ment	**C_2H_4 Flow rate (STP ml/min)**	**CO Flow rate (STP ml/min)**	**% MeOH conver-sion**	**Space time calculated at reactor inlet, τ_{in} min**	**Space time calculated at reactor outlet, τ_{out} min**	**Aver age space time, $\tau_{ave=(\tau_{in} + \tau_{out})/2}$ min**	**%difference in space time calculations = =100 * (τ_{in} - τ_{out})/ τ_{in} min**	**%CO conversion**	**%C2H4 conversion**
1	0.1	0.65	2.71	5.99	6.41	6.20	-7.0	3.88	29.06
2	0.15	0.608	1.74	6.00	6.26	6.13	-4.3	2.67	12.42
3	0.20	0.566	2.37	6.00	6.19	6.10	-3.2	3.90	12.69
4	0.25	0.524	1.50	6.00	6.22	6.11	-3.7	2.67	6.40
5	0.05	0.692	2.47	5.99	6.37	6.18	-6.3	3.32	53.00

Table 8.13. Ethylene capillary data.

A comparison between the capillary and the autoclave initial rates data is shown in Figure 8.16. The LN of the ethylene partial pressure is plotted on the horizontal axis of the graph while the LN of TOF (molMeP/molPd/h) is plotted on the vertical axis.

Appendix D contains the thermodynamic VLE calculations which concluded that the liquid vapours amount to 33% of the gas phase inside the capillary microreactor. Simulation with Aspen Custom Modeller (ACM) gave very similar results; 34% of the gas phase is methanol and methyl propionate vapours. For the capillary data, the partial pressures of ethylene data included in the figure below were corrected for VLE taking into account that out of the 10bar total reactor pressure, 3.4 bar is contributed by the evaporation of the volatiles (methanol and methyl propionate) according to Aspen Custom Modeller (ACM).

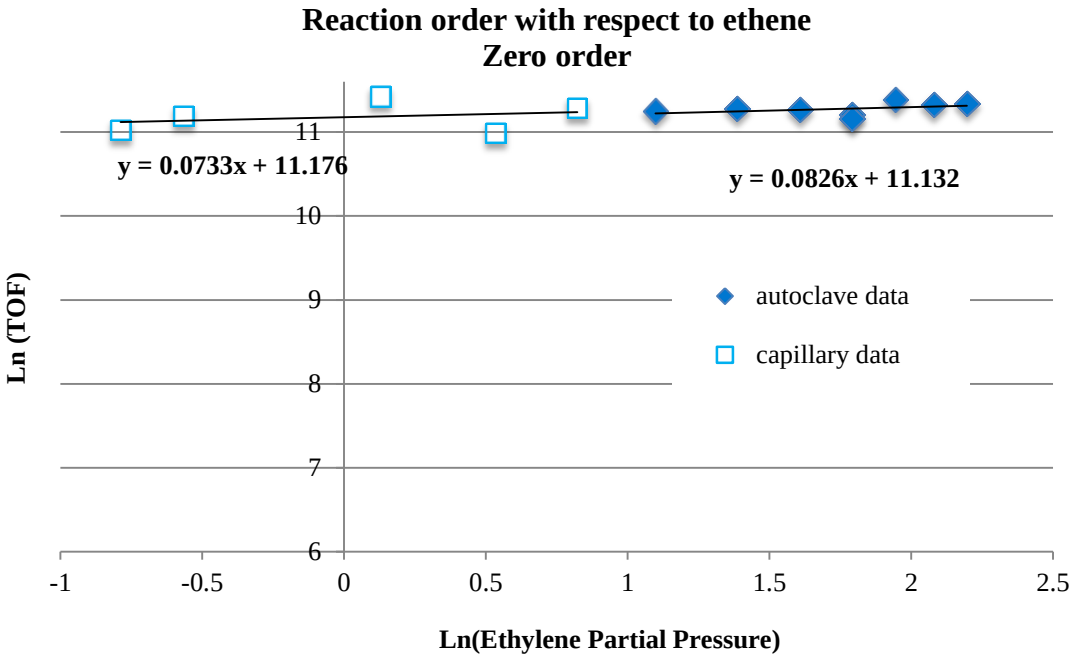

Figure 8.16. Comparison of capillary with autoclave data for determination of reaction order with respect to ethylene.

The autoclave LI data shown in the figure above are kinetic data as verified experimentally and by calculations. The increase of ethylene dissolved concentration shows a marginal positive effect on the reaction rate. The results show a practically zero reaction order with respect to ethylene.

8.3.4 CO series of Experiments

A series of experiments was performed with the capillary reactor in order to determine the partial order with respect to CO. All experiments were conducted at (P,T)=(10bar, 100^{o}C). The reactor space time calculated at the reactor inlet was maintained at 7.67min for all the experiments of this series apart from experiment 2 for which 7.25 min space time was used accidentally.

Experimental Conditions		
Parameter	**Unit**	**Value**
CO flow rate	**ml/min, STP**	**0.04-0.314**
C2H4 flow rate	ml/min, STP	0.302-0.63
Liquid flow rate	μl/min	5
MeOH:MeP composition of reactant mixture	%(w/w)	70:30
Pd catalyst	mol/lt	2.4 10^{-5}
Pressure	bar	10
Temperature	^{o}C	100

Table 8.14. Experimental conditions for the CO series.

Table 8.15 contains all the data collected in this series.

CO Capillary Data- constant reactor space time										
No	**Liquid flow rate µl/min**	**CO flow Rate, ml/min**	**C2H4 flow Rate ml/min**	**Space time calculated at reactor inlet, τ_{in}**	**Space time calculated at reactor outlet, τ_{out}**	**Average space time, $\tau_{ave=(}\ \tau_{in}$ $_{+}\ \tau_{out)/2}$**	**%difference in space time calculations= =100 * (τ_{in} – τ_{out})/ τ_{in}**	**%MeOH conversion**	**%CO conversion**	**%C2H4 conversion**
1	5	0.04	0.63	7.67	7.92	7.79	-3.26	1.02	23.75	1.70
2	10	0.07	0.594	7.25	7.83	7.54	-8.00	1.28	34.07	4.59
3	5	0.1	0.558	7.67	8.11	7.89	-5.74	1.78	16.58	3.39
4	5	0.13	0.522	7.67	8.07	7.87	-5.22	1.62	11.61	3.29
5	5	0.16	0.486	7.67	8.21	7.94	-7.04	2.15	12.52	4.71
6	5	0.19	0.450	7.67	8.22	7.94	-7.17	2.17	10.64	5.14
7	5	0.21	0.426	7.67	8.19	7.93	-6.78	2.06	9.14	5.15
8	5	0.24	0.390	7.67	8.04	7.86	-4.82	1.48	5.75	4.04
9	5	0.27	0.354	7.68	7.97	7.81	-3.78	1.23	4.24	3.69
10	5	0.3	0.318	7.68	7.94	7.81	-3.39	1.12	3.48	3.74
11	5	0.314	0.302	7.67	8.07	7.87	-5.22	1.66	4.92	5.86

Table 8.15. CO Capillary Data.

Figures 8.17 and 8.19 depict the data obtained with the capillary reactor for the determination of partial reaction order with respect to CO. All the capillary data were corrected for VLE in terms of CO partial pressures in the reactor after taking into account the evaporation of the methanol and MeP.

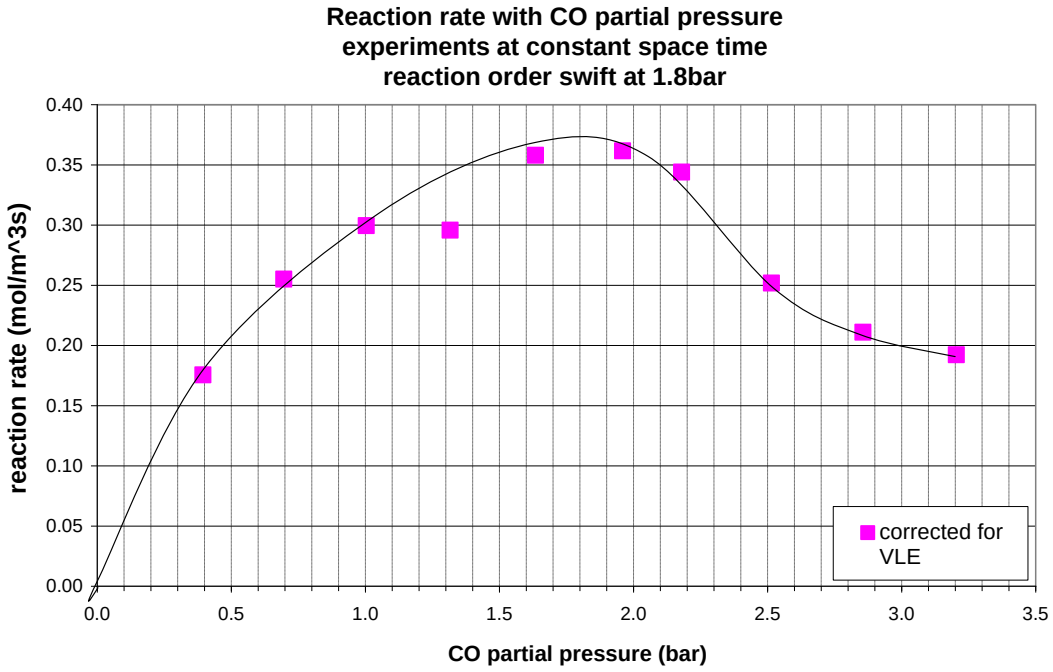

Figure 8.17. Reaction Rate with Respect to CO Partial Pressure. Capillary Data.

Figure 8.18 compares the results obtained with the capillary reactor are compared with the autoclave initial rates data. The rate plotted is a normalised rate=(reaction rate at CO partial pressure p)/(reaction rate at p=0.4 bar). This was done to avoid the catalyst activity effect due to the fact that the catalyst used for the capillary experiments had lost a significant part of its activity due to the catalyst storage bottle having been opened and in use for about 2-3 weeks. It should be mentioned that due to limited resources (one catalyst bottle available at any time) there was no alternative catalyst to use. It is estimated by comparing the results obtained under the Alpha conditions with the standard results obtained in the past with fresh material, that the catalyst used for the CO experiments with the capillary reactor presented here, had 55% of the activity one would expect from a catalyst contained in a freshly opened bottle but still worth using.

It should be mentioned here that the catalyst solution for all the capillary experiments apart from the ***Catalyst Concentration Series of Experiments*** (Section 8.3.7) was not prepared at UCL but it was provided ready to use by LI in 1 L glass bottles. The catalyst solution once it is exposed in the air degrades due to Pd-ligand dissociation which eventually leads to formation and precipitation of Pd black and consequently the catalyst activity is reduced. The physical meaning of this unavoidable phenomenon is a decrease of the effective Pd concentration and therefore reduced reaction rates were observed. A significant effort was made in this research work to minimise the effect of catalyst deactivation when conducting capillary experiments by performing experiments of the same series in close consequence with a maximum of four experiments performed in one day. A higher scattering of the autoclave data compared to the capillary data is evident from Figure 8.18 which can be attributed to the difficulty of determining the initial reaction rates.

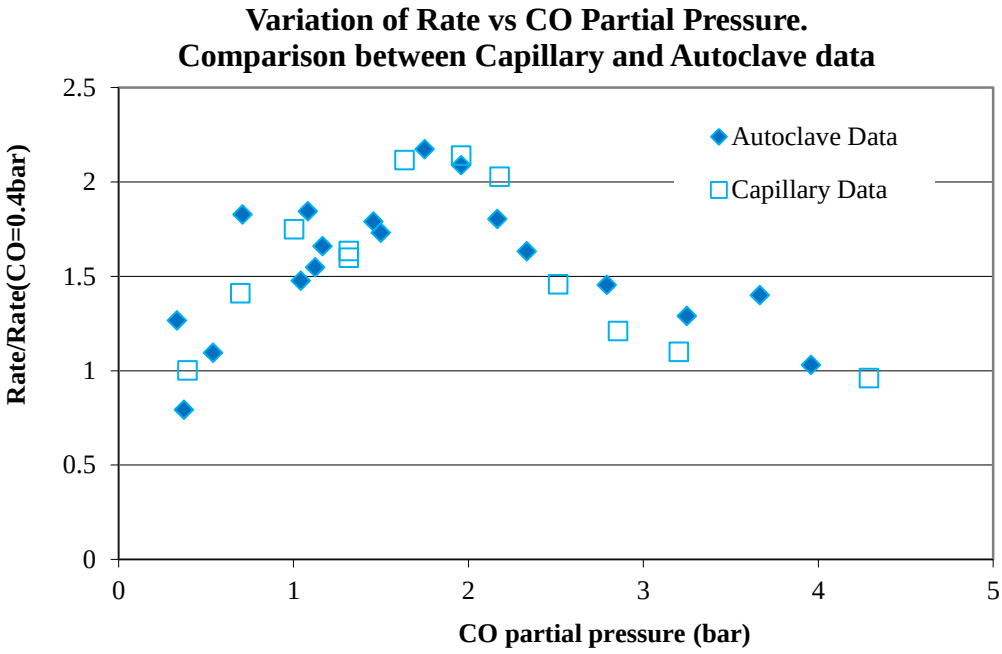

Figure 8.18. Reaction rate with respect to CO partial pressure. Capillary data and autoclave data comparison.

Figure 8.19 is the plot of LN(reaction rate) versus LN(partial CO partial pressure) in order to determine the partial reaction order with respect to CO using the differential method. The shifting reaction order from positive to negative depending on the CO partial pressure is clearly evident.

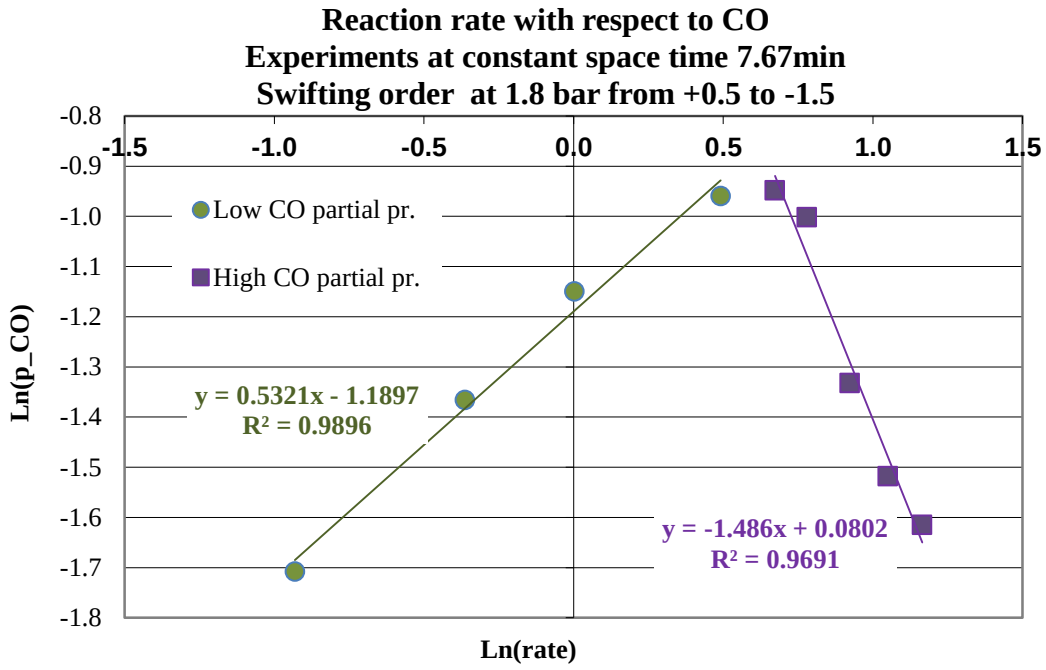

Figure 8.19. Determination of partial reaction order with respect to CO for low and high partial presssures. Initial rates Method. Capillary data.

Figure 8.20 is the initial rates plot for CO based on the autoclaves data. A reaction induction time of several minutes was reported for autoclave experiments performed for CO partial pressures of 2.35 bar and above. In these cases, the data were extrapolated to t=0 in order to find the initial rate.

The shift in the reaction order signifies the existence of the concentration term [CO] in the nominator and of the $[CO]^3$ in the denominator of the reaction rate law. This

agrees with the mechanistically derived reaction rate law as it will be shown in Section 8.4.

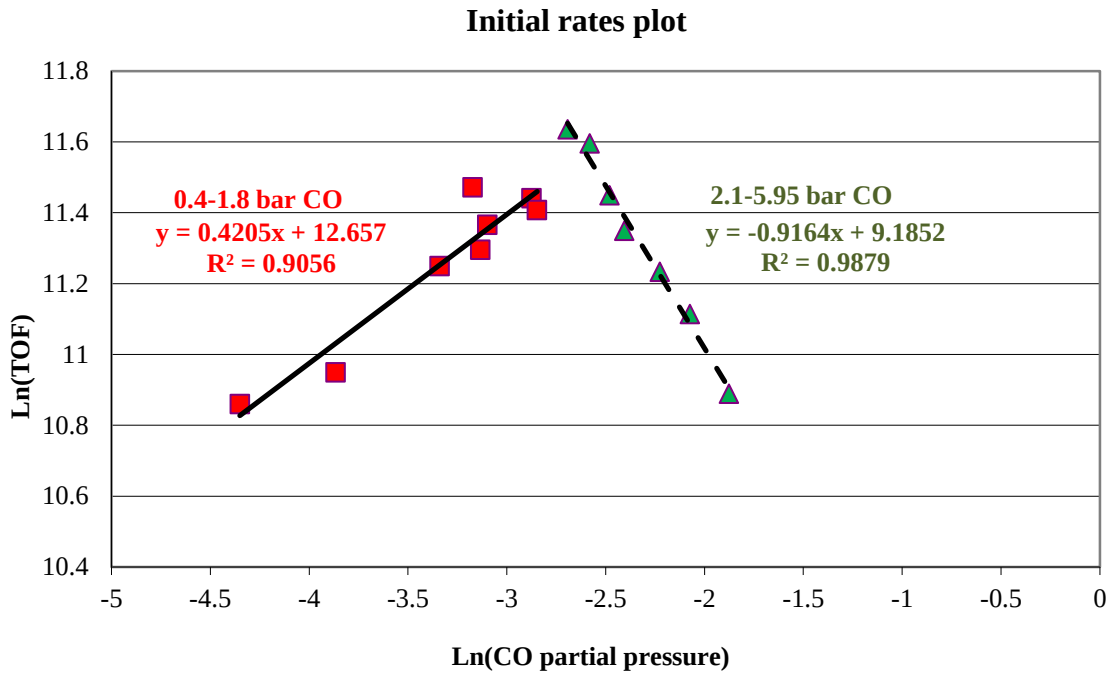

Figure 8.20. Autoclave data for determination of reaction order with respect to CO.

The partial reaction order for CO using the capillary microreactor (please refer to Figure 8.19) was found to be:

- $0.5321 \approx 0.5$ for partial pressures 0-1.8 bar
- $-1.486 \approx -1.5$ for partial pressures above 1.8 bar

Very similar reaction kinetics was found from capillary microreactor and autoclave (batch) experiments. In detail, experiments with autoclave reactors led to the following conclusions regarding the partial reaction orders:

- Autoclave experiments conducted in 2001 (LI report 91, 2001): order 0.5724 and -1.4715 for pressures below and above 2 bar respectively.

- Autoclave experiments described in Chapter Five (please refer to Figure 8.20): order $0.4172 \approx 0.4$ and $-0.9232 \approx -0.9$ for pressures below and above the CO critical partial pressure respectively. It should be noted though, that if the autoclave data for CO partial pressures of 2.35 bar and above were not extrapolated to t=0, the reaction order would be -1.5 instead of -0.9. The CO critical partial pressure where the reaction order shifts could not be determined with accuracy and it was found to be in the range [1.75-2.1 bar].

8.3.5 Methanol Series of Experiments

In order to find the reaction order with respect to methanol the content of methanol in the liquid mixture was varied in the range of [20 %-60 %] while keeping the gas flow rates at the constant values of CO=0.1 ml/min and C_2H_4=0.9 ml/min maintaining in this manner the gas ratio C_2H_4/CO=9:1 in agreement with the Alpha standards. The liquid flow rate was 5 μl/min (please refer to Table 8.16). The flow rates were chosen so that the space time calculated at the inlet conditions is always 5.20 min which was large enough to give a MeOH conversion that could be measured with good analytical accuracy. Please note that for this series of experiments the catalyst was replaced with material from a newly opened catalyst bottle.

Experimental Conditions		
Parameter	**Unit**	**Value**
CO flow rate	ml/min, STP	0.1
C_2H_4 flow rate	ml/min, STP	0.9
Liquid flow rate	μl/min	5
MeOH concentration	**wt%**	**[20-60]**
MeP concentration	wt%	[80-40]
Pd catalyst concentration	mol/lt	$2.4\ 10^{-5}$
Pressure	bar	10
Temperature	^oC	100

Table 8.16. Experimental conditions.

The data obtained are shown in Table 8.17 and Figure 8.21 provides a comparison between the results obtained with the capillary and the autoclave reactors.

Methanol Capillary Data									
Experiment	**%MeOH in the liquid mixture- the rest is MeP**	**MeOH concen-tration mol/m^3**	**% MeOH conversion**	**Space time calculated at reactor inlet, τ_{in} min**	**Space time calculated at reactor outlet, τ_{out} min**	**Average space time, $\tau_{ave=(}\ \tau_{in}+\ \tau_{out)/2}$ min**	**%difference in space time calculations= =100 * (τ_{in} – τ_{out})/ τ_{in} min**	**%CO conversion**	**%C_2H_4 conversion**
1	27.59	7565	2.08	5.20	5.41	5.31	-4.04	17.87	2.25
2	35.95	9735	2.37	5.20	5.52	5.36	-6.15	26.20	3.32
3	39.75	10764	2.01	5.20	5.50	5.35	-5.77	24.57	3.11
4	55.59	15242	2.87	5.20	5.84	5.52	-12.31	49.68	6.32
5	25.37	6956	2.21	5.20	5.41	5.31	-4.04	17.46	2.20
6	19.41	5322	1.78	5.20	5.31	5.26	-2.12	10.76	1.34

Table 8.17. Methanol capillary data.

The LN of the Methanol concentration versus the LN of TOF (molMeP/molPd/h) is plotted below (Figures 8.21 and 8.22) using the capillary data and the autoclave initial rates data. The two sets of experimental data agree very well and show essentially a first order dependency with respect to methanol if one takes into account the data for methanol concentrations 30 %-70 % (% w/w) as the gradient of the plot is 0.9. Methanol has a higher impact on the reaction rate at lower concentrations (15 %-25 %) as it was found by autoclave experiments. That is the reason why if the data over the whole range of concentations (15-70 %) are taken into account, the gradient is higher than 1; at 1.25.

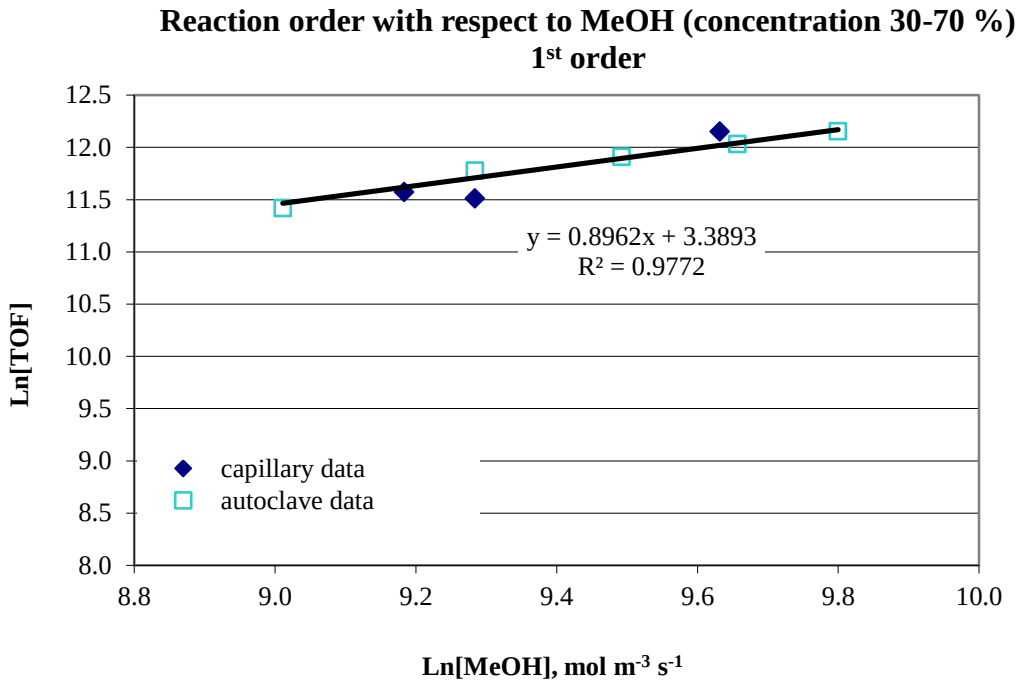

Figure 8.21. Comparison between capillary and autoclave experimental data for determination of reaction order with respect to methanol. Methanol concentration 30 %-70 % (% w/w) in the liquid mixture.

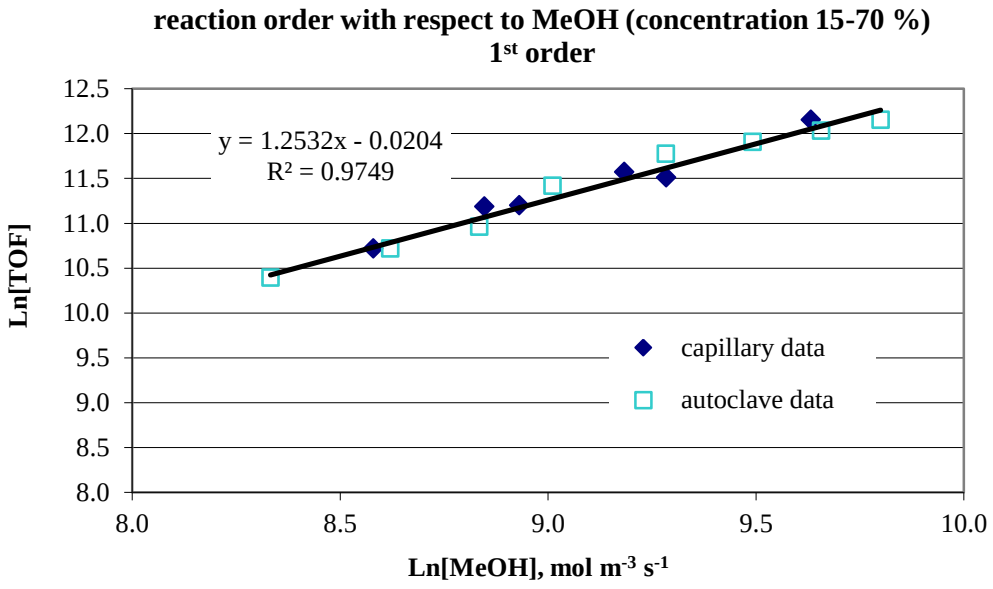

Figure 8.22. Comparison between capillary and autoclave experimental data for determination of reaction order with respect to methanol. Methanol concentration 15 %-70 % (% w/w) in the liquid mixture.

8.3.6 Temperature Series of Experiments

Experiments were performed using gas flow rates: for CO=0.1ml/min, for C_2H_4=0.9ml/min, the standard liquid mixture 70:30 MeP:CO with liquid flow rate L=5 μl/min, pressure P=10 bar and variable reaction temperature in the range 80 to 120 ^oC in order to investigate the dependence of the reaction rate on temperature.

Experimental Conditions		
Parameter	**Unit**	**Value**
CO flow rate	ml/min, STP	0.1
C_2H_4 flow rate	ml/min, STP	0.9
Liquid flow rate	μl/min	5
MeOH concentration	wt%	30

Parameter…*Continued*	**Unit**	**Value**
MeP concentration	wt%	70
Pd catalyst concentration	mol/lt	2.4 10^{-5}
Pressure	bar	10
Temperature	**^{o}C**	**[80-120]**

Table 8.18. Experimental conditions.

The increase in temperature increased the reaction rate as it was expected until the temperature 110 ^{o}C. A sudden drop in reaction rate was observed at 120 ^{o}C to the reaction level corresponding to 100 ^{o}C. The reaction rate decrease at 120 ^{o}C was also observed from autoclave experiments performed in 2001 by Lucite International. The reason for the decrease is believed to be catalyst deactivation at higher temperatures due to cleavage of the Pd-P bonds. The table below contains the data obtained with the capillary reactor.

Effect of temperature on Methanol conversion.	
Temperature (^{o}C)	**% MeOH conversion**
80	1.7
90	2.1
100	2.8
110	8.9
120	3.0

Table 8.19. Effect of Temperature on methanol conversion.

The capillary data are compared against early autoclave data **obtained in 2001** and provided by Lucite International in Figure 8.23. The normalised rate=(reaction rate

at a temperature T/reaction rate at 363 K) was plotted against the reaction temperature instead of the reaction rate, in order to avoid the catalyst effect as the catalyst used for the capillary experiments was not fresh and its exact effectiveness was not known but more importantly the early autoclave experiments were performed using 4.5 10^{-5} mol/lt [Pd] instead of 2.4 10^{-5} mol/lt for the capillary experiments.

A very good agreement was found between the two sets of results at all temperatures apart from 110 ^{o}C when the reaction rate obtained with the autoclaves was surprisingly low. This could be due to mass transfer limitations for the early autoclave experiment at this temperature as it is known that as temperature elevates diffusional effects become more important. Another reason could be side reactions that consume the methanol and can affect the esterification reaction forming MeP as it is explained below.

Methanesulfonic acid is a component of the catalytic system and can react with methanol to create an ester and water as follows:

$$CH_3OH + CH_3SO_3H \leftrightarrow CH_3SO_3CH_3 + H_2O \qquad (8.12a)$$

Water can also form from acid-catalysed alcohol etherification, particularly at temperatures above 100 ^{o}C (Kiss, 2001). A hydrogen atom protonates one methanol molecule giving it a positive charge:

$$CH_3OH + H^+ \rightarrow CH_3OH_2^+ \qquad (8.12b)$$

A nucleophilic oxygen atom of unprotonated methanol displaces a water molecule from the electrophilic (protonated) methanol yielding water, a hydrogen ion and dimethyl ether:

$$CH_3OH_2^+ + CH_3OH \rightarrow H_2O + H^+ + CH_3OCH_3 \qquad (8.12c)$$

Water can have an important influence in an esterification system because it creates hydrogen via the homogeneously catalysed gas water shift reaction (8.12d). The occurrence of this reaction can affect catalyst selectivity, activity and stability.

$$H_2O + CO \leftrightarrow H_2 + CO_2 \qquad (8.12d)$$

The mechanism of the homogeneously Pd-catalysed Water Gas Shift Reaction (WGSR) involves the formation of a Pd-hydride (Zudin et al., 1989) and as Alpha process also proceeds via the hydride mechanism where the Pd-hydride is the catalyst precursor, the WGSR can accelerate the esterification, a fact which has been reported by a number of other research groups too (Kiss, 2001).

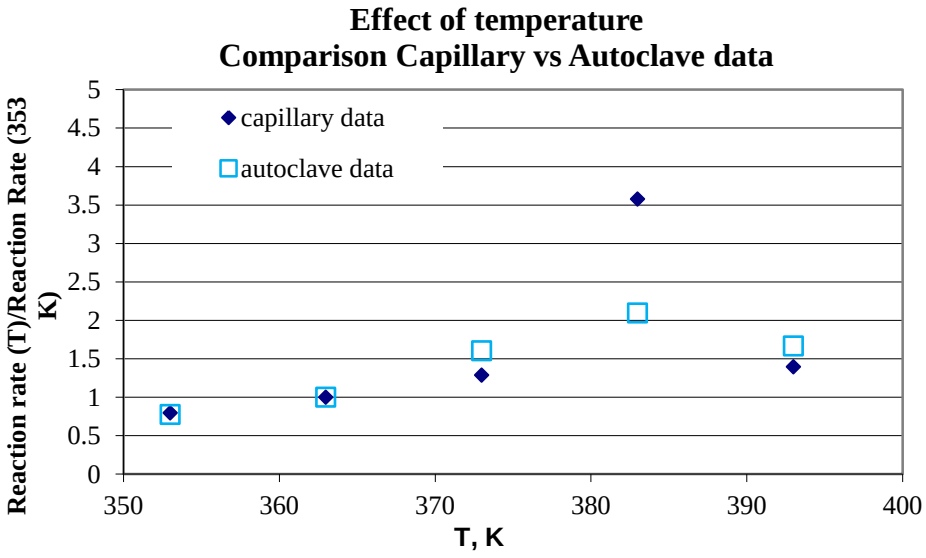

Figure 8.23. Comparison between capillary and autoclave data (2001). Significant difference only at 110 ^{o}C.

According to Ramachandran & Chaudrari (1983) mass transfer controlling processes for multiphase reactions have low activation energy (4-12 kJ/mol) while if there are no mass transfer limitations, the activation energy would be greater than 40 kJ/mol. If there are some mass transfer resistances, the estimated activation energy would be half (20-50 kJ/mol) of what it would be under kinetic control. However, it should be taken into account that as the temperature increases, the diffusional effects become important, so for every point a check should ensure that the process is controlled by the chemical reaction at all the temperatures studied (Vavasori et al., 2003). Kreutzer (2003) used the activation energy not only as an indication of the existence of mass transfer effects but also for the assessment of the degree of limitation.

Figure 8.24 is the comparative Arrhenius plot between the capillary and the autoclave data. The plot was found to be linear, but what does this signify for complex kinetics? According to Espenson (1981), it signifies a reaction mechanism composed of successive steps and one step is rate-limiting. The plot would be curved downwards if the rates of the consecutive steps are comparable. Conversely, if the mechanism is composed of parallel pathways then the plot will be curved upwards. The apparent activation energy using the capillary data for temperatures 80, 90, 100 and 110 ^{o}C was calculated and found equal to 53 kJ/mol while the apparent activation enthalpy and entropy were calculated 50 kJ/mol and -164 J/K respectively. By comparison, an average value of 36 kJ/mol and 39 kJ/mol for the apparent activation energy was determined by the autoclave experiments conducted in 2001 and 2005 respectively by LI. It should be noted that capillary experiments were not performed at 130 ^{o}C as this temperature is above the recommended by the manufacturer operating temperature for the plastic capillary tubing.

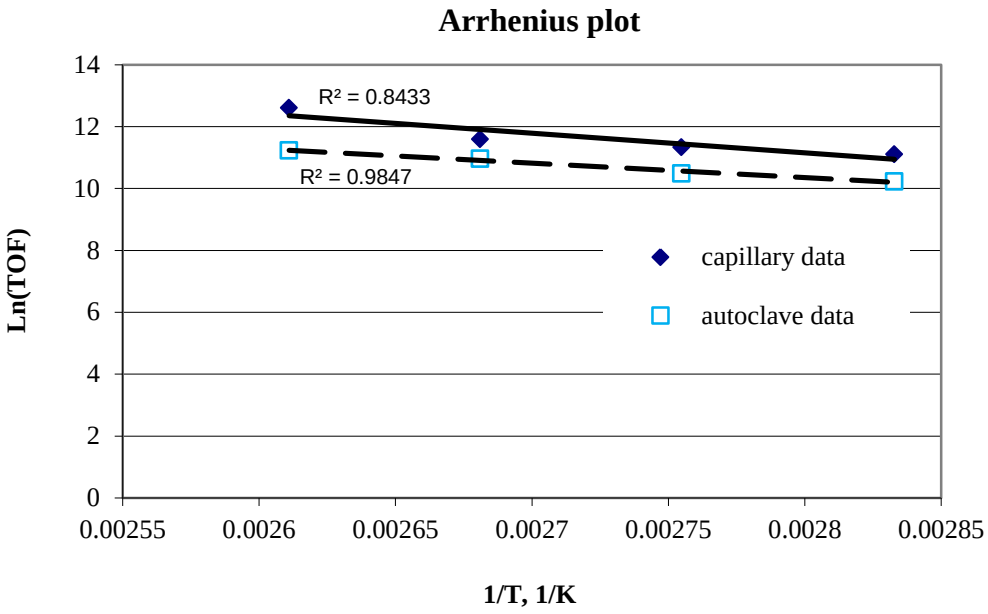

Figure 8.24. Arrhenius plot obtained with Capillary and Autoclave Data – Comparison.

In the current study, the activation energy for the methoxycarbonylation of ethylene yielding methyl propionate was calculated as 53 kJ/mol. But, what does the magnitude of activation energy actually mean? In general, a rate of reaction will depend on three factors: the pre-exponential factor, the activation energy and the concentrations of the reactants and more often the activation energy is the most influential factor of the three. That is the reason why frequently, rates of different reactions can be compared based on their activation energy and as a guide the lower the activation energy, the faster is the reaction. The magnitude of the activation energy also denotes the degree at which the reaction rate increases when the temperature increases under similar concentration conditions. An activation energy 53 kJ/mol means that the reaction rate at 100 ^{o}C roughly increases by 60 % for every 10 ^{o}C temperature increase.

The value of the activation energy depends on factors like the catalyst used, the substrate and the solvent. In general, the more polar the solvent the lower the activation energy which means the faster is the reaction. The 53 kJ/mol calculated for the methoxycarbonylation of ethylene with the d^tbpx ligand (Alpha process) at 1 bar of CO and 10 bar of total pressure is less than half of the activation energy measured for the methoxycarbonylation of 1-heptene with catalyst $[(C_6H_5)_3P]_2PdCl_2 - SnCl_2$ at 134 bar of CO (Knifton, 1976). Conversely, it is higher than the activation for the asymmetric hydrogenation of methyl Z-acetamidocinamate with a [Rh (S,S-BDPPTS)]$^+$ water soluble catalyst at conditions [20-70 ^{o}C] and [3-11 bar], found equal to 31 kJ/mol and 40 kJ/mol using a microdevice and a batch reactor system respectively, as reported by de Bellefon and co-workers in 2003. The researchers explained this difference to the difficulty of performing experiments with a very low material inventory in addition to the probability of poor temperature and residence time control in the microreactor. Abdallah et al. (2006) investigating the fast hydrogenation of α-methylstyrene with Rh/γ-alumina catalyst using a mesh microreactor, concluded that the reactor likely operated in the kinetic regime since the activation energy of 40 kJ/mol was obtained. The same conclusion can be derived for the Alpha process in this work; since the activation energy is 53 kJ/mol (i.e. larger than 40 kJ/mol), the capillary microreactor used was operating in the kinetic regime.

In the current work, the activation enthalpy for the Alpha process was calculated at 50 kJ/mol from the formula (Nakamura & Tsutsui, 1980):

$$\Delta H = E_\alpha - RT \tag{8.13}$$

The activation enthalpy is a measure of the energy barrier which must be overcome in order to attain the transition state. It is associated with bond strengths inside and between the reactants. It is known that the lower the activation enthalpy, the faster the reaction when the other parameters are equal.

The entropy of activation, ΔS, is associated with the probability of a reaction occurring and includes contributions from the orientation and steric bulk of the reactants and their solvation. Negative values of ΔS result from bringing together different species with different orientations and can also reflect anionic charges. Positive values of activation entropy relate to dissociation such as bond breaking within a species (Espenson, 1981).

The entropy of activation can be calculated from the enthalpy of activation:

$$\Delta S = R \ln\left(\frac{\Delta H \cdot h}{k_b \cdot T}\right) \tag{8.14}$$

For the reaction under study, ΔS was calculated at -164J/K and the negative value signifies that two ionic species collide to form a transition state (Nakamura & Tsutsui, 1980).

8.3.7 Catalyst Concentration Series of Experiments

Experiments were conducted at standard conditions (P,T) (10 bar,100 ^{o}C), 70:30 MeP: MeOH mixture and flow rates CO=0.1 ml/min, C_2H_4=0.9 ml/min, L=5 μl/min but using variable catalyst concentration from 4.30 10^{-5} to 6.86 10^{-5} mol/L .

Parameter	**Unit**	**Value**
CO flow rate	ml/min, STP	0.1
C_2H_4 flow rate	ml/min, STP	0.9
Liquid flow rate	μl/min	5
MeOH concentration	wt%	30
Parameter...*Continuued*	**Unit**	**Value**
MeP concentration	wt%	70
Pressure	bar	10
Temperature	^{o}C	100
Pd catalyst concentration	**mol/lt**	**[4.30 10^{-5} -6.86 10^{-5}]**

Table 8.20. Experimental conditions.

This series showed that the increase in catalyst has a positive effect on the reaction rate. Furthermore, for low catalyst concentrations the process is under kinetic control but for concentrations above 5.88 10^{-5} mol/L the reaction rate is controlled by mass transfer.

The method followed here to determine whether kinetics control the capillary reactor operation was based on a suggestion made by Ramachandra & Chaudhari (1983). They proposed that for reactions which are first order with respect to gaseous reactant *A* there is a simple method to check if reactor operation in the kinetic

regime. The method consists of varying the catalyst loading and measure and rate of gas absorption R_A. A plot of $[A^*]/R_A$ versus $1/w$ where w is the catalyst loading will be a straight line passing from the centre of the axes (or the intercept is close to zero) and with a slope $1/\kappa_1$ if the process is controlled by kinetics. If the process is controlled by diffusion, the plot will be a straight line almost horizontal (a line parallel to the $1/w$ axis). In the intermediate case (regime between 1 and 2) the line will have a slope equal to $1/\kappa_1$ and an intercept equal to $1/k_L\alpha$ (please refer to Figure 8.25). Figure 8.26 shows plots of $[A^*]/R_A$ versus $1/w$ for different reaction orders.

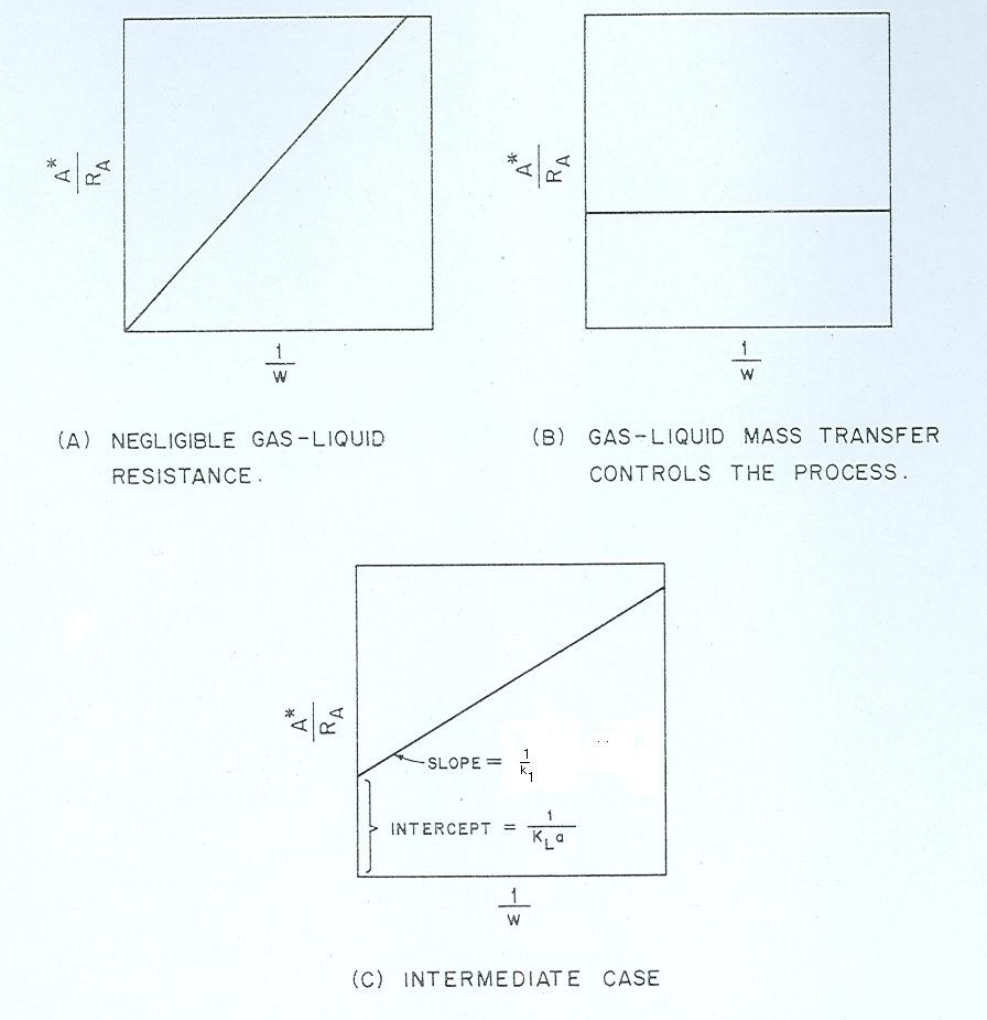

Figure 8.25. Plots of $[A^*]/R_A$ versus $1/w$ for various controlling regimes. First order reaction.

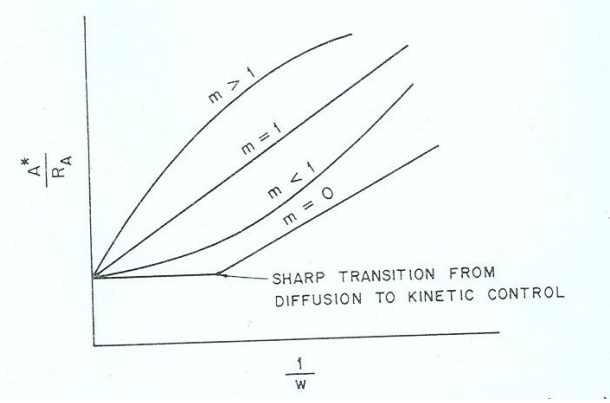

Figure 8.26. A schematic plot of $[A^*]/R_A$ versus $1/w$ for different reactions orders with respect to the dissolved gas.

Figure 8.27 is a plot of the data obtained with the capillary reactor and shows the transition from a kinetically controlled reaction to a reaction dominated by mass transfer as the catalyst concentration in the liquid mixture is increased. The standard catalyst concentration used for the capillary experiments presented in the previous sections of this Chapter was only 2.4 10^{-5} mol/L which means that reaction operation was under the kinetic control.

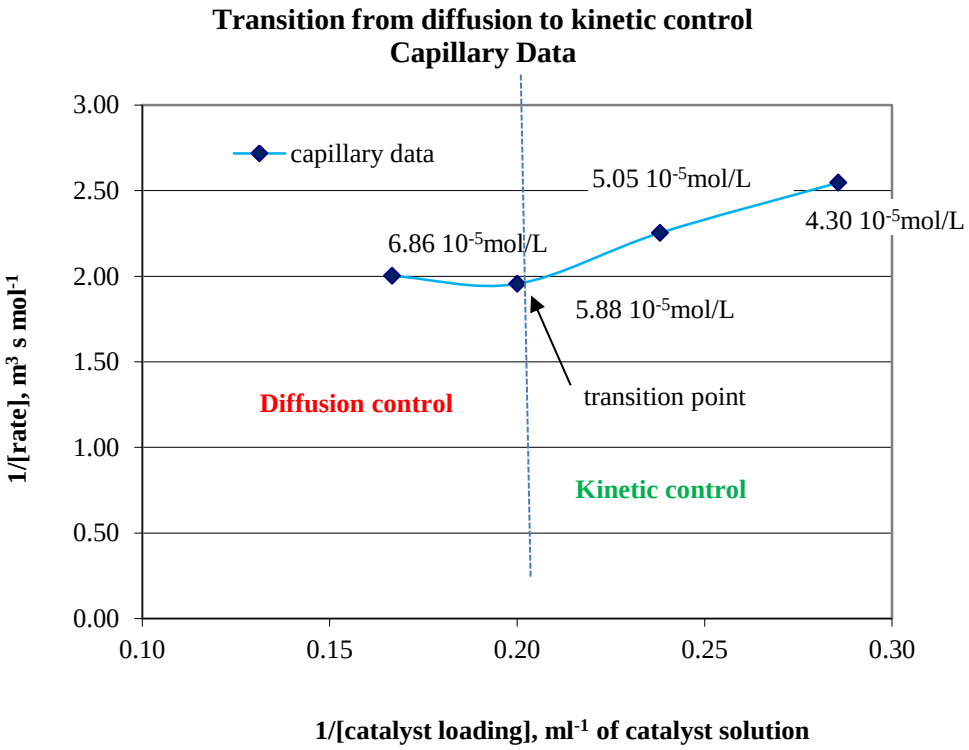

Figure 8.27. Transition from diffusion to kinetic control. Capillary data.

A similar graph was produced based on old autoclave data provided by LI but the experimental conditions were not Alpha Standards as it is presented below.

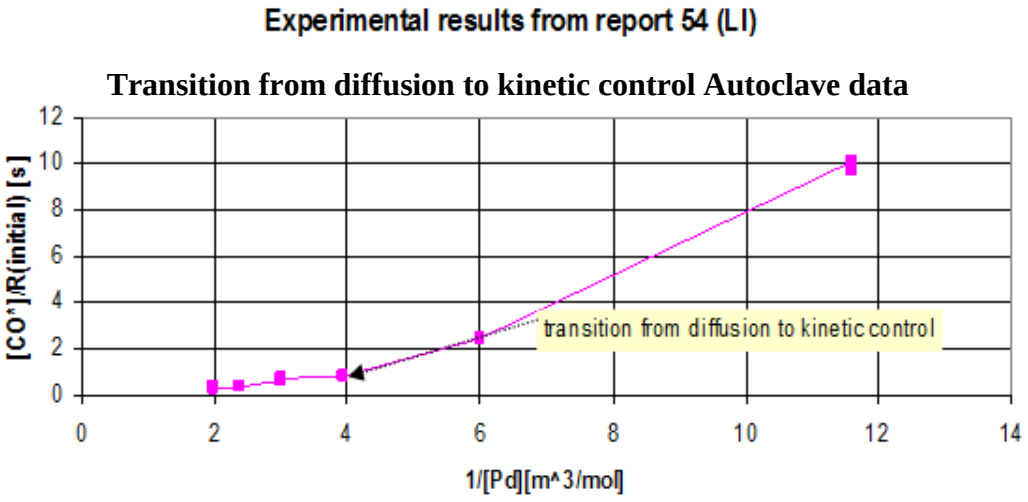

Figure 8.28. Transition from Diffusion to Kinetic Control. Autoclave data.

The data obtained with the capillary reactor were used to find the partial reaction order and the results are shown in the graph below.

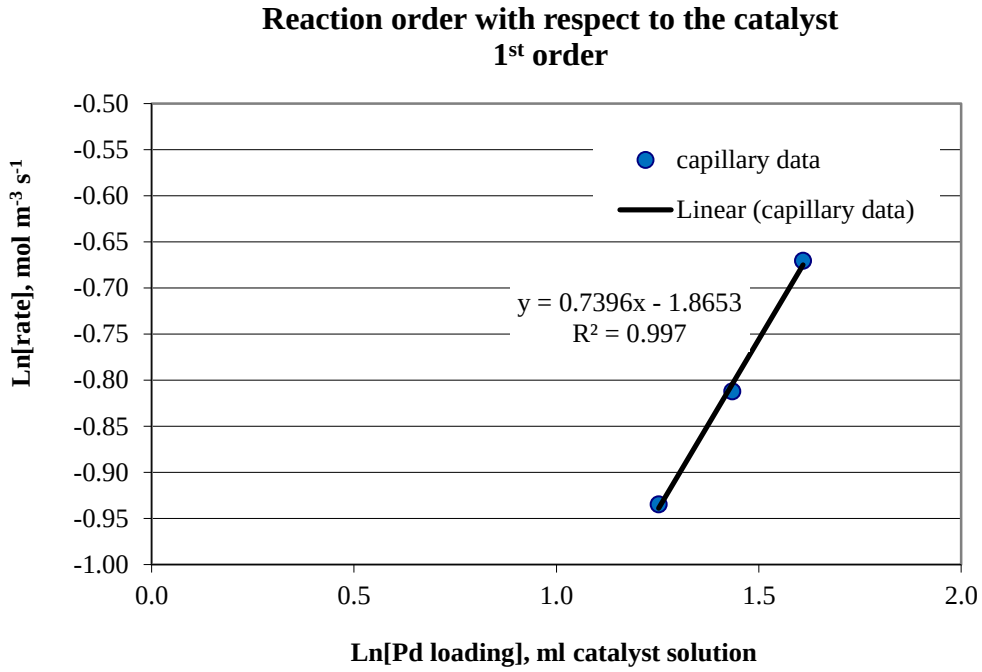

Figure 8.29. Determination of reaction order with respect to the Pd catalyst. Capillary data.

Figure 8.29 shows that the catalyst concentration has a positive effect on the reaction rate. The partial reaction order with respect to the catalyst was found to be +0.74. Based on the catalytic cycle of the methoxycarbonylation of ethylene with the Alpha process, a first order dependency would be anticipated. Moreover, a first order reaction was found from early autoclave experiments conducted by LI. The same conclusion was derived from NMR experiments under reaction conditions conducted at the University of Liverpool, also participating in this project (Lucite Research Conference, November 2007). However, it is possible that other interactions in the chemical system, like solvent interactions for instance, reduce the apparent reaction order to a fractional number.

8.3.8 Catalyst Degradation Experiments

During the course of the experimental program with the capillary reactor it was noticed that the Pd catalyst activity would deteriorate with time. The catalyst provided by LI was stored in glass bottles in the lab cupboard and not kept under a nitrogen atmosphere. After three months storage in a sealed bottle a drop in activity would be noticed and once the bottle was opened the catalyst would become unusable for the capillary reactor experiments after a month, as no record of the methoxycarbonylation reaction taking place was longer possible (no measurable difference in MeP concentration between the reactor inlet and outlet). Another characteristic of catalyst degradation which occurred after prolonged storage was the increased formation of a formaldehyde by-product resulting from methanol oxidation.

Two series of experiments were conducted under the same conditions of pressure, temperature, gas ratio and liquid composition of 70:30 MeP:MeOH in order to find the effect of catalyst deactivation on the reaction rate (please see Table 8.21). The first series used fresh catalyst while the second one used three months old catalyst previously stored in a sealed bottle.

Experimental Conditions for Comparison between Fresh and 3months Old Catalyst		
Parameter	**Unit**	**Value**
CO flow rate	ml/min, STP	0.1
C_2H_4 flow rate	ml/min, STP	1.0
Liquid flow rate	µl/min	5
MeOH concentration	wt%	30

Parameter…*Continued*	Unit	Value
MeP concentration	wt%	70
Pd catalyst concentration	mol/lt	2.4 10^{-5}
Pressure	bar	6
Temperature	^{o}C	100

Table 8.21. Experimental conditions-catalyst degradation experiments.

The comparison between the two sets of data is shown in Figure 8.30 from which it can be concluded that fresh and old catalyst produced different results. The old catalyst produced higher reaction rate at high residence time but in this case the product was not only methyl propionate but also formaldehyde.

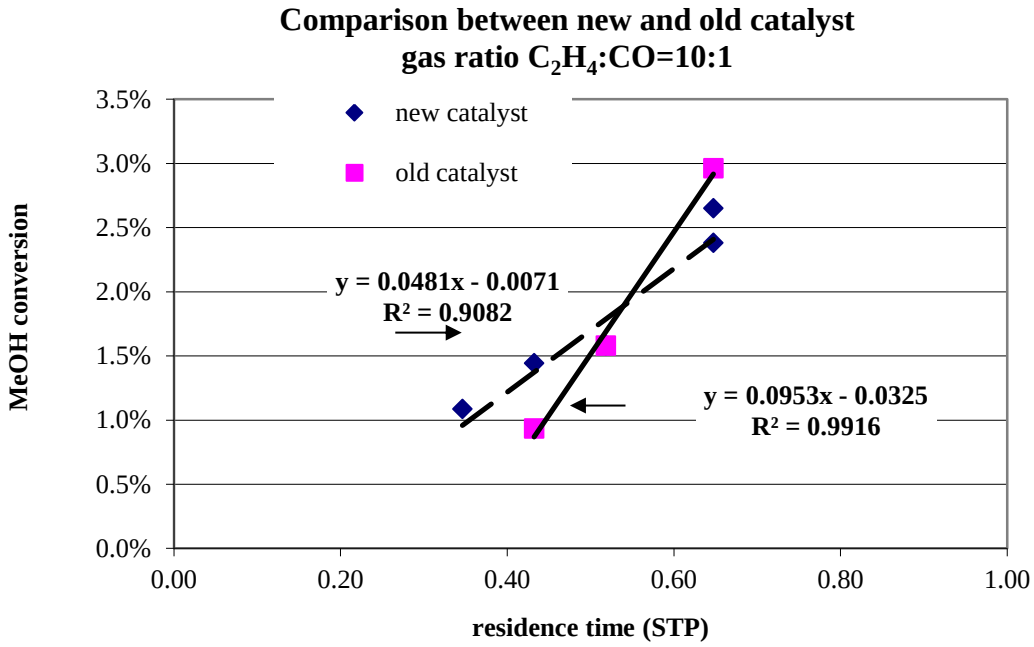

Figure 8.30. Catalyst Degradation. Higher Reaction Rates Obtained from using the Old Catalyst but reaction also leads to formaldehyde formation through methanol oxidation.

The following GC reports show the increased production of a formaldehyde by-product when the catalyst is old. The first and second peaks correspond to the

methanol and the MeP composition of the liquid mixture while the third one corresponds to the concentration of the un-known component which might be dimethoxy-methane $CH_2(OCH_3)_2$ formed by the reaction of methanol and formaldehyde.

In conclusion, old catalyst slows down the main reaction and it enhances formaldehyde formation. A plausible mechanism is as follows:

Methanol oxidation: (8.15)

$2CH_3OH+2O_2 \rightarrow 2CH_2O+2H_2O$

Dimethoxymethane formation: (8.16)

$CH_2O+2CH_3OH \rightarrow CH_2(OCH_3)_2+H_2O$

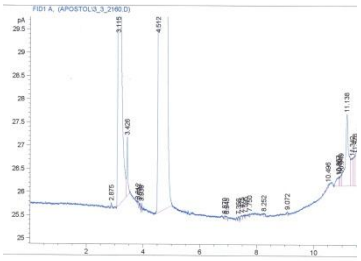

New catalyst used, no reaction, 3rd peak relative area 0.066%

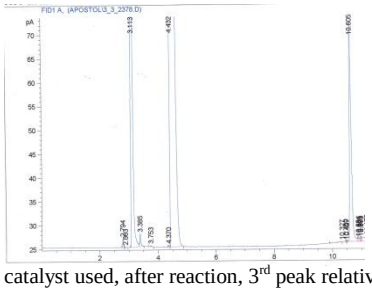

New catalyst used, after reaction, 3rd peak relative area 0.34%

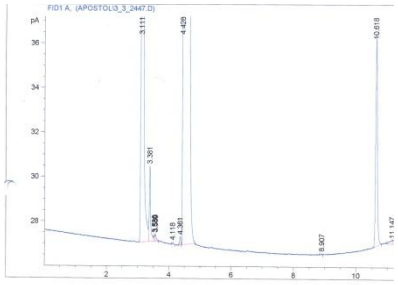

Old catalyst used, no reaction, 3rd peak relative area 0.19%

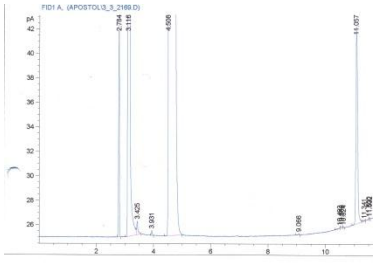

Old catalyst used, after reaction, 3rd peak relative area 0.99%

Figure 8.31. GC reports showing increased production of a reaction by-product (3rd peak). Experiments at 6 bar.

8.4 Reaction Scheme and Kinetic Model

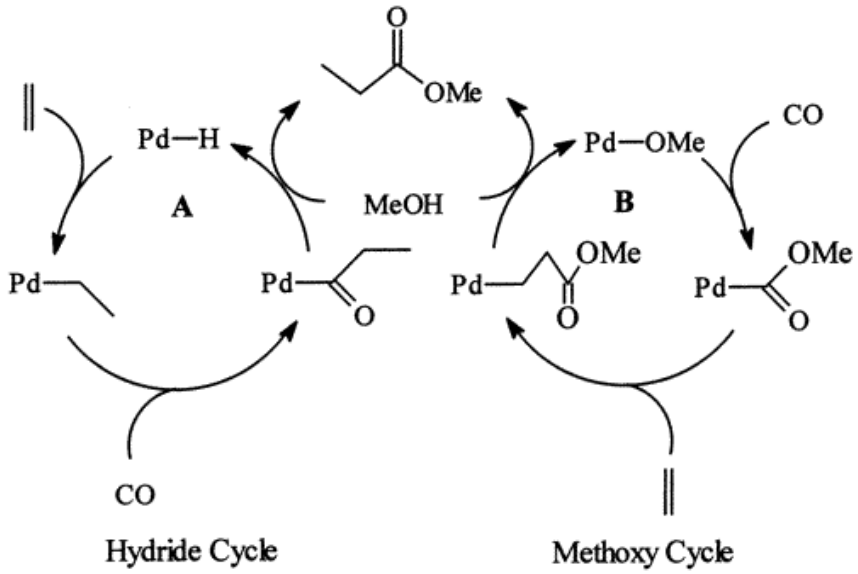

Figure 8.32. The Possible catalytic cycles for the methoxycarbonylation of ethylene to methyl propionate. A: Hydride cycle, B: Methoxy cycle (Torres, 2009).

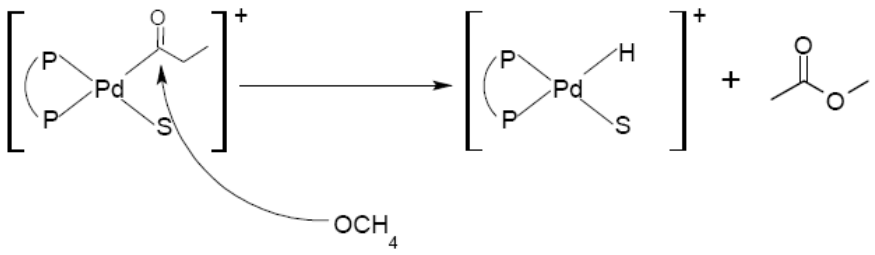

Figure 8.33a. Methanolysis as the termination step for the production of methyl propionate (intermolecular mechanism). From Torres (2009).

A probable reaction scheme resulting in product formation and catalyst deactivation is described below based on the following assumptions:

- The Pd-hydride is the predominant catalytic cycle (W. Clegg et al, 2002).
- The catalyst deactivation is induced through the formation of the $[Pd(L-L)H(CO)]^{+}$ and followed by the addition of more CO molecules which eventually leads to the formation of palladium black.
- The nucleophilic attack on the acyl complex (methanolysis) is the rate determining step. In addition to this being reported in the literature for other carbonylation reactions, different rate equations were derived in the context of this work assuming different steps as rate controlling but they were found to contradict the experimental data gathered from autoclave and capillary reactor experiments.
- The reverse reaction of the MeP decomposition and the formation of CO, ethylene and methanol under the Alpha Standards is negligible which agrees with observations from the autoclave experiments.
- The quasi-state approximation was used for the analysis which assumes that the intermediate complexes formed are very reactive and they never accumulate to considerable amounts compared to the concentrations of the initial reactants (CO, ethylene, methanol). This situation is a common one and can be applied to many chemical systems. The method entails setting to zero the first derivatives to all the intermediates.

The various complexes were named with letters, e.g (α), (b) etc for simplicity.

$$(L-L)Pd(H)]^{+} + CO \overset{K_1}{\longleftrightarrow} (L-L)Pd(H)(CO) \quad \text{(r1)}$$

(α) (b)

$$(L-L)Pd(H)(CO) + CO \overset{K_2}{\longleftrightarrow} (L-L)Pd(CO)_2 + H^{+} \quad \text{(r2)}$$

(b) (c)

$$(L-L)Pd(CO)_2 + CO \overset{K_3}{\longleftrightarrow} (L-L)Pd(CO)_3 \quad \text{(r3)}$$

(c) (d)

$$(L-L)Pd(CO)_3 + CO \overset{K_4}{\longleftrightarrow} Pd(CO)_4 \downarrow + (L-L) \quad \text{(r4)}$$

(d) (e)

$$(L-L)Pd(H)]^{+} + CH_2 = CH_2 \overset{K_5}{\longleftrightarrow} (L-L)Pd(CH_2CH_3)]^{+} \quad \text{(r5)}$$

(α) (f)

$$(L-L)Pd(CH_2CH_3)]^{+} + CO \overset{K_6}{\longleftrightarrow} (L-L)Pd(CO)(CH_2CH_3)]^{+} \quad \text{(r6)}$$

(f) (g)

$$(L-L)Pd(CO)(CH_2CH_3)]^{+} + CH_3OH \xrightarrow{k_6} (L-L)Pd(H)]^{+} + CH_3CH_2COOCH_3$$

(r7)

(g) (α)

At high CO partial pressures r1-r4 become important and lead to the formation of the inactive species $(L-L)Pd(CO)_3$ and $Pd(CO)_4$ which reduce the amount of the effective catalyst in the system and therefore diminish the reaction rate.

Analysis using the steady state approximation for reactions (r1-r7) gives:

$$K_1 = \frac{[b]}{[a][CO]} \tag{8.17}$$

$$K_2 = \frac{[c][H^+]}{[b][CO]} \tag{8.18}$$

$$K_3 = \frac{[d]}{[c][CO]} \tag{8.19}$$

$$K_4 = \frac{[e][L-L]}{[d][CO]} \tag{8.20}$$

$$K_5 = \frac{[f]}{[a][C2H4]} \tag{8.21}$$

$$K_6 = \frac{[g]}{[f][CO]} \tag{8.22}$$

$$R = k_7[g][CH_3OH] \tag{8.23}$$

$$[Pd]_{tot} = [a]+[b]+[c]+[d]+[e]+[f]+[g] \tag{8.24}$$

After rearranging we end up with the reaction rate:

$$R = \frac{K_5K_6k_7[Pd][C_2H_4][CO][CH_3OH]}{K_5K_6[CO][C_2H_4]+K_1[CO]+\frac{K_1K_2}{[H^+]}[CO]^2+\frac{K_1K_2K_3}{[H^+]}[CO]^3+\frac{K_1K_2K_3K_4}{[H^+][[L-L]}[CO]^4+K_5[C_2H_4]+1} \tag{8.25}$$

If the following definitions apply:

$$X_1 = K_5K_6 \tag{8.26}$$

$$X_2 = \frac{K_1K_2}{[H^+]} \tag{8.27}$$

$$X_3 = \frac{K_1K_2K_3}{[H^+]} \tag{8.28}$$

$$X_4 = \frac{K_1 K_2 K_3 K_4}{[H^+][L-L]} \tag{8.29}$$

Equation (8.25) takes the form:

$$R = \frac{X_1 k_7 [Pd][C_2H_4][CO][CH_3OH]}{X_1[C_2H_4][CO] + K_1[CO] + X_2[CO]^2 + X_3[CO]^3 + X_4[CO]^4 + K_5[C_2H_4] + 1} \tag{8.30}$$

And after rearranging:

$$R = \frac{X_1 k_7 [Pd][C_2H_4][CO][CH_3OH]}{K_1[CO] + X_2[CO]^2 + X_3[CO]^3 + X_4[CO]^4 + K_5[C_2H_4](1 + K_6[CO]) + 1} \tag{8.31}$$

It should be noted that the proton concentration $[H]^+$ is considered to be stable for two reasons: Firstly, its role is to protonate the phosphine contributing in this way to the Pd-hydride formation with no further participation in the catalytic cycle and secondly its concentration in the liquid mixture is very high and equal to 450 times that of Pd. The phosphine ligand is also in large excess in comparison to Pd catalyst and its concentration $[L-L]$ assumed constant too.

Equation (8.31) is in accordance with the general experimental trends of dependence of reaction rate with respect to the concentration of CO, ethylene, catalyst and particularly with the shifting reaction order with respect to CO. The theoretical kinetic model must be coupled with the experimental results for the determination of the reaction rate constant k_7 and the equilibrium constants for the elementary reactions in the catalytic cycle $K_1, K_2, K_3, K_4, K_5, K_6$.

It is not uncommon in homogeneous and enzymatic catalysis, complex rate equations to reduce to simplified forms if one of the terms in the equation denominator is orders of magnitude larger than the other terms. If this is true for the reaction under study, there is a number of possible simplified forms of equation (8.25) and are included in the following Table.

Dominant term in the denominator of eq.(8.25)	**(8.25) Reduced to the simplified form**
1	$R = X_1 k_7 [Pd][C_2H_4][CO][CH_3OH]$
$X_1[CO][C_2H_4]$	$R = k_7 [Pd][CH_3OH]$
$K_1[CO]$	$R = (K_{56} k_7 K_1^{-1})[Pd][C_2H_4][CH_3OH]$
$X_2[CO]^2$	$R = (X_1 k_7 X_2^{-1})[Pd][C_2H_4][CH_3OH][CO]^{-1}$
$X_3[CO]^3$	$R = (X_1 k_7 X_3^{-1})[Pd][C_2H_4][CH_3OH][CO]^{-2}$
$X_4[CO]^4$	$R = (X_1 k_7 X_4^{-1})[Pd][C_2H_4][CH_3OH][CO]^{-4}$
$K_5[C_2H_4]$	$R = K_6 k_7 [Pd][CO][CH_3OH]$

Table 8.22. Possible simplified forms of reaction rate equation if one of the terms in the denominator is dominant over the rest of the terms.

Other possible reactions in the catalytic cycle leading to alcohol oxidation and formation of formaldehyde and Pd^0 are:

$$(L-L)Pd(H)]^+ + H^+ \leftrightarrow (L-L)Pd]^{2+} + H_2 \uparrow \text{(r8)}$$

$$(L-L)Pd]^{2+} + CH_3OH \leftrightarrow (L-L)Pd]^0 + HCHO + H_2 \uparrow \text{(r9)}$$

Even though a small amount of formaldehyde is always formed during the course of every experiment, (r8-r9) are predominant when the catalyst is old. In this case, it was noticed that methanol mostly oxidises to formaldehyde and only a very small amount of methyl propionate is produced.

Other possible reaction that can lead to the formation of Pd black is the formation of the Pd-dimers or trimers are according to the study by Tromp at al. (2003):

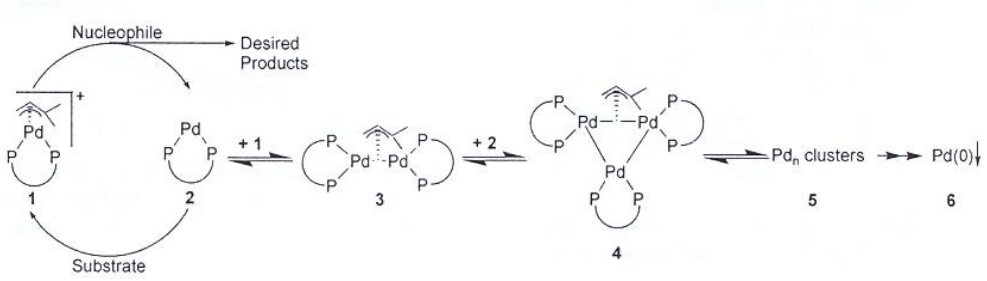

Figure 8.33. Deactivation mechanism by the formation of Pd dimers, trimers.

One of the conclusions derived from the same research work was that the phosphine ligand bite angle plays a significant role on whether formation of Pd-dimers will lead to Pd-trimers. Large bite angles facilitate formation of dimers only, while both dimers and trimers are formed for ligands with small bite angles like the d^{t}bpx phosphine ligand used in the Alpha process. However, the minimal amount of Pd catalyst used in the Alpha process makes the deactivation route depicted in the Figure 8.33 not very plausible.

8.5 Parameter Estimation

The statistical package SPSS was used to evaluate the parameters of the kinetic equation (8.30) which was derived from the theoretical approach described in the preceding section.

The SPSS analysis suggested that the terms $K_1[CO]$, $X_3[CO]^3$ and $K_5[C_2H_4]$ were not significant and therefore, equation (8.30) was simplified to:

$$R = \frac{X_1 k_7 [Pd][C_2H_4][CO][CH_3OH]}{X_1[C_2H_4][CO] + X_2[CO]^2 + X_4[CO]^4 + 1} \tag{8.32}$$

The parameters provided by SPSS are listed below:

Parameter	Value	Unit
$X_1 k_7$	3.31 10^{-7}	(mol/(m^3 s))$^{-3}$
X_1	6.57 10^{-5}	(mol/(m^3 s))$^{-2}$
X_2	2.34 10^{-4}	(mol/(m^3 s))$^{-2}$
X_4	5.28 10^{-7}	(mol/(m^3 s))$^{-4}$

Table 8.23. Kinetic parameters.

At very low CO partial pressures the terms 1 and $X_1[C_2H_4][CO]$ are the most significant and as the CO pressure increases $X_2[CO]^2$ becomes comparable to the term $X_1[C_2H_4][CO]$. The term $X_4[CO]^4$ becomes important at very high CO partial pressures.

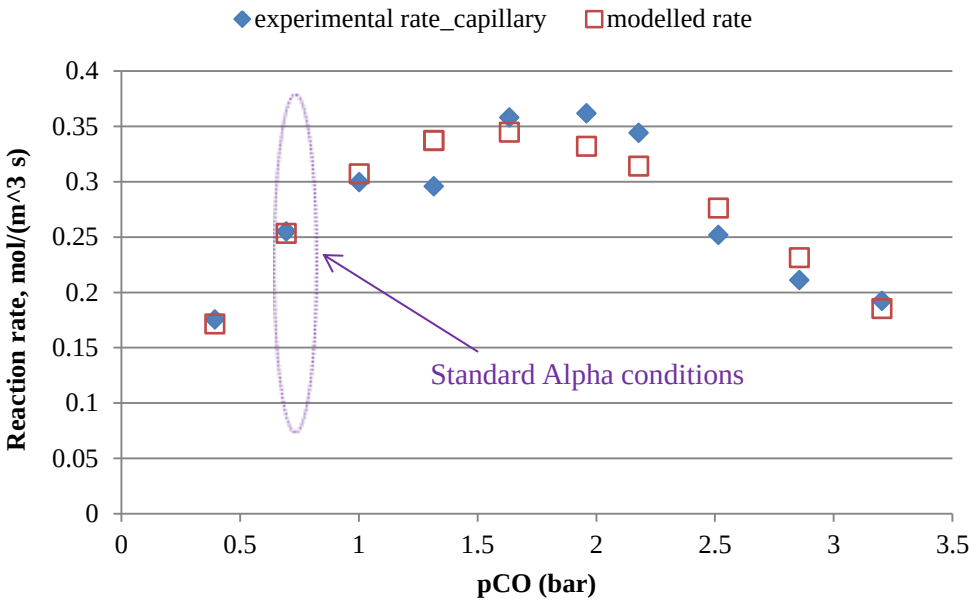

Figure 8.34. Comparison between experiment and modelling. CO data.

The residuals and the error of fit were calculated from the following formulas:

$$\mathrm{Re}\,sidual = Rate_{\exp} - Rate_{\mathrm{mod}} \tag{8.33}$$

$$Error = \sqrt{\frac{\sum(\mathrm{Re}\,siduals)^2}{n}} \tag{8.34}$$

The sum of the squares of the residual and the error were calculated equal to 8.62 10^{-2} and 2.94 10^{-2} (2.94 %) respectively. The difference between the predicted and the experimental rates were found to be within the range -8.8 % to +13.9 %. For the standard conditions of the Alpha process the difference was evaluated at -0.7 %. The residuals do not follow a pattern and they take both positive and negative values, a fact which denotes goodness of fit as it is evident from Figure 8.35.

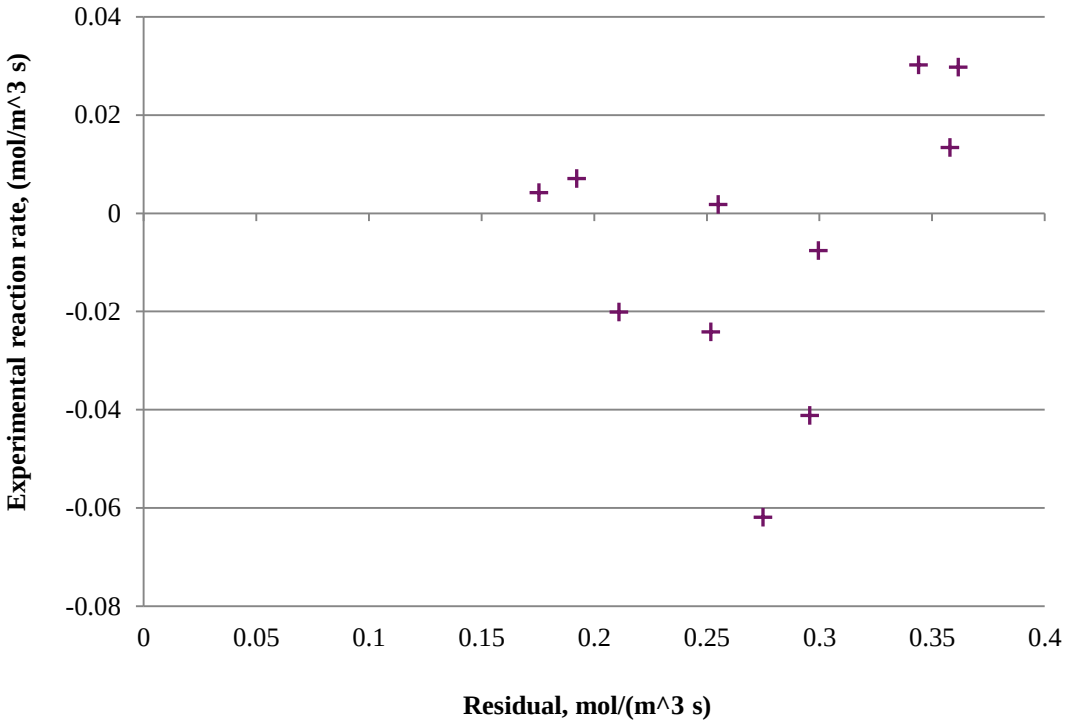

Figure 8.35. Residuals against experimental rates.

Equation (8.32) not only predicts very well the CO series data but it also predicts well the methanol data in a range of methanol concentrations above and below the standard one. The difference between the predicted and the experimental rates were found to vary within the range -9.8 % to +22.6 % for methanol concentrations above 5544 mol m^{-3} which corresponds to a liquid mixture MeOH:MeP equal to 20:80 (% w/w). For lower methanol concentrations, the model over-predicts the reaction rate. It should be mentioned though that the standard methanol concentration for the Alpha process is 8203 mol m^{-3} (liquid mixture MeOH:MeP 30:70 % w/w) for which the difference between the predicted rate and the experimental one is 0.4 %.

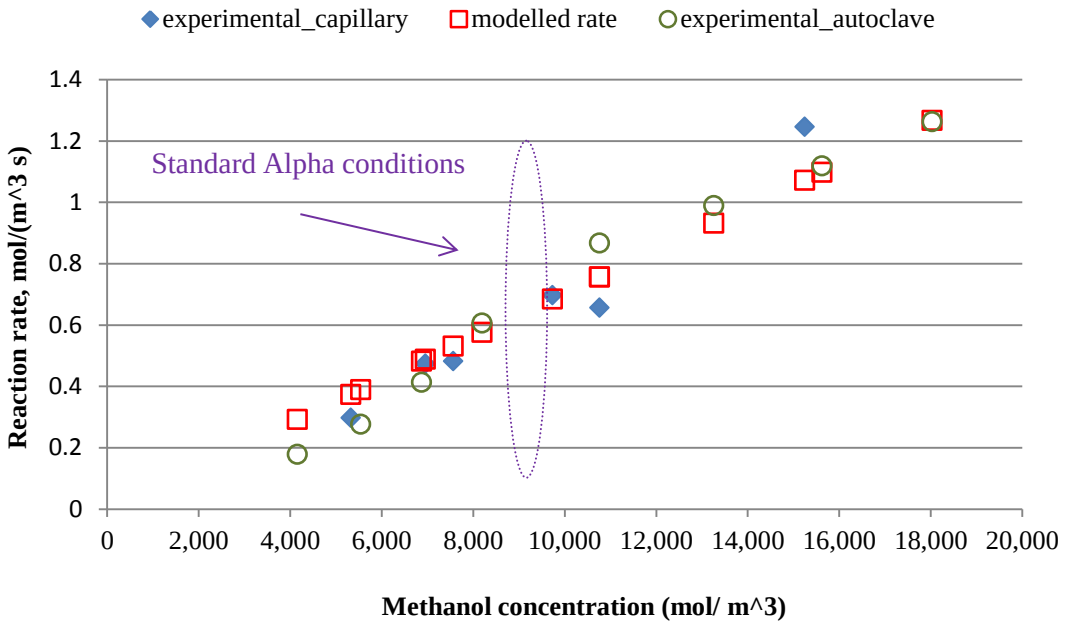

Figure 8.36. Comparison between experiment and modelling. Methanol data.

The parity plot for the CO and methanol data is illustrated below:

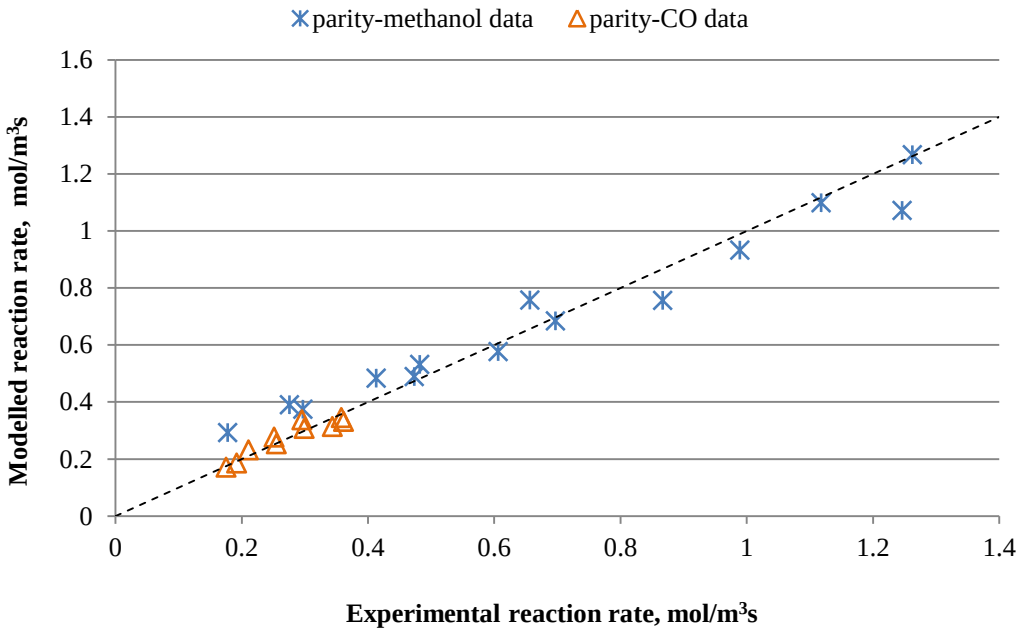

Figure 8.37. Parity plot.

Several empirical rate equations were evaluated for fitting the kinetic data. These were selected based on the trends observed. The following table lists all the kinetic equations used and the corresponding parameters. Φ_{min} is the minimized sum of the squares of the differences between observed and predicted rates (residuals). The equation derived based on the mechanistic analysis of the catalytic scheme gives the lowest Φ_{min} equal to 4.78 10^{-3}.

Number	Rate model	*kappa*	A'_2	A'_4	A'_6	Φ_{min}
1	$R = \frac{kappa \cdot [Pd][C_2H_4][CO][CH_3OH]}{A'_2[CO]^2 + A'_4[CO]^4 + A'_6[C_2H_4][CO] + 1}$	3.31 10^{-7}	2.34 10^{-4}	5.28 10^{-7}	6.57 10^{-5}	4.78 10^{-3}
2	$R = \frac{kappa \cdot [Pd][C_2H_4][CO][CH_3OH]}{(1 + A'_4[CO]) + (1 + A'_6[C_2H_4][CO])}$	1.02 10^{-7}	6.98 10^{-4}	-2.44 10^{-4}	-	1.04 10^{-1}
3	$R = \frac{kappa \cdot [Pd][C_2H_4][CO][CH_3OH]}{(1 + A'_4[CO])^4 + (1 + A'_6[C_2H_4][CO])}$	1.02 10^{-7}	6.98 10^{-4}	-2.44 10^{-4}	-	1.07 10^{-1}
4	$R = \frac{kappa \cdot [Pd][C_2H_4][CO][CH_3OH]}{(1 + A'_4[CO]^4) + (1 + A'_6[C_2H_4][CO])}$	5.71 10^{-7}	7.76 10^{-7}	3.46 10^{-3}	-	9.49 10^{-3}
5	$R = \frac{kappa \cdot [Pd][C_2H_4][CO][CH_3OH]}{(1 + A'_4\sqrt{[CO]})^4 + (1 + A'_6[C_2H_4][CO])}$	7.41 10^{-8}	1.53 10^{-2}	-1.13 10^{-3}	-	6.63 10^{-2}

Table 8.24. Models examined to fit the experimental data on the methoxycarbonylation of ethylene in the Alpha process.

8.6 Conclusions

Numerous experiments were conducted with the capillary micro reactor for the kinetic study of the methoxycarbonylation of ethylene with the Alpha process. Experimental data were collected under different conditions in order to establish the partial reaction orders with respect to ethylene, methanol, CO and the catalyst as well as to investigate the effect of the temperature on the reaction rate and calculate the apparent activation energy. The data obtained with the capillary reactor are intrinsic kinetic data as it was shown by calculations as well as derived experimentally. It is known that intrinsic data are characteristic of the chemical system and do not depend on the scale of the operation. This is why the data collected with the capillary micro reactor which has a volume of 0.573 ml agree so well with the data obtained using semi-batch autoclave reactors with volume of 2000 ml presented in detail in Chapter Two. The Differential Method was used for the analysis of the experiments which entailed calculation of the reaction rate and plotting *LN[Reaction Rate]* versus *LN[Reactant Concentration]* (or *LN[Partial Pressure of Gas]* for investigation of CO and ethylene partial pressure). The rate was calculated by experimentally measuring the inlet and outlet concentration of methanol and calculating the reactor space time by taking into account the gas and liquid flow rates used, the reaction conditions and the stoichiometry of the reaction. A similar method was used by Enache et al. (2005). The experiments were conducted under conditions so that the difference between the space time calculated at the reactor inlet or outlet was less than 12 % in all cases. The space time was also measured experimentally using a dye pulse and the result showed a very good agreement with the calculated space time at the reactor outlet.

From the experiments conducted with the capillary reactor, significant conclusions can be made:

- The effect of the increase of the ethylene concentration on the reaction rate is marginal. The reaction order with respect to ethylene is practically zero.
- The reaction is first order with respect to methanol.
- The reaction order with respect to CO shifts from +0.5 to -1.5 at a CO partial pressure of 1.8 bar.
- The apparent activation energy was calculated to be 53 kJ/mol from the linear Arhenius plot. The value was higher than 40 kJ/mol, a fact which the operation of the capillary reactor was under kinetic control.
- The catalyst concentration has a positive effect on the reaction rate. Experiments using variable catalyst concentration also verified that the reaction is very slow and that the operation of the capillary reactor in the kinetic regime as the catalyst concentration generally used is lower than the concentration at which mass transfer effects become significant.

A kinetic reaction model was developed which not only agrees with the hydride catalytic cycle established by previous studies but also accounts for the catalyst deactivation by the formation of electron-poor CO-complexes which eventually lead to the formation of Pd black.

Based on the rate data obtained with the capillary and autoclave reactors, a rate equation was proposed also after examining various other empirical models and the kinetic parameters were reported (a similar analysis was used by Divekar et al.

(1993) examining the kinetics of the hydroformylation of 1-decene using initial reaction rate data):

$$R = \frac{3.31 \cdot 10^{-7}[Pd][C_2H_4][CO][CH_3OH]}{6.57 \cdot 10^{-5}[C_2H_4][CO] + 2.34 \cdot 10^{-4}[CO]^2 + 5.28 \cdot 10^{-7}[CO]^4 + 1} \quad (8.35)$$

This rate equation derived from the reaction mechanism, composed of a series of consecutive steps and assuming that nucleophilic attack/methanolysis is the rate determining step, was found to agree with the observed trends and it predicts the rate satisfactorily. Under Alpha conditions the difference between the predicted and the observed rate was less than 1 %. Overall, this model is applicable for the following conditions:

- √ Methanol concentration in the liquid mixture in the range [4158 mol m^{-3}-18028 mol m^{-3}], or 15-70 % (w/w) with balance methyl propionate.
- √ CO at 0.5-5 bar nominal pressure in the reactor overhead space for batch operation or in the reactor feed for continuous operation with balance ethylene.
- √ Ethylene in excess in the reactor overhead space for batch operation or in the reactor feed for continuous operation.
- √ Reactor pressure, 10 bar (11 barA).
- √ Reactor temperature, 100 ^{o}C.

--//--

CHAPTER 9

Summary and Discussion

This final chapter of the Thesis restates the research problem, and reviews the main methods used in the study. The major sections of this Chapter summarise the results and discuss their implications.

9.1 Statement of the Problem

The kinetics of the methoxycarbonylation of ethylene with a Pd homogeneous catalyst as the first stage of the production of methyl methyl acrylate (MMA) using the LI Alpha Process formed the subject of this study and the ultimate goal was the development of the kinetic model suitable for reactor design.

9.2 Review of the Experimental Equipment and Methodology

As explained in previous chapters, this study primarily focused on determining the kinetics of the Alpha process by using traditional laboratory reactors (autoclaves) and a number of microreactors.

9.2.1 Autoclave Reactors

The autoclave reactor had a 2 L volume with a hollow stirrer shaft for the gas reactants (CO and ethylene) to be mixed with the liquid reactant mixture (MeOH in an MeP solution with methanosulphonic acid) by means of a 4-blade stirrer turbine characterised by a high rotating speed of the blades (up to 2330 rpm) to allow for efficient dispersion of the gas bubbles. Reactor heating was provided by the outer surface while the cooling was achieved by an internal cooling coil. A temperature control system enabled the reactor to operate within a range of two degrees below and one degree above the programmed temperature. As the reaction is in progress, the consumed gas is replenished with new supply from a reservoir tank containing the reactants in composition reflecting the reaction stoichiometry and through a regulator valve ensuring that the reactor pressure is at constant set-point. Measurements of the pressure of the gas reservoir and the reactor temperature are logged automatically every 5 s onto a personal computer and are available for further elaboration. The pressure readings are translated into mol of gas consumed and these in turn to mol of the desired product, MeP, formed. This collection of data of mol MeP during the course of the reaction will eventually be converted to reaction rate data as TOF (mol MeP/mol Pd/h) with the help of a software program. The TOF values plotted against reaction constitute the reaction rate profile.

Detailed description of the methodology for the autoclave experiments is provided in Chapter Five, but the main steps include firstly, the preparation of the Pd catalyst in a glove box, followed by transfer of the catalyst in a glass flask and the addition of the other liquid components of the mixture (MeP, MeOH and acid) under stirring. The

active catalyst, the hydride complex, [P-P-Pd^{II}-H-MeOH] is formed at this stage which is marked from the colour change of the solution from yellow to red. It should be mentioned that preparation of the catalyst solution happens under nitrogen as the catalyst is oxygen sensitive. The reactant solution in then transferred by vacuum into the reactor. The reactor's stirrer is turned on and the temperature of the reactor is starting to rise to the set-point of 100^{o}C. When set-point has been reached, the pressure inside the reactor is 2.2 bar which corresponds to the vapour pressure of MeOH and MeP. At this point, the pre-treatment of the liquid mixture with ethylene is initiated, consisting of manual addition of 8 bar of ethylene and maintenance under stirring for a duration of 30 min. The addition of an ethylene/CO 1:1 mixture from an external to the reactor gas reservoir follows next, until the reactor pressure reaches 12.2 bar. Once, the addition is complete, the pressure in the gas reservoir is monitored and a drop shortly afterwards, indicates the reaction onset. The reaction is normally allowed to proceed for 3 h and after the end of the run the reactor is cooled down, the stirrer is tuned off, the gas is vented-off, the liquid is emptied from the draining valve into a sample bottle for weighing and finally, the reactor is washed clean with methanol. The experimental conditions (temperature, pressure, reactant compositions) and methodology followed characterise a standard experiment performed under the *Alpha Standards*.

Numerous experiments were conducted with the autoclave reactor altering the reactant concentrations to determine the reaction order with respect to methanol, CO and ethylene. After the elimination of the mass transfer resistances as it was verified by calculations and empirically, the kinetic data collected were analysed using the

methods of initial rates and the integral method as described in a Chemical Kinetics textbook.

9.2.2 Microreactors

A bespoke mesh microreactor of rectangular shape with dimensions (3 cm x 3 cm x 1.38 mm) was developed in the context of this study whose basic characteristics were a silicon nitrate mesh with open pores where the contact between the gas and the liquid reactants takes place, a gas channel with 215 μm width x 370 μm depth and 1,357.6 mm length etched in silicon above the mesh, and a liquid channel of 225 μm width x 120 μm depth and 1,359.2 mm length below the mesh. The mesh characteristics were; pore size 5 μm, silicon nitrate membrane of thickness 1 μm, vertical pore walls and a 1:1 pitch. The design and microfabrication sequence were developed at UCL but fabrication was outsourced to Aquamatijn Ltd, Netherlands, due to lack of micro-engineering facilities at the university. Microfabrication entailed the following steps; thermal oxidation of silicon to produce SiO_2, chemical vapour deposition to create the silicon nitrate layer on the Si wafer, optical lithography to pattern the mesh pores, deep reactive ion etching to create the channel where the gas would flow and powder blasting to create the liquid channel. The three layers were sandwiched together by four-electrode anodic bonding to create one solid structure. Inlet and outlet holes for the gas and liquid flows were also fabricated using powder blasting. Four identical mesh microreactors were fabricated.

Prior to being used for kinetic experiments, the mesh microreactors were subjected to pressure testing as one of the requirements of the Alpha process is operation under 10

bar pressure. Unfortunately, this concluded that the maximum operating pressure was just above atmospheric and below 2.7 bar following the breakage of one unit and the leakage from the periphery of a second one. This characterised the mesh microreactor unsuitable for the Alpha process and subsequently the focus of the Author was directed to employing other type of micro-reactors for the kinetic study.

Firstly, the Author tested a nickel mesh microreactor designed and built by CRL (Central Research Laboratories, London) for a previous research project. The micromesh had been fabricated by a two-stage electroplating method, had 5 μm pores and an open area of approximately 20-25 %. The cavity above the mesh was fed with the gas and the bottom cavity was the reacting chamber and was fed with liquid. This device was pressure-tested to check its suitability to conduct the reaction under study, but to the Author's disappointment this effort was proven unsuccessful too due to leakage.

Secondly, the micronit lab on-a chip 4515 kit was tested, an "off the shelf" piece of equipment manufactured by Micronit Microfluidics DV, the Netherlands. It consisted of the microreactor holder, two microreactor chips (single channel capillary microreactor), the fittings and the tubing. Maximum operating pressure and temperature were 100 bar and 100 ^{o}C according to the manufacturer. The holder comprised of two plates, the bottom was PEEK while the top one was stainless steel. The fittings and the tubing provided are Teflon. The chip size was made out of borosilate glass and had dimensions l x w x d, 45 x 15 x 1.8 mm and comprised of two plates. The structured bottom plate where the capillary channel had been etched using powder blasting had a thickness of 0.7 mm. The dimensions of the capillary channel

were 676 length x 0.15 width x 0.15 depth mm which gives a volume of 15 μl. Fruitful cold runs using de-ionised water and nitrogen gas were performed first to test the sound operation of the bespoke experimental set-up as a whole and its various components. Then, experiments were conducted under reaction conditions but with limited success due to channel blockage caused by deposition of Pd particles (otherwise referred to as *Pd black*). At this point, the research changed focus and turned to the design of a bespoke capillary microreactor as a tool for the kinetic study.

In a second phase of this project, a capillary reactor consisting of a FEP tube 0.25 mm ID tube, 1.6 mm OD and of maximum length 7.6 m was developed to study the hydrodynamic of Taylor flow. In particular, the objectives of this work were firstly to provide an understanding of the gas-liquid Taylor flow under reaction conditions, secondly to investigate what factors affect the flow homogeneity and how this could be improved and thirdly, to investigate the possibility of getting preliminary kinetic data by measuring the decrease in bubble size as the gas gets consumed travelling along the capillary tube.

The capillary was wrapped in a spiral form and was enclosed in a pan- type structure comprising of a SS bottom plate etched to accommodate the capillary channel and the top one made out of Perspex for optical transparency. The two plates had ¼" thickness and 7" diameter so that they fitted exactly on top of the heater and were sealed together by means of six screws around the periphery. Experiments were conducted under reaction conditions, and photographs of liquid slugs and gas bubbles were taken at the reactor inlet, outlet and as well as at intermediate positions for visualisation and analysis of the flow development along the 6 m (actual length)

capillary. The visualisation system was mounted on top of the microreactor and consisted of a microscope, and a high-speed camera connected to a PC employing a suitable software program. Different gas-liquid SS tee-contactors with boreholes ranging 0.15 mm, 0.25 mm, 0.5mm and 1 mm as well as a plastic tee with 10 μm frit were tried extensively to determine the one producing the best results in terms of flow homogeneity and small size of liquid slugs at the reactor entrance. The effect of pieces of equipment of the experimental set-up (pump, pulse dampener, pressure controller), on the gas-liquid flow pattern produced was also investigated. The repeatability of the flow achieved in the spiral reactor was checked too.

Kinetic experiments were performed using another capillary microreactor, made of transparent FEP polymeric material with 0.25 mm ID and 1.6 mm OD and 11.7 m length wrapped in a coil form and immersed in a thermal bath of an ethylene glycol solution contained in a custom-made SS vessel with 6.5 cm diameter and 9 cm height placed on top of the heater. The vessel also had a cover with 0.3 cm thickness accommodating a thermocouple that was dipped inside the thermal bath and connected to the temperature control system in order to maintain constant temperature in the bath. The SS vessel was encased inside a 3.3 mm borosilicate glass cover fitted on top of the heater to minimise heat losses. A number of series of experiments were conducted to elucidate the effect of CO, ethylene, methanol and catalyst on the reaction rate. The influence of temperature on the rate was also investigated and the activation energy was calculated from the Arrhenius plot. A kinetic model was developed for parameter estimation using a molecular-type approach based on the catalytic cycle.

9.3 Summary of the Results

9.3.1 Hydrodynamics of Taylor flow

Numerous photographs of the flow were obtained at the reactor inlet and outlet as well as at various intermediate positions along the spiral. Bubble and slug coalescence was evident and therefore size increase was observed and measured along the capillary tube. Size distributions of bubbles and slugs were derived from these experiments (on average 100 data points collected for each distribution) and were proven to be narrow at the reactor inlet but due to the coalescence phenomenon very wide at the reactor outlet. The good repeatability of the gas-liquid flow achieved by the spiral reactor under reaction conditions was established after the completion of a series of experiments performed at various dates utilizing different gas flow rates while the liquid flow rate was maintained at 5 μl/min for all experiments.

The search of the most suitable tee-contactor in terms of homogeneous flow and small slug size to avoid mass transfer limitations under reaction conditions, pointed to the 0.5 mm borehole contactor. The contactors with the smaller boreholes although produced smaller liquid slugs but the flow was more inhomogeneous. Comparatively, the 0.15 mm performed relative better when low gas flow rates were utilised and the opposite was true for the 0.25 mm tee but the plastic micro-mixing tee with 0.50 mm borehole and 10 μm SS frit performed the best in terms of flow homogeneity amongst the small-borehole tees due to the frit-induced turbulence. The results obtained with the static mixing tee agree well with the scaling law developed by Garstecki (2006). The 1 mm tee was rejected as it produced very long slugs, in the range of 3 mm.

The parameters found to have an effect on the gas-liquid flow pattern in micro channels were the gas superficial velocity, the geometry and size of the tee-contactor, the size of the main channel as compared to the inlet, the orientation of gas and liquid streams at the reactor inlet, the degree of gas-liquid pre-mixing and the pressure fluctuations, particularly at the reactor outlet. The influence of the pressure fluctuations is minimised when the gas gets consumed almost in its entirety and the reaction exit stream is full liquid.

Next, one of the main factors that was noted to have an effect on bubble and slug sizes was the gas velocity as it increases the length of the bubbles and decreases the size of the liquid slugs. Additionally, an increase in the gas velocity increased the non-uniformity of the gas bubbles and also yielded a broader bubble and slug size distribution. Other factors include the gas-liquid premixing, the orientation of the tee-contactor, the size of the tee's borehole, the size of the tubing preceding the tee and the length of the capillary as coalescence and broader distribution of sizes was noted along the channel. Finally, the flow pattern can be affected by the type of pump used probably due to pump-induced pulsations.

Bubble and slug coalescence occurred along the capillary reactor which rendered impossible the estimation of the extent of reaction by measuring the bubble size changes along the tube.

The experimental results in terms of liquid slug lengths and pressure drop were compared with correlations found in the literature; some showed convergence and some did not.

Finally, by materialising certain set-up improvements like the use of the correct tee-contactor and its orientation amongst others, the range of operating conditions under which Taylor flow was homogeneous was expanded significantly. In the remainder of cases, the flow pattern was bubble-train flow consisting of bubbles broken in various parts in a random manner with very short liquid slugs in-between. The number of bubbles pertaining to the train seemed to increase with the proportion of gas in the flow.

9.3.2 Kinetics of the Alpha process

Numerous experiments were conducted with the capillary micro reactor and the autoclave reactors for the kinetic study of the methoxycarbonylation of ethylene in the Alpha process. The experiments were performed under kinetic regime conditions, that is conditions not affected by diffusional limitations as it was demonstrated theoretically by calculations. Experimental data were collected under different conditions in order to establish the partial reaction orders. It is known that intrinsic data are characteristic of the chemical system and do not depend on the scale of the operation. This is why the data collected with the capillary micro reactor which has a volume of 0.573 ml agree so well with the data obtained using semi-batch autoclave reactors with volume of 2000 ml.

From the experiments conducted, significant conclusions can be made. The effect of the increase of the ethylene concentration on the reaction rate is marginal. The reaction order with respect to ethylene is practically zero while the reaction is first order with respect to methanol. The reaction order with respect to CO shifts from +0.5

to -1.5 at a CO partial pressure of 1.8 bar. The catalyst concentration has a positive effect on the reaction rate and the order was calculated as +0.74. Finally, the methanolysis step was proven to be the rate-determining one in the catalytic cycle. The effect of the temperature was studied and the apparent activation energy was calculated to be 53 kJ/mol from the linear Arhenius plot. The value was higher than 40 kJ/mol, a fact indicating that the operation of the capillary reactor was under kinetic control. The apparent activation enthalpy and entropy were found to be 50 kJ/mol and -164 J/K respectively. A higher reaction rate recorded at 110 ^{o}C can be attributed to side reactions taking place. The drop of reaction rate observed at 120^{o}C must be due to the Pd-phosphine cleavage.

The reaction was proven to be very slow and that the operation of the capillary reactor was verified in the kinetic regime as the catalyst concentration generally used was lower than the concentration at which mass transfer effects become significant. Calculations also excluded the presence of mass-transfer limitations for the autoclave and capillary reactors.

The pre-treatment of the liquid reactant mixture under an ethylene atmosphere at reaction temperature when autoclaves are used, hastens the onset of the catalytic cycle and increases the product yield. Saturation of the liquid mixture with ethylene and formation of the alkyl complex is much faster in the capillary microreactor due to its inherent characteristics and pre-treatment is unnecessary in this case.

By employing the stationary-state approximation for the unstable intermediates appearing in the reaction mechanism a kinetic reaction model was developed. This not

only agrees with the hydride catalytic cycle established by previous studies but also accounts for the catalyst deactivation by the formation of electron-poor CO-complexes which eventually lead to the formation of Pd black. Based on the rate data obtained with the capillary and autoclave reactors, a rate equation was proposed also after examining various other empirical models and the kinetic parameters were derived with the aid of a statistical software package:

$$R = \frac{3.31 \cdot 10^{-7}[Pd][C_2H_4][CO][CH_3OH]}{6.57 \cdot 10^{-5}[C_2H_4][CO] + 2.34 \cdot 10^{-4}[CO]^2 + 5.28 \cdot 10^{-7}[CO]^4 + 1}$$

Under Alpha conditions the difference between the predicted and the observed rate was less than 1%.

9.4 Discussion of the Results

9.4.1 Interpretation of the Findings

This study is important because it sheds light on the kinetics of the Alpha process which is a novel industrial process for the production of MMA presenting various advantages as compared to the conventional manufacturing routes like a significant reduction in production costs and the elimination of by-products. Two routes were chosen to tackle this research question; the conventional method using laboratory reactors (autoclaves) and the development of microreactors - either mesh or capillary. The reaction in question entails gas reactants dissolving into a liquid mixture where the reaction occurs by means of an homogeneous catalyst. Therefore, the issue of the

elimination of mass transfer resistances to enable the collection of intrinsic kinetic data had to be tackled first. Then the autoclaves produced some interesting results mostly in terms of partial reaction orders for the various reactants and these results were complemented and reconfirmed by data produced by the capillary microreactor developed in the framework of this project. A major finding of this work is the kinetic model developed taking into account the experimental results collected with the autoclave and the capillary reactors.

This research work extended to the area of hydrodynamics trying to clarify the flow pattern in very narrow (0.25 mm ID) and very long (7.6 to 11.7 m) capillaries. Taylor flow and bubble-train flow under Alpha reaction conditions have been identified and a flow map was created. Moreover, liquid slugs, gas bubbles sizes and pressure drop have been measured and compared to correlations found in the literature. It was interesting to see the number of parameters affecting bubble and slug sizes and the Author embarked on a quest to find ways to improve homogeneity of the flow. These improvement steps were made prior to the initiation of the kinetic experiments. A significant amount of work was put in developing a novel mesh microreactor but unfortunately, this was proven unsuitable to operate under reaction conditions.

9.4.2 Relationship of the Current Study to Previous Research

In terms of kinetics of the Alpha process, current work built upon previous research done by LI using autoclave reactors. This past research provided indications of the kinetics but most of these experiments were under mass transfer control and were conducted under slightly different experimental conditions, and therefore not exactly

comparable to current work. The Thesis agrees with previous studies on the Alpha process suggesting that the methanolysis step is rate-determining (see for example Jimenez et al., 2004). Regarding partial reaction orders, the shifting reaction order in terms of CO is in-line with conclusions from studies on carbonylation reactions (for instance Gavino et al., 2001, Kiss et al., 1999 and Divekar et al., 1993). It also agrees with previous research by LI who reported a shift from positive to negative but failed to determine the point of shift accurately. The zero-order with respect to the substrate (ethylene) agrees with the findings from the study of the carbonylation of styrene and (Seayad et al., 1998). The first order with respect to methanol and the positive effect of catalyst loading on the reaction rate agrees with the findings of Torres (2009) who reported a first order with respect to the catalyst. More experiments would be necessary in order to ascertain the effect of the catalyst on the reaction rate as a fractional reaction order has been reported for another carbonylation reaction; the hydroformylation of 1-decene with a Pd catalyst (Divekar et al., 2003). The positive effect of the pre-treatment of the liquid mixture with ethylene for 30 min was inferred from this study in accordance with previous research by LI. Moreover, this work substantiated the importance of reactor temperature during pre-treatment.

The use of capillary microreactors for kinetic studies in the literature was limited (for instance refer to Dummann et al., 2003 and Enache et al. 2005). Moreover, the capillaries were of much larger diameter and of shorter length and reaction conditions were milder. This study is the first one that used the micro capillary with 0.250 mm ID and 11.7 m length at 10 bar pressure.

A comparison of the experimental data with the calculated values using the correlations reported in the literature suggests a relative agreement with the one proposed by Qian & Laval (2006) applicable for capillaries with diameter 0.25-1.0 mm. Conversely, the correlations brought forward by Laborie et al. (1999) and Liu et al. (2005) do not agree with the experimental data which was not surprising as these were developed for larger capillaries. Particularly the latter showed the opposite trend with slug length increasing with the gas superficial velocity instead of decreasing.

According to Kreutzer (2003) Taylor flow does not exhibit coalescence but in the system and for the experimental conditions used in this project, slug coalescence was observed starting at distances above 1 m from the spiral inlet and at around 0.5 m for the bubbles. A possible reason for that might have been the pressure fluctuations at the capillary inlet or outlet. Second, a significant amount of work was dedicated to investigating flow homogeneity and the factors that affect it. It was discovered that a number of previous researchers had also recorded flow instability like for instance Duducovic (2002), Kreutzer (2005) and Laborie et al. (1999) and instability criteria were established and flow maps were drawn. However, the findings of current work do not validate these criteria and this could be explained by the fact that they were developed for much larger capillaries, up to a few mm diameter. The bubble-train flow pattern which was encountered in this project at higher gas velocities when liquid velocity remained the same, was also seen in few studies like for instance by Yue et al. (2008). Churn flow, slug-annular and annular flow patterns were not encountered in this study due to the pressure of 10 bar utilised.

There are similarities found amongst the findings in this study and previous research efforts in terms of factors affecting bubble and slug lengths. For instance the fact that when the gas superficial velocity increases the bubble length increases and the slug length decreases (for example Laborie et al., 1999, Kumar et al., 2007). Current work also found that when the superficial liquid velocity rises, the slug length increases and bubble length decreases which is in accordance with Qian & Lawal (2006) but not with Laborie et al. (1999). Other effects like pre-mixing, inlet geometry and in particular the size of the gas and liquid inlets, were reported as influential factors in this work and the work of Qian & Laval (2006). On the other hand, the results from the current work do not confirm the findings of Qian & Laval (2006) in terms of inlet orientation.

Finally, with regards to microengineering and the development of the mesh reactor, the fabrication process was novel and more sophisticated as compared to mesh microreactors developed previously (see for example Wenn et al., 2003). However, it was unsuitable for operation at high pressure. Previous studies focused on operation of these devices under mild conditions.

9.4.3 Recommendations for Additional Research

Additional research seems needed on the kinetics to assess with certainty the effect of catalyst on the reaction rate. As noted above, the reaction rate with respect to the catalyst was found to be +0.74 instead of +1 and this was unanticipated somewhat. Fractional reaction orders have been reported previously in the study of hydroformylation of ethylene with $CO_2(Co)_8$ homogeneous catalyst (Chaudhari et al., 2001) or the hydroformylation of 1-decene (Divekar et al., 1993) and were attributed

to other interactions in the system; one example being solvent interactions. More experiments are necessary to investigate in detail the phenomenon of catalyst deactivation in terms of mechanism, products and rate and to find ways of decelerating it beyond empirical observations. It was also found from this study that the precipitation of particles/clusters of Pd black arise more in a glass channel than in one made of polymeric material. Could Pd have a better affinity with glass than plastic? This merits more research.

It is difficult to suggest that mesh microreactors are not suitable for operation at high temperature on the basis of the current study alone. However, a couple of improvements to the design can be made, like for instance to increase the thickness of the top and bottom plates to be larger than the 0.5 mm in this study. Secondly, the 4.5 mm margins at the reactor periphery allowed for the anodic bonding should be wider to enable better cohesion amongst the different parts of the reactor chip. Reactions that could be tried at atmospheric conditions to verify sound operation of the mesh microreactor could be:

- Hydrogenation of methyl Z-(a) acetamidocinamate with a rhodium /(S,S-BDPPTS) catalyst in an aqueous phase (de Bellefon et al., 2003):

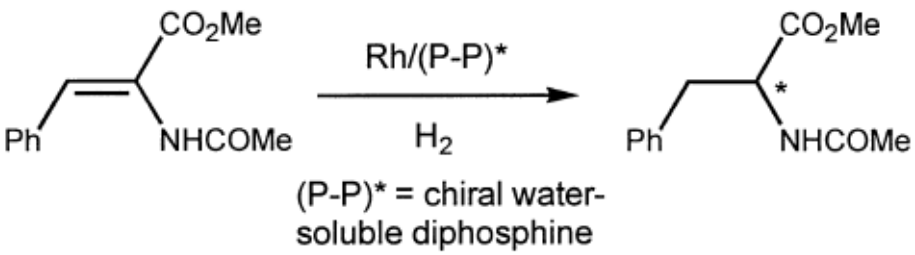

(9.1)

- Fluorination of di(m-nitrophenyl) disulphide to create sulphur pentafluoride derivative. Conditions are MeCN (5 ml h^{-1}), 10% in N_2 (10 ml min^{-1}) at room temperature. (Chambers & Spink, 1999):

(9.2)

- Fluorination of *β*-Dicarbonyl compounds (also by Chambers & Spink, 1999):

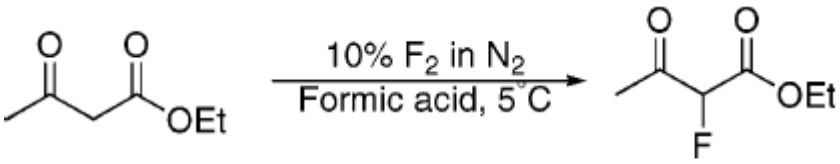

99% Conversion, 73% Yield (9.3)

- Catalyst-screening reactions.

Development and work with novel mesh microreactors has already offered and will offer further valuable insight in the field of microengineering in terms of microfabrication and operation of these sensitive equipment. Very interesting conclusions are expected to be drawn from future experiments about the microreactors' usefulness as tools for study of reactions occurring at high temperatures and low pressures.

--//--

APPENDICES

APPENDIX A

Experimental Set-Up: Description of Components

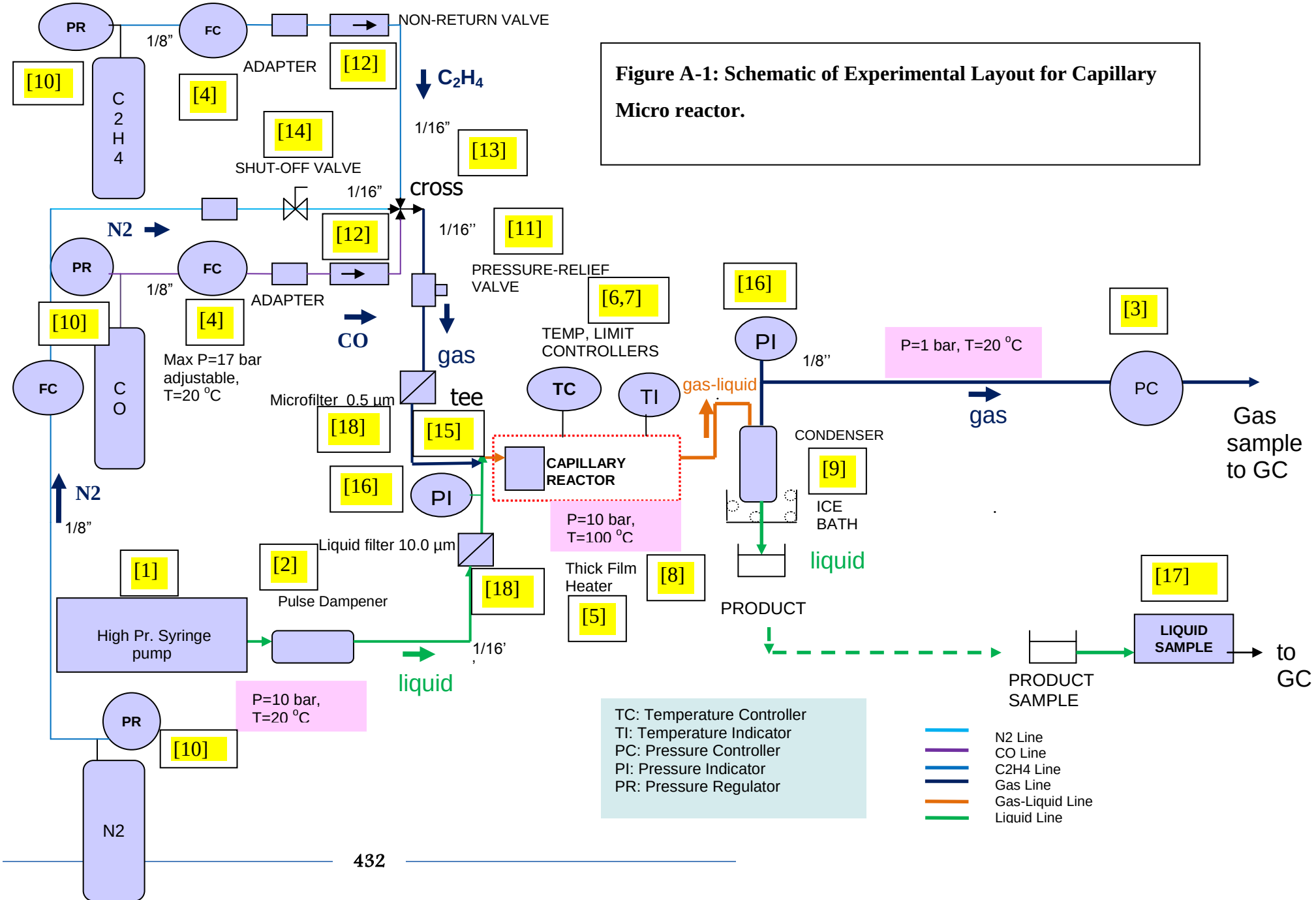

Figure A-1: Schematic of Experimental Layout for Capillary Micro reactor.

Component	Description
[1] Kds 410 High Pressure Syringe pump ***Provider: Presearch Ltd***	Can deliver at high pressure. Operates with 20 ml or 8 ml SS syringe with 1/16'' Swagelok fittings. The minimum and maximum flow rates are 0.03 µl/h and 38.25 ml/min respectively and the maximum pressure is at least 16 bar. The typical accuracy of the pump is 1% or better and the linear force is higher than 100 lbs.
FlatLine Pulse Damper ***Provider: Presearch Ltd(ASI)***	The FlatLine Pulse Damper manufactured by ASI was fitted in the liquid inlet stream after the syringe pump in order to achieve a uniform flow with minimised pulsations.
[3] 5866 Brooks Pressure Controller ***Provider: Flotech Instruments (Brooks Instr.)*** 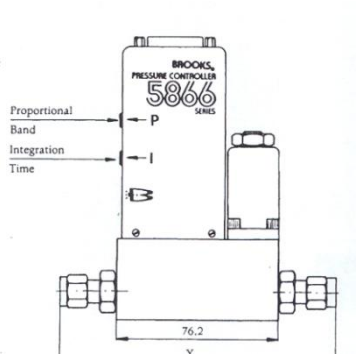	The Brooks Pressure Controller 5866 is used for pressure control on the gas line downstream of the reactor. It is an analogue instrument with an accuracy of 0.5 % full scale. It contains an accurate pressure transducer, a control valve and the electronics. The controller is an upstream one because our objective is to maintain the pressure at 10barg before the controller. Other characteristics are the Teflon/Kalrez O rings and Kalrez valve seat. The range of the instrument is 0-10 bar. The maximum operating temperature is 60 ^{o}C. The inlet/outlet connections are 1/8'' compression fittings.

[4] 5860 Brooks Mass Flow Controller

Provider: Flotech Instruments (Brooks Instr.)

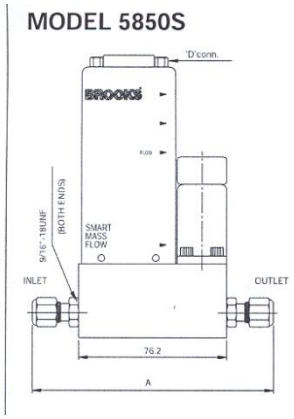

Two Brooks 5850S thermal gas mass flow controllers are used for the reactor feed with ethylene and CO. The instruments were calibrated for the specific gas (CO or ethylene respectively) at atmospheric conditions and for the flow range 0.06-3 ml/min. They are analogue instruments with an accuracy of 0.2 % full scale. The instruments are fitted with PTFE/Karlez O rings and valve seat for chemical resistance to the reactant mixture. The inlet/outlet connections are 1/8'' compression fittings. The Brooks instruments are powered and controlled through 0154 Readout/Power Unit with the capability of accommodating 4 instruments. The control unit is fitted with a RS-232 connection for PC communication. Please refer to Figure A-2 for the connection schematic of the analogue instruments.

[5] Thick Film Heater

Provider: Watlow

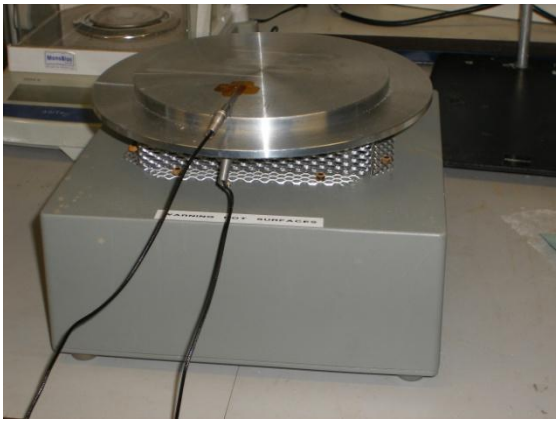

The 430 Stainless steel Thick Film Heater, part No: TF4A6AA07EL18C, was chosen for heating because it has several advantages: Fast response but mainly temperature uniformity at a moderate cost. The 430SS is a ferritic stainless steel with good thermal stability. The manufacturer WATLOW Ltd guaranteed upon purchase 100 % temperature uniformity, a fact which was also verified by experiments. The heater has a rectangular shape of 15cmX10cm and consists of three separate plates; the heater, the mica insulator and the clamping plate. The mica insulator acts as a thermal barrier and forces the heat to the part being

heated as well as a protective layer of the heater. The clamping plate distributes the pressure evenly across the entire surface of the heater and promotes intimate contact between the heater and the part being heated. Its wattage output at 25 ^{o}C is 725 W and 4.7 W/cm^2. An aluminium plate, made at UCL, was fitted above the thick heater. The glass cover was fitted tightly on top of the aluminium cover.

[6] Temperature Controllers

Provider: WATLOW

The other component of the temperature control system is the WATLOW DIN-A-MITE A solid state power controller with the catalogue No is DA10-24C0-0000.

The power controller is connected to a PID temperature controller; the WATLOW Series F4 controller, catalogue No: F4SH-CAA0-01RG which provides powerful and precise control in the most demanding applications. Other benefits are easy set-up and operation. It includes a 16-bit microprocessor for accuracy and performance.

The last component of the temperature control system is a Single Loop Limit Controller the WATLOW Series LV Limit Controller, Part No: LVC6JW00000300A. The controller ensures that the power supply to the heating assembly will be cut if the temperature exceeds a certain set point.

[7] Thermocouples

Provider: WATLOW

They are AF style T/Cs (which means metal transition with strain relief), MI (mineral insulated). The sheath is made of 316 SS with a 2 mm diameter and have a length of 41mm. They are J calibration-standard limits, grounded junction T/C with fibreglass leads and standard split termination.

The accuracy or 'tolerance' is $\pm 2.2\,^{o}C$

[8] Glass Cover

Provider: Custom-made by Scott-Glass Ltd

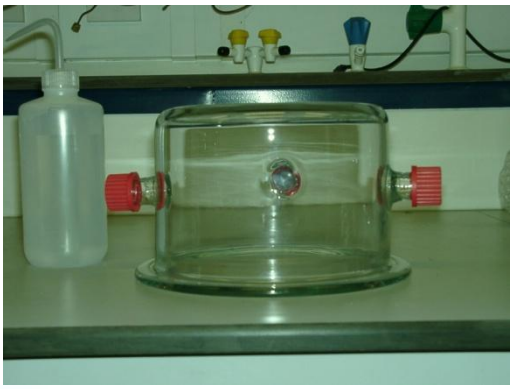

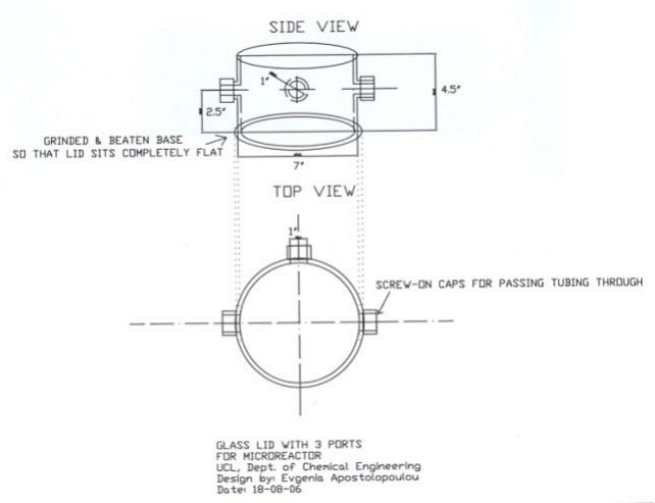

The glass cover was custom-made in order to maintain the temperature around the microreactor and minimise heat loses.

The glass cover fits exactly on the thick film heater. The cover has three ports of which two are used for inlet-outlet lines and the third one is available for future use. It is manufactured from borosilicate glass with a 3.3 mm thickness.

[9] Gas Condenser

Provider: Made at UCL, Design: E. Apostolopoulou

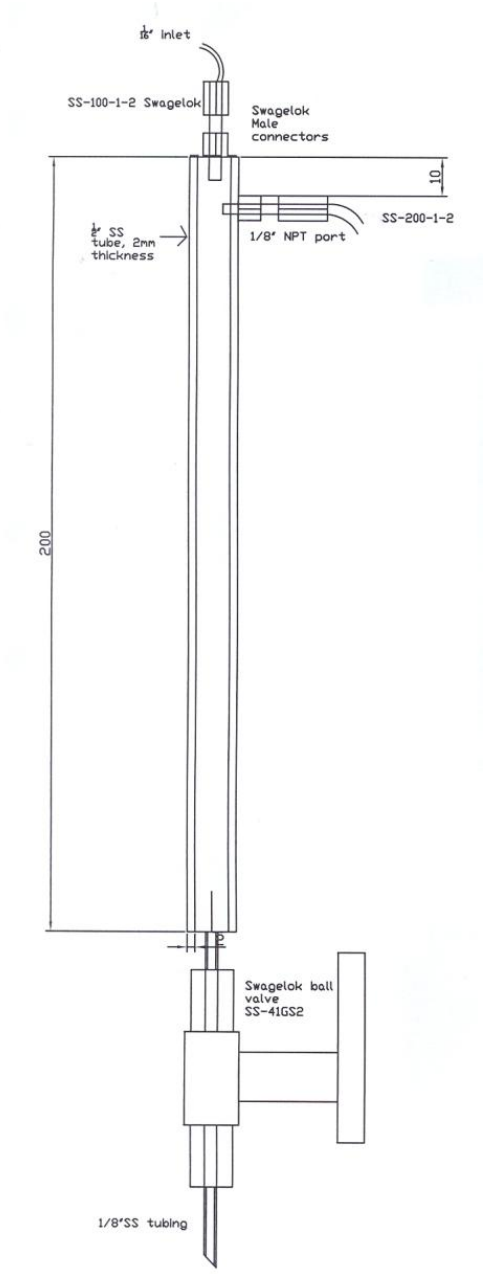

The condenser is placed on the high pressure gas side before the pressure regulator to avoid condensation inside the tubing as the temperature drops. Stainless steel was chosen as the material for manufacture as the condenser needs to withstand pressure of 13 bar. It is a bespoke device with a 1/16" inlet and a 1/8" outlet with suitable Swagelok fittings at the top surface which were welded onto the cylinder. The bottom piece is separate with a conical shape and a Swagelok fitting at the end, also welded on the cylinder. The condenser has a dead volume of 11 ml. The dimensions were chosen so that the condenser has not only the minimum amount of volume but also adequate volume so that the an experiment can be performed utilising the full volume of the syringe (8 ml) and a safety margin of 30 % without the liquid overflowing the condenser and coming out the gas line through the pressure controller. In case of an overflow the pressure controller would be ruined as it is designed to handle only gases and not liquids.

Condenser Fittings

Provider: Swagelok

The fittings at the condenser are all Swagelok; SS-100-1-2 for a 1/8" NPT connection with 1/116" OD tubing for the inlet gas stream, SS-200-1-2 for a 1/8" NPT connection with 1/8" OD tubing for the outlet gas steam. For the removal of the condensed drops, at the bottom of the condenser we fitted the

	part SS-42GS-4 which is a 40G series ball valve for ¼" OD tubing and with 0.6Cv. The ¼" tubing was chosen because it is rigid and it will not bend when we open and close the valve.
[10] High pressure regulators for the gas cylinders ***Provider:BOC*** 	Three pressure regulators for the carbon monoxide, ethylene cylinder and nitrogen were bought from BOC Gases. The catalogue no is HP1702B.GL-BS4-1/8" Comp and each one is a two stage regulator for corrosive or non-corrosive gases. It has a brass body and stainless steel diaphragm. The inlet is a BS4 cylinder connection and the outlet is a diaphragm-seal valve with 1/8" compression fitting. The maximum inlet and outlet maximum pressure is 100 and 17 bar respectively.
[11] Pressure relief valve ***Provider: Presearch Ltd (Upsearch Scientific)*** 	The purpose of the pressure relief valve is to protect the system from over pressurisation. It is designed to direct flow out the tee when the pressure exceeds the set limit of 17 bar. It is placed on the gas line before the micro-filter upstream of the microreactor. The parts purchased from Upchurch Scientific are the U-469 stainless steel back pressure holder (including two-piece F-300 Fingertight fittings), the P-764 250psi (17 bar), back pressure regulator cartridge and the P-612 pressure relief valve tee for 1/16" tubing. Extra Stainless Steel Fingertight Fittings F-140 are used, with 10-32 threads and either F-142 PEEK ferrule or F-142N Tefzel ferrules.

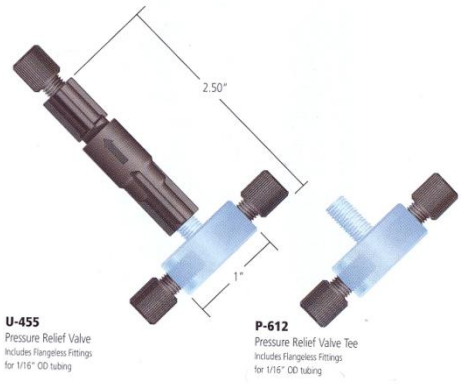

[12] Check valves (Non-return valves)

Provider: Presearch Ltd (Upsearch Scientific)

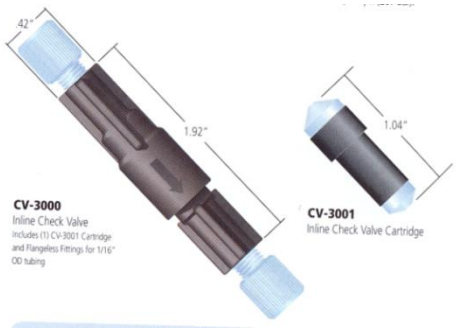

The Check Valves (or non-return valves) are designed to limit the flow in one direction. Two check valves were placed on the two gas lines; ethylene and CO. The parts bought from Upchurch Scientific are the CV-3000: inline check valve assembly for 1/16" tubing and is accompanied with the CV-3001 cartridge and Flangeless fittings P-235 Short Flangeless PEEK Nuts with P-200 Flangeless ETFE Ferrules. The assembly can withstand pressures of 69 bar. The cartridge incorporates a gold-plated stainless steel spring and a perfluoelastomer seal.

[13] Cross-type contactor

Provider:Presearch Ltd (Upchurch Scientific Ltd)

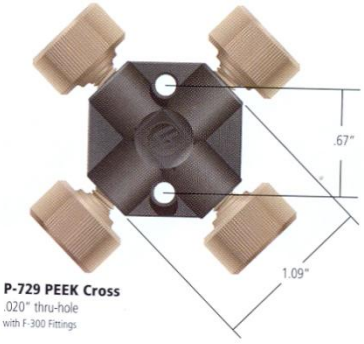

The cross connection P-729 from Upchurch Scientific is made of PEEK, has 10-32 threads and comes with Fingertight Fittings F-300 PEEK 10-32 Nuts with P-142 PEEK ferrules for 1/16" tubing allowing maximum operating pressure 241 bar. The gases CO, ethylene and nitrogen meet at the cross junction upstream of the microreactor.

[14] Shut-off valve

Provider:Presearch Ltd (Upchurch Scientific Ltd)

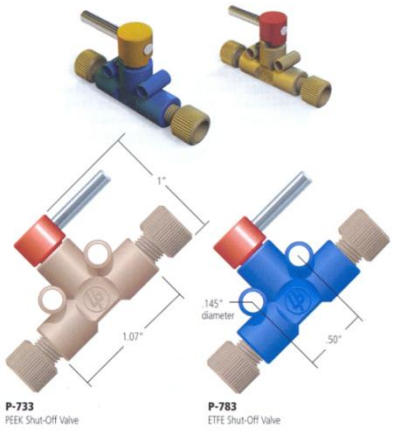

The shut –off valve from Upchurch Scientific is the P-732 for 1/16" tubing and comes with P-235 Short Flangeless PEEK Nuts with P-200 Flangeless ETFE Ferrules allowing maximum pressure 34 bar.

[15] Tee contactor

Provider:Presearch Ltd (Upchurch Scientific Ltd)

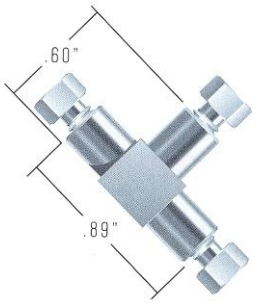

The tee U-428 is used to connect the liquid and gas flows upstream of the microreactor. It is rated to 690 bar of pressure, has 10-32 threads, a 0.020" (0.50mm) thru-hole with U-400/U-401 fittings.

[16] Pressure transducers

Provider: Sensor Technics Ltd

Two pressure transducers like the one shown in the adjacent Figure were used to measure the pressure of the liquid inlet and the gas outlet lines. The transducers have the catalogue no 40PC250G2A. Their gage pressure range is [0-250 psi]. They are connected to the tubing through a tee. The reading from the instrument are in V and by means of a Volt-meter are translated into psi using a formula provided by the manufacturer.

[17] Limited volume inserts for GC sampling ***Provider: GRACE ALTECH Ltd*** 	The limited volume inserts or micro-inserts for vials (12 x 32 mm) with standard mouth (4mm), cat. no 95201, purchased from GRACE ALTECH Ltd have a volume of 0.1 ml and dimensions 30 x 5 mm and 15 mm top, made of clear glass and are being used for taking small samples. It was found that if the vial insert is full, the GC analysis can be repeated three times in a reliable way.
[18] Microfilters ***Provider:Presearch Ltd (Upchurch Scientific Ltd)***	The filter M-550 with 0.5 μm withbstainless steel frit was used on the gas line before the reactor inlet to retain any particles present. The stainless steel A-314 inline solvent filter assembly with stainless steel frit was used for the liquid line.
[19] Gas Monitor ***Provider: Crowcon Detection Instruments Ltd***	The portable monitor Triple Plus + from Crowcon Detection Instruments Ltd was necessary as a safety measure. The standard instrument is suitable for detection of oxygen, toxic (like carbon monoxide) and flammable gases and it was fitted with a special sensor to detect also ethylene and methanol. This instrument promises reliable and robust performance.

Table A-1. Experimental set-up components.

Figure A-2 illustrates the way the connections between the different analogue instruments and the power supply are effectuated:

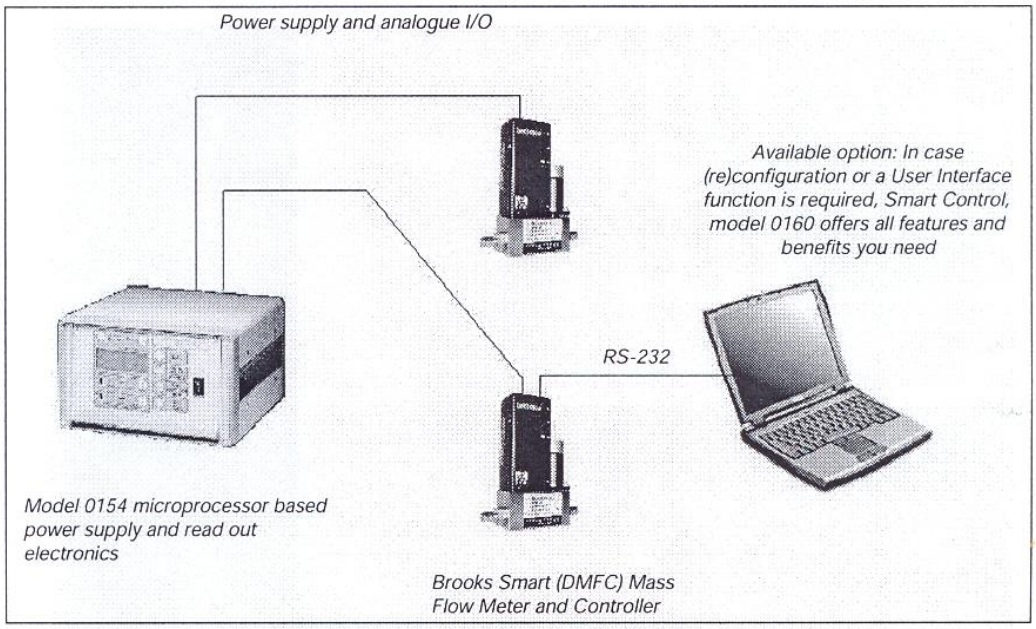

Figure A-2. Set-up of analogue instruments.

The installed experimental set-up is shown below:

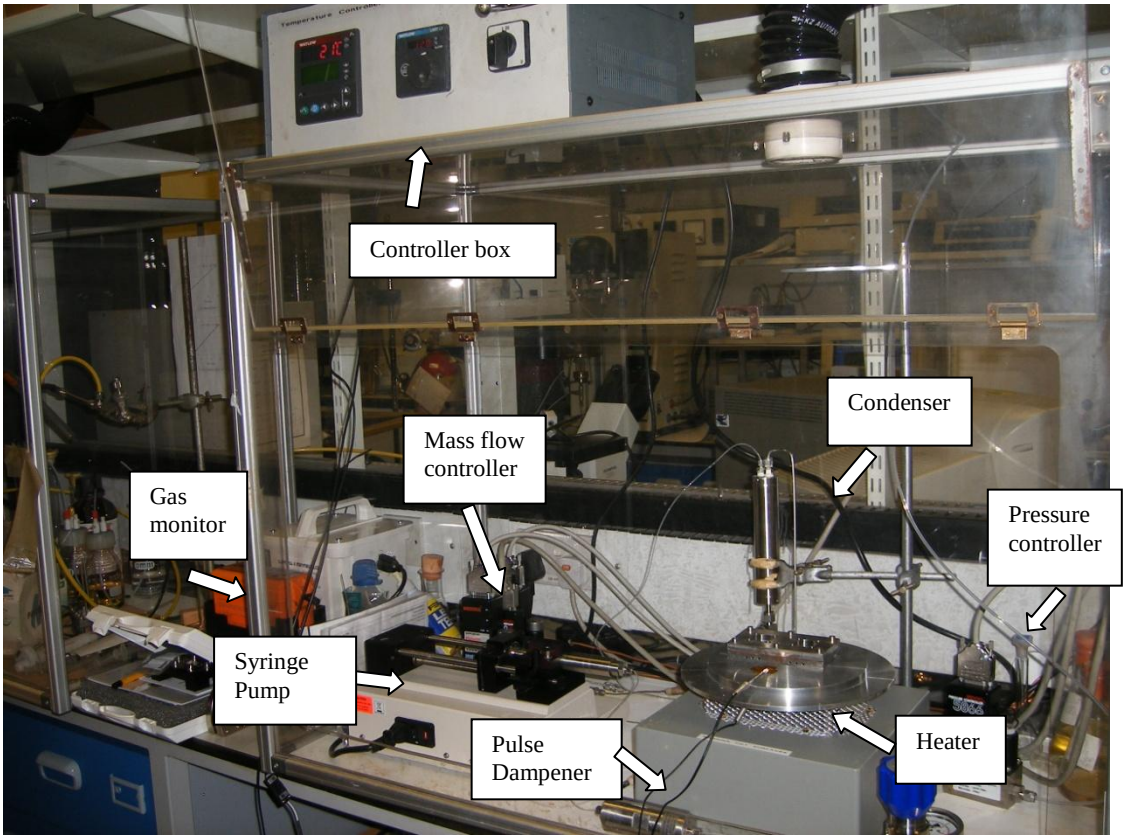

Figure A-3. Experimental set-up.

APPENDIX B

Calculation of Reaction Rate - Example

Date of experiment		**02/05/08**	
Condition	**Symbol**	**Value**	**Unit**
Pressure	P	11	bara
Temperature	T	100	^{o}C
Liquid Flowrate	Q_L	5	µl/min
Ethylene Flowrate	Q_{C2H4}	0.558	ml/min
CO Flowrate	Q_{CO}	0.1	ml/min
MeOH conversion	X_{MeOH}	1.78	%
Initial MeOH concentration in the liquid mixture*	C_{MeOH0}	8203	mol/m^3
Conversion factor** for CO flow rate under different conditions(STP→11bara, 100^{o}C)		0.1244	
Conversion factor** for C_2H_4 flow rate under different conditions(STP→11bara, 100^{o}C)		0.103733	
Conversion factor** for liquid flow rate under different conditions(STP→11bara, 100 ^{o}C)		0.8694	

Table B-1. Experimental Conditions and Data

*mixture consists of 70:30 (% w/ % w) MeP:MeOH

**Conversion factors derived from the thermodynamic and fluid mechanics database FLUIDAT

Assumptions:

- Perfect mixing in the liquid slug where the reaction takes place
- Perfect temperature and pressure homogeneity in the reactor system
- Not significant difference existing between reactor space time calculated at the reactor inlet or outlet (in reality, due to the utilisation of high flow rates, the difference is typically in the range of 6 % or less)
- No liquid vapours escape from the condenser (thermodynamics calculations showed 2 % of MeP and MeOH vapours leave the condenser, but physically there was never condensation observed in the gas stream exiting the condenser)
- The evaporation of the liquid mixture during the sampling procedure is insignificant

CALCULATIONS FLOWCHART

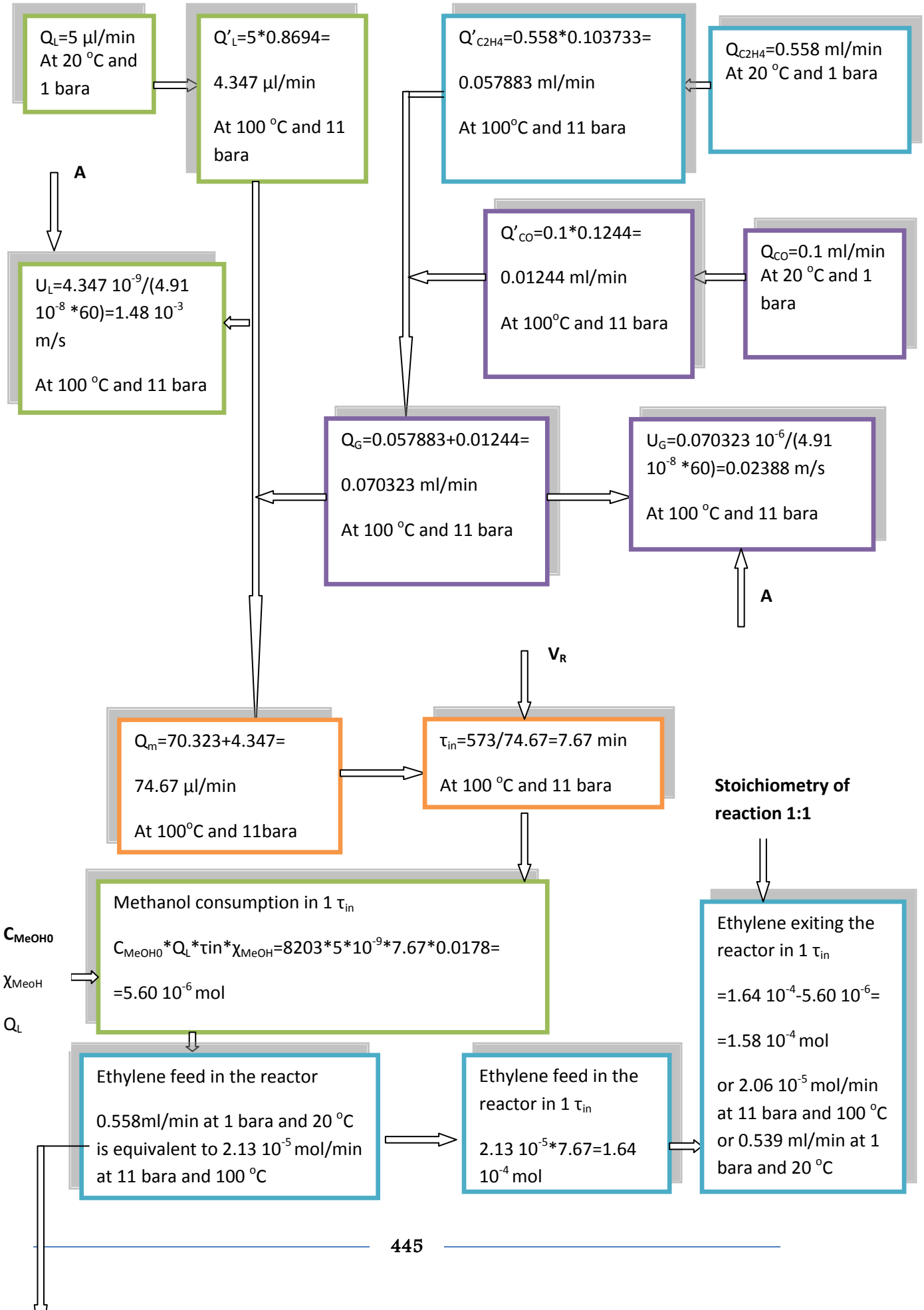

CO feed in the reactor

0.1 ml/min at 1 bara and 20 °C is equivalent to 4.40 10^{-6} mol/min at 11 bara and 100 °C

Ethylene consumption due to reaction

(2.13-2.06)/2.13=3.3 %

CO feed in the reactor in 1 τ_{in}

4.40 10^{-6}*7.67=3.37 10^{-5} mol

CO exiting the reactor in 1 τ_{in}

=3.37 10^{-5}-5.60 10^{-6}=

=2.81 10^{-5} mol

or 3.66 10^{-6} mol/min at 11 bara and 100 °C or 0.082 ml/min at 1 bara and 20 °C

CO consumption due to reaction

=(3.37-2.81)3.37=16.6 %

$Q_{G,out}$=0.539+0.082=0.621 ml/min

At 11 bara and 20 °C or

0.539*0.103733+0.082*0.1244=

=0.0661 ml/min at 11 bara and 100 °C

Q'_L

$Q_{m,out}$=66.113+4.347=

=70.460 µl/min

At 100 °C and 11 bara

V_R

τ_{out}=573/70.460=8.13 min

At 100 °C and 11 bara

Reaction rate

$R=N_{MeOH0}\chi_{MeoH}/\tau_{out}$=

=8203*0.0178/8.13/60=
=0.300 mol m^{-3} s^{-1}

C_{MeOH0}

χ_{MeoH}

APPENDIX C

Mass transfer Resistances – Example of Calculations

Date of experiment		**02/05/08**	
Condition	**Symbol**	**Value**	**Unit**
Pressure	P	11	bara
Temperature	T	100	^{o}C
Liquid Flowrate	Q_L	5	µl/min
Ethylene Flowrate	Q_{C2H4}	0.558	ml/min
CO Flowrate	Q_{CO}	0.1	ml/min
MeOH conversion	X_{MeOH}	1.78	%
Length of the liquid slug	L_{slug}	1.23	mm

Table C-1. Experimental conditions and data.

Condition	Symbol	Value	Unit
Diameter of the capillary reactor	d	0.00025	m
Cross sectional area of the capillary reactor	A	$4.91\ 10^{-8}$	m^2
Surface tension of the liquid mixture* at 100^{o}C	σ	0.02237	N/m
Viscosity of the liquid mixture* at 100^{o}C	μ	$2.884\ 10^{-4}$	Pa s
Diffusion coefficient of CO in the liquid mixture at 100^{o}C	D	$1.87\ 10^{-9}$	$m^2\ s^{-1}$
Reaction rate calculated	R	0.300	mol $m^{-3}\ s^{-1}$
CO solubility at 100 ^{o}C, 11bara	[CO*]	17.784	mol m^{-3}

***mixture consists of 70:30 (%w/%w) MeP:MeOH**

Table C-2. Other data.

CALCULATIONS FLOWCHART

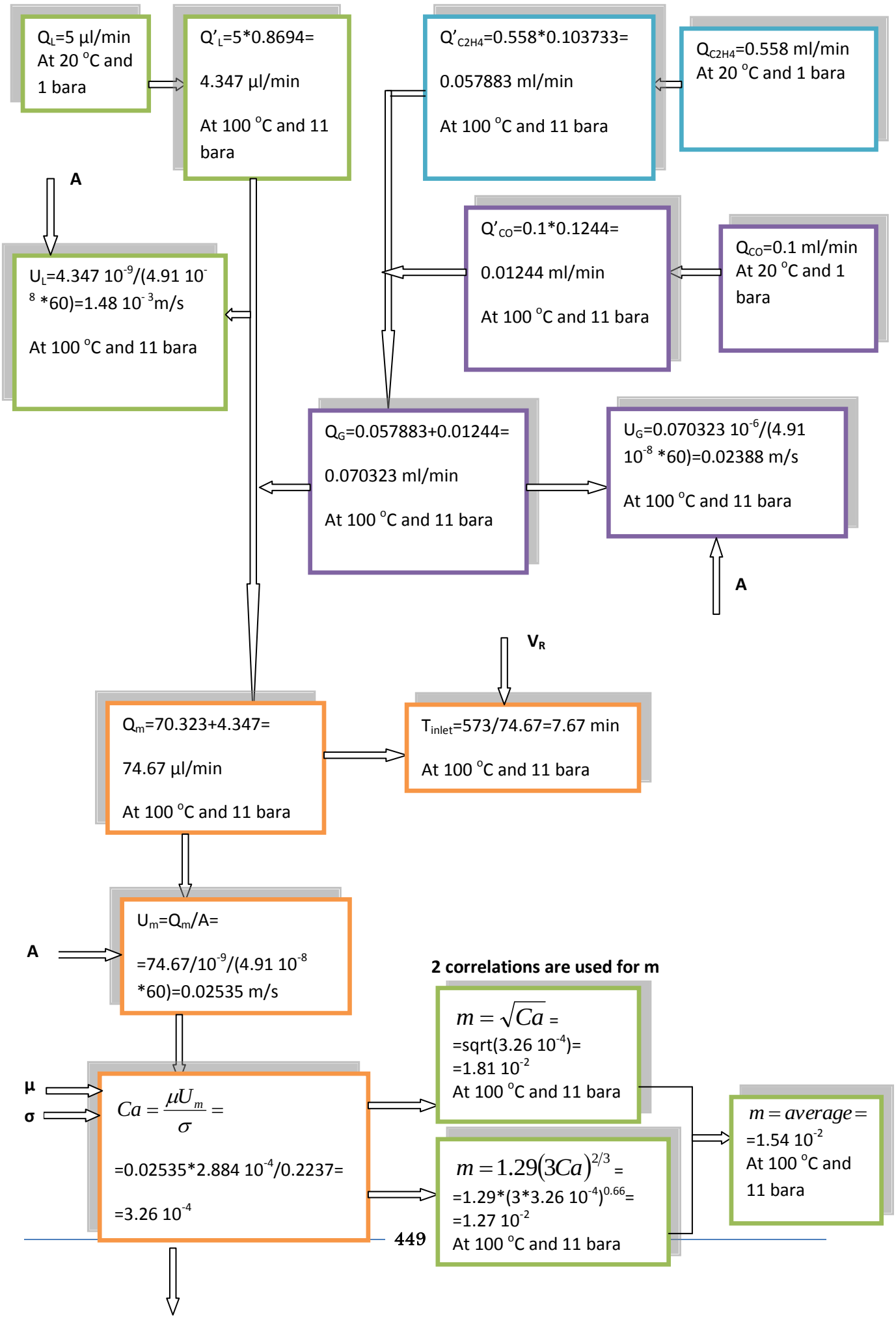

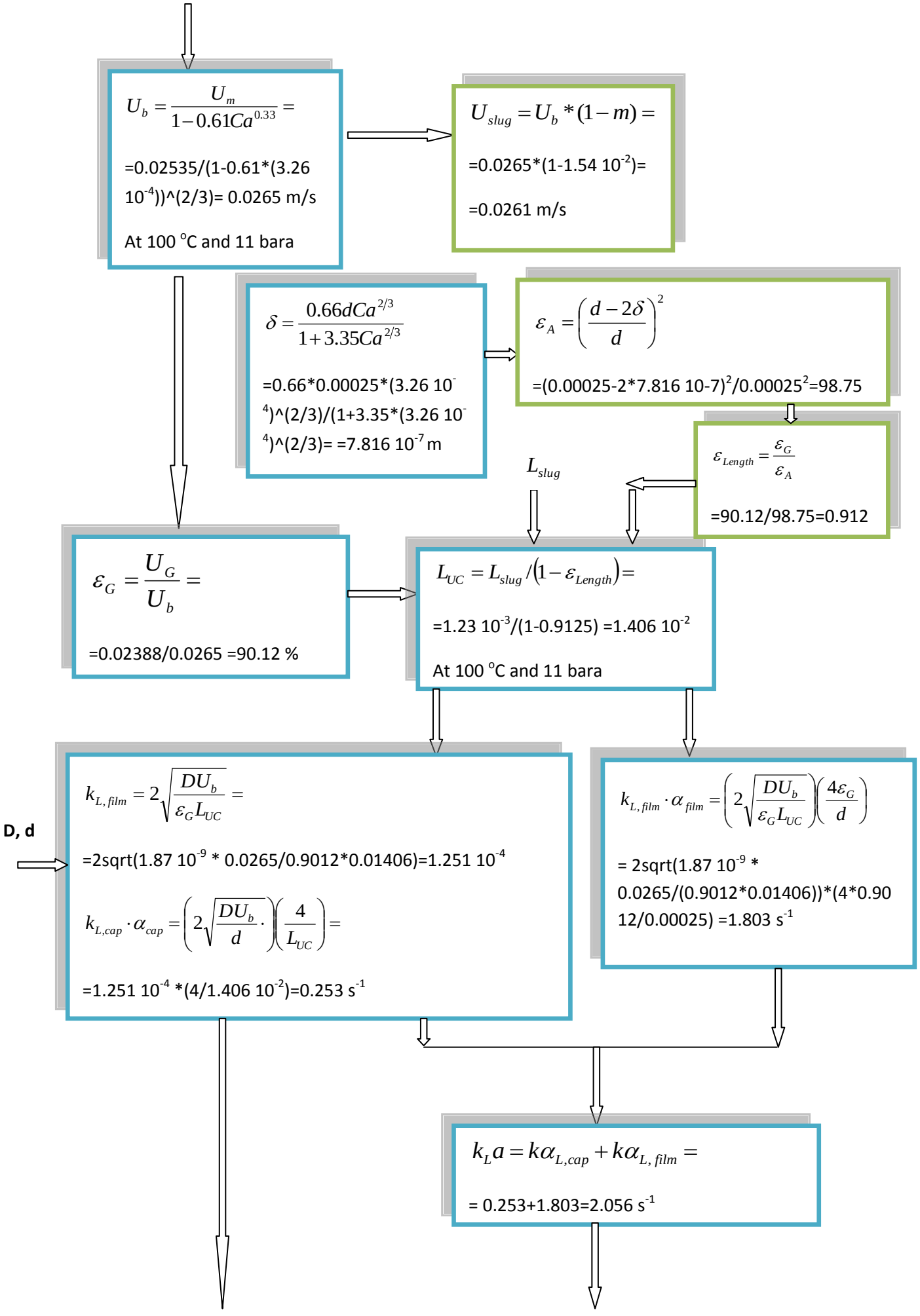
$U_b = \frac{U_m}{1-0.61Ca^{0.33}} =$
=0.02535/(1-0.61*(3.26 10-4))^(2/3)= 0.0265 m/s
At 100 °C and 11 bara
$U_{slug} = U_b * (1-m) =$
=0.0265*(1-1.54 10-2)=
=0.0261 m/s
$\delta = \frac{0.66dCa^{2/3}}{1+3.35Ca^{2/3}}$
=0.66*0.00025*(3.26 10-4)^(2/3)/(1+3.35*(3.26 10-4)^(2/3)= =7.816 10-7 m
$\varepsilon_A = \left(\frac{d-2\delta}{d}\right)^2$
=(0.00025-2*7.816 10-7)2/0.000252=98.75
$\varepsilon_{Length} = \frac{\varepsilon_G}{\varepsilon_A}$
=90.12/98.75=0.912
L_{slug}
$\varepsilon_G = \frac{U_G}{U_b} =$
=0.02388/0.0265 =90.12 %
$L_{UC} = L_{slug} / (1-\varepsilon_{Length}) =$
=1.23 10-3/(1-0.9125) =1.406 10-2
At 100 °C and 11 bara
D, d
$k_{L,film} = 2\sqrt{\frac{DU_b}{\varepsilon_G L_{UC}}} =$
=2sqrt(1.87 10-9 * 0.0265/0.9012*0.01406)=1.251 10-4
$k_{L,cap} \cdot \alpha_{cap} = \left(2\sqrt{\frac{DU_b}{d}} \cdot\right)\left(\frac{4}{L_{UC}}\right) =$
=1.251 10-4 *(4/1.406 10-2)=0.253 s-1
$k_{L,film} \cdot \alpha_{film} = \left(2\sqrt{\frac{DU_b}{\varepsilon_G L_{UC}}}\right)\left(\frac{4\varepsilon_G}{d}\right)$
= 2sqrt(1.87 10-9 * 0.0265/(0.9012*0.01406))*(4*0.9012/0.00025) =1.803 s-1
$k_L a = k\alpha_{L,cap} + k\alpha_{L,film} =$
= 0.253+1.803=2.056 s-1

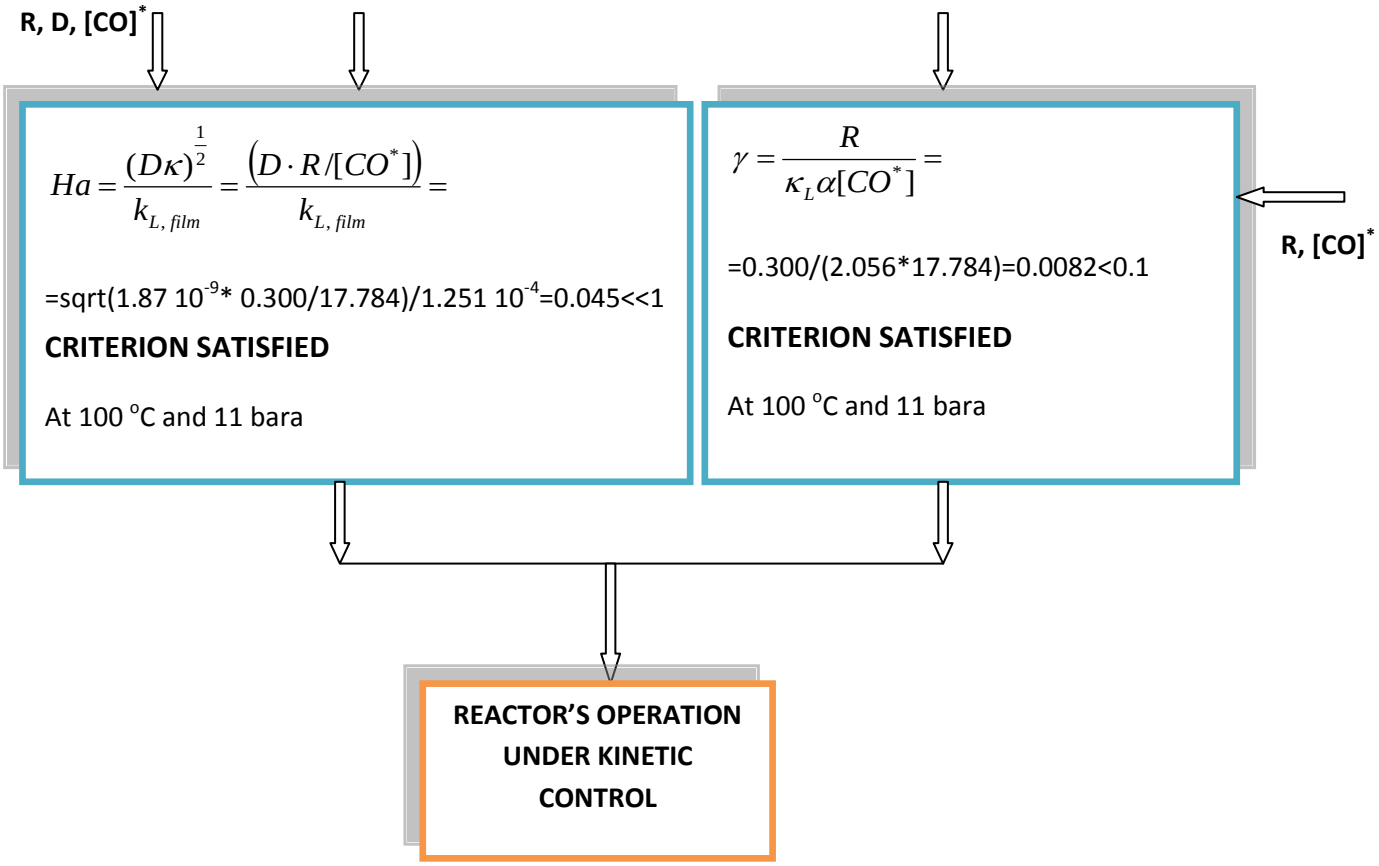
R, D, [CO]*
$Ha = \frac{(D\kappa)^{\frac{1}{2}}}{k_{L,\,film}} = \frac{\left(D \cdot R/[CO^*]\right)}{k_{L,\,film}} =$
=sqrt(1.87 10-9* 0.300/17.784)/1.251 10-4=0.045<<1
CRITERION SATISFIED
At 100 °C and 11 bara
$\gamma = \frac{R}{\kappa_L \alpha [CO^*]} =$
=0.300/(2.056*17.784)=0.0082<0.1
CRITERION SATISFIED
At 100 °C and 11 bara
R, [CO]*
REACTOR'S OPERATION UNDER KINETIC CONTROL

APPENDIX D

Thermodynamic VLE Prediction

1. Objective and Assumptions

The aim of this exercise is to predict the composition of the gas phase if the liquid phase is the system methanol:methyl propionate of composition 30 %:70 % at 10 bar pressure and 100 ^{o}C. It is also assumed that there is a permanent gas in the gas phase, that is ethylene. In the calculations the presence of CO in the gas phase is ignored for simplicity as the composition of CO under the Alpha Standard Conditions is nine times less compared to that of ethylene. Finally, the system is regarded as like a closed box where no reaction and no flow in or out of the microreactor is considered.

As there is limited amount of thermodynamics data about the two components system methanol-methyl propionate, mainly data for the pure components had to be used.

2. Theory

One of the first pieces of information needed for the calculations is the vapour pressure of each of the mixture components at 100 ^{o}C.

Vapour pressure of the pure components

Methanol

The methanol vapour pressure data with respect to temperature was obtained from the DETHERM database.

As it is known the vapour pressure of a pure component is a function of the temperature according to the equation Clausius-Clapeyron:

$$\frac{dP^S}{dT} = \frac{\Delta H_V}{T \cdot \Delta V} = \frac{\Delta H_V}{(RT^2 / P^S)\Delta z} \qquad \text{(D-1)}$$

where:

- dP^S/dT is the slope of the of the vapour pressure curve,
- ΔV is the difference between the molar volumes of the saturated liquid and the saturated vapour and
- Δz is the difference between the compressibility factors of the saturated liquid and the saturated vapour.

All the above parameters are calculated at temperature T.

If it is assumed that the term $\Delta H_V/\Delta z$ is independent of the temperature then the above equation is simplified to the form:

$$\ln P^S = A - B/T, \qquad \text{(D-2)}$$

where A is the integration constant and $B = \Delta H_V/R\Delta z$.

The above equation shows that if a limited amount of vapour pressure data is available, we can plot the linear relationship between $\ln P^S$ and $1/T$ which can be used for interpolation and extrapolation.

The plot for the methanol vapour pressure data with respect to the temperature obtained from the Detherm database was constructed as follows:

T(K)	Ps(bar)	1/T	ln(Ps)
340	1.111	0.002941	0.105261
360	2.299	0.002778	0.832474
380	4.37	0.002632	1.474763
400	7.743	0.0025	2.046789
420	12.92	0.002381	2.558776

Table D-1. Methanol vapour pressure data.

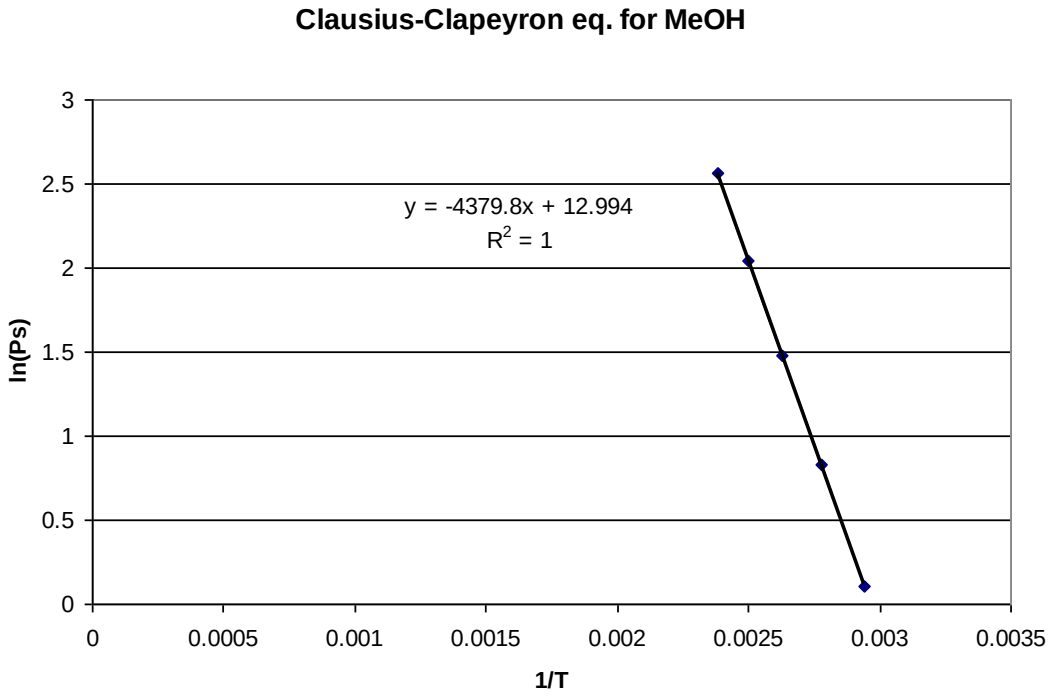

Figure D-1. Clausius-Clapeyron equation for methanol.

At T=373 K the calculated vapour pressure for the methanol is 3.497 bar≈3.5 bar.

Methyl Propionate

The same procedure was followed for methyl propionate with the data shown in Table D-2.

T(K)	Ps(bar)	1/T	ln(Ps)
343.15	0.730607	0.002914	-0.31388
353.15	1.027916	0.002832	0.027533
363.15	1.39322	0.002754	0.331618
373.15	1.874513	0.00268	0.628349
383.15	2.471797	0.00261	0.904945
393.15	3.207737	0.002544	1.165566
403.15	4.094331	0.00248	1.409603
413.15	5.183575	0.00242	1.645495
423.15	6.439472	0.002363	1.862447

Table D-2. Methyl propionate vapour pressure data.

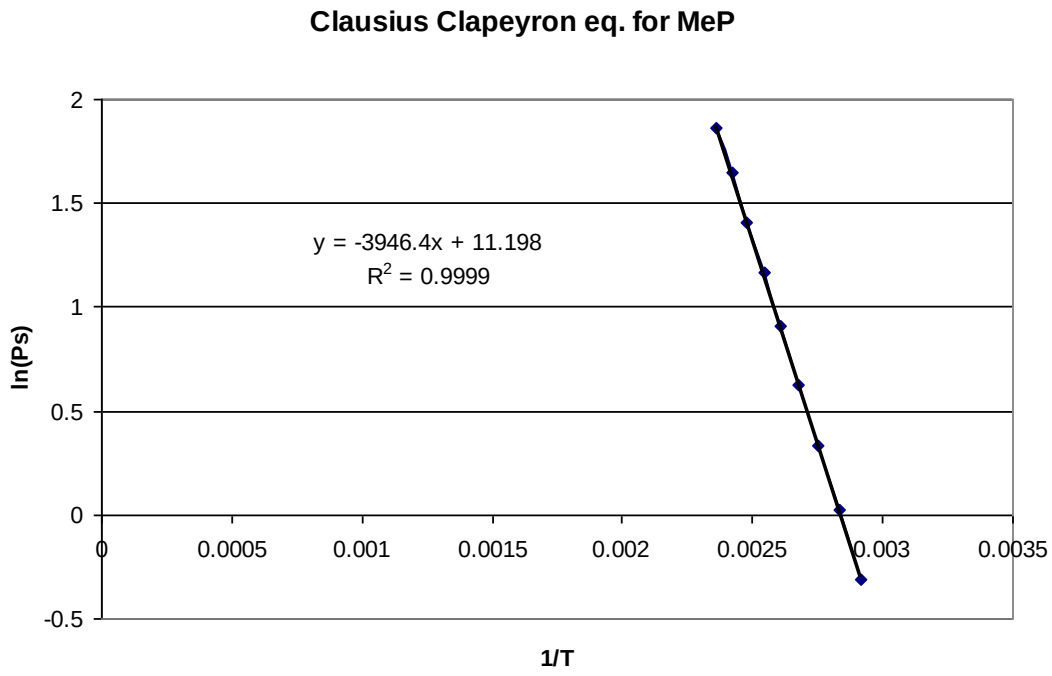

Figure D-2. Clausius-Clapeyron equation for methyl propionate.

At T=373 K the calculated vapour pressure for the methyl propionate is 1.85 bar≈1.9 bar.

From the difference in the vapour pressure it can be seen how much more volatile methanol is compared to methyl propionate.

Estimation of the activity coefficients

The isothermal VLE data for the system methanol-methyl propionate presented in the following table were obtained from DETHERM:

T of the system (K)	$P_{saturated}$ of the system (bar)	x_{MeoH}	x_{MeP}
	2.547	0.4987	0.5013
363.3	2.588	0.5576	0.4424

Table D-3. Isothermal VLE data for the system methanol-methyl propionate.

The activity coefficient, which signifies basically the divergence of the behaviour of the liquid phase from that of an ideal mixture, depends greatly on the mixture composition. The mixture composition in our case is x_{MeoH} =0.54 mol/mol and x_{MeP}=0.46 mol/mol (30 %:70 % w/w).

It will be attempted to estimate the value of the activity coefficient for the two components in the liquid phase using the data in the above table. Firstly, the fact which had to be investigated, is that the data do not correspond exactly to out conditions of T and P and whether this difference will have a significant effect on γ_i or not.

The activity coefficient can show a strong dependence from temperature according to the equation:

$$\left(\frac{\partial \ln \gamma_i}{\partial T}\right)_{x,P} = -\frac{\overline{H}_i^E}{RT^2} \qquad \text{(D-3)}$$

where $\overline{H}_i^E$ is the residual enthalpy of mixing which reflects the difference between the components' intramolecular forces.

The activity coefficient is a weak function of pressure:

$$\left(\frac{\partial \gamma_i}{\partial P}\right)_{x,T} = \frac{\overline{V}_i^E}{RT} \qquad \text{(D-4)}$$

where $\overline{V}_i^E$ is the residual partial molar volume of the i component in the liquid phase which has a very small value at low pressures.

Let us remember that residual properties signify the difference between the value M of a property of a mixture at given (T, P) and the value M(id) for the ideal mixture under the same conditions.

Coming back to the data in Table D-3, it can be assumed that the value of the activity coefficients that we will calculate at 363 K will not differ substantially from the value at 373 K. Furthermore, the mixture composition in our problem is x_{MeoH} =0.54 mol/mol and x_{MeP}=0.46 mol/mol (30 %:70 % w/w) which is close to the compositions in Table . We can also ignore the dependence of γ_i on the system pressure P.

At equilibrium the following equation applies:

$$P^{Sat} = x_1\gamma_1 P_1^S + x_2\gamma_{21}P_2^S, \qquad \text{(D-5)}$$

where the subscripts 1 and 2 denote methanol and methyl propionate respectively.

From the equation Clausius-Clapeyron we obtain P_1^S =2.5559 bar and P_{21}^S =1.3984 bar.

The solution of the 2 x 2 system:

$$1.2746 \cdot \gamma_1 + 0.7010 \cdot \gamma_2 = 2.5470$$

$$1.4252 \cdot \gamma_1 + 0.6187 \cdot \gamma_2 = 2.5880$$

gives γ_1 =1.1319 and γ_2 =1.5757

If the above values are compared with the values γ_1 =1.2051 and γ_2 =1.1973 from VLE data at 148^{o}C for the liquid composition x_{MeoH} =0.54 mol/mol and x_{MeP}=0.46 mol/mol obtained by ASPEN PHYS PROPS we can comment on the correct trend of the activity coefficient to decrease when temperature increases for the methyl propionate. On the contrary, the trend for methanol is the opposite; the activity coefficient decreases when temperature decreases and this was expected due to the presence of hydrogen bonds in the methanol hydroxide.

Equation of state

A Vapour-Liquid Equilibrium is characterised by the equality of fugacities of component i in the gas and liquid phase:

$$f_i^V = f_i^L \tag{D-6}$$

The fugacity of the vapour phase is expressed as:

$$f_i^V = \hat{\phi}_i \cdot y_i \cdot P\,, \tag{D-7}$$

where $\hat{\phi}_i$ is the fugacity coefficient of the vapours which can be expressed using an Equation of State for example the Virial EOS.

The fugacity of the liquid phase is given by the equation:

$$f_i^L = x_i \cdot \gamma_i \cdot f_i^o = x_i \cdot \gamma_i \cdot P_i^S \phi_i^S \exp \int_{P_i^S}^{p} \left(V_{li} \big/ RT \right) dP\,, \tag{D-8}$$

where:

- f_i^o is the fugacity of component i at the chosen standard state at which the activity coefficient is equal to 1.0 and usually corresponds to the state of the pure component i at conditions (P,T).
- P_i^S is the vapour pressure of pure i at temperature T.
- ϕ_i^S is the fugacity coefficient of the saturated vapour which again is calculated using a EOS and
- V_{li} is the molar volume of liquid i at temperature T and in the pressure range $\left[P_i^S, P\right]$.

For conditions below the critical point, the molar volume of the liquid does not practically depend on pressure so we can replace V_{li} with an average value $V_{li}(avg)$ for the range $\left[P_i^S, P\right]$. In this case the above equation becomes:

$$f_i^L = x_i \cdot \gamma_i \cdot P_i^S \phi_i^S \exp\left(V_{li}(avg) \cdot \left(P - P_i^S\right) \big/ RT \right) \tag{D-9}$$

The exponential term is called the Poynting Effect or $(PE)_i$ and basically shows the effect of the pressure on the fugacity of the pure liquid i for pressures from P_i^S to P

.

Thus, at VLE the equality of fugacities of i in the two phases becomes:

$$y_i \cdot \hat{\phi}_i \cdot P = x_i \cdot \gamma_i \cdot P_i^S \phi_i^S \exp\left(V_{li} \cdot \left(P - P_i^S\right) \Big/ RT\right) \quad \text{(D-10)}$$

From the DETHERM database we obtain the data for the critical point for the components methanol, methyl propionate and ethylene as shown in the following table:

	Symbol	**Component 1**	**Component 2**	**Component 3**
	Units	**Methanol**	**Methyl propionate**	**Ethylene**
critical temperature	Tc(K)	512.6	530.8	282.0
critical pressure	Pc(bar)	81	40	50.39
critical compressibility factor	Zc	0.224	0.256	0.276
critical volume	Vc(m^3/mol)	0.000118	0.000282	9.06E-05
accentric factor	Ω	0.559	0.352	0.086

Table D-4. Critical data for the components.

As it was mentioned earlier, one equation that can be used to model the gas phase and is reliable for non-polar and slightly polar mixtures, is the Virial EOS cut-off after the second Virial coefficient. Strict mixing rules apply when we are dealing with mixtures due to the fact that the Virial EOS was developed from statistical mechanics. Thus:

$$B = \sum\sum B_{ij} y_i y_j \quad \text{(D-11)}$$

where B_{ii} is the second Virial coefficient of the pure component i while B_{ij} corresponds to the couple of components (i-j) and obviously $B_{ij} = B_{ji}$. For a three component system the above equation becomes:

$$B = y_1^2 B_{11} + y_2^2 B_{22} + y_3^2 B_{33} + 2y_1 y_2 B_{12} + 2y_1 y_3 B_{13} + 2y_2 y_3 B_{23} \quad \text{(D-12)}$$

The following table shows the second virial coefficients for our mixtures components as obtained from the DETHERM database:

	Symbol	Component 1	Component 2	Component 3
	Units (m^3/mol)	Methanol	Methyl Propionate	Ethylene
second virial coefficient for MeOH at 373.15K	B11	-0.000534921		
second virial coefficient for MeP at 369.95K	B22		-0.00113	
second virila coefficient for ethylene at 373 K	B33			-7.63E-05

Table D-5. Second Virial coefficients.

Due to the fact that there are no data for the B_{ij}, an estimation technique had to be used but first the couple (i-j) the parameters had to be calculated:

- Critical temperature ($T_{C_{ij}}$).
- Critical pressure ($P_{C_{ij}}$).
- Critical compressibility factor ($z_{C_{ij}}$).
- Critical specific volume ($V_{C_{ij}}$).
- Accentric factor (ω_{ij}).

The following empirical combination rules were applied:

$$T_{C_{ij}} = (T_{C_i} T_{C_j})^{0.5}$$

$$z_{C_{ij}} = (z_{C_i} + z_{C_j})/2$$

$$V_{C_{ij}} = \left\{ \left[\left(V_{C_i}\right)^{1/3} + \left(V_{C_j}\right)^{1/3} \right] / 2 \right\}^3 \qquad \text{(D-13)}$$

$$P_{C_{ij}} = z_{C_{ij}} R T_{C_{ij}} / V_{C_{ij}}$$

$$\omega_{C_{ij}} = (\omega_i + \omega_j)/2$$

The Virial EOS cut-off after the second coefficient is valid in the pressure range:

$$P \leq \frac{T}{2}\frac{P_C}{T_C} \qquad \text{(D-14)}$$

To calculate B_{ij} the Tsonopoulos correlations were used:

$$\frac{B_{ij}P_{C_{ij}}}{RT_{C_{ij}}} = f^{(0)} + \omega_{ij} f^{(1)}, \tag{D-15}$$

where

$$f^{(0)} = 0.1445 - \frac{0.330}{T_{rij}} - \frac{0.1385}{T_{r_{ij}}^2} - \frac{0.0121}{T_{r_{ij}}^3} - \frac{0.000607}{T_{r_{ij}}^8} \text{ and}$$

$$f^{(1)} = 0.0637 + \frac{0.331}{T_{r_{ij}}^2} - \frac{0.423}{T_{r_{ij}}^3} - \frac{0.008}{T_{r_{ij}}^8} \tag{D-16}$$

$T_{r_{ij}}$ is the reduced temperature for the couple (i-j) and equal to:

$$T_{r_{ij}} = \frac{T}{T_{C_{ij}}} \tag{D-17}$$

3. Calculations

Using the combination rules the critical properties for the sets of the components were calculated. The results are shown in the next table:

Critical property	Value
Tc12=sqrt(Tc1*Tc2) (K)	521.6
Pc12=zc12RTc12/Vc12 (Pa)	5528704.5
ω12=(ω1+ω2)/2	0.456
zc12=(zc1+zc2)/2	0.24
Vc12={[(Vc1)^(1/3)+(Vc2)^(!/3)]/2}^3 (m^3/mol)	0.000188258
Tc13=sqrt(Tc1*Tc3) (K)	380.4
Pc13=zc13RTc13/Vc13 (Pa)	7624768.8
ω13=(ω1+ω3)/2	0.323
Vc13={[(Vc1)^(1/3)+(Vc3)^(1/3)]/2}^3 (m^3/mol)	0.000103697
Tc23=sqrt(Tc2*Tc3) (K)	406.55
Pc23=zc13RTc23/Vc23 (Pa)	5332429.095
ω23=(ω2+ω3)/2	0.323
zc23=(zc2+zc3)/2	0.266
Vc23={[(Vc2)^(1/3)+(Vc3)^(1/3)]/2}^3 (m^3/mol)	0.000168609

Table 6.Calculated critical properties.

Subsequently, the value $(\frac{T}{2}\frac{P_{C\,ij}}{T_{C\,ij}})$ was calculated to see whether the condition $P \le \frac{T}{2}\frac{P_{C_{ij}}}{T_{C_{ij}}}$ apply or not. Table D-7 contains the results:

(T/2)*Pc12/Tc12 (bar)	20
(T/2)*Pc13/Tc13 (bar)	37
(T/2)*Pc23/Tc23 (bar)	24

Table D-7. Validation check for the Virial EOS.

As it can be seen from the above table, the Virial EOS is valid for P=12 bar and thus, the calculations process was continued to estimate firstly the virial coefficients for

the components sets using the Tsonopoulos correlations (the results are shown in Table D-8) and subsequently the fugacity coefficients.

B12 (m^3/mol)	-0.000695137
B13(m^3/mol)	-0.00015173
B23(m^3/mol)	-0.000273206

Table D-8. Second Virial coefficients for the components sets.

The fugacity coefficient of the component i in the vapour phase for a mixture of m components is given by the formula:

$$\ln \hat{\phi}_i = \left[2\sum_{j=1}^{m} y_j B_{ij} - B \right] \frac{P}{RT} \qquad \text{(D-18)}$$

For a three-component system it becomes:

$$\ln \hat{\phi}_1 = \left[2\left(y_1 B_{11} + y_2 B_{12} + y_3 B_{13} \right) - B \right] \frac{P}{RT}$$

$$\ln \hat{\phi}_2 = \left[2\left(y_1 B_{12} + y_2 B_{22} + y_3 B_{23} \right) - B \right] \frac{P}{RT} \qquad \text{(D-19)}$$

The fugacity coefficient of the pure saturated vapour of i is given by:

$$\ln \phi_i^S = \frac{B_{ii} P_i^S}{RT} \qquad \text{(D-20)}$$

and the calculated values are as follows:

Φ^s_1	0.9415
Φ^s_2	0.9346

Table D-9. Fugacity coefficients of the saturated vapour for methanol and methyl propionate

The Poynting Effect (PE) is calculated using the data for the specific liquid volume of methanol and methyl propionate attained from DETHERM:

average molar volume for the $MeOH_{(l)}$ (m^3/mol)	V1	4.49E-05
Conditions: at 373.15K		
average molar volume for the $MeP_{(l)}$ (m^3/mol)	V2	9.23E-05
Conditions: data for T in the range [318.15-328.15K] and then extrapolation to 373K		

Table D-10. Molar volume for liquid methanol and methyl propionate for calculation of the PE.

(PE)1=exp(V1*(P-Ps1)/(RT)	1.0124
(PE)2=exp(V2*(P-Ps2)/(RT)	1.0307

Table D-11. Poynting Effect from methanol and methyl propionate.

The fugacity coefficient of component i in the gas phase depends on its concentration y_i. By the method of trial and error we get the results that are summarised in the following table.

		component 1	component 2
Fugacity coefficient of the gas phase	Φ_i	0.8711	1.0000
Fugacity coefficient of the saturated liquid	Φ^s_i	0.9415	0.9346
activity coefficient	γ_i	1.1319	1.5757
Poynting effect	$(PE)_i$	1.0124	1.0307
Composition of i in the gas phase	$\mathbf{y_i}$	**0.21230**	**0.11739**

Table D-12. Summary of the results

It is thus estimated that the gas phase will consist of approximately 21 % methanol(v), 12 % methyl propionate(v). **The total fraction of liquid vapours in the gas phase is 33 %.**

APPENDIX E

Experimental Procedure for the Capillary Microreactor

Initial checks

Check that the following systems are sound and ready for operation prior to commencing the experiment:

- ✓ GC ready.
- ✓ Pressure relief valve set up ok.
- ✓ Pressure control system ready.
- ✓ Temperature control system ready.
- ✓ Flow control system ready.
- ✓ Filters clean.
- ✓ Reactant mixture in the syringe pump ok.
- ✓ Pressure regulators on the cylinders ok.
- ✓ Gas in the gas cylinders ok.
- ✓ Gas monitoring system ok.

Start –up sequence, experimental procedure, turn-off sequence

- Start the heating system with a set point of 100^{o}C.
- Open the valves of the H_2 and Air cylinders
- Start GC (enter method etc) and FID detector.
- Initially the pressure control system is off.
- Take sample from the syringe pump and analyse it in the GC.
- Start the pressure controlling system.
- Set the pressure controller to the desired set point.
- Start the gas flow meters (N_2, ethylene and CO).
- Open the outlet valves at the gas cylinders (N_2, Ethylene, CO).
- Check the system for leaks using the appropriate spray. This action should be repeated at intervals during the course of experiment as well.
- Build up the pressure in the reactor to the desired set point.
- Program the syringe pump to the desired flow rate.
- Start syringe pump.
- See the gas-liquid flow going through the micro reactor.
- Start the camera and the VISIFLOW software and monitor the flow.
- Once everything is flowing ok at the correct temperature and pressure, wait until you reach steady state and then empty the phase separator and discard the liquid collected.
- After one hour of steady state operation take a liquid from the bottom of the liquid separator in a glass vial with the limited volume inserts and analyse it in the GC.
- Continue the experiment and take a liquid sample every hour.
- If you want to take pressure measurements connect the voltmeter to the pressure transducers, monitor the voltage and convert it to pressure using the calibration line.
- Before you take a liquid sample switch off the gas flow and make sure that you open the valve of the phase separator only slightly so that the pressure

drop incurred because of sampling is 0.3 bar or less. Then, switch the gas flow on again and continue the experiment.

- Take photographs of the flow and measure the size of the slugs and the bubbles using the Aequitas software.
- If you want to measure the experimental space time then inject for 1-2 s blue dye (ink) and with a stop watch measure the time necessary for the tiny liquid slug to pass through the capillary reactor.
- When you want to stop the experiment switch off the gas by turning off the mass flow controllers.
- Switch off the syringe pump.
- Change the GC method to COOLDOWN.
- Switch off the valves at the cylinders H_2 and Air.
- Open the bottom of the phase separator to empty it and release the pressure.
- Open the valve of the pressure regulator.
- Turn off the gas at the cylinders (N_2, ethylene, CO) by closing the main valve at the top of the cylinder.
- Turn down the temperature of the heating system to the off position.
- If you want to zero the regulators open fully the valves of the gas flow meters and empty the lines.
- Once the lines are empty the manometers on the gas cylinders will show zero and then you can close the outlet valve on the cylinder and the valves of the gas mass flow controllers.
- Turn off the heating system.

Personal Protective Equipment (PPE)

From the risk assessment initially compiled on 10-01-07 by E. Apostolopoulou, it was concluded that the following (PPE) are necessary when performing experiments:

- Lab coat to be worn at all times.
- Lab goggles to be worn at all times.
- Insulated gloves to be worn when working near the thick film heater and plastic inert gloves at all other times.
- Organic Vapour Respirator to be worn at all times.
- Polycarbonate helmet bound to face shield to be worn when working near the microreactor or when de-pressurising the system.

APPENDIX F

Comparison of Results obtained with Different Tee Contactors

Five series of experiments were carried out under the same conditions with five different tees.

Condition	Symbol	Value	Unit
Pressure	P	6	bar
Temperature	T	100	^{o}C
Liquid Flowrate	Q_L	5	µl/min
Ethylene /CO Flowrate Ratio		3/1	ml/min

Table F-1. Experimental conditions.

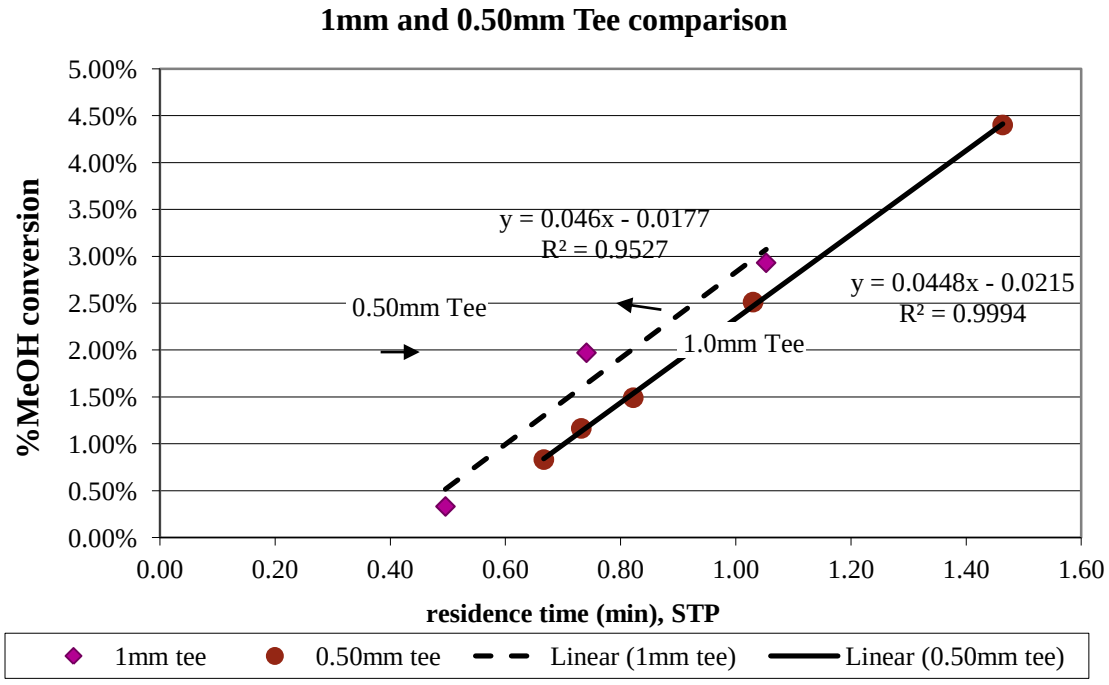

Figure F-1. MeOH conversion versus residence time for gas ratio 3/1. Comparison of results obtained with the 1mm tee and 0.50mm t-contactors.

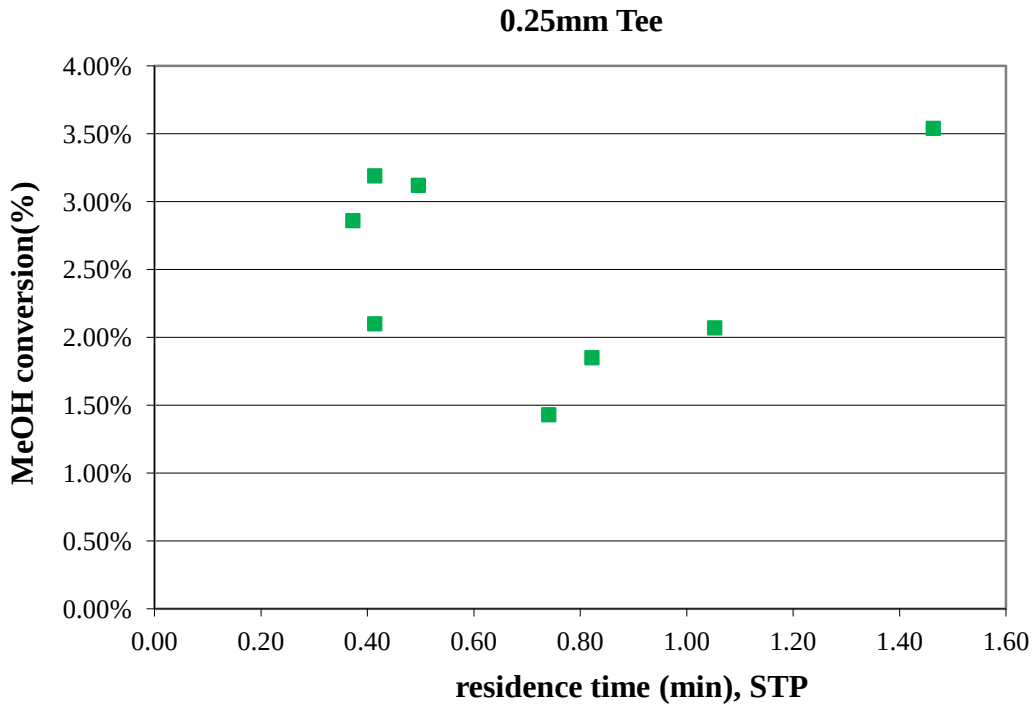

Figure F-2. MeOH conversion versus residence time for gas ratio 3/1. Results obtained with the 0.25mm tee contactor.

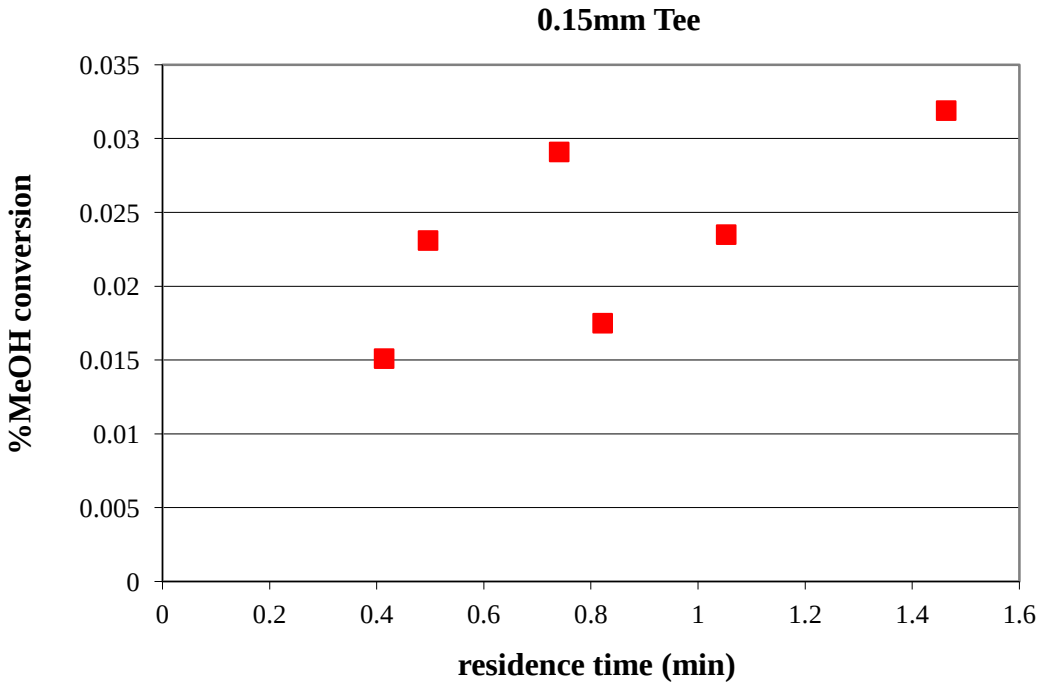

Figure F-3. MeOH conversion versus residence time for gas ratio 3/1. Results obtained with the 0.15mm tee contactor.

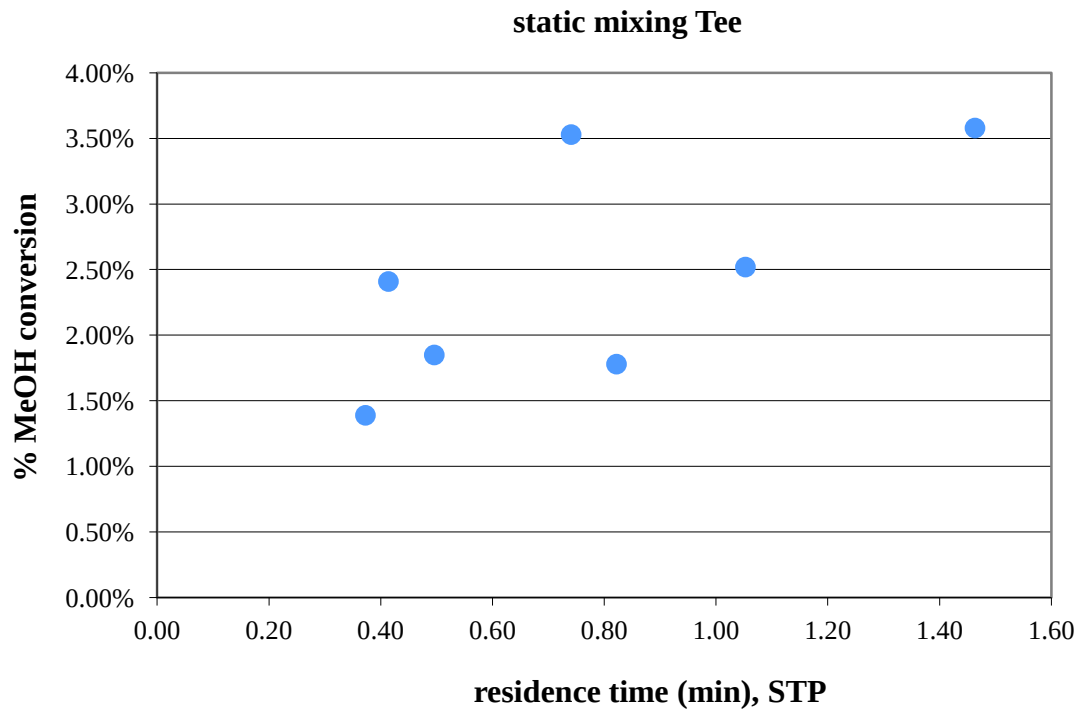

Figure F-4. MeOH conversion versus residence time for gas ratio 3/1. Results obtained with the static mixing tee.

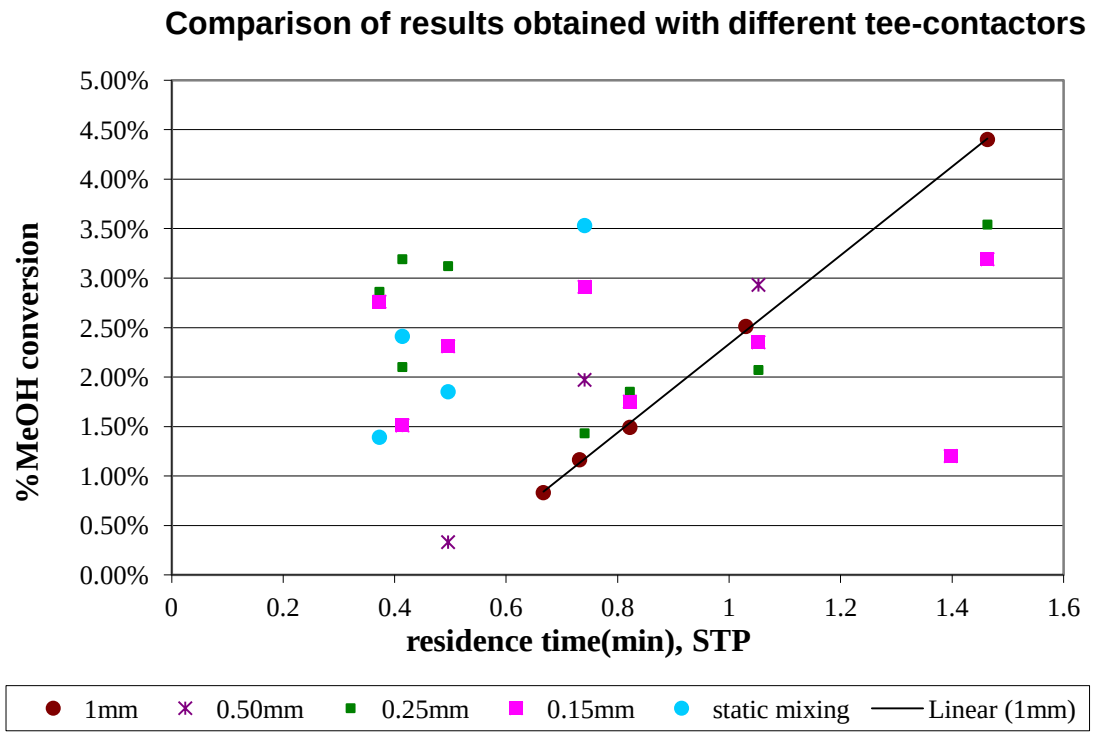

Figure F-5. MeOH conversion versus residence time for gas ratio 3/1. Comparison of results obtained with the five tee contactors.

APPENDIX G

Reactor Carbon Balance Closure

The carbon balance was closed for two experiments performed under the conditions listed in the Table below:

Experiment No	**1**	**2**	
Condition	**Symbol**	**Value**	**Unit**
Reaction Pressure	11	11	bara
Reaction Temperature	100	100	^{o}C
Liquid Flowrate	5	5	µl/min (STP)
Ethylene Flowrate	0.20	0.50	ml/min (STP)
CO Flowrate	0.20	0.25	ml/min (STP)
Mass Fraction of MeOH in the liquid mixture feed to the capillary reactor*	0.30	0.30	(w/w)
Mass Fraction of MeP in the liquid mixture feed to the capillary reactor*	0.70	0.70	(w/w)
Mass Fraction of C2H4 in the gas exit stream from the capillary reactor*	43.15	64.10	(% w/w)
Mass Fraction of CO in the gas exit stream from the capillary reactor*	58.85	35.90	(% w/w)
Mass Fraction of C2H4 in the gas exit stream from the capillary reactor (calculated)**	45.45	64.30	(% w/w)
Mass Fraction of CO in the gas exit stream from the capillary reactor (calculated) **	54.55	34.70	(% w/w)

Table G-1. Experimental Conditions and Data

*Measured by the GC at STP conditions.

**Calculated gas compositions at the reactor inlet. The difference between the calculated and the measured gas compositions was found to be [3 % - 7 %].

Reactor inlet and outlet conditions calculated using the ACM and the measured gas and liquid compositions at the reactor outlet, are shown below:

Experiment No	**1**	**2**	
Condition	**Value**	**Value**	**Unit**
Reactor Liquid Feed			
Mass flow rate	5.78e-8	5.06e-8	Kg/s
Mass Fraction of MeOH at reaction conditions	0.28	0.26	(w/w)
Mass Fraction of MeP at reaction conditions	0.71	0.73	(w/w)
Mass Fraction of C2H4 at reaction conditions	7.53e-3	1.05e-2	(w/w)
Mass Fraction of CO at reaction conditions	1.88e-3	1.24e-3	(w/w)
Reactor Gas Feed			
Mass flow rate	1.75e-8	3.28e-8	Kg/s
Mass Fraction of MeOH at reaction conditions	0.20	0.20	(w/w)
Mass Fraction of MeP at reaction conditions	0.28	0.29	(w/w)
Mass Fraction of C2H4 at reaction conditions	0.25	0.34	(w/w)
Mass Fraction of CO at reaction conditions	0.27	0.17	(w/w)
Reactor Liquid Exit			
Mass flow rate	6.19e-8	5.56e-8	Kg/s
Mass Fraction of MeOH at reaction conditions	0.28	0.26	(w/w)
Mass Fraction of MeP at reaction conditions	0.71	0.73	(w/w)

Condition...*continued*	**Value**	**Value**	**Unit**
Mass Fraction of C2H4 at reaction conditions	6.40e-3	1.01e-2	(w/w)
Mass Fraction of CO at reaction conditions	2.13e-3	1.35e-2	(w/w)
Reactor Gas Exit			
Mass flow rate	1.35e-8	2.45e-8	Kg/s
Mass Fraction of MeOH at reaction conditions	0.20	0.20	(w/w)
Mass Fraction of MeP at reaction conditions	0.28	0.29	(w/w)
Mass Fraction of C2H4 at reaction conditions	0.21	0.32	(w/w)
Mass Fraction of CO at reaction conditions	0.30	0.19	(w/w)
Difference between compositions at the reactor inlet and the outlet <5 %			

Table G-2. Calculated inlet and outlet reactor conditions.

The carbon balance is closed with a discrepancy of 2 % as it is shown in the following Table:

Carbon at reactor inlet			
Experiment No	**1**	**2**	
Carbon from MeOH	7.40 e-09	7.42e-09	Kg/s
Carbon from MeP	2.51e-08	2.52e-08	(w/w)
Carbon from C2H4	4.09e-09	1.00e-08	(w/w)
Carbon from CO	2.04e-09	2.46e-09	(w/w)
Total Carbon at reactor inlet	3.87e-08	4.51e-08	(w/w)
Carbon at reactor outlet			
Carbon from MeOH	7.58e-09	7.47e-09	Kg/s
Carbon from MeP	2.60e-08	2.74e-08	(w/w)
Carbon from C2H4	2.78e-09	7.34e-09	(w/w)
Carbon from CO	1.80e-09	2.00e-09	(w/w)
Total Carbon at reactor outlet	3.82e-09	4.42e-08	(w/w)
Carbon difference between outlet-inlet	**-1.27**	**-1.91**	**%**

Table G-3. Carbon balance closure.

APPENDIX H

Experimental Error Estimation

The experimental error can be expressed as absolute error (E_{abs}) or relative error (E_{rel}). The absolute experimental error is defined as the difference between the measured value or calculated value X_m and T_v is the true value and has three components as follows:

$$E_{abs} = X_m - T_v = e_s + e_r + e_b \tag{H-1}$$

e_s is the systematic error, e_r is the random error and e_b is the error due to blunders or gross mistakes.

The estimation of the systematic error depends on the number of observations, the standard deviation of the observations and the chosen confidence level (usually 90 %, 95 % or 99 %). For a number N of observations, the systematic error is calculated as follows:

$$e_s = t\frac{s}{\sqrt{N}} \tag{H-2}$$

where s is the standard deviation of the sample of observations and t is the value from the t-distribution which depends on the confidence level and the $(N-1)$ degrees of freedom equal to $(n-1)$. Thus, the confidence interval for the true mean of the population of the observations μ is given:

$$\mu = \overline{X} \pm e_s \tag{H-3}$$

where $\overline{X}$ is the mean of the sample of observations.

The relative systematic error δ_x can be calculated from the formula:

$$\delta_x = \frac{e_s}{\bar{X}}, \tag{H-4}$$

which gives $\mu = \bar{X}(1 \pm \delta_x)$ (H-5)

Autoclave reactors

Three standard experiments performed by LI under the Alpha standard conditions and produced the following results:

No of experiment	Date of experiment	Max TOF achieved (molMePproduced/molPd/h)
1	16/09/04	79838
2	20/09/04	82526
3	28/09/04	90696

Table H-1. Experimental data.

The systematic error is calculated as follows:

Mean of TOF	84354
Standard deviation of TOF	5655
For 90% confidence level and (3-1)=2 degrees of freedom, t	2.92
Systematic absolute error	2.92*5655/sqrt(3)=9534
Systematic relative error	9534/84354=0.113
Repeatability	2.96*sqrt(2)*5655=23353

Table H-2. Calculation of experimental error- Autoclave.

Therefore, it can be said with 90 % certainty that the maxTOF achieved from a standard experiment will lie in the range 84354 ± 9534.

It should be mentioned here that the number of experiments (observations) was only three. A greater number of experiments would allow better accuracy and smaller error, thus, a narrower confidence interval for the maxTOF. For example, is we wanted to estimate the TOF from a standard experiment with an accuracy of ±5000, then we would require data

from $n \approx \left(\frac{ts}{c}\right)^2$ = (2.92*5655/5000)^2=10.9 or 11 experiments. Regarding the calculated repeatability, it can be concluded with 90 % certainty that the difference between the maxTOF obtained from two consecutive experiments performed under repeatable conditions should not be greater than 23353. If it is greater, means that something had gone wrong with the experiment.

Capillary reactor

Conditions: T=100^{o}C, P=7bara, Q_{C2H4}=0.54ml/min, Q_{CO}=0.54ml/min, L=5μl/min

No of experiment	Date of experiment	% MeOH conversion achieved
1	25/06/07	2.16
2	25/06/07	1.96
3	25/06/07	2.57
4	25/06/07	1.85
5	26/06/07	2.22
6	26/06/07	1.68
7	26/06/07	1.64
8	26/06/07	1.74

Table H-3. Experimental data.

Mean of MeOH conversion	2.26
Standard deviation of conversion	0.33
For 90% confidence level and (8-1)=7 degrees of freedom, t	1.89
Systematic absolute error	1.89*0.33/sqrt(8)=0.22
Systematic relative error	0.22/2.26=0.097=9.7%
Repeatability	1.89*sqrt(2)*0.33=0.88

Table H-4. Calculation of experimental error.

Therefore, it can be concluded with 90 % confidence, that the true conversion of MeOH should lie in the interval 2.26 % ± 0.22 % and two consecutive experiments performed under the same repeatable conditions should not differ by 0.88 %. If a 95 % confidence level is chosen instead of 90 %, then the interval produced for the conversion would be 2.26 % ± 0.27 %, the relative error would equate 0.121 and the repeatability of the experimental method would be 1.09 %.

GC Analysis

Two sets of measurements were taken by the GC as it is shown in the Table H-5 to estimate the measurement error.

No of measurement	**Set 1**	**Set 2**
Date	27-03-07	27-03-07
1	1.22	1.36
2	1.18	1.37
3	1.20	1.38

Table H-5. Experimental data- GC measurements.

	Set 1	**Set 2**
Mean of MeOH conversion	1.20	1.37
Standard deviation of conversion	0.020	0.010
For 90 % confidence level and (3-1)=2 degrees of freedom, *t*	2.92	2.92
Systematic absolute error	2.92*0.02/sqrt(3)=0.034	2.92*0.01/sqrt(3)=0.017
Systematic relative error	0.034/1.20=0.028=2.8 %	0.017/1.20=0.012=1.2 %
Repeatability	2.92*sqrt(2)*0.020=0.083	2.92*sqrt(2)*0.010=0.041

Table H-6. Calculation of experimental error of conversion measurement using the GC.

The analysis showed that the confidence interval for the MeOH conversion measurements from set 1 was 1.20 % ± 0.034 % while for set 2 was 1.37 % ± 0.017 %. In addition, it

was found that the difference between two consecutive conversion measurements should be no greater than 0.083 % or 0.041 % as resulted from set 1 or 2 respectively.

Slug and bubble size measurement

The results of two sets of bubble and slug size measurements are presented overleaf in order to assess the experimental error involved in the measurement procedure.

	Experiment 1		**Experiment 2**	
Exp. Conditions	0.50 mm tee contactor		0.50 mm tee contactor	
	T=100 ^{o}C		T=100 ^{o}C	
	P=11 bara		P=11 bara	
	L=5 µl/min		L=5 µl/min	
	CO=1 ml/min		CO=0.12 ml/min	
	C2H4=0.3 ml/min		C2H4=0.36 ml/min	
	Experiment 1		Experiment 2	
	size measurements (mm)		size measurements (mm)	
	slug	bubble	slug	bubble
1	1.012	4.665	0.831	5.915
2	1.008	4.672	0.908	5.999
3	1.032	4.845	0.943	6.842
4	1.035	5.347	0.898	6.134
5	1.116	5.514	0.950	6.311
6	1.097	5.209	0.920	6.020
7	1.047	5.378	0.940	6.413

Calculations				
	slug	bubble	slug	bubble
Mean, mm	1.050	5.090	0.913	6.233
Standard deviation,mm	0.041	0.355	0.041	0.322
t for (7-1=6) degrees of freedom and 90 % confidence level	1.94	1.94	1.94	1.94
N (No of observations)	7	7	7	7
Absolute systematic error	0.030	0.261	0.030	0.236
Systematic relative error, %	2.9	5.1	3.3	3.8
Repeatability, mm	0.114	0.975	0.113	0.882

Table H-7. Calculation of experimental error for slug and bubble size measurements.

It is derived from the calculations above that the 90 % confidence interval for the slug size and bubble size in Experiment 1 are 1.05 ± 0.03 mm and 5.09 ± 0.26 mm which means a 2.9 and 5.1 % relative experimental error respectively. Regarding Experiment 2, the confidence interval for the slugs was found to be 0.91 ± 0.03 mm while for the bubbles 6.23 ± 0.24 mm. The relative error was calculated as 3.3 % and 3.8 % respectively.

APPENDIX I

Investigation of Mass Transfer Resistances in the Autoclave Reactor

Criterion 1: $\mathrm{Ha} = \frac{\sqrt{D_L \frac{R}{[A]^*}}}{k_L} < 0.16$	
[1] mass transfer coefficient, k_L, m s^{-1}	5.40E-03
[2] Diffusion coefficient, D_L, m s^{-2}	1.87E-09
[3] reaction rate *R*, mol m^{-3} s^{-1}	6.54E-01
[4] Solubility of CO at 12 bara and 373 K - molar fraction (solubility data from Torres, 2009)	8.05E-04
[5] molality of liquid mixture, mol m^{-3}	1.52E+04
[6] Solubility of CO, CO*, mol m-3=[4]*[5]	1.22E+01
Ha=sqrt([2]*[3]/[6])/[1]	0.002
CRITERION 1 SATISFIED?	**TRUE**
Criterion 2: $\gamma = \frac{R}{\kappa_L \alpha C_{CO}^*} << 1$	
[7] Volumetric mass transfer coefficient, $k_L\alpha$, s^{-1}	0.64
γ=[3]/([7]*[6])	0.08
CRITERION 2 SATISFIED?	**TRUE**

Table I-1. Example of calculations.

APPENDIX J

Evaluation of Mass Transfer Coefficients $k_L\alpha$ and k_L

Evaluation of $k_L\alpha$

Three correlations found in the literature were used to estimate the volumetric mass transfer coefficient $k_L\alpha$ in the autoclave reactor.

The first correlation was proposed by Chaudhari & Gholap (1987):

$$k_L\alpha = 1.48\times10^{-3} N^{2.18}\left(\frac{V_G}{V_L}\right)^{1.88}\left(\frac{d_I}{d_T}\right)^{2.16}\left(\frac{h_1}{h_2}\right)^{1.66} \tag{J-1}$$

where N is the agitation speed (Hz), d_I the impeller diameter (m), d_T the tank diameter (m), h_1 the distance of the impeller from the bottom (m), h_2 the liquid height in the reactor from the bottom (m), V_G the volume of gas-phase (m^3), V_L the volume of liquid phase (m^3).

The correlation is applicable when the following conditions are satisfied:

$$\left.\begin{array}{l} N > 8.33Hz \\ \dfrac{d_I}{d_T} > 0.5 \\ \dfrac{V_G}{V_L} > 1 \\ \dfrac{h_1}{h_2} > 0.3 \end{array}\right\} \tag{J-2}$$

Furthermore, it is applicable for a single stirrer blade and when the gas is fed into the reactor with a dip-tube. When there is no-dip tube the actual mass-transfer coefficient is lower than the one predicted.

The geometrical characteristics of the autoclave reactors at LI values are included in Table J.1. These were used for the correlations of the mass transfer coefficient.

Characteristic	**Value**
d_I	2 in
d_T	4 in
V_L	0.3 L
V_G	1.7 L
h_1/h_2	1/3

Table J-1. Geometrical characteristics of autoclave reactors at LI.

For the agitation speed of 1000 rpm equation (J-1) gives:

$k_L\alpha$ =0.642 s^{-1}

The second correlation used was reported by Trambouze et al. (1988):

$$\frac{k_L\alpha d_I^2}{D} = 0.06\left(\frac{d_I^2 N\rho_L}{\mu_L}\right)^{1.5}\left(\frac{d_I N^2}{g}\right)^{0.19}\left(\frac{\mu_L}{\rho_L D}\right)^{0.5}\left(\frac{\mu_L V_{SG}}{\sigma}\right)^{0.6}\left(\frac{N d_I}{V_{SG}}\right)^{0.32} \quad \text{(J-3)}$$

V_{SG} is the surface aeration speed (m/s), μ_L is the viscosity of the liquid (Ns/m^2), ρ_L is the density of the liquid (Kg/m^3), surface tension of the liquid (N/m) and D is the diffusion coefficient of the CO into the liquid (m^2/s).

The following physical properties for the system CO/methanol were used in the calculations.

Physical property	Value
σ	0.02237 N/m
ρ_L	791.7 kg/m^3
μ_L	2.88 10^{-4} Ns/m^2
D	1.87 10^{-9} m^2/s

Table J-2. Physical properties of the system CO/methanol.

The value of V_{SG}, necessary for correlation (J-3), was obtained using the VISIMIX software as the *surface aeration rate* which represents the gas flow rate per tank cross-section and describes the entrainment of gas into the liquid caused by the turbulence at the surface. A reactor with the geometrical characteristics given in Table J-1, in addition to having an elliptical bottom tank, 4 tubular-baffles and a radial turbine with 4 blades was assumed for the simulation. Furthermore, 1000 rpm was used as the agitation speed in the calculations as well as the average gas consumption of 1.84 10^{-4} mol/s. The latter was derived from batch experimental data collected in September 2004 at LI. From the simulation with VISIMIX, it was found that V_{SG}=0.0233 m/s.

For 1000 rpm agitation speed, it was derived from equation (J-3) that the value of $k_L\alpha$ is 0.641 s^{-1}.

VISIMIX software is a simulation package of mixing-related processes for chemical engineers. It is based on physical and mathematical models of phenomena that occur in mixing tanks. These models have been developed from all the known data published on mixing and are the product of 30 years systematic theoretical and experimental research. The basic equations used are the fundamental equations of turbulent transport of energy, momentum and mass. Experimental data and correlations to describe specific conditions are also used. The models in VISIMIX have been tested on industrial scale and they form part of the engineering practice for years.

The third correlation was derived by Meille et al. (2004) who determined experimentally the volumetric mass transfer coefficient in small laboratory batch

reactors with volume 0.025 - 0.3 L and correlated the experimental data with a power expression of the form:

$$k_L\alpha = AN^B \quad \text{(J-4)}$$

The parameters A and B for the reactor with 0.3 L volume and also equipped with a four-blade gas inducing turbine and four baffles are: A=9.7 and B=2.3. The above equation for 1000 rpm=16.67 Hz gives $k_L\alpha$ =0.62 s^{-1}.

Evaluation of k_L

Slip velocity model approach

Two relationships were used depending on the bubble diameter, in line with the 'slip velocity' models which assume a gross mean flow of fluid relative to the bubble (called the slip velocity) and that the renewal of the liquid on the bubble surface is controlled by the bubble surface mobility. Large bubbles have a completely mobile surface but this is not true for small bubbles and this is the reason behind the distinction based on bubble size. Linek et al. (2005) argued that the distinction between the two categories was unclear and depended significantly on the presence of surfactants.

According to Trambouze et al. (1988) the following two correlations for k_L can be utilized. These mostly apply to sieve-trays:

Small bubbles: bubble diameter<25mm

$$k_L = 0.31\left(\frac{g\mu_L}{\rho_L}\right)^{\frac{1}{3}}\left(\frac{D_L\rho_L}{\mu_L}\right)^{\frac{2}{3}} \quad \text{(Calderbank, 1961)} \quad \text{(J-5)}$$

The values of k_L =1.4 10^{-4} m s^{-1} and a=4560 m^2/m^3 (from $k_L\alpha / k_L$ and $k_L\alpha = 0.64\,s^{-1}$) were obtained.

Large bubbles: bubble diameter >25mm

$$k_L = 0.42\left(\frac{g\mu_L}{\rho_L}\right)^{\frac{1}{3}}\left(\frac{D_L\rho_L}{\mu_L}\right)^{\frac{1}{2}} \qquad \text{(Reith, 1968)} \qquad \text{(J-6)}$$

The values of k_L =4.6 10^{-4} ms^{-1} and a=1398 m^2/m^3 were obtained.

It is likely that correlations (J-5) and (J-6) underestimate the mass transfer coefficient because they are applicable for sieve trays when obviously there is no stirrer.

Specific interfacial area approach

The volumetric mass transfer coefficient $k_L\alpha$ has two contributions; one from the mass transfer coefficient k_L and one from the specific interfacial area a. The latter can be calculated from the gas hold-up and the bubble diameter assuming spherical bubbles (Stenberg & Andersson, 1988):

$$\alpha = \frac{6\varepsilon_G}{d_b} \qquad \text{(J-7)}$$

$$\frac{\varepsilon_G}{1-\varepsilon_G} = 0.819\frac{V_{SG}^{2/3}N^{2/5}d_I^{4/15}}{g^{1/3}}\left(\frac{\rho_L}{\sigma}\right)^{1/5}\left(\frac{\rho_L}{\rho_L-\rho_G}\right)\left(\frac{\rho_L}{\rho_G}\right)^{-1/15} \qquad \text{(J-8)}$$

(derived from Garcia-Ochoa & Gomez, 2004, for Rushton turbines)

$$d_b = \frac{4.15\sigma^{0.6}\varepsilon_G^{0.5}}{\left(\frac{P_G}{V_L}\right)^{0.4}\rho_L^{0.2}} + 0.0009 \qquad \text{(Calderbank, 1958)} \qquad \text{(J-9)}$$

$$\frac{P_G}{V_L} = \frac{0.83}{V_L}\left[\frac{N_p d_I^8 \rho_L N^4 V_L}{V_{SG}^{0.56}}\right]^{0.45} \qquad \text{(Lemoine \& Morsi, 2005)} \qquad \text{(J-10)}$$

N_P=6 (for Rushton turbines)

The density of the gas was calculated as follows:

$$\rho_G = 0.1\rho_{CO} + 0.9\rho_{Eth} = 9.313 \text{ Kg m}^{-3} \quad \text{(J-11)}$$

$$k_L = \frac{k_L \alpha}{a} \quad \text{(J-12)}$$

Using the above formulas, the following parameters were determined:

$\frac{P_G}{V_L} = 29.04 \text{ W m}^{-3}$

$\varepsilon_G = 0.364$

d_b=0.018 m

A=119.0 m^2 m^{-3}, and finally,

$k_L = 5.4\ 10^{-3}$ m s^{-1}

Visimix approach

Using the same parameters specified earlier and the VISIMIX software for 1000 rpm agitation speed we obtained:

$k_L = 3.5\ 10^{-3}$ m s^{-1} and a=720 m^2/m^3

Eddy model approach

The 'eddy model' assumes that the liquid renewal on the bubble surface is due to small-scale eddies of the turbulent field. Mass transfer is therefore affected by these small motions which are much smaller in scale that the gas bubbles and therefore, the bubble size is not a critical parameter for the estimation of mass transfer coefficient. In this context, Linek et al. in a study published in 2005, proposed that the mass transfer coefficient can be correlated satisfactorily by the following relation:

$$k_L = 0.448\left(\frac{P_g \mu_L}{V_L \rho_L^2}\right)^{0.25}\left(\frac{D_L \rho_L}{\mu_L}\right)^{0.5} \quad \text{(J-13)}$$

Many researchers have also related the volumetric mass transfer coefficient with the agitation power per unit volume $\left(\frac{P_g}{V_L}\right)$, the superficial gas velocity V_{SG} and the stirring speed as follows:

$$k_L\alpha = 0.04\left(\frac{P_g}{V_L}\right)^{0.47} V_{SG}^{0.6} \tag{J-14}$$

Eq. (J-13) was derived from a study of reactor with a reactor diameter 0.211 m, gas volumetric flow rate $1 \le Q_g \le 15$ L/min and agitation speed $6.67 \le N \le 13.33$ rev/s. This correlation is independent of the flow hydrodynamics and the flow regimes in the stirred tank reactor according to Kapic & Heindel (2006).

Smith et al. (1977) proposed a similar general correlation for conventional mechanically agitated reactors operating with coalescing systems:

$$k_L\alpha = 0.01\left(\frac{P_g}{V_L}\right)^{0.475} V_{SG}^{0.4} \tag{J-15}$$

Correlations for a stirred reactor with gas-inducing impeller were put forward by Joshi & Sharma (1977):

$$k_L\alpha = 0.0068\left(\frac{P_g}{V_L}\right)^{0.55} V_{SG}^{0.25} \quad \text{applicable for } V_{SG}<0.005\text{m s}^{-1} \tag{J-16}$$

$$k_L\alpha = 0.00326\left(\frac{P_g}{V_L}\right)^{0.55} V_{SG}^{0.25} \quad \text{applicable for } V_{SG}>0.005\text{m s}^{-1} \tag{J-17}$$

However, the correlations of Joshi & Sharma were found to slightly under-predict results obtained by the experiments of Poncin et al. (2002) using a mechanically agitated reactor of 0.6 m internal diameter equipped with four baffles and gas-inducing impeller.

Using one of the equations (J-14) to (J-17) and the value of $k_L\alpha$ equal to 0.64 s^{-1}, the energy dissipation per unit of liquid volume $\left(\frac{P_g}{V_L}\right)$ can be calculated and subsequently the mass transfer coefficient can be determined from correlation (J-13).

APPENDIX K

Representative Photographs of Flow Patterns obtained in the 250 µm Capillary

Date of experiment	Liquid flow rate, µl/min (STP)	Ethylene flow rate, ml/min (STP)	CO flow rate, ml/min (STP)	Flow pattern	Photograph
23/10/07	5	0.6	0.2	Bubble train	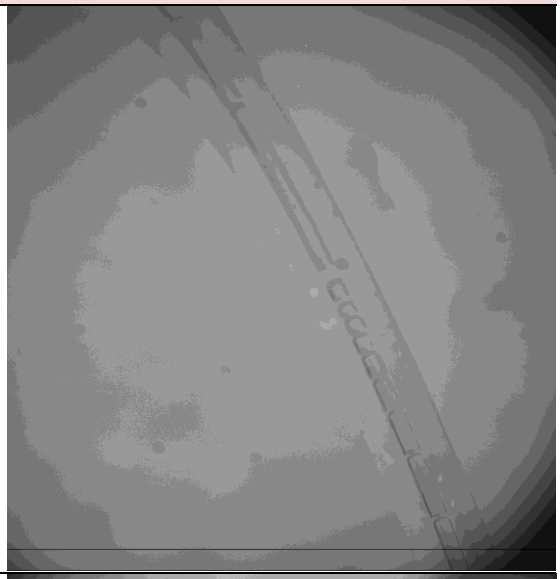
30/10/2007	5	0.45	0.15	Bubble train	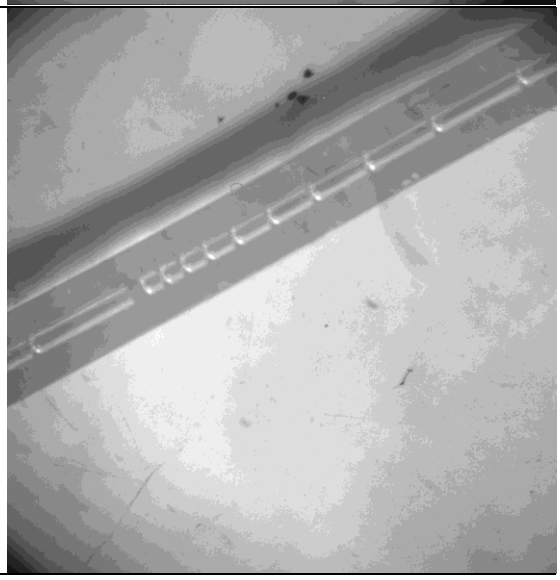

Date of experiment	Liquid flow rate, µl/min (STP)	Ethylene flow rate, ml/min (STP)	CO flow rate, ml/min (STP)	Flow pattern	Photograph
13/11/2007	5	0.15	0.05	Taylor flow	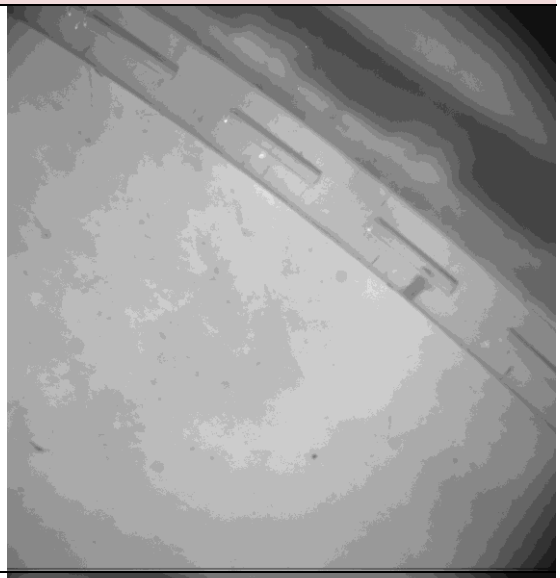
13/11/2007	5	0.12	0.04	Bubble train	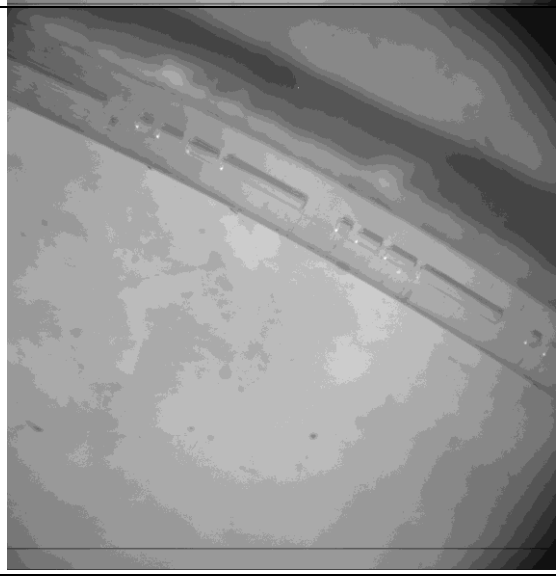

Date of experiment	Liquid flow rate, µl/min (STP)	Ethylene flow rate, ml/min (STP)	CO flow rate, ml/min (STP)	Flow pattern	Photograph
15/11/2007	5	0.8	0.08	Bubble train	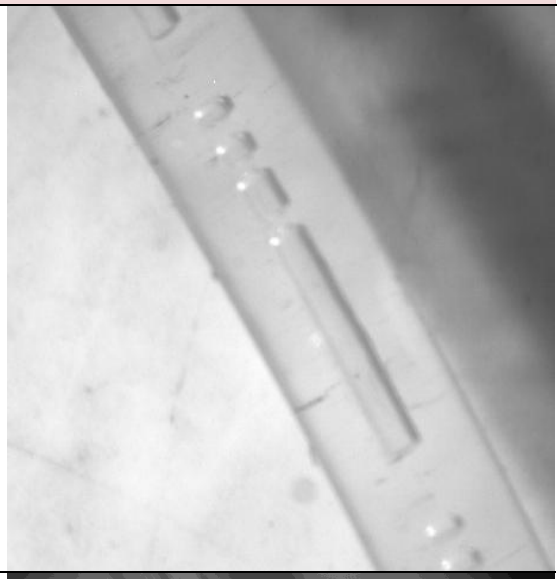
16/11/07	5	1.2	0.12	Bubble Train	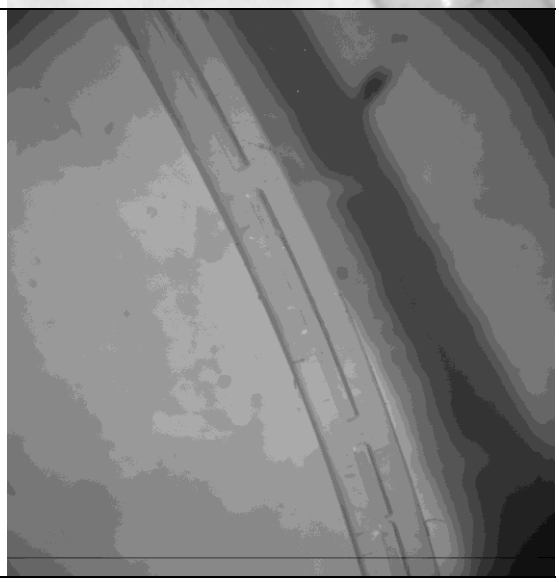

Date of experiment	Liquid flow rate, µl/min (STP)	Ethylene flow rate, ml/min (STP)	CO flow rate, ml/min (STP)	Flow pattern	Photograph
29/11/2007	5	0.5	0.05	Bubble train	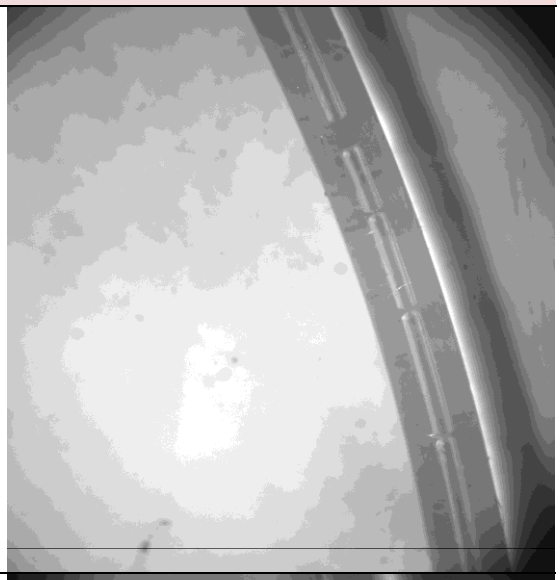
30/11/2007	5	1.0	0.1	Bubble train	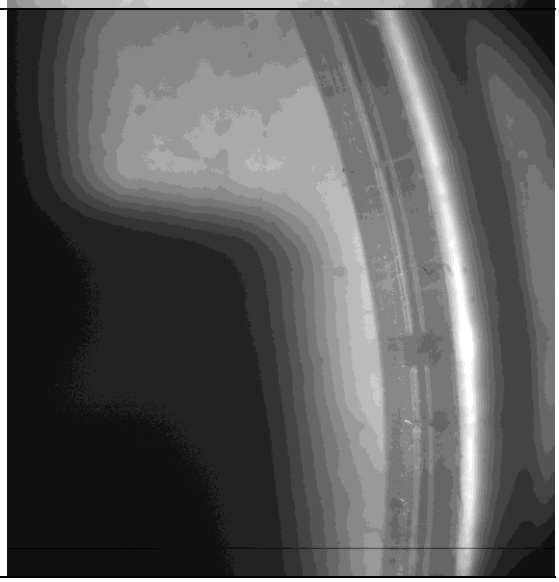

Date of experiment	Liquid flow rate, µl/min (STP)	Ethylene flow rate, ml/min (STP)	CO flow rate, ml/min (STP)	Flow pattern	Photograph
03/12/07	5	1.2	0.12	Bubble train	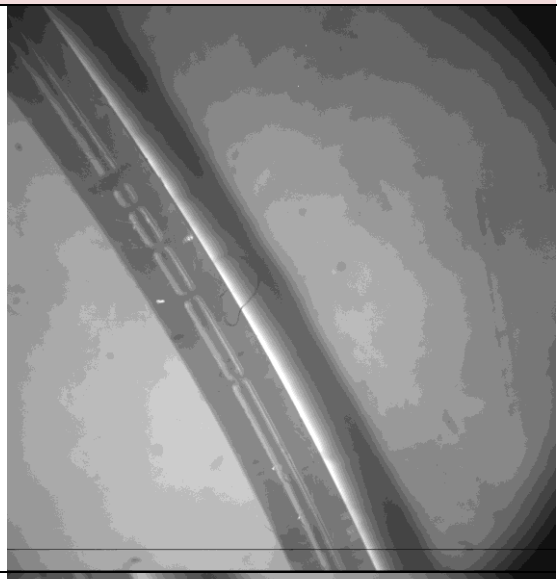
5/12/2007	5	1.0	0.1	Bubble train	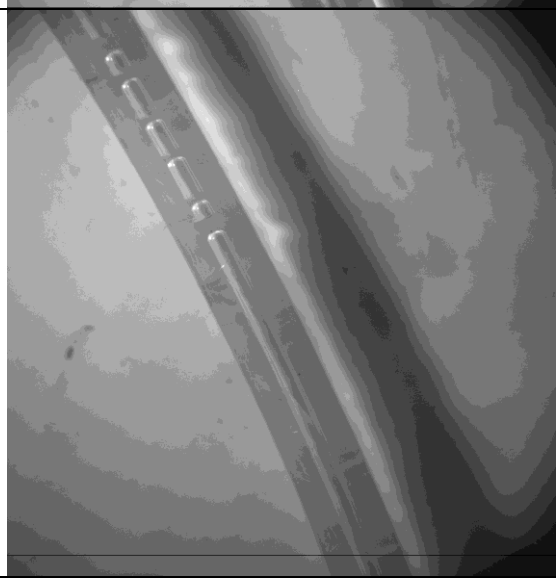

Date of experiment	Liquid flow rate, µl/min (STP)	Ethylene flow rate, ml/min (STP)	CO flow rate, ml/min (STP)	Flow pattern	Photograph
10/12/07	5	0.15	0.15	Bubble train	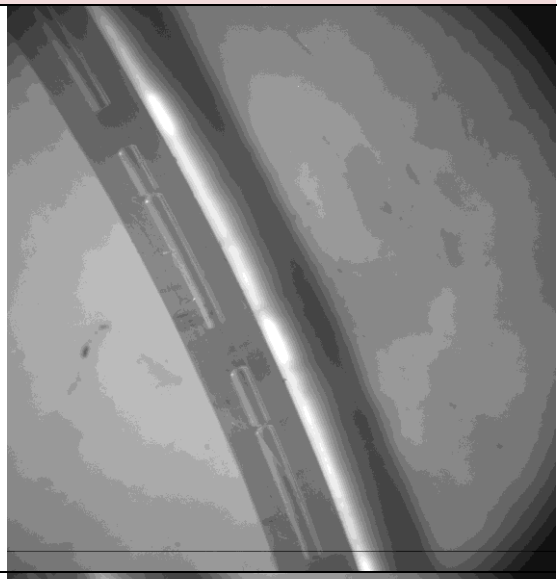
10/12/2007	5	0.1	0.1	Taylor flow but unstable	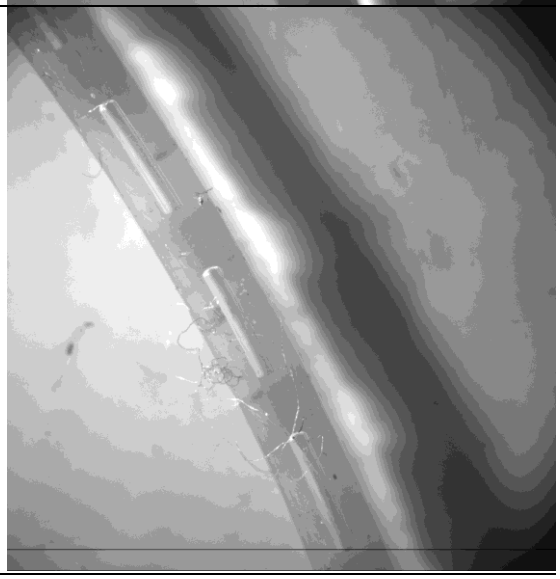

Date of experiment	Liquid flow rate, µl/min (STP)	Ethylene flow rate, ml/min (STP)	CO flow rate, ml/min (STP)	Flow pattern	Photograph
11/12/2007	5	0.2	0.2	Taylor flow	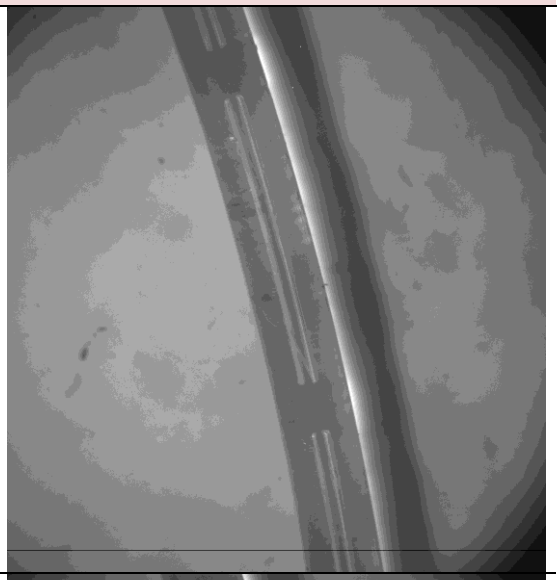
11/12/2007	5	0.174	0.174	Taylor flow	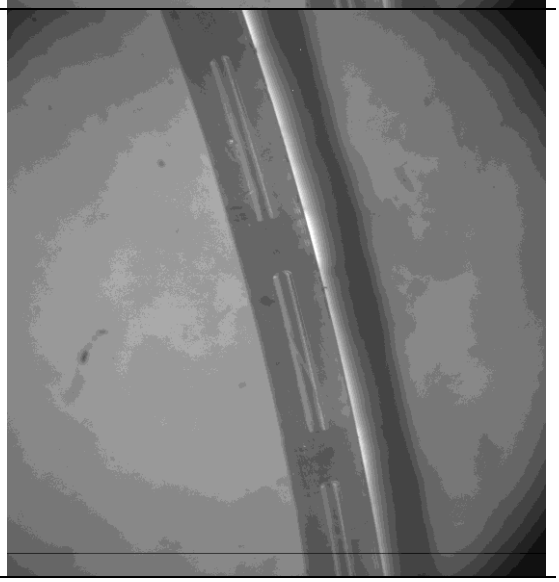

Date of experiment	Liquid flow rate, µl/min (STP)	Ethylene flow rate, ml/min (STP)	CO flow rate, ml/min (STP)	Flow pattern	Photograph
17/12/07	5	0.452	0.226	Taylor flow but unstable	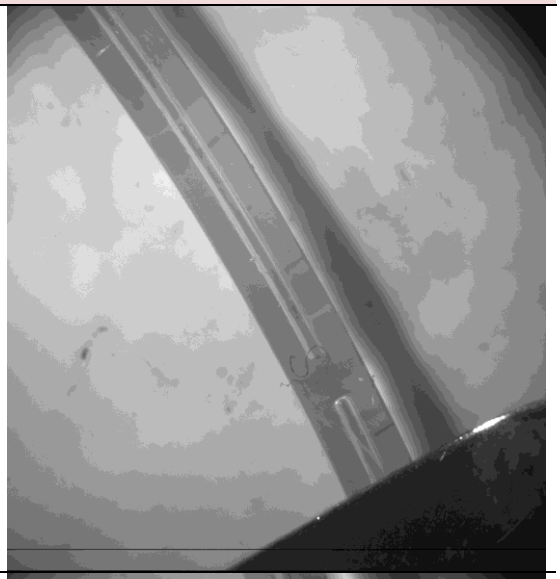
18/12/07	5	0.6	0.3	Bubble train	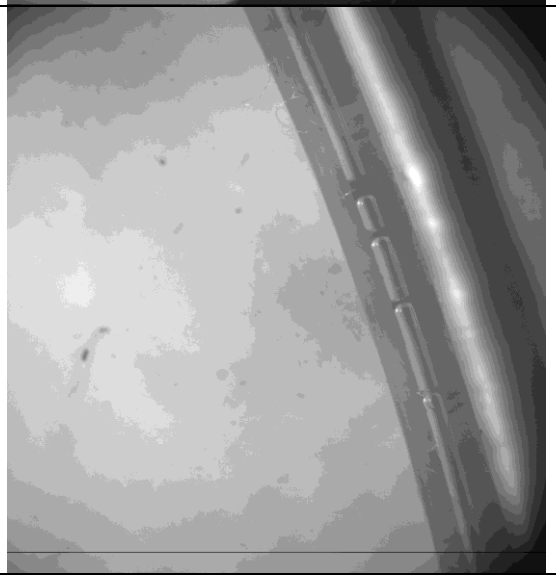

Date of experiment	Liquid flow rate, µl/min (STP)	Ethylene flow rate, ml/min (STP)	CO flow rate, ml/min (STP)	Flow pattern	Photograph
03/01/2008	5	0.21	0.07	Bubble train	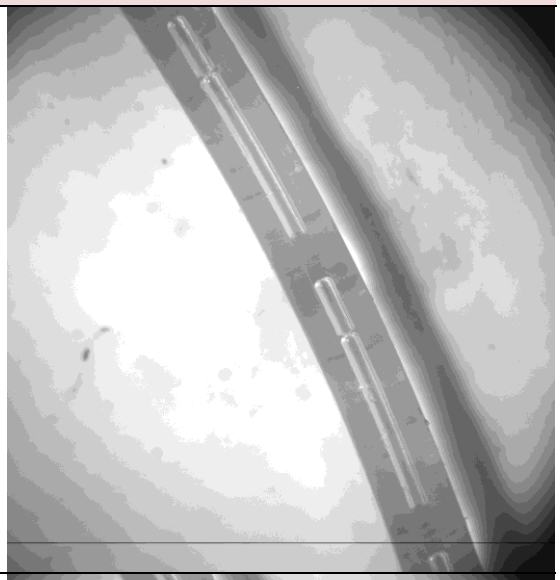
08/01/2008	5	0.24	0.08	Bubble train	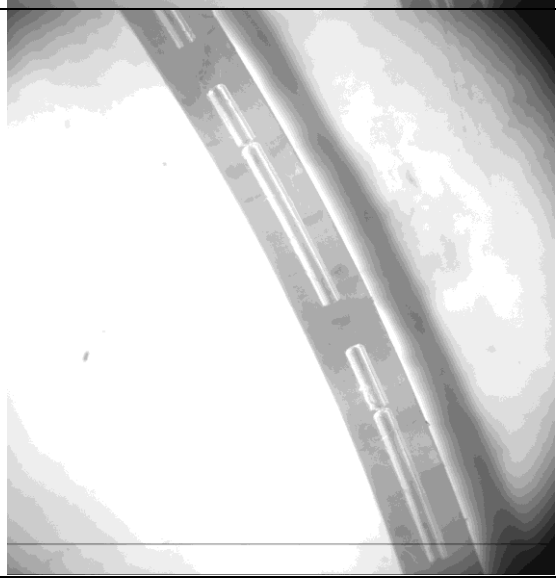

Date of experiment	Liquid flow rate, µl/min (STP)	Ethylene flow rate, ml/min (STP)	CO flow rate, ml/min (STP)	Flow pattern	Photograph
08/01/2008	5	0.36	0.12	Taylor flow	
08/01/2008	5	0.45	0.15	Bubble train	

Date of experiment	Liquid flow rate, µl/min (STP)	Ethylene flow rate, ml/min (STP)	CO flow rate, ml/min (STP)	Flow pattern	Photograph
10/01/2008	5	0.5	0.1	Bubble train	
11/01/2008	5	0.6	0.12	Bubble train	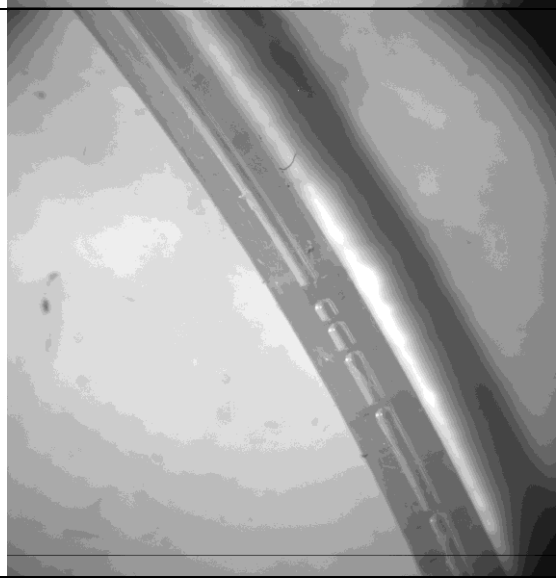

Date of experiment	Liquid flow rate, µl/min (STP)	Ethylene flow rate, ml/min (STP)	CO flow rate, ml/min (STP)	Flow pattern	Photograph
14/01/2008	5	0.75	0.15	Bubble train	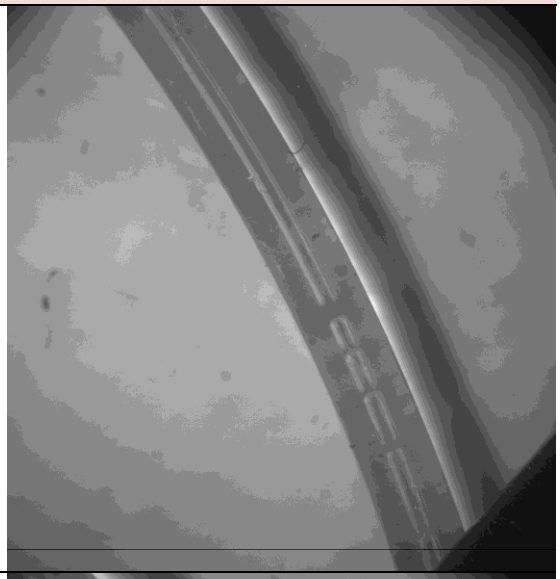
15/01/2008	5	0.1	0.2	Bubble train	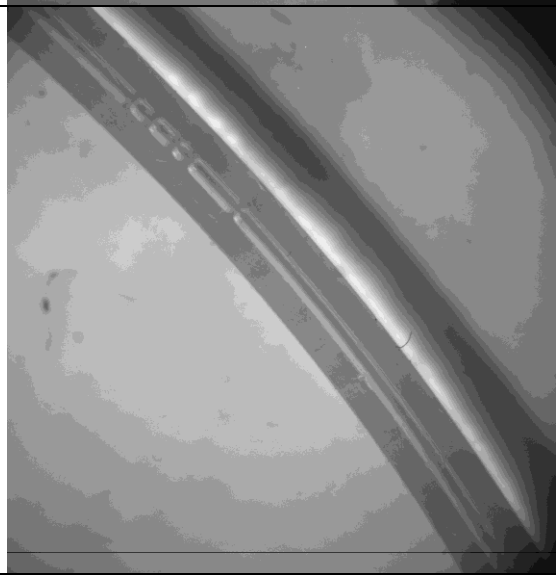

Date of experiment	Liquid flow rate, µl/min (STP)	Ethylene flow rate, ml/min (STP)	CO flow rate, ml/min (STP)	Flow pattern	Photograph
11/04/2008	5	0.2	0.7	Bubble train	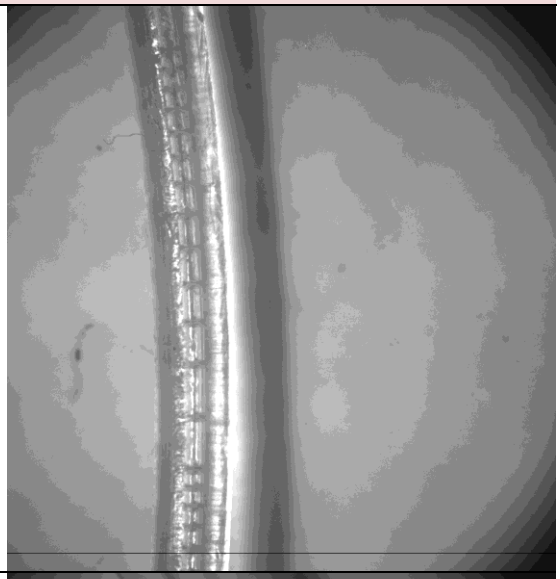
15/04/2008	5	0.05	0.7	Bubble train	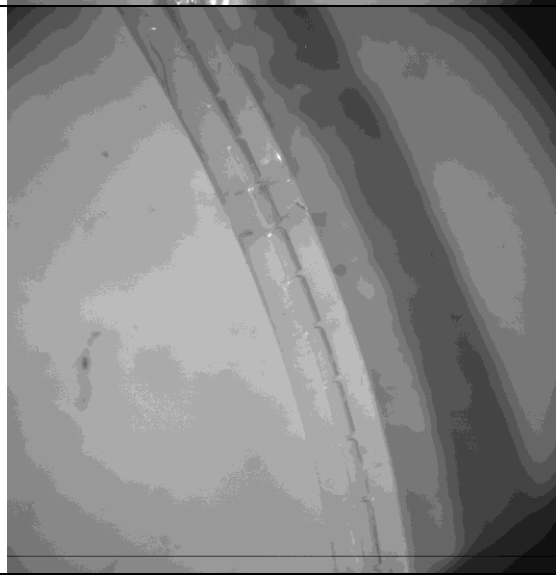

Date of experiment	Liquid flow rate, µl/min (STP)	Ethylene flow rate, ml/min (STP)	CO flow rate, ml/min (STP)	Flow pattern	Photograph
15/04/2008	5	0.426	0.21	Bubble train	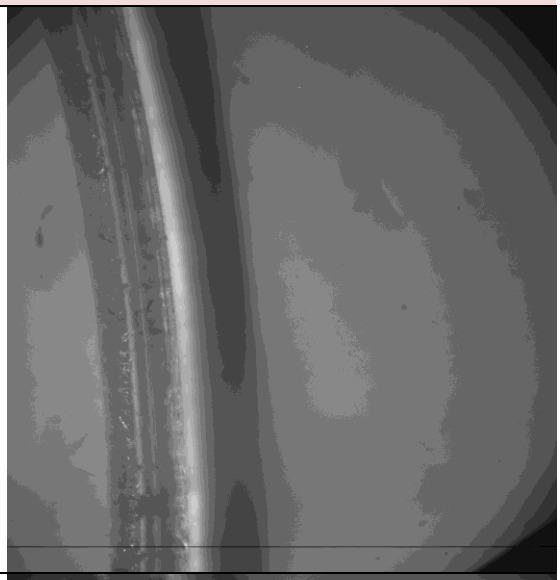
17/04/2008	5	0.1	0.65	Taylor flow	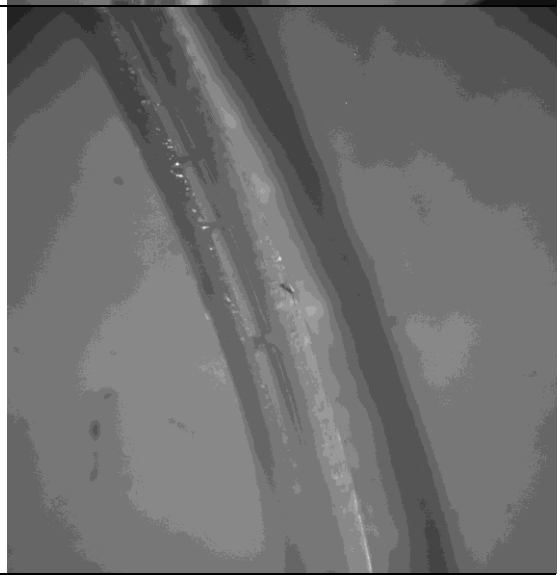

Date of experiment	Liquid flow rate, µl/min (STP)	Ethylene flow rate, ml/min (STP)	CO flow rate, ml/min (STP)	Flow pattern	Photograph
22/04/2008	5	0.25	0.524	Bubble train	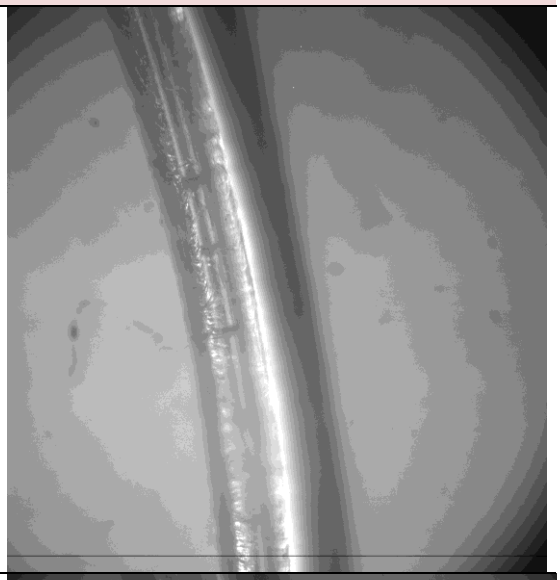
25/04/2008	5	0.7	0.04	Bubble train	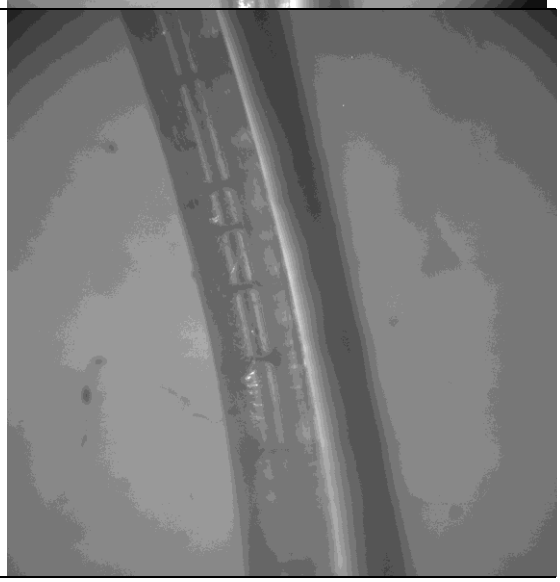

Date of experiment	Liquid flow rate, µl/min (STP)	Ethylene flow rate, ml/min (STP)	CO flow rate, ml/min (STP)	Flow pattern	Photograph
29/04/2008	5	0.188	0.350	Bubble train	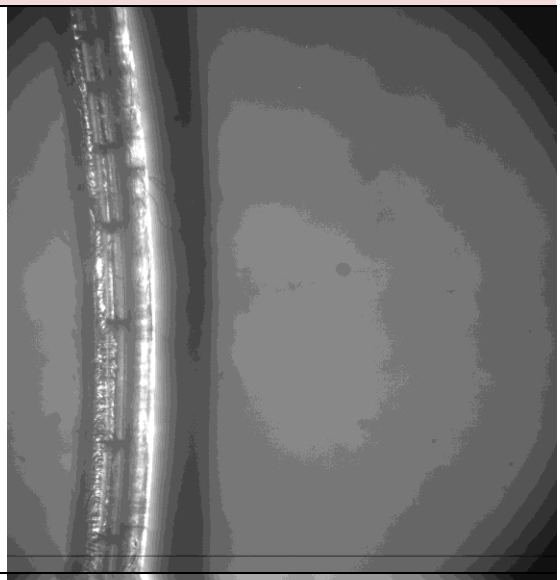
02/05/2008	5	0.588	0.1	Bubble train	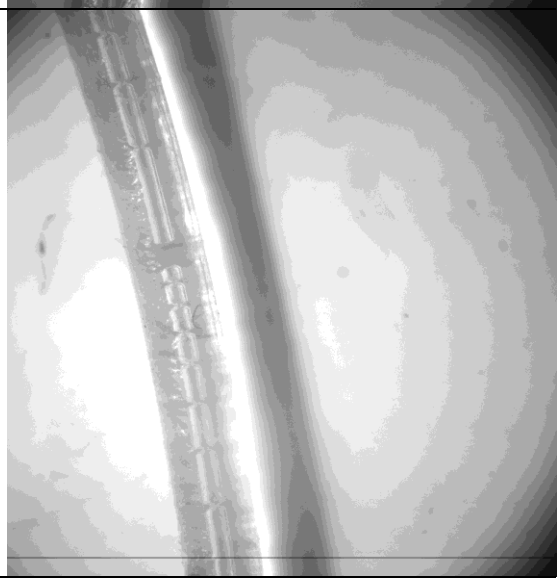

Date of experiment	Liquid flow rate, µl/min (STP)	Ethylene flow rate, ml/min (STP)	CO flow rate, ml/min (STP)	Flow pattern	Photograph
15/04/2008	5	0.426	0.21	Bubble train	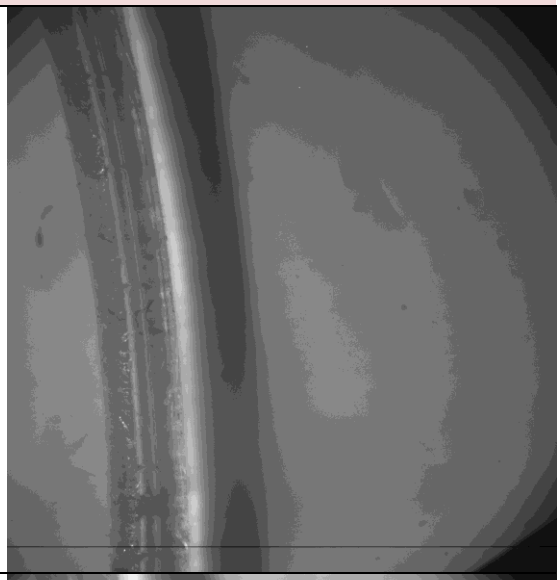
16/05/2008	5	0.39	0.24	Bubble train	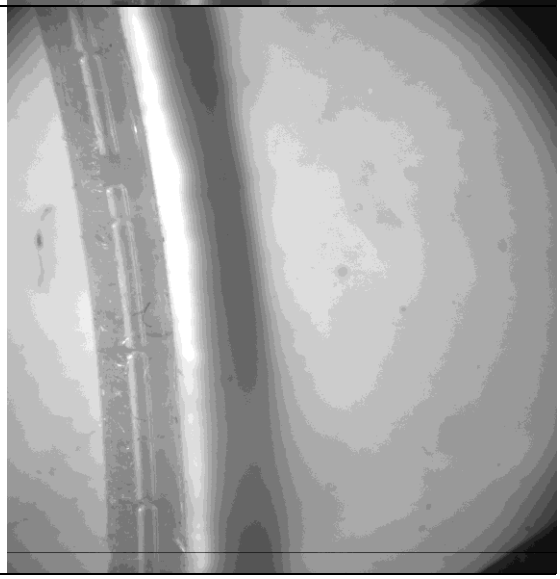

Date of experiment	Liquid flow rate, µl/min (STP)	Ethylene flow rate, ml/min (STP)	CO flow rate, ml/min (STP)	Flow pattern	Photograph
19/05/2008	5	0.354	0.27	Bubble train	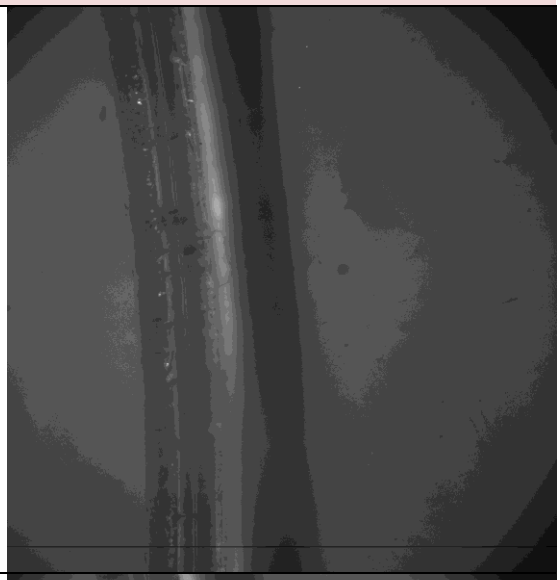
22/05/08	5	0.354	0.27	Bubble train	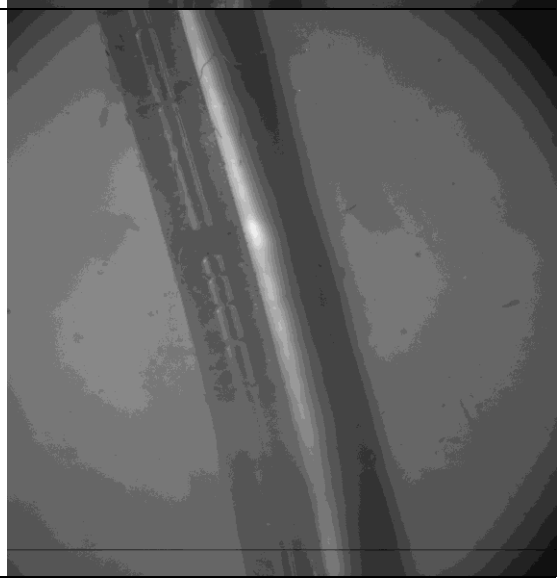

Date of experiment	Liquid flow rate, µl/min (STP)	Ethylene flow rate, ml/min (STP)	CO flow rate, ml/min (STP)	Flow pattern	Photograph
06/06/08	5	0.522	0.13	Bubble train	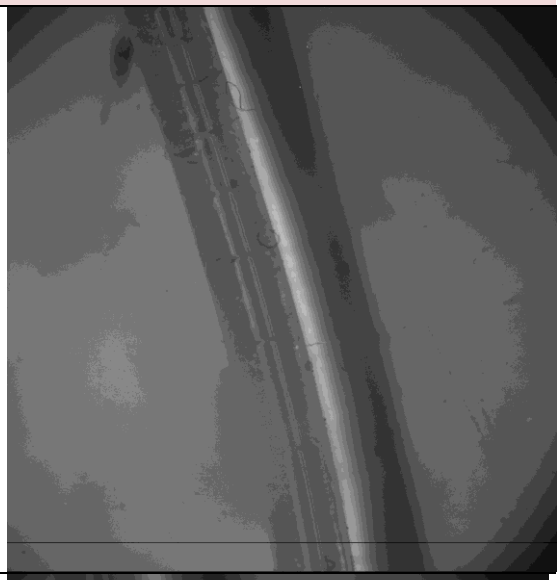
09/06/2008	5	0.9	0.1	Bubble train	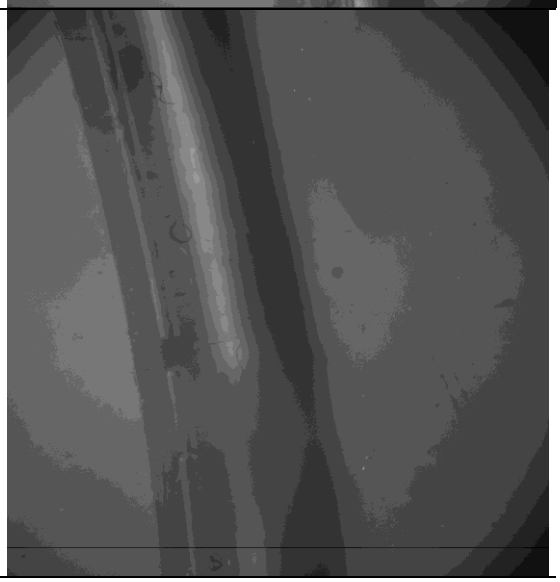

Date of experiment	Liquid flow rate, µl/min (STP)	Ethylene flow rate, ml/min (STP)	CO flow rate, ml/min (STP)	Flow pattern	Photograph
10/06/2008	5	0.9	0.1	Bubble train	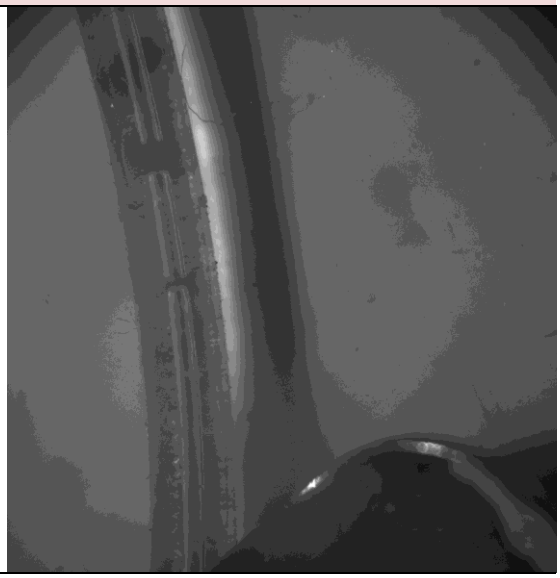

References

1. Abdallah, R ., Magnico, P., Fumey, B. and de Bellefon, C. (2006) CFD and kinetic methods for mass transfer determination in a mesh microreactor. *AIChe*, 52 (6), 2230-2237.

2. Abdallah, R., Meille, V., Shaw, J., Wenn, D. and de Bellefon, C. (2004) Gas-liquid and gas-liquid-solid catalysis in a mesh microreactor. *Chemical Communications*, 2004 (4), 372-373.

3. Abiev, R. Sh. (2010) Method for calculating the void fraction and relative length of bbbles under slug flow in capillaries. *Theoretical Foundations of Chemical Engineering*, 44 (1), 86-101.

4. Akbar, M. K. and Ghiaasiaan S. M. (2006) Simulation of Taylor flow in capillaries based on the volume-of-fluid technique. *Industrial Engineering Chemistry Research*, 45 (15), 5396-5403.

5. Akbar, M. K., Plummer, D. A. and Ghiaasiaan, S. M. (2003) On gas-liquid two-phase flow regimes in microchannels. *International Journal of Multiphase Flow*, 29 (5), 855-865.

6. Amador C., Salman, W., Sanguanpiyapan, S., Gavriilidis, A. and Angeli, P. (2004) Effect of gas-liquid inlet conditions on slug length in Taylor flow. *Proceedings of the 5th International Conference on Multiphase Flow, Japan, 2004*.

7. Angeli, P., and Gavriilidis, A. (2008) Hydrodynamics of Taylor flow in small channels: a review. *Proc. IMechE, Vol. 222, Part C: J. Mechanical Engineering Science*, 737-751.

8. Aussilous P., and Quéré, D. (2000) Quick deposition of a fluid on a wall of a tube. *Physical Fluids*, 12 (10), 2367-2371.

9. Barnard C. F. (2008) Palladium-Catalyzed Carbonylation- A reaction Come of Age. *Organometallics*, 27 (21), 5402-5422.

10. Basheer, C., Shahitha Jahir Hussain, F., Kee Lee, H. and Valiyaveettil S. (2004) Design of a capillary-microreactor for efficient Suzuki coupling reactions. *Tethahedron Letters*, 45 (39), 729-730.

11. Beller, M., Cornils, B., Frohning, C. D., Kohlpaintner, C. W. (1995) Progress in hydroformylation and carbonylation. *Journal of Molecular Catalysis A*: 104, 17-85.

12. Bendiksen, K. H. (1984) An experimental investigation on the motion of long bubbles in inclined tubes. *International Journal of Multiphase Flow*, 10 (4), 467-483.

13. Bendiksen, K. H. (1985) On the motion of long bubbles in vertical tubes. *International Journal of Multiphase Flow*, 11 (6), 797-812.

14. Benedeck, C., Toros, S. and Heil, B. (1999) Comparative investigation of the regioselectivity instyrene and *a*-methylstyrene hydroalkoxycarbonylation as a function of palladium catalyst structure. *Journal of Organometallic Chemistry*, 586 (1), 85-93.

15. Bercic, G. and Pintar, A. (1997) The role of gas bubbles and liquid slug lengths on mass transport in Taylor flow through capillaries. *Chemical Engineering Science*, 52 (21-22), 3709-3719.

16. Brennfuhrer, A., Neumann, H. and Beller, M. (2009) Palladium Catalyzed Carbonylation Reactions of Alkenes and Alkynes. *Chem Cat Chem*, 2009, 1 (1), 28-41.

17. Bretherton, F. P. (1961) The motion of long bubbles in tubes. *Journal of Fluid Mechanics*, 10 (2), 166-188.

18. Calderbank, P. H. (1959) Physical rate processes in industrial fermentation 2. Mass transfer coefficients in gas-liquid contacting with and without mechanical agitation. *Chemistry and Industry*, (9), 284-284.

19. Calderbank, P. H. (1961) The interfacial area in gas-liquid contacting with mechanical agitation. *Transactions of the Institution of Chemical Engineers*, 39, 337-347.

20. Cavinato, G., Vavasori, A., Toniolo, L. and Dolmella, A. 'Synthesis, characterization and catalytic activity in the carbonylation of ethene of $cis-[Pd(H_2O)_2(PPh_3)_2]X_2 \cdot nH_2O$ $(X = p-CH_3C_6H_4SO_3, n=2; X = CH_3SO_3, n=0)$.X-ray structure of $cis-[Pd(H_2O)_2(PPh_3)_2](p-CH_3C_6H_4SO_3)_2 \cdot 2H_2O$ and of $cis-[Pd(H_2O)_2(PPh_3)_2](CH_3SO_3)_2 \cdot 2CH_2Cl_2$. *Inorganica Chimica Acta*, 357 (9) 2004, 2737-2747.

21. Cavinato, G., Toniolo, L. and Vavasori, A. (2004) Characterization and catalytic activity of $trans-[Pd(COCH_2CH_3)(TsO)(PPh_3)_2]$ isolated from the hydro-methoxycarbonylation of ethene catalyzed by $[Pd(TsO)_2(PPh_3)_2]$. *Journal of Molecular Catalysis A: Chemical*, 219 (2), 233-240.

22. Chambers R. D. and Spink R. C. H. (1999) Microreactors for elemental fluorine. *Chemical Communications*, (10), 883-884.

23. Chaudhari, R.V. and Gholap, R.V. (1987) Gas-Liquid Mass Transfer in Dead-End Autoclave Reactors. *The Canadian Journal of Chemical Engineering*, 65 (5), 744-751.

24. Chaudhari, R.V., Seayad, A., Jayasree, S. (2001) Kinetic modeling of homogeneous catalytic processes. *Catalysis Today*, 66 (2-4), 371-380.

25. Chen, W. L., Twu, M. C. and Pan, C. (2002) Gas-liquid two-phase flow in microchannels. *International Journal of Multiphase flow*, 28 (7), 1235-1247.

26. Chen, G. W., Yue, J. And Yuan, Q. (2008) Gas-liquid Microreaction technology: Recent developments and future challenges. *Chinese Journal of Chemical Engineering*, 16 (5), 663-669.

27. Chiusoli, G. P. (1991) Advances in catalytic carbonylation with transition metal complexes in homogeneous phase. *Transition Metal Chemistry*, 16 (6), 553-564.

28. Clegg, W., Eastham, G. R., Elsegood, M. R. J., Tooze, R. P., Lan Wang, X. and Whiston, K. (1999) Highly active and selective catalysts for the production of methyl propanoate via the methoxycarbonylation of ethene. *Chemical Communications*, (18), 1877-1878.

29. Clegg, W., Eastham, G. R., Elsewood, M. R. J., Heaton, B. T., Iggo, J.A., Tooze, R.P., Whyman, R. and Zacchini, S. (2002) Synthesis and reactivity of palladium hydro-solvento complexes, including a key intermediate in the catalytic methoxycarbonylation of ethene to methylpropionate. *Journal of Chemical Society Dalton Transactions*, 3300-3308.

30. Clegg, W., Eastham, G. R., Elsegood, M. R. J., Heaton, B.T., Iggo, J. A., Tooze, P. R., Whyman, R., Zacchini, S. (2002a) Characterization and

Dynamics of $[Pd(L-L)H(solv)]^+, [Pd(L-L)CH_2CH_3]^+, [Pd(L-L)C(OEt)(THF)]^+$ $L-L = 1,2-(CH_2PBu^t_2)_2C_6H_4$: Key Intermediates in the Catalytic Methoxycarbonylation of Ethene to Methylpropanoate. *Organometallics*, 21 (9), 1832-1840.

31. Chisholm, D. (1967) A theoretical basis for the Lockhart-Martinelli correction for two-phase flow. *International Journal Heat Mass Transfer*, 10 (12), 1767-1778.

32. Cox, B. G. (1964) An experimental investigation of the streamlines in viscous fluid expelled from a tube. *Journal of Fluid Mechanics*, 20 (2), 193-200.

33. Collins, R., de Moraes, F. F., Davidson J. F. and D. Harrison (1978) The motion of large bubbles rising through liquid flowing in a tube. *Journal of Fluid Mechanics*, 89 (3), 487-514.

34. Dai, L., Cai, W., Xin, F. (2009) Numerical Study on Bubble Formation of a Gas-Liquid Flow in a T-Junction Microchannel. *Chemical Engineering Technology*, 32 (12), 1984-1991.

35. de Bellefon, C., Pestre, N., Lamouille, T., Grenouillet, P., Hessel, V. (2003) High Throughput Kinetic Investigations of Asymmetric Hydrogenations with Microdevices. *Advanced Synthesis and Catalysis*, 345 (1-2), 190-193.

36. Deshpande, R. M., Chaudhari, R.V. (1988) Kinetics of Hydroformylation of 1-hexene using homogeneous HRH(CO)$(PPH3)_3$ complex catalyst. *Industrial and Engineering Chemical Research*, 27 (11), 1996-2002.

37. Divekar, S. S., Deshpande, R. M., Chaudhari, R.V. (1993) Kinetics of Hydroformylation of 1-decene using homogeneous $HRH(CO)(PPH_3)_3$ catalyst-A molecular level approach. *Catalysis Letters*, 21 (1-2), 191-200.

38. Dudokovic, M.P., Larachi, F., Mills, P. L. (2002) Multiphase catalytic reactors: Multiphase catalytic reactors: A perspective on current knowledge and future trends. *Catalysis Reviews – Science and Engineering*, 44 (1), 123-246.

39. Dummann, G., Quittmann, U., L. Gröschel, L., Agar, D.W., Wörz O. and Morgenschweis, K. (2003) The capillary-microreactor: a new reactor concept for the intensification of heat and mass transfer in liquid-liquid reactions. *Catalysis Today*, 79-80, 433-439.

40. Eastham, G. R., Heaton, B.T., Iggo, J.A., Tooze, R. P., Whyman, R., Zacchini, S. (2000) Synthesis and spectroscopic characterisation of all the intermediates in the Pd-catalysed methoxycarbonylation of ethene. *Chemical Communications*, (7), 609-610.

41. Eastham, G. R., Tooze, G. R., Kilner, M., Foster, D. F., Cole-Hamilton, D. J. (2002) Deuterium Labelling evidence for a hydride mechanism in the formation of methyl propanoate from carbon monoxide, ethene and methanol catalysed by a palladium complex. *Journal Chemical Society, Dalton Transactions*, (8), 1613-1617.

42. Edvinsson, R. K., Irandoust, S., (1996) Finite-element analysis of Taylor flow. *AICHE JOURNAL*, 42 (7), 1815-1823.

43. Enache, D. I., Hutchings, G. J., Taylor, S. H., Natividad, R., Raymahasay, S., Winterbottom, J.M., Stitt, E. H. (2005) Experimental Evaluation of a Three-

Phase Downflow Capillary Reactor. *Industrial Engineering Chemical Research*, 44 (16), 6295-6303.

44. Enright T.E. and Cunningham M. F., Keoshkerian, B. (2005) Direct fluorination of toluene using elemental fluorine in gas/liquid microreactors. *Macromolecular Rapid Communications*, 2005, 26 (4), 221-225.

45. Fairbrother F. and Stubbs, A. E. (1935) Studies in electro-endosmosis Part VI: The "bubble-tube" method of measurement. *Journal of Chemical Society*, 1, 527-529.

46. Fries, D. M and von Rohr, P. R. (2009) Impact of inlet design of mass transfer in gas-liquid rectangular microchannels. *Microfluid Nanofluid*, 6, 27-35.

47. Fu, T., Ma, Y. Funfschilling, D., Li, H. Z. (2009) Bubble formation and break-up mechanism in a microfluidic flow-focusing device. *Chemical Engineering Science*, 64 (10), 2392-2400.

48. Fukano, T. Kariyasaki, A (1993) Characteristics of gas-liquid 2-phase flow in a capillary-tube. *Nuclear Engineering and Design*, 141 (1-2), 59-68.

49. Garcia-Ochoa, F. and Gomez, E. (2004) Theoretical prediction of gas-liquid mass transfer coefficient, specific area and hold-up in sparged stirred tanks. *Chemical Engineering Science*, 59 (12), 2489-2501.

50. Garstecki, P., Fuerstman, M.T., Stone, H. A., Whitesides, G. M. (2006) Formation of droplets and bubbles in a microfluidic T-junction –scaling and mechanism of break-up. *Lab on a Chip*, 6 (3), 437-446.

51. Gavino, R., Pellegrini, S., Castanet, Y., Mortreux, A., Mentre, O. (2001) CO pressure as a key factor for the palladium catalysed methoxycarbonylation

of benzyl chloride under mild conditions. *Applied catalysis A:General*, 217 (1-2), 91-99.

52. Giavetoni M. D. and Saita, F. A. (1997) The axisymmetric and plane case of a gas phase steadily displacing a Newtonian liquid- a simultaneous solution to the governing equations. *Physical Fluids*, 9 (8), 2420-2428.

53. Gielens, F.C., Tong, H. D., Van Rijn, C. J. M., Vorstman, M. A. G., Keurentjes, J. T. F. (2002) High-flux palladium-silver alloy membranes fabricated by microsystem technology. *Desalination*, 147 (1-3), 417-423.

54. Gielens, F. C., Tong, H. D., van Rijn, C. J. M., Vorstman, M. A. G., Keurentjes, J. T. F. (2004) Microsystem technology for high-flux hydrogen separation membranes. *Journal of Membrane Science*, 243 (1-2), 203-213.

55. Grolman, E., Commandeur, N.C.J., deBaat, E.C. (1996) Wavy to slug flow transition in slightly inclines gas-liquid pipe flow. *AICHE JOURNAL*, 42 (4), 901-909.

56. Guangwen, C., Jun Y. and Quan, Y. (2008) Gas-Liquid Microreactor Technology: Recent Development and Future Challenges. *Chinese Journal of Chemical Engineering*, 16 (5), 663-669.

57. Haverkamp, V., Hessel, V., Lowe, H., Menzes, G., Warnnier, M. J. F., Rebrov, E., de Croon, M., Shouten, J. C., Liauw, M. A. (2006) Hydrodymanics and mixer-induced bubble formation in mico bubble columns with single and multiple channels. *Chemical Engineering Technology*, 29 (9), 1015-1026.

58. .Heiszwolf, R., Kreutzer, M. T., van den Eijnden, M. G., Kapteijn, F., Moulijn, J. A. (2001) Mass transfer of Taylor flow in momoliths. *Catalysis Today*, 69 (1-4), 51-55.

59. Hessel, V., Angeli, P., Gavriilidis, A. and Lowe, H. (2005) Gas-Liquid and Gas-Liquid Solid Microstructured Reactors: Contacting Principles and Applications. *Industrial Engineering Chemical Research*, 44 (25), 9750-9769.

60. Ming Hsing, I., Srinivasan, R., Harold, M. P., Jensen, K. F., Schmidt, M. A. (2000) Simulation of micromachined chemical reactors for heterogeneous partial oxidation reactions. *Chemical Engineering Science*, 55 (1), 3-13.

61. Irandoust, S., B. Andersson, B. (1989) Liquid film in Taylor flow through a capillary. *Industrial and Engineering Chemistry Research*, 28 (11), 1684-1688.

62. Jähnisch, K., Baerns, M., Hessel, V., Ehrfeld, W., Haverkamp, V., Löwe, H., Wille, Ch. and Guber. A. (2005) Direct fluorination of toluene using elemental fluorine in gas/liquid microreactors. *Journal of Fluorine Chemistry*, 2000, 105 (1), 117-128.

63. Jauregui-Haza, U. J., Pardillo-Fontdevila, E., Kalck, Ph., Wilhelm, A.M., Delmas, H. (2003) Supported aqueous phase catalysis: a new kinetic model of hydroformylation of octane in gas-liquid-liquid-solid system. *Catalysis Today*, 79-80, 409-417.

64. Jimenez Rodriguez, C., Foster, D. F., Eastham, G. R., Cole-Hamilton, D. J. (2004) Highly selective formation of linear estersfrom terminal and internal alkenes catalysed by Pd complexes of bis-(di-tert-butylphosphinomethyl)benzene, *Chemical Communications*, (15), 1720-1721.

65. Joshi, J. B.; Sharma, M. M. (1977) Mass transfer and hydrodynamics characteristics of gas inducing type of agitated contactors. *Canadian Journal of Chemical Engineering*, 55 (6), 683-695.

66. Kapic A. and Heindel, T.J (2006) Correlating Gas-Liquid Mass Transfer in a Stirred-Tank Reactor. *Chemical Engineering Research and Design*, 84 (3), 239-245.

67. Knight, J. G., Doherty, S., Harriman, A., Robins, E. G., Betham, M., Eastham, G. R., Tooze, R. P., Elsegood, M. R. J., Champkin, P., Clegg, W. (2000) Remarkable differences in catalyst activity and selectivity for the production of Methyl Propanoate versus CO-Ethylene Copolymer by a series of Palladium complexes of related C_4-bridged diphosphines. *Organometallics*, 19 (24), 4957-4967.

68. Kiss, G. (2001) Palladium catalysed Reppe Carbonylation. *Chemical Reviews*, 101 (11), 3435-3456.

69. Kiss, G., Mozeleski, E. J., Nadler, K. C., Van Driessche, E., De Roover, C. (1999) Hydroformylation of ethene with triphenylphosphine modified rhodium catalysts:kinetc and mechanistic study. *Catalysis A: Chemical* 138 (2-3), 155-176.

70. Kiwi-Minsker, L. and Renken, A. (2005) Microstructured reactions for catalytic reactions. *Catalysis Today*, 110 (1-2), 2–14.

71. Knifton, J. F. (1976) Linear carboxylic acid esters from *a*-olefins 2. Catalysis by homogeneous palladium complexes. *Journal of Organic Chemistry*, 41 (17), 2885-2890

72. Kreutzer, M. T. (2003) Hydrodynamics of Taylor in capillaries and monolith reactors. *PhD Thesis, Technical University of Delft*, 2003.

73. Kreutzer, M. T., Kapteijn, F., Moulijn, J. A., Kleijn, C.R., Heiszwolf, J. J. (2005a) Inertial and interfacial effects on pressure drop of Taylor flow in capillaries. *AIChEJ*, 51 (9), 2428-2440.

74. Kreutzer, M. T., Bakker, J. J. W., Kapteijn, F., Moulijn, J. A., Verheijen, P. J. T., (2005b) Scaling-up multiphase monolith reactors: linking residence time distribution and feed maldistribution. *Industrial and Engineering Chemistry Research*, 44 (14), 4898-4913.

75. Kreutzer, M. T., Bakker , J. J. W., Kapteijn, F., Moulijn, J. Heiszwolf, , J. J. (2005c) Multiphase monolith reactors: chemical reaction engineering of segmented flow in microchannels. *Chemical Engineering Science*, 60 (21), 5895-5916.

76. Kuiper, S., van Rijn, C. J. M., Nijdam, W., Elwenspoek, M.C. (1998) Development and applications of very high flux microfiltration membranes. *Journal of membrane Science*, 150 (1), 1-8.

77. Kuiper, S., Brink, R., Nijdam W., Krijnen, G. J. M., Elwenspoek, M. C. (2002) Ceramic microsieves: influence of perforation shape and distribution on flow resistance and membrane strength. *Journal of Membrane Science*, 196 (2), 149-157.

78. Kulkarni, A. A., Gorasia, A. K., Ranade V. V. (2007) Hydrodynamics and liquid phase residence time distribution in a mesh microreactor. *Chemical Engineering Science*, 62 (24), 7484-7493.

79. Kumar, V. S., Vashisth, Y., Hoarau and Nigam, K. D. P. (2007) Slug flow in curved microreactors: Hydrodynamics study', *Chemical Engineering Science*, 26 (24), 7494-7504.

80. Laborie, S., Cabassud, C., Durand-Bourlier, L., Lainé, J. M. (1999) Characterisation of gas-liquid two-phase flow inside capillaries. *Chemical Engineering Science*, 54 (23), 5723-5735.

81. Lente G., L., Bazsa G., Fabian I., (2007) What is and what isn't a clock reaction? *New Journal of Chemistry*, 31 (10), 1707-1707.

82. Lebens, P. J. M., van der Meijden, R, Edvinsson, R. K. (1997) Hydrodynamics of gas liquid countercurrent flow in internally finned monolithic structures. *Chemical Engineering Science*, 52 (21-22), 3893-3899.

83. Lemoine, R. and Morsi, B. I. (2005) Hydrodynamics and Mass Transfer in Agitated Reactors Part II: Gas-Hold, Volumetric Mass Transfer Coefficients, Gas-Liquid Interfacial Areas and Liquid Side Mass Transfer Coefficients. *International Journal of Chemical Engineering*, 3, A20.

84. Linek, V., Moucha, T., Prokopova E. and Rejl, J. F. (2005) Simultaneous determination of vapour- and liquid- side volumetric mass transfer coefficients in distillation column. *Chemical Research and Design*, 83 (A8), 979-986.

85. Liu, S. Fukuyama, T., Sato, M. and Ryu, I. (2004) Continuous Microflow Synthesis of Butyl Cinnamate by a Mizoroki−Heck Reaction Using a Low-Viscosity Ionic Liquid as the Recycling Reaction Mediu. *Organic Process Research & Development*, 8 (3), 477-481.

86. Liu, H., Vandu, C.O., Krishna, R. (2005) Hydrodynamics of Taylor flow in vertical capillaries: Flow regimes, Bubble rise velocity, Liquid slug length, and Pressure drop. Industrial Engineering Chemistry Research, 44 (14), 4884-4897.

87. Mantle, M. D., Sederman, A. J., Gladden L.F, Raymahasay, S., Winterbottom, J.M. AND Stitt, E. H. (2002) Dynamic MRI Visualisation of two-phase phase flow in a ceramic monolith, *AICHE JOURNAL*, 48 (4), 909-912.

88. Marchessault, R. N. and Mason, S. G. (1986) Flow of entrapped bubbles inside a capillary. *Journal of Colloid Interface Science*, 109 (7), 341-349.

89. Mason, B. P., Price, K. E., Steinbacher, J. L., Bogdan, A. R., and Tyler McQuade, D. (2007) Greener Approaches to Organic Synthesis using Microrecator Technology. *Chemical Reviews*, 107 (5), 2300-2318.

90. Meille, V., Pestre, N., Fongarland, P., de Bellefon, C. (2004) Gas/Liquid Mass Transfer in Small Laboratory Batch Reactors: Comparison of Methods. *Industrial Engineering Chemical Research*, 2004 (4), 43, 924-927.

91. Menech, M.D., Gastercki, C. P., Jousse, F., Stone, A. (2008) Transition from squeezing to dripping in a microfluidic T-shaped junction. *Journal of Fluid Mechanics*, 595, 141-161.

92. Milles, P. L., Quiram D. J. and Ryley, J. F. (2007) Microreactor technology and process miniaturization for catalytic reactions-A perspective on recent developments and emerging technologies. *Chemical Engineering Science*, 62 (24), 6992-7010.

93. Mishima, K. and Hibiki, T. (1996) Some characteristics of air-water two-phase flow in small diameter vertical tubes. *International Journal of Multiphase Flow*, 22 (4), 703-712.

94. Morimoto, T. and Kakiuchi, K. (2004) Evolution of Carbonylation Catalysis: No Need for Carbon Monoxide. *Angewandte Chemie International Edition*, 43 (42), 5380-5588.

95. Önal, Y., Lucas, M., Claus, P. (2005) Application of a Capillary Microreactor for selective hydrogenation of α,β Unsaturated Aldehydes in Acqueous Multiphase Catalysis. *Chemical Engineering Technology*, 28 (9), 972-978.

96. Pohorecki, R. (2007) Effectiveness of interfacial area for mass transfer in two-phase flow in microreactors. *Chemical Engineering Science*, 62 (22), 6495-6498.

97. Pohorecki, P. and Kula, K. (2008) A simple mechanism of bubble and slug formation in Taylor flow in microchannels. *Chemical Engineering Research and Design*, 86 (9), 997-1001.

98. Pugh, R.I., Drent, E., Pringle, P. G. (2001) Tandem isomerisation-carbonylation catalysis: highly active palladium catalysts for the selective methoxycarbonylation of internal alkenes to linear esters. *Chemical Communications*, (16), 1476-1477.

99. Pugh, R. I., Drent, E. (2002) Methoxycarbonylation versus hydroacylation of ethene;dramatic influence of the ligand in cationic palladium catalysis. *Advanced synthesis & catalysis*, 344 (8), 837-840.

100. Reinecke, N., Petrisch, G., Boddem M. and Mewes, D. (1997) Tomographic imaging of the imaging of the phase distribution in two phase slug flow. *International Journal of Multiphase Flow*, 24 (4), 617-634.

101. Russum, J. P., Jones, C. W. and Schork, F.J. (2006) Impact of flow regime on polydispersity in tubular RAFT microemulsion pokymerization. *AIChE*, 52 (4), 1566-1576.

102. Qian D. and Lawal, A. (2006) Numerical study on gas and liquid slugs for Taylor flow in a T-junction microchannel. *Chemical Engineering Science,* 61 (23), 7609-7625.

103. Santacesaria, E. (1999) Fundamental Chemical Kinetics: the first step to reaction modelling and reaction engineering. *Catalysis Today*, 52 (2-3), 113-123.

104. Schwartz, L. W., Princen, H. M. and Kiss, A. D. (1986) On the motion of bubbles in capillary tubes', *Journal of Fluid Mechanics*, 172, 259-275.

105. Seayad, A., Kelkar, A. A. and Chaudhari, R.V. (1998) Kinetics of Carbonylation of Styrene Using Homogeneous Palladium Complex Catalyst. *Industrial Engineering Chemical Research*, 37 (6), 2180-2187.

106. Smith, J. M., van´t Riet, K. and Middleton, J.C. (1977) Proc.2nd Eur. Conf. on Mixing, St. John.s College, Cambridge, England, *BHRA Fluid Eng*., Cranfield, England, F4-51.

107. Sobieszuk, P., Cyganski, P. and Pohorecki, R. (2010) Bubble lengths in the gas-liquid flow in microchannels', *Chemical Engineering Research and Design*, 88 (3), 263-269.

108. Stenberg, O. and Andersson, B. (1988) Gas-liquid Mass Transfer in Agitated Vessels- II. Modelling of Gas-liquid Mass Transfer. *Chemical Engineering Science*, 43 (3), 725-730.

109. Tan J., Li, W., Wang, K. and Luo, G.S. (2009) Gas-liquid flow in T-junction microfluidic devices with a new perpendicular rupturing flow route. *Chemical Engineering Journal*, 146 (3), 428-433.

110. Taylor, G. I. (1961) Deposition of a viscous fluid on the wall of a tube', *Journal of Fluid Mechanics*, 10, 161-165.

111. Tesser, R., Di Serio, M., Santacesaria, E. (2003) Influence of the vapor-liquid equilibria (VLE) on the kinetics in gas-liquid and gas-liquid-solid systems. *Catalysis Today*, 79-80, 323-331.

112. Thulasidas, T. C., Abraham, M. A., Cerro, R. L (1995) Bubble-train flow in capillaries of circular and square cross-section. *Chemical Engineering Science*, 50 (2), 183-199.

113. Thulasidas, T. C., Abraham, M. A., Cerro, R. L. (1999) Dispersion during bubble-train flow in capillaries. *Chemical Engineering Science*, 54(1), 61-76.

114. Tong, H. D. , Berenschot, J.W. E., De Boer, M. J., Gardeniers, J. G. E., Wenink, H., Jansen, H. V., Nijdam, W., Elwensopek, M. C., Gielens, F.C. , Van Rijn, C. J. M (2003) Microfabrication of Palladium-Silver Alloy Membranes for Hydrogen Separation. *Journal of Electromechanical Systems*, 12 (5).

115. Torres A. (2009) Measuring gas solubility using NMR. PhD Thesis, *University of Liverpool, UK*.

116. Triplett, K. A., Ghiaasiaan, S. M., Abdel-Khalik, S. I. and Sadowski, D. L. (1999) Gas–liquid two-phase flow in microchannels Part I: two-phase flow patterns. *International Journal of Multiphase Flow*, 25 (3), 377-394.

117. Tromp, M. (2003) Deactivation process of homogeneous Pd catalysts using in situ time resolved spectroscopic techniques. Chemical *Communications*, (1), 128-129.

118. Trzeciak, A. M., Ziolkowski, J. J. (2005) Structural and mechanistic studies of Pd-catalyzed C-C bond formation: The case of carbonylation and Heck reaction., *Coordination Chemistry Reviews*, 249 (21-22), 2308-2322.

119. van Baten, J. M., Krishna, R. (2004) CFD simulations of mass transfer from Taylor bubbles rising in circular capillaries. *Chemical Engineering Science* 59, 2535–2545.

120. van Rijn, C. J. M., Nijdam, W. ,Kuiper, S. , Veldhuis, G. J., van Wolferen, H. and Elwenspoek, M. (1999) Microsieves made with laser interference lithography for micro-filtration applications. *Journal of Micromechanics and Microengineering* 9 (2), 170-172.

121. Vandu, C. O., Liu, H., Krishna, R. (2005) Mass transfer from taylor bubbles in single capillaries. *Chemical Engineering Science*, 60 (22), 6430-6437.

122. Vavasori, A. ,Cavinato, G. , Toniolo, L. (2001) Effect of a hydride source (water, hydrogen, p-toluenesulfonic acid) on the hydroesterification of ethylene to methyl propionate using a $Pd(PPh_3)_2(TsO)_2$ ($TsO = p-toluenesulfonic$ anion) catalyst precursor. *Journal of Molecular Catalysis A: Chemical*, 176 (1), 11-18.

123. Vavasori, A., Toniolo, L., Cavinato, G. (2003) Hydroesterifiacation of cyclohexene using the complex $Pd(PPh_3)_2(TsO)_2$ as catalyst precursor. Effect of a hydrogen source ($TsOH, H_2O$) on the TOF and a kinetic study ($TsOH = p-toluenesulfonic \cdot acid$). *Journal of Molecular Catalysis A: Chemical*, 191 (1), 9-21.

124. Warnier, M. J. F., de Croon, M .H. J. M., Rebrov, E. V., Schouten, J. C. (2010) Pressure drop of gas-liquid Taylor flow in round micro-capillaries for low to intermediate Reynolds numbers. *Microfluid Nanofluid*, 8 (1), 33-45.

125. Wenn, D. A., Shaw, J. E. A., Mackenzie, B. (2003) A mesh microreactor for 2-phase reactions. *Lab on a Chip*, 3, 180-186.

126. Wilhite, B. A., Schmidt, M. A., Jensen, K. F. (2004) Palladium-Based Micromembranes for Hydrogen Separation: Device Performance and Chemical Stability. *Industrial Engineering Chemistry Research*, 43 (22), 7083-7091.

127. Wolowska, J., Eastham, G. R., Heaton, B. T., Iggo, J. A., Jacob, C., Whyman, R. (2002) The effect of mechanistic pathway on activity in the Pd and Pt catalysed methoxycarbonylation of ethene. *Chemical Communications*, (23), 2784-2785.

128. Xia, G. D., Cui, Z. Z., Liu, Q., Zhou, F. D., Hu, M. S (2009) A model for liquid slug distribution in vertical gas-liquid slug flow. *Journal of Hydrodynamics*, 21(4), 491-498.

129. Yue, J., Chen, G. W., Yuan, Q., Luo, L., Gonthier, Y. (2007) Hydrodynamics and mass transfer characteristics in gas-liquid flow through a rectangular microchannel. *Chemical Engineering Science*, 62 (7), 2096-2108.

130. Yue, J., Luo, L., Gonthier, Y., Chen, G. and Yuan, Q. (2008) An experimental investigation of gas-liquid two-phase flow in single microchannel contactors. *Chemical Engineering Science*, 63 (16), 4189-4202.

131. Zanfir, M., Sun, X. and Gavriilidis, A. (2008) Microstructured Mesh Contactor for Asymmetric Transfer Hydrogenation with Simultaneous Stripping: Modelling and Experiments. *Industrial Engineering Chemistry Research*, 47 (23), 8995-9005.

132. Zhao, L., Rezkallah, K. S. (1993) Gas- liquid flow patterns at microgravity conditions. *International Journal of Multiphase Flow*, 19 (5), 751-763.

133. Zudin, V. N., Chinakov, V. D., Nekipelov, V. M., Rogov, V. A. Likholobov and Yermakov Yu. I. (1989) Determination of key intermediates for homogeneous water-gas shift reaction and hydrocarbonylation of ethylene to diethyl ketone catalyzed by the 'Pd$(OAc)_2$-PPh_3-CF_3COOH/H_2O' system. *Journal of Moleculal Catalysis, 52 (1), 27-48*.

134. Zukoski, E. E. (1966) Influence of viscosity, surface tension and inclination angle on motion of long bubbles in closed tubes. Journal of Fluid Mechanics, 25, 821-837.

Bibliography

135. Bailey P. S. Jr, C. Bailey, C. (1985) Organic Chemistry: A brief survey of concepts and applications, *ALLYN AND BACON INC*.

136. Bhaduri, S., Mukesh, D. (2000) Homogeneous Catalysis, Mechanisms and Industrial Applications, *J. Wiley & SONS*.

137. Cornils, B., Herrmann, W. A., Schlogl, R., Wong, C. (2003) Catalysis from A to Z, A Concise Encyclopedia, *WILEY-VCH*.

138. Coulson, J. M, Richardson, J. F., Backhurst, J. R., Harker, J. H., (1999) Chemical Engineering, Vol 1, 6th ed., *Elsevier Science*.

139. Doraiswamy, L.K., Sharma, M. M. (1984) Heterogeneous reactions: analysis, examples and reactor design. *John Wiley & sons*.

140. Espenson, J. H. (1981) Chemical Kinetics and Reaction Mechanisms, *McGraw-Hill Book Company*.

141. Espenson, J. H. (1995) Chemical kinetics and reaction mechanisms', 2nd ed., *Mc-Graw-Hill*.

142. Levenspiel, O. (1992) Chemical Reaction Engineering, 2nd ed., *WILEY-VCH*.

143. Nakamura, A., Tsutsui, M. (1980) Principles and Applications of Homogeneous Catalysis', *J. Wiley & SONS*.

144. Ramachandran, P. A., Chaudhari, R. V. (1983) Three-Phase Catalytic Reactors. *Gordon and Breach Science Publishers*.

145. Smith, J.M. (1981) Chemical Engineering kinetics, 3rd ed., *Mc-Graw-Hill*.

146. Solomons, G., Fryhle, C. (2000) Organic Chemistry, 7th ed., *John Wiley*.

147. Trambouze, P., Van Landenghem, H., Wauquier, J. P. (1983). Institut Francais Du Petrole, *Gulf Publishing Company*.